GEOLOGICAL SURVEY OF DENMARK AND GREENLAND BULLETIN 11 · 2006

Precambrian crustal evolution and Cretaceous–Palaeogene faulting in West Greenland

Edited by
Adam A. Garde and Feiko Kalsbeek

GEOLOGICAL SURVEY OF DENMARK AND GREENLAND
DANISH MINISTRY OF THE ENVIRONMENT

Geological Survey of Denmark and Greenland Bulletin 11

Keywords
Archaean, Cretaceous–Palaeogene, deformation, faulting, geochronology, Kangâmiut dykes, Nagssugtoqidian, Rinkian, West Greenland

Cover
Flat-lying, grey Archaean orthogneisses cut by Palaeoproterozoic dolerite dykes (black), which have been deformed and rotated into near-parallellism with their host rocks during the Nagssugtoqidian orogenesis. The whole succession is cut by late- to postkinematic Nagssugtoqidian pegmatites (pink). South coast of island 11 km east of Aasiaat in the northern Nagssugtoqidian orogen. The Nagssugtoqidian deformation of Archaean rocks in this region is the main subject of Mazur *et al.* (this volume) and van Gool & Piazolo (this volume). Photo: Adam A. Garde.

Frontispiece: facing page
Archaean, syn- to postkinematic granitic sheets cutting grey orthogneiss and variably folded with their host. Coastal exposure on the north coast of Saqqarput 30 km south-east of Kangaatsiaq, within an Archaean block in the northern Nagssugtoqidian orogen that has largely escaped Palaeoproterozoic deformation. Compare with the cover photograph displaying an example of Palaeoproterozoic deformation, and see articles by Mazur *et al*. and Thrane & Connelly (this volume). Photo: Adam A. Garde.

Receipt/acceptance dates of manuscripts: see end of individual articles
Printed: 5 December 2006

ISSN 1604-8156
ISBN-10: 87-7871-188-6
ISBN-13: 978-87-7871-188-5

Geological Survey of Denmark and Greenland Bulletin
The series *Geological Survey of Denmark and Greenland Bulletin* replaces *Geology of Denmark Survey Bulletin* and *Geology of Greenland Survey Bulletin*.

Citation of the name of this series
It is recommended that the name of this series is cited in full, viz. *Geological Survey of Denmark and Greenland Bulletin*.
If abbreviation of this volume is necessary, the following form is suggested: *Geol. Surv. Den. Green. Bull.* 11, 204 pp.

Available from
Geological Survey of Denmark and Greenland (GEUS)
Øster Voldgade 10, DK-1350 Copenhagen K, Denmark
Phone: +45 38 14 20 00, fax: +45 38 14 20 50, e-mail: geus@geus.dk
or
Geografforlaget ApS
Rugårdsvej 55, DK-5000 Odense C, Denmark
Phone: +45 63 44 16 83, fax: +45 63 44 16 97, e-mail: go@geografforlaget.dk

Contents

Preface

The present volume marks the completion of a large research project by the Geological Survey of Denmark and Greenland (GEUS), focused on the northern part of the Palaeoproterozoic Nagssugtoqidian orogen of central West Greenland, and carried out by a team of Danish and international participants. The project comprised geological mapping as well as structural, geochronological, geochemical and economic geological studies. This volume contains reports on both Archaean and Palaeoproterozoic geology as well as a study of neotectonic brittle structures. The field work was carried out in 2000–2003 in the region between Nordre Strømfjord and Jakobshavn Isfjord (see e.g. van Gool & Piazolo 2006, this volume, fig. 1). The project had two immediate purposes, namely to establish an overview of the mineral resource potential of supracrustal rocks in the region between 66° and 70°15′N, and produce four new geological sheets in the Survey's 1:100 000 map series.

The first collection of papers about the Nagssugtoqidian orogen, published by the Geological Survey of Greenland (GGU, now part of GEUS), dates back to 1979 (Korstgård 1979). The investigations in this period were mainly based on field descriptions and structural analysis of coastal areas in the southern and central parts of the orogen, combined with limited petrographical, palaeomagnetic and geochronological studies; the results also comprised the first 1:100 000 geological map from within the Nagssugtoqidian orogen (Olesen 1984). The Proterozoic age of the orogen had been established, but it was believed that most, if not all of the quartzofeldspathic basement gneisses were of Archaean origin.

Subsequent work in the Nagssugtoqidian orogen by GGU in the 1980s showed that besides Archaean orthogneisses and supracrustal rocks, the central part of the orogen also comprises the root zone of a Palaeoproterozoic magmatic arc and associated panels of Palaeoproterozoic volcanic and metasedimentary rocks (Kalsbeek *et al.* 1987). These results were confirmed during further investigations by the Danish Lithosphere Centre (DLC) in 1994–1999, and the plate-tectonic collisional history of the southern and central Nagssugtoqidian orogen was described in detail (van Gool *et al.* 2002). However, these studies added little to previous knowledge of the northern parts of the orogen in the Kangaatsiaq–Aasiaat–Qasigiannguit region, knowledge that was largely based on coastal reconnaissance by Henderson (1969) at the time when the entire orogen was still believed to consist of Archaean rocks.

Another project preceding the present work was carried out by GGU in 1988–1991 immediately north of the Nagssugtoqidian orogen, in the southernmost part of the likewise Palaeoproterozoic Rinkian fold belt (Disko Bugt project, Kalsbeek 1999). It was shown that also the latter region comprises Palaeoproterozoic (meta)sedimentary rocks, and that most of the Archaean basement is strongly overprinted by Palaeoproterozoic structures that were formed during overall W- or NW-directed lateral tectonic transport. Although these structures might be related to similar structures in the Nagssugtoqidian orogen, the relationship between the Nagssugtoqidian orogen and the Rinkian fold belt remained speculative.

The only previous economic geological study of regional extent in central West Greenland was an airborne reconnaissance study supplemented by local field work, which was carried out in the early 1960s by Kryolitselskabet Øresund A/S. This work resulted in the discovery of a massive sulphide deposit at Naternaq (Lersletten), which was studied again in some detail in 2001 by the Survey (Østergaard *et al.* 2002) but not reported on in the present volume.

The present volume comprises 12 papers with topics ranging geochronologically from mid-Archaean to Palaeogene, and geographically from the southern Nagssugtoqidian foreland to the central part of the Rinkian fold belt. Many of the papers deal with the northern part of the Nagssugtoqidian orogen and are related to the recent field work in that region, while a few contributions are rooted in DLC- or other projects. The papers have been arranged in approximate chronological order and are grouped in terms of their main subjects.

The two first papers, by Hollis *et al.* and Moyen & Watt, deal with Archaean supra- and infracrustal rocks in the northern Nagssugtoqidian orogen: their origin, ages, and structural and metamorphic evolution. These papers provide insight into the age and origin of the continental crustal orthogneisses and granites that underlie most of the region, and discuss the relationships between the supracrustal and plutonic components, using zircon U-Pb age determinations and major and trace element geochemical characteristics. Also the question of Palaeoproterozoic tectonic overprint is discussed, with the conclusion

from both study areas that most of the observed structures are Archaean.

The third paper with focus on Archaean geology, by Stendal *et al.*, describes a small gold prospect at Attu likewise in the northern Nagssugtoqidian orogen, and discusses the age of the prospect and its host rocks using Pb-Pb geochronology of magnetite. It is concluded that the host rocks at Attu may be as old as 3162 ± 43 Ma, and that the gold prospect itself is around 2650 Ma in age.

The fourth paper, by Mayborn & Lesher, is a thorough review of the Kangâmiut dyke swarm in the southern Nagssugtoqidian orogen and its foreland. It includes new whole-rock and mineral chemical data, and a list of sampling sites and corresponding field data. The emplacement mechanism and depth of the dyke swarm are discussed in detail, and it is concluded that the dykes were emplaced during the initial rifting prior to the Nagssugtoqidian collision and that they are unrelated to subduction processes (contrary to the belief by some previous authors).

The next three papers provide geochronological constraints on the ages of supra- and infracrustal rocks and the deformation and metamorphism in the northern Nagssugtoqidian orogen, and on late orogenic uplift in the central Rinkian fold belt. In the first of these papers Thrane & Connelly employ zircon U-Pb age determinations (mainly using the laser ICP-MS method), and for the first time provide unequivocal documentation that the Naternaq supracrustal belt is of Palaeoproterozoic age. Other zircon age data from a synkinematic granite southeast of Kangaatsiaq show that the large fold structures in this region are of Archaean age. The subsequent paper by Stendal *et al.* presents Pb-Pb ages and isotopic signatures of magnetite in amphibolites; the obtained ages are younger than 1800 Ma and are related to cooling of the orogen. Stepwise leaching Pb-Pb ages of monazite and allanite in pegmatites fall in the range of 1750–1800 Ma, and are interpreted to date the emplacement of these rocks. The third paper in this group, by Sidgren *et al.*, deals with new $^{40}Ar/^{39}Ar$ ages of around 1790 Ma (hornblende) and 1680 Ma (muscovite) from Archaean and Palaeoproterozoic rocks in the central Rinkian fold belt, which are interpreted as orogenic cooling ages. The hornblende ages are significantly older than such hornblende ages previously obtained from the central and northern Nagssugtoqidian orogen, pointing to different uplift histories in the two regions. This may in turn suggest that the Rinkian continental collision preceded that in the Nagssugtoqidian orogen.

Four of the remaining five papers deal with the Nagssugtoqidian structural evolution. In the first of these, van Gool & Piazolo present a new method of structural analysis, where a geographical information system (GIS) is used as a framework for visualisation and analysis of large amounts of structural data. The paper graphically presents an overview of thousands of data points within an area of approximately 160 × 180 km in the central and northern parts of the Nagssugtoqidian orogen. This interesting data set points directly towards the two next papers, where crustal-scale structures in the same region and their origin are discussed: Sørensen *et al.* address the prominent Nordre Strømfjord shear zone just south of this block, and describes the structural and metasomatic transition into the shear zone by means of aeromagnetic and lithological map patterns and geochemical data. Another paper, by Mazur *et al.*, addresses a prominent break in the structural pattern within the Kangaatsiaq–Aasiaat area, where the southern part acted as a rigid block during the Nagssugtoqidian orogeny and thus preserved its Archaean structure. The fourth paper in this group, by Korstgård *et al.*, combines rock and aeromagnetic data to discuss the relationship between structure, metamorphic facies and total magnetic field intensity anomalies in the southern Nagssugtoqidian orogen. The authors show that static metamorphic boundaries are gradual, whereas boundaries along deformation zones are abrupt.

The last paper, by Wilson *et al.*, is a novel remote sensing and field geological analysis of onshore brittle structures related to the complex Ungava fault zone in the Davis Strait, which developed during the Cretaceous–Palaeogene opening of the Labrador Sea – Davis Strait – Baffin Bay seaway. The study area is located in the central Nagssugtoqidian orogen, and the authors carefully establish a distinction between old Nagssugtoqidian and younger structures in the basement rocks and identify five main sets of young lineaments. They conclude that the onshore fault patterns are predominantly of strike-slip nature, and that they reflect the stress fields that governed the opening of the seaway.

Acknowledgements

The editors are grateful to the 14 external reviewers, each of whom reviewed one or more of the individual papers, for their thorough and constructive work.

References

Henderson, G. 1969: The Precambrian rocks of the Egedesminde–Christianshåb area, West Greenland. Rapport Grønlands Geologiske Undersøgelse 23, 37 pp.

Kalsbeek, F. (ed.) 1999: Precambrian geology of the Disko Bugt region, West Greenland. Geology of Greenland Survey Bulletin 181, 179 pp.

Kalsbeek, F., Pidgeon, R.T. & Taylor, P.N. 1987: Nagssugtoqidian mobile belt of West Greenland: a cryptic 1850 Ma suture between two Archaean continents – chemical and isotopic evidence. Earth and Planetary Science Letters 85, 365–385.

Korstgård, J.A. (ed.) 1979: Nagssugtoqidian geology. Rapport Grønlands Geologiske Undersøgelse 89, 146 pp.

Olesen, N.Ø. 1984: Geological map of Greenland, 1:100 000, Agto 67 V.1 Nord. Copenhagen: Geological Survey of Greenland.

Østergaard, C., Garde, A.A., Nygaard, J., Blomsterberg, J., Nielsen, B.M., Stendal, H. & Thomas, C.W. 2002: The Precambrian supracrustal rocks in the Naternaq (Lersletten) and Ikamiut areas, central West Greenland. Geology of Greenland Survey Bulletin 191, 24–32.

van Gool, J.A.M. & Piazolo, S. 2006: Presentation and interpretation of structural data from the Nagssugtoqidian orogen using a GIS platform: general trends and features. In: Garde, A.A. & Kalsbeek, F. (eds): Precambrian crustal evolution and Cretaceous–Palaeogene faulting in West Greenland. Geological Survey of Denmark and Greenland Bulletin 11, 125–144 (this volume).

van Gool, J.A.M., Connelly, J.N., Marker, M. & Mengel, F.C. 2002: The Nagssugtoqidian orogen of West Greenland: tectonic evolution and regional correlation from a West Greenland perspective. Canadian Journal of Earth Sciences 39, 665–686.

Adam A. Garde and Feiko Kalsbeek

Evolution of Neoarchaean supracrustal belts at the northern margin of the North Atlantic Craton, West Greenland

Julie A. Hollis, Marie Keiding, Bo Møller Stensgaard, Jeroen A.M. van Gool and Adam A. Garde

The Archaean North Atlantic Craton of West Greenland collided at *c.* 1.9 Ga with a lesser-known Archaean craton to the north, to form the Nagssugtoqidian orogen. The Palaeoproterozoic metamorphic grade and strain intensity decrease northward through the orogen, allowing investigation of the reworked Archaean components in its northern part. Two Archaean supracrustal belts in this region – the Ikamiut and Kangilinaaq belts – are investigated here using field mapping, aeromagnetic data, zircon geochronology, and geochemistry. Both belts comprise quartzo-feldspathic and pelitic metasedimentary rocks, amphibolite, and minor calc-silicate rocks, anorthosite and ultramafic rocks. Pb-Pb and U-Pb dating of detrital zircons and host orthogneisses suggest deposition at *c.* 2800 Ma (Kangilinaaq belt) and after 2740 Ma (Ikamiut belt); both belts have zircons with Neoarchaean metamorphic rims. Metasedimentary rocks and orthogneisses at Ikamiut share similar steep REE signatures with strong LREE enrichment, consistent with local derivation of the sediment and deposition directly onto or proximal to the regional orthogneiss precursors. Zircon age data from Kangilinaaq indicate both local and distal sources for the sediment there. Geochemical data for Kangilinaaq amphibolites indicate bimodal, mixed felsic–mafic source rocks with island-arc basaltic affinities, consistent with a shelf or arc setting. Both belts experienced a similar tectono-metamorphic history involving Neoarchaean amphibolite facies peak metamorphism at *c.* 2740–2700 Ma, possibly due to continued emplacement of tonalitic and granodioritic magmas. Nagssugtoqidian lower amphibolite facies metamorphism at *c.* 1850 Ma was associated with development of the large-scale F_2 folds and shear zones that control the present outcrop pattern. The observed differences in the sources of the Kangilinaaq and Ikamiut belts and their shared post-Archaean history suggest they were formed in different Neoarchaean environments proximal to and on a continental plate, and were amalgamated in a convergent margin setting shortly after their deposition.

Keywords: North Atlantic Craton, northern Nagssugtoqidian orogen, LA-ICP-MS, SIMS, zircon

---

J.A.H., B.M.S., J.A.M.v.G. & A.A.G., *Geological Survey of Denmark and Greenland, Øster Voldgade 10, DK-1350 Copenhagen K, Denmark.* E-mail: *jho@geus.dk*
M.K., *Geological Museum, University of Copenhagen, Øster Voldgade 5–7, DK-1350 Copenhagen K, Denmark.*

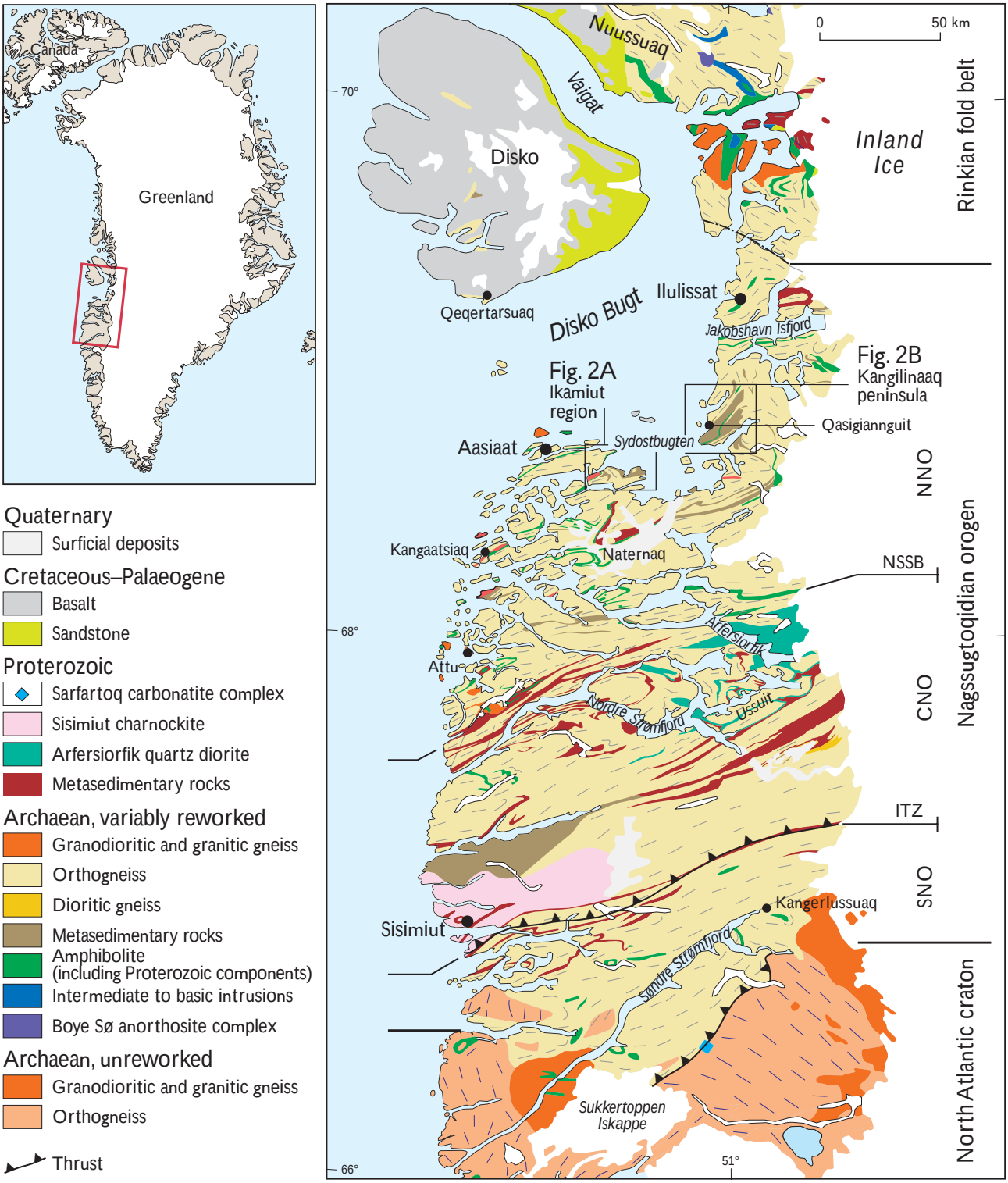

Fig. 1. Geological map of the Nagssugtoqidian orogen, West Greenland, from van Gool *et al.* (2002b). Frames show locations of Figs 2 and 3.

The Palaeoproterozoic Nagssugtoqidian orogen, central West Greenland, comprises Archaean and less abundant Proterozoic orthogneiss and metasedimentary rocks deformed and metamorphosed at *c*. 1850 Ma during collision of the North Atlantic Craton with a lesser-known, likewise Archaean craton to the north (Kalsbeek *et al*. 1987; Taylor & Kalsbeek 1990; Kalsbeek & Nutman 1996; Connelly *et al*. 2000; van Gool *et al.* 2002a). The orogen extends from Søndre Strømfjord in the south, northward to Disko Bugt and possibly farther into the largely contemporaneous Rinkian fold belt (Fig. 1). The metamorphic grade associated with orogenesis decreases from granulite facies in the collisional core (the central Nagssugtoqidian orogen) to amphibolite facies in the southern foreland and the northern part of the orogen. Also the penetrative Palaeoproterozoic deformation diminishes toward the north in the northern Nagssugtoqidian orogen (NNO), and heterogeneous strain distribution may have been important in the preservation of pre-Nagssugtoqidian, i.e. Archaean structural fabrics and metamorphic assemblages and textures (van Gool *et al*. 2002a; Garde *et al*. 2004; Hollis *et al*. 2004; Piazolo *et al*. 2004; Mazur *et al*. 2006, this volume). As a consequence of the northward decrease in the Palaeoproterozoic thermal overprint and deformation, the NNO provides an opportunity for investigation of the pre-Nagssugtoqidian history of its Archaean components. In particular, its supracrustal belts can provide valuable information on the tectonic environment(s) of their formation, their relationship to the plate-tectonic configuration, and whether different parts of the craton experienced the same or different Archaean histories.

Here we investigate two supracrustal belts within the NNO – the kilometre-wide Ikamiut and Kangilinaaq belts – that crop out on the western and eastern sides of Sydostbugten in southern Disko Bugt (Fig. 1). Parts of the NNO were mapped by the Geological Survey of Greenland in the 1960s for its 1:500 000 scale geological map series (Noe-Nygaard & Ramberg 1961; Henderson 1969) and also by the Geological Survey of Denmark and Greenland (GEUS) in 2000–2003 for the 1:100 000 scale geological map series (see below). Henderson (1969) identified a complex map-scale fold structure that dominates the Ikamiut peninsula and adjacent inland areas in the western Sydostbugten region, and also outlined many of the dominant lithologies and large structural elements in the Kangilinaaq region.

In this paper we present geological, geochemical, geochronological and geophysical data from work carried out in the period 2000–2003 by GEUS mapping teams for the Kangersuneq and Ikamiut 1:100 000 scale geological map sheets (van Gool 2005; Garde in press); part of this work is reported in more detail in Keiding (2004). Aeromagnetic data for the Sydostbugten region are correlated with major lithological and structural elements. Geochemical data from amphibolites in the Kangilinaaq region interpreted as deformed and metamorphosed basaltic volcanic rocks, and interlayered pelitic rocks, are used to determine the likely depositional environment. Zircon Pb-Pb and U-Pb geochronology on granodioritic orthogneisses and a metasedimentary rock from the Ikamiut region is compared with existing data from the Ikamiut and Kangilinaaq regions. Finally, the implications for regional Neoarchaean tectonics are discussed.

Ikamiut belt and host rocks west of Sydostbugten

The Ikamiut belt is a deformed, kilometre-thick sequence of biotite schists, with less abundant siliceous and pelitic rocks, amphibolite and minor ultramafic rocks. The belt forms a ten kilometre-scale antiform in the north-western part of Sydostbugten (Fig. 2A). It is everywhere in contact with *c*. 2830–2760 Ma old, tonalitic to granodioritic orthogneiss (Pb-Pb whole rock, Kalsbeek *et al*. 1987; U-Pb zircon, Connelly & Mengel 2000 and this study), which dominates the region. The original nature of the contacts between the supracrustal belt and the regional orthogneiss is obscured by later ductile deformation (see also Østergaard *et al*. 2002). Rb-Sr data for 12 metasedimentary samples from this belt, near Ikamiut, gave an age of *c*. 1880 Ma for closure of the Rb-Sr system and a very high initial ^{87}Sr-^{86}Sr ratio of *c*. 0.712, suggesting that these rocks were deposited at around 2.8 Ga and isotopically strongly reset during Nagssugtoqidian metamorphism (Kalsbeek & Taylor 1999).

Structure

The structural pattern is dominated by kilometre-scale, closed, upright F_2 folds folding an S_1 foliation and associated with a moderate to intense, ENE-striking S_2 foliation (Fig. 2A). Preservation of S_1 fabrics is found in areas of low D_2 strain, typically within the cores of large F_2 folds. Outcrop-scale, parasitic F_2 folds associated with weak to moderately developed mineral lineations (L_2) plunge at shallow angles to the WSW. In the eastern Ikamiut region, L_2 lineations are shallow and, in some cases, plunge to the east. Some F_2 folds may be doubly plunging and/or refolded, consistent with localised outcrop-scale refolded

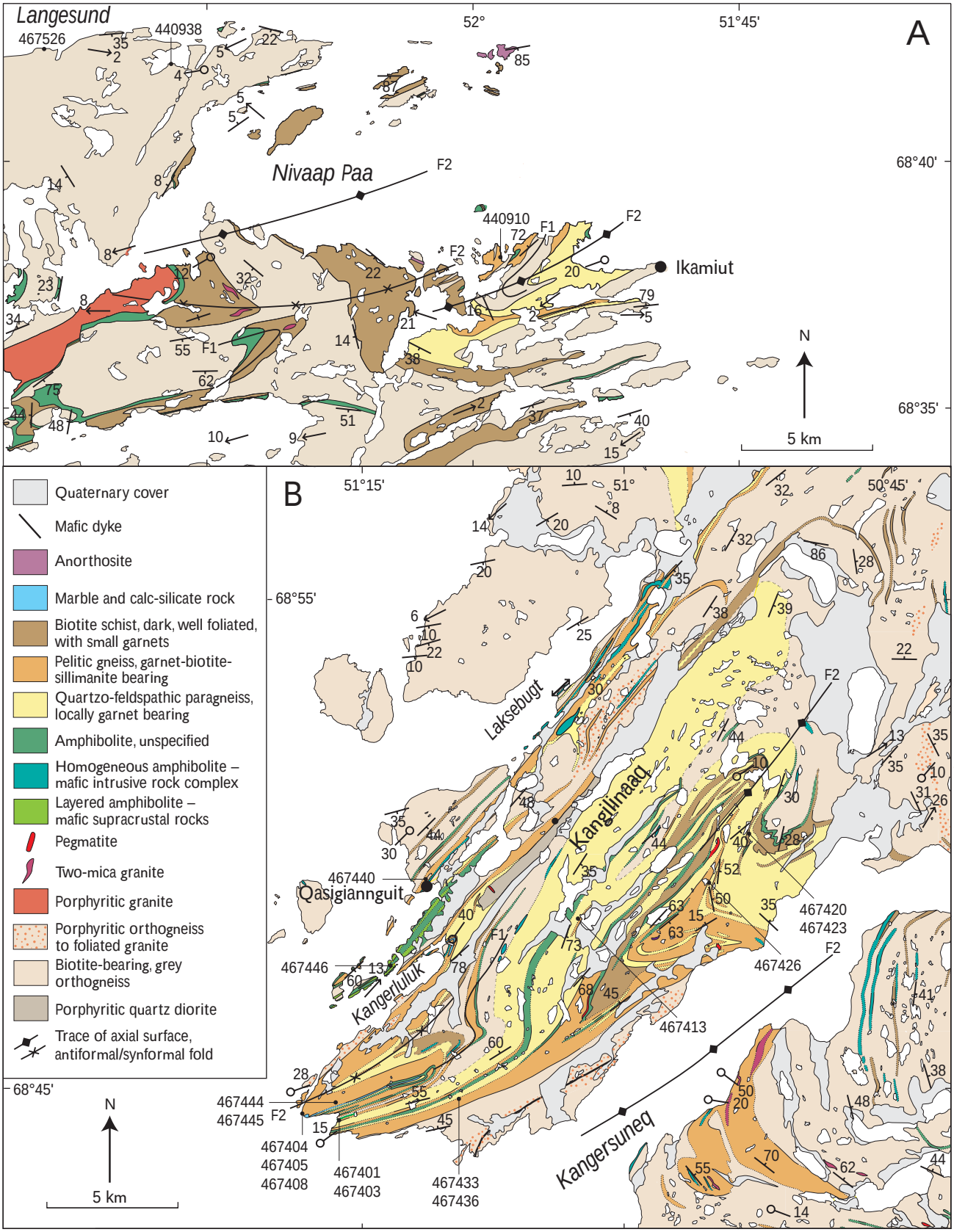

Fig. 2. Preliminary geological interpretation maps on (a) the Ikamiut region and (b) the Kangilinaaq peninsula, showing representative structural data, sample numbers and localities. For regional location see frames in Fig. 1.

folds. The kilometre-scale, upright F_2 folds are probably parasitic on the major antiformal structure that dominates the outcrop pattern. Ten to hundred metre-scale, shallowly W-plunging F_2 folds of flat-lying S_1 foliation are abundant in the tonalitic to granodioritic orthogneiss inland at the head of Nivaap Paa (Fig. 2A). These folds are difficult to trace for long distances along strike. The inland outcrop is relatively poor, and available outcrop suggests that some of the folds die out towards the west, apparently because of homogeneity and lack of ductility contrast within the orthogneiss.

Lithologies, mineral assemblages and fabrics

The tonalitic to granodioritic orthogneiss is a compositionally layered, medium-grained, pale pink and grey rock dominantly comprising plagioclase and quartz, with lesser K-feldspar and disseminated biotite. A medium- to coarse-grained gneissic layering (S_1) is discontinuous on a scale of metres to tens of metres and commonly displays intrafolial isoclinal folds. The orthogneiss typically also holds a moderate, ENE-striking S_2 foliation that is a partially to completely transposed S_1 fabric, and a weakly to moderately developed, shallow W-plunging L_2 mineral lineation. Medium- to coarse-grained, centimetre-scale granitic veins indicate variable D_2 strain: they form a layering that is typically transposed into S_2, but in some cases they are slightly discordant.

The supracrustal sequence is dominated by biotite schists to gneissic rocks that typically comprise plagioclase, quartz, biotite, and rarely garnet. Interlayered with these rocks occur local, more mica-rich and aluminous layers up to 20 m thick, which commonly display a schistose S_1 fabric. These rocks typically comprise biotite, plagioclase, quartz, muscovite, sillimanite, and garnet, with accessory tourmaline. Locally, in the most micaceous parts, a D_2 crenulation of S_1 biotite, plagioclase and quartz ± sillimanite is developed, with axial planes parallel to the dominant regional S_2 gneissosity of the tonalitic–granodioritic orthogneiss host, and fine-grained biotite and muscovite along the crenulations. Aggregates of fine-grained sillimanite and biotite in biotite-rich schists form blocky, centimetre-scale patches interpreted as pseudomorphs after andalusite. This suggests that the S_1 fabrics and assemblages were formed at low-pressure (< 3.85 kbar), lower amphibolite facies metamorphic conditions, followed by increasing temperature (and possibly also pressure) into sillimanite-grade conditions.

A distinct unit of siliceous paragneiss, locally garnet-bearing, is also volumetrically important. It is distinguished from the biotite schist/gneiss by its more quartz-rich and mica-poor composition. It is often difficult to distinguish this lithology from the tonalitic to granodioritic orthogneiss, particularly in inland areas where outcrop is poor.

Amphibolite layers, which are 10–50 m thick and laterally discontinuous on a kilometre-scale, are associated with the metasedimentary sequence. They commonly occur at or near boundaries between the metasedimentary rocks and orthogneiss. The amphibolites are medium grained and comprise hornblende with lesser plagioclase and quartz, and locally clinopyroxene ± garnet. In some cases they show distinct mafic–felsic layering, and they commonly contain thin (0.5–5 cm), discontinuous felsic layers.

A few isolated occurrences of intensely deformed anorthosite occur at tectonised boundaries between the tonalitic to granodioritic orthogneiss and metasedimentary rocks. The largest occurrence is in the northern island group of Nivaap Paa (Fig. 2A). The anorthositic rock is coarse grained and 'zebra-striped', and consists of hornblende and calcic plagioclase with a variably developed foliation and an intense linear fabric. The mafic parts are commonly boudinaged within the more felsic component.

An extensive body of medium- to coarse-grained granite is located within the hinge zone of the large antiformal structure along the southern coast of Nivaap Paa. The granite is porphyritic and white to red in colour, and holds a weak gneissose fabric. Its northern contact with the regional orthogneiss is tectonised and possibly tectonically repeated. The relatively undeformed nature of the granite suggests it intruded into the orthogneiss after formation of the regional gneissose fabric (S_2). The granite contains thin lenses and layers of medium-grained amphibolite, and is bounded to the south by a layer of amphibolite 50–400 m thick, the outcrop of which defines a tight synformal fold closure (Fig. 2A).

Kangilinaaq belt and host orthogneiss east of Sydostbugten

The Kangilinaaq peninsula (Fig. 2B) is dominated by a kilometre-scale synformal structure comprising a series of NE-trending, upright, isoclinal F_1 and F_2 folds that repeat a thick supracrustal sequence. The most common lithologies are quartzo-feldspathic and pelitic metasedimentary rocks, with lesser amphibolite and subordinate marble and calc-silicate rocks. An equivalent supracrustal sequence is found south of Kangersuneq fjord, on the southern limb of an antiformal fold running through the fjord. A lithologically distinct unit of amphibolite and associated metasedimentary rocks runs through the town

of Qasigiannguit in the west of the peninsula. For ease of reference this unit is named the Qasigiannguit amphibolite in the following. It is separated from the main supracrustal sequence by 200–500 m of high-strain Archaean orthogneiss. The significance of this high-strain zone in terms of the original supracrustal stratigraphy is uncertain, and thus the Qasigiannguit amphibolite may or may not be part of an originally continuous supracrustal series on the Kangilinaaq peninsula. For descriptive reasons the two supracrustal sequences are collectively termed the Kangilinaaq belt in the following.

Pelitic rocks from the main supracrustal sequence contain Archaean detrital zircon populations in the range 2820–2760 Ma, with a minimum depositional age constrained by an intrusive two-mica granite at 2723 ± 15 Ma (Thrane & Connelly 2006, this volume). Metamorphic zircon growth occurred at 1920–1820 Ma in various rocks (Keiding 2004; Thrane & Connelly 2006, this volume). Age data are addressed in more detail in the discussion.

Structure

The structural pattern is dominated by large, tight to isoclinal folds. Especially along the south-eastern side of the peninsula, the quartzo-feldspathic and pelitic rocks are intensely folded into upright folds on scales from decimetres to tens of metres with shallowly NE-plunging fold axes. Older, isoclinal, often intrafolial folds indicate that the upright folds are at least second-generation (F_2). A shear zone containing mylonitic orthogneiss bounds the supracrustal rocks to the south-east. It can be traced from the south-western part of the peninsula to half-way up Kangersuneq fjord, where it meets the water (Fig. 2B). Kinematic indicators and a lineation suggesting sinistral/top to the west movement are poorly developed in the shear zone. The continuation of the shear zone may be found in a poorly developed, but continuous SE-trending shear zone south of Kangersuneq fjord, marked by a sliver of metasedimentary rocks. North-west of the supracrustal sequence, no similar shear zone was found, although some smaller zones of high strain were recognised.

Lithologies, mineral assemblages and fabrics

The predominant regional lithologies are layered, grey tonalitic to granodioritic orthogneisses interleaved with supracrustal rocks. The orthogneisses contain variable proportions of plagioclase, quartz and biotite, with minor K-feldspar and hornblende. Compositional layering of orthogneiss with thin amphibolite layers interpreted as highly attenuated enclaves, give the rocks a layered appearance. The orthogneisses are intersected by concordant to slightly discordant, medium- to coarse-grained, centimetre- to half metre-scale granitic veins interpreted as derived from local melts. The orthogneisses show intrusive contacts into part of the supracrustal sequence (see below), although it is not certain that this relationship applies to all of the supracrustal rocks on the peninsula. The gneissic fabric of orthogneiss in the core of the peninsula is locally disturbed by pods and sweats of partial melt, which can contain millimetre-sized garnets. Garnet formation in the orthogneiss is restricted to the core of the peninsula, a region of abundant metasedimentary rocks. The garnet formation may be the product of contamination during partial melting of the metasedimentary rocks, either during intrusion of the precursors to the orthogneiss, or during metamorphism.

Variably deformed quartz diorite occurs in two localities. Typically it has tectonised contacts with the supracrustal rocks, but east of Qasigiannguit it has intrusive contacts to the latter and has yielded a U-Pb zircon emplacement age of 2801 ± 34 Ma (Thrane & Connelly 2006, this volume).

The main supracrustal sequence is dominated by medium-grained, quartzo-feldspathic metasedimentary rocks that commonly contain garnet. Where garnet is absent in these rocks, they are difficult to distinguish from the orthogneisses. The quartzo-feldspathic paragneiss alternates on metre- to 100 metre-scale with pelitic rocks, amphibolite and rare calc-silicate rocks. The pelitic rock comprises quartz, plagioclase, biotite, garnet, and sillimanite. Locally, it has a large component of granitic partial melt, commonly occurring in boudinaged lenses, indicative of upper amphibolite facies metamorphic conditions. Amphibolites are commonly dark and subtly layered, fine to medium grained and few metres to 50 m wide. Remnants of deformed pillows are locally present. In the eastern part of the sequence isolated lenses of metamorphosed ultramafic rocks occur in a few locations, commonly within amphibolites. They comprise predominantly amphibole and orthopyroxene, with or without clinopyroxene, olivine, phlogopite, and serpentinite. Minor calc-silicate rocks are layered, with variable grain size, and comprise calcite, phlogopite, quartz, tremolite and locally actinolite. Pelitic rocks in this sequence are commonly coarse grained and comprise quartz, biotite, garnet, plagioclase, and sillimanite. Large lumps of fibrous sillimanite (up to 3 cm in diameter) are likely pseudomorphs after andalusite. Rare pseudomorphs of sillimanite after kyanite were also found.

This may indicate variability in pressure conditions in the Kangilinaaq belt or prograde Barrovian-style metamorphism. Quartzo-feldspathic metasedimentary rocks in the central/northern part of the synform are coarse grained, heterogeneous, and rarely garnet-bearing.

The Qasigiannguit sequence comprises mafic and felsic metavolcanic rocks intercalated with clastic sequences and isolated layers and lenses of strongly deformed, zebra-striped anorthosite. The sequence is *c*. 700 m wide, trends SW–NE, and is well exposed on the islands south-west of Qasigiannguit. The rocks are isoclinally folded with an intrafolially folded gneissic fabric. As mentioned above it is separated from the predominantly clastic sequence of Kangilinaaq by 200–500 m of high-strain Archaean orthogneiss (Fig. 2B; see also below). In contrast with the main supracrustal belt, the metamorphic grade is lower amphibolite facies. The fine- to medium-grained, layered amphibolite contains hornblende and plagioclase, and minor clinopyroxene, epidote, biotite, quartz, and possibly also chlorite. Only along Laksebugt is the amphibolite locally garnet-bearing. Felsic layers can be up to several metres wide and contain predominantly plagioclase and quartz, with minor amphibole, white mica and titanite. Pelitic and semipelitic layers up to 50 m wide occur mainly on the islands south-west of Qasigiannguit. These layers are generally schistose and contain predominantly quartz, plagioclase, biotite and minor garnet, while sillimanite and muscovite are rare. In exposures 25 km north-east of Qasigiannguit, an outcrop of kyanite-bearing pelite shows no indications of replacement by sillimanite. This is the only known occurrence in the north-eastern part of the Nagssugtoqidian orogen of stable kyanite, although this mineral has also been described from Archaean supracrustal rocks within the southern part of the Rinkian fold belt (Garde & Steenfelt 1999). Fine-grained, dark grey biotite-rich schist/gneiss forms layers 50–80 m wide that grade locally into layered amphibolites. Homogeneous, medium-grained, greyish green, quartzo-feldspathic gneisses form layers up to 30 m wide that are generally platy and contain quartz, plagioclase, white mica, and amphibole. Their origin is uncertain. Their occurrence in a layered supracrustal sequence, without obvious intrusive contacts, could indicate that these rocks are also of supracrustal origin, but similar rocks in the main Kangilinaaq sequence grade into low-strain megacrystic granodiorite to quartz diorite. The contacts between the Qasigiannguit amphibolite and the regional Archaean orthogneiss are always tectonised, and their original contact relationships are uncertain. However, lenses of amphibolite, and locally also anorthosite, occur abundantly as inclusions in the regional Archaean orthogneiss close to its contacts with the supracrustal sequence. These lenses are unlikely to be tectonic because they occur in an irregular pattern, not along zones of high strain. It is more likely that they are xenoliths, suggesting that the orthogneiss precursors intruded into the supracrustal sequence.

Aeromagnetic characteristics

Aeromagnetic data covering the Ikamiut and Kangilinaaq regions (Thorning 1993) allow us to image geological features in terms of magnetic responses, also in areas covered by lakes, sea and overburden. A spacing of flight lines of 1 km and a survey altitude of 500 m control the resolution of the aeromagnetic data. In order to enhance the anomaly patterns from shallow-seated geological features, a separation filter has been applied (Jacobsen 1987). The filter enhances magnetic anomalies caused by geological features within a specific depth interval in the crust. The rationale of the filter is that the upward continuation of a potential field to a selected height represents the field from sources in the crust below half the selected height. The difference, or residual, between fields at two different heights can then be viewed as representing the field from sources within the corresponding depth interval in the crust. Thus, a total magnetic field that has been continued upward to a height of 2 km represents sources in the crust below 1 km. Likewise, the field observed at 500 m represents sources below 250 m. Consequently, the residual obtained from these two fields by subtraction represents an enhanced image of the anomaly pattern of geological features in the depth interval 250 m – 1 km. The resulting 'subsurface' total magnetic field for the Ikamiut–Kangilinaaq region is shown in Figs 3–5. In view of the fundamental ambiguity and complexity of the magnetic field separation, the filtering should only be used as a tool for detection of anomalies and discrimination of patterns, and qualitative interpretations should be supported by other types of geological data.

Aeromagnetic patterns in the Ikamiut region

The supracrustal rocks in the Ikamiut region appear as intermediate to low magnetic anomalies in the separation-filtered total magnetic field intensity map (–1 to –30 nT, A's in Fig. 4). The orthogneisses are expressed as slightly higher magnetic anomalies (5–20 nT, B and C in Fig. 4), although these show considerable variability that may be a consequence of differing contributions from other subsurface lithologies. From the aeromagnetic anomalies it is

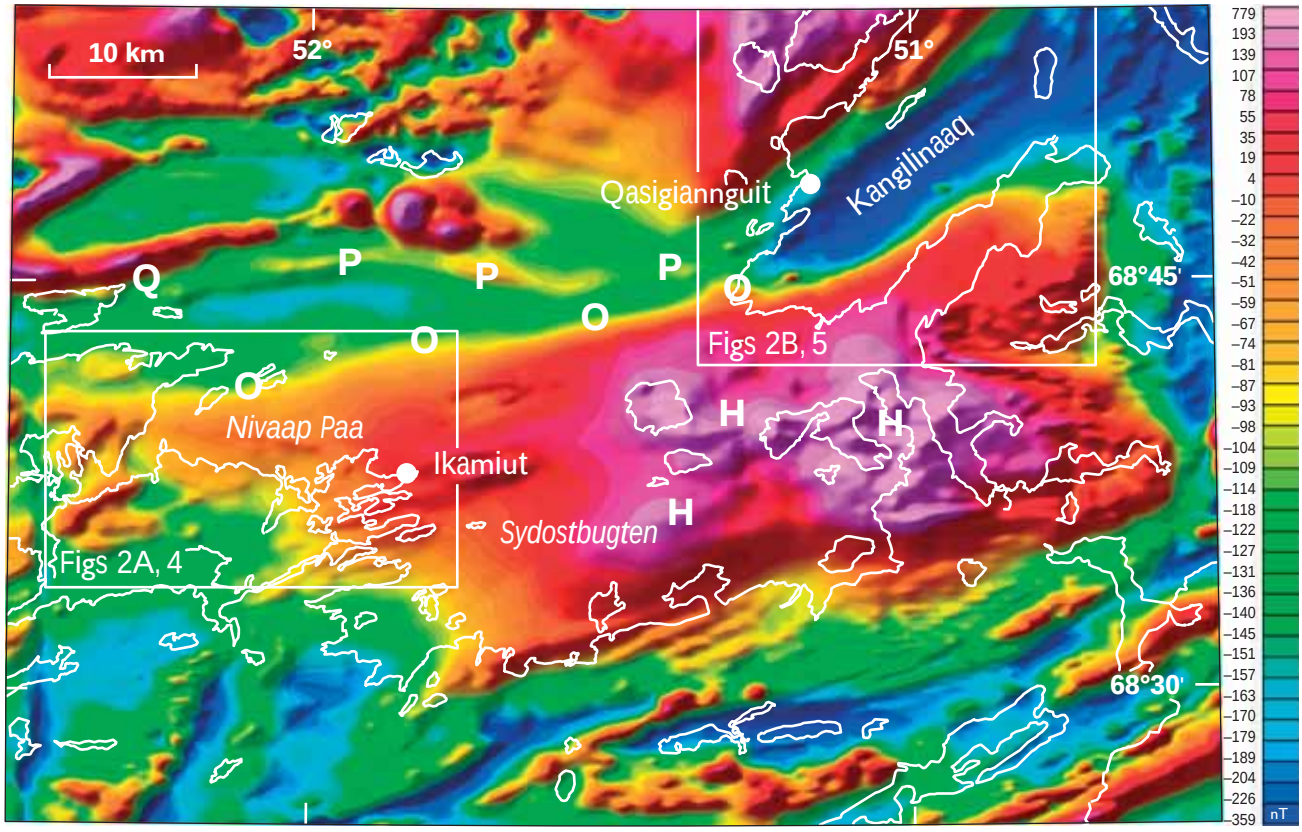

Fig. 3. Total magnetic field intensity for the Ikamiut and Kangilinaaq regions. The labels H, O, P and Q are referred to in the main text. A shadowing effect from NW (315°N) with an inclination of 45° has been applied. The areas of Figs 4 and 5 are outlined by white frames.

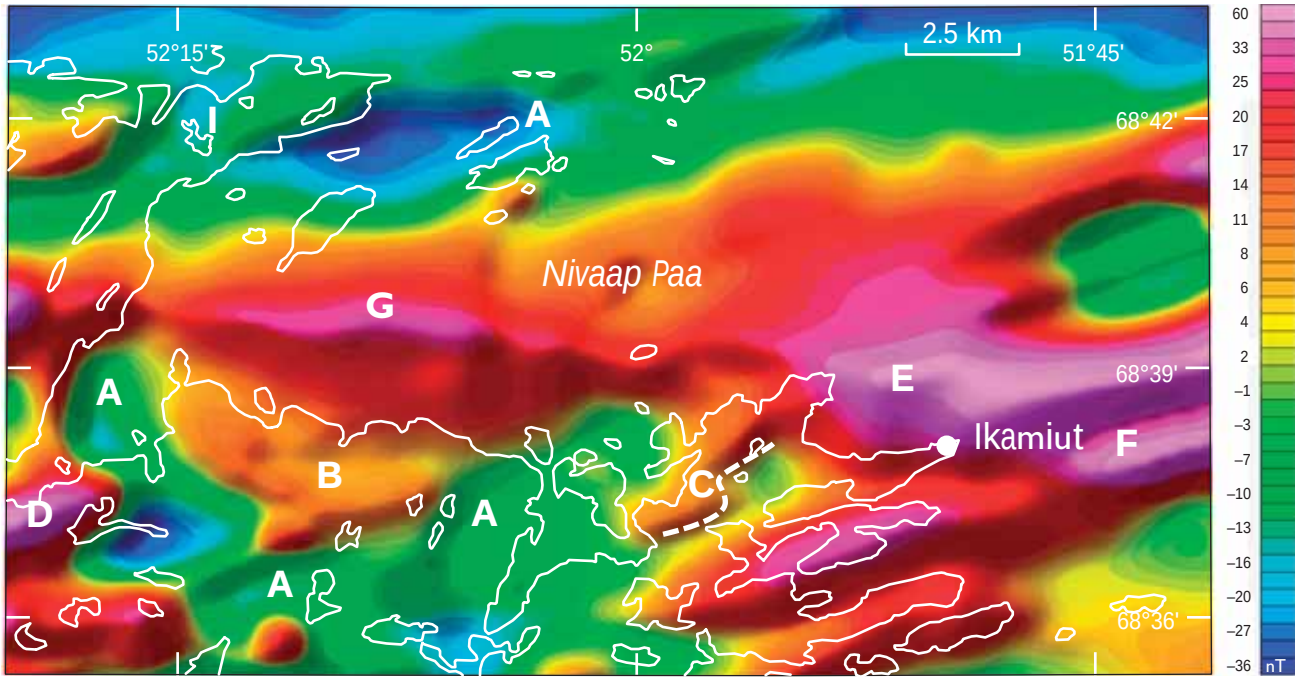

Fig. 4. The separation-filtered total magnetic field intensity in the interval from 0.250 m – 1 km for the Ikamiut area. Shadowing effect as in Fig. 3. The labels A–I are referred to in the main text.

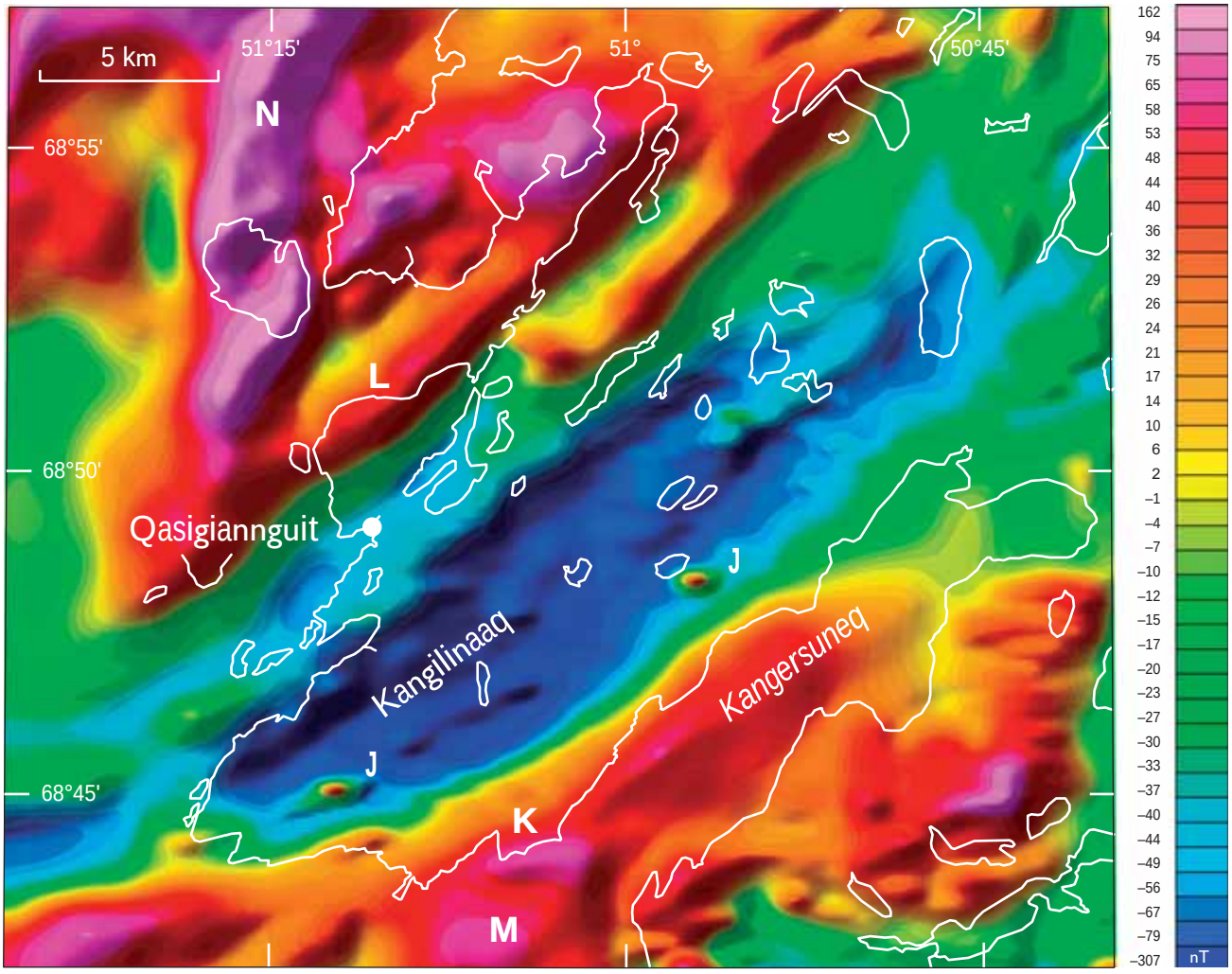

Fig. 5. The separation-filtered total magnetic field intensity in the interval from 0.250 m – 1 km for the Kangilinaaq area. Shadowing effect as in Fig. 3. The labels J–N are referred to in the main text.

possible to recognise folding of the orthogneiss (e.g. east of C, Fig. 4), which correlates closely with the geological mapping (Fig. 2A). Similarly, a strong magnetic low visible between B and D (Fig. 4) defines a refolded fold structure in pelitic gneiss identified during mapping. Exposed granitic rocks are visible as high positive anomalies (D, Fig. 4). Similar anomalies are visible beneath the sea north and east of Ikamiut and beneath the bay of Nivaap Paa (E, F and G, Fig. 4). The orthogneiss north of Nivaap Paa (I, Fig. 4) shows slightly lower magnetic anomalies than the orthogneisses to the south.

Aeromagnetic patterns in the Kangilinaaq region

The supracrustal belt on the Kangilinaaq peninsula appears as a distinct, rather homogeneous, low negative magnetic anomaly (–35 to –300 nT, Fig. 5), possibly reflecting the dominance of quartzo-feldspathic rocks with low magnetite contents. Small positive, short-wavelength, ovoid anomalies within the supracrustal rocks reflect small ultramafic bodies (J's, Fig. 5, too small to appear on the map of Fig. 2B). The biotite-bearing orthogneiss south of the supracrustal belt shows a positive magnetic anomaly (0–55 nT, K in Fig. 5). The change is rather abrupt and correlates with the ENE-trending mylonitic shear zone along the south-eastern margin of the supracrustal rocks close to the coast of the peninsula (see also Fig. 2B). The north-western boundary of the supracrustal belt on the opposite side of the peninsula, where supracrustal rocks and orthogneiss are interleaved, is less well defined. Farther north in the vicinity of Qasigiannguit, an abrupt change to a high positive magnetic anomaly field to the north-west corresponds with the northern contact of the amphibolite sequence against the orthogneiss (L in Fig.

5). The positive magnetic anomalies within the orthogneiss domains immediately north and south of the Kangilinaaq peninsula (M and N in Fig. 5) are much stronger than found within the orthogneiss in the north-eastern region of Fig. 5 (e.g. at 68°55′N, 50°45′W). Based on similar strong positive anomalies associated with granitic rocks in the Ikamiut area (Fig. 4) and the porphyritic granite on the south-western tip of the Kangilinaaq peninsula (Fig. 5), the former anomalies may correspond to large deep-seated granitic intrusives. Likewise, the large magnetic high at eastern Sydostbugten may represent granitic intrusive rocks hidden 1–2 km below the present surface (H's, Fig. 3; Thorning 1993; Nielsen & Rasmussen 2004).

Geochronology

Zircon separates from three samples from the Ikamiut region were analysed to determine (1) the age of emplacement of the regional tonalitic to granodioritic orthogneiss, (2) the age distribution, provenance and minimum age of deposition of the sedimentary precursor to the Ikamiut metasedimentary rocks, and (3) the timing of metamorphism. Samples of two granodioritic orthogneisses and a quartzo-feldspathic metasedimentary rock were analysed, see below. Sample descriptions of these and other rocks are given in Table 1, and the age data are presented in Tables 2–3 and Figs 6–7. All age data in the text are quoted with 2σ absolute uncertainty.

Methodology

Samples were crushed and sieved to < 400 µm. The fraction < 45 µm was removed via washing and sieving and the remaining sample panned in water to concentrate the heavy fraction. The heavy, nonmagnetic fraction was separated using heavy liquids (3.30 gcm^{-3}) and a Frantz magnetic separator. Zircons were hand-picked and mounted in epoxy resin. For secondary ion mass spectrometry (SIMS) analysis, grains were mounted together with 1065 Ma zircons from reference sample 91500, Ontario, Canada (Wiedenbeck *et al*. 1995). For laser inductively-coupled plasma mass spectrometry (LA-ICP-MS) analysis no zircon standard was used. The mounted samples were ground to expose the mid-sections of the zircons and polished. The polished samples were examined using backscattered electron (BSE) imaging on a Philips XL 40 scanning electron microscope at GEUS, operating at 20kV and a working distance of 10 mm. Backscattered electron

Table 1. Sample descriptions

Sample	Region	Rock type	Paragenesis
		Amphibolite	
467403	Kangilinaaq	Fine-grained, layered amphibolite	hbl-pl ± cpx ± grt, accessory Fe-Ti oxides
467405	Kangilinaaq	Fine-grained, layered amphibolite	
467413	Kangilinaaq	Fine-grained, layered amphibolite	
467426	Kangilinaaq	Fine-grained, layered amphibolite	
467436	Kangilinaaq	Fine-grained, layered amphibolite	
467440	Kangilinaaq	Fine-grained, layered amphibolite	
467444	Kangilinaaq	Fine-grained, layered amphibolite	
467445	Kangilinaaq	Fine-grained, layered amphibolite	
467446	Kangilinaaq	Fine-grained, layered amphibolite	
		Orthogneiss	
440938	Ikamiut	Medium-grained granodioritic orthogneiss	pl-qtz-ksp-bi
467526	Ikamiut	Medium-grained granodioritic orthogneiss	pl-qtz-ksp-bi
467401	Kangilinaaq	Medium-grained tonalitic orthogneiss	pl-qtz-bi
		Metasedimentary rocks	
440910	Ikamiut	Quartzo-feldspathic gneiss	pl-qtz-grt-bi, minor sill-ksp
440931	Ikamiut	Quartzo-feldspathic gneiss	pl-qtz-bi, minor ksp-mag. Bi partly replaced by chl
467503	Ikamiut	Quartzo-feldspathic gneiss	pl-qtz-bi, minor ksp-mag-mu
467404	Kangilinaaq	Garnet-bearing schist	qtz-pl-bi-sill-grt. Bi partly replaced by sill
467408	Kangilinaaq	Cummingtonite gneiss	qtz-pl-bi-cu, minor hbl
467417	Kangilinaaq	Biotite-hornblende gneiss	qtz-pl-bi-hbl
467420	Kangilinaaq	Fine-grained schist	qtz-pl-bi-ep, accessory al & zn
467423	Kangilinaaq	Hornblende gneiss	hbl-pl, minor qtz, bi
467433	Kangilinaaq	Hornblende gneiss	hbl-pl, minor qtz, bi

Mineral abbreviations: al: allanite, bi: biotite, cpx: clinopyroxene, cu: cummingtonite, ep: epidote, grt: garnet, hbl: hornblende, ksp: K-feldspar, mag: magnetite, mu: muscovite, pl: plagioclase, qtz: quartz, sill: sillimanite, ti: titanite, zn: zircon.

Table 2. Zircon LA-ICP-MS ^{207}Pb-^{206}Pb data

Spot	^{206}Pb (cps)	$^{207}Pb/^{206}Pb$	Age (Ma)	2σ %
440938 Granodioritic orthogneiss				
1	44913	0.207628	2847	4.8
2	54464	0.206401	2843	6.1
3	51744	0.211202	2865	10.9
5	66847	0.205833	2818	12.1
6	45663	0.239096	3072	7.3
7	114515	0.203027	2811	4.9
10	29662	0.206933	2835	8.2
12	81235	0.200267	2785	5.6
15	63304	0.204663	2825	8.7
16	58962	0.203500	2813	7.4
17	32961	0.211432	2888	7.4
20	86073	0.205326	2830	9.7
21	125993	0.199600	2796	4.5
25	60136	0.185466	2664	6.1
26	48587	0.207014	2855	5.6
27	98098	0.202412	2838	8.0
28	46100	0.198084	2836	11.7
29	44476	0.209520	2878	6.4
30	55984	0.205825	2836	9.9
31	52515	0.204633	2835	7.3
33	60481	0.205708	2838	7.2
34	41693	0.217275	2967	29.6
40	16473	0.210866	2905	33.5
41	63641	0.205836	2847	6.9
42	26576	0.199429	2802	10.4
43	34970	0.210589	2882	6.9
44	66299	0.200725	2807	4.9
47	76450	0.185001	2778	5.5
48	344404	0.196981	2819	6.9
50	94026	0.206532	2859	4.6
54	32535	0.206805	2838	17.7
55	18887	0.185070	2753	19.3
57	45001	0.201119	2811	5.3
59	63523	0.203583	2830	8.1
60	35435	0.205041	2842	6.2
61	23531	0.190093	2715	6.2
63	112296	0.208790	2878	4.6
64	39902	0.195071	2763	6.6
74	19592	0.202403	2820	6.2
75	30652	0.204612	2837	11.0
77	41961	0.195999	2774	6.8
78	64028	0.206406	2860	6.1
80	30243	0.209704	2877	6.2
81	106313	0.203552	2844	6.4
82	47863	0.206121	2857	7.4
83	58886	0.201354	2817	6.6
84	119357	0.209519	2882	4.0
86	93017	0.206130	2857	4.8
87	59542	0.208843	2878	4.8
88	80384	0.190889	2738	6.0
89	56425	0.198658	2797	6.6
90	52868	0.194667	2773	5.8
91	54794	0.203058	2825	6.2
92	86828	0.211233	2895	4.7
93	86433	0.207258	2863	4.4
94	41347	0.203007	2830	5.5
467526 Granodioritic orthogneiss				
5	56698	0.200720	2804	5.3
6	33787	0.193076	2748	6.6
7	55326	0.195289	2762	4.8
8	76699	0.182851	2652	4.9
10	31196	0.183045	2654	6.6
11	4904	0.204104	2807	12.9
13	39648	0.191787	2718	5.5
15	40707	0.202256	2816	5.0
17	29635	0.217163	2844	19.1
18	6853	0.206028	2827	14.9
19	9339	0.206467	2995	5.7
440910 Metasedimentary rock				
1	35535	0.200401	2828	6.5
2	31197	0.211066	2824	10.1
3	41461	0.193703	2741	6.1
4	30241	0.204419	2821	6.0
5	25534	0.191383	2718	5.6
6	46366	0.198531	2774	6.1
7	86549	0.207000	2846	5.7
8	48635	0.201767	2807	5.3
9	36751	0.209132	2858	7.0
10	27744	0.183921	2654	9.9
11	43029	0.194263	2742	6.7
12	29314	0.172110	2520	8.6
13	47160	0.206249	2841	5.9
14	49306	0.201659	2804	7.0
15	29978	0.198089	2779	6.0
17	53134	0.194413	2748	5.4
18	27856	0.201215	2810	6.9
19	30082	0.205162	2842	5.9
20	55684	0.198413	2780	5.1
21	147594	0.191303	2722	5.3
22	25436	0.210142	2870	7.0
23	29257	0.196016	2766	7.0
24	20655	0.203877	2826	6.4
25	26159	0.201727	2796	6.6
26	82319	0.215426	2917	4.5
27	112103	0.194672	2751	5.1
30	15491	0.200465	2794	7.1
31	21709	0.204749	2831	8.0
32	14364	0.206770	2843	11.0
33	41967	0.201274	2800	6.8
34	56320	0.189864	2710	5.6
35	23757	0.202176	2801	9.1
36	30037	0.201451	2808	6.6
37	31254	0.193787	2730	7.6
38	22041	0.205579	2827	10.1
39	52491	0.162084	2504	10.1
40	40780	0.194811	2741	5.7
42	61409	0.195555	2747	4.9
43	103057	0.171459	2534	10.0
44	40828	0.200096	2744	7.8
45	58477	0.197715	2764	5.3
46	20270	0.206049	2843	8.7
47	33049	0.196133	2748	6.5
48	28126	0.193760	2738	6.3
50	19721	0.207732	2845	6.6
51	86891	0.232092	2997	11.6
52	58228	0.201806	2799	5.0
53	50522	0.190800	2710	5.8
54	60856	0.195334	2736	5.6
55	35515	0.198275	2772	5.4
56	51577	0.196653	2758	5.9
58	27007	0.203361	2811	5.7
59	49414	0.202192	2798	5.8
62	10375	0.207836	2855	9.5
63	120563	0.189864	2717	4.2
64	23252	0.187771	2722	7.0
65	26567	0.202492	2801	6.5
69	89976	0.191213	2728	4.7
70	25130	0.199809	2796	6.1
71	68881	0.206577	2861	4.6
72	53407	0.199076	2805	5.1
73	51707	0.194570	2755	4.9
74	67393	0.179579	2625	5.3
75	30132	0.198104	2773	6.6
76	36875	0.197163	2802	7.8
77	28362	0.198893	2790	5.4
78	27133	0.201214	2812	5.7
79	133087	0.188329	2702	4.7
80	45162	0.206677	2856	4.4
81	51961	0.194173	2749	4.6
83	27444	0.201457	2807	5.6
84	26057	0.208900	2868	5.4
85	31842	0.198490	2789	7.0
86	114220	0.180764	2635	5.5
87	62748	0.189371	2717	5.5
88	42113	0.198204	2782	5.2
89	24400	0.199600	2793	6.6
90	29322	0.208314	2861	5.3
91	75430	0.205029	2835	6.0
93	24848	0.198066	2773	6.3
95	60703	0.191617	2717	6.7
96	40762	0.207364	2850	4.1
97	131809	0.193200	2737	6.3
98	43657	0.197222	2778	5.6
99	17404	0.199360	2767	19.2

Table 3. Zircon ion probe (SIMS) U-Th-Pb data

Spot	U ppm	Th ppm	Pb ppm	Th/U measured	f^{206} %	$^{207}Pb/^{206}Pb$	σ %	$^{207}Pb/^{235}U$	σ %	$^{206}Pb/^{238}U$	σ %	Discordance % (conventional)	Ages (Ma) $^{207}Pb/^{206}Pb$	Ages (Ma) σ
440938 Granodioritic orthogneiss														
3	155	94	113	0.607	0.04	0.19819	0.28	14.5789	1.06	0.53352	1.03	–2.4	2811.3	4.6
4	575	274	417	0.502	0.07	0.19781	0.18	14.8262	1.04	0.54361	1.03	–0.4	2808.2	2.9
8	192	24	127	0.117	0.05	0.19575	0.28	14.5329	1.07	0.53845	1.03	–0.6	2791.1	4.6
14	164	23	109	0.140	0.02	0.19767	0.38	14.7352	1.09	0.54065	1.03	–0.9	2807.1	6.1
20a	206	56	134	0.222	0.09	0.19216	0.30	13.6935	1.07	0.51684	1.03	–3.3	2760.7	5.0
24	175	37	117	0.170	0.05	0.19891	0.31	14.7222	1.07	0.53682	1.03	–2.1	2817.2	5.0
29	578	153	384	0.217	0.23	0.19498	0.17	14.2171	1.04	0.52885	1.03	–2.1	2784.6	2.8
41	632	35	391	0.054	0.01	0.19138	0.14	13.5355	1.04	0.51295	1.03	–3.8	2754.1	2.4
54	273	155	199	0.555	0.09	0.19767	0.29	14.6540	1.07	0.53768	1.03	–1.5	2807.0	4.8
66	251	227	191	0.878	0.07	0.19836	0.23	14.3381	1.05	0.52425	1.03	–4.2	2812.7	3.7
72	203	158	150	0.762	0.09	0.19789	0.29	14.2560	1.07	0.52248	1.03	–4.3	2808.9	4.7
76	157	49	107	0.307	0.02	0.20014	0.33	14.6609	1.09	0.53127	1.04	–3.5	2827.4	5.4
440910 Metasedimentary rock														
22	850	51	526	0.057	0.01	0.18523	0.20	13.1609	1.78	0.51532	1.77	–0.9	2700.3	3.4
29	480	2	308	0.002	0.03	0.18986	0.27	14.0987	1.79	0.53857	1.77	1.6	2740.9	4.4
42	609	3	390	0.003	0.05	0.18800	0.22	13.9521	1.78	0.53823	1.77	2.3	2724.8	3.6
54	554	2	344	0.004	0.01	0.18507	0.22	13.3561	1.78	0.52342	1.77	0.7	2698.8	3.6
58c	106	32	71	0.275	0.23	0.19043	0.43	14.0439	1.82	0.53488	1.77	0.7	2745.9	7.1
58r	610	2	378	0.003	0.04	0.18916	0.21	13.6001	1.79	0.52146	1.77	–1.3	2734.8	3.5
82	1178	7	730	0.004	0.07	0.18473	0.17	13.3129	1.78	0.52267	1.77	0.7	2695.8	2.9

Errors on ratios and ages are quoted at the 1σ level.
c: core; r: rim; f^{206} %: The fraction of common ^{206}Pb, estimated from the measured ^{204}Pb.
Discordance %: Degree of discordance of the zircon analysis (at the centre of the error ellipse).

(BSE) images of some of the analysed grains showing sites of analysis and ages obtained are presented in Fig. 6.

All three samples were analysed at GEUS using a PerkinElmer 6100 DRC quadrupole inductively-coupled plasma mass spectrometer combined with a Cetac LSX 200 laser ablation unit based on a solid-state Nd-YAG laser, emitting at a wavelength of 266 nm. The laser was operated at 20 Hz with a spot size of 30 µm, producing pits of *c*. 50 µm depth. The masses ^{208}Pb, ^{207}Pb, ^{206}Pb, and ^{204}Pb were analysed in line scans run at 1 µm per second. Each analysis comprised 150 time-resolved replicates (duration of total analysis 150 s). In the case of small grains with diameters < 100 µm, only 100 replicates over 100 s were collected. If inconsistencies in the measured ratios were identified within the time span of each analysis, such as spikes relating to inclusions, or significant changes in Pb-Pb ratios indicative of sampling of different age zones, then the whole analysis was discarded. The analyses were standardised against NIST 610 glass (Pearce *et al*. 1997) to account for instrument drift. The influence of common Pb cannot be assessed using this method, since ^{204}Pb was generally below the detection limit. Also, because U isotopes could not be measured, the significance of Pb loss cannot be assessed, and therefore the ages determined should be regarded as minimum ages. In addition, the age resolution on any individual analysis was restricted owing to relatively low count rates obtained. However, it is a great advantage of the LA-ICP-MS method that a large number of analyses can be made within a short time period, allowing analysis of large numbers of grains in samples with isotopically simple zircon. The LA-ICP-MS age data are presented in Table 2 and as histograms coupled with relative probability curves (Fig. 7).

SIMS analysis of zircon from two samples (440938, 440910) was carried out using a CAMECA IMS 1270 secondary ion mass spectrometer at the NORDSIM laboratory, Swedish Museum of Natural History, Stockholm. The polished zircon mounts were coated with a *c*. 30 nm layer of gold. Analytical procedures and common lead corrections are similar to those described by Whitehouse *et al*. (1997). A primary O^{2-} ion beam is focussed into a spot with a diameter of 20 µm that sputters material from the sample to leave a flat-bottomed crater. Positive ions sputtered from the crater are extracted and mass-separated into the peaks of interest: $^{90}Zr_2{}^{16}O$, ^{204}Pb, ^{206}Pb, ^{207}Pb, ^{208}Pb, ^{238}U, $^{232}Th^{16}O$, and $^{238}U^{16}O$. Calibrations of Pb/U ratios are based on the observed relationship between Pb/U and UO_2/U. Weighted average $^{207}Pb/^{206}Pb$ ages were calculated using ISOPLOT (Ludwig 2000). SIMS age data are presented in Table 3 and on Tera-Wasserburg diagrams in Fig. 7.

Orthogneiss

The two samples of granodioritic orthogneiss selected for geochronology (440938 and 467526) were collected at the south coast of Langesund (Fig. 2A). Sample descriptions and chemical composition are presented in Tables 1 and 4. Sample 440938 yielded abundant zircon and contains common thin, transposed granitic layers, whereas sample 467526 does not contain such granitic leucosome. The zircons from both samples are 100–600 µm (mostly *c*. 200–300 µm) in length and translucent with a heterogeneous orange colour. The crystals are euhedral with slightly rounded terminations and aspect ratios from 1:2.5–1:4, typically *c*. 1:3. Broad oscillatory zones *c*. 10–30 µm wide are very common, with rare development of bright, presumably metamorphic rims (see below). The zircons are commonly weakly to moderately fractured, both concentrically and radially, and often show partial fracture healing within bright oscillatory zones (Fig. 6).

LA-ICP-MS analyses of 57 oscillatory zoned grains from sample 440938 give a weighted mean age of 2831 ± 23 Ma (2σ, MSWD = 0.36; Table 2; Fig. 7A). Ten SIMS analyses of cores of oscillatory zoned grains and two of bright rims reveal more age complexity, with seven of the cores yielding an important 2820–2810 Ma age component (Table 3; Fig. 7B, black data ellipses). Four of these seven analyses lie slightly off concordia. Another, slightly older and likewise discordant grain (2827 Ma, blue in Fig. 7B) belongs to the 2831 ± 23 Ma LA-ICP-MS age group. Many of the analysed grains show slight discordance indicating partial Pb loss, the timing of which is unclear from the data available. Two bright rims with significantly younger ages of 2761 ± 10 Ma and 2754 ± 5 Ma are interpreted as metamorphic. This is supported by the very low Th/U of the latter (0.054), though the former is not anomalous in this respect (Th/U = 0.22). The SIMS data are slightly but significantly younger than the LA-ICP-MS data for the same sample (but from different analysed grains), although the 2σ error on the LA-ICP-MS age spectrum encompasses most of the SIMS data. It is difficult to establish the reason for this, particularly given the apparent complexity of the zircons (Fig. 7B). It is possible that a larger proportion of older material has been sampled in the LA-ICP-MS work. It may also be that matrix effects had some influence in standardising zircon data against NIST610 glass, though such effects are not generally regarded as significant.

The few zircons separated from sample 467526 were analysed via LA-ICP-MS. Eleven analyses of cores displaying oscillatory zonation yield a poorly constrained weighted mean age of 2741 ± 53 Ma (2σ, MSWD = 0.55; Fig. 7C).

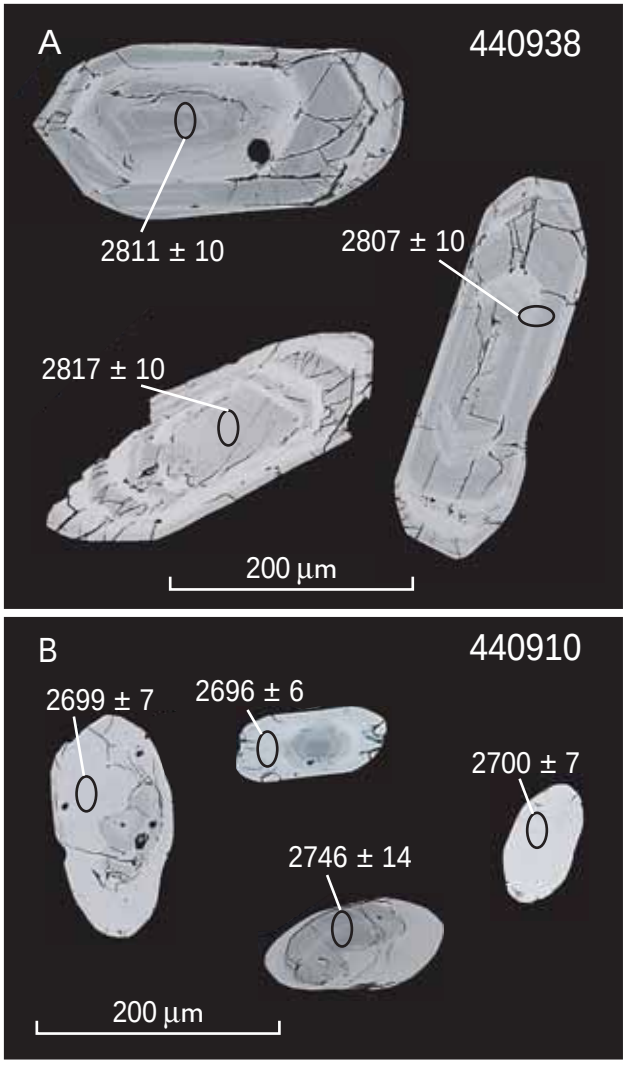

Fig. 6. Backscattered electron images of zircons in samples 440938 (orthogneiss) and 440910 (metasediment) analysed via SIMS, showing analysed areas and ages obtained.

It might be considered that the large analytical error for this sample leaves room for age complexity, possibly involving analysis of both inherited grains and Pb loss (similar to sample 440938). However, all analyses statistically belong to the same population, and there are no significant differences in internal zircon morphology that might account for different age groups.

Metasedimentary rocks

Sample 440910 from the Ikamiut belt (Fig. 2A) is a medium-grained, garnet-bearing quartzo-feldspathic, gneissic rock. Colourless, pale yellow and pale pink zircon grains are abundant. They are elongate and generally 100–200

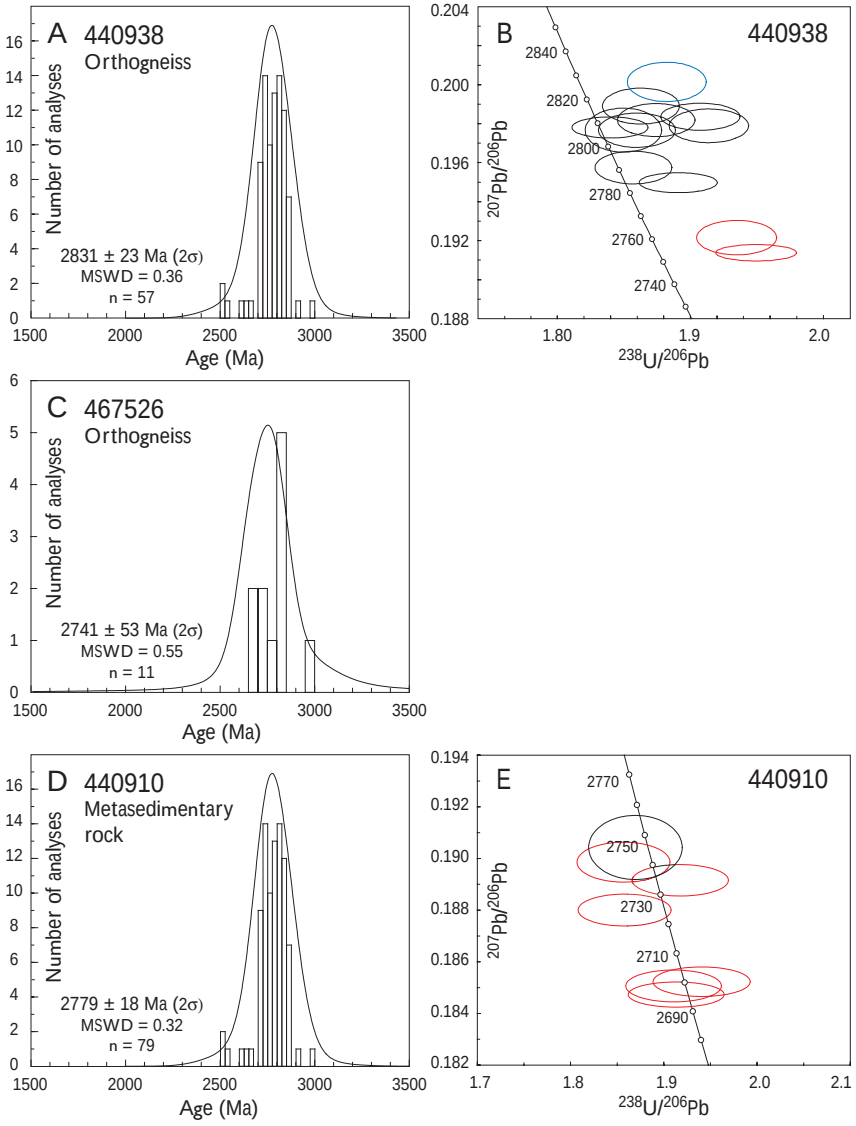

Fig. 7. LA-ICP-MS $^{207}Pb/^{206}Pb$ histograms and SIMS U-Pb Tera-Wasserburg concordia plots of zircon age data from the Ikamiut region. A: Histogram of $^{207}Pb/^{206}Pb$ ages from orthogneiss sample 440938. B: Tera-Wasserburg plot for orthogneiss sample 440938 showing nine cores of oscillatory-zoned grains (black), an older core (blue), and two bright rims (red). C, D: Histograms of $^{207}Pb/^{206}Pb$ ages from orthogneiss 467526 and metasedimentary sample 440910. E: Tera-Wasserburg plot for metasedimentary sample 440910 showing one core (black) and six metamorphic rims (red). The histogram bin size is 25 Ma (A, D) or 50 Ma (C). Error ellipses on concordia diagrams are drawn at 68.3% confidence (1σ).

µm in length, with rounded terminations and aspect ratios of 1:1–1:3, typically *c.* 1:2. BSE imaging reveals relatively wide (*c.* 10–30 µm) oscillatory zoned cores with moderate to well-developed bright rims *c.* 10–60 µm wide, which in many cases have annealed former fractures (Fig. 6).

^{207}Pb-^{206}Pb ages from 87 LA-ICP-MS analyses of oscillatory zoned zircon cores are shown in Fig. 7D. The vast majority (79) define a tightly clustered peak at *c.* 2800 Ma. The complete age range spans 2997–2520 Ma. The youngest ages (< 2700 Ma) may reflect mixed core–rim data, although most of them are statistically within the main age population. If a few anomalous old and young ages are disregarded, a weighted mean age of 2779 ± 18 Ma is obtained (2σ, MSWD = 0.32, n = 79). This group is interpreted as comprising a homogeneous population of detrital zircons, consistent with local derivation from orthogneiss of this age (see above). Seven SIMS analyses, of one core with oscillatory zonation and six bright rims, all fall on concordia (Fig. 7E). The core gives the oldest age of 2746 ± 14 Ma (Th/U = 0.275). The six analyses of bright rims give ages between 2741 ± 9 and 2696 ± 6 Ma. All have very low Th/U (0.004–0.06), consistent with a metamorphic origin. These metamorphic ages are comparable to the few young ages also identified in the LA-ICP-MS analyses, and suggest that this sample underwent metamorphism at *c.* 2740–2700 Ma, shortly after its deposition. An alternative, and in our view less likely interpretation is that the metamorphic rims were developed during metamorphism of the source rock prior to erosion and deposition of the sediment.

Geochemistry

Whole-rock geochemical analysis of amphibolites, felsic orthogneiss and metasedimentary rocks from the Ikamiut and Kangilinaaq regions was undertaken to (a) geochemically characterise these rock types, (b) investigate the likely tectonic environment of formation and provenance of the amphibolites and metasedimentary rocks, and (c) investigate likely regional correlations. Sample descriptions are presented in Table 1, and major and trace element compositions in Table 4.

Analytical procedure

Major and trace element analyses (Table 4) were performed by GEUS. The samples were ground in tungsten (Ikamiut samples) or agate (Kangilinaaq samples) mills, and dried. For major elements the rock powders were fluxed with sodium tetraborate and fused to glass discs and analysed with a Philips PW1606 X-ray fluorescence (XRF) mass spectrometer. Na and Cu were determined by atomic absorption spectrometry, and volatiles were analysed by gravimetry. Refer to Kystol & Larsen (1999) for the complete analytical procedure. For trace element analyses, powdered samples were brought into solution and analysed using a PerkinElmer 6100 DRC Quadrupole ICP-MS instrument. For the Ikamiut samples Zr, Cr, REEs and Hf were determined by dissolving a piece of the borate glass used in the major element XRF analyses, in order to obtain complete contributions of these elements from chromite and zircon. The ICP-MS results were corrected for the relevant oxide interferences using BHVO-1 and GH as standards.

For the Kangilinaaq samples some trace elements were also analysed by XRF performed directly on pressed powder tablets at the Geological Institute, University of Copenhagen, using a Phillips PW 1400 XRF spectrometer. The data were corrected for matrix variations using the major element compositions, and AGV-1 was run as standard.

Orthogneisses

Two orthogneiss samples from the Ikamiut region were analysed (440938 and 467526), and one from Kangilinaaq (467401; Table 4a; Fig. 2). The two Ikamiut samples show very similar granodioritic major element chemistry, while the Kangilinaaq sample is more tonalitic. The Kangilinaaq sample has low REE concentrations and a fairly steep REE curve with La_N/Lu_N ~ 16 (Fig. 8B). In contrast, the two Ikamiut samples have higher REE concentrations and significant negative Eu anomalies, consistent with the more evolved composition of these rocks.

Amphibolites from the Kangilinaaq belt

Nine amphibolites *s.s.* from the Kangilinaaq belt were analysed for major and trace elements (Table 4a); no amphibolite samples have been analysed from the Ikamiut region, where amphibolites only constitute a minor component of the supracrustal rocks. The nine samples from Kangilinaaq show only a small range in chemical composition. They have relatively primitive signatures with low SiO_2 (46–49 wt%) and high MgO (7–11 wt%), and flat REE patterns that group tightly around ten times chondrite values (Fig. 8A). Their Ti/V ratios display a narrow range of 16–19, and in a Ti-V diagram (Shervais 1982) they plot just within the island arc field (Fig. 9). The positive correlation between Ti and V could reflect fractionation of olivine and plagioclase. The geochemical resemblance between all nine samples and their well-defined Ti/V trend are consistent with formation within a single volcanic suite.

Metasedimentary rocks and hornblende-bearing gneisses from the Kangilinaaq belt

Metasedimentary sample 467404 is characterised by high alumina (19 wt%) coupled to low CaO (0.7 wt%) and high concentrations of REE and Ba (605 ppm), consistent with a clay-rich precursor. The REE curve is steep (La_N/Lu_N = 30, La = 140 times chondrite), and has a significantly negative Eu anomaly. Sample 467420 is siliceous (75 wt% SiO_2), consistent with a relatively mature sedimentary precursor. Its REE concentrations lie just below those of sample 467404, with a similar steep REE pattern. For sample 467417, both major and trace elements agree well with the average composition of Archaean mudstone from Taylor & McLennan (1985, table 7.8). The REE curve resembles that of sample 467408 (see below), although it has slightly lower concentrations of the HREE.

The hornblende-bearing gneisses 467423 and 467433 were collected from thin (< 1 m) amphibolite units within metasedimentary sequences. The geochemical compositions of these two samples are close to those of the nine amphibolite samples described above, and they can only be distinguished from the latter by their higher concentrations of LREE, Ba, and Sr, and higher K_2O and Rb in

Table 4a. Chemical analyses of amphibolite and orthogneiss

	Amphibolite, Kangilinaaq belt									Orthogneiss		
	467403	467405	467413	467426	467436	467440	467444	467445	467446	440938	467526	467401
SiO_2	48.73	48.72	49.3	46.86	48.39	47.37	48.01	48.25	46.00	71.93	71.70	68.86
TiO_2	1.03	0.87	0.83	0.60	0.64	0.66	0.90	0.88	0.75	0.24	0.39	0.22
Al_2O_3	13.16	15.81	14.61	16.21	15.68	16.36	13.29	12.18	16.25	14.58	14.64	16.93
Fe_2O_3	1.67	2.54	2.7	1.88	2.13	2.79	1.90	1.88	2.83	1.99	2.09	0.09
FeO	10.64	8.89	9.11	7.48	7.85	8.14	8.04	8.82	7.94	0.00	0.00	1.68
FeO*	12.14	11.17	11.53	9.17	9.77	10.65	9.75	10.51	10.49	1.79	1.88	1.76
MnO	0.22	0.21	0.20	0.18	0.17	0.16	0.13	0.19	0.17	0.01	0.02	0.02
MgO	8.82	6.90	7.73	8.30	8.34	9.37	10.74	11.15	10.04	0.57	0.57	0.98
CaO	11.46	12.72	11.51	14.17	12.78	10.91	12.31	12.43	10.42	2.02	2.12	4.02
Na_2O	2.25	1.28	1.58	1.60	1.36	2.00	1.97	1.56	2.38	4.47	4.70	5.17
K_2O	0.11	0.23	0.25	0.31	0.25	0.08	0.52	0.10	0.48	3.08	2.31	1.05
P_2O_5	0.06	0.06	0.05	0.04	0.04	0.04	0.06	0.06	0.05	0.07	0.08	0.07
Volatiles	1.58	1.5	1.57	1.48	1.57	1.6	1.43	1.53	2.06	0.27	0.10	0.53
Sum	99.74	99.72	99.43	99.11	99.21	99.47	99.29	99.02	99.36	99.23	98.71	99.62
Sc	53.6	49.0	54.8	44.1	44.2	38.7	49.6	52.3	49.7	5.5	8.1	4.6
V	347	283	308	214	237	220	301	297	256	16	13.8	24.1
Cr	106	301	380	444	450	207	521	485	411	5.0	2.6	35.9
Co	53.5	55.1	51.6	51.2	56.1	58.0	70.3	56.6	54.0	17.2	14.7	6.0
Ni	117	150	160	221	222	254	214	221	159	3.6	3.4	12.9
Cu	64.2	89.0	82.7	39.1	90.3	89.5	4.8	82.8	80.8	2.4	8.1	7.3
Zn	91.9	86.0	92.2	74.3	74.8	80.1	40.0	77.3	74.6	40.9	39.8	45.2
Ga	15.7	16.3	15.7	14.2	14.2	14.8	14.8	14.1	15.4	18.2	20.8	23.2
Rb	1.1	7.6	9.1	12.4	10.9	1.2	9.5	2	10.6	82.1	91.4	92.9
Sr	124	111	91	118	150	100	94	109	155	385	303	375
Y	19.6	19.5	19.6	13.6	14.3	14.2	18.1	17.4	17	3	7.8	2.8
Zr	29.7	11.8	12.5	9.4	9.4	15.8	18.4	11.6	16.2	143	117	57.9
Nb	3.1	2	1.9	1.5	1.4	1.1	2.4	2.2	1.7	2.5	4.9	15.4
Cs	0.0	0.3	0.2	0.7	0.8	0.0	0.1	0.0	0.2	1.2	2.6	5.6
Ba	18	56	43	47	25	6	31	20	60	748	446	210
La	3.2	2.2	2.4	1.7	1.6	1.6	3.5	2.5	2.2	34.1	18.9	4.0
Ce	8.4	6.0	6.3	4.5	4.3	4.3	8.0	6.5	6.0	65.0	37.8	8.3
Pr	1.3	1.0	1.0	0.7	0.7	0.7	1.2	1.0	0.9	7.2	4.2	1.0
Nd	6.7	5.3	5.3	3.7	3.7	3.7	6.0	5.6	5.1	24.2	14.9	3.7
Sm	2.2	1.8	1.8	1.4	1.4	1.3	1.9	1.9	1.7	3.3	2.5	0.8
Eu	0.7	0.7	0.7	0.5	0.5	0.6	0.7	0.7	0.6	0.6	0.6	0.3
Gd	3.0	2.7	2.6	1.6	1.7	1.6	2.4	2.3	2.2	3.4	2.6	1.0
Tb	0.5	0.5	0.5	0.3	0.3	0.3	0.5	0.4	0.4	0.2	0.3	0.1
Dy	3.3	3.2	3.1	2.3	2.3	2.3	3.1	2.9	2.8	0.9	1.5	0.6
Ho	0.7	0.7	0.7	0.5	0.5	0.5	0.6	0.6	0.6	0.1	0.3	0.1
Er	1.9	1.9	2.0	1.3	1.4	1.4	1.8	1.7	1.6	0.3	0.7	0.2
Tm	0.3	0.3	0.3	0.2	0.2	0.2	0.3	0.2	0.2	0.0	0.1	0.0
Yb	1.8	1.9	2.0	1.3	1.5	1.4	1.7	1.6	1.6	0.2	0.7	0.2
Lu	0.3	0.3	0.3	0.2	0.2	0.2	0.3	0.3	0.3	0.0	0.1	0.0
Hf	1.0	0.6	0.6	0.4	0.5	0.6	0.7	0.6	0.6	3.8	3.3	1.5
Ta	0.2	0.1	0.1	0.1	0.1	0.1	0.1	0.1	0.1	0.5	1.1	1.9
Pb	1.4	1.5	1.1	1.3	0.8	0.5	0.6	1.3	1.2	9.5	7.6	7.4
Th	0.4	0.2	0.2	0.2	0.2	0.1	0.3	0.3	0.2	10.1	4.2	0.9
U	0.1	0.1	0.1	0.1	0.1	0.0	0.2	0.1	0.0	0.5	0.9	0.4
Total REE	34	28	29	20	20	20	32	28	26	140	85	20

Major elements (in wt%) by XRF at GEUS. Trace elements (in ppm) by ICP-MS at GEUS.
FeO* = total Fe calculated as FeO. Volatiles = loss on ignition corrected for oxygen uptake due to oxidation of iron.

Table 4b. Chemical analyses of various supracrustal rocks

	440910	440931	467503	467404	467408	467417	467420	467423	467433
SiO_2	63.27	69.36	74.26	62.76	61.37	59.87	75.29	49.25	49.94
TiO_2	0.59	0.49	0.03	0.61	0.67	0.64	0.34	0.61	0.78
Al_2O_3	17.61	16.08	14.81	19.09	13.90	16.78	13.01	16.21	15.53
Fe_2O_3	5.19	2.38	0.01	1.17	1.32	1.25	0.51	3.63	1.80
FeO	0.00	0.00	0.37	5.82	6.73	5.38	1.26	6.97	8.34
FeO*	4.67	2.14	0.38	6.87	7.92	6.50	1.72	10.24	9.96
MnO	0.05	0.01	0.00	0.05	0.11	0.15	0.01	0.19	0.16
MgO	2.31	1.03	0.10	2.80	6.41	3.97	0.57	7.70	7.78
CaO	2.26	3.17	2.02	0.75	4.60	3.68	5.62	9.21	10.73
Na_2O	3.84	3.85	4.89	1.60	1.82	2.73	1.05	2.63	1.88
K_2O	3.02	1.79	2.81	3.20	1.46	3.21	0.62	1.63	0.50
P_2O_5	0.13	0.11	0.02	0.03	0.07	0.08	0.05	0.13	0.16
Volatiles	1.00	0.75	0.29	1.64	1.26	1.28	0.90	1.39	1.48
Sum	99.27	99.02	99.62	99.52	99.71	99.01	99.23	99.55	99.06
Sc	18.0	10.2	0.8	17.6	39.3	26.6	7.7	43.8	39.7
V	98.5	38.2	1.7	56.7	208	149	43.5	204	209
Cr	89.1	25.0	0.4	120.0	667	312	66.1	268	318
Co	22.3	17.2	26.9	16.3	44.8	28.4	14.0	51.2	50.7
Ni	32.3	5.2	1.3	54.7	194.0	106.0	34.0	148.0	145.0
Cu	21.9	8.8	5.2	4.8	20.0	26.3	26.9	25.1	34.8
Zn	71.4	38.9	4.4	37.8	89.5	104.5	41.4	81.8	87.4
Ga	20.8	19.6	16.0	25.7	17.5	23.1	15.5	16.3	15.9
Rb	82.7	48.2	58.5	96.9	51.1	197.0	41.6	59.1	8.0
Sr	210	314	402	47	117	177	137	270	288
Y	16.0	6.4	2.4	11.1	15.4	16.7	11.1	17.4	17.0
Zr	134	151	70.8	57.7	82.4	83.1	73.9	38.4	24.0
Nb	5.6	5.6	0.8	8.7	3.3	6.9	2.9	2.3	2.0
Cs	4.1	4.7	0.5	2.0	2.5	8.1	2.7	2.4	0.0
Ba	417	286	591	581	386	377	310	153	97
La	28.2	20.0	7.9	34.5	11.0	9.6	28.3	11.9	13.4
Ce	58.3	40.6	16.1	64.7	29.1	28.5	56.0	29.5	37.5
Pr	6.9	4.4	2.1	7.4	2.9	2.6	6.5	3.8	4.5
Nd	25.3	15.7	7.7	26.4	11.8	10.5	24.5	16.8	19.7
Sm	4.3	2.6	1.8	4.4	2.7	2.5	4.0	3.9	4.4
Eu	1.2	0.7	0.4	0.7	0.7	0.7	1.0	1.2	1.1
Gd	4.5	2.6	1.5	5.0	3.6	2.3	3.9	3.5	3.8
Tb	0.6	0.3	0.2	0.5	0.5	0.4	0.4	0.5	0.5
Dy	3.0	1.4	0.6	2.4	2.8	2.4	2.3	2.9	3.0
Ho	0.6	0.2	0.1	0.4	0.6	0.6	0.4	0.6	0.6
Er	1.6	0.6	0.2	1.1	1.6	1.9	1.1	1.7	1.7
Tm	0.2	0.1	0.0	0.1	0.2	0.3	0.1	0.3	0.3
Yb	1.5	0.5	0.2	0.9	1.5	2.1	0.8	1.6	1.6
Lu	0.2	0.1	0.0	0.1	0.2	0.3	0.1	0.2	0.2
Hf	3.7	3.9	2.8	1.5	2.2	2.2	1.8	1.0	0.8
Ta	0.9	2.6	1.9	0.6	0.3	0.6	0.2	0.1	0.1
Pb	12.7	5.2	11.8	3.7	4.7	9.5	6.1	6.6	4.2
Th	6.2	3.3	4.8	8.5	3.5	6.0	4.2	2.0	2.0
U	1.5	0.9	1.3	0.8	0.9	3.1	0.9	0.7	0.6
Total REE	137	90	39	149	69	65	129	79	92

Major elements (in wt%) by XRF at GEUS. Trace elements (in ppm) by ICP-MS at GEUS.
Volatiles: loss on ignition corrected for oxygen uptake due to oxidation of iron.
FeO*: total Fe calculated as FeO.

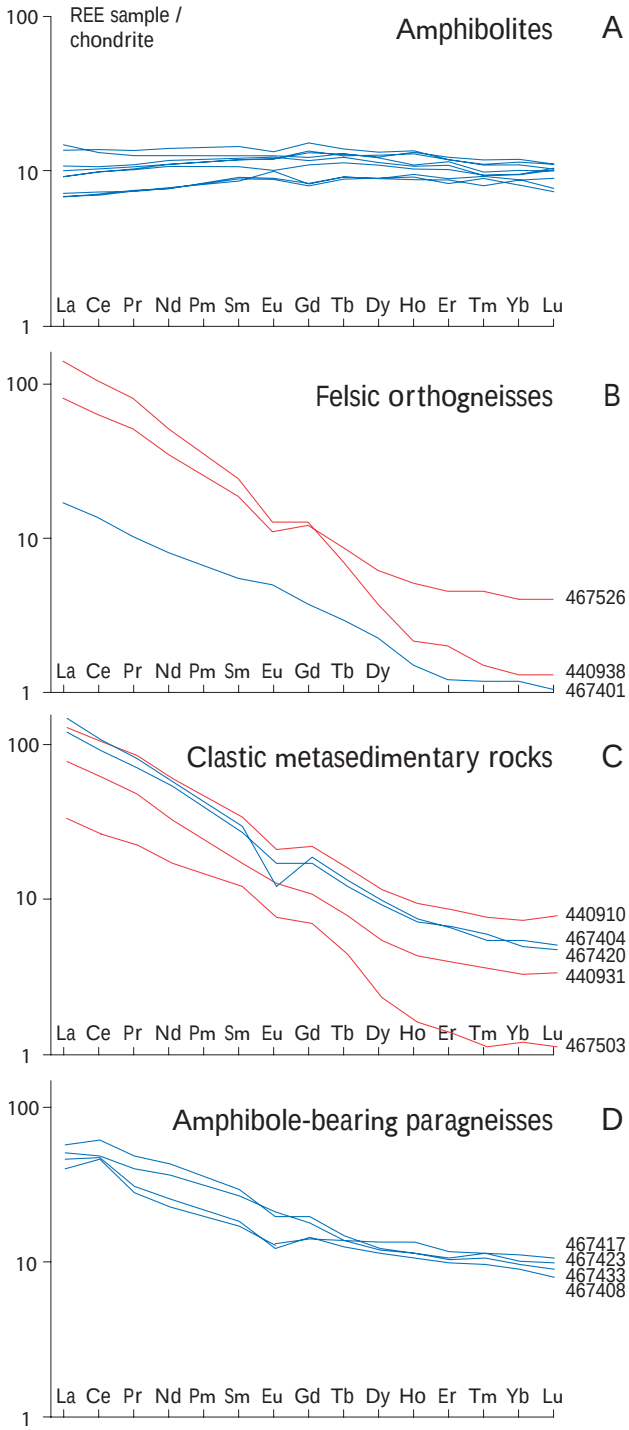

Fig. 8. Chondrite-normalised REE plots. A: amphibolites. B: felsic orthogneiss. C: quartzo-feldspathic metasedimentary rocks. D: mafic metasedimentary rocks. Blue: Samples from the Kangilinaaq region. Red: Samples from the Ikamiut region.

sample 467423. Sample 467408 has an intermediate silica content (61.37 wt% SiO_2), is cummingtonite-bearing, and has high concentrations of MgO (6.41 wt%) and FeO* (7.92 wt%) as well as Cr and N (627 and 186 ppm, respectively). It also has high Ba (405 ppm). The REE curve is almost flat, with ten times chondritic HREE and a weak LREE enrichment (La_N/Lu_N = 5). There is a small positive Ce anomaly in addition to a negative Eu anomaly.

Metasedimentary rocks from the Ikamiut belt

Sample 440910 is the most aluminous (18 wt% Al_2O_3, Table 4), has high REE concentrations, and a fairly steep REE curve with La_N/Lu_N = 15 (Fig. 8C). Samples 440931 and 467503 are more siliceous (69 and 74 wt% SiO_2, respectively) with lower Al, Fe and Mg. Both have lower REE concentrations and slightly steeper REE curves than sample 440910.

Interpretation

The metasedimentary rocks and amphibole-bearing gneisses of supracrustal origin described above from the Ikamiut and Kangilinaaq belts can be divided into two groups based on their geochemical compositions and REE patterns. Five of them, namely all three Ikamiut samples and samples 467404 and 467420 from Kangilinaaq, are typical metasedimentary lithologies with steep REE curves (Fig. 8C). Although they have varying REE concentrations, all five samples have fairly steep REE curves that are comparable to the REE patterns seen in the Kangilinaaq and Ikamiut orthogneisses. The group shows a trend of increasing REE concentrations with decreasing SiO_2 and increasing Al_2O_3, consistent with the general presumption that the REE are preferentially concentrated in the clay fraction of sediments. One exception from this is the siliceous sample 467420 that has REE concentrations comparable to the most aluminous metasediments. Its unusual REE enrichment may be due to high contents of detrital allanite and zircon, as these minerals incorporate high REE concentrations.

The REE curves for the four amphibole-bearing gneisses (467408, 467417, 467423, and 467433; Fig. 8D) have $La_N/Lu_N \sim 5$, showing significantly flatter patterns. These four samples all have high concentrations of mafic minerals and may represent intermediate tuffaceous rocks or mildly chemically altered mafic volcanic rocks. The rather peculiar composition of sample 467408, with high Ni and Cr, suggests that it is a metamorphosed, hydrothermally

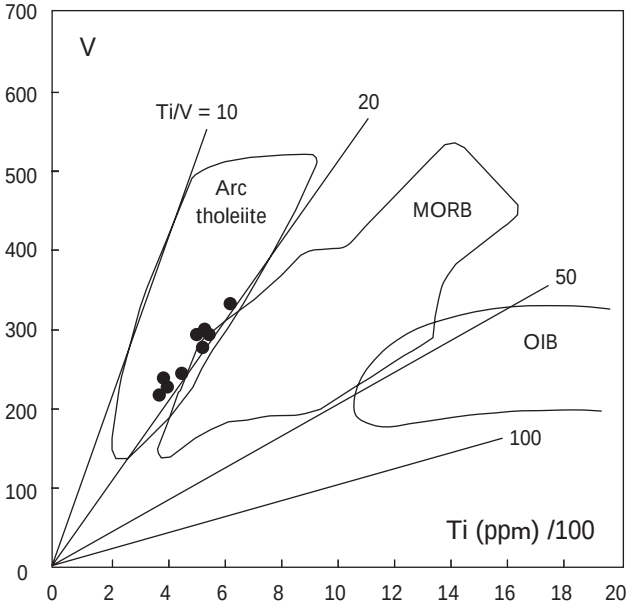

Fig. 9. Ti/V discrimination diagram (Shervais 1982) for nine amphibolite samples from the Kangilinaaq peninsula (Fig. 2B), illustrating their island arc affinities. Note that Ti and V are both immobile elements, considered to be stable during hydrothermal alteration and regional metamorphism (e.g. Nicollet & Andriambololona 1980; Mottl 1983). The partition coefficient of V varies with the oxygen fugacity of the magma, whereas the partition coefficient of Ti remains unchanged.

altered mafic volcanic rock. Alternatively, such high Ni and Cr in a clastic sedimentary precursor would require an abundance of heavy minerals such as garnet and spinel.

Discussion

Regional structures

Both the Ikamiut and Kangilinaaq regions preserve complex tectono-metamorphic histories, and although they show similarities in lithologies and metamorphic grade (amphibolite facies mineral assemblages defining D_1 and D_2 structures) and lie roughly along strike, the large structures are sufficiently different to make a direct correlation between the two regions and their supracrustal belts difficult and dubious. Both regions show evidence for at least two generations of fold structures, with kilometre- to ten kilometre-scale F_2 folds dominating the outcrop pattern. However, there is considerable variation in the typical strike of foliation and plunge of large-scale folds and lineations between the two regions. Furthermore, the aeromagnetic data do not suggest a strong link between the two regions. On the basis of geological mapping and the aeromagnetic data it seems likely that the Kangilinaaq belt forms a synformal fold closure at the south-western tip of the Kangilinaaq peninsula, with little or no westward continuation. We cannot rule out the possibility that there is continuation of this belt across Sydostbugten into the Ikamiut region along an abrupt change in the aeromagnetic response across northern Sydostbugten (boundary O in Fig. 3). This could be interpreted as an extension of the linear aeromagnetic anomaly marking the northern contact of the Qasigiannguit amphibolite sequence with the surrounding orthogneiss, which appears to extend westward to several kilometres north of the Nivaap Paa bay (boundary P in Fig. 3). However, there is no strong field evidence to support this, since no comparable amphibolite sequence occurs on land at Q (Fig. 3). It is possible that this linear aeromagnetic anomaly relates instead to an interpreted granitic body beneath Sydostbugten, represented by outcrop on the south-eastern tip of the Kangilinaaq peninsula, and on the south-west coast of Nivaap Paa.

Magmatism

Geochronological data show that the magmatic precursors to granodioritic orthogneiss from the Ikamiut region were emplaced in the Late Archaean. Sample 440938, with a LA-ICP-MS Pb-Pb zircon age of 2831 ± 23 Ma U-Pb zircon ages of 2820–2810 Ma, is significantly older than sample 467526, which was collected from a nearby locality (LA-ICP-MS Pb-Pb zircon age = 2741 ± 53 Ma). The latter compares well with a homogeneous undeformed granite collected a few kilometres west of the head of Nivaap Paa, which yielded an upper intercept U-Pb zircon age of 2778 +7/–3 Ma (Connelly & Mengel 2000). Similarly, a grey tonalitic orthogneiss sampled close to Aasiaat yielded a U-Pb concordia age of 2727 +36/–22 Ma and consistent Pb-Pb and Rb-Sr whole-rock ages of 2759 +87/–92 Ma and 2752 ± 656 Ma respectively (Kalsbeek *et al.* 1987).

Available data on emplacement ages of the precursors to the tonalitic orthogneiss in the Kangilinaaq region suggest these may be slightly older than those in the Ikamiut region. Kalsbeek & Nutman (1996) reported ion probe data for a few zircon grains from a granodioritic to granitic orthogneiss in the Kangilinaaq area, which gave an emplacement age between 2900 and 2750 Ma. Keiding (2004) presented LA-ICP-MS $^{207}Pb/^{206}Pb$ zircon age data for a tonalitic orthogneiss of 2818 ± 1 Ma, interpreted as an igneous crystallisation age.

Sedimentation

Deposition of the sedimentary precursors to the Ikamiut and Kangilinaaq belts likely occurred in the Neoarchaean, as indicated by the metamorphic ages of *c*. 2800–2700 Ma of zircon from both belts. The age of the Kangilinaaq belt is further constrained by the 2723 ± 15 Ma emplacement age of a two-mica granite, which cross-cuts pelitic metasedimentary rocks of this belt on the south shore of Kangersuneq fjord (Thrane & Connelly 2006, this volume). As regards the Ikamiut belt, its detrital zircon ages do not preclude deposition after the Archaean. Neoarchaean metamorphic rims have been observed on some detrital grains, but these might have formed already during metamorphism of the source and survived during erosion and deposition. However, we consider this possibility unlikely. A Neoarchaean depositional age is furthermore in agreement with the Rb-Sr isotopic data for 12 metasedimentary samples from Ikamiut reported by Kalsbeek & Taylor (1999), which likewise show that their source was Archaean. Finally, the Ikamiut belt has experienced a more complex structural history than the Naternaq supracrustal belt of Palaeoproterozoic age to its south (Østergaard *et al*. 2002; Garde 2004; Thrane & Connelly 2006, this volume). This likewise points to an Archaean age of the Ikamiut belt.

The depositional sources themselves are constrained by detrital zircon populations. The detrital age spectrum for zircon grains (with igneous zonation) from metasedimentary sample 440910 from the Ikamiut region forms a tightly clustered peak at *c*. 2800 Ma, consistent with the age of the older tonalitic orthogneiss in this area. Furthermore, the steep REE pattern of this sample mimics that of the granodioritic to tonalitic orthogneiss that dominates the region. Thus the sedimentary precursor to this rock was probably derived locally from (and possibly deposited onto) the igneous precursor to the Neoarchaean orthogneiss basement. This requires a tectonic environment conducive to rapid erosion of the precursor to the source orthogneiss shortly after its emplacement at *c*. 2800 Ma.

Similarly, a metasedimentary rock from the Kangilinaaq region contains Archaean detrital zircon, with a strong peak at *c*. 2800 Ma (Thrane & Connelly 2006, this volume, $^{207}Pb/^{206}Pb$ zircon). However, there is also evidence for a significant older component, not recognised in metasedimentary rocks from the Ikamiut region: Keiding (2004) reported detrital zircon ages for two metasedimentary samples from the Kangilinaaq region with grains as old as 3600 Ma, and down to 2500 Ma, although the youngest grains (< 2800 Ma) were suspected of having suffered lead loss. Both samples show a large spread of ages, but neither has a significant Neoarchaean component at *c*. 2800 Ma. These data contrast with those of sample 440910 from the Ikamiut region, which has a tightly clustered detrital zircon population at *c*. 2800 Ma. This suggests that at least some of the Kangilinaaq metasedimentary rocks were derived from different, older, and distal source rocks: the older (> 2900 Ma) component may be derived from a presently unexposed region within the Nagssugtoqidian orogen or possibly from the lesser-known craton to the north (Keiding 2004).

A difference in the depositional sources of the Ikamiut and Kangilinaaq belts is also apparent from the geochemical data. The metasedimentary rocks form two groups based on their REE patterns. The first group (three Ikamiut and two Kangilinaaq samples) shows steep REE curves (Fig. 8C), interpreted as indicative of derivation from a felsic source, based on their similarity with REE patterns seen in the Kangilinaaq and Ikamiut orthogneisses. The second group (four Kangilinaaq samples, Fig. 8D) shows flatter patterns, consistent with derivation from a bimodal source, i.e. detritus of both felsic (steep REE patterns) and mafic (flat REE patterns) igneous rocks. The precursors to the amphibole-bearing gneisses are interpreted as volcaniclastic material that may have been mixed with clastic material during deposition or by tectonic interleaving. Given the intensity of deformation and paucity of information on the depositional environment(s) we consider it imprudent to establish a single stratigraphic-structural interpretation. In view of the different dominant lithologies of the Qasigiannguit amphibolite and the remainder of the Kangilinaaq belt, it would be interesting to investigate further whether they represent the same or different settings. The geochemistry of their amphibolite samples fall within the same range, but no metasedimentary rocks associated with the Qasigiannguit amphibolite have been analysed, and these may be important for identifying links between the latter unit and the Kangilinaaq belt.

Metamorphism

Age data for metamorphic zircon from orthogneiss and metasedimentary samples from the Ikamiut region indicate an important Neoarchaean thermal event. Two analyses of metamorphic rims from the 2831 ± 23 Ma orthogneiss 440938 yield ages of 2761 ± 10 Ma and 2754 ± 5 Ma, within error the same as the 2741 ± 53 Ma emplacement age of sample 467526 (Fig. 7). This may suggest that continued synkinematic emplacement of Neoarchaean granitoids at *c*. 2760–2700 Ma resulted in metamorphism

of slightly older (*c*. 2800 Ma) crust. This is also supported by U-Pb zircon data from the metasedimentary sample 440910. The six SIMS ages of metamorphic rims fall in two ranges, 2741 ± 9 Ma and 2696 ± 6 Ma, and similar young ages were identified in the LA-ICP-MS data (Fig. 7). These ages probably relate to the growth of S_1 garnet, biotite, plagioclase, quartz, minor sillimanite and K-feldspar in this and other metasedimentary rocks, indicative of amphibolite facies conditions only shortly after deposition, and predating regional F_2 folding. Neoarchaean metamorphism has also been recognised from zircon age data in the Kangilinaaq region. Keiding (2004) reported *c*. 2800 and 2760 Ma LA-ICP-MS ages of zircon rims and discrete grains, interpreted as metamorphic in origin, in a 2818 ± 1 Ma tonalitic orthogneiss. These ages correlate reasonably well with 2810–2720 Ma metamorphic U-Pb zircon and monazite ages in 2870–2810 Ma orthogneisses from throughout the Nagssugtoqidian orogen (Connelly & Mengel 2000).

It is likely that Neoarchaean amphibolite facies metamorphism in the Ikamiut and Kangilinaaq regions was the product of tectonism along a convergent margin (see also Connelly & Mengel 2000) on the basis of (1) the tonalitic to granodioritic composition of the Neoarchaean regional orthogneisses, (2) the apparent island arc geochemical character of amphibolites of the Kangilinaaq belt, (3) differences in the ages of sediment sources in the two supracrustal belts, and (4) the rapidity of the cycle of magmatism, erosion, sedimentation, and metamorphism.

Proterozoic zircon ages are known from the Kangilinaaq region. Keiding (2004) reported 1920–1820 Ma LA-ICP-MS ages of zircon rims and discrete grains in Archaean tonalitic orthogneisses, and also reported weighted mean age of 1919 ± 11 Ma from three rims of detrital grains in a metasedimentary rock from the Kangilinaaq belt. Thrane & Connelly (2006, this volume) report metamorphic ages of *c*. 1850 Ma for a metasedimentary rock collected on the south shore of Kangersuneq fjord, attributed to the peak of regional Nagssugtoqidian metamorphism. Given the consistency of ENE-trending D_2 structures in the Kangilinaaq and Ikamiut regions with ENE-trending Palaeoproterozoic structures throughout the orogen, these are interpreted as the product of the *c*. 1850 Ma Nagssugtoqidian orogenesis. The significance of the slightly older, *c*. 1920 Ma metamorphic age is not clear, but may indicate that part of this region experienced a thermal event prior to the main regional Nagssugtoqidian orogenesis.

By contrast, no significant indications of Palaeoproterozoic resetting are found in our Ikamiut data. The slightly discordant zircon data in sample 440938 suggest some Pb loss in this sample, although the timing is not clear. Similarly, three titanite U-Pb analyses of 2778 +7/–3 Ma reported by Connelly & Mengel (2000) from a homogeneous, undeformed granite plot on a discordia line between 2789 ± 100 and 1775 ± 10 Ma. This indicates that Palaeoproterozoic metamorphic temperatures were too low to completely reset titanite in this region. Likewise, no indication of U-Pb resetting in zircon was found in the 2727 +36/–22 Ma age from a tonalitic gneiss reported by Kalsbeek *et al*. (1987). This contrasts with zircon U-Pb analyses of samples from the Nordre Strømfjord region in the core of the Nagssugtoqidian orogen, which experienced significant Pb-loss at *c*. 1850 Ma (Kalsbeek *et al*. 1987).

Conclusions

New mapping, geochemical, geochronological and geophysical studies of two supracrustal belts from Sydostbugten, southern Disko Bugt region, West Greenland, shed light on the Neoarchaean tectonic evolution of the northern Nagssugtoqidian basement. The Kangilinaaq belt was deposited at *c*. 2800 Ma, whereas the deposition of the Ikamiut belt may postdate *c*. 2740 Ma. The geochemical signatures of the majority of metasedimentary samples from the Kangilinaaq region show REE patterns indicative of mixed felsic and mafic sources with distal Meso- and Palaeoarchaean components that are not currently known *in situ* in this part of West Greenland. Island-arc geochemical affinities of intercalated amphibolites are consistent with deposition in an arc setting. In contrast, the Ikamiut belt was sourced locally from, and deposited onto or proximal to the igneous precursors of Neoarchaean granodioritic to tonalitic orthogneisses. This is constrained by (1) the similarity in REE signatures of metasedimentary rocks and local orthogneisses and (2) the zircon emplacement ages of orthogneisses (*c*. 2820–2810 Ma; 2831 ± 23 Ma; 2741 ± 53 Ma) and detrital zircons in metasediment (2779 ± 18 Ma).

Zircon U-Pb data and $S_{1–2}$ sillimanite-bearing mineral assemblages (this study and existing data) indicate that *c*. 2800–2700 Ma amphibolite facies metamorphism affected both regions, shortly after the emplacement of the regional orthogneiss precursors and deposition of the supracrustal rocks. The rather rapid cycle of magmatic emplacement, island arc volcanism, erosion and sedimentation, and subsequent amphibolite facies metamorphism is consistent with Neoarchaean convergent tectonism at the northern margin of the present Nagssugtoqidian orogen.

Subsequently, both regions underwent Palaeoproterozoic regional deformation and lower amphibolite facies

metamorphism at *c.* 1850 Ma during the Nagssugtoqidian orogenesis, the effects of which control outcrop patterns in both areas. In the Ikamiut region, the supracrustal belt defines a broad, shallowly W-plunging antiformal structure with associated kilometre-scale parasitic F_2 folds. S_1 fabrics are folded into metre- to kilometre-scale F_2 folds and variably transposed into ENE-striking, steeply dipping S_2 fabrics and shallow W-plunging mineral lineations defined by biotite and muscovite.

In the Kangilinaaq region, the supracrustal belt defines a broad, NE-plunging F_2 fold structure. A pervasive, NE-striking, moderately dipping S_2 fabric, defined by medium- to coarse-grained garnet-hornblende-biotite-sillimanite-bearing assemblages in pelitic rocks, is folded into F_3 folds, and attests to amphibolite facies metamorphic conditions during deformation. Lack of Palaeoproterozoic resetting of the zircon U-Pb isotopic system in the Ikamiut region, cf. the Kangilinaaq region, suggests that temperatures were relatively lower in the former region during the Nagssugtoqidian orogenesis.

Acknowledgements

Mads Sylvest Christensen, Jane Gilotti, Christian Knudsen, Stanislaw Mazur, Mac Persson, Sandra Piazolo and Thomas V. Rasmussen contributed to field work in 2002–2003 reported here and part of the GEUS project *Archaean and Proterozoic crustal evolution in the Aasiaat region, central West Greenland.* Dirk Frei, Mark T. Hutchison, Lev Ilyinsky, Jørgen Kystol, Ingerlise Nørgaard, Thomas V. Rasmussen, Mikkel Vognsen, and Martin Whitehouse provided support and assistance in sample preparation and collection of analytical data. The Nordsim laboratory is funded and operated under agreement between the research funding agencies of Denmark, Norway, and Sweden, GTK, Finland, and Naturhistoriska Riksmuseet, Sweden; this is Nordsim contribution no. 164. Clark Friend, Lotte Melchoir Larsen and an anonymous reviewer are thanked for critical reviews.

References

Connelly, J.N. & Mengel, F.C. 2000: Evolution of Archean components in the Paleoproterozoic Nagssugtoqidian orogen, West Greenland. Geological Society of America Bulletin 112, 747–763.

Connelly, J.N., van Gool, J.A.M. & Mengel, F.C. 2000: Temporal evolution of a deeply eroded orogen: the Nagssugtoqidian orogen, West Greenland. Canadian Journal of Earth Sciences 37, 1121–1142.

Garde, A.A. 2004: Geological map of Greenland, 1:100 000, Kangaatsiaq, 68 V.1 Syd. Copenhagen: Geological Survey of Denmark and Greenland.

Garde, A.A. in press: Geological map of Greenland, 1:100 000, Ikamiut, 68 V.1 Nord. Copenhagen: Geological Survey of Denmark and Greenland.

Garde, A.A. & Steenfelt, A. 1999: Precambrian geology of Nuussuaq and the area north-east of Disko Bugt, West Greenland. Geology of Greenland Survey Bulletin 181, 6–40.

Garde, A.A., Christiansen, M.S., Hollis, J.A., Mazur, S. & van Gool, J.A.M. 2004: Low-pressure metamorphism during Archaean crustal growth: a low-strain zone in the northern Nagssugtoqidian orogen, West Greenland. Geological Survey of Denmark and Greenland Bulletin 4, 73–76.

Henderson, G. 1969: The Precambrian rocks of the Egedesminde–Christianshåb area (sheets 68V.1 and 68V.2). Rapport Grønlands Geologiske Undersøgelse 23, 1–37.

Hollis, J.A., Garde, A.A., van Gool, J.A.M. & Thrane K. 2004: Polymetamorphism in the northern Nagssugtoqidian orogen: a review and presentation of recent data. Danmarks og Grønlands Geologiske Undersøgelse Rapport 2004/17, 25–27.

Jacobsen, B.H. 1987: A case for upward continuation as a standard separation filter for potential-field maps. Geophysics 52, 1138–1148.

Kalsbeek, F. & Nutman A.P. 1996: Anatomy of the Early Proterozoic Nagssugtoqidian orogen, West Greenland, explored by reconnaissance SHRIMP U-Pb zircon dating. Geology 24, 515–518.

Kalsbeek, F. & Taylor, P.N. 1999: Review of isotope data for Precambrian rocks from the Disko Bugt region, West Greenland. Geology of Greenland Survey Bulletin 181, 41–47.

Kalsbeek, F., Pidgeon, R.T. & Taylor, P.N. 1987: Nagssugtoqidian mobile belt of West Greenland: a cryptic 1850 Ma suture between two Archaean continents – chemical and isotopic evidence. Earth and Planetary Science Letters 85, 365–385.

Keiding, M. 2004: Petrologiske og geokronologiske unders¿gelser af prækambriske bjergarter fra Kangilinaaq, Vestgrønland, 70 pp. Unpublished Master thesis, Københavns Universitet, Danmark.

Kystol, J. & Larsen, L.M. 1999: Analytical procedures in the Rock Geochemical Laboratory of the Geological Survey of Denmark and Greenland. Geology of Greenland Survey Bulletin 184, 59–62.

Ludwig, K.R. 2000: Isoplot/Ex version 2.2: a geochronological toolkit for Microsoft Excel. Berkeley: Berkeley Geochronology Center.

Mazur, S., Piazolo, S. & Alsop, G.I. 2006: Structural analysis of the northern Nagssugtoqidian orogen, West Greenland: an example of complex tectonic patterns in reworked high-grade metamorphic terrains. In: Garde, A.A. & Kalsbeek, F. (eds): Precambrian crustal evolution and Cretaceous–Palaeogene faulting in West Greenland. Geological Survey of Denmark and Greenland Bulletin 11, 163–178 (this volume).

Mottl, M.J. 1983: Metabasalts, axial hot springs, and the structure of hydrothermal systems at mid-ocean ridges. Geological Society of America Bulletin 94, 161–180.

Nicollet, C. & Andriambololona, D.R. 1980: Distribution of transition elements in crustal metabasic igneous rocks. Chemical Geology 28, 79–90.

Nielsen, B.M. & Rasmussen, T.M. 2004: Mineral resources of the Precambrian shield of central West Greenland (66° to 70°15′N). Part

3. Implications of potential field data for the tectonic framework. Danmarks og Grønlands Geologiske Undersøgelse Rapport 2004/21, 165 pp.

Noe-Nygaard, A. & Ramberg, H. 1961: Geological reconnaissance map of the country between latitudes 69°N and 63°45′N, West Greenland. Meddelelser om Grønland 123, 1–9.

Østergaard, C., Garde, A.A., Nygaard, J., Blomsterberg, J., Nielsen, B.M., Stendal, H. & Thomas, C.W. 2002: The Precambrian supracrustal rocks in the Naternaq (Lersletten) and Ikamiut areas, central West Greenland. Geology of Greenland Survey Bulletin 191, 24–32.

Pearce, N.J.G., Perkins, W.T., Westgate, J.A., Gorton, M.P., Jackson, S.E., Neal., C.R. & Cheney, S.P. 1997: A compilation of new and published major and trace element data for NIST SRM 610 and NIST SRM 612 glass reference material. Geostandards Newsletter 21, 115–144.

Piazolo, S., Alsop, G.I., Nielsen, B.M. & van Gool, J.A.M., 2004: The application of GIS to unravel patterns of deformation in high grade terrains: a case study of indentor tectonics from West Greenland. In Alsop, G.I. & Holdsworth, R.E. (eds): Flow processes in faults and shear zones. Geological Society Special Publication (London) 224, 63–78.

Shervais, J.W. 1982: Ti-V plots and the petrogenesis of modern and ophiolitic lavas. Earth and Planetary Science Letters 59, 101–118.

Taylor, P.N. & Kalsbeek, F. 1990: Dating the metamorphism of Precambrian marbles: examples from Proterozoic mobile belts in Greenland. Chemical Geology 86, 21–28.

Taylor, S.R. & McLennan, S.M. 1985: The continental crust: its composition and evolution, 312 pp. Oxford: Blackwell Scientific Publications.

Thorning, L. 1993: Project AEROMAG-92: a new high resolution aeromagnetic survey of the Lersletten area, central West Greenland (68°15′ to 68°55′N, 50°25′ to 53°35′W). Open File Series Grønlands Geologiske Undersøgelse 93/2, 36 pp.

Thrane, K. & Connelly, J.N. 2006: Zircon geochronology from the Kangaatsiaq–Qasigiannguit region, the northern part of the 1.9–1.8 Ga Nagssugtoqidian orogen, West Greenland. In: Garde, A.A. & Kalsbeek, F. (eds): Precambrian crustal evolution and Cretaceous–Palaeogene faulting in West Greenland. Geological Survey of Denmark and Greenland Bulletin 11, 87–99 (this volume).

van Gool, J.A.M. 2005: Geological map of Greenland, 1:100 000, Kangersuneq, 68 V.2 Syd. Copenhagen: Geological Survey of Denmark and Greenland.

van Gool, J.A.M., Connelly, J.N., Marker, M. & Mengel, F.C. 2002a: The Nagssugtoqidian orogen of West Greenland: tectonic evolution and regional correlations from a West Greenland perspective. Canadian Journal of Earth Sciences 39, 665–686.

van Gool, J.A.M. *et al.* 2002b: Precambrian geology of the northern Nagssugtoqidian orogen, West Greenland: mapping in the Kangaatsiaq area. Geology of Greenland Survey Bulletin 191, 13–23.

Whitehouse, M.J., Claesson, S., Sunde, T. & Vestin, J. 1997: Ion microprobe U-Pb zircon geochronology and correlation of Archaean gneisses from the Lewisian Complex of Gruinard Bay, northwestern Scotland. Geochimica et Cosmochimica Acta 61/20, 4429–4438.

Wiedenbeck, M., Alle, P., Corfu, F., Griffin, W.L., Meier, M., Oberli, F., von Quadt, A., Roddick, J.C. & Spiegel, W. 1995: Three natural zircon standards for U-Th-Pb, Lu-Hf, trace element and REE analyses. Geostandards Newsletter 19/1, 1–23.

Manuscript received 4 October 2004; revision accepted 15 February 2006

Pre-Nagssugtoqidian crustal evolution in West Greenland: geology, geochemistry and deformation of supracrustal and granitic rocks north-east of Kangaatsiaq

Jean-François Moyen and Gordon R. Watt

The area north-east of Kangaatsiaq features polyphase grey orthogneisses, supracrustal rocks and Kangaatsiaq granite exposed within a WSW–ENE-trending synform. The supracrustal rocks are comprised of garnet-bearing metapelites, layered amphibolites and layered, likewise grey biotite paragneisses. Their association and geochemical compositions are consistent with a metamorphosed volcano-sedimentary basin (containing both tholeiitic and calc-alkali lavas) and is similar to other Archaean greenstone belts. The Kangaatsiaq granite forms a 15 × 3 km flat, subconcordant body of deformed, pink, porphyritic granite occupying the core of the supracrustal synform, and is demonstrably intrusive into the amphibolites. The granite displays a pronounced linear fabric (L or L > S). The post-granite deformation developed under lower amphibolite facies conditions (400 ± 50°C), and is characterised by a regular, NE–SW-trending subhorizontal lineation and an associated irregular foliation, whose poles define a great circle; together they are indicative of highly constrictional strain. The existence of a pre-granite event is attested by early isoclinal folds and a foliation within the amphibolites that is not present in the granite, and by the fact that the granite cuts earlier structures in the supracrustal rocks. This early event, preserved only in quartz-free lithologies, resulted in high-temperature fabrics being developed under upper amphibolite to granulite facies conditions.

Keywords: Archaean, deformation, supracrustal rocks, granite, Nagssugtoqidian

J.-F.M., *Department of Geology, University of Stellenbosch, 7602 Matieland, South Africa.* E-mail: *jfmoyen@wanadoo.fr*
G.R.W., *Marchmyres Cottage, Breda, Alford AB33 8NQ, Aberdeenshire, U.K.*

Introduction and regional geology

The northern part of the Nagssugtoqidian orogen (NNO) is a domain of predominantly Archaean rocks that have been deformed and metamorphosed during Nagssugtoqidian orogenic activity at *c.* 1.8 Ga (Hollis *et al.* 2006, this volume; Mazur *et al.* 2006, this volume; Thrane & Connelly 2006, this volume; van Gool & Piazolo 2006, this volume). Palaeoproterozoic rocks are sparse, and apparently confined to some supracrustal belts, the most prominent one being the Naternaq supracrustal belt (Østergaard *et al.* 2002). A few small granitic-pegmatitic plugs and dykes are also related to the Palaeoproterozoic evolution. Therefore, while the structures probably reflect Nagssugtoqidian deformation, the rocks themselves (and their protoliths) largely reflect Archaean formations and evolution.

Among the Archaean units, the ubiquitous orthogneissic basement has previously been studied (Moyen *et al.* 2003a; Steenfelt *et al.* 2005); it is mostly made up of classical tonalite-trondhjemite-granodiorite (TTG) gneisses, with minor components either related to TTG partial melting, or to the participation of peridotitic mantle in their petrogenesis. All these components are well known in the Archaean, and are probably related to the subduc-

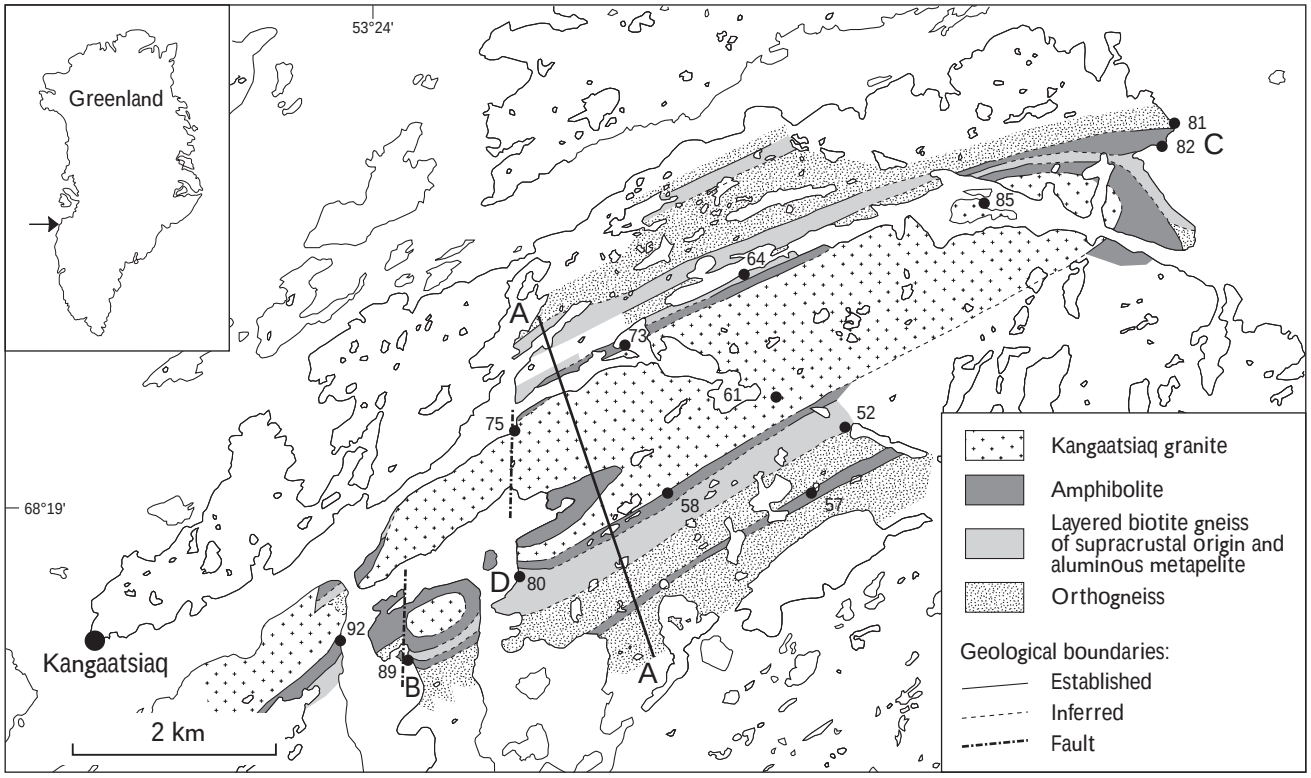

Fig. 1. Geological map of the Kangaatsiaq granite and surrounding synform, with sample localities from Table 1. Geology mostly from 2002 field work; some parts are drawn from 2001 data (J.A.M. van Gool, G.I. Alsop, S. Piazolo and S. Mazur). A–A, approximate position of section on Fig. 2; B, loc. 89, see Fig. 3; C, locs 81–82, see Fig. 4; D, loc. 80, see Fig. 5.

tion of hot oceanic lithosphere in an arc setting (Martin 1986, 1994; Moyen *et al.* 2003b; Steenfelt *et al.* 2005). Several components of the gneissic basement have been dated (Kalsbeek & Nutman 1996; Connelly & Mengel 2000; Thrane & Connelly 2002, 2006, this volume), yielding ages in the range 2.9–2.6 Ga.

Supracrustal assemblages are common, and have been mapped in many places in the Kangaatsiaq, Aasiaat and Kangersuneq map sheet areas (Marker *et al.* 1995; Mengel *et al.* 1998; Østergaard *et al.* 2002; van Gool *et al.* 2002a; Garde 2004; Hollis *et al.* 2006, this volume). They are of two main types, either amphibolites or metasedimentary rocks, that may be either aluminous, biotite ± muscovite ± sillimanite ± garnet-bearing metapelites, or quartz-rich, psammitic rocks. The age of the supracrustal rocks is, however, poorly constrained. Whilst some of them are of demonstrated Palaeoproterozoic age (*c.* 1.95 Ga, the Naternaq supracrustal belt, Østergaard *et al.* 2002; Thrane & Connelly 2002, 2006, this volume), others are likely to be of Archaean age, for instance anatectic metapelites in Saqqarput fjord in the southern part of the Kangaatsiaq map sheet area (Thrane & Connelly 2006, this volume).

Lastly, small intrusions, plugs and sheets of granite and pegmatite cut across the lithologies described above. Some of them have been dated (Kalsbeek & Nutman 1996; Thrane & Connelly 2002, 2006, this volume) and yielded late Archaean ages (2.7–2.6 Ga); it is commonly agreed that most magmatic activity in this region was related to late Archaean events, Palaeoproterozoic *P–T* conditions being such that anatexis was hardly achieved in the NNO (Mazur 2002; Piazolo 2002). The very homogeneous and porphyritic Kangaatsiaq granite north-east of Kangaatsiaq, 15 by 3 km in outcrop size, is among the largest granitic bodies of presumed late Archaean age in the southern Disko Bugt region. Altogether, the three components outlined above are representative of the usual trilogy of Archaean terranes (Windley 1995): grey TTG gneisses; volcanic and volcano-sedimentary deposits (greenstones); and late, K-rich granites. The area east and north-east of the town of Kangaatsiaq (Fig. 1) is dominated by a synform of supracrustal rocks (mafic and felsic volcanic rocks associated with sediments), into which the Kangaatsiaq granite was emplaced. It is, therefore, a good place to study the Archaean components and local history in the NNO.

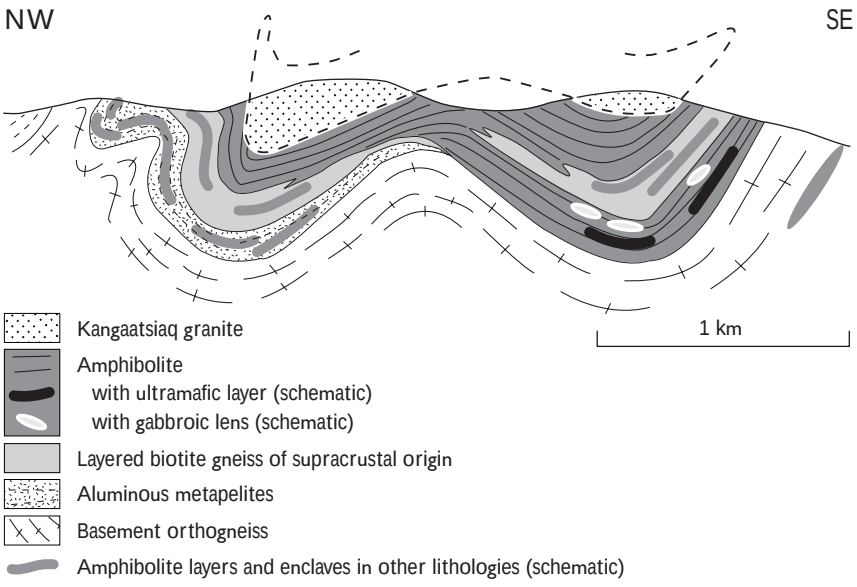

Fig. 2. Schematic NNW–SSE cross-section across the Kangaatsiaq granite and the surrounding synform. The laccolith shape (dashed line) is inferred, see text for details.

Previous work

Previous studies in the Kangaatsiaq area included reconnaissance mapping by Noe-Nygaard & Ramberg (1961), 1:250 000 scale mapping by Henderson (1969), and visits to key localities during the Danish Lithosphere Centre project (Marker *et al.* 1995; Mengel *et al.* 1998), as a result of which most published ages were obtained (Kalsbeek & Nutman 1996; Connelly & Mengel 2000). Mapping of the area was predominantly based on coastal exposures, while map information for large parts of the inland areas was based only on photogeological interpretation. Therefore, the Kangaatsiaq granite, which happens to crop out mostly inland and occupies the high grounds at the core of a synform, was at that time simply considered to be part of the polyphase gneissic basement.

The Geological Survey of Denmark and Greenland (GEUS) and its partners undertook more detailed mapping of the Kangaatsiaq map sheet in the summer of 2001. This included limited inland work, and the Kangaatsiaq granite was recognised for the first time as belonging to the group of the late Archaean intrusives. Its overall shape was mapped, as well as the supracrustal rocks into which it intrudes. Metasedimentary rocks in the area were also sampled, allowing for metamorphic studies (Mazur 2002; Piazolo 2002).

Finally, re-evaluation of the area in the summer of 2002 by the present authors led to the refinement of geological boundaries and the production of the map of Fig. 1. Sampling of the whole supracrustal series was also undertaken. Thin sections were cut at Université Claude-Bernard (Lyon, France), and samples were analysed at GEUS using XRF as well as ICP-MS (Table 1). In addition, other supracrustal rocks from the same area (obtained from A.A. Garde, personal communication 2003) have been used for the interpretation presented here, as they show similar geochemical features.

Map pattern

As mentioned in the introduction, the studied area (Fig. 1) is mainly made up of three main components: basement orthogneisses discussed by Moyen *et al.* (2003a) and Steenfelt *et al.* (2005), a succession of supracrustal rocks which comprise a sequence of amphibolite and metasedimentary rocks described below (Figs 1, 2), and the Kangaatsiaq granite, an intrusion of pink, coarse-grained, strongly lineated (L or L > S fabric) granite with K-feldspar phenocrysts. The foliated basement gneisses and the supracrustal rocks, together with early folds and structures, are refolded into a complex synform which is locally overturned, in particular on its north-western rim (see below). The granite occupies the core of the synform; it is intrusive within the top amphibolitic layer of the supracrustal sequence (Fig. 3) and is also folded together with the supracrustal rocks. The geometry of the granite suggests that it constitutes a single sheet within the supracrustal unit, and that the original intrusion had an overall flat, laccolith-like shape (Fig. 2). We consider that the mapped contact always corresponds to the bottom of the laccolith, and that the top surface has been removed by erosion (Fig. 2).

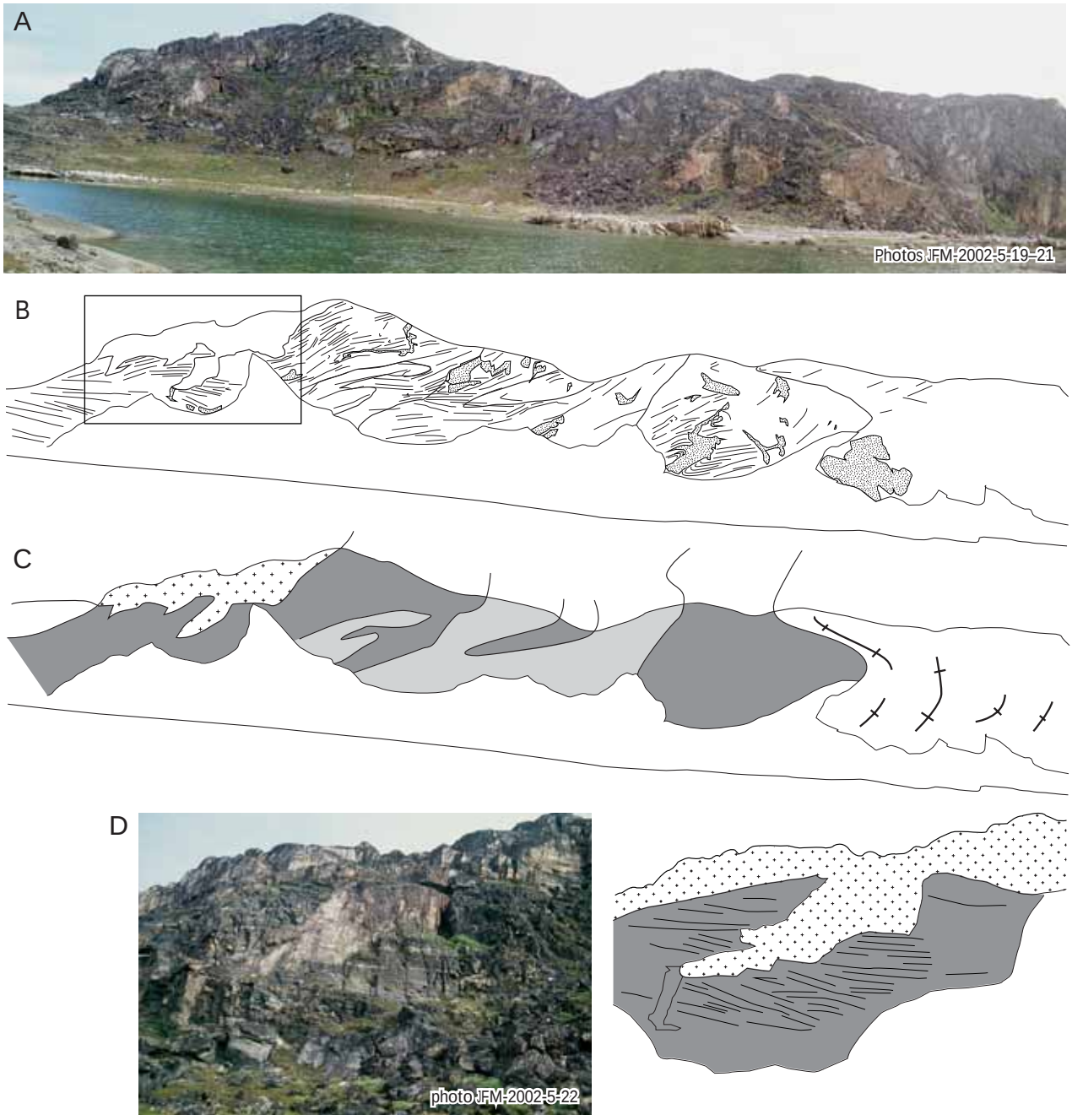

Fig. 3. Contact of the Kangaatsiaq granite and the south-western limb of the synform, loc. 89. The granite clearly intrudes the supracrustal pile, and at the same time occupies the core of the (here, slightly overturned) synform with apparently conformable relationships. A: Photomosaic of cliff face, facing east. B: Structural interpretation (stippled: pegmatites; rectangle: location of enlargement D). C: Lithological interpretation. crosses: granite; dark grey: amphibolite; light grey: layered gneiss. D: Detail of a small granitic apophysis which clearly cuts across the foliation of the amphibolite.

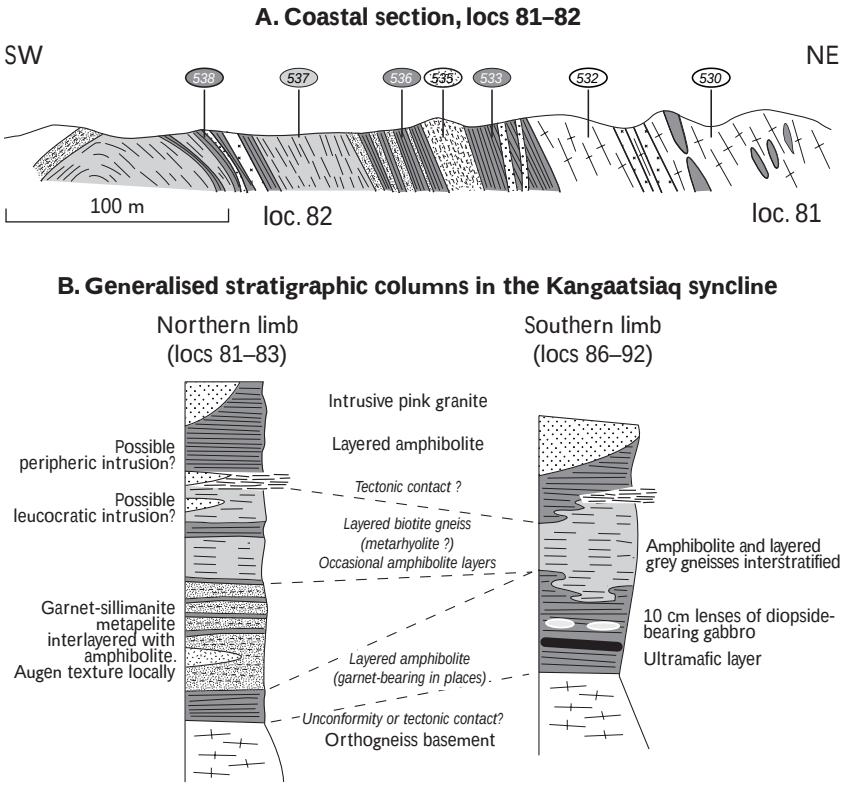

Fig. 4. Stratigraphic succession of the Kangaatsiaq synform. A: Detailed section of the overturned northern limb of the synform in its eastern extremity (locs 81–82), with sample numbers (all with prefix '485'). B: Inferred generalised logs in the north-eastern and south-western parts of the synform. Legend: see Fig. 2.

The early structures are associated with syntectonic aplites and pegmatites that cut across the amphibolite but occasionally occupy shear zones or fold hinges.

The supracrustal series

Stratigraphy

The supracrustal rocks that define the synform occur as largely discontinuous layers (Figs 2–4), that could either correspond to an original, discontinuous geometry (therefore suggesting lava flows), or simply be a result of tectonic stretching during the multiphase deformation witnessed by the area. Indeed, some of the contacts between the lithological units appear to be tectonic (Figs 4, 5), suggesting that the present-day 'stratigraphy' might not be original. Nevertheless, our mapping suggests that three main units can be recognised, allowing the following tentative stratigraphic sequence (Figs 2, 4).

1. The lowermost, *c.* 100 m thick part consists of an association of amphibolite interlayered with garnet-sillimanite metapelites, sometimes with augen textures. Some of the amphibolites are garnet-bearing, while others contain centimetre-sized lenses of diopside-bearing gabbro and small ultrabasic layers (pyroxenite or serpentinite, observed in the south-western part of the synform). The pelitic rocks seem to be more abundant in the northern limb and north-eastern extremity of the synform, while the ultramafic rocks and gabbros were found only in its south-western part.

2. The middle part is a sequence about 100 m thick of layered biotite gneiss, i.e. quartzo-feldspathic gneiss with no discriminant minerals and a compositional layering at a scale of *c.* 10 cm. The layered biotite gneiss is commonly interstratified with layers and lenses of amphibolite 10–100 cm thick. The contact with the lower amphibolite is gradational. As will be discussed below, the layered biotite gneiss likely represents meta-rhyolite. The middle unit of layered biotite gneiss probably does not have a constant thickness; furthermore, in poor, inland outcrops, it is readily confused with basement orthogneisses. A detailed log of the lower and middle parts of the sequence as described in the foregoing was made in the overturned, north-eastern part of the synform, displaying its complex and composite nature (Fig. 3A, locs 81–82).

3. A horizon 50–100 m thick of fine grained, dark, layered amphibolite forms the highest observed level. The

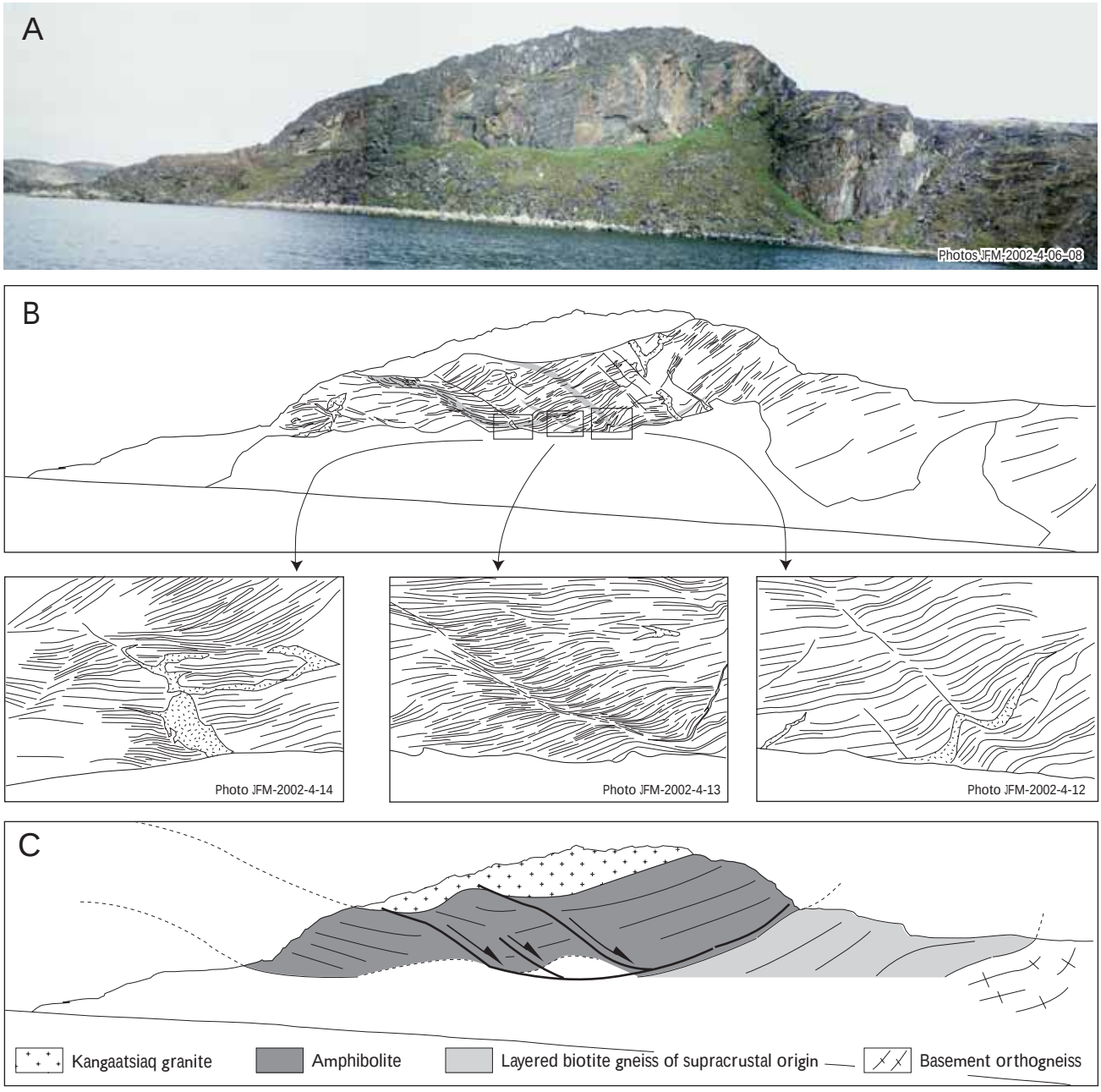

Fig. 5. Photomosaic (A) and structural interpretation (B) of the cliff face at loc. 80 (photo facing east). Stippled: pegmatites; grey: high-strain zones. Evidence for pre- to syn-granite, apparently extensional deformation is preserved in the amphibolite bodies intruded by the granite. Details of the cliff face display the apparently extensive deformation in the amphibolite. Cross-cutting pegmatites (see photo 4-12) are occasionally affected by this deformation, suggesting that it is synchronous or nearly synchronous with granite emplacement. C: Schematic relationships between the granite, the early extensional deformation, and the supracrustal pile, inspired from loc. 80.

Fig. 6. Field and thin sections photographs of lithologies of the supracrustal series (XPL: crossed polarised light; PPL: plane polarised light). Microphotographs are *c.* 5 mm across. A1: Outcrop of sillimanite-bearing metapelite, loc. 64 (sample 485525). Hammer is 80 cm long. A2: Thin section (XPL) of the same. B1: Outcrop of layered biotite gneiss interstratified with amphibolite at loc. 81 (sample 485537). Pen is 15 cm long. B2: Thin section (XPL) of same. C1: Outcrop of the top amphibolite at loc. 58 (sample 485523). Pocket knife is 10 cm long. C2: Thin section (PPL) of same. C3: Outcrop of gabbroic inclusions in the basal amphibolite layer at loc. 92 (sample 485541). Compass 5 cm wide. C4: Thin section (XPL) of clinopyroxene cluster in amphibolite. C5: Thin section (XPL) of sample 485540 (ultramafic layer, same locality).

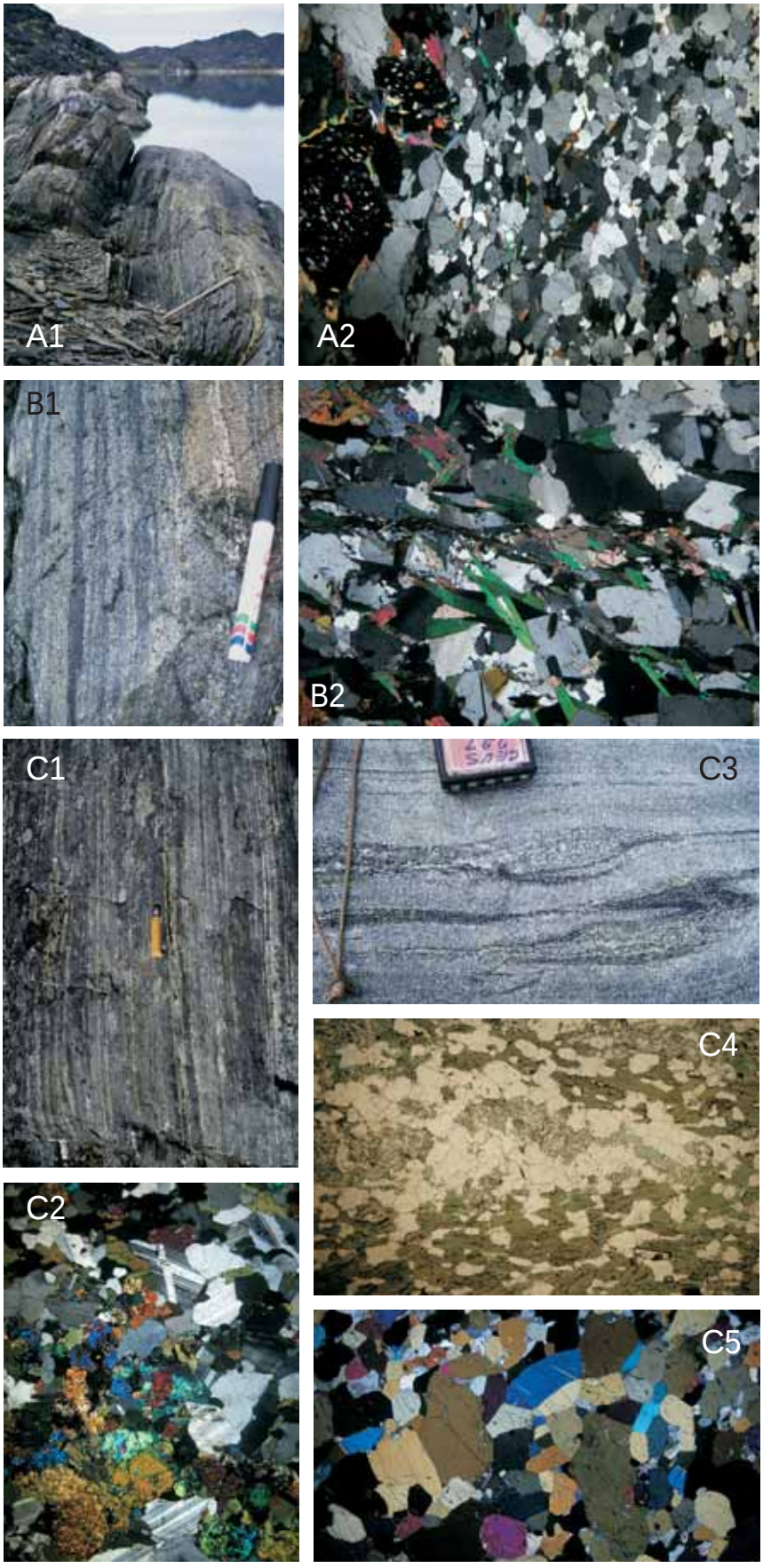

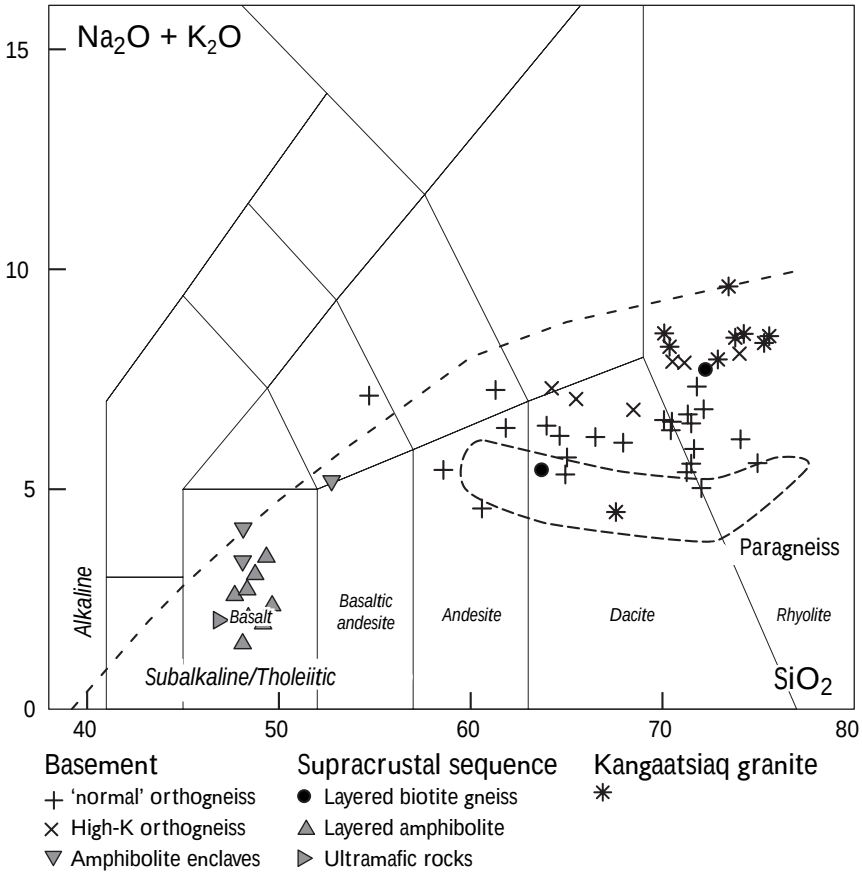

Fig. 7. Total alkali vs. silica (TAS) diagram (Le Maître *et al.* 1989) for the magmatic components of the supracrustal rocks and the surrounding orthogneisses.

upper boundary of this unit is not observed, since it is everywhere intruded by the granite. This 'top amphibolite' is continuous and can be traced all around the exposed granite contact; it is also rather homogeneous, much more so than any of the other components of the supracrustal sequence. In loc. 80 (Fig. 5), it appears to be in tectonic contact with the underlying layered biotite gneiss.

Field description and petrology

As mentioned above, three main components are observed in the supracrustal succession: aluminous metapelite, layered biotite gneiss and amphibolite. Field aspects together with photographs of thin sections are presented in Fig. 6. The aluminous metapelites occur as slaty, fine-grained (0.5–1 mm), grey to yellowish paragneisses (Fig. 6A1). Garnet or sillimanite is commonly seen in outcrop. In thin section, they display biotite, plagioclase and quartz with either sillimanite or poikiloblastic garnet (Fig. 6A2) cutting across an earlier weak foliation marked by preferred orientation of biotite flakes and elongation of plagioclase crystals.

The layered biotite gneisses appear as grey, relatively massive, fine grained (0.5–1 mm), finely layered rocks. They are interstratified at all scales with amphibolite (Figs 3C, 6B1) and generally form discontinuous bodies on a 100 m scale. They consist of quartz, plagioclase, K-feldspar and biotite; the foliation is defined by the preferred orientation of biotite and elongation of quartz grains (Fig. 6B2).

The amphibolites are dark, massive rocks that also show a strong compositional banding (Fig. 6C1–C2). Regardless of their mode of outcrop either as a thick continuous layer, as in the 'top amphibolite', or as discontinuous layers interstratified with other lithologies, they are very similar in visual aspect and mineralogy. They mostly consist of a fine-grained (0.5–1 mm) hornblende-plagioclase assemblage, with preferred orientation of minerals defining the foliation. Commonly, small clusters of clinopyroxene surrounded by felsic (mostly plagioclase) rims are observed (Fig. 6C4).

At one locality, gabbroic lenses on a scale of 5–10 cm have been observed within the amphibolite (loc. 92, Fig. 6C3). They are medium grained (2–5 mm) and greenish in aspect, and composed of a clinopyroxene-plagioclase association with diffuse contacts with the neighbouring amphibolite (Fig. 6C4). At the same locality, an ultrama-

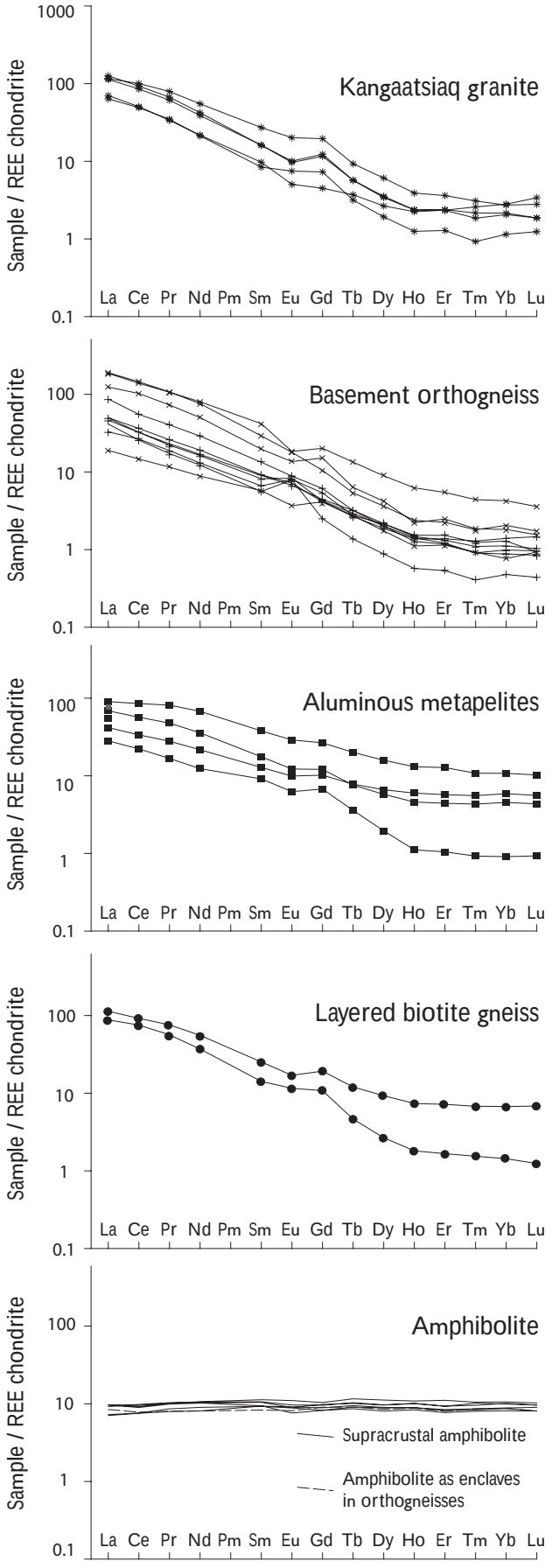

Fig. 8. REE patterns (chondrite normalised, Boynton 1984) for the lithologies in and around the Kangaatsiaq synform.

fic layer *c.* 0.5 m thick has been observed. It is slightly coarser grained (2–5 mm) than the amphibolite, and solely consists of amphibole grains (Fig. 6C5), which are optically similar to the hornblende in the surrounding amphibolite.

Geochemistry and origin

Figures 7–8 and Table 1 summarise the major and trace element (especially REE) characteristics and relationships of the three main supracrustal components: amphibolites, metapelites and layered biotite gneisses. There is little, if any doubt of the fact that the amphibolites correspond to metamorphosed and deformed mafic igneous rocks. Elsewhere, similar field characteristics in amphibolites as those observed here have been interpreted as corresponding to transposition of former pillow lavas in high strain domains (e.g. Myers 2001). The metapelites obviously have a sedimentary origin and probably represent terrigeneous sediments. The origin of the layered biotite gneisses, however, is less obvious. They could represent either sedimentary or felsic volcanic rocks. Therefore, they are plotted on geochemical diagrams for both magmatic and sedimentary rocks (see below), allowing comparisons.

Origin of the amphibolites

The supracrustal amphibolites and their counterparts, enclaves in the basement orthogneisses, appear to be very similar in composition. They plot mostly as basalts in a TAS diagram (Fig. 7; Le Maître *et al.* 1989), and an AFM diagram (Fig. 9; Irvine & Baragar 1971) reveals that they belong to a tholeiitic series. This, together with their spectacularly flat REE pattern at about 10 times chondritic values (Fig. 8), is consistent with the amphibolites corresponding to former MORB basalts, possibly formed as part of an oceanic crust. Many discriminant diagrams for basaltic rocks have been proposed on geochemical grounds (e.g. Pearce 1982; Shervais 1982; Mullen 1983). However, some caution should be exercised when using such diagrams for the Archaean, since the existence of modern-style tectonic settings in the Archaean is not certain, and the palaeogeodynamical contexts might not be similar to those of modern settings (Hamilton 1998; McCall 2003; van Kranendonk 2003). Nevertheless, in

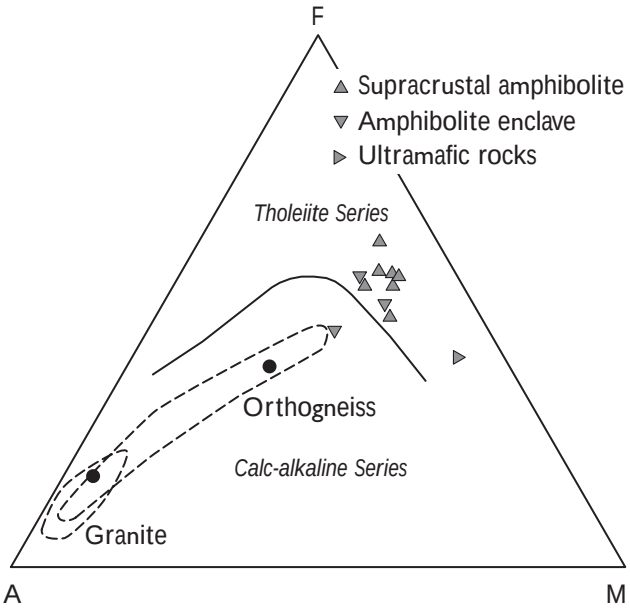

Fig. 9. AFM diagram (Irvine & Baragar 1971) showing the tholeiitic affinity of both the supracrustal amphibolites and the enclaves in the gneisses. A, $Na_2O + K_2O$; F, FeO_{total}; M, MgO. The fields of the basement orthogneisses and the Kangaatsiaq granite are also shown for comparison.

such diagrams, the amphibolites plot either as MORB or as rocks originated in oceanic arcs (arc tholeiites), leaving some ambiguity about their original setting.

Origin of the aluminous metapelites

The geochemistry of metasedimentary rocks is commonly used to discuss their source, in terms of (1) the nature of the original sediments, (2) the nature of the weathered/eroded source material, and (3) the degree of weathering of the source (see e.g. Taylor & McLennan 1985; Herron 1988; Roser & Korsch 1988; Nesbitt & Young 1989; Bohlar *et al.* 2005). While several authors also use the geochemistry of sediments to discuss their geodynamical setting (Bhatia 1983; Bhatia & Crook 1986; Roser & Korsch 1988), some caution should be exercised when dealing with Archaean environments, as mentioned above. In terms of classification, the metasedimentary rocks from the Kangaatsiaq area plot mostly as shales or greywackes, using either of the two schemes proposed by Herron (1988). One of these is shown on Fig. 10A; the ambiguity and possible (chemical) confusion between the two groups, shales and greywackes, which are poorly separated by this diagram, has been outlined by these authors. Nevertheless, the conclusion points to relatively immature sediments which have undergone limited transport from their source.

The nature of the source itself can be discussed using major or trace elements. Roser & Korsch (1988) proposed a scheme for source determination of clastic sediments on the basis of major elements. In this instance, the studied samples straddle the P2–P3 boundary (Fig. 10B), suggesting a felsic to intermediate source. Also trace elements can be used to refine this conclusion. As pointed out by Taylor & McLennan (1985), some elements (high field strength elements, rare earth elements (REE), Y, Sc, Th) only undergo limited fractionation during sedimentary processes; thus, their ratios reflect the signature of their source. Plotting these elements against each other shows that the Kangaatsiaq metasedimentary rocks (Fig. 10E–H) have element ratios that are generally consistent with derivation from an orthogneissic source (amphibolites generally have too low trace element contents and incorrect ratios to be a possible source). The only exception is for heavy REE (Figs 8, 10G). Indeed, the relatively high Yb contents of the metasedimentary rocks precludes their derivation solely from a low-Yb gneissic basement, and implies that they must, at least in part, have been derived from higher-Yb rocks such as the amphibolites; this is hardly a surprise, since amphibolite occurs as enclaves intercalated within the orthogneisses. Modelling the REE contents of such a mixture shows that mixing of ortho-

Facing page:

Fig. 10. Major and trace element geochemistry (A–D and E–H) of the metasedimentary rocks (paragneisses, and layered biotite gneisses). Dotted fields show the compositions of the major regional lithologies (orthogneiss and high-K orthogneiss, Moyen *et al.* 2003a; Steenfelt *et al.* 2005; amphibolite; Kangaatsiaq granite). A: $Log(SiO_2/Al_2O_3)$ vs. $log(Fe_2O_3/K_2O)$, from Herron (1988). B: Discriminant diagrams for the metapelites, from Roser and Korsch (1988). The sources for each group are P1, mafic to intermediate volcanic rocks; P2, intermediate (andesitic, dacitic, occasionally rhyolitic) volcanic rocks; P3, felsic volcanic rocks; P4, evolved sediments, sandstones, etc. The discriminant functions are: $F1 = -1.773\ TiO_2 + 0.607\ Al_2O_3 + 0.760\ Fe_2O_3 - 1.500\ MgO + 0.616\ CaO + 0.509\ Na_2O - 1.224\ K_2O - 9.090$; $F2 = 0.445\ TiO_2 + 0.070\ Al_2O_3 - 0.250\ Fe_2O_3 - 1.142\ MgO + 0.438\ CaO + 1.475\ Na_2O + 1.426\ K_2O - 6.861$. C, D: Triangular diagrams (from Nesbitt & Young 1989). Stars: theoretical mineral compositions; il, illite; ms, muscovite; pg, plagioclase; ksp, K-feldspar; cpx, clinopyroxene; hbl, hornblende; chl, chlorite; bt, biotite; sm, smectite. Dashed arrows: trends for (1) weathering and (2) K-metasomatism, after Nesbitt & Young (1989) and Bohlar *et al.* (2005). E, F: U vs. Th and Ti vs. Zr (log scale) diagrams, showing that the metasedimentary rocks have trace elements ratios comparable to the gneisses, but mostly different from the amphibolites. G, H: La/Yb vs. Yb and Ti/Zr vs. Ni (log scale) diagrams displaying the same relationships as E–F, also showing the mixing between an amphibolite-like and an orthogneiss-like source (ticks at 10% increments).

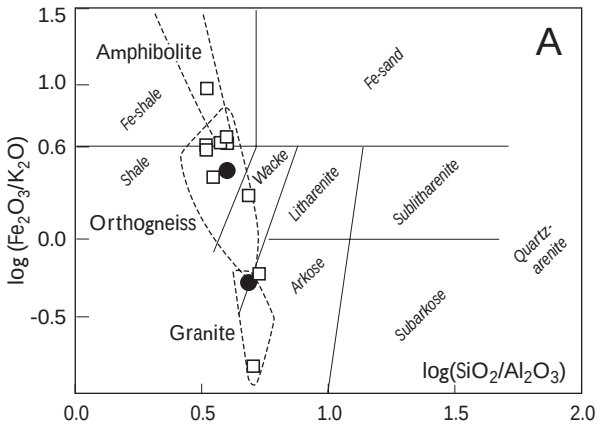
A
Amphibolite
Fe-shale
Fe-sand
Shale
Wacke
Litharenite
Sublitharenite
Orthogneiss
Quartz-arenite
Arkose
Granite
Subarkose
log (Fe2O3/K2O)
log(SiO2/Al2O3)

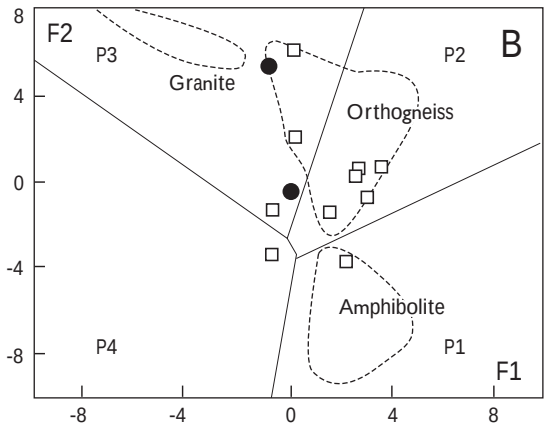
B
F2
P3
P2
Granite
Orthogneiss
Amphibolite
P4
P1
F1

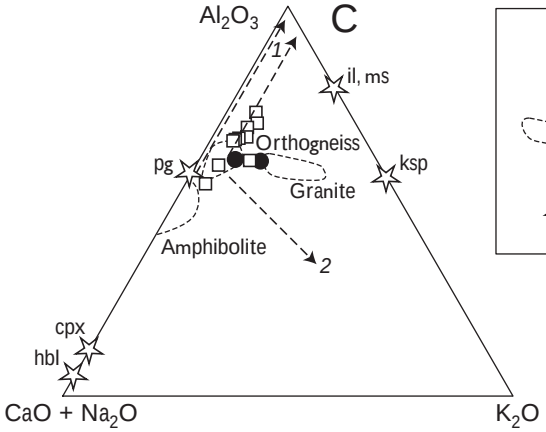
C
Al2O3
1
il, ms
Orthogneiss
pg
ksp
Granite
Amphibolite
2
cpx
hbl
CaO + Na2O
K2O

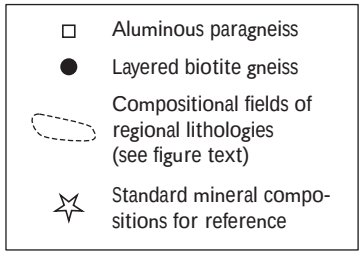
Aluminous paragneiss
Layered biotite gneiss
Compositional fields of regional lithologies (see figure text)
Standard mineral compositions for reference

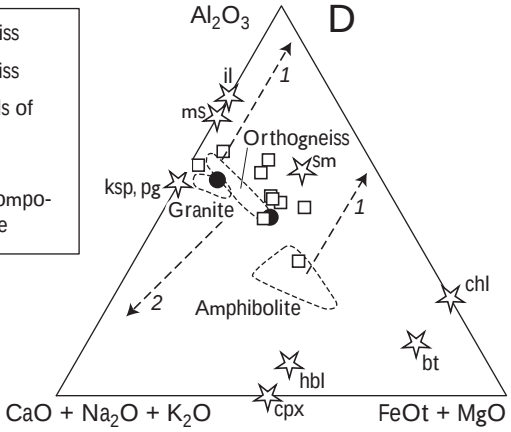
D
Al2O3
il
1
ms
Orthogneiss
sm
ksp, pg
Granite
1
2
chl
Amphibolite
bt
hbl
cpx
CaO + Na2O + K2O
FeOt + MgO

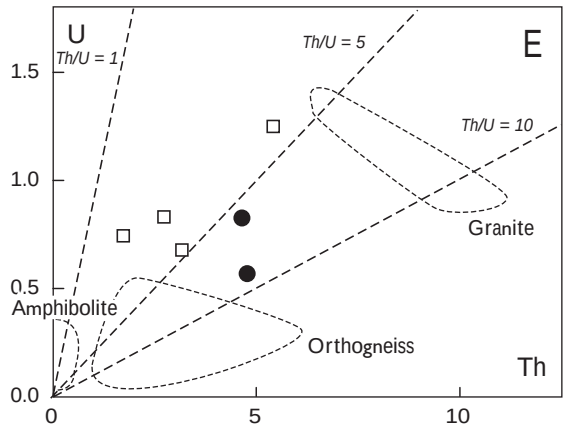
U
Th/U = 1
Th/U = 5
E
Th/U = 10
Granite
Amphibolite
Orthogneiss
Th

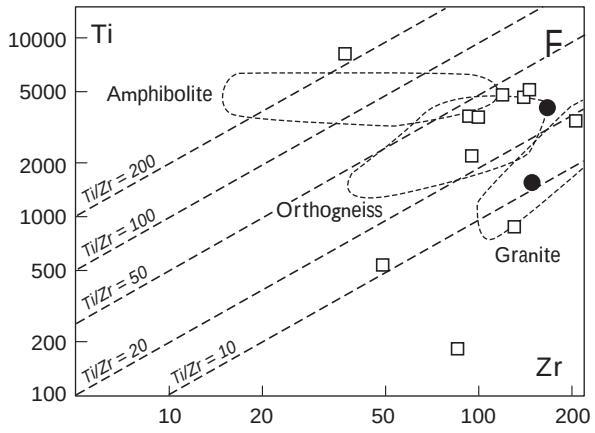
Ti
F
Amphibolite
Ti/Zr = 200
Ti/Zr = 100
Orthogneiss
Granite
Ti/Zr = 50
Ti/Zr = 20
Ti/Zr = 10
Zr

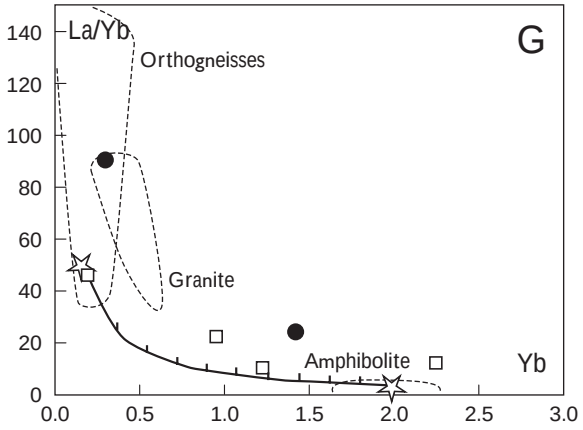
La/Yb
G
Orthogneisses
Granite
Amphibolite
Yb

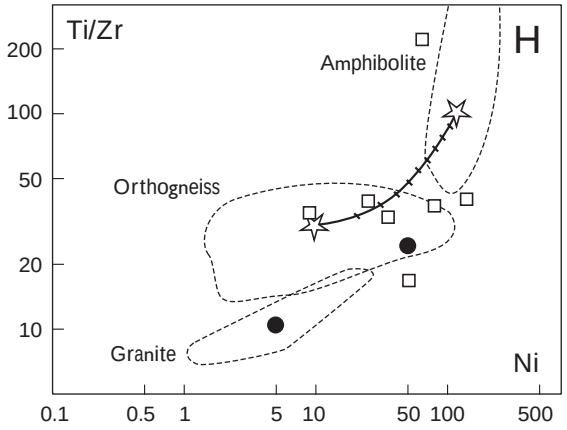
Ti/Zr
H
Amphibolite
Orthogneiss
Granite
Ni

Table 1. Chemical analyses of rocks in and around the Kangaatsiaq syncline

	Basement			Kangaatsiaq granite						Amphibolite						Biotite-bearing gneiss		Aluminous metased.	
	Orthogneiss		Amphibolite enclave	Main granitic mass					Peripheric granitic dyke	Amphibolite in lower layer associated with felsic rocks			Massive amphibolite, top		Ultramafic layer in amphibolite	Layered biotite gneiss	Pale leucocratic gneiss	Qz-Bt-Sill-Gt schist	Qz-Bt-Gt gneiss
Sample No.	485530	485532	485522	485524	485527	485529	485539	470529	485534	485533	485536	485538	485523	485528	485540	485537	485531	485535	485525
Locality	81	81	57	61	73	75	85	gia 2001-217	81	81	81	81	58	73	92	81	52	81	64
SiO_2	70.81	70.03	47.52	69.00	74.08	72.92	72.88	70.21	66.04	47.05	47.14	48.77	48.74	48.08	45.87	62.29	70.97	63.10	66.03
TiO_2	0.29	0.31	0.74	0.37	0.18	0.27	0.21	0.43	0.62	0.95	0.81	0.87	0.77	0.72	0.51	0.68	0.26	0.61	0.62
Al_2O_3	15.08	15.15	14.94	15.16	13.22	13.48	13.87	15.14	16.01	14.68	14.72	14.67	15.82	14.69	11.54	15.69	14.88	16.97	18.98
Fe_2O_3*	2.47	2.06	12.46	2.46	1.33	1.48	1.61	2.50	3.94	12.99	10.90	12.60	12.14	10.77	11.74	5.68	1.85	5.92	4.27
MnO	0.02	0.02	0.19	0.02	0.01	0.01	0.02	0.04	0.01	0.22	0.26	0.24	0.21	0.20	0.21	0.09	0.02	0.10	0.03
MgO	0.90	0.64	8.32	0.79	0.31	0.44	0.46	0.89	1.27	6.80	4.74	6.70	7.18	7.90	14.19	3.13	0.48	2.17	1.45
CaO	2.88	2.39	11.22	2.07	1.01	1.17	1.29	2.17	5.07	13.30	17.89	11.51	12.18	13.14	11.78	4.71	2.13	4.60	2.19
Na_2O	4.42	4.61	2.48	4.18	3.63	3.64	4.06	3.93	3.31	2.02	1.40	2.67	1.64	2.55	1.39	3.31	4.23	2.94	3.20
K_2O	2.02	3.13	0.83	4.23	4.56	4.74	4.28	4.29	1.07	0.53	0.08	0.76	0.31	0.52	0.58	2.03	3.38	1.41	1.70
P_2O_5	0.06	0.15	0.04	0.16	0.05	0.07	0.08	0.17	0.39	0.06	0.06	0.06	0.05	0.03	0.04	0.22	0.08	0.07	0.10
H_2O	0.18	0.26	0.54	0.22	0.16	0.17	0.26		0.80	0.36	1.19	0.51	0.45	0.30	0.79	0.98	0.18	0.69	0.59
K/Na	0.30	0.45	0.22	0.67	0.83	0.86	0.69	0.72	0.21	0.17	0.04	0.19	0.12	0.13	0.27	0.40	0.53	0.32	0.35
Mg#	42	38	57	39	32	37	36	41	39	51	46	51	54	59	71	52	34	42	40
A/CNK	1.03	0.99	0.59	1.00	1.04	1.02	1.02	1.01	1.01	0.52	0.42	0.56	0.63	0.51	0.47	0.97	1.03	1.15	1.71
C.I.A.																60.95	60.44	65.47	72.80
V	25	20	254	28	11	10	11	33	36	271	237	271	244	225	177	100	12	133	88
Cr	22	3	332	7	3	3	4	14	11	207	308	284	247	425	1734	68	2	136	61
Ni	12.9	7.6	147.8	8.1	3.5	4.4	5.5	bdl	22.7	153.1	167.6	121.7	175.7	197.5	728.1	50.1	5.0	79.1	25.1
Co	71.4	46.4	72.3	37.0	44.6	79.4	68.8		50.7	72.1	59.9	57.1	57.5	61.0	81.6	47.8	86.3	100.8	103.0
Cu	5.4	3.2	40.3	3.3	2.6	2.6	1.7	13.0	329.1	78.7	73.7	30.3	12.6	24.1	2.2	14.2	3.7	101.4	14.9
Zn	43.6	42.7	86.2	36.2	21.5	20.6	27.9	25.0	31.9	90.1	76.7	108.2	77.4	74.8	103.3	67.0	34.7	78.3	57.3
Rb	74.4	92.0	7.7	114.7	115.5	118.7	125.8	56.0	96.0	9.1	1.7	9.4	32.4	6.5	14.8	46.9	83.2	44.7	79.8
Sr	504	839	93	735	252	342	340	712	1913	93	117	117	92	94	78	803	822	231	213
Ba	558	1049	39	1476	463	672	593	1384	2095	64	22	118	46	37	82	819	1430	314	262
Y	3.0	4.5	17.6	8.5	2.7	5.7	5.5	bdl	7.2	21.1	18.8	20.6	18.5	17.1	11.6	16.2	3.8	12.5	9.2
Zr	862	117	334	178	104	132	140	219	203	19	16	20	32	16	24	165	147	98	93
Nb	5.4	5.6	2.1	8.4	3.8	6.0	4.8	bdl	7.0	2.8	2.2	2.4	4.1	2.7	1.8	8.3	3.5	4.5	5.1
Ta	2.5	3.2	1.0	4.2	3.1	3.5	3.7		4.6	0.9	0.6	0.9	1.1	0.7	0.8	3.9	3.8	2.7	2.4
Hf	11.4	7.9	3.1	5.4	2.2	10.5	2.6		4.7	1.1	0.8	0.8	0.7	1.3	0.6	3.6	3.5	3.3	2.3
Sc	5.0	3.7	43.8	2.4	0.9	1.5	1.5		3.9	41.6	38.2	40.9	41.2	38.3	31.3	14.2	2.3	23.4	13.0
Ga	20.8	22.4	15.1	19.1	17.6	17.8	18.2		21.3	16.4	14.5	16.1	16.5	14.8	11.9	18.6	19.6	19.7	24.1
Cs	1.0	1.3	0.0	1.0	0.4	0.6	1.9		6.2	0.1	0.1	0.0	0.3	0.0	0.3	4.7	1.2	2.2	1.5
Pb	9.6	15.6	2.6	15.6	16.5	12.8	17.3		6.9	2.9	2.8	3.5	1.7	3.2	1.3	8.6	15.4	7.1	7.8
Th	1.9	5.1	0.2	10.8	6.8	9.8	9.2		14.0	0.4	0.2	0.3	0.2	0.2	0.2	4.7	4.8	2.7	3.2
U	0.5	1.7	0.3	0.9	1.4	1.0	0.9		2.6	0.2	0.1	0.1	0.3	0.1	0.3	0.8	0.6	0.8	0.7
Th/U	3.8	3.0	0.7	12.1	5.0	10.0	9.8		5.4	1.8	3.5	3.2	0.9	1.4	0.5	5.6	8.2	3.3	4.7
Ti/Zr	20.4	15.9	134	12.6	10.4	12.3	9.0	11.8	18.2	296	303	266	142	270	125	24.8	10.5	37.0	39.7
La	10.2	38.4	2.6	35.9	19.8	35.2	39.1	29.0	151.7	3.0	2.2	3.0	2.2	2.9	2.6	35.3	27.3	12.9	21.3
Ce	21.4	82.7	6.3	81.2	39.7	68.9	75.1	105.0	313.7	7.7	6.2	7.2	6.1	7.9	5.2	74.4	61.0	27.2	46.0
Pr	2.3	8.9	1.0	9.7	4.2	7.5	8.2		37.7	1.2	1.0	1.2	1.0	1.3	0.8	9.3	6.9	3.4	5.8
Nd	7.8	30.1	4.9	33.0	12.8	23.3	25.4		126.4	6.3	5.4	6.1	4.9	6.1	3.7	33.4	22.2	13.0	21.5
Sm	1.3	3.8	1.6	5.3	1.6	3.2	3.1		13.4	2.1	1.8	2.0	1.8	1.8	1.2	4.9	2.8	2.5	3.4
Eu	0.6	1.0	0.6	1.5	0.6	0.7	0.7		2.4	0.7	0.6	0.7	0.7	0.6	0.4	1.3	0.9	0.7	0.9
Gd	1.4	3.9	2.3	5.1	1.9	3.0	3.2		12.5	2.5	2.1	2.5	2.3	2.1	1.4	5.0	2.8	2.6	3.1
Tb	0.13	0.30	0.43	0.44	0.15	0.27	0.27		0.83	0.49	0.43	0.48	0.45	0.41	0.28	0.57	0.22	0.37	0.36
Dy	0.69	1.35	2.74	1.96	0.62	1.14	1.10		2.81	3.12	2.85	3.10	2.89	2.60	1.72	2.99	0.86	2.13	1.86
Ho	0.11	0.16	0.63	0.28	0.09	0.17	0.17		0.25	0.72	0.64	0.73	0.64	0.60	0.40	0.53	0.13	0.43	0.33
Er	0.32	0.52	1.68	0.76	0.27	0.50	0.49		0.98	1.96	1.77	1.95	1.72	1.62	1.13	1.51	0.35	1.20	0.93
Tm	0.04	0.06	0.28	0.10	0.03	0.07	0.06		0.07	0.31	0.28	0.33	0.27	0.26	0.18	0.22	0.05	0.18	0.14
Yb	0.27	0.38	1.82	0.57	0.24	0.45	0.43		0.47	2.12	1.85	2.08	1.82	1.70	1.20	1.41	0.30	1.23	0.95
Lu	0.03	0.05	0.26	0.09	0.04	0.06	0.06		0.06	0.31	0.29	0.31	0.26	0.26	0.17	0.22	0.04	0.18	0.14
La/Yb	37.8	102	1.44	63.0	83.3	79.0	89.8		320	1.42	1.22	1.43	1.20	1.68	2.19	25.0	91.8	10.5	22.3
Eu/Eu*	1.34	0.78	0.94	0.87	0.96	0.70	0.71		0.56	0.96	1.01	0.90	1.00	0.87	0.99	0.77	0.93	0.87	0.82

Sample numbers refer to GEUS databases; localities are shown on Figs 1 and 4, except gia 2001-217 outside the map area (UTM 396540, 7575984).
Major elements in wt%; trace elements in ppm. Analytical data obtained at GEUS by XRF (major elements and approximate trace elements in 470529) and ICP-MS (all other trace elements).
K/Na: Molecular K/Na ratio. Mg#: Molecular 100Mg/(Mg + Fe). A/CNK: Molecular Al/(Ca + Na + K). C.I.A.: Continental Index of Alteration (Nesbitt & Young 1989); metased.: metasedimentary rock; bdl: below detection limit.

gneisses with amphibolite (Fig. 10G, H) can explain the Yb contents of the sediments; since the amphibolites are, collectively, less enriched in trace elements than the gneisses, their involvement would only have little effect on the other incompatible elements in the metasedimentary rocks. In contrast, the latter display higher Ni and Cr contents than the orthogneisses, also consistent with a contribution from amphibolite or its precursor rocks in their formation (Fig. 10H). Finally, the degree of alteration of the source can be discussed. The metasedimentary rocks display C.I.A. values (Chemical Index of Alteration, Nesbitt & Young 1989) of *c.* 60–70 (Table 1), slightly lower than for shales or similar rocks (70–75, Taylor & McLennan 1985). In the triangular diagrams proposed by Nesbitt & Young (1989; Fig. 10C, D), they also depart only moderately from their protoliths, suggesting a relatively unweathered source. Very little or no evidence for secondary K-enrichment is observed.

Taking the above-mentioned limitations into account, the geoynamic setting inferred from the geochemistry gives consistent results regardless of the classification scheme used. Both the major elements classifications of Bhatia (1983) and Roser & Korsch (1988) and the trace element systems of Bhatia & Crook (1986) suggest an oceanic or continental island-arc setting. However, this only reflects the characteristics outlined above: relatively immature sediment derived from poorly weathered felsic to intermediate magmatic rocks, with a possible mafic component.

Origin of the layered biotite gneiss (felsic volcanic rocks?)

The two samples analysed of the layered biotite gneisses give ambiguous geochemical signatures and can be interpreted either as sedimentary or igneous (Figs 7–10). In general, they seem to share more similarities with the granite or the orthogneisses than with any other member of the supracrustal group. In particular, Fig. 10 (C, D) shows that if these rocks are of sedimentary origin, they are indeed very similar to their source and were derived from a largely unweathered protolith. This implies that the layered biotite gneiss can be interpreted in two ways. It may represent very immature sediment derived from a mostly unweathered protolith with a very similar bulk composition, such as a conglomerate made of pebbles of unweathered orthogneiss, in which case the banding could be a trace of the transposed pebbles. Alternatively the layered biotite gneiss represents calc-alkali or TTG-type felsic lavas, whose composition would of course be very similar to that of their plutonic counterparts.

Origin of the supracrustal sequence as a whole

Based on the foregoing discussion two interpretations can be proposed for the supracrustal sequence.

1. The succession could represent a dismembered ophiolite sequence intermingled with clastic sediments eroded from a nearby continent. The combined sequence could then be interpreted as an accretionary prism. The likely tectonic nature of the contact between members of the sequence (see above and Figs 4, 5) supports this hypothesis.

2. The whole supracrustal pile consists of a bimodal, calc-alkaline, probably subduction-related volcanic suite associated with immature terrigeneous sediments directly derived from their weathering. This is consistent with an arc situation, in which a back- or fore-arc basin is being filled with both volcanic products and detrital sediments largely derived from the weathering of these lavas. At the same time, tonalitic plutons are emplaced at depth from the same magmas. The plutonic rocks are quickly uplifted and eroded, and, besides intruding into the supracrustal pile, may in some cases also represent the basement for subsequent volcano-detritic basin fill.

In both cases, the rocks were formed in a convergent setting, probably above or close to an active subductions margin. In general, arc- or subduction-related origins for Archaean volcanic suites are preferred by most workers (e.g. Card 1990; Lowe 1994; Windley 1995; Chadwick *et al.* 1996), although the issue remains controversial (Hamilton 1998; McCall 2003; van Kranendonk 2003).

Nature and origin of the Kangaatsiaq granite

The Kangaatsiaq granite is pink, porphyritic, and displays a distinct rodding (Fig. 11A) showing that it has been intensely deformed (see below). While YZ sections (perpendicular to the main stretching direction) display a preserved magmatic texture, sections parallel to X clearly show the gneissic texture of the rock. The mineralogical paragenesis is K-feldspar + quartz + sodic plagioclase + biotite, with accessory zircon, titanite, apatite and oxides.

The granite has moderate K/Na ratios (0.67–0.86), is slightly metaluminous with A/CNK ratios of 1.00–1.04, and has low Mg# of 32– 41 (Table 1). Ni and Cr contents are also low, while Rb, Sr and Ba contents are moderate;

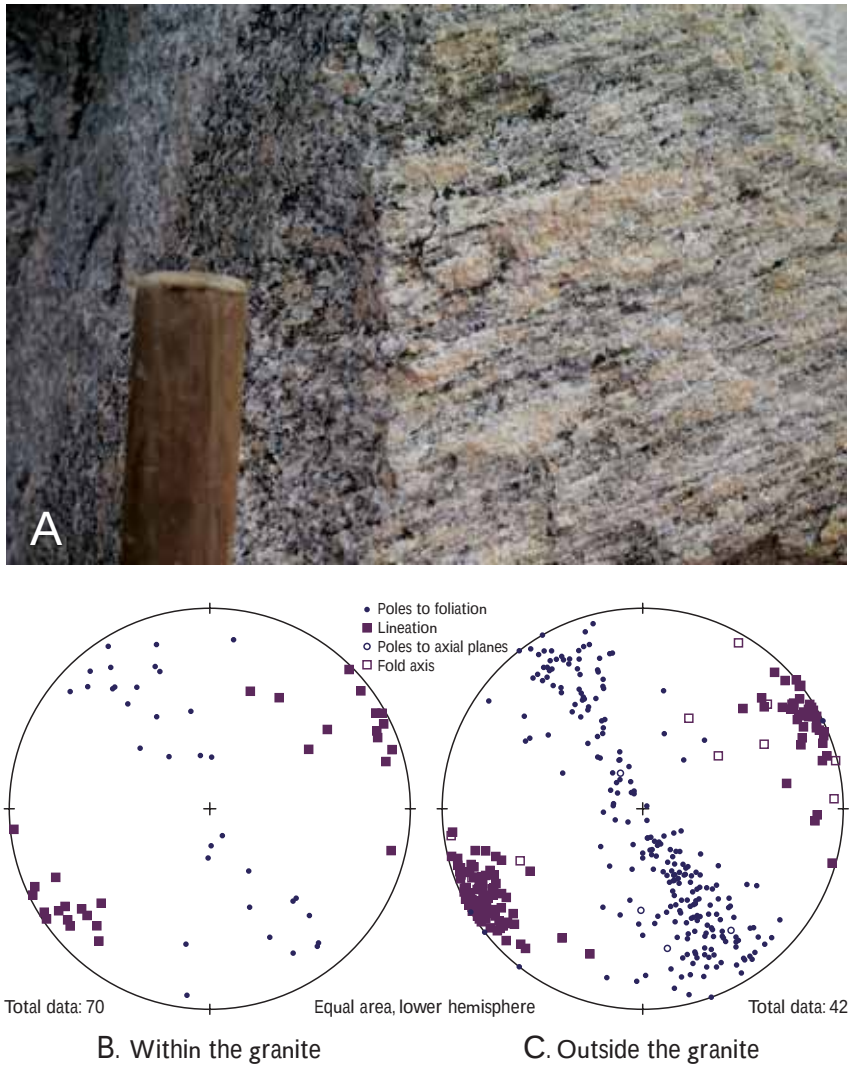

Fig. 11. A: Macroscopic view of the Kangaatsiaq granite at loc. 75 (corresponding to sample 485529), showing strong rodding. Hammer shaft about 4 cm wide. B, C: Stereograms of poles to foliation (circles) and lineations (squares) within and outside the granitic intrusion. The strain patterns are similar in both units and define a highly constrictional, NE–SW-trending and subhorizontal deformation.

this composition corresponds to the biotite-bearing granites of Moyen *et al.* (2003b), which are interpreted to have been derived from partial melting of TTG gneisses. This conclusion is consistent with the highly migmatitic nature of the surrounding gneissic basement (van Gool *et al.* 2002a).

Structure and deformation history

As mentioned above, the granite displays a strong rodding and L > S fabrics (Fig. 11A). The strain pattern in the granite (Fig. 11B) is consistent with highly constrictional deformation, with foliation poles plotting on a great circle, and lineations clustered near the pole of this great circle. This corresponds to subhorizontal, ENE–WSW stretching, consistent with the general orientation of the structures in Kangaatsiaq area (Fig. 1), and more generally with the structural grain of the region (van Gool *et al.* 2002a; Piazolo *et al.* 2004; Mazur *et al.* 2006, this volume). The surrounding gneissic basement and supracrustal rocks show the same strain pattern when plotted (Fig. 11C), although in the field, the rocks commonly have a LS or S > L fabric. This suggests that pre-existing foliations have been reoriented during the latest constrictional deformation event, leading to their present distribution. The fact that intense constriction (rather than shortening) can produce folded structures has previously been demonstrated by e.g. Leloup *et al.* (1995) in the Red River shear zone in Yunnan, China, where the ductile deformation in gneisses resulted in the development of elongate synclines and anticlines with axes parallel to the shear zone and the X-axis of deformation.

The study of deformation-related textures allows the conditions of deformation to be roughly constrained. In the granite and felsic components of the supracrustal se-

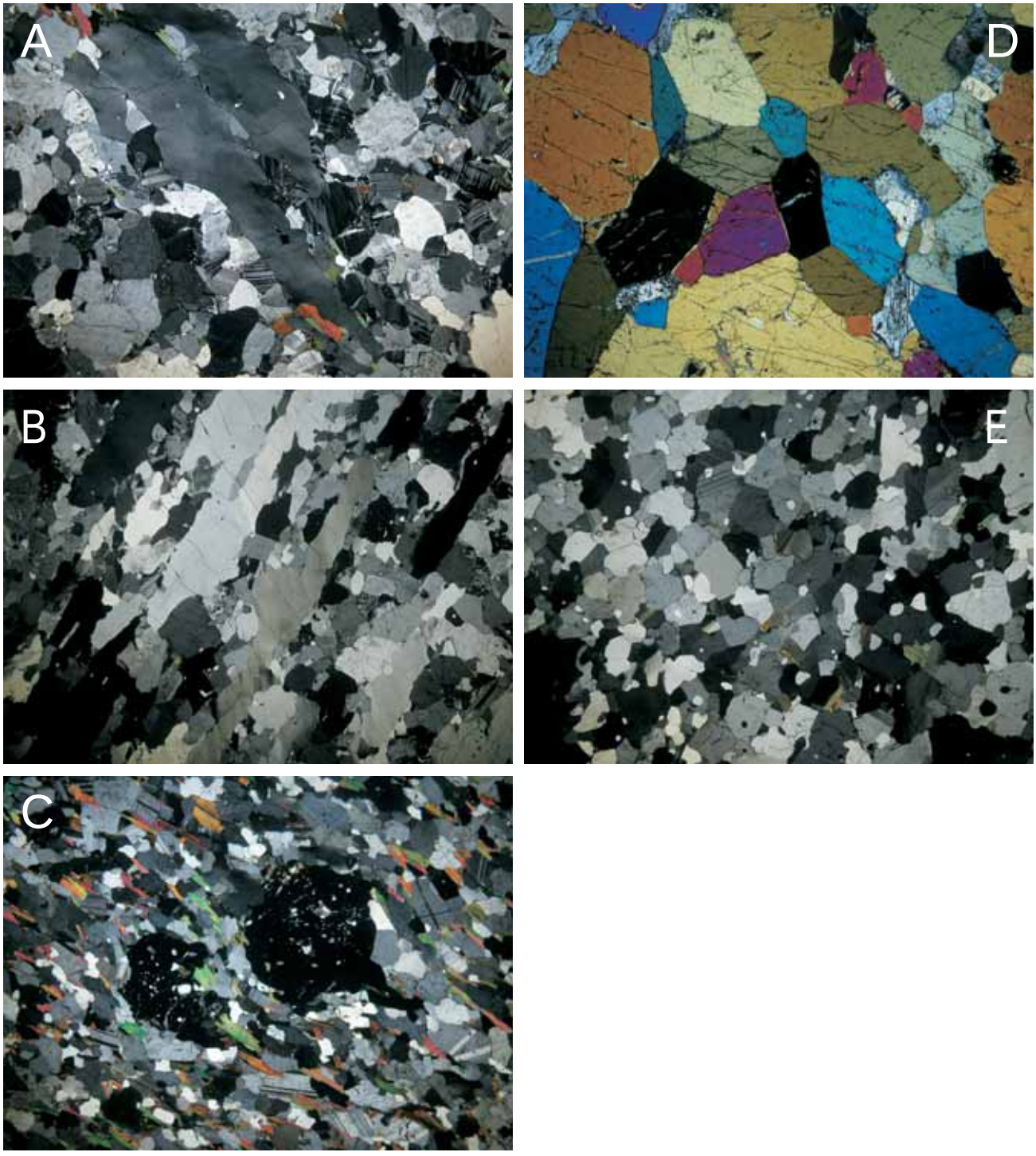

Fig. 12. Deformation textures either related to the latest, constrictional deformation (A–C) or not compatible with low-T deformation (D, E). See comments in the main text. A: Quartz ribbons in the Kangaatsiaq granite (sample 485527). B: Quartz subgrains in felsic supracrustal gneiss (sample 485531). C: Poikiloblastic garnet in metapelite cutting across an earlier foliation (sample 485535). D, E: High-temperature recrystallisation with 120° triple junctions in amphibolite (sample 485540) and felsic rocks (sample 485530). In E, the quartz also shows low-temperature deformational features such as undulating extinction and quartz subgrains, indicating that this rock witnessed two successive deformation events.

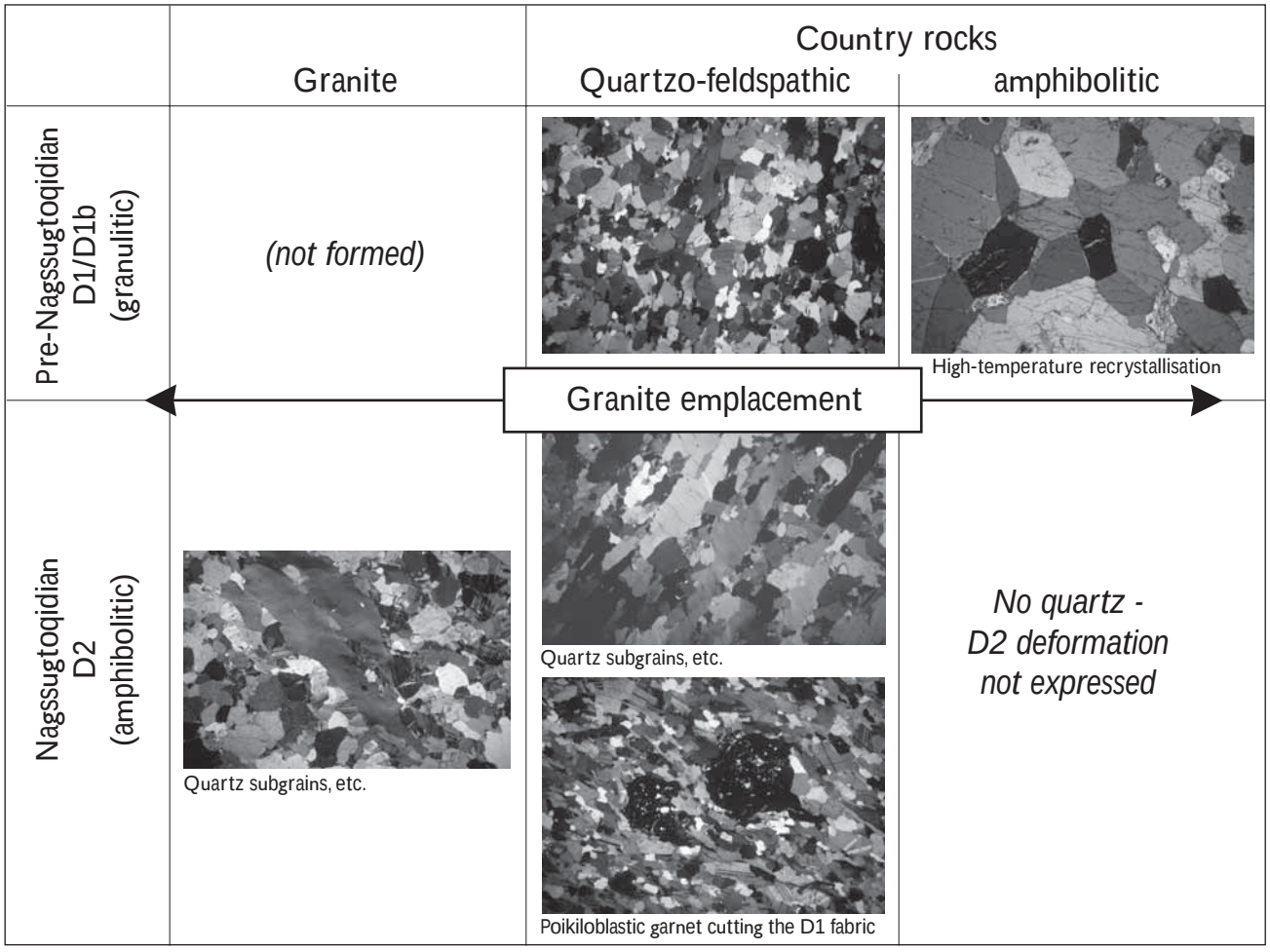

Fig. 13. Summary of the deformation history of the Kangaatsiaq synform and Kangaatsiaq granite. See comments in the main text. Photos from Fig. 12.

ries (Fig. 12A, B), the deformation led to the development of quartz subgrains and recrystallised quartz ribbons. This corresponds to deformation under lower amphibolite facies conditions (400± 50°C; Bouchez & Pécher 1976; Gapais & Barbarin 1986; Gapais 1989; Hirth & Tullis 1992; Vernon 2000). Under these conditions, only the quartz is ductile, such that all deformation is accommodated by quartz recrystallisation or deformation. In the Al-rich lithologies, deformation-related textures are mostly seen in the formation of poikiloblastic, syn- to post-tectonic garnets (Fig. 12C). Piazolo (2002) estimated that the chemistry of garnet in similar pelites nearby is compatible with a long duration of temperature conditions at around 500°C, which is in broad agreement with the above estimate. Willigers *et al.* (2002) described the cooling history of the NNO close to our study area from Ar-Ar dating of various minerals, and likewise concluded that the cooling history of the NNO was slow, from 400°C (muscovite closure) at 1.7 Ga to 200°C (K-feldspar closure) at 1.5 Ga. Therefore, it can be considered that a constrictional deformation event post-dating the granite emplacement occurred during cooling to lower amphibolite facies conditions. Since this event is apparently responsible for the regional-scale structures (Mazur 2002; van Gool *et al.* 2002b; Piazolo *et al.* 2004), and is of lower Proterozoic age (Willigers *et al.* 2002), we propose that it corresponds essentially to the Nagssugtoqidian deformation proper.

However, some textures are not compatible with the above conditions. In amphibolites, high-temperature fabrics with polygonal textures and 120° triple junctions are preserved (Fig. 12D). In some of the felsic supracrustal rocks or basement gneisses (but never in the granite), evidence is preserved for a similar high-temperature fabric, overprinted by later quartz recrystallisation (Fig. 12E). According to Kretz (1969), Gower & Simpson (1992), Kretz (1994) and Martelat *et al.* (1999), such fabrics are

likely to develop under granulite facies conditions (600–800°C). This points to the existence of one or more older (D1?) deformation event(s). Since no evidence for this deformation is found in the granite, we suggest that it was pre-granite, and therefore likely corresponds to late Archaean deformation. *P–T* estimates for metapelites and metabasites in the Kangaatsiaq area by Piazolo (2002) also indicated the existence of an early metamorphic phase with *P–T* conditions between 650°C, 3–5 kbar and 780°C, P unknown. This estimate is in good agreement with the textural evidence for D1 deformation under lower granulite facies conditions. The pre-granite deformation is also evidenced by the early isoclinal folds, the existence of a foliation within the supracrustal rocks that does not exist in the granite, and the fact that the granite apparently cuts earlier structures (Fig. 5). At loc. 80, the granite is clearly observed cutting across the foliation and shear bands in the amphibolite; these shear bands are injected by pegmatites that might also be cut by the granite. This suggests that there were actually two pre-granite events, the first of which corresponds to the granulite facies formation of the foliation and isoclinal folds, and the second one to the pegmatite-injected shear bands. However, the floor of the granitic intrusion is also apparently offset by the shear bands (Fig. 5B). Furthermore, the geometry of the shear bands and the foliation suggests extensional deformation; since the cliff face studied here almost corresponds to a YZ section relative to the regional constrictional deformation, this geometry is likely to correspond to the original, preserved pre-constriction geometry. Finally, the fact that the granite both cuts across, and is offset by the shear bands, suggests that the granite emplacement may actually have been syn-extension as sketched in Fig. 5C.

Altogether, the simplest possible deformation history (with the smallest number of episodes) can be summarised as follows (Fig. 13).

1. A first deformation event (D1) under lower granulite facies conditions (*c.* 5 kb, 600–800°C), resulted in the development of granulitic (polygonal) textures in all the existing lithologies, the formation of a main foliation, and isoclinal folding. It probably corresponds to compression of the original, likely accretionaly wedge or arc sequence.

2. This may have been followed by a second event (D1b) of probably extensional deformation, maybe associated with (or shortly followed by) the emplacement of the granite sheet. This event, only witnessed by the shear zones cutting the D1 foliation, e.g. at locality 80, is poorly recorded and probably just represents the final stage of D1 deformation. Assuming the granite has a late Archaean age, which is very likely in the regional context, this deformation could correspond to the later stages of the evolution of an arc or active continental margin, with strain relaxation and syn-extension granite emplacement.

3. A final event of constrictional deformation under lower amphibolite conditions (D2). Due to the relatively low-temperature conditions, only the quartz-bearing lithologies were affected. Therefore, the granite shows strong recrystallisation, the felsic supracrustal rocks display overprinting of the D1/D1b fabric by this event, and the quartz-free amphibolites were essentially unaffected by this event. The D2 event corresponds to the purely constrictional, regional structures which have been interpreted by Piazolo *et al.* (2004) and Mazur *et al.* (2006, this volume) as resulting from the indentation of the NNO by a solid, north-moving block immediately north of the Arfersiorfik shear zone (for the latter, see e.g. Sørensen *et al.* 2006, this volume). This Palaeoproterozoic deformation gave the studied area its present synformal structure.

Conclusions

While the present-day synclinal structure of the Kangaatsiaq area essentially results from N60 constriction related to the Palaeoproterozoic Nagssuqtoqidian deformation, the lithologies together with early preserved structures give insight into the late Archaean crustal evolution. The basement gneisses genetically belong to the TTG suite (Moyen *et al.* 2003a; Steenfelt *et al.* 2005), which is generally interpreted as generated by partial melting of a subducting slab (e.g. Martin 1994). Some components of the basement display implications of mantle wedge involvement in their genesis (Steenfelt *et al.* 2005), which is unusual in the Archaean but nevertheless consistent with an active margin setting. The supracrustal succession is composed of discontinuous layers of mafic MORB-like or arc tholeiite lavas, and together with immature, terrigeneous shales or greywackes derived from erosion of the basement TTG gneisses or volcanic counterparts to them, with a likely small contribution from tholeiitic lavas. Part of the succession could also have been felsic rocks derived from erosion of the basement TTG gneisses or volcanic counterparts to the latter, with a likely small contribution from tholeiitic lavas. The whole series is capped by a layer *c.* 100 m thick of mafic volcanic rocks likewise of tholeiitic affinity. All these lithological components are in good

agreement with either an arc-related setting, with a plutonic arc developing simultaneously with the filling of volcano-detritic basins with lavas of similar affinities and immature sediments; or with an accretionary wedge environment involving ocean floor juxtaposed together with similar sediments. In both cases, they correspond to an active subduction margin. Intense migmatisation of the basement is probably associated with the emplacement of the anatectic, likely synkinematic Kangaatsiaq granite. This was apparently synchronous with an early, lower granulite facies (D1/D1b) deformation event that may have ended with strain relaxation and exhumation of the rocks from the active margin at the end of the Archaean cycle.

The supracrustal association and the sequence of events in the Kangaatsiaq area are comparable to the evolution of many Archaean greenstone belts (e.g. Card 1990; Chadwick *et al.* 1996; Hunter *et al.* 1998). On the other hand, classical Archaean components such as orthochemical sediments and plume-related komatiites (Arndt 1994) or orthochemical components (Lowe 1994) are completely missing from the Kangaatsiaq area. However, this apparently rather uncommon absence is known from other mid- to late Archaean greenstones, also in West Greenland (e.g. Garde 1997). The setting is sometimes interpreted as being arc-related (Card 1990; Lowe 1994). In contrast, widespread melting and granite emplacement at the end of the Archaean is a very common situation, which has been described in many studies (among others, e.g. Gorman *et al.* 1978; Card 1990; Sylvester 1994; Windley 1995; Chadwick *et al.* 1996; Moyen *et al.* 2003b).

Acknowledgements

J.A.M. van Gool, G.I. Alsop, S. Piazolo and S. Mazur visited the area in 2001, and their work was used as a basis for the subsequent mapping. They also provided useful comments on the geology and metamorphic history of the region. A.A. Garde kindly supplied analyses of the basement gneisses; his editorial help with the figures and manuscript is also gratefully acknowledged. Reviews by A.G. Leslie and a second reviewer greatly improved the original manuscript. Linguistic corrections by R.W. Belcher were also of greatest help. Chemical analyses were performed at GEUS.

References

Arndt, N.T. 1994: Archean komatiites. In: Condie, K.C. (ed.): Archean crustal evolution. Developments in Precambrian Geology 11, 11–44.

Bhatia, M.R. 1983: Plate tectonics and geochemical composition of sandstones. Journal of Geology 91, 611–627.

Bhatia, M.R. & Crook, K.A.W. 1986: Trace element characteristics of graywackes and tectonic discrimination of sedimentary basins. Contribution to Mineralogy and Petrology 92, 181–193.

Bohlar, R., Kamber, B.S., Moorbath, S., Whitehouse, M.J. & Collerson, K.D. 2005: Chemical characterization of Earth's most ancient clastic metasediments from the Isua greenstone belt, southern West Greenland. Geochimica and Cosmochimica Acta 69(6), 1555–1573.

Bouchez, J.-L. & Pécher, A. 1976: Plasticité du quartz et sens de cisaillement dans des quartzites du Grand Chevauchement Central himalayen. Bulletin de la Société Géologique de France XVIII, 1377–1385.

Boynton, W.V. 1984: Geochemistry of the rare earth elements: meteorite studies. In: Henderson, P. (ed.): Rare earth element geochemistry, 63–114. Amsterdam: Elsevier.

Card, K.D. 1990: A review of the Superior Province of the Canadian shield, a product of Archean accretion. Precambrian Research 48, 99–156.

Chadwick, B., Vasudev, V.N. & Ahmed, N. 1996: The Sandur Schsit Belt and its adjacent plutonic rocks. Implications for Late Archaean crustal evolution in Karnataka. Journal of the Geological Society of India 47, 37–57.

Connelly, J.N. & Mengel, F.C. 2000: Evolution of Archean components in the Paleoproterozoic Nagssugtoqidian Orogen, West Greenland. Geological Society of America Bulletin 112 (5), 747–763.

Gapais, D. 1989: Shear structures within deformed granites: mechanical and thermal indicators. Geology 17, 1144–1147.

Gapais, D. & Barbarin, B. 1986: Quartz fabric transition in a cooling syntectonic granite (Hermitage massif, France). Tectonophysics 125, 357–370.

Garde, A.A. 1997: Accretion and evolution of an Archaean high-grade grey gneiss – amphibolite complex: the Fiskefjord area, southern West Greenland. Geology of Greenland Survey Bulletin 177, 115 pp.

Garde, A.A. 2004: Geological map of Greenland, 1:100 000, Kangaatsiaq 68 V.1 Syd. Copenhagen: Geological Survey of Denmark and Greenland.

Gorman, B.E., Pearce, T.H. & Birkett, T.C. 1978: On the structure of Archean greenstone belts. Precambrian Research 6, 23–41.

Gower, R.J.W. & Simpson, C. 1992: Phase boundary mobility in naturally deformed, high-grade quartzo-feldspathic rocks: evidence for diffusional creep. Journal of Structural Geology 14, 301–313.

Hamilton, W.B. 1998: Archean magmatism and deformation were not products of plate tectonics. Precambrian Research 91, 143–179.

Henderson, G. 1969: The precambrian rocks in the Egedesminde–Christianshåb area, West Greenland. Rapport Grønlands Geologiske Undersøgelse 19, 37 pp.

Herron, M.M. 1988: Geochemical classification of terrigeneous sands

and shales from core or log data. Journal of Sedimentary Petrology 58, 820–829.

Hirth, G. & Tullis, J. 1992: Dislocation creep regimes in quartz aggregates. Journal of Structural Geology 14, 145–159.

Hollis, J.A., Keiding, M., Stensgaard, B.M., van Gool, J.A.M. & Garde, A.A. 2006: Evolution of Neoarchaean supracrustal belts at the northern margin of the North Atlantic Craton, West Greenland. In: Garde, A.A. & Kalsbeek, F. (eds): Precambrian crustal evolution and Cretaceous–Palaeogene faulting in West Greenland. Geological Survey of Denmark and Greenland Bulletin 11, 9–31 (this volume).

Hunter, M.A., Bickle, M.J., Nisbet, E.G., Martin, A. & Chapman, H.J. 1998: Continental extensional setting for the Archean Belingwe Greenstone Belt, Zimbabwe. Geology 26, 883–886.

Irvine, T.N. & Baragar, W.R.A. 1971: A guide to the chemical classification of the common volcanic rocks. Canadian Journal of Earth Sciences 8, 523–548.

Kalsbeek, F. & Nutman, A.P. 1996: Anatomy of the Early Proterozoic Nagssugtoqidian orogen, West Greenland, explored by reconnaissance SHRIMP U-Pb zircon dating. Geology 24, 515–518.

Kretz, R. 1969: On the spatial distribution of crystals in rocks. Lithos 2, 39–66.

Kretz, R. 1994: Metamorphic crystallisation. Chichester: J. Wiley and Sons.

Le Maître, R.W. *et al.* 1989: A classification of igneous rocks and glossary of terms, 193 pp. Oxford: Blackwell.

Leloup, P.H., Lacassin, R., Tapponnier, P., Schärer, U., Dalai, Z., Xiaohan, L., Liangshang, Z., Shaocheng, J. & Trong Trinh, P. 1995: The Ailao Shan – Red River shear zone (Yunnan, China), Tertiary transform boundary of Indochina. Tectonophysics 251, 3–10.

Lowe, D.R. 1994: Archean greenstone-related sedimentary rocks. In: Condie, K.C. (ed.): Archean crustal evolution. Developments in Precambrian Geology 11, 121–169.

Marker, M., Mengel, F., van Gool, J.[A.M.] & field party 1995: Evolution of the Palaeoproterozoic Nagssugtoqidian orogen: DLC investigations in West Greenland. Rapport Grønlands Geologiske Undersøgelse 165, 100–105.

Martelat, J.-E., Schulmann, K., Lardeaux, J.-M., Nicollet, C. & Cardon, H. 1999: Granulite microfabrics and deformation mechanisms in southern Madagascar. Journal of Structural Geology 21, 671–687.

Martin, H. 1986: Effect of steeper Archean geothermal gradient on geochemistry of subduction-zone magmas. Geology 14, 753–756.

Martin, H. 1994: The Archean grey gneisses and the genesis of the continental crust. In: Condie, K.C. (ed.): Archean crustal evolution. Developments in Precambrian Geology 11, 205–259.

Mazur, S. 2002: First impressions on structural evolution of the northern Nagssugtoqidian foreland. In: Nielsen, B.M. & Thrane, K. (eds): Workshop on Nagssugtoqidian and Rinkian geology, West Greenland. Danmarks og Grønlands Geologiske Undersøgelse Rapport 2002/9, 28–29.

Mazur, S., Piazolo, S. & Alsop, G.I. 2006: Structural analysis of the northern Nagssugtoqidian orogen, West Greenland: an example of complex tectonic patterns in reworked high-grade metamorphic terrains. In: Garde, A.A. & Kalsbeek, F. (eds): Precambrian crustal evolution and Cretaceous–Palaeogene faulting in West Greenland. Geological Survey of Denmark and Greenland Bulletin 11, 163–178 (this volume).

McCall, G.J.H. 2003: A critique of the analogy between Archaean and Phanerozoic tectonics based on regional mapping of the Mesozoic–Cenozoic plate convergent zone in the Makran, Iran. Precambrian Research 127, 5–17.

Mengel, F., van Gool, J.A.M., Krogstad, E. & the 1997 field crew 1998: Archaean and Palaeoproterozoic orogenic processes: Danish Lithosphere Centre studies of the Nagssugtoqidian orogen, West Greenland. Geology of Greenland Survey Bulletin 180, 100–110.

Moyen, J.-F., Garde, A.A. & Steenfelt, A. 2003a: Plain, boring orthogneisses? Geochemistry of the Archaean grey gneisses in the northern Nagssugtoqidian belt. Workshop on Precambrian geology of central West Greenland, February 28 and March 1, 2003, p. 10. Copenhagen: Geological Survey of Denmark and Greenland.

Moyen, J.-F., Martin, H., Jayananda, M. & Auvray, B. 2003b: Late Archaean granites: a typology based on the Dharwar Craton (India). Precambrian Research 127, 103–123.

Mullen, E.D. 1983: MnO/TiO2/P2O5: a minor element discriminant for basaltic rocks of oceanic environments and its implications for petrogenesis. Earth and Planetary Science Letters 62, 53–62.

Myers, J.S. 2001: Protoliths of the 3.8–3.7 Ga Isua greenstone belt, West Greenland. Precambrian Research 105, 129–141.

Nesbitt, H.W. & Young, G.M. 1989: Formation and diagenesis of weathering profiles. Journal of Geology 97, 129–147.

Noe-Nygaard, A. & Ramberg, H. 1961: Geological reconnaissance map of the country between latitudes 69°N and 63°45′ N, West Greenland, 1:500 000. Geological Map Grønlands Geologiske Undersøgelse 1, 9 pp., 2 maps (also Meddelelser om Grønland 123(5)).

Østergaard, C., Garde, A.A., Nygaard, J., Blomsterberg, J., Møller Nielsen, B., Stendal, H. & Thomas, C.W. 2002: The Precambrian supracrustal rocks in the Naternaq (Lersletten) and Ikamiut areas, central West Greenland. Geology of Greenland Survey Bulletin 191, 24–32.

Pearce, J.A. 1982: Trace element characteristics of lavas from destructive plate boundaries. In: Thorpe, R.S. (ed.): Andesites, 525–548. Chichester: Wiley.

Piazolo, S. 2002: Overview of the metamorphic evolution of tonalitic gneisses and metasedimentary sequences from the Kangaatsiaq, Lersletten and Sydostbugten area – first comparison to adjacent areas. In: Nielsen, B.M. & Thrane, K. (eds): Workshop on Nagssugtoqidian and Rinkian geology, West Greenland. Danmarks og Grønlands Geologiske Undersøgelse Rapport 2002/9, 32–33.

Piazolo, S., Alsop, G.I., Møller Nielsen, B. & van Gool, J.A.M. 2004: The application of GIS to unravel patterns of deformation in high grade terrains: a case study of indentor tectonics from West Greenland. In: Alsop, G.I. & Holdsworth, R.E. (eds): Flow processes in faults and shear zones. Geological Society Special Publication (London) 224, 63–78.

Roser, B.P. & Korsch, R.J. 1988: Provenance signature of sandstone-mudstone suite determined using discriminant function analysis of major-element data. Chemical Geology 67, 119–139.

Shervais, J.W. 1982: Ti-V plots and the petrogenesis of modern and ophiolitic lavas. Earth and Planetary Science Letters 59, 101–118.

Sørensen, K., Glassley, W., Korstgård, J. & Stensgaard, B.M. 2006: The Nordre Strømfjord shear zone and the Arfersiorfik quartz diorite in Arfersiorfik, the Nagssugtoqidian orogen, West Greenland. In: Garde, A.A. & Kalsbeek, F. (eds): Precambrian crustal evolution and Cretaceous–Palaeogene faulting in West Greenland. Geological Survey of Denmark and Greenland Bulletin 11, 145–161 (this volume).

Steenfelt, A., Garde, A.A. & Moyen, J.-F. 2005: Mantle wedge involvement in the petrogenesis of Archaean grey gneisses in West Greenland. Lithos 79, 207–228.

Sylvester, P.J. 1994: Archean granitic plutons. In: Condie, K.C. (ed.): Archean crustal evolution. Developments in Precambrian Geology 11, 261–314.

Taylor, S.R. & McLennan, S.M. 1985: The continental crust: its composition and evolution, 312 pp. Oxford: Blackwell.

Thrane, K.T. & Connelly, J. 2002: Linking the Nagssugtoqidian orogen and the Rinkian belt: preliminary ages from the Disko Bugt region. In: Nielsen, B.M. & Thrane, K. (eds): Workshop on Nagssugtoqidian and Rinkian geology, West Greenland. Danmarks og Grønlands Geologiske Undersøgelse Rapport 2002/9, 46–48.

Thrane, K. & Connelly, J.N. 2006: Zircon geochronology from the Kangaatsiaq–Qasigiannguit region, the northern part of the 1.9–1.8 Ga Nagssugtoqidian orogen, West Greenland. In: Garde, A.A. & Kalsbeek, F. (eds): Precambrian crustal evolution and Cretaceous–Palaeogene faulting in West Greenland. Geological Survey of Denmark and Greenland Bulletin 11, 87–99 (this volume).

van Gool, J.A.M. & Piazolo, S. 2006: Presentation and interpretation of structural data from the Nagssugtoqidian orogen using a GIS platform: general trends and features. In: Garde, A.A. & Kalsbeek, F. (eds): Precambrian crustal evolution and Cretaceous–Palaeogene faulting in West Greenland. Geological Survey of Denmark and Greenland Bulletin 11, 125–144 (this volume).

van Gool, J.A.M. *et al*. 2002a: Precambrian geology of the northern Nagssugtoqidian orogen, West Greenland: mapping in the Kangaatsiaq area. Geology of Greenland Survey Bulletin 191, 13–23.

van Gool, J.A.M., Connelly, J.N., Marker, M. & Mengel, F.C. 2002b: The Nagssugtoqidian orogen of West Greenland: tectonic evolution and regional correlations from a West Greenland perspective. Canadian Journal of Earth Sciences 39, 665–686.

van Kranendonk, M.J. 2003: Archaean tectonics in 2001: an Earth odyssey. Precambrian Research 127, 1–3.

Vernon, R.H. 2000: Review of microstructural evidence of magmatic and solid-state flow. Electronic Geosciences 5(2).

Willigers, B.J.A., van Gool, J.A.M., Wijbrans, J.R., Krogstad, E.J. & Mezger, K. 2002: Posttectonic cooling of the Nagssugtoqidian orogen and a comparison of contrasting cooling histories in Precambrian and Phanerozoic orogens. Journal of Geology 110, 503–517.

Windley, B.F. 1995: The evolving continents, 3rd ed., 526 pp. Chester: John Wiley and Sons.

Manuscript received 7 June 2004; revision accepted 1 February 2006

A lead isotope study of an Archaean gold prospect in the Attu region, Nagssugtoqidian orogen, West Greenland

Henrik Stendal, Robert Frei and Bo Møller Stensgaard

This paper presents a lead isotope investigation of a gold prospect south of the village Attu in the northern part of the Nagssugtoqidian orogen in central West Greenland. The Attu gold prospect is a replacement gold occurrence, related to a shear/mylonite zone along a contact between orthogneiss and amphibolite within the Nagssugtoqidian orogenic belt. The mineral occurrence is small, less than 0.5 m wide, and can be followed along strike for several hundred metres. The mineral assemblage is pyrite, chalcopyrite, magnetite and gold. The host rocks to the gold prospect are granulite facies 'brown gneisses' and amphibolites. Pb-isotopic data on magnetite from the host rocks yield an isochron in a $^{207}Pb/^{204}Pb$ vs. $^{206}Pb/^{204}Pb$ diagram, giving a date of 3162 ± 43 Ma (MSWD = 0.5). This date is interpreted to represent the age of the rocks in question, and is older than dates obtained from rocks elsewhere within the Nagssugtoqidian orogen. Pb-isotopic data on cataclastic magnetite from the shear zone lie close to this isochron, indicating a similar origin. The Pb-isotopic compositions of the ore minerals are similar to those previously obtained from the close-by ~2650 Ma Rifkol granite, and suggest a genetic link between the emplacement of this granite and the formation of the ore minerals in the shear/mylonite zone. Consequently, the age of the gold mineralisation is interpreted to be late Archaean.

Keywords: Archaean, gold, magnetite, Pb isotopes, geochronology, West Greenland

H.S. & B.M.S., *Geological Survey of Denmark and Greenland, Øster Voldgade 10, DK-1350 Copenhagen K, Denmark.*
E-mail: *hst@geus.dk*
R.F., *Geological Institute, University of Copenhagen, Øster Voldgade 10, DK-1350 Copenhagen K, Denmark.*

Discovery of the gold prospect described in this study was due to the find of a mineralised sample, which Karl Markussen from Attu submitted to the Bureau of Minerals and Petroleum in Greenland. The Geological Survey of Denmark and Greenland (GEUS) visited the locality in 2001 and in 2002 (Stendal *et al.* 2002, 2004), and the present paper reports Pb-isotopic data for minerals from the prospect and its surroundings.

The Attu gold prospect lies within the Nagssugtoqidian orogen of West Greenland (Fig. 1), where geological mapping and exploration has been carried out for decades by the Geological Survey, the Danish Lithosphere Centre, university research groups and exploration companies (e.g. Kalsbeek *et al.* 1987; Connelly *et al.* 2000; van Gool *et al.* 2002). In addition to the general investigations, Steenfelt (2001) has summarised geochemical signatures from stream sediments, Rasmussen & van Gool (2000) have described geophysical aspects, and Steenfelt *et al.* (2002), Stendal & Schønwandt (2003) and Stendal *et al.* (2004) have described mineral occurrences and their economic potential. An overview of the mineral occurrences in the entire region has been presented by Stendal *et al.* (2004).

Detailed, mainly zircon U-Pb geochronological data from the Nagssugtoqidian orogen have been presented by Kalsbeek & Nutman (1996), Connelly & Mengel (2000) and Connelly *et al.* (2000), and Pb-Pb, Rb-Sr and Sm-

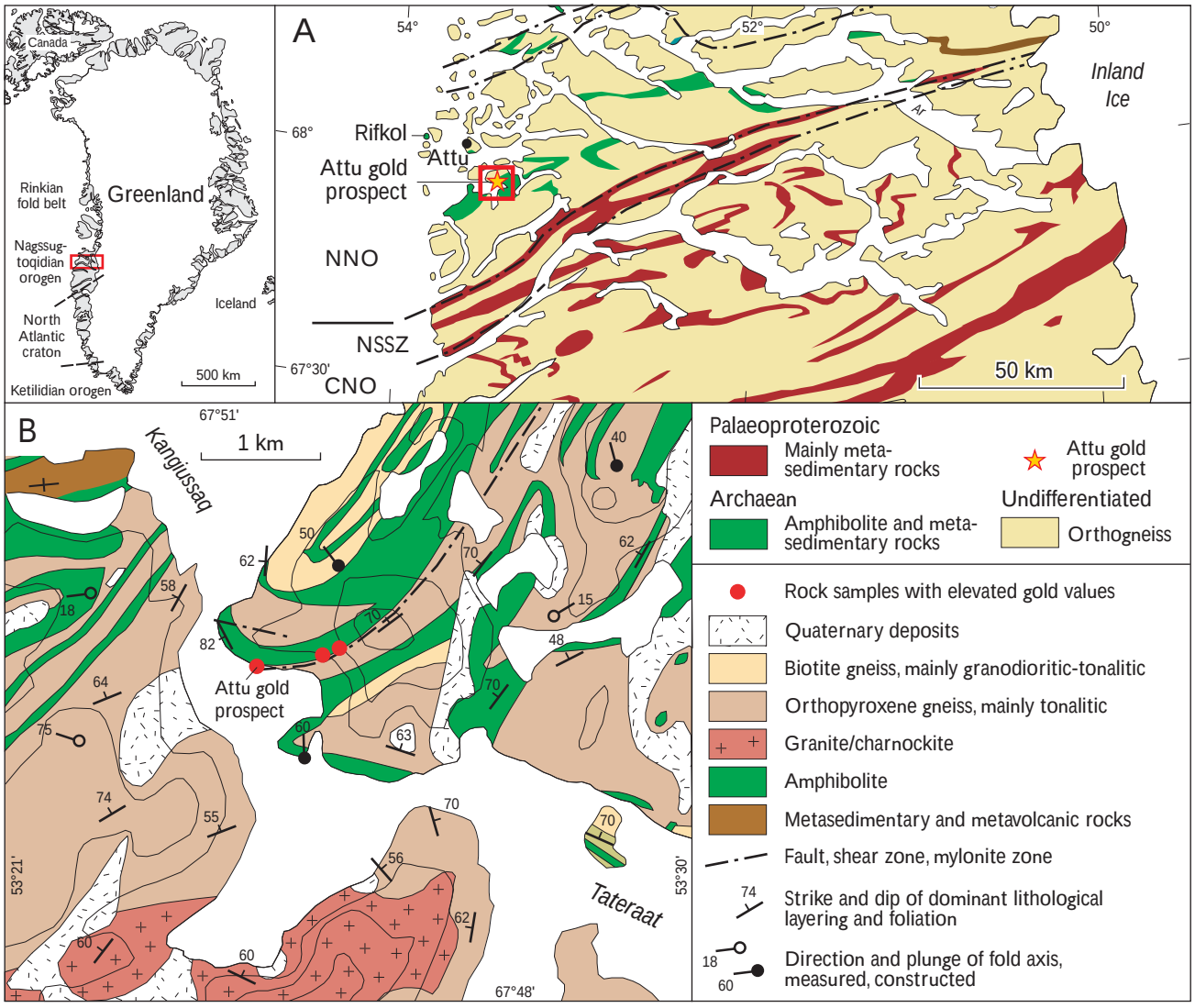

Fig. 1. A: Geological map of the Attu region with index map of Greenland. CNO, central Nagssugtoqidian orogen; NNO, northern Nagssugtoqidian orogen; NSSZ, Nordre Strømfjord shear zone. B: Geological map of the Attu gold prospect area (modified from Olesen 1984).

Nd whole-rock isotope data from the region have been reported by Kalsbeek *et al.* (1984, 1987), Taylor & Kalsbeek (1990) and Whitehouse *et al.* (1998). In addition, some Pb-isotopic work has been carried out on sulphide separates, mainly pyrite, from mineral occurrences in the Disko Bugt region (Stendal 1998).

Geological setting

The Palaeoproterozoic Nagssugtoqidian orogen of West Greenland (van Gool *et al.* 2002) is located between the Archaean North Atlantic craton to the south and a lesser-known continental mass to the north that includes the Palaeoproterozoic Rinkian fold belt. Most of the orogen consists of variably reworked Archaean orthogneisses. Several thin belts of supracrustal and intrusive igneous rocks occur within this gneiss terrain. Granitoid rocks and numerous pegmatites intrude the gneisses. Formations of Palaeoproterozoic age are limited to the Arfersiorfik and Sisimiut igneous suites and minor supracrustal sequences (Connelly *et al.* 2000).

The Attu area itself is located in the southern part of the northern Nagssugtoqidian orogen (NNO; Fig. 1). The metamorphic grade is granulite facies; metamorphism and deformation of the Archaean granitoid rocks in the NNO gradually decrease northwards, from granulite to amphibolite facies, and from high strain to lower strain with more open structures. Steeply and shallowly dipping shear and fault zones are common in contact zones between

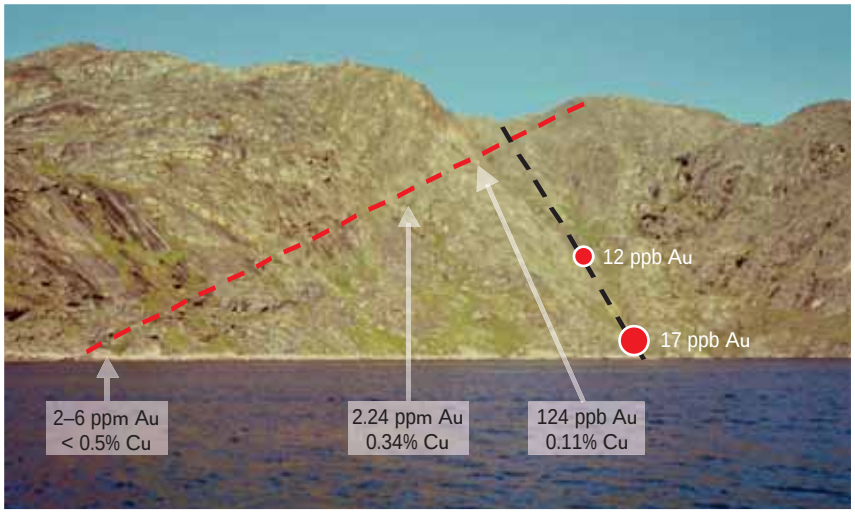

Fig. 2. The site of the Attu gold prospect. Gold values are given for rock samples. Red circles are sample sites with gold values obtained from fine-grained stream sediments (see Fig. 1 for geographical location). The red line shows the approximate position of the gold-bearing zone in the shear/mylonite zone. The black line shows the approximate position of a stream.

different lithologies. Major fault zones generally strike NNE to NE. The major Nordre Strømfjord shear zone (van Gool 2002) is located *c*. 20 km south of the study area. The shear zone is traceable from the coast to the Inland Ice and forms the southern boundary of the NNO. The gneisses of the NNO are late Archaean, with ages between 2870 and 2700 Ma (Kalsbeek & Nutman 1996; Connelly & Mengel 2000; Hollis *et al*. 2006, this volume; Thrane & Connelly 2006, this volume). Discordant sheets of granitoid rocks of Archaean age occur in the centre of the NNO and large charnockite/granite bodies including the Rifkol granite are situated 20 km to the northwest and just south of the study area (Fig. 1; Hansen 1979; Kalsbeek *et al*. 1984). Only a few younger Palaeoproterozoic ages have been obtained from the NNO: Thrane & Connelly (2006, this volume) have obtained an approximate depositional age of the Naternaq supracrustal belt some 80 km north-east of Attu of *c*. 1950–1900 Ma, and an undeformed pegmatite between Attu and Aasiaat has yielded an age of *c*. 1790 Ma (Connelly & Mengel 2000).

The Attu gold prospect

The Attu gold prospect is located south of the village Attu within a 100–330 m wide, complex tract hosting several parallel shear/mylonite zones and faults that strike NNE to NE and dip 60–70°W (Figs 1, 2). The fault zone can be followed along strike in a north-easterly direction for several kilometres. The host rocks are layered, brown

Fig. 3. Layered brown gneiss with black bands of amphibolite. The hammer shaft is 50 cm long.

Fig. 4. The gold bearing mylonite zone. K-feldspar occurs on the right side of the yellow magnet pen (10 cm long). The zone also contains pyrite, chalcopyrite and magnetite.

weathering gneiss and amphibolite (Fig. 3). At the western border of the tract a gold-bearing shear/mylonite zone follows the contact between brown gneisses and amphibolites. The gold-bearing shear/mylonite zone (Fig. 4) is invaded by pegmatite sheets as well as centimetre-wide veins consisting of red alkali-feldspar and quartz with occasional pyrite and magnetite. The estimated relative volume of pegmatite in the tract varies from 1 to 10% (Stendal *et al*. 2002, 2004).

The most promising gold showings are found in a coastal profile along the shear/mylonite zone, which can be followed along strike for several hundreds of metres (Figs 1, 2). The studied site is a cliff exposure consisting of mylonite (Fig. 4) and a rusty weathered band (10–20 cm in width) mineralised with pyrite, magnetite and some chalcopyrite (Fig. 5). Pyrite and chalcopyrite replace magnetite. The magnetite is predominantly cataclastic in nature, but recrystallised ore also occurs. The gold is found within pyrite and chalcopyrite. The gangue mineralogy comprises quartz, K-feldspar, muscovite, biotite and carbonates (calcite, dolomite and/or ankerite).

The mylonite zone is silicified at the contact with the mineralised zone, and sulphide-rich parts are weathered. Secondary goethite and malachite are common (Fig. 5). The ore is structurally controlled by and confined to favourable sites (sulphide-bearing zones) within the mylonite/shear/fault zone.

The Attu gold prospect has returned reproducable gold

Table 1. Pb-isotopic ratios of magnetite, pyrite and K-feldspar from the Attu gold prospect and its host rocks

Sample number	Mineral	$^{206}Pb/^{204}Pb$	± 2σ*	$^{207}Pb/^{204}Pb$	± 2σ	$^{208}Pb/^{204}Pb$	± 2σ	r1**	r2†
Amphibolite and orthogneiss (host rocks)									
446601	magnetite	14.631	0.007	14.642	0.009	44.688	0.033	0.961	0.939
446602	magnetite	15.051	0.014	14.752	0.015	36.702	0.040	0.969	0.942
446610	magnetite	17.540	0.051	15.361	0.046	37.613	0.112	0.977	0.988
446614	magnetite	17.002	0.025	15.225	0.024	38.086	0.061	0.976	0.967
Shear zone and mineralised rock									
446616	magnetite	15.423	0.023	14.844	0.023	41.598	0.068	0.979	0.957
2000368	magnetite	15.286	0.009	14.832	0.010	41.201	0.034	0.962	0.936
481093	magnetite	14.247	0.042	14.625	0.044	41.821	0.130	0.982	0.960
446615	pyrite	14.241	0.009	14.587	0.010	42.001	0.035	0.963	0.934
481078	pyrite	14.447	0.011	14.633	0.012	40.805	0.039	0.967	0.925
446616	K-feldspar	15.123	0.008	14.893	0.010	36.451	0.029	0.958	0.932

* Errors are two standard deviations absolute (Ludwig 1990).
** r1 = $^{206}Pb/^{204}Pb$ versus $^{207}Pb/^{204}Pb$ error correlation (Ludwig 1990).
† r2 = $^{206}Pb/^{204}Pb$ versus $^{208}Pb/^{204}Pb$ error correlation (Ludwig 1990).

Fig. 5. The gold bearing zone (10 cm wide) within the mylonite zone, with malachite and rusty weathered sulphides.

concentrations in the range 2.3–5.8 ppm. Other localities in the same fault structure yielded 2.24 ppm and 124 ppb Au (Fig. 2). The gold concentrations are positively correlated with concentrations of copper, and gold-bearing samples often contain magnetite. Two stream sediment samples yielded anomalous gold concentrations of 12 ppb and 17 ppb Au, respectively (Fig. 2).

The host gneisses are brownish in colour and comprise orthopyroxene, amphibole, biotite and feldspar, but little quartz. Magnetite is in equilibrium with the rock forming minerals and has the same granular texture. In the amphibolites magnetite forms up to millimetre-thick layers, and also occurs in disseminated form. Within the mylonite zone, magnetite occurs as a primary phase in the host gneiss as cataclastic grains with cracks filled with pyrite and chalcopyrite, and as a residual phase resulting from sulphide replacement. Ten samples were analysed for Pb-isotopic compositions.

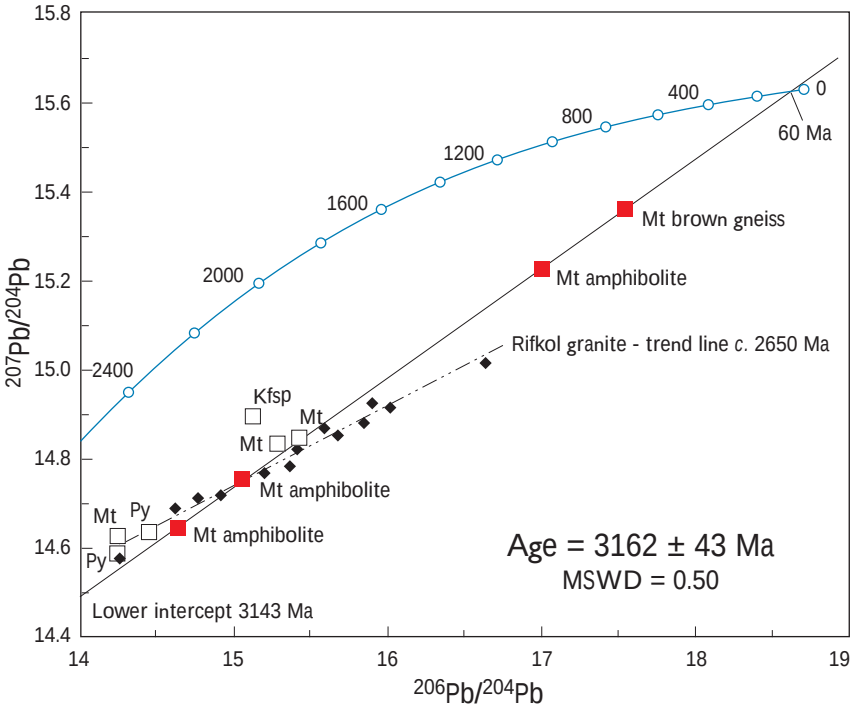

Fig. 6. $^{206}Pb/^{204}Pb$–$^{207}Pb/^{204}Pb$ diagram for minerals from the Attu area listed in Table 1. Open squares, mineral separates from the gold-bearing mylonite zone. Red squares, host rock data. Black diamonds, whole-rock samples from the Rifkol granite for comparison (data from Kalsbeek *et al.* 1984). Mt, magnetite; Py, pyrite; Kfsp, K-feldspar. Blue curve, the Pb-isotopic growth curve from Stacey & Kramers (1975).

Analytical methods

The Pb-isotopic study was carried out on magnetite from host gneisses and amphibolites, and on K-feldspar, magnetite and pyrite from the shear zone-hosted mineralised zone (Table 1). The isotope analyses were carried out at the Danish Centre for Isotope Geology, Geological Institute, University of Copenhagen. Near-pure mineral fractions were separated from dry split aliquots of crushed and sieved (100–200 µm) rock powders using a hand magnet, a Frantz isodynamic separator and heavy liquid techniques. Ore minerals were dissolved in concentrated *aqua regia*. Total procedural blanks for Pb amounted to < 120 pg which is considered insignificant for the measured Pb-isotopic results, relative to the amount of sample Pb estimated from the mass spectrometer signal intensities. Isotope analyses were carried out on a VG Sector 54-IT instrument in static collection mode. Fractionation for Pb was controlled by repetitive analysis of the NBS 981 standard (values of Todt *et al.* 1993) and amounted to 0.103 ± 0.007% / amu (2 σ; n = 11). All results are quoted with 2 σ precisions.

Results

The Pb-isotopic compositions of mineral separates from the gold-bearing mylonite zone and its host rocks are listed in Table 1. In the $^{207}Pb/^{204}Pb$ vs. $^{206}Pb/^{204}Pb$ diagram shown in Fig. 6, the Pb-isotopic compositions of magnetite from the four host rock samples of brown gneiss and amphibolite (red squares) define a straight line with a slope corresponding to 3162 ± 43 Ma (MSWD = 0.50). This line has intercepts with the Stacey & Kramers (1975) Pb-isotopic growth curve at 3143 and 60 Ma. Based on the good fit of the data points on the isochron, and the agreement of the isochron age with the intercepts of the growth curve, we interpret the 3162 Ma date as the age of the rocks in question. However, farther south, in the central part of the Nagssugtoqidian orogen, Palaeoproterozoic granulite facies metamorphism has led to U loss in Archaean rocks, resulting in Pb-isotopic compositions plotting above and to the left of an 2800 Ma reference isochron (Whitehouse *et. al.* 1998). If this process had also taken place in the area of the present study, the 3162 Ma date might give a false impression of the age of the rocks. However, the good fit of the data points on the isochron and the agreement of the intercepts with the Stacey & Kramers (1975) growth curve with the isochron age would then be accidental, a coincidence which we regard as very unlikely.

Six mineral separates from the gold-bearing mylonite zone (Fig. 6, open squares) lie close to or slightly above the isochron obtained for magnetite from the host rocks. The most primitive $^{206}Pb/^{204}Pb$ and $^{207}Pb/^{204}Pb$ ratios have been measured in pyrite and magnetite from the ore-bearing zone, whereas the two primary magnetites with cataclastic texture from within the shear zone plot very close to the host rock magnetite isochron. This suggests that their crystallisation took place at about the same time as the magnetites from outside the shear zone. Whole-rock Pb-isotopic ratios from the Rifkol granite (Kalsbeek *et al.* 1984) are also plotted on Fig. 6 for comparison, and the isotopic values are listed in Table 1. The errorchron defined by these samples has a slope corresponding to an age of 2653 ± 110 Ma, which has been interpreted as emplacement age of the granite (Kalsbeek *et al.* 1984). This errorchron is oblique and discordant to the isochron obtained for magnetite from the host rocks, but the three least radiogenic data points from ore minerals associated with native gold from within the shear zone are conformable with this younger trend. This suggests that the fluids in the shear zone from which the gold mineralisation was deposited were somehow genetically linked to the intrusion of the Rifkol granite. Alkali feldspar from the shear zone has its own Pb-isotopic signature, which is neither compatible with a 'Rifkol' source nor with a source typical of the immediate host rocks.

The uranogenic vs. thorogenic isotopic pattern (not shown in a figure) is more disperse than the uranogenic pattern and does not add to the understanding of the uranogenic Pb-isotopic data; as expected, it mostly reflects the differences in U and Th concentrations in the different analysed minerals.

Summary, discussion and conclusions

The Attu gold prospect is small. The gold mineralised zone does not exceed 0.5 m in width, and its length is now known to be only a few hundred metres. Gold has also been detected along strike several kilometres away, but the mineralisation does not show a continuous outcrop pattern. However, the fact that gold is present indicates that the NE-striking shear/mylonite zone is mineralised and that hydrothermal activity seems to have occurred in most of the prominent lineaments in the region. The gold-bearing sulphide deposit is of replacement type, where pyrite and chalcopyrite grew at the expense of e.g. magnetite. It is envisaged that gold was introduced contemporaneously with the replacement processes.

Reworked Archaean orthogneisses dominate all segments of the Nagssugtoqidian orogen. Published age deter-

minations range from 2870–2700 Ma (e.g. Kalsbeek & Nutman 1996; Connelly & Mengel 2000), but no chronological information has yet been available from the Attu region. The 3162 ± 43 Ma magnetite age obtained from the Attu host rocks suggests that the rocks in this part of the Nagssugtoqidian orogen may be significantly older than similar rocks elsewhere in the orogen. However, Sm-Nd isotope data from Archaean gneisses in the central part of the orogen suggest the involvement of pre-2800 Ma crustal material (possibly 3100 Ma or older) in their source (Whitehouse *et al.* 1998). Large parts of the Nagssugtoqidian orogen underwent Palaeoproterozoic granulite facies metamorphism around 1850 Ma (e.g. Willigers *et al.* 2001), which resulted in severe disturbance of the Pb-isotopic evolution of the rocks (Whitehouse *et al.* 1998). In view of the well-preserved 3162 Ma isochron relationships for the Attu gneisses it appears possible that these rocks escaped high-grade Nagssugtoqidian metamorphism and that granulite facies metamorphism here is of Archaean age, in agreement with the conclusions of Mazur *et al.* (2006, this volume) and Thrane & Connelly (2006, this volume).

The Pb-isotopic data of the gold bearing samples (Fig. 6) suggest a genetic link between the Rifkol granite intrusion and the fluids percolating through the shear zone, implying an Archaean age of the mineralisation. Without further analytical work we are unable to elaborate and comment on a possible source of the Pb that has been incorporated into the K-feldspar in the shear zone.

Acknowledgements

The authors acknowledge F. Kalsbeek, P.M. Holm and an anonymous reviewer for thorough criticism and constructive suggestions, which greatly improved the manuscript. The authors would also like to thank the participants in the resource assessment programme *Mineral resources of the Precambrian shield of central West Greenland (66°–70°15′N)* for valuable discussions concerning mineralising events in the region. Input from other scientists in the region is also gratefully acknowledged. Special thanks go to Karl Markussen, Attu, who submitted the first gold bearing sample, for showing us the exact sample locality.

References

Connelly, J.N. & Mengel, F.C. 2000: Evolution of Archean components in the Paleoproterozoic Nagssugtoqidian orogen, West Greenland. Geological Society of America Bulletin 112, 747–763.

Connelly, J.N., van Gool, J.A.M. & Mengel, F.C. 2000: Temporal evolution of a deeply eroded orogen: the Nagssugtoqidian orogen, West Greenland. Canadian Journal of Earth Sciences 37, 1121–1142.

Hansen, B.F. 1979: Some charnockitic rocks in the Nagssugtoqidian of West Greenland. Rapport Grønlands geologiske Undersøgelse 89, 85–96.

Hollis, J.A., Keiding, M., Stensgaard, B.M., van Gool, J.A.M. & Garde, A.A. 2006: Evolution of Neoarchaean supracrustal belts at the northern margin of the North Atlantic Craton, West Greenland. In: Garde, A.A. & Kalsbeek, F. (eds): Precambrian crustal evolution and Cretaceous–Palaeogene faulting in West Greenland. Geological Survey of Denmark and Greenland Bulletin 11, 9–31 (this volume).

Kalsbeek, F. & Nutman, A.P. 1996: Anatomy of the Early Proterozoic Nagssugtoqidian orogen, West Greenland, explored by reconnaissance SHRIMP U-Pb zircon dating. Geology 24, 515–518.

Kalsbeek, F., Taylor, P.N. & Henriksen, N. 1984: Age of rocks, structures, and metamorphism in the Nagssugtoqidian mobile belt, West Greenland – field and Pb-isotope evidence. Canadian Journal of Earth Sciences 21, 1126–1131.

Kalsbeek, F., Pidgeon, R.T. & Taylor, P.N. 1987: Nagssugtoqidian mobile belt of West Greenland: a cryptic 1850 Ma suture between two Archaean continents – chemical and isotopic evidence. Earth and Planetary Science Letters 85, 365–385.

Mazur, S., Piazolo, S. & Alsop, G.I. 2006: Structural analysis of the northern Nagssugtoqidian orogen, West Greenland: an example of complex tectonic patterns in reworked high-grade metamorphic terrains. In: Garde, A.A. & Kalsbeek, F. (eds): Precambrian crustal evolution and Cretaceous–Palaeogene faulting in West Greenland. Geological Survey of Denmark and Greenland Bulletin 11, 163–178 (this volume).

Olesen, N.Ø. 1984: Geological map of Greenland, 1:100 000, Agto 67 V.1 Nord. Copenhagen: Geological Survey of Greenland.

Rasmussen, T.M. & van Gool, J.A.M. 2000: Aeromagnetic survey in southern West Greenland: project Aeromag 1999. Geology of Greenland Survey Bulletin 186, 73–77.

Stacey, J.S. & Kramers, J.D. 1975: Approximation of terrestrial lead isotope evolution by a two-stage model. Earth and Planetary Science Letters 26, 207–221.

Steenfelt, A. 2001: Geochemical atlas of Greenland – West and South Greenland. Danmarks og Grønlands Geologiske Undersøgelse Rapport 2001/46, 39 pp., 1 CD-ROM.

Steenfelt, A., Stendal, H., Nielsen, B.M. & Rasmussen, T.M. 2004: Gold in central West Greenland – known and prospective occurrences. Geological Survey of Denmark and Greenland Bulletin 4, 65–68.

Stendal, H. 1998: Contrasting Pb isotopes of Archaean and Palaeoproterozoic sulphide mineralisation, Disko Bugt, central West Greenland. Mineralium Deposita 33, 255–265.

Stendal, H. & Schønwandt, H.K. 2003: Precambrian supracrustal rocks

and mineral occurrences, Northeast Disko Bugt. Danmarks og Grønlands Geologiske Undersøgelse Rapport 2003/24, 57 pp.

Stendal, H., Blomsterberg, J., Jensen, S.M., Lind, M., Madsen, H.B., Nielsen, B.M., Thorning, L. & Østergaard, C. 2002: The mineral resource potential of the Nordre Strømfjord – Qasigiannguit region, southern central West Greenland. Geology of Greenland Survey Bulletin 191, 39–47.

Stendal, H., Nielsen, B.M., Secher, K. & Steenfelt, A. 2004: Mineral resources of the Precambrian shield of central West Greenland (66° to 70°15′). Part 2. Mineral occurrences. Danmarks og Grønlands Geologiske Undersøgelse Rapport 2004/20, 212 pp.

Taylor, P.N. & Kalsbeek, F. 1990: Dating the metamorphism of Precambrian marbles: examples from Proterozoic mobile belts in Greenland. Chemical Geology 86, 21–28.

Thrane, K. & Connelly, J.N. 2006: Zircon geochronology from the Kangaatsiaq–Qasigiannguit region, the northern part of the 1.9–1.8 Ga Nagssugtoqidian orogen, West Greenland. In: Garde, A.A. & Kalsbeek, F. (eds): Precambrian crustal evolution and Cretaceous–Palaeogene faulting in West Greenland. Geological Survey of Denmark and Greenland Bulletin 11, 87–99 (this volume).

Todt, W., Cliff, R.A., Hanser, A. & Hofmann, A.W. 1993: Re-calibration of NBS lead standards using a $^{202}Pb + {}^{205}Pb$ double spike. Terra Abstracts 5, Supplement 1, 396 only.

van Gool, J.A.M., Connelly, J.N., Marker, M. & Mengel, F. 2002: The Nagssugtoqidian orogen of West Greenland: tectonic evolution and regional correlations from a West Greenland perspective. Canadian Journal of Earth Sciences 39, 665–686.

Whitehouse, M.J., Kalsbeek, F. & Nutman, A.P. 1998: Crustal growth and crustal recycling in the Nagssugtoqidian orogen of West Greenland: constraints from radiogenic isotope systematics and U-Pb zircon geochronology. Precambrian Research 91, 365–381.

Willigers, B.J.A., Krogstad, E.J. & Wijbrans, J.R. 2002: Comparison of thermochronometers in a slowly cooled granulite terrain: Nagssugtoqidian orogen, West Greenland. Journal of Petrology 42, 1729–1749.

Manuscript received 4 October 2004; revision accepted 19 December 2005

Origin and evolution of the Kangâmiut mafic dyke swarm, West Greenland

Kyle R. Mayborn and Charles E. Lesher

The Kangâmiut dyke swarm in West Greenland intruded Archaean terrains at 2.04 Ga, and its northern portion was subsequently metamorphosed to granulite facies during the Nagssugtoqidian orogeny (*c*. 1.8 Ga). Mineral and whole-rock major and trace element compositions show that the parental magmas for the dyke swarm differentiated by the fractionation of olivine, clinopyroxene, plagioclase and late stage Fe-Ti oxides. Petrographical observations and the enrichment of K_2O during differentiation argue that hornblende was not an important fractionating phase. Field observations suggest emplacement at crustal levels above the brittle–ductile transition, and clinopyroxene geothermobarometry constrains dyke emplacement depths to less than 10 km. Granulite facies metamorphism of the Kangâmiut dykes and their host rocks in the northern portion of the swarm requires subsequent burial to *c*. 30 km, related to roughly 20 km of crustal thickening between the time of dyke emplacement and peak metamorphism during the Nagssugtoqidian orogeny. Kangâmiut dykes are characterised by low Ba/La ratios (12 ± 5), and high Nb/La ratios (0.8 ± 0.2), compared to subduction related basalts (Ba/La *c*. 25; Nb/La *c*. 0.35). These geochemical characteristics argue that the Kangâmiut dykes are not related to subduction processes. Forward modelling of rare-earth element data requires that primitive magmas for the Kangâmiut dykes originated from a moderately depleted mantle source with a mantle potential temperature of *c*. 1420°C. The inferred potential temperature is consistent with potential temperature estimates for ambient mantle at 2.0 Ga derived from secular cooling models and continental freeboard constraints. The geochemistry and petrology of the Kangâmiut dykes support a model that relates the dyke activity to passive rifting of the proposed Kenorland supercontinent rather than to mantle plume activity or subduction.

Keywords: dyke swarm, Laurentia, Palaeoproterozoic, rifting

K.R.M., *Department of Geology, Western Illinois University, Macomb, IL 61455, USA.* E-mail: *KR-Mayborn@wiu.edu*
C.E.L., *Department of Geology, University of California-Davis, Davis, CA 95616, USA.*

The 2.04 Ga Kangâmiut dyke swarm of West Greenland has been the subject of numerous investigations over the past 35 years (Windley 1970; Escher *et al.* 1976; Bridgwater *et al.* 1995; Cadman *et al.* 1999), yet there is still considerable disagreement over many aspects of the swarm's history. Since the work of Escher *et al.* (1976), who associated the dykes with synkinematic shearing during N–S compression, the swarm has often been cited as a type example of dykes that are emplaced into crustal regions undergoing shear deformation (Cadman *et al.* 1999). The proposed compressional setting led Cadman *et al.* (2001) to speculate that the swarm formed in a subduction-related environment. Nevertheless, recent geochronology has shown that many of the shear zones originally thought to be consanguineous with the dykes are actually significantly older or younger than the dykes themselves (Connelly & Mengel 2000). The field area for Escher *et al.*'s (1976) investigations is now known to contain Archaean shear

zones and post-Kangâmiut dyke shearing associated with the Nagssugtoqidian orogeny. Despite these complications, the Kangâmiut dyke swarm offers a unique opportunity to constrain the magmatic and tectonic evolution of the province spanning the period from dyke emplacement to the Nagssugtoqidian orogeny (2.04 to *c.* 1.8 Ga). The present work discusses the constraints on the magmatic and metamorphic history of the Kangâmiut dykes provided by field observations, petrology, geochemistry, and geochronology and critically evaluates previous and newly proposed models for their origin and subsequent metamorphism during the Nagssugtoqidian orogeny.

Regional geology

Figure 1 is a geological map of central West Greenland showing the Nagssugtoqidian orogen and the Kangâmiut dykes. The Nagssugtoqidian orogen is bounded to the north by the Palaeoproterozoic Rinkian orogen (Escher & Pulvertaft 1976) and to the south by the Archaean Nain craton (Nutman & Bridgwater 1986; Nutman & Collerson 1991; Friend & Nutman 1994). The orogen is divided into four parts based on lithology, structure, stream sediment geochemistry, and aeromagnetic data. From north to south, these are the northern Nagssugtoqidian orogen (NNO), the central Nagssugtoqidian orogen (CNO), the southern Nagssugtoqidian orogen (SNO), and the southern Nagssugtoqidian foreland (SNF). These terrains are separated by three shear zones. The Nordre Strømfjord shear zone separates the NNO from the CNO, the Ikertôq shear zone separates the CNO from the SNO, and the Nagssugtoqidian Front separates the SNO from the SNF.

The NNO contains Archaean granitic gneisses and supracrustal rocks (van Gool *et al.* 2002), whereas the CNO is characterised by reworked Archaean granitic and tonalitic gneisses, the 1.92 Ga Arfersiorfik quartz diorite, the 1.92 Ga Sisimiut charnockite, and supracrustal rocks (Bak *et al.* 1975; Kalsbeek *et al.* 1987; Manatschal *et al.* 1998; Kalsbeek & Manatschal 1999; Nutman *et al.* 1999; van Gool *et al.* 1999). The SNO and SNF are composed of Archaean granitic and tonalitic gneisses and the Kangâmiut dykes. In the SNO the dykes are metamorphosed to amphibolite facies in the south and granulite facies in the extreme north. The transition from amphibolite facies to granulite facies occurs within the Ikertôq shear zone (Korstgård 1979). In the SNF, most of the Kangâmiut dykes retain igneous textures and mineralogies.

Figure 1 shows that the Ikertôq shear zone is the most continuous structure within the Nagssugtoqidian orogenic belt and represents an important lithological boundary between the SNO and the CNO. It is traceable from the western shoreline, just south of the village of Sisimiut, to the inland icecap. The shear zone contains panels of Kangâmiut dyke-bearing tonalitic gneiss alternating with layers of garnet-sillimanite-kyanite-bearing metapelites, marbles, and quartzites that dip steeply NNW. The repetition of lithological units, the presence of down-dip lineations and S-vergent kinematic indicators show that this structure is a reverse fault (Grocott 1979). Deformed Kangâmiut dykes are restricted to the southern footwall, while Palaeoproterozoic felsic igneous rocks, including the 1.92 Ga Sisimiut charnockite and the 1.92 Ga Arfersiorfik quartz diorite, are found only north of the shear zone. U/Pb dates for detrital zircons from the supracrustal rocks of the region require that these units were deposited after 2.10 Ga (Nutman *et al.* 1999), while $^{40}Ar/^{39}Ar$ dating of hornblende from metamorphosed Kangâmiut dykes and orthogneisses from within the shear zone gives cooling ages of *c.* 1.73 Ga (Willigers *et al.* 1999).

The Itivdleq shear zone is located to the south of the Ikertôq shear zone within the SNO and is *c.* 6 km wide with E–W-trending lineations (Hanmer *et al.* 1997). It contains multiple bands of sheared Kangâmiut dykes and Archaean orthogneisses that Connelly & Mengel (2000) used to document shearing during the Archaean and the Palaeoproterozoic Nagssugtoqidian orogeny. For example, some of the shear bands are cut by weakly deformed tonalites that yield a magmatic age of 2498 ± 4 Ma with a metamorphic overprint at 1782 ± 12 Ma (Connelly & Mengel 2000). This shows that some of the shear bands near Itilleq fjord developed prior to *c.* 2.5 Ga and were subsequently intruded by tonalite. The metamorphic overprint age of 1782 Ma and the presence of shear bands that cut the Kangâmiut dykes indicate reactivation during the Nagssugtoqidian orogeny. Metamorphic hornblende from a recrystallised Kangâmiut dyke within the Itivdleq shear zone gives an $^{40}Ar/^{39}Ar$ age of 1873 ± 13 Ma, consistent with the age of Nagssugtoqidian metamorphism (Willigers *et al.* 1999).

The Nagssugtoqidian Front is the southernmost structural expression of the Nagssugtoqidian orogenic event (Fig. 1). Hageskov (1995) showed that it is a discontinuous, en échelon array of NW-dipping, low-angle thrust

Facing page:
Fig. 1. Geological map of the Nagssugtoqidian orogen and its southern foreland in West Greenland. NNO, northern Nagssugtoqidian orogen; CNO, central Nagssugtoqidian orogen; SNO, southern Nagssugtoqidian orogen; SNF, southern Nagssugtoqidian foreland. Modified from van Gool *et al.* (2002).

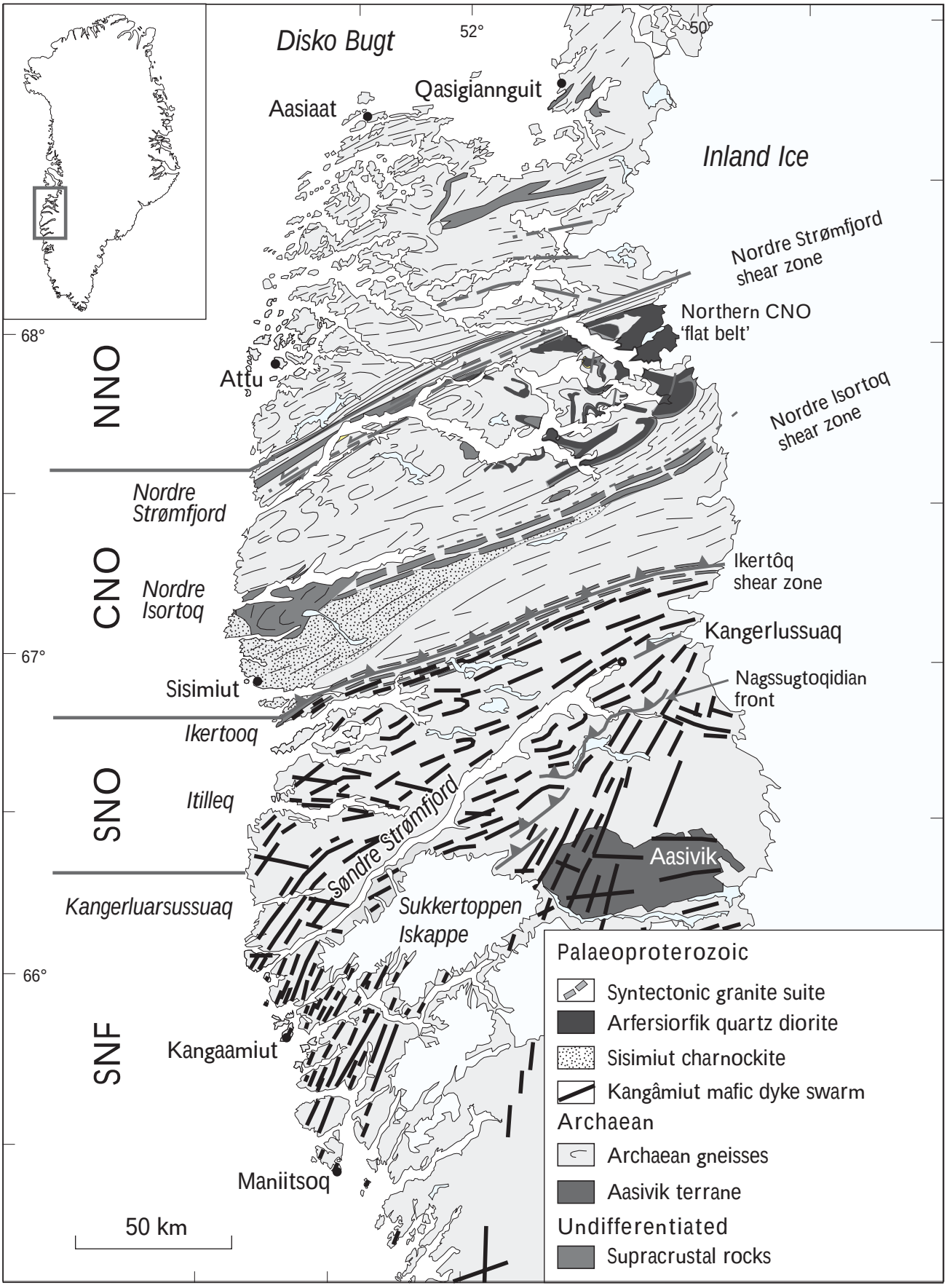
Disko Bugt
52°
50°
Qasigiannguit
Aasiaat
Inland Ice
Nordre Strømfjord shear zone
Northern CNO 'flat belt'
68°
Attu
NNO
Nordre Isortoq shear zone
Nordre Strømfjord
CNO
Nordre Isortoq
Ikertôq shear zone
Kangerlussuaq
67°
Sisimiut
Nagssugtoqidian front
Ikertooq
SNO
Itilleq
Søndre Strømfjord
Aasivik
Kangerluarsussuaq
Sukkertoppen
Iskappe
66°
SNF
Kangaamiut
Maniitsoq
50 km
Palaeoproterozoic
Syntectonic granite suite
Arfersiorfik quartz diorite
Sisimiut charnockite
Kangâmiut mafic dyke swarm
Archaean
Archaean gneisses
Aasivik terrane
Undifferentiated
Supracrustal rocks

faults that deformed the Kangâmiut dykes in this region. The Nagssugtoqidian Front is well defined in the eastern portion of the orogen but is difficult to trace to the west approaching the Sukkertoppen Iskappe. It is not known whether the Nagssugtoqidian Front dies out beneath the icecap or swings to the NNW merging with the Itivdleq shear zone (Hageskov 1995).

Geological history

The Precambrian history of central West Greenland involves five major events: (1) genesis and metamorphism of Archaean crust; (2) emplacement of the Kangâmiut dykes (2.04 Ga); (3) deposition of sediments (*c*. 2.00–1.92 Ga); (4) emplacement of the Sisimiut and Arfersiorfik intrusions (*c*. 1.92–1.87 Ga); and (5) metamorphism and deformation accompanying the Nagssugtoqidian orogeny (*c.* 1.82–1.77 Ga).

Genesis and metamorphism of Archaean crust

Connelly & Mengel (2000) and Kalsbeek & Nutman (1996) present U/Pb dates and field observations that document the genesis and metamorphism of a large portion of the central West Greenland crust during the Late Archaean. Igneous zircons from foliated granulite facies gneisses give ages between 2.87 and 2.81 Ga. Granitoids that cut the foliation in these gneisses give ages between 2.81 and 2.72 Ga. These cross-cutting relationships and dates indicate widespread genesis of granitic crust between 2.87 and 2.81 Ga, immediately followed by metamorphism at 2.81–2.72 Ga.

Emplacement of the Kangâmiut dykes

The emplacement of the Kangâmiut dykes occurred after the formation of the Archaean host rocks and before the Nagssugtoqidian orogeny. U/Pb geochronology on igneous zircons from three dykes gives ages of 2036 ± 5 Ma, 2046 ± 8 Ma (Nutman *et al.* 1999), and 2048 ± 4 Ma (Connelly *et al.* 2000). The analysed zircons come from dioritic centres in wide composite dykes and cover most of the N–S extent of the dyke swarm. $^{40}Ar/^{39}Ar$ dating of hornblende from the Kangâmiut dykes from the SNF by Willigers *et al.* (1999) gives emplacement related ages of 2.05–2.02 Ga.

Deposition of sediments

Dating of detrital zircons from metasedimentary units just south of the Nordre Strømfjord shear zone and within the Ikertôq shear zone (Fig. 1) yields ages between 3.4 and 1.95 Ga (Nutman *et al.* 1999). Some metasediments containing 1.95 Ga zircons are cut by 1.92 Ga quartz-diorites, requiring that deposition of the sediments occurred between 1.95 and 1.92 Ga. Metasediments found within thrust-bounded panels in the Ikertôq shear zone contain zircons that yield ages between 2.1 and 2.0 Ga. There are no known granitic intrusive rocks with ages between 2.5 and 1.92 Ga within the central West Greenland field area, suggesting that the sediments originated from a distal source. Nutman *et al.* (1999) propose that the Archaean and Palaeoproterozoic terranes of eastern Canada are possible source regions. Sediments derived from these terranes would support the existence of the supercontinent Kenorland (Williams *et al.* 1991; Aspler & Chiarenzelli 1998). Additionally, the deposition of sediments suggests the presence of basins that may have developed during the rifting and break-up of Kenorland (van Gool *et al.* 2002).

The Nagssugtoqidian orogeny and emplacement of Sisimiut and Arfersiorfik intrusions

Ramberg (1949) and Noe-Nygaard (1952) first recognised the Nagssugtoqidian orogen based on the deformation and metamorphism of the Kangâmiut dykes and the occurrence of shear zones with steeply dipping foliations. Geochronological data show that the Nagssugtoqidian orogenic event occurred between 1.91 and 1.77 Ga (Connelly *et al.* 2000) and resulted in granulite to amphibolite grade metamorphism and the development of discrete shear zones. Pre-orogenic magmatism includes the emplacement of the 1.92 Ga Arfersiorfik quartz diorite (Kalsbeek *et al.* 1987) and the 1.92 Ga Sisimiut charnockite. The orogenic event is proposed to be the result of continental collision that produced thrust stacking, folding and associated metamorphism (van Gool *et al.* 2002). The suture between the two continents is not easily identifiable, but Kalsbeek *et al.* (1987) proposed that the suture is located in what is now the boundary between the NNO and the CNO.

Previous work on the origin of the Kangâmiut dykes

Many early workers suggested that the emplacement of the Kangâmiut dykes was directly related to the Nagssugtoqidian orogeny. Escher *et al.* (1976) stated that the dykes were emplaced into conjugate sets of active shear zones during NNW–SSE compression. They based this hypothesis on their observations of conjugate sets of dykes that show a variety of cross-cutting relationships. They, and Hanmer *et al.* (1997), proposed that the emplacement of both dyke sets occurred during shearing. Bridgwater *et al.* (1995) expanded on the Escher *et al.* (1976) hypothesis by proposing that the dykes formed during thrusting of amphibolite facies crust from the north under the granulite facies terrain in the southern Nagssugtoqidian orogen. They invoked this hypothesis because the Kangâmiut dykes contain hornblende suggesting they crystallised from a hydrous magma. Bridgwater *et al.'s* (1995) hypothesis seeks to explain the hydrous nature of the Kangâmiut dyke magmas by placing a hydrous source beneath the granulite facies host rocks. A potential problem with the Escher *et al.* (1976) and Bridgwater *et al.* (1995) hypotheses is that neither easily explains how partial melting of hydrous lower crust would directly produce melt of basaltic composition. If the Escher *et al.* (1976) and Bridgwater *et al.* (1995) hypotheses of dyke emplacement during compression are correct, then subduction related magmatism becomes a possibility. Cadman *et al.* (2001) explicitly consider this possibility and proposed that the Kangâmiut dyke swarm formed by adiabatic decompression of metasomatised mantle during passage of a slab window.

The recent work of Kalsbeek & Manatschal (1999), Connelly & Mengel (2000) and van Gool *et al.* (2002), offer alternatives to the subduction hypothesis and suggest that the swarm was emplaced during continental rifting. Van Gool *et al.* (2002) cite evidence of 2.0 Ga rift related sediments in support for the rifting hypothesis. Kalsbeek & Manatschal (1999) speculate that the Kangâmiut dykes are the product of mantle plume-related rifting based on the presence of ultramafic rocks found within the Nagssugtoqidian orogeny. Although these authors discuss the origin of the Kangâmiut dykes, they do so only briefly, because their primary focus is on the Nagssugtoqidian orogeny.

Field setting

The Kangâmiut dyke swarm intruded granulite facies Archaean orthogneisses and is exposed over an 18 000 km^2 area. Figure 1 shows that the swarm extends for 150 km from just south of the village of Maniitsoq towards Sisimiut in the north and from the coast eastward to the ice cap. The dykes are most abundant near the coast and less so towards the ice cap. Dyke widths range from a few centimetres to greater than 140 m. Escher *et al.* (1975) estimated that dyke emplacement was accommodated by 2–3% crustal extension. Appendix A provides locality and field characteristics of all the dykes examined in this study.

Field observations show that there are three dyke suites (Mengel *et al.* 1996). Two of these trend east–west, while the third has a NE trend. The NE-trending suite of dykes represents the vast majority of the dykes in the area and is the only suite that contains dykes with dioritic centres. The three sets of zircon populations used to date three separate dykes all come from these dioritic centres (Nutman *et al.* 1999; Connelly *et al.* 2000). Thus, the NE-trending suite is dated at 2.04 Ga and will be referred to as the 'Kangâmiut dykes' proper as suggested by Mengel *et al.* (1996).

Although the Kangâmiut dykes have an overall NE trend, there are some systematic deviations. Figure 1 shows that the southern portion of the swarm trends NNE. Moving northward, the orientation gradually changes to ENE. Changes in the orientation of the swarm correlate with increased dyke deformation and recrystallisation. Escher *et al.* (1975) suggested that the bend in the swarm resulted from deformation during the Nagssugtoqidian. Hanmer *et al.* (1997) argue that this change in orientation is a primary feature related to the regional stress field during dyke emplacement.

The majority of dykes south of the Nagssugtoqidian Front retain igneous mineralogies and textures with the exception of a small number of composite dykes with sheared dioritic centres. Shearing was parallel to the dyke contacts, and mostly affected the large composite dykes. Windley (1970) worked in an area just north of Maniitsoq village where he observed cross-cutting dykes. He described a set of cross-cutting dykes where a younger dyke cuts the internal foliation of an older dyke. Not all of the composite dykes show internal deformation. Some dykes show irregular intrusive contacts between the dioritic centre and mafic host dyke showing that they formed by successive injections, closely spaced in time.

Large composite dykes show structural and petrological features not seen in the smaller non-composite dykes. For example, a 140 m wide dyke in Kangerluarsussuaq fjord has fine-grained (*c.* 0.1–0.5 mm) equigranular mafic contacts. Twelve metres from the contact the grain size is *c.* 1 mm with some contact-parallel primary layering. Halfway towards the dyke centre the grain size increases

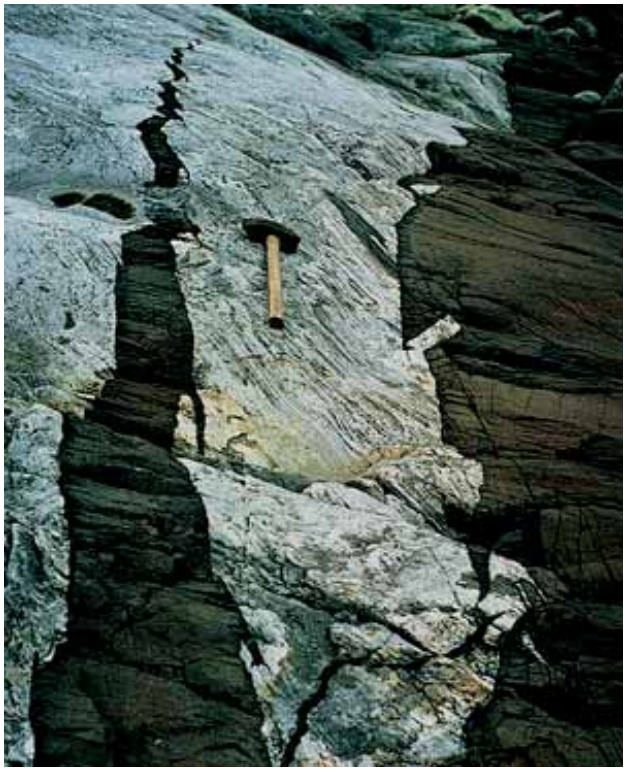

Fig. 2. Kangâmiut dyke with angular bridges within the chilled margin (Photo: David Bridgwater).

to *c*. 3 mm with primary clinopyroxene mostly replaced by hornblende. Near its centre the dyke is slightly foliated and recrystallised to a garnet amphibolite. The centre of the dyke is a strongly foliated garnet-plagioclase-hornblende schist with a dioritic composition. A 10 cm wide epidote-calcite-quartz vein originates from the sheared centre and cuts the non-sheared mafic portion of the dyke.

There are a variety of intrusive relationships between dykes and host rocks including en échelon steps, bridges, and forks. Figure 2 shows bridges with sharp, angular edges contained within the chilled margin of a Kangâmiut dyke. Some dykes have chilled margins up to 40 cm thick, while others have no chilled margins. Chilled margins contain fine-grained plagioclase and clinopyroxene phenocrysts in a microcrystalline groundmass. Some chilled margins contain dismembered bridges of host rock, whereas dyke interiors contain no bridges or xenoliths.

In the northern portion of the dyke swarm, metamorphic minerals and deformation features replace igneous minerals and primary intrusive features. In the Itilleq fjord region, most of the dykes are partly to completely altered during static or shear-related recrystallisation. Some dykes show penetrative foliation, whereas other dykes are deformed only at the contacts and form boudins within the deformed country rock. The central portions of these boudins are partially recrystallised. On the south shore of Itilleq fjord, away from most of the Nagssugtoqidian deformation, the dykes preserve primary emplacement structures, but are statically recrystallised to garnet amphibolites. Dykes at the northern extent of the swarm within Ikertooq fjord are completely recrystallised to granulite facies.

Petrography

The chilled margins of the Kangâmiut dykes contain 0.2–0.8 mm phenocrysts of clinopyroxene and plagioclase in a microcrystalline groundmass of plagioclase, clinopyroxene, hornblende, quartz, and Fe-Ti oxides. Plagioclase phenocrysts are euhedral to subhedral and weakly zoned, whereas the clinopyroxene phenocrysts are subhedral to anhedral. Some chilled margins contain 0.2–1.5 mm hornblende crystals. Figure 3A shows that these hornblende crystals contain abundant inclusions of Fe-Ti oxides, which are absent from the clinopyroxene and plagioclase phenocrysts. These hornblende crystals also enclose plagioclase and clinopyroxene phenocrysts suggesting they are a later phase that crystallised *in situ*.

The interiors of most Kangâmiut dykes are fine- to medium-grained with subophitic textures. Subhedral to anhedral clinopyroxene, plagioclase, and Fe-Ti oxides are the primary constituents along with interstitial quartz, hornblende, and trace amounts of apatite. In some of the dykes, anhedral clinopyroxene fills interstitial areas between subhedral to euhedral plagioclase. Clinopyroxene displays two types of exsolution. The first type is laminar exsolution of low-Ca pyroxene. The second type appears to be granular exsolution of low-Ca pyroxene around the outer parts of the original clinopyroxene crystal. Additionally, most clinopyroxene grains have rims of hornblende (Fig. 3B).

Kangâmiut dyke samples from Itilleq fjord are variably metamorphosed to fine-grained (0.2–1.0 mm) amphibolites with well-developed foliations. Metamorphic assemblages include hornblende, plagioclase, quartz, garnet, titanite, and biotite. Hornblende replaces clinopyroxene, whereas plagioclase and garnet form at contacts between hornblende and plagioclase (see also Mengel *et al.* 1996). Titanite replaces Fe-Ti oxides.

Metamorphic orthopyroxene occurs within Kangâmiut dykes in Ikertooq fjord near the northern extent of the swarm (Fig. 1), marking the transition from amphibolite to granulite facies. The typical assemblage in these granulite facies dykes is plagioclase + hornblende + orthopyroxene + clinopyroxene ± garnet ± titanite (see also Korstgård

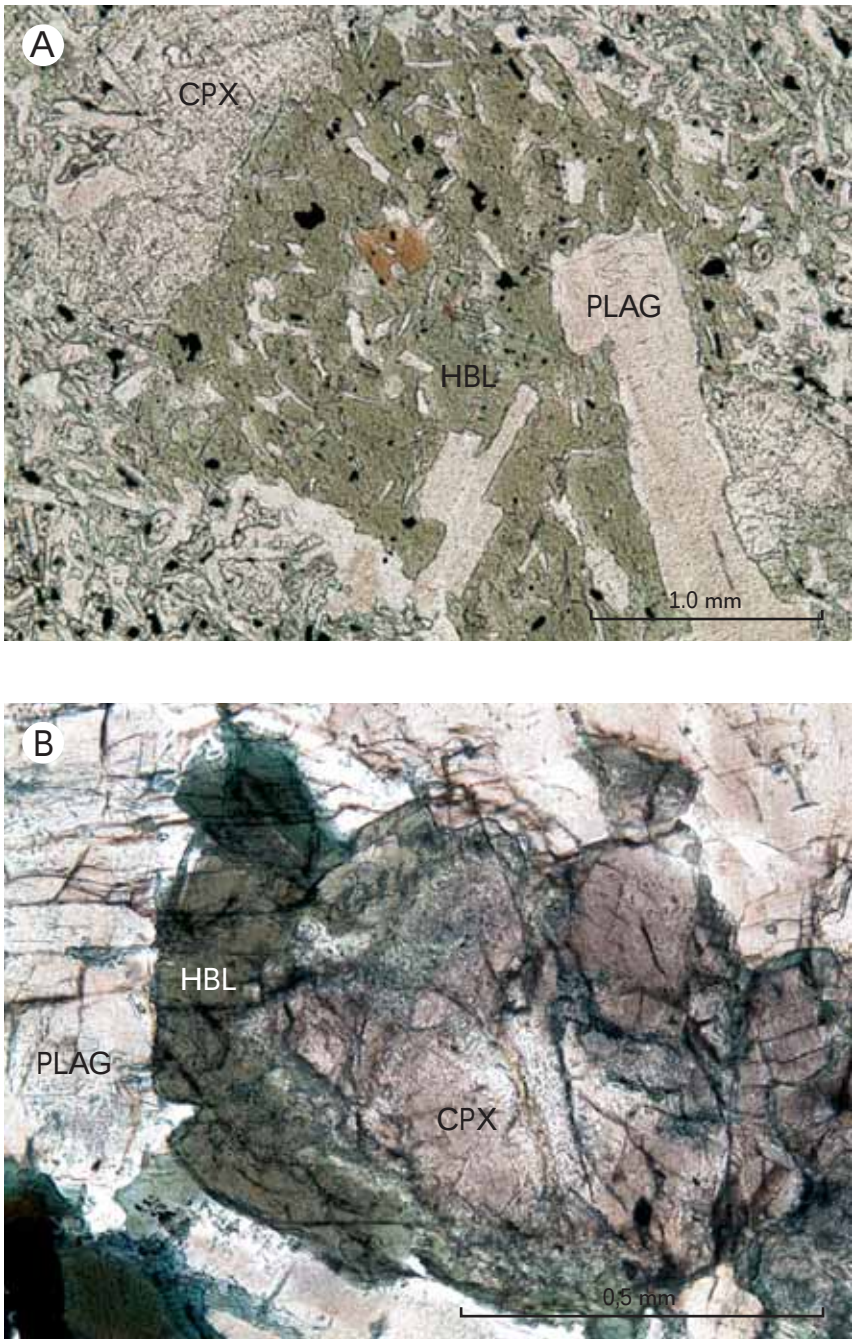

Fig. 3. A: Photomicrograph of a chilled margin of a Kangâmiut dyke with clinopyroxene (CPX) and plagioclase (PLAG) phenocrysts in a groundmass of the same plus Fe-Ti oxides. The large crystal in the centre is hornblende (HBL) with inclusions of a plagioclase phenocryst and groundmass plagioclase and Fe-Ti oxides. Sample GGU 430267, plane polarised light. B: Photomicrograph of a sample from the interior of a Kangâmiut dyke showing hornblende (HBL) rims on clinopyroxene (CPX). Sample GGU 430999, plane polarised light.

1979). These dykes are weakly foliated and fine-grained (0.1–1.0 mm).

Petrology and geochemistry

Whole-rock major and trace elements

A total of 122 dyke samples were analysed for most major and minor elements on fused glass discs using a wavelength dispersive x-ray fluorescence (XRF) spectrometer at the Geological Survey of Denmark and Greenland (GEUS) in Copenhagen. Na_2O was determined by atomic absorption spectrometry. Kystol & Larsen (1999) describe the analytical methods, precision, and accuracy of the GEUS lab and report that the standard error for all major and minor elements is less than 0.25 wt%, based on multiple analyses of international standards.

Trace element concentrations for 73 dyke samples were measured at the University of California-Davis using a

Table 1. Major and trace element data for representative Kangâmiut dykes

Sample	430904	430923	430926	430931	430952	430970	430981	430988	430997	432102	432108	432115	432118	432122	432133	432138	432143	432158
Dyke	5	13	14	16	27	37	42	45	54	86	60	64	64	64	71	70	76	75
SiO_2	50.87	52.78	50.64	50.73	52.19	48.90	50.71	49.30	56.06	57.18	48.97	51.01	56.84	50.25	51.00	49.46	50.57	50.48
TiO_2	2.47	2.31	1.94	0.88	1.62	1.66	1.02	1.45	0.79	1.65	1.69	1.92	2.12	1.82	1.64	2.70	1.33	1.34
Al_2O_3	12.62	13.65	13.29	12.57	13.19	13.14	14.09	13.34	21.46	14.37	13.75	12.97	13.07	13.67	13.96	15.57	13.14	13.59
Fe_2O_3	4.27	3.53	4.26	1.74	4.14	2.52	1.55	1.91	1.24	2.15	4.73	2.21	1.98	2.17	2.06	2.54	1.26	1.75
FeO	11.67	11.34	9.99	9.10	11.05	11.98	9.89	11.40	4.34	8.94	9.48	12.73	10.99	12.22	11.59	11.51	11.99	11.84
MnO	0.24	0.20	0.22	0.21	0.24	0.24	0.21	0.22	0.08	0.16	0.23	0.24	0.19	0.23	0.21	0.20	0.23	0.23
MgO	4.27	3.51	5.55	8.90	4.57	6.40	7.43	6.60	0.92	2.34	6.12	5.08	2.14	5.81	4.78	3.44	6.98	6.12
CaO	8.93	8.24	9.86	12.31	8.48	10.85	11.27	11.39	9.07	6.11	10.72	9.46	6.17	10.12	9.53	8.61	11.40	10.59
Na_2O	2.47	2.91	2.55	2.27	2.80	2.28	2.15	2.25	4.19	3.69	2.44	2.57	3.37	2.45	2.46	2.99	2.11	2.07
K_2O	0.69	1.13	0.58	0.18	0.87	0.28	0.18	0.30	0.51	1.14	0.39	0.52	1.43	0.33	0.47	1.02	0.22	0.35
P_2O_5	0.26	0.29	0.19	0.07	0.19	0.13	0.09	0.13	0.16	0.35	0.15	0.19	0.39	0.10	0.18	0.44	0.10	0.13
LOI	0.84	0.63	0.94	0.91	1.07	1.34	0.79	1.31	0.79	1.43	1.41	1.01	1.17	0.91	1.64	1.35	1.11	1.06
Sum	99.60	100.52	100.03	99.88	100.40	99.72	99.39	99.58	99.61	99.50	100.08	99.90	99.86	100.07	99.53	99.83	100.44	99.55
Sc	38	30	36	58	44	46	47	45	14	20	38	41	22	41	36	29	49	45
V	368	355	333	389	318	381	296	362	29	155	348	393	207	558	303	259	390	336
Cr	47	14	63	145	43	63	153	98	5	33	134	83	22	94	61	33	174	103
Ni	40	28	65	113	40	74	88	60	1	17	82	54	15	66	49	23	78	74
Co	46	44	47	52	44	61	51	56	14	28	53	46	32	54	49	32	53	52
Rb	22	33	16	3.9	25	5.6	4.3	6.1	10	31	7.4	13	45	8.0	12	28	4.6	8.5
Sr	171	201	241	117	207	160	136	160	290	306	235	164	247	164	200	213	138	142
Y	47	34	29	19	35	27	18	27	34	35	26.2	37	48	23	30	53	24	28
Zr	182	168	139	47	133	99	46	92	157	194	106	133	326	78	110	200	58	84
Nb	14.7	10.9	11.8	3.3	9.2	9.2	3.2	8.2	11.3	18.1	9.3	10.0	23.9	6.2	7.3	15.8	4.6	5.2
Ba	204	321	156	50	306	90	50	95	192	392	104	145	454	98	156	366	69	106
La	17.5	20.5	17.1	4.4	12.7	9.2	4.4	8.4	12.3	27.8	10.86	12.9	42.0	7.4	11.4	18.2	5.8	7.6
Ce	43.8	46.0	40.2	10.6	31.9	21.8	10.7	20.7	32.0	63.9	26.28	30.6	94.4	18.1	26.7	40.4	14.1	18.0
Pr	6.07	6.13	5.41	1.49	4.43	3.10	1.70	3.00	4.54	8.66	3.73	4.36	11.96	2.58	3.83	5.58	2.07	2.67
Nd	27.8	27.1	22.7	7.37	18.8	14.2	7.31	13.9	20.6	36.2	16.93	19.1	49.7	11.6	17.3	25.7	9.90	12.2
Sm	7.14	6.11	5.44	2.45	4.58	3.93	2.32	3.71	5.09	8.12	4.35	5.05	10.85	3.02	4.71	6.91	2.72	3.24
Eu	2.08	1.84	1.66	0.82	1.56	1.33	0.89	1.22	1.88	2.49	1.45	1.68	2.93	1.10	1.47	2.20	1.02	1.20
Gd	7.52	6.84	5.55	3.01	5.42	4.51	2.76	4.16	5.41	6.98	4.46	5.27	10.02	3.51	4.86	7.39	3.27	3.99
Tb	1.33	1.12	0.87	0.51	0.95	0.79	0.50	0.73	0.90	1.11	0.75	0.99	1.47	0.60	0.82	1.32	0.57	0.68
Dy	8.17	6.80	5.22	3.12	5.63	4.61	3.10	4.37	5.44	6.31	4.47	6.23	8.26	3.75	5.01	8.56	3.68	4.51
Ho	1.62	1.28	1.06	0.68	1.22	0.99	0.69	0.93	1.15	1.20	0.98	1.24	1.60	0.81	1.08	1.88	0.82	1.04
Er	4.76	3.73	2.96	1.90	3.39	2.75	2.12	2.56	3.23	3.19	2.44	3.71	4.22	2.28	2.92	5.03	2.36	2.89
Tm	0.70	0.52	0.42	0.30	0.52	0.42	0.29	0.38	0.48	0.45	0.34	0.57	0.61	0.34	0.41	0.70	0.36	0.41
Yb	4.52	3.34	2.67	1.97	3.53	2.61	1.96	2.54	3.11	2.89	2.31	3.45	3.90	2.20	2.67	4.97	2.31	2.81
Lu	0.63	0.49	0.39	0.29	0.54	0.42	0.29	0.37	0.45	0.44	0.35	0.55	0.55	0.32	0.43	0.74	0.35	0.41
Hf	4.78	4.60	3.68	1.27	3.54	2.77	1.44	2.47	4.13	4.68	2.83	3.49	7.64	2.10	2.78	5.19	1.59	2.36
Ta	1.03	0.76	0.82	0.26	0.64	0.54	0.24	0.52	0.72	1.27	0.64	0.66	1.55	0.41	0.50	0.98	0.30	0.34
Pb	4.04	5.81	3.26	1.49	6.50	1.84	1.08	3.35	3.78	3.65	1.92	2.63	4.89	1.73	3.07	6.66	1.03	1.88
Th	2.83	3.80	2.12	0.50	3.47	0.90	0.42	0.90	1.88	4.52	1.19	1.73	7.92	1.00	1.61	3.88	0.60	1.04
U	0.71	0.93	0.54	0.14	0.79	0.24	0.11	0.24	0.49	1.10	0.29	0.46	1.92	0.28	0.40	0.87	0.16	0.29

Major element oxides in wt%; trace elements in ppm. Sample numbers refer to GEUS databases. Dyke localities shown in Fig. A1 (appendix).

Perkin-Elmer ELAN 500 inductively coupled plasma mass spectrometer (ICP-MS). Samples were prepared for analyses using the method described by Jenner *et al.* (1990) with the exception that we utilised microwave digestion bombs to insure total dissolution.

Table 1 presents representative major and trace element data for the Kangâmiut dykes, and Figs 4 and 5 show these data in covariation diagrams. The full data set is available upon request from the first author. The Kangâmiut dykes cover a range from 9.0–0.9 wt% MgO and the majority of the dykes would be classified as medium-K basalts or low-K basalts based on their K_2O and SiO_2 contents (Le Maitre 2002). First order observations of the major and compatible trace element data, as described below, indicate that the differentiation of the parental magma(s) of the Kangâmiut dykes was influenced by the fractionation of plagioclase, clinopyroxene, late stage Fe-Ti oxides and possibly olivine. First order observations based on covariation diagrams neither support nor refute the involvement of hornblende as a fractionating phase.

Figure 4C shows Al_2O_3 concentrations that range between 11.4 and 15.8 wt%. The highest MgO sample has a low Al_2O_3 concentration, whereas the next group of dykes at *c.* 7.0–7.5 wt% MgO have higher concentrations of Al_2O_3. This increase of Al_2O_3 between *c.* 9 and 7 wt% MgO likely reflects olivine and/or clinopyroxene fractionation. Clustering of data between 7.5 and 4.5 wt% MgO defines a trend of decreasing Al_2O_3 with decreasing MgO, indicative of plagioclase fractionation. The initial increase in total FeO ($FeO + 0.9 \times Fe_2O_3$) between *c.* 8.0 and 4.5

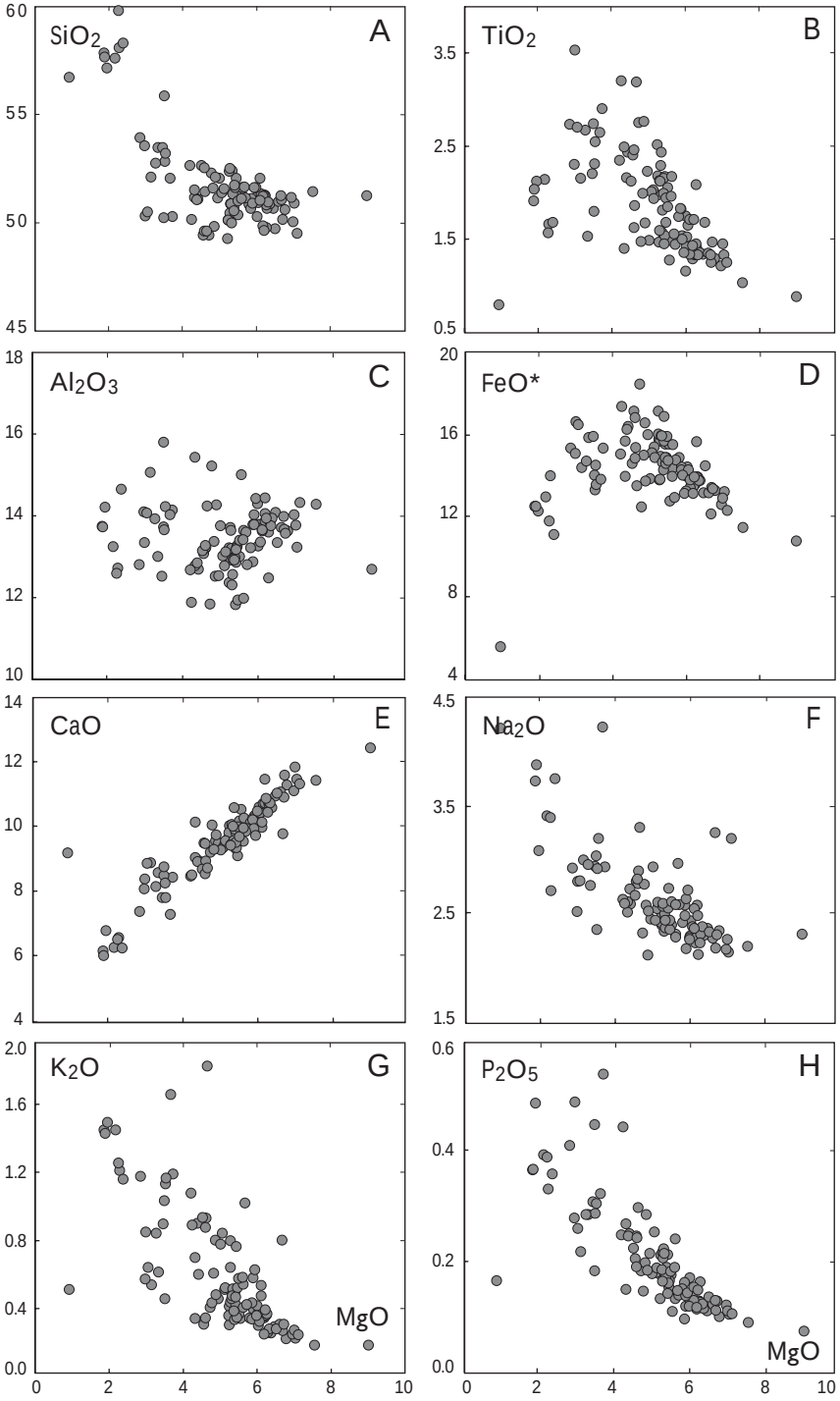

Fig. 4. Variations of SiO_2, TiO_2, Al_2O_3, FeO, CaO, Na_2O, K_2O, P_2O_5 with MgO (in wt%) for the Kangâmiut dykes. All analyses are recalculated on an anhydrous basis with all iron as FeO.

wt% MgO is also indicative of plagioclase fractionation (Fig. 4D).

Figure 4E shows that CaO ranges from 12.4 to 6.0 wt% and correlates positively with MgO, indicating that clinopyroxene and/or plagioclase was part of the fractionating assemblage. Figure 6 shows the CaO/Al_2O_3 ratio for the Kangâmiut dykes decreases with decreasing MgO, and Fig. 5A shows decreasing Sc with increasing Zr. Both of these observations further indicate that clinopyroxene was a fractionating phase. The decrease in nickel with increasing zirconium, shown in Fig. 5C, is related to clinopyroxene and/or olivine fractionation.

Figure 4B shows TiO_2 concentrations that range from 0.9–3.5 wt% with trends that show increasing TiO_2 from 9–4.5 wt% MgO that changes to decreasing TiO_2 below *c.* 4.5 wt% MgO. Figure 4D shows that a similar trend is

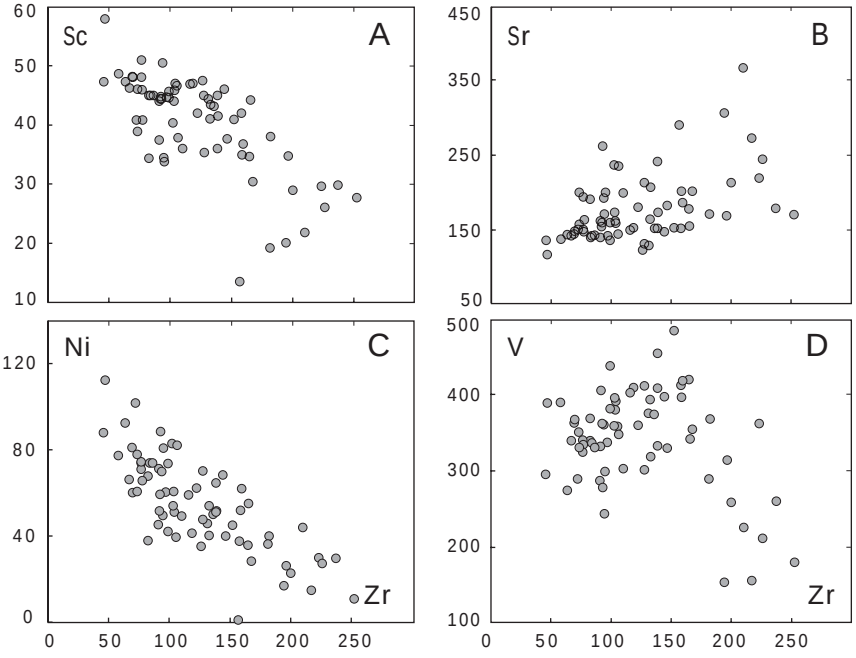

Fig. 5. Variation of Sc, Sr, Ni, and V with Zr (in ppm) for the Kangâmiut dykes.

observed for total FeO. Additionally, vanadium (Fig. 5D) shows an initial increase, then decrease with increasing zirconium. These changes from increasing to decreasing TiO_2, FeO and vanadium concentrations suggest Fe-Ti oxides fractionated when the magmas reached *c.* 4.5 wt% MgO.

Mineral chemistry

Major element compositions of pyroxenes, plagioclase, and hornblende were acquired using a Cameca SX-50 microprobe at the University of California-Davis. Analyses were made using a 15 kV accelerating voltage, a 10 nA beam current, and a 1 µm beam. Elements were calibrated using mineral standards. The data in Tables 2–4 give the compositions of clinopyroxene, plagioclase, and hornblende phenocrysts from chilled margins.

Table 2 presents major and minor element compositions of clinopyroxene phenocrysts from chilled margins based on the average of 2–4 spot analyses of 4–7 grains per sample. The proportions of enstatite, ferrosilite, and wollastonite components are 0.48–0.52, 0.13–0.23, and 0.28–0.35, respectively. Al_2O_3 concentrations range from 3.93–2.75 wt%, while Na_2O varies from 0.36–0.26 wt%.

Table 3 presents plagioclase phenocryst compositions from chilled margins. Plagioclase phenocryst cores have an anorthite (An) component range of An_{69}–An_{55}. Table 4 presents compositions of the hornblendes found in the chilled margins of some Kangâmiut dykes. They would be classified as ferrohornblende and ferrotschermakite based on the classification of Leake *et al.* (1997).

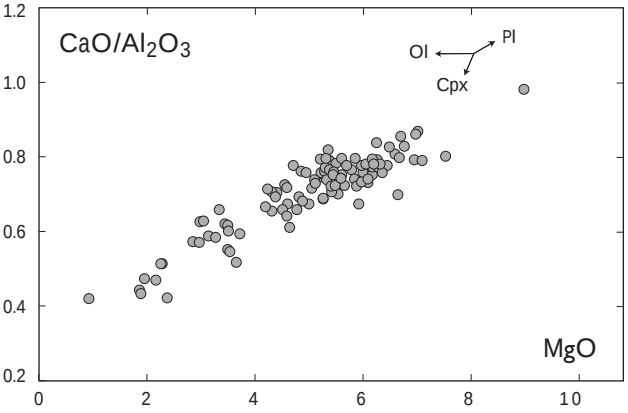

Fig. 6. Variation of CaO/Al_2O_3 with MgO. Arrows show path caused by fractionation of olivine, clinopyroxene, or plagioclase from a starting composition with 9 wt% MgO and Ca/Al_2O_3 = 1.0.

Whole-rock and mineral compositions in projection space

Figure 7 shows pseudo-ternary projections of whole-rock and mineral data for the Kangâmiut dykes. The components CPX, PLAG, OL, and QTZ were calculated using major and minor elements and the scheme of Tormey *et al.* (1987). In the projection from QTZ (Fig. 7A), the dyke data form a cluster that is displaced from the centre

Table 2. Microprobe analyses of clinopyroxene phenocrysts from chilled margins

Sample	430988	432108	432145	432148	432158	430211	430267	430283
Dyke	45	60	76	77	75	82	84	85
	n = 7	n = 8	n = 6	n = 8	n = 8	n = 8	n = 10	n = 10
SiO_2	52.34	50.68	51.88	51.17	52.01	51.36	51.85	51.59
TiO_2	0.47	0.65	0.44	0.61	0.45	0.34	0.44	0.60
Al_2O_3	3.17	3.93	3.14	3.21	3.34	2.75	3.63	2.68
Cr_2O_3	0.11	0.19	0.18	0.21	0.22	0.08	0.18	0.07
FeO	8.29	9.83	8.76	12.45	9.43	13.79	9.72	12.94
MgO	16.46	15.18	15.70	15.62	15.54	16.94	15.62	15.37
CaO	19.59	19.18	18.96	16.16	19.01	14.32	18.01	16.52
Na_2O	0.29	0.32	0.26	0.29	0.28	0.36	0.31	0.26
Sum	100.72	99.96	99.31	99.72	100.28	99.94	99.76	100.03
Si	1.917	1.886	1.927	1.913	1.920	1.922	1.920	1.928
Al(IV)	0.083	0.114	0.073	0.087	0.080	0.078	0.080	0.072
Al(VI)	0.053	0.058	0.065	0.055	0.065	0.074	0.079	0.046
Ti	0.013	0.018	0.012	0.017	0.012	0.011	0.012	0.017
Cr	0.003	0.006	0.005	0.006	0.007	0.001	0.005	0.002
Fe^{3+}*	0.022	0.039	0.000	0.013	0.004	0.016	0.000	0.010
Fe^{2+}	0.232	0.266	0.274	0.377	0.287	0.401	0.308	0.395
Mn	0.000	0.000	0.000	0.000	0.000	0.000	0.000	0.000
Mg	0.899	0.842	0.870	0.871	0.855	0.858	0.862	0.856
Ca	0.768	0.765	0.755	0.647	0.752	0.611	0.715	0.661
Na	0.021	0.025	0.020	0.021	0.020	0.036	0.022	0.019
K	0.000	0.000	0.000	0.000	0.000	0.000	0.000	0.000
Total	4.011	4.020	4.001	4.006	4.002	4.008	3.996	4.005
Mg#	0.78	0.73	0.76	0.69	0.75	0.67	0.74	0.68
Wo	0.35	0.34	0.35	0.29	0.34	0.28	0.33	0.30
En	0.52	0.51	0.50	0.50	0.49	0.49	0.50	0.48
Fs	0.13	0.16	0.16	0.22	0.17	0.23	0.18	0.22

Oxides in wt%; n = number of grains. Fe^{3+}* calculated using the method of Papike *et al.* (1974). Dyke localities shown in Fig. A1 (appendix).

Table 3. Microprobe analyses of plagioclase phenocrysts from chilled margins

Sample	430988	432108	432145	432148	432158	430211
Dyke	45	60	76	77	75	82
	n = 8	n = 8	n = 8	n = 8	n = 7	n = 8
SiO_2	52.18	49.74	53.36	53.79	51.23	54.13
$Al2O_3$	30.45	31.49	29.65	29.65	30.91	29.03
FeO	0.65	0.57	0.59	0.74	0.96	0.92
CaO	13.11	14.13	12.43	12.23	13.34	11.24
Na_2O	4.02	3.36	4.33	4.64	3.89	4.84
K_2O	0.05	0.05	0.09	0.07	0.09	0.17
Sum	100.46	99.34	100.45	101.12	100.41	100.34
Ab	35	30	38	40	34	43
An	64	69	61	59	65	55
Or	0.3	0.3	0.5	0.4	0.5	1.0

Oxides in wt%; n = number of grains. Dyke localities shown in Fig. A1 (appendix).

of the ternary plot towards the PLAG apex. In this projection all the dykes lie within the phase volumes defined by the joins between olivine, clinopyroxene and plagioclase (Ol:Cpx:Pl) or hornblende, clinopyroxene and plagioclase (Hbl:Cpx:Pl). In the projection from the CPX component (Fig. 7B), the dykes define an array that projects away from both the Pl:Ol and the Pl:Hbl joins. Similarly, in the projection from the PLAG component (Fig. 7C), the dykes form an array that intersects both the Cpx:Ol and Cpx:Hbl joins. These observations show that plagioclase, clinopyroxene and either olivine or hornblende were co-fractionating phases.

A and C in Fig. 7 also show experimentally determined 1 atm and 0.8 GPa Ol:Cpx:Pl cotectics derived from melting experiments using a primitive Kangâmiut dyke (dyke #45) as the starting material (Mayborn 2000). The whole-rock data form a cluster near the low pressure Ol:Cpx:Pl cotectic in the projection from the QTZ component. Similarly, in the projection from the PLAG component the whole-rock data also plot close to the low-pressure cotectic.

Incompatible trace element behaviour

Figure 8 shows representative chondrite normalised rare-earth element (REE) patterns for the Kangâmiut dykes. The dykes are slightly light rare-earth element (LREE) enriched with a La/Sm_N ratio ranging from 1.16 to 2.50, with an average of 1.50. The heavy rare-earth (HREE) patterns have shallow slopes with a Dy/Yb_N range of 1.05

Table 4. Microprobe analyses of amphiboles from chilled margins

Sample	432158	430267	430283
Dyke	75	84	85
	n = 12	n = 14	n = 6
SiO_2	43.90	42.63	40.88
TiO_2	1.04	1.92	1.64
Al_2O_3	10.69	10.05	9.98
FeO	21.09	21.73	24.02
MnO	0.22	0.19	0.21
MgO	8.09	8.05	6.44
CaO	10.93	10.78	10.58
Na_2O	1.18	1.63	1.58
K_2O	0.99	0.90	0.90
Cl	0.57	0.67	0.65
F	0.09	0.05	0.14
Sum	98.79	98.60	97.02
Si	6.549	6.425	6.346
Ti	0.117	0.218	0.192
Al(IV)	1.451	1.575	1.654
Al(VI)	0.427	0.209	0.172
Fe^{3+}	0.767	0.799	0.922
Fe^{2+}	1.864	1.940	2.196
Mn	0.027	0.025	0.027
Mg	1.798	1.809	1.491
Ca	1.747	1.741	1.760
Na(M4)	0.253	0.259	0.240
Na(a)	0.089	0.217	0.237
K(a)	0.189	0.172	0.178
Total	15.28	15.39	15.41

Oxides, Cl and F in wt%. Dyke localities shown in Fig. A1 (appendix).

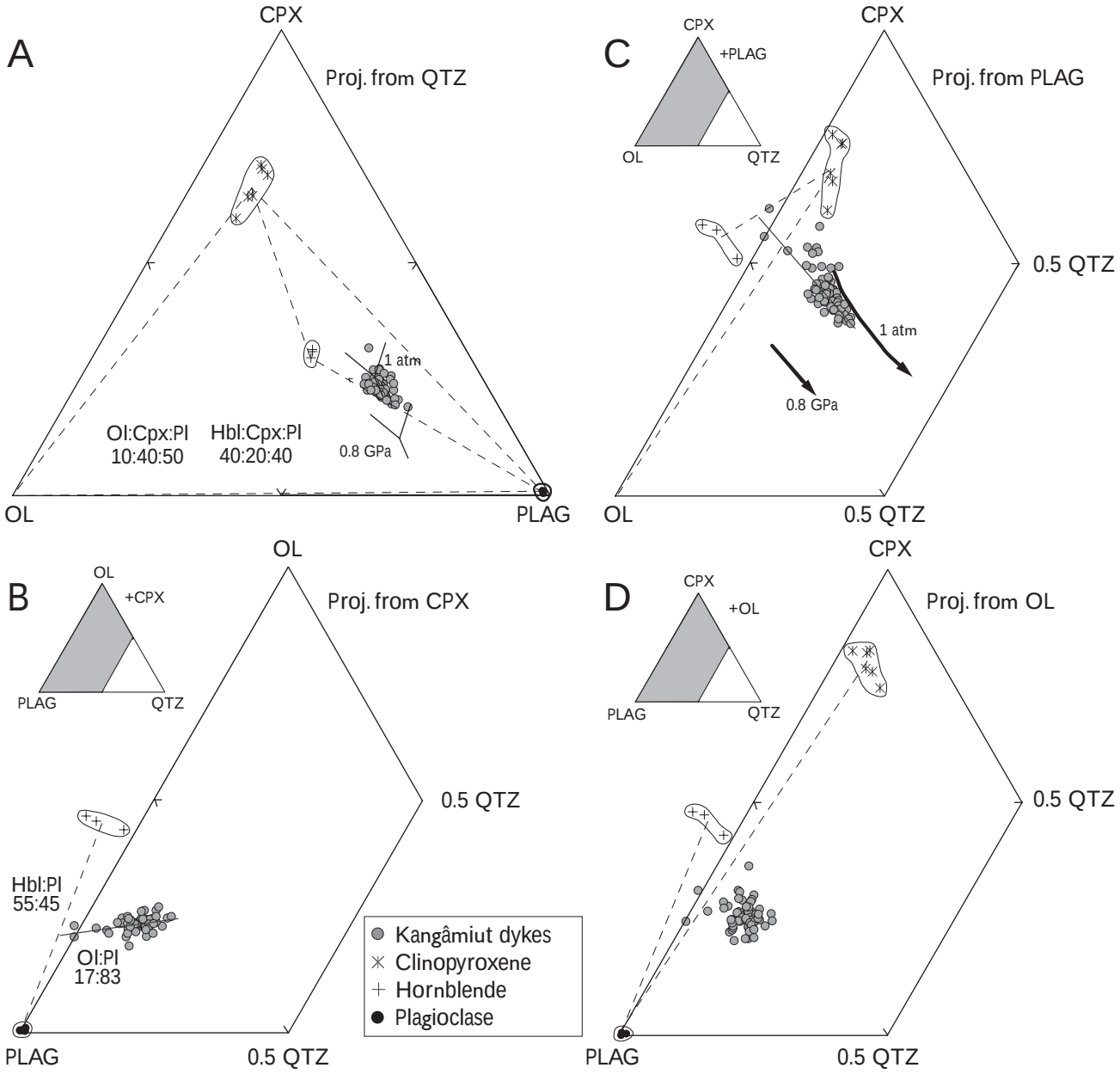

Fig. 7. Pseudo-ternary projections of whole-rock and mineral compositions from the Kangâmiut dykes using the projection scheme of Tormey *et al*. (1987). Dashed lines connect possible crystallisation assemblages. Solid lines through data show the trend of Kangâmiut dykes where this is well defined, and the locations of the olivine:clinopyroxene:plagioclase cotectics at 0.8 GPa and 1 atm. A: Projection from the QTZ component. B: Projection from the CPX component. C: Projection from the PLAG component. D: Projection from the OL component.

to 1.46 and an average of 1.15. The two most LREE-enriched samples come from sheared dioritic centres and have Dy/Yb_N ratios of 1.46 and 1.42, respectively. The patterns for the sheared dioritic centres cross-cut the patterns for non-sheared dykes.

Figure 9A shows incompatible trace elements for the Kangâmiut dykes on primitive mantle normalised compatibility diagrams (Thompson 1982). The elements on the right hand side of Fig. 9A are moderately incompatible, with incompatibility increasing towards the left using the element order from Sun & McDonough (1989). The most primitive Kangâmiut dykes have the lowest concentration of incompatible elements and have flat patterns with small negative Nb and Zr anomalies. The negative Sr anomaly seen in the more evolved samples reflects plagioclase fractionation. The two most evolved samples

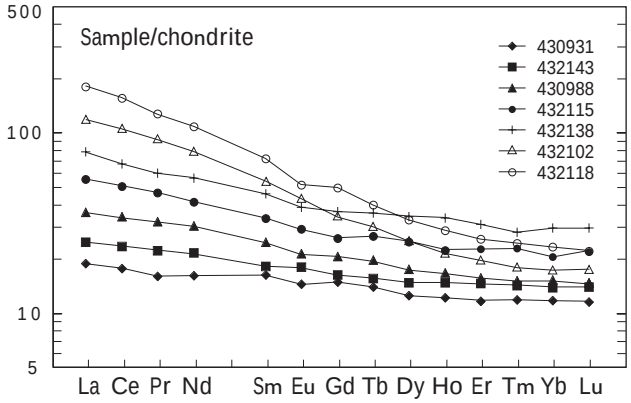

Fig. 8. Rare-earth element compositions of representative Kangâmiut dykes normalised to C1 chondrite. Chondrite normalising values from Sun & McDonough (1989).

(432102 and 432118) are sheared dioritic centres and display negative Ti anomalies. They also show a depletion of HREE, as noted in Fig. 8.

Figure 9B shows representative patterns for basalts from a variety of tectonic settings and a pattern representing the average of Kangâmiut dykes with MgO > 6 wt%. Notable features in the Kangâmiut pattern are a smooth, slightly increasing trend from right to left through the moderately incompatible elements (Lu to Sm), small negative anomalies of Nb, Sr, and Zr, and a relatively flat trend for Th, Ba and Rb. The Kangâmiut dyke pattern is distinct relative to the ocean island basalt (OIB), mid-ocean ridge basalt (MORB), island arc basalt (IAB), and continental arc basalt (CAB) patterns. For example, the Kangâmiut dykes do not display the enrichment of highly incompatible elements, or the positive Nb anomaly seen in the OIB pattern, or depletions seen in the MORB pattern. Relative to IAB and CAB, the Kangâmiut dyke patterns do not exhibit the large negative Nb anomaly or the positive Sr anomaly. Overall, the Kangâmiut dyke pattern most closely resembles the pattern for continental flood basalts (CFB), including the shallow slope of the pattern, and the small negative Nb and Sr anomalies.

Discussion

Tectonic setting

One of the primary goals of this study is to constrain the tectonic environment during emplacement of the Kangâmiut dykes. Experimental melting studies over the past 40 years have shown that basalts are products of partial melting of peridotite (Reay & Harris 1964; Takahashi 1986; Baker & Stolper 1994). Since the dominant source of peridotite is the mantle, then the basaltic nature of the Kangâmiut dykes indicates that they resulted from partial melting of mantle peridotite followed by intracrustal differentiation. Three settings where mantle melting occurs beneath continental crust are (1) subduction zones, (2) active rifts associated with mantle plumes, and (3) passive rift settings. Each of these settings can have distinctive mantle compositions and conditions for melting

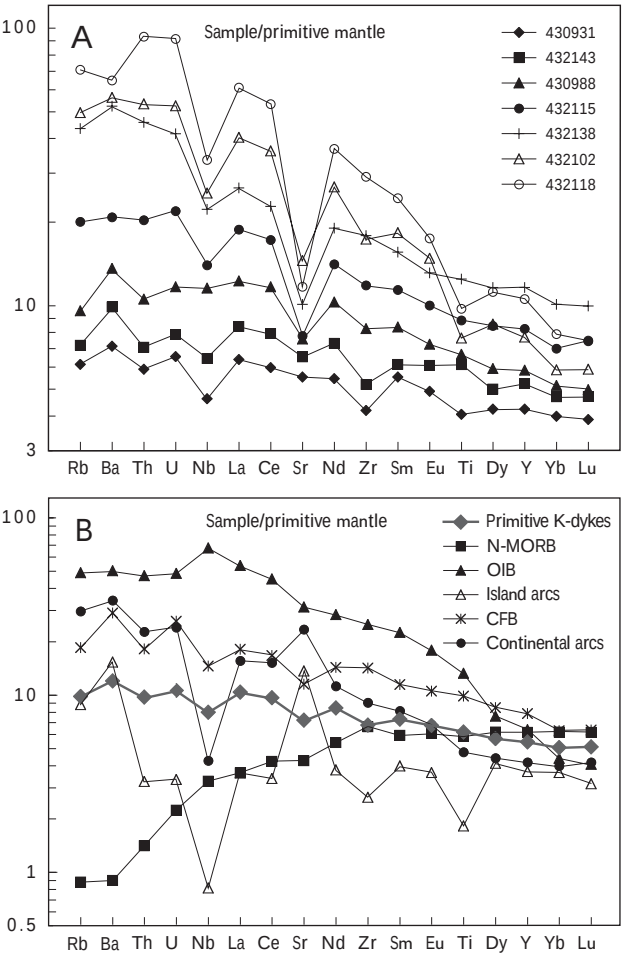

Fig. 9. A: Normalised incompatible trace element compositions of representative Kangâmiut dykes. B: Comparison of the Kangâmiut dykes with normal mid-ocean ridge basalts (N-MORB), ocean-island basalts (OIB), island arc basalts, continental flood basalts (CFB), and continental arcs. Representative 'Primitive Kangâmiut dykes' is the average composition of 18 Kangâmiut dykes with a MgO range of 8.9–6.1 wt%. Data for N-MORB and OIB are from Sun & McDonough (1989). Island arc data compiled from Bailey *et al.* (1989), Pearce *et al.* (1995), and Gust *et al.* (1997). CFB data compiled from Hooper & Hawkesworth (1993), Lightfoot *et al.* (1993), Wooden *et al.* (1993), Peate & Hawkesworth (1996) and Storey *et al.* (1997). Continental arc data compiled from Tormey *et al.* (1991) and Bacon *et al.* (1997).

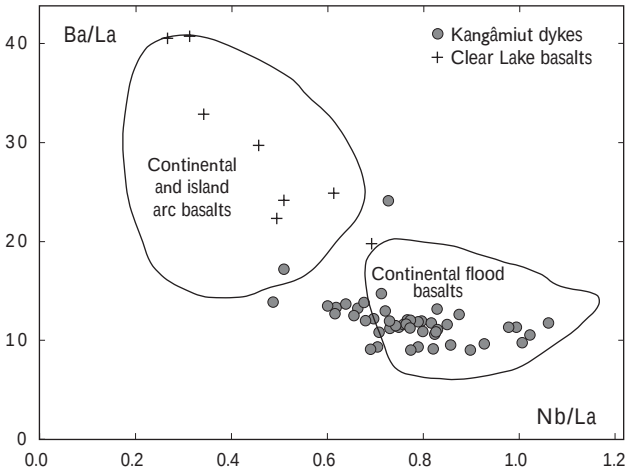

Fig. 10. Ba/La versus Nb/La showing the differences between arc basalts, the Kangâmiut dykes, and basalts from the Clear Lake Volcanic Field. Data for the arc field are from Bailey *et al.* (1989), Tormey *et al.* (1991), Francalanci *et al.* (1993), Pearce *et al.* (1995), Bacon *et al.* 1997), Gust *et al.* (1997), and Kelemen *et al.* (2003). Data for the continental flood basalt field are from Hooper & Hawkesworth (1993), Lightfoot *et al.* (1993), Wooden *et al.* (1993), Peate & Hawkesworth (1996), and Storey *et al.* (1997). Data for the Clear Lake Volcanic Field are from Charles Lesher (unpublished data).

that are reflected in the trace element compositions of the associated basalts.

The Kangâmiut dykes have evolved compositions with a Mg-number (defined as 100Mg/(Mg + Fe) on a molecular basis) range of 0.60–0.21. Magmas in equilibrium with mantle peridotite will have a Mg-number close to 0.71 (Roeder & Emslie 1970; Langmuir *et al.* 1992) showing that even the most primitive Kangâmiut dykes represent somewhat evolved magmas. Thus, the major elements reflect both the fractionation and mantle melting histories. However, most incompatible trace element ratios remain relatively constant during crystallisation and can be used to constrain primary source characteristics. The following discussion examines some characteristics of the mantle source and the conditions of mantle melting revealed by examining incompatible trace elements from the more primitive dyke samples (with MgO > 4.5 wt%).

Subduction hypothesis for generation of Kangâmiut dykes

Subduction environments generate basaltic melts by two different mechanisms of partial melting. The first is melting induced by lowering the solidus temperature of the peridotite by the introduction of volatiles from the subducting slab and subsequent decompression melting within the mantle wedge (Jakes & Gill 1970; Tatsumi 1989; Arculus 1994). The second is decompression melting associated with back-arc spreading (Tatsumi *et al.* 1989; Gribble *et al.* 1998). Although the mechanisms of melting in these settings are different from each other, they both produce magmas with a compositional 'subduction component' that is indicative of a hydrated and metasomatised mantle. Some important characteristics of subduction zone basalts are HFSE depletions, LILE enrichment, and high Al_2O_3. The available data can be used to evaluate the subduction hypothesis for the Kangâmiut dyke swarm implied by Escher *et al.* (1976) and Bridgwater *et al.* (1995), and explicitly proposed by Cadman *et al.* (2001).

As shown in Fig. 9B, arc basalts have distinctive depletions in HFSE. These HFSE depletions occur in Palaeozoic, Proterozoic, and Archaean arc-related basalts, suggesting that modern style subduction occurred in the Archaean (Stern *et al.* 1994; Blichert-Toft *et al.* 1995). In addition to HFSE depletions, arc basalts are enriched in LILE (e.g. Pb, K, Ba, Rb, and Cs) relative to basalts from other tectonic settings. This enrichment is proposed to

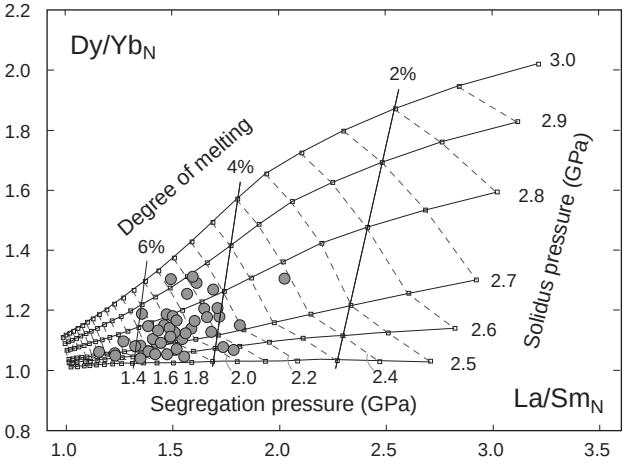

Fig. 11. Chondrite-normalised DyYb versus La/Sm ratios for the Kangâmiut dykes and mantle melting models using the algorithm of Fram & Lesher (1993) based on a 0.5% depleted PM source composition, where F is the melt proportion. The model assumes partial melting proceeds by incremental non-modal batch melting at 1% per kbar of decompression in a corner flow melting regime. Melts are pooled after each kbar of decompression. REE distribution coefficients are taken from Green (1994). The garnet-spinel transition is modelled as a gradual change between 30 and 25 kbar. The spinel–plagioclase transition is modelled as a gradual change between 14 and 10 kbar. Residues are recalculated after each melting increment and adjusted for pressure dependent phase transitions using melting reactions as given by Fram & Lesher (1993). Model curves, for melting starting at 3.0, 2.9, 2.8, 2.7, 2.6 and 2.5 GPa and ending at 0.5 GPa, define a melting grid, where solid subvertical lines contour constant mean melt fraction, whereas the dashed subvertical lines contour final pooled melt segregation pressure (i.e. the top of the melting column). Slightly modified from Mayborn & Lesher (2004).

occurduring the flux of fluids from the slab into the mantle wedge (Miller *et al.* 1994; Pearce *et al.* 1995; Becker *et al.* 1999). Mafic rock suites in volcanic arc settings also typically contain a large proportion of high-alumina basalts (Perfit *et al.* 1980; Brophy & Marsh 1986; Kelemen *et al.* 2003).

If the Kangâmiut dykes are arc-related, they should show LILE enrichment, HFSE depletions, and high Al_2O_3. Figure 10 shows a comparison of the Nb/La and Ba/La ratios for the Kangâmiut dykes, island arcs, continental arcs, and continental flood basalts. Relative to arc basalts, the Kangâmiut dykes have lower Ba/La and Nb/La ratios – unlike arc-related basalts. Additionally, subduction zone basalts typically have Al_2O_3 contents of 19–15 wt% (Plank & Langmuir 1988, 1992; Kelemen *et al.* 2003), whereas all of the Kangâmiut dykes have lower Al_2O_3 concentrations (16–12 wt%). Thus, the Kangâmiut dykes have none of the geochemical characteristics of subduction related basalts, contrary to previous conjecture (Cadman *et al.* 2001).

A more detailed analysis of the Cadman *et al.* (2001) hypothesis also raises significant questions about its viability. Cadman *et al.* (2001) propose that the Kangâmiut dykes formed after ridge subduction resulting in a 'slab window' passing beneath metasomatised mantle. The resulting mantle upwelling lead to melting within hydrated mantle wedge material. Although Cadman *et al.*'s hypothesis would explain elevated water contents postulated for Kangâmiut dyke magmas, such an origin would also be expected to impart an arc geochemical signature to the magmas. It is instructive to directly compare the composition of the Kangâmiut dykes with those from the Clear Lake Volcanic Field located in the coastal region of northern California and associated with the development of a slab window after passage of the Mendocino Triple Junction (Furlong & Schwartz 2004). Figure 10 compares the Ba/La and Nb/La ratios for Clear Lake basalts, with typical arc basalts, the Kangâmiut dykes and continental flood basalts. It is evident from these, among other, geochemical indices that the Kangâmiut dykes lack the expected arc signature postulated by Cadman *et al.* (2001). Rather the Kangâmiut dykes have compositions consistent with their derivation from asthenospheric mantle supplying normal continental flood basalts.

Active rifting, plume and passive rifting hypotheses

The temperature of the mantle is an important difference between plume associated rifting and passive rifting. Mayborn & Lesher (2004) presented a detailed analysis of the

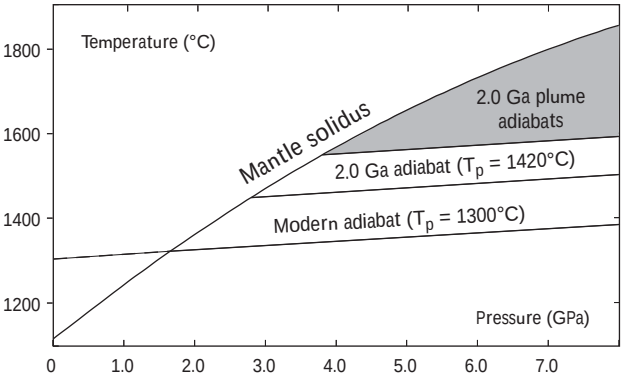

Fig. 12. Plot showing the fertile peridotite solidus and adiabats for modern mantle, 2.0 Ga mantle, and plume mantle associated with potential temperatures of 100 to 300°C greater than 2.0 Ga mantle. Pressures and temperatures for the fertile peridotite from Hirschmann (2000). Slightly modified from Mayborn & Lesher (2004).

temperature of the mantle during Kangâmiut dyke magma genesis as constrained by REE systematics. They used the algorithm of Fram & Lesher (1993), as shown in Fig. 11, to propose that the Kangâmiut dykes are the results of mantle melting with a mean solidus pressure of *c.* 2.75 GPa and a mean extent of melting of 5%. When compared to the solidus for nominally anhydrous mantle (Fig. 12), this mean solidus temperature would correspond with a potential mantle temperature of 1420°C. This temperature estimate falls at the lower end of potential temperatures estimated for *c.* 2.0 Ga mantle by Richter (1984, 1420–1600°C) and Abbott *et al.* (1994, 1380–1680°C) based on secular cooling models and geochemical data for Precambrian MORB-type basalts, respectively. Addition-

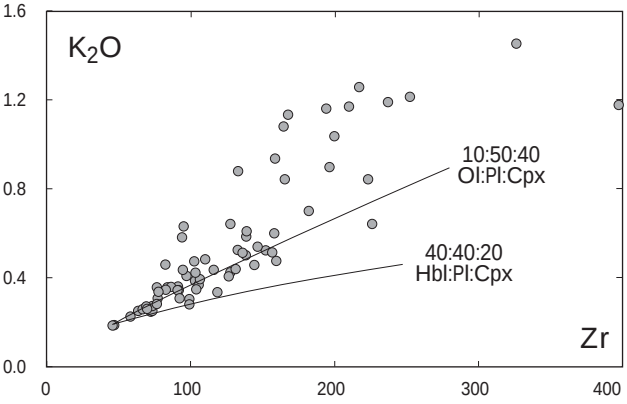

Fig. 13. Variation of K_2O (in wt%) with Zr (in ppm) for the Kangâmiut dykes. Solid lines show results of fractional crystallisation models using mineral proportions of 10:50:40 Ol:Pl:Cpx and 40:40:20 Hbl:Pl:Cpx. The model starting composition is the sample with lowest K_2O and Zr, which are 0.19 wt% K_2O and 47 ppm Zr. Based on Cadman *et al.* (2001).

ally, an ambient mantle potential temperature of 1420°C at 2.0 Ga. is consistent with constraints from continental freeboard that suggests that mantle temperatures were below 1430°C by the mid-Archaean (Galer 1991). Thus, the 1420°C mantle temperature for the Kangâmiut dykes is consistent with ambient mantle temperatures for that time, reducing the need for anomalously high potential temperatures commonly associated with plume magmatism. The explanation that best fits both the geochemical and field data is that the Kangâmiut dykes formed by decompression melting in a rift environment under ambient mantle conditions. This conclusion implies that the dykes are the products of rifting of Kenorland supercontinent between 2.1 and 2.0 Ga (Williams *et al.* 1991). The implications of these findings for the temperature of the Palaeoproterozoic mantle, the occurrence of Palaeoproterozoic mantle plumes, and for Palaeoproterozoic continental crustal growth are discussed in Mayborn & Lesher (2004).

Fractionation of the Kangâmiut dykes

As noted previously, the range in Mg-number (0.60–0.21) of the Kangâmiut dykes shows that they are not in equilibrium with mantle peridotite and do not represent direct mantle melts. Thus, even the most primitive sampled Kangâmiut dyke represents an evolved magma. First order observations of the whole-rock and mineral data show that the dykes evolved by Ol:Cpx:Pl or Hbl:Cpx:Pl fractionation with the late-stage introduction of Fe-Ti oxides into the fractionating assemblage. Windley (1970) and Bridgwater *et al.* (1995) proposed that hornblende was a primary crystallising phase from the Kangâmiut dyke magmas partly based on the occurrence of large hornblende crystals in chilled margins. However, our petrographical studies of the chilled margins show that these amphiboles grew *in situ* during the final stage of solidification (see Fig. 3). This does not preclude the possibility that hornblende was a stable and fractionating phase at depth and thus influenced the composition of evolved Kangâmiut dyke magmas prior to their emplacement.

The main difference between Hbl:Cpx:Pl and Ol:Cpx:Pl crystallisation to explain the magmatic evolution of the dykes is the relative cotectic proportions of hornblende and olivine. In the projection from QTZ (Fig. 6A) the dyke compositions lie within both the Hbl:Cpx:Pl and Ol:Cpx:Pl phase volumes. If hornblende is a fractionating phase its cotectic proportion would be *c.* 0.40 (based on the projections from QTZ, CPX, and PLAG), with plagioclase and clinopyroxene at 0.40 and 0.20, respectively. If olivine, and not hornblende, is a fractionating phase, the cotectic proportions would be *c.* 0.10 olivine, 0.50 plagioclase, and 0.40 clinopyroxene.

These different cotectic proportions can be used to determine if hornblende or olivine was a fractionating phase by examining the partitioning behaviour of potassium. Experimentally determined amphibole-basaltic melt Kds for potassium range between 1 and 2 (Green 1994). In contrast, the olivine-basaltic melt Kd is *c.* 0.0005 (Green 1994) for potassium between olivine and basaltic liquid. Figure 13 shows the results of fractional crystallisation modelling for K_2O and Zr. The cotectic assemblage 40:40:20 Hbl:Cpx:Pl gives a bulk distribution coefficient (D) of 0.52 for K and 0.094 for Zr. The olivine-bearing assemblage, 10:50:40 Ol:Cpx:Pl, gives a bulk D of 0.16 for K and 0.026 for Zr. As shown in Fig. 13, the hornblende-bearing assemblage underestimates the concentration of K_2O and is not consistent with the trend defined by the dyke data, whereas the olivine-bearing assemblage provides a better fit to the data. Thus, these relationships show that the Kangâmiut dykes evolved by the fractionation of olivine, clinopyroxene, plagioclase and late stage Fe-Ti oxides, and that hornblende was not a significant fractionating phase at any stage of their evolution. Support for this conclusion comes from the 0.8 GPa melting experiments of Mayborn (2000) showing that the cotectic assemblage for a water-bearing Kangâmiut dyke starting material is olivine, clinopyroxene, and plagioclase, but no hornblende.

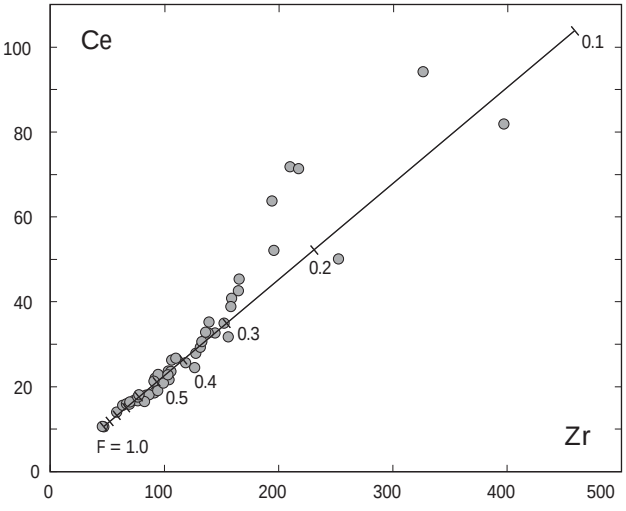

Fig. 14. Variation of Ce with Zr (in ppm) showing the results of a fractional crystallisation model where F is the melt proportion. Tic marks on model curve are drawn at 0.1 intervals of F.

Origin of water in the Kangâmiut dykes

Based on the presence of hornblende in the Kangâmiut dykes, Bridgwater *et al.* (1995) speculated that the parental magmas for the dykes were derived from a hydrous protolith during thrusting of an amphibolite facies terrain beneath the granulite facies terrain in the southern Nagssugtoqidian orogen. Although this model does offer an explanation for the proposed high water contents of the dykes, the presence of hornblende itself, often as reaction rims on clinopyroxene or poikilitic grains enclosing plagioclase and clinopyroxene, only argues for elevated water contents during final stages of crystallisation of the dykes. It is, therefore, possible that the high water contents sufficient to stabilise hornblende resulted solely from its enrichment during crystal fractionation.

The modal abundance of hornblende in dykes not affected by Nagssugtoqidian deformation is *c*. 5–20% for dolerites and 10–35% for dioritic centres. Since amphiboles contain *c*. 2 wt% water, these modes would indicate a whole-rock water concentration of 0.1 wt% in the primitive dolerites and 0.7 wt% in the more evolved dioritic centres. Whether these differences in concentrations between the primitive and evolved samples are related to enrichment during crystal-liquid fractionation can be evaluated using the following equation for fractional crystallisation:

$$C_L = C_0 \times F^{(D-1)} \qquad (1)$$

where C_0 is the initial concentration, C_L is the liquid concentration, F is the proportion of liquid, and D is the bulk distribution coefficient. Danyuschevsky *et al.* (2000) showed that in mafic systems water will have a bulk distribution coefficient of *c*. 0.01. Starting with a magma with 0.1 wt% (C_0) H_2O, representing the primitive dolerites, and ending with 0.7 wt% (C_L) H_2O, representing the evolved dioritic centres, requires 86% crystallisation (F = 0.14) of the primitive magma. Figure 14 shows the relative enrichment of highly incompatible elements Zr and Ce during fractional crystallisation, where Ce is used as a proxy for water given their similar incompatibilities (Danyuschevsky *et al.* 2000). The amount of fractionation required to relate the primitive samples to dioritic centres is 0.3–0.13, corresponding to 70–87% crystallisation. Thus, the evolved dykes reflect sufficient fractionation to explain the difference in water concentrations between the primitive dykes and dioritic centres.

The origin of the water in the primitive dykes can also be addressed using equation 1. The most primitive Kangâmiut dykes (MgO > 6 wt%) have a modal hornblende content of 5–10% indicating a maximum of 0.1–0.2 wt% water content in the rocks. This suggests that the amount of water in the parental magma derived from the mantle is less than 0.2 wt%. Equation 1 can also approximate fractional mantle melting and can help constrain the amount of water in the mantle source needed to produce a primitive magma containing 0.2 wt% H_2O. In this case, the unknown variable is C_0, the initial concentration in the mantle. The concentration in the liquid (C_L) is 0.2 wt%, and D is equal to 0.01. The evaluation of REE systematics, presented by Mayborn & Lesher (2004) and illustrated in Fig. 11, shows that the average F value for mantle melting leading to the Kangâmiut dykes was 0.05. Thus, using these values in equation 1 results in a concentration in the mantle source (C_0) of 0.01 wt% (100 ppm). This is well within the range of 28–300 ppm H_2O given by Bell & Rossman (1992) for the upper mantle containing nominally anhydrous phases. As such, the water present in the hornblende within the Kangâmiut dykes can be reasonably accounted for given estimates of its original concentration in primary melts and enrichment through subsequent differentiation. Although these considerations do not rule out Bridgwater *et al.*'s (1995) model for the Kangâmiut dykes derived from an amphibolite facies protolith, we show that differentiation of partial melts derived from depleted upper mantle can readily explain the occurrence of late crystallising hornblende in the evolved Kangâmiut magmas.

The Kangâmiut dykes and the Nagssugtoqidian orogeny

The preservation of both igneous and metamorphic features in the Kangâmiut dyke swarm provides an excellent opportunity to evaluate the amount of crustal thickening that likely occurred during the Nagssugtoqidian orogeny. Determining the amount of thickening requires knowledge of the depths associated with emplacement and peak metamorphism for currently exposed dykes.

Field relationships show brittle deformation of host rocks and segmentation of the Kangâmiut dykes into en échelon arrays during emplacement. Reches & Fink (1988) proposed that the segmentation of dykes into en échelon arrays occurs when they cross from the ductile into the brittle regime. In modern continental crust the brittle–ductile transition is observed as the seismic to aseismic transition at depths of 10–15 km (Chen & Molnar 1983). Chen & Molnar (1983) and Williams (1996) give temperature estimates for the brittle–ductile transition between 450 and 250°C.

Fahrig & Bridgwater (1976) presented Palaeomagnetic data from dykes and host rocks unaffected by Nagssugtoqidian metamorphism, and showed that the host rocks and dykes record different declinations. These differences in declination show that the host rocks were below their Curie temperature during dyke emplacement. Fahrig & Bridgwater (1976) do not discuss the magnetic carrier in the host rocks, but an examination of host rock samples suggests that the magnetic carrier(s) are magnetite and/or ilmenite. The Curie temperatures of these minerals vary due to solid solutions amongst magnetite-ulvöspinel and hematite-ilmenite, but the upper limit is 580°C if the magnetic carrier is pure magnetite.

Additional support for dyke emplacement into host rocks with temperatures below 580°C comes from $^{40}Ar/^{39}Ar$ dating of dykes and host rocks. Willigers *et al.* (1999) presented $^{40}Ar/^{39}Ar$ cooling ages from dykes in the southern foreland that gave a mean age of 2.02 Ga. This age is within error of the 2.04 Ga emplacement age determined by dating of igneous zircons (Nutman *et al.* 1999). The $^{40}Ar/^{39}Ar$ cooling age of a regional granitic host rock is 2.5 Ga (Willigers *et al.* 1999). This older age indicates that the host rocks have remained below 480°C, the closure temperature of argon in hornblende (Harrison 1981), since 2.5 Ga.

Field evidence of brittle deformation, Palaeomagnetic data, and $^{40}Ar/^{39}Ar$ cooling ages all indicates that the peak crustal temperatures of exposed basement hosting the Kangâmiut dykes were less than *c*. 450°C at the time of dyke emplacement. Estimates of the geothermal gradient appropriate for continental crust at 2.0 Ga can help to constrain the depth of the 450°C isotherm and thus the depth of dyke emplacement. The geotherm is computed from

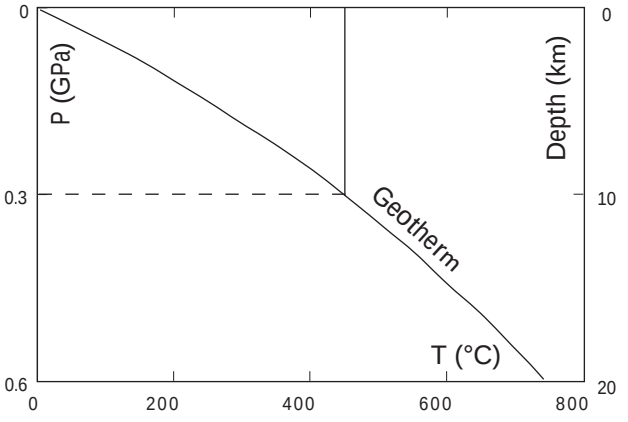

Fig. 15. Model continental geotherm constructed using the heat flow equation shown in text (equation 2). Solid vertical line represents the 450°C isotherm that intersects the geotherm at *c*. 0.3 GPa (10 km) as shown by dashed horizontal line.

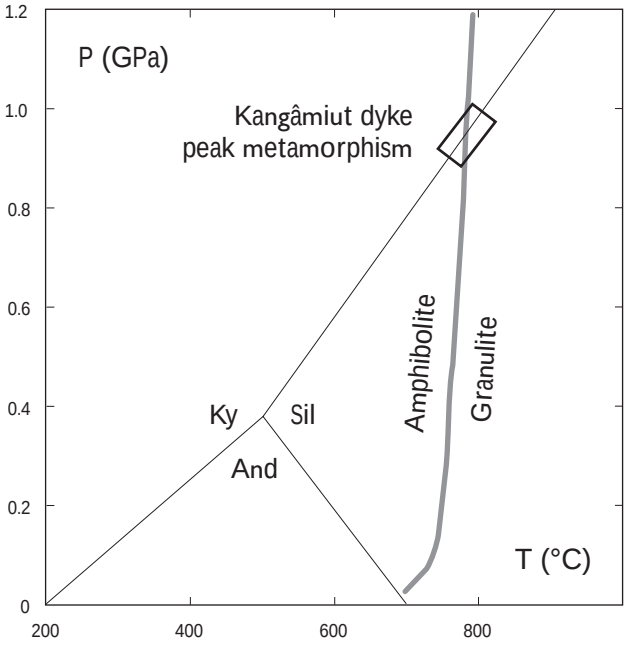

Fig. 16. Pressure versus temperature diagram showing the intersection of the amphibolite/granulite facies transition with the kyanite–sillimanite transition. The black rectangle around the intersection shows possible temperature and pressure ranges of peak metamorphism of the Kangâmiut dykes and metasediments in Ikertooq fjord. The Al_2SiO_5 phase diagram is from Holdaway (1971) and the amphibolite to granulite transition is based on the first occurrence of orthopyroxene in experiments on mafic rocks by Spear (1981).

the heat flow equation assuming an exponential distribution of heat producing elements that includes contributions from heat conduction, advection, and production (Carslaw & Jaeger 1959):

$$T = \frac{Q^* z}{k} + \frac{A^o D^2}{k}\left(1 - e^{-z/Hr}\right) \qquad (2)$$

where T is temperature in °C, Q* is the reduced heat flow at the crust-mantle boundary in mWm^{-2}, z is the depth in km, k is the thermal conductivity of the crust in $Wm^{-1}K^{-1}$, A^o is the concentration of heat producing elements at the earth's surface in μWm^{-3}, D is crustal thickness in km, and Hr is the length scale for the decrease in heat producing elements with depth in km. Current average values are Q = 30 mWm^{-2}, k = 2.25 $Wm^{-1}K^{-1}$, A^o = 0.75 μWm^{-3}, D = 35 km, and Hr = 15 km. The model geotherm shown in Fig. 15 uses these values with the exception of A^o = 1.2 to account for higher heat production during the Palaeoproterozoic and Archaean (Stein 1995). Using the geotherm in Fig. 15 and a maximum host rock tempera-

ture of 450°C require that the dykes intruded to a minimum depth of 10 km corresponding to a lithostatic pressure of *c*. 0.3 GPa. This estimate of a shallow emplacement level for the dykes is also supported by the clustering of whole-rock data near the low-pressure Ol:Cpx:Pl cotectics as previously shown in Fig. 7.

Application of the clinopyroxene geothermobarometry developed by Putirka *et al.* (1996) provides another independent estimate of the depth of dyke emplacement. This geothermobarometer uses compositions of clinopyroxenes and their host rocks to estimate the pressure and temperature of clinopyroxene crystallisation. There are two important assumptions when applying this geothermobarometer to chilled margins in the Kangâmiut dykes. First, we assume that the whole-rock composition is a close approximation of the original liquid composition. Second, we assume that the cores of the clinopyroxene phenocrysts were once in equilibrium with this liquid. One test of equilibrium between the whole-rock and clinopyroxene phenocrysts is given by the FeO/MgO ratios in the whole rocks and pyroxenes. The FeO/MgO ratios in the clinopyroxenes from eight chilled margins and the FeO/MgO ratio in their host rocks yield an average $K_D^{Fe\text{-}Mg}$ for clinopyroxene and liquid of 0.32 ± 4. Based on experimental work, $K_D^{Fe\text{-}Mg}$ for basaltic systems between 1 atm and 1.5 GPa ranges from 0.22–0.36 (Baker & Eggler 1987; Putirka *et al*. 1996). Our estimates for the Kangâmiut dykes fall within this range.

Applying the Putirka *et al.* (1996) geothermobarometer to clinopyroxene phenocrysts cores and whole-rock compositions from chilled margins of eight Kangâmiut dykes gives temperatures of 1199–1170°C and pressures of 0.75–0.35 GPa. The upper pressure limit of 0.75 GPa indicates a maximum recorded depth of fractionation recorded by clinopyroxene phenocrysts of *c*. 25 km. The lower pressure estimate of 0.35 GPa constrains a maximum emplacement depth of *c*. 12 km, since the clinopyroxene phenocrysts in the chilled margins must have formed at a depth greater or equal to the final depth of dyke emplacement. This is consistent with the preceding results from temperature estimates of the host rocks during emplacement that indicate a maximum of *c*. 0.3 GPa or a depth of *c*. 10 km.

If these independent estimates of the Kangâmiut dyke emplacement depths are taken as representative of the dyke swarm in general, then a consideration of peak metamorphic conditions during the Nagssugtoqidian orogeny can be used to constrain the amount of crustal thickening during orogenesis. The majority of the metamorphism of the northern portion of the swarm during the Nagssugtoqidian orogeny occurred at amphibolite facies, with the exception of the northernmost portion within Ikertooq fjord where the transition to granulite facies metamorphism occurs. The amphibolite to granulite facies transition is marked by the first appearance of orthopyroxene in mafic rocks and is known to occur at *c*. 800°C (Spear 1981). The constraint on the pressure of the granulite facies metamorphism comes from the presence of kyanite-sillimanite paragneisses that are interleaved with sheets of dyke-bearing orthogneisses. The presence of granulite facies metamorphosed Kangâmiut dykes and the alumina-silicate-bearing gneisses indicates that peak metamorphism occurred at conditions corresponding to both the amphibolite to granulite and kyanite to sillimanite transitions. Figure 16 shows that these transitions indicate a peak metamorphic pressure of *c*. 0.9 GPa. This pressure is consistent with the results of Mengel *et al*. (1995) who determined metamorphic pressures on the Kangâmiut dykes in the Ikertooq region using TWEEQU geothermobarometry (Berman 1991).

Knowing the approximate depth of emplacement and the pressure of peak metamorphism provides constraints on the amount and style of burial during the Nagssugtoqidian orogeny. Emplacement at 0.3 GPa of pressure followed by peak metamorphism at 0.9 GPa requires an increase of 0.6 GPa. This indicates a minimum of 20 km of crustal thickening between dyke emplacement and peak metamorphism. A probable mechanism of crustal thickening in this case is thrust imbrication and crustal loading of material from north to south. The structural feature associated with this imbrication is most likely the Ikertôq shear zone (Fig. 1). The imbrication of rock types, the lithostratigraphic changes, including the disappearance of the Kangâmiut dykes, and the lateral continuity of the Ikertôq shear zone suggest that it is a major structure capable of accommodating displacement of material that buried the northern portion of the dyke swarm with 20 km of overburden. Crustal thickening must have occurred over a minimum map distance of 50 km extending from the Ikertôq shear zone to at least the Itivdleq shear zone (Fig. 1) and farther to the south approaching the Nagssugtoqidian front where the last significant metamorphism occurs.

Summary and conclusions

The 2.04 Ga Kangâmiut dyke swarm in West Greenland is composed of tholeiitic dykes that intruded during passive rifting of Archaean continental crust. The current level of exposure corresponds to emplacement depths less than 10 km based on estimated host rock temperatures less than 450°C during emplacement and geothermobarometry for

Kangâmiut dyke clinopyroxenes. Major and trace element systematics show that the parental magmas for the Kangâmiut dykes differentiated by fractionation of plagioclase, clinopyroxene, olivine, and late state Fe-Ti oxides. The rare-earth element systematics of the dykes indicate initiation of mantle melting at *c.* 2.75 GPa, corresponding to a potential mantle temperature of *c.* 1420°C. This temperature is consistent with ambient mantle temperature estimates for 2.0 Ga and shows that the Kangâmiut dyke swarm formed during passive rifting of the Kenorland supercontinent. Anomalously hot plume mantle is not required for their generation. Subsequent metamorphism of the northern portion of the swarm reached granulite facies, with an estimated temperature of 800°C and pressure of 0.9 GPa. The emplacement pressure of less than 0.3 GPa and peak metamorphism at 0.9 GPa indicate a minimum of 20 km of crustal thickening associated with the Nagssugtoqidian orogeny. Crustal thickening likely occurred during thrusting of material from the central Nagssugtoqidian orogen southward over the southern Nagssugtoqidian orogen along the Ikertôq shear zone.

Acknowledgements

We are especially grateful to the late David Bridgwater, whose boundless energy and enthusiasm for the Kangâmiut dykes inspired this work from beginning to end. We also thank Flemming Mengel, Jim Connelly, and Minik Rosing for their support of this project at various stages, and Andy Saunders and Karen Hanghøj for their constructive reviews of the final manuscript. This work was partially supported by the Danish Lithosphere Centre and grants from the US National Science Foundation (EAR 97-06677 and OCE 98-11453).

References

Abbott, D., Burgess, L., Longhi, J. & Smith, W.H.F. 1994: An empirical thermal history of the Earth's upper mantle. Journal of Geophysical Research 99(7), 13835–13850.

Arculus, R.J. 1994: Aspects of magma genesis in arcs. Lithos 33(1–3), 189–208.

Aspler, L.B. & Chiarenzelli, J.R. 1998: Two Neoarchean supercontinents? Evidence from the Paleoproterozoic. Sedimentary Geology 120(1–4), 75–104.

Bacon, C.R., Bruggman, P.E., Christiansen, R.L., Clynne, M.A., Donnelly-Nolan, J.M. & Hildreth, W. 1997: Primitive magmas at five Cascade volcanic fields; melts from hot, heterogeneous sub-arc mantle. Canadian Mineralogist 35(4), 397–423.

Bailey, J.C., Frolova, T.I. & Burikova, I.A. 1989: Mineralogy, geochemistry and petrogenesis of Kurile island-arc basalts. Contributions to Mineralogy and Petrology 102(3), 265–280.

Bak, J., Korstgård, J. & Sørensen, K. 1975: A major shear zone within the Nagssugtoqidian of West Greenland. Tectonophysics 27(3), 191–209.

Baker, D.R. & Eggler, D.H. 1987: Compositions of anhydrous and hydrous melts coexisting with plagioclase, augite, and olivine or low-Ca pyroxene from 1 atm to 8 kbar; application to the Aleutian volcanic center of Atka. American Mineralogist 72(1–2), 12–28.

Baker, M.B. & Stolper, E.M. 1994: Determining the composition of high-pressure mantle melts using diamond aggregates. Geochimica et Cosmochimica Acta 58(13), 2811–2827.

Becker, H., Jochum, K.P. & Carlson, R.W. 1999: Constraints from high-pressure veins in eclogites on the composition of hydrous fluids in subduction zones. Chemical Geology 160(4), 291–308.

Bell, D.R. & Rossman, G.R. 1992: Water in Earth's mantle; the role of nominally anhydrous minerals. Science 255(5050), 1391–1397.

Berman, R.G. 1991: Thermobarometry using multi-equilibrium calculations; a new technique, with petrological applications. The Canadian Mineralogist 29, 833–855.

Blichert-Toft, J., Rosing, M.T., Lesher, C.E. & Chauvel, C. 1995: Geochemical constraints on the origin of the late Archean Skjoldungen alkaline igneous province, SE Greenland. Journal of Petrology 36(2), 515–561.

Bridgwater, D., Mengel, F., Fryer, B., Wagner, P. & Hansen, S.C. 1995: Early Proterozoic mafic dykes in the North Atlantic and Baltic cratons: field setting and chemistry of distinctive swarms. In: Coward, M.P. & Ries, A.C. (eds): Early Precambrian processes. Geological Society Special Publication (London) 95, 193–220.

Brophy, J.G. & Marsh, B.D. 1986: On the origin of high alumina arc basalt and the mechanics of melt extraction. Journal of Petrology 27(4), 763–789.

Cadman, A.C., Noble, S.R., Tarney, J., Park, G., Ryan, A.B. & Royse, K.R. 1999: U-Pb ages of syndeformational dykes associated with the Mesoproterozoic Nain Plutonic Suite, Labrador. Canadian Journal of Earth Sciences 36(3), 339–348.

Cadman, A.C., Tarney, J., Bridgwater, D., Mengel, F.C., Whitehouse, M.J. & Windley, B.F. 2001: The petrogenesis of the Kangâmiut dyke swarm, W. Greenland. Precambrian Research 105, 183–203.

Carslaw, H.S. & Jaeger, J.C. 1959: Conduction of heat in solids, 510 pp., Oxford: Clarendon Press.

Chen, W. & Molnar, P. 1983: Focal depths of intracontinental and intraplate earthquakes and their implications for the thermal and mechanical properties of the lithosphere. Journal of Geophysical Research 88(5), 4183–4214.

Connelly, J.N. & Mengel, F.C. 2000: Evolution of Archean components in the Paleoproterozoic Nagssugtoqidian orogen, West Greenland. Geological Society of America Bulletin 112(5), 747–763.

Connelly, J.N., van Gool, J.A.M. & Mengel, F.C. 2000: Temporal evolution of a deeply eroded orogen: the Nagssugtoqidian Orogen, West Greenland. Canadian Journal of Earth Sciences 37, 1121–1142.

Danyuschevsky, L.V., Eggins, S.M., Falloon, T.J. & Christie, D.M. 2000: H_2O abundance in depleted to moderately enriched mid-ocean ridge magmas; Part 1: Incompatible behavior, implications for mantle stor-

age, and origin of regional variations. Journal of Petrology 41, 1329–1364.

Escher, A. & Pulvertaft, T.C.R. 1976: Rinkian mobile belt of West Greenland. In: Escher A. and Watt W.S. (eds): Geology of Greenland, 104–119. Copenhagen: Geological Survey of Greenland.

Escher, A., Escher, J.C. & Watterson, J. 1975: The reorientation of the Kangâmiut dike swarm, West Greenland. Canadian Journal of Earth Sciences 12, 158–173.

Escher, A., Jack, S. & Watterson, J. 1976: Tectonics of the North Atlantic Proterozoic dyke swarm. Philosophical Transactions of the Royal Society of London, Series A: Mathematical and Physical Sciences 280(1298), 529–539.

Fahrig, W.F. & Bridgwater, D. 1976: Late Archean – early Proterozoic paleomagnetic pole positions from West Greenland. In: Windley, B.F. (ed.): Early history of the Earth, 427–439. New York: John Wiley & Sons.

Fram, M.S. & Lesher, C.E. 1993: Geochemical constraints on mantle melting during creation of the North Atlantic basin. Nature 363, 712–715.

Francalanci, L., Taylor, S.R., McCulloch, M.T. & Woodhead, J.D. 1993: Geochemical and isotopic variations in the calc-alkaline rocks of Aeolian arc, southern Tyrrhenian Sea, Italy; constraints on magma genesis. Contributions to Mineralogy and Petrology 113(3), 300–313.

Friend, C.R.L. & Nutman, A.P. 1994: Two Archaean granulite-facies metamorphic events in the Nuuk–Maniitsoq region, southern West Greenland; correlation with the Saglek Block, Labrador. Journal of the Geological Society (London) 151, 421–424.

Furlong, K.P. & Schwartz, S.Y. 2004: Influence of the Mendocino triple junction on the tectonics of coastal California. Annual Review of Earth and Planetary Sciences 32, 403–433.

Galer, S.J.G. 1991: Interrelationships between continental freeboard, tectonics and mantle temperature. Earth and Planetary Science Letters 105(1–3), 214–228.

Green, T.H. 1994: Experimental studies of trace-element partitioning applicable to igneous petrogenesis; Sedona 16 years later. Chemical Geology 117(1–4), 1–36.

Gribble, R.F., Stern, R.J., Newman, S., Bloomer, S.H. & O'Hearn, T. 1998: Chemical and isotopic composition of lavas from the northern Mariana Trough; implications for magmagenesis in back-arc basins. Journal of Petrology 39(1), 125–154.

Grocott, J. 1979: Shape fabrics and superimposed simple shear strain in a Precambrian shear belt, West Greenland. Journal of the Geological Society (London) 136(7), 471–489.

Gust, D.A., Arculus, R.J. & Kersting, A.B. 1997: Aspects of magma sources and processes in the Honshu Arc. Canadian Mineralogist 35(4), 347–365.

Hageskov, B. 1995: Structural evolution of the southern Nagssugtoqidian front and the role of the Kangâmiut dykes. Terra Nova 7, 107 only.

Hanmer, S., Mengel, F., Connelly, J. & van Gool, J. 1997: Significance of crustal-scale shear zones and synkinematic mafic dykes in the Nagssugtoqidian Orogen, SW Greenland; a re-examination. Journal of Structural Geology 19(1), 59–75.

Harrison, T.M. 1981: Diffusion of ^{40}Ar in hornblende. Contributions to Mineralogy and Petrology 78(3), 324–331.

Hirschmann, M.M. 2000: Mantle solidus: experimental constraints and the effects of peridotite composition. Geochemistry, Geophysics, Geosystems 1(10) (http://dx.doi.org/10.1029/2000GC000070).

Holdaway, M.J. 1971: Stability of andalusite and the aluminum silicate phase diagram. American Journal of Science 271(2), 97–131.

Hooper, P.R. & Hawkesworth, C.J. 1993: Isotopic and geochemical constraints on the origin and evolution of the Columbia River Basalt. Journal of Petrology 34(6), 1203–1246.

Jakes, P. & Gill, J. 1970: Rare earth elements and the island arc tholeiitic series. Earth and Planetary Science Letters 9(1), 17–28.

Jenner, G.A., Longerich, H.P., Jackson, S.E. & Fryer, B.J. 1990: ICP-MS; a powerful tool for high-precision trace-element analysis in earth sciences; evidence from analysis of selected U.S.G.S. reference samples. Chemical Geology 83(1–2), 133–148.

Kalsbeek, F. & Manatschal, G. 1999: Geochemistry and tectonic significance of peridotitic and metakomatiitic rocks from the Ussuit area, Nagssugtoqidian Orogen, West Greenland. Precambrian Research 94, 101–120.

Kalsbeek, F. & Nutman, A.P. 1996: Anatomy of the early Proterozoic Nagssugtoqidian Orogen, West Greenland, explored by reconnaissance SHRIMP U-Pb zircon dating. Geology 24(6), 515–518.

Kalsbeek, F., Pidgeon, R.T. & Taylor, P.N. 1987: Nagssugtoqidian mobile belt of West Greenland; a cryptic 1850 Ma suture between two Archaean continents; chemical and isotopic evidence. Earth and Planetary Science Letters 85(4), 365–385.

Kelemen, P.B., Hanghøj, K. & Greene, A.R. 2003: One view of the geochemistry of subduction-related magmatic arcs, with an emphasis on primitive andesite and lower crust. In: Rudnick, R.L., Holland, H.D. & Turekian, K.K. (eds): Treatise on Geochemistry: the Crust 3, 593–659.

Korstgård, J.A. 1979: Metamorphism of the Kangâmiut dykes and the metamorphic and structural evolution of the southern Nagssugtoqidian boundary in the Itvidleq–Ikertôq region, West Greenland. Rapport Grønlands Geologiske Undersøgelse 89, 63–75.

Kystol, J. & Larsen, L.M. 1999: Analytical procedures in the Rock Geochemical Laboratory of the Geological Survey of Denmark and Greenland. Geology of Greenland Survey Bulletin 184, 59–62.

Langmuir, C.H., Klein, E.M. & Plank, T. 1992: Petrological systematics of mid-ocean ridge basalts: constraints on melt generation beneath ocean ridges. In: Morgan, J.P., Blackman, D.K. & Sinton, J.M. (eds): Mantle flow and melt generation at mid-ocean ridges. Geophysical Monograph 71, 183–280. Washington D.C.: American Geophysical Union.

Le Maitre, R.W. 2002: A classification of igneous rocks and glossary of terms, 2nd edition., 236 pp. Cambridge: Cambridge University Press.

Leake, B.E. *et al.* 1997: Nomenclature of amphiboles; report of the Subcommittee on Amphiboles of the International Mineralogical Association, Commission on New Minerals and Mineral Names. American Mineralogist 82(9–10), 1019–1037.

Lightfoot, P.C., Hawkesworth, C.J., Hergt, J., Naldrett, A.J., Gorbachev, N.S., Fedorenko, V.A. & Doherty, W. 1993: Remobilisation of the continental lithosphere by a mantle plume; major-, trace-element, and Sr-, Nd-, and Pb-isotope evidence from picritic and tholeiitic

lavas of the Noril'sk District, Siberian Trap, Russia. Contributions to Mineralogy and Petrology 114(2), 171–188.

Manatschal, G., Ulfbeck, D. & van Gool, J. 1998: Change from thrusting to syncollisional extension at a mid-crustal level; an example from the Palaeoproterozoic Nagssugtoqidian Orogen, West Greenland. Canadian Journal of Earth Sciences 35(7), 802–819.

Mayborn, K.R. 2000: Petrogenesis of the Paleoproterozoic Kangâmiut dike swarm, West Greenland: implications for the tectonic history of northeast Laurentia and the evolution of basaltic magmas, 318 pp. Unpublished Ph.D. thesis, University of California-Davis, USA.

Mayborn, K.R. & Lesher, C.E. 2004: Paleoproterozoic mafic dike swarms of northeast Laurentia: products of plumes or ambient mantle? Earth and Planetary Science Letters 225(3), 305–317.

Mengel, F., van Gool, J. & Marker, M. 1995: Mafic dykes as monitors of orogenic development: an example from the southern margin of the Palaeoproterozoic Nagssugtoqidian Orogen, West Greenland. Proceedings, First DLC Workshop on the Nagssugtoqidian Orogen in West Greenland, 6–7 April, 15–18. Copenhagen, Denmark: Danish Lithosphere Centre.

Mengel, F., Bridgwater, D. & Hageskov, B. 1996: Southern Nagssugtoqidian foreland: tectonic and thermal evolution monitored by the Proterozoic Kangâmiut dyke swarm. LITHOPROBE Report 57, 177–191.

Miller, D.M., Goldstein, S.L. & Langmuir, C.H. 1994: Cerium/lead and lead isotope ratios in arc magmas and the enrichment of lead in the continents. Nature 368(6471), 514–520.

Noe-Nygaard, A. 1952: A new orogenic epoch in the pre-Cambrian of Greenland. International Geological Congress, Part 13(59), 199–204. International Geological Congress.

Nutman, A.P. & Bridgwater, D. 1986: Early Archaean Amitsop tonalites and granites of the Isukasia area, southern West Greenland; development of the oldest-known sial. Contributions to Mineralogy and Petrology 94(2), 137–148.

Nutman, A.P. & Collerson, K.D. 1991: Very early Archean crustal-accretion complexes preserved in the North Atlantic Craton. Geology 19(8), 791–794.

Nutman, A.P., Kalsbeek, F., Marker, M., van Gool, J. & Bridgwater, D. 1999: U-Pb zircon ages of Kangâmiut dykes and detrital zircons in metasediments in the Palaeoproterozoic Nagssugtoqidian Orogen (West Greenland); clues to the pre-collisional history of the orogen. Precambrian Research 93(1), 87–104.

Papike, J.J., Cameron, K.L. & Baldwin, K. 1974: Amphiboles and pyroxenes; characterization of other than quadrilateral components and estimates of ferric iron from microprobe data. Abstracts with Programs – Geological Society of America 6, 1053–1054.

Pearce, J.A., Baker, P.E., Harvey, P.K. & Luff, I.W. 1995: Geochemical evidence for subduction fluxes, mantle melting and fractional crystallization beneath the South Sandwich island arc. Journal of Petrology 36(4), 1073–1109.

Peate, D.W. & Hawkesworth, C.J. 1996: Lithospheric to asthenospheric transition in low-Ti flood basalts from southern Parana, Brazil. Chemical Geology 127, 1–24.

Perfit, M.R., Gust, D.A., Bence, A.E., Arculus, R.J. & Taylor, S.R. 1980: Chemical characteristics of island-arc basalts; implications for mantle sources. Chemical Geology 30(3), 227–256.

Plank, T. & Langmuir, C.H. 1988: An evaluation of the global variations in the major element chemistry of arc basalts. Earth and Planetary Science Letters 90(4), 349–370.

Plank, T. & Langmuir, C.H. 1992: Effects of the melting regime on the composition of the oceanic crust. Journal of Geophysical Research 97(13), 19749–19770.

Putirka, K., Kinzler, R., Longhi, R. & Walker, D. 1996: Thermobarometry of mafic igneous rocks based on clinopyroxene-liquid equilibria, 0–30 kbar. Contributions to Mineralogy and Petrology 123(1), 92–108.

Ramberg, H. 1949: On the petrogenesis of the gneiss complexes between Sukkertoppen and Christianshaab, West-Greenland. Meddelelser fra Dansk Geologisk Forening 11, 312–327.

Reay, A. & Harris, B. 1964: The partial fusion of peridotite. Bulletin of Volcanology 27, 115–127.

Reches, Z. & Fink, J. 1988: The mechanism of intrusion of the Inyo Dike, Long Valley Caldera, California. Journal of Geophysical Research 93(5), 4321–4334.

Richter, F.M. 1984: Regionalized models for the thermal evolution of the Earth. Earth and Planetary Science Letters 68(3), 471–484.

Roeder, P.L. & Emslie, R.F. 1970: Olivine-liquid equilibrium. Contributions to Mineralogy and Petrology 29(4), 276–289.

Spear, F.S. 1981: An experimental study of hornblende stability and compositional variability in amphibole. American Journal of Science 281(6), 697–734.

Stein, C.A. 1995: Heat flow of the Earth. In: Ahrens, T.J. (ed.): Global earth physics: a handbook of physical constants, 144–158. Washington D.C.: American Geophysical Union.

Stern, R.A., Percival, J.A. & Mortensen, J.K. 1994: Geochemical evolution of the Minto Block; a 2.7 Ga continental magmatic arc built on the Superior proto-craton. Precambrian Research 65(1–4), 115–153.

Storey, M., Mahoney, J.J. & Saunders, A.D. 1997: Cretaceous basalts in Madagascar and the transition between plume and continental lithosphere mantle sources. In: Mahoney, J.J. & Coffin, M.F. (eds): Large igneous provinces; continental, oceanic, and planetary flood volcanism, 95–122. Washington D.C.: American Geophysical Union.

Sun, S.S. & McDonough, W.F. 1989: Chemical and isotopic systematics of oceanic basalts; implications for mantle composition and processes. In: Saunders, A.D. & Norry, M. J. (eds): Magmatism in the ocean basins. Geological Society Special Publication (London) 42, 313–345.

Takahashi, E. 1986: Melting of a dry peridotite KLB-1 up to 14 GPa; implications on the origin of peridotitic upper mantle. Journal of Geophysical Research 91(9), 9367–9382.

Tatsumi, Y. 1989: Migration of fluid phases and genesis of basalt magmas in subduction zones. Journal of Geophysical Research 94(4), 4697–4707.

Tatsumi, Y., Otofuji, Y., Matsuda, T. & Nohda, S. 1989: Opening of the Sea of Japan back-arc basin by asthenospheric injection. Tectonophysics 166(4), 317–329.

Thompson, R.N. 1982: Magmatism of the British Tertiary volcanic province. Scottish Journal of Geology 18, 49–107.

Tormey, D.R., Grove, T.L. & Bryan, W.B. 1987: Experimental petrol-

ogy of normal MORB near the Kane fracture zone; 22 degree–25 degree N, Mid-Atlantic Ridge. Contributions to Mineralogy and Petrology 96(2), 121–139.

Tormey, D.R., Hickey-Vargas, R., Frey, R.A. & Lopez-Escobar, L. 1991: Recent lavas from the Andean volcanic front (33–42 degrees S); interpretations of along-arc compositional variations. In: Harmon, R.S. (ed.): Andean magmatism and its tectonic setting. Geological Society of America Special Paper 265, 57–77.

van Gool, J.A.M., Kriegsman, L.M., Marker, M. & Nichols, G.T. 1999: Thrust stacking in the inner Nordre Strømfjord area, West Greenland; significance for the tectonic evolution of the Palaeoproterozoic Nagssugtoqidian Orogen. Precambrian Research 93(1), 71–85.

van Gool, J.A.M., Connelly, J.N., Marker, M. & Mengel, F.C. 2002: The Nagssugtoqidian Orogen of West Greenland: tectonic evolution and regional correlations from a West Greenland perspective. Canadian Journal of Earth Sciences 39(5), 665–686.

Williams, C.F. 1996: Temperature and the seismic/aseismic transition; observations from the 1992 Landers earthquake. Geophysical Research Letters 23(16), 2029–2032.

Williams, H., Hoffman, P.F., Lewry, J.F., Monger, J.W.H. & Rivers, T. 1991: Anatomy of North America; thematic geologic portrayals of the continent. Tectonophysics 187(1–3), 117–134.

Willigers, B.J.A., Mengel, F.C., Bridgwater, D., Wijbrans, J.R. & van Gool, J.A.M. 1999: Mafic dike swarms as absolute time markers in high-grade terranes; $^{40}Ar/^{39}Ar$ geochronological constraints on the Kangâmiut dikes, West Greenland. Geology 27(9), 775–778.

Windley, B.F. 1970: Primary quartz ferro-dolerite/garnet amphibolite dykes in the Sukkertoppen region of West Greenland. In: Newall, G. & Rast, N. (eds): Mechanism of igneous intrusion, 79–92. Liverpool: Seel House Press.

Wooden, J.L., Czamanske, G.K., Fedorenko, V.A., Arndt, N.T., Chauvel, C., Bouse, R.M., King, B.W., Knight, R.J. & Siems, D.F. 1993: Isotopic and trace-element constraints on mantle and crustal contributions to Siberian continental flood basalts, Noril'sk area, Siberia. Geochimica et Cosmochimica Acta 57(15), 3677–3704.

Manuscript received 8 June 2004; revision accepted 15 August 2005

Appendix

Table A1. Field data for Kangâmiut dykes examined for this study

Dyke	Location	Latitude	Longitude	Trend	Thickness (m)	Samples
1	Søndre Strømfjord	66°05.266'N	053°33.211'W	010	2	430901 middle of dyke, 430902 near contact
2	Søndre Strømfjord	66°05.26'N	053°33.5'W	080	20	430903 ~7 m from dyke contact
3	Søndre Strømfjord	66°05.26'N	053°33.5'W	010	0.4	none
4	Søndre Strømfjord	66°05.26'N	053°33.7'W	020	?	none
5	Itilleq	66°33.3'N	053°02.5'W	086	6	430904 ~2 m from contact
6	Itilleq	66°33.3'N	053°02.5'W	?	1.5	430905 middle of dyke
7	Ikertooq	66°58.1'N	052°28.9'W	079	0.3	none
8	Ikertooq	66°58.1'N	052°28.9'W	123	0.15	none
9	Ikertooq	66°57.55'N	052°31.7'W	010	2	430910 0.5 m from dyke margin
10	Ikertooq	66°58.95'N	052°26.8'W	080	2	430915 middle of dyke
11	Ikertooq	66°49.7'N	052°16.7'W	054	0.3	430917 middle of dyke
12	Ikertooq	66°50.1'N	052°19.2'W	?	?	430919 middle of dyke
13	Itilleq	66°32.25'N	052°45.0'W	080	8	430923 middle of dyke
14	Itilleq	66°32.85'N	052°47.15'W	?	0.1	430926 whole width of dyke
15	Itilleq	66°33.3'N	052°51.3'W	095	1	430929 middle of dyke
16	Itilleq	66°33.03'N	052°53.54'W	035	8	430930 ~2.5 m from contact, 430931 dyke contact
17	Itilleq	66°33.5'N	052°56.0'W	080	2	430933 0.3 m from contact
18	Itilleq	66°34.7'N	052°56.0'W	062	10	430935 middle of dyke
19	Itilleq	66°34.7'N	052°56.0'W	090	14	430936 middle of dyke
20	Itilleq	66°35.1'N	052°49.0'W	090	8	430939 middle of dyke
21	Itilleq	66°35.1'N	052°47.5'W	079	8	430940 middle of dyke
22	Itilleq	66°34.75'N	052°48.5'W	?	?	430942 middle of dyke
23	Itilleq	66°34.75'N	052°48.5'W	?	?	430943 middle of dyke
24	Itilleq	66°33.1'N	053°04.0'W	?	25	430946 middle of dyke
25	Itilleq	66°33.7'N	052°55.1'W	087	16	430948 middle of dyke, 430950 dyke contact
26	Itilleq	66°33.25'N	052°38.5'W	100	1	430951 middle of dyke
27	Itilleq	66°33.25'N	052°33.0'W	096	20	430952 middle of dyke
28	Itilleq	66°32.6'N	052°27.0'W	057	30	430953 middle of dyke
29	Itilleq	66°31.8'N	052°41.0'W	061	5	430955 ~1.5 m from contact, 430956 ~5 m from contact
30	Itilleq	66°31.9'N	052°38.5'W	085	15	430957 dyke contact, 430959 ~5 m from contact
31	Itilleq	66°31.8'N	052°36.2'W	065	18	430960 middle of dyke
32	Itilleq	66°31.7'N	052°34.0'W	078	22	430961 middle of dyke
33	Mouth of Itilleq	66°29.9'N	053°33.5'W	022	20	430965 middle of dyke
34	Mouth of Itilleq	66°30'N	053°34.8'W	065	25	430966 ~7 m from contact
35	Mouth of Itilleq	66°30.05'N	053°35.8'W	117	40	430967 ~7 m from contact
36	Mouth of Itilleq	66°30.5'N	053°36.4'W	006	10	430969 middle of dyke
37	South of Maniitsoq	65°22.7'N	052°47.3'W	345	4.5	430970 middle of dyke
38	East of Maniitsoq	65°25.5'N	052°24.0'W	?	15	430972 middle of dyke
39	East of Maniitsoq	65°25.4'N	052°23.0'W	054	0.4	430973 middle of dyke
40	East of Maniitsoq	65°25.5'N	052°18.0'W	117	12	430974 middle of dyke
41	East of Maniitsoq	65°26.0'N	052°14.8'W	354	7	430975 middle of dyke
42	East of Maniitsoq	65°35.15'N	052°46.0'W	002	49	430977 dyke contact, 430979 1 m from contact, 430981 5 m from contact, 430982 17 m from contact
43	North of Maniitsoq	65°39.85'N	052°37.0'W	003	25	430983 middle of dyke, 430984 dyke contact
44	North of Maniitsoq	65°44.4'N	052°38.5'W	344	0.5	430986 middle of dyke
45	North of Maniitsoq	65°38.75'N	052°37.5'W	002	16	430987 middle of dyke, 430988 ~6 cm from contact
46	North of Maniitsoq	65°36.9'N	052°43.5'W	005	10	430990 ~4 m from contact, 430991 ~0.5 m from contact

Table A1 *(continued)*

Dyke	Location	Latitude	Longitude	Trend	Thickness (m)	Samples
47	North of Maniitsoq	65°40.1'N	052°49.0'W	010	17	430992 middle of dyke
48	North-east of Kangaamiut	65°54.9'N	053°14.5'W	050	12	430993 ~2 m from contact
49	North-east of Kangaamiut	65°53.95'N	053°16.0'W	045	27	430994 middle of dyke
50	North-east of Kangaamiut	65°53.4'N	053°14.95'W	033	1	none
51	North-east of Kangaamiut	65°53.4'N	053°14.95'W	110	0.2	none
52	North-east of Kangaamiut	65°53.4'N	053°14.95'W	030	1.5	430995 middle of dyke
53	North-east of Kangaamiut	65°53.4'N	053°14.95'W	110	2	430996 middle of dyke
54	North-east of Kangaamiut	65°52.6'N	053°14.0'W	063	60	430997 andesitic portion of dyke, 430998 mafic portion of dyke
55	North-east of Kangaamiut	65°50.8'N	053°13.0'W	064	1.5	432101 middle of dyke
56	North-east of Kangaamiut	65°50.8'N	053°13.0'W	015	15	430999 middle of dyke
57	Søndre Strømfjord	66°01.4'N	053°28.65'W	028	60	432103 middle of dyke
58	Kangerluarsussuaq	66°17.5'N	053°05.65'W	065	40	432104 dyke contact, 432105 middle of dyke
59	Kangerluarsussuaq	66°17.5'N	053°05.8'W	057	40	432107 middle of dyke
60	Kangerluarsussuaq	66°17.25'N	053°07.5'W	022	1	432108 middle of dyke
61	Kangerluarsussuaq	66°17.25'N	053°07.5'W	145	45	432106 1 m from contact, 432108 middle of dyke
62	Kangerluarsussuaq	66°17.15'N	053°08.5'W	045	21	432111 middle of dyke
63	Kangerluarsussuaq	66°17.05'N	053°11.25'W	028	40	432112 ~7 m from contact
64	Kangerluarsussuaq	66°16.9'N	053°09.7'W	031	140	432115 dyke contact, 432116 ~2.5 m from W contact, 432118 ~45 m from W contact, 432119 ~70 m from W contact, 432120 ~95 m from W contact, 432121 ~19 m from E contact, 432122 ~18 m from W contact, 432136 ~40 m from W contact, 432137 middle of dyke
65	Kangerluarsussuaq	66°39.5'N	053°03.0'W	065	50	432123 middle of dyke
66	East of Itilleq	66°29.3'N	052°25.0'W	065	15	432125 middle of dyke
67	East of Itilleq	66°29.1'N	052°24.0'W	050	8	432128 middle of dyke
68	East of Itilleq	66°33.1'N	052°07.5'W	072	1	432129 middle of dyke
69	East of Itilleq	66°31.75'N	052°18.0'W	050	4	432130 middle of dyke
70	East of Itilleq	66°30.5'N	052°27.5'W	090	25	432138 middle of dyke
71	East of Itilleq	66°27.9'N	052°27.0'W	022	70	432133 middle of dyke
72	East of Itilleq	66°26.0'N	052°40.5'W	080	5	432134 middle of dyke
73	East of Itilleq	66°27.45'N	052°45.5'W	055	4	432135 middle of dyke
74	Kangerluarsussuaq	66°16.6'N	053°17.0'W	032	17	432139 middle of dyke
75	Kangerluarsussuaq	66°15.3'N	053°22.5'W	036	18	432140 middle of dyke, 432151 9 m from N contact, 432152 6 m from N contact, 432153 4 m from N contact, 432154 2 m from N contact, 432155 1 m from N contact, 432156 0.5 m from N contact, 432157 0.25 m from N contact, 432158 dyke contact, highly jointed
76	Kangerluarsussuaq	66°14.6'N	053°33.0'W	020	25	432143 middle of dyke, 432144 5 m from E contact, 432145 E contact
77	Kangerluarsussuaq	66°14.7'N	053°31.7'W	044	0.4	432147 NW contact, 432148 middle of dyke 432149 SE contact
78	Kangerluarsussuaq	66°15.15'N	053°29.0'W	086	2	432150 middle of dyke
79	Mouth of Itilleq	66°30.05'N	053°35.8'W	090	50	430206 and 430207 middle of dyke
80	Mouth of Itilleq	66°30.05'N	053°35.8'W	090	15	430208 and 430209 middle of dyke
81	Mouth of Itilleq	66°30.05'N	053°35.8'W	090	?	430210 middle of dyke
82	Mouth of Itilleq	66°30.05'N	053°35.8'W	090	0.1	430211 whole width of dyke
83	Søndre Strømfjord	66°01.4'N	053°28.65'W	?	?	430258 dyke contact
84	North-east of Kangaamiut	65°52.6'N	053°14.9'W	022	30	430267 dyke contact, 430265 middle of dyke
85	North-east of Kangaamiut	65°53.6'N	053°14.9'W	045	30	430283 dyke contact, 430284 middle of dyke
86	North-west of Kangaamiut	65°56.6'N	053°28.0'W	25	60	158074 and 430288 dyke contact, 432102 and 158077 middle of dyke

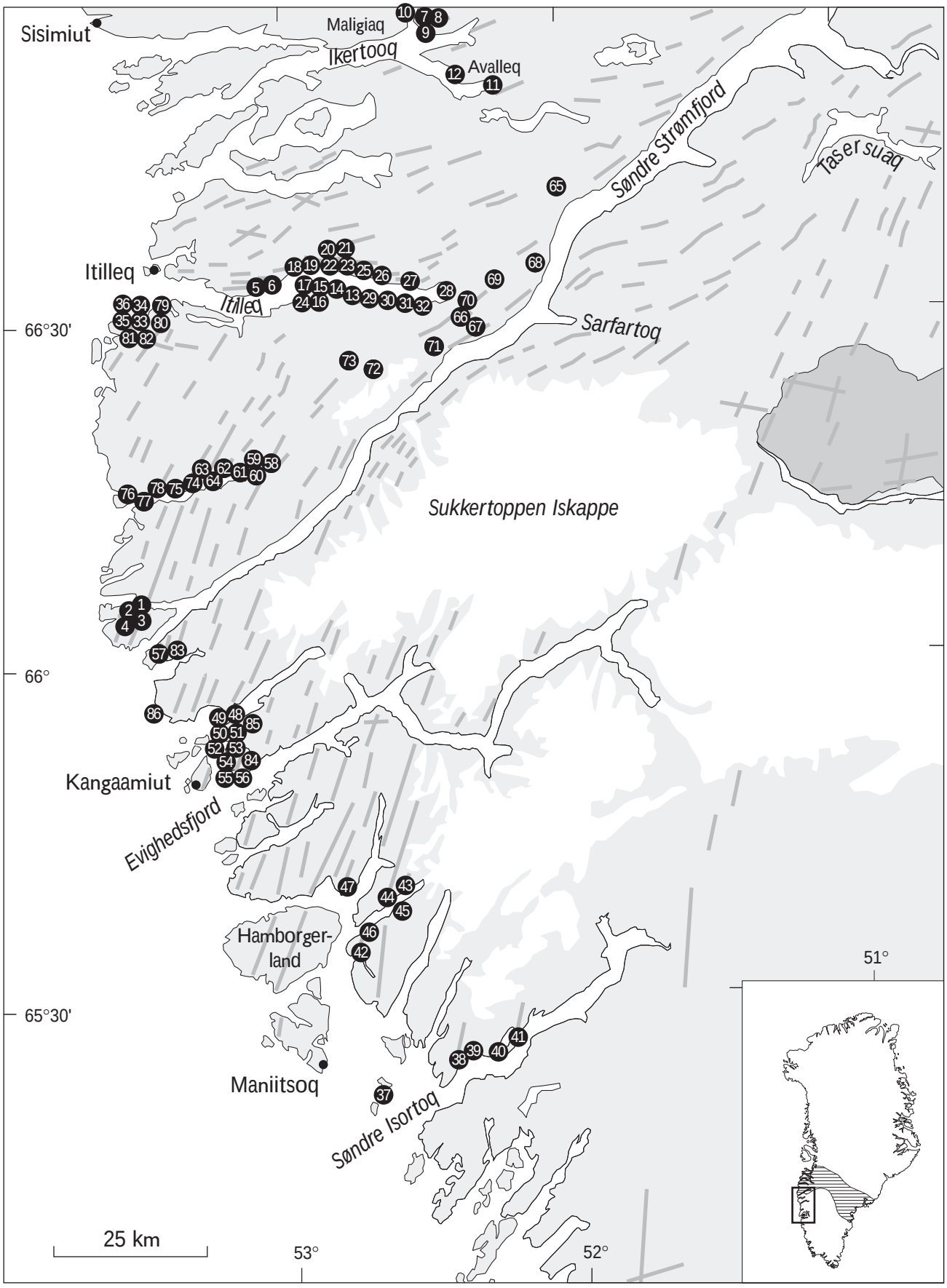

Fig. A1. Map showing the locations of dykes examined in this study.

Zircon geochronology from the Kangaatsiaq–Qasigiannguit region, the northern part of the 1.9–1.8 Ga Nagssugtoqidian orogen, West Greenland

Kristine Thrane and James N. Connelly

The Kangaatsiaq–Qasigiannguit region in the northern part of the Palaeoproterozoic Nagssugtoqidian orogen of West Greenland consists of poly-deformed orthogneisses and minor occurrences of interleaved, discontinuous supracrustal belts. Laser ablation ICP-MS $^{207}Pb/^{206}Pb$ analyses of detrital zircons from four metasedimentary rocks (supplemented by ion probe analysis of one sample) and igneous zircons from six granitoid rocks cutting metasedimentary units indicate that the supracrustal rocks in the Kangaatsiaq–Qasigiannguit (Christianshåb) region are predominantly Archaean in age. Four occurrences of metasedimentary rocks are clearly Archaean, two have equivocal ages, and only one metasedimentary unit, from within the Naternaq (Lersletten) supracrustal belt, is demonstrably Palaeoproterozoic and readily defines a large fold complex of this age at Naternaq. The 2.9–2.8 Ga ages of detrital Archaean grains are compatible with derivation from the local basement orthogneisses within the Nagssugtoqidian orogen. The detrital age patterns are similar to those of metasediments within the central Nagssugtoqidian orogen but distinct from age patterns in metasediments of the Rinkian belt to the north, where there is an additional component of pre-2.9 Ga zircons. Synkinematic intrusive granitoid rocks constrain the ages of some Archaean deformation at 2748 ± 19 Ma and some Palaeoproterozoic deformation at 1837 ± 12 Ma.

Keywords: Nagssugtoqidian orogen, deformation, LA-ICP-MS, zircon, metasediment

K.T., *Geological Institute, University of Copenhagen, Øster Voldgade 10, DK-1350 Copenhagen K, Denmark.*
E-mail: *kthrane@geol.ku.dk*
J.N.C., *Department of Geological Science, University of Texas at Austin, Austin, TX 78712, USA.*

The Kangaatsiaq–Qasigiannguit area that is the focus of this paper (Fig. 1) forms a large part of the northern Nagssugtoqidian orogen, which is interpreted as the southern part of a major collisional orogenic system that crops out in central and northern West Greenland and adjacent parts of eastern Canada (Connelly *et al.* 2006). The northern Nagssugtoqidian orogen, which was re-investigated in 2001–2003 by the Geological Survey of Denmark and Greenland (GEUS) in co-operation with external partners, is underlain by poly-deformed, variably reworked grey Archaean orthogneiss interleaved with dismembered Archaean and Palaeoproterozoic supracrustal rocks of volcanic and sedimentary origin. Only few significant time marker horizons (such as distinct suites of mafic dykes or one or more groups of characteristic supracrustal rocks with known ages) are present. The primary objectives of this geochronological study were therefore to determine the extent of Palaeoproterozoic metasedimentary rocks and attempt to directly date different phases of deformation and metamorphism.

A number of lithological, structural and metamorphic features, especially in the Kangaatsiaq–Aasiaat area (Fig. 1),

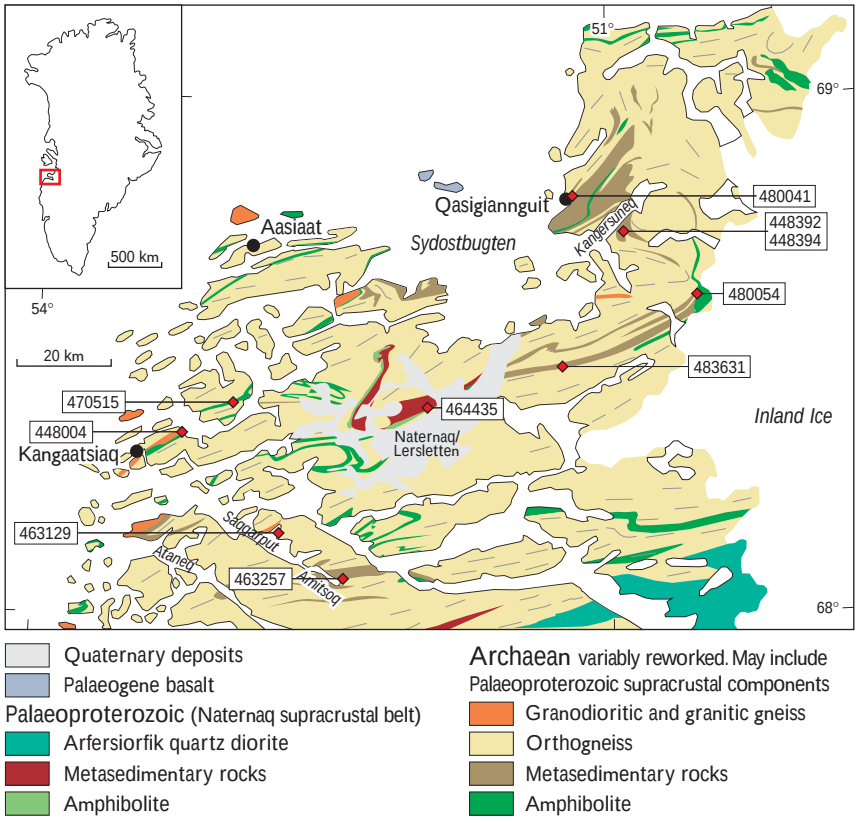

Fig. 1. Simplified geological map of the Kangaatsiaq–Qasigiannguit region, with sample locations.

provide some immediate constraints on the Archaean and Palaeoproterozoic geological evolution of the northern Nagssugtoqidian orogen, and are outlined here as an introduction to the geochronological study. The study area may be divided into two different tracts based on metamorphism and structural style (Piazolo *et al.* 2004; Mazur *et al.* 2006, this volume). The tract south-west and south-east of Kangaatsiaq is metamorphosed at granulite facies grade and is characterised by a general WSW–ENE-trending structural grain with large, moderately to steeply plunging fold structures and undeformed to weakly deformed, synkinematic granitic neosome (van Gool *et al.* 2002; Garde 2004). Several E–W-trending mafic dykes occur south of Kangaatsiaq around 68°N. They are undeformed and discordant to the main structures and lithological boundaries, but variably metamorphosed (Glassley & Sørensen 1980; Árting 2004). These dykes are presumed to be of Palaeoproterozoic age and perhaps related to pre-Nagssugtoqidian rifting (Árting 2004), and if so would constrain the deformation and granulite facies metamorphism south of Kangaatsiaq to be Archaean in age, whereas the thermal event recorded by the dykes themselves would be Palaeoproterozoic.

The remainder of the study area, to the north and east of Kangaatsiaq, is at amphibolite grade (e.g. Hollis *et al.* 2006, this volume), and does not display any signs of retrogression from granulite facies except within a *c.* 10 km thick transition zone adjacent to the granulite facies terrain. These northern and eastern areas generally possess a much more intense planar and linear tectonic fabric than in the south, commonly including a strong subhorizontal extension lineation that also penetrates the late granitic neosome. Furthermore, a structural discordance occurs in the Naternaq area (Fig. 1) between WNW–ESE-trending amphibolite to the west and the structurally overlying, NE–SW-trending Naternaq supracrustal belt in the east, suggesting that the respective structures of the two supracrustal units are unrelated to each other and of different age (Mazur *et al.* 2006, this volume). In addition, the northern and eastern areas also host occasional mafic dykes on islands north-east of Aasiaat and on the southern coast of Sydostbugten (Fig. 1). Although these dykes are still largely coherent and unmigmatised, they are intensely deformed, almost concordant with their host rocks, and tectonically thinned to about 1–2 m thick. Both the granitic neosome, the Naternaq supracrustal rocks, and the deformed dykes provide relative age constraints on the intense deformation in the northern and eastern parts of the study area. If it is again assumed that the deformed dykes in the north are Palaeoproterozoic, it would follow

Table 1. Zircon LA-ICP-MS ^{207}Pb-^{206}Pb data

Spot	^{206}Pb (cps)	$^{207}Pb/^{206}Pb$	Age (Ma)	2σ %
448004 Metasediment NE of Kangaatsiaq				
1	22419	0.21046	2909	7.7
2	30428	0.20444	2862	4.9
3	27946	0.20011	2827	5.9
4	41739	0.20405	2859	4.8
5	66864	0.20548	2870	5.8
6	52963	0.20846	2894	4.2
7	70422	0.18216	2673	3.9
8	46147	0.20058	2831	5.2
9	73807	0.20449	2862	3.7
10	41046	0.20919	2899	5.9
11	75396	0.20183	2841	6.5
12	84403	0.20242	2846	4.2
13	27932	0.20390	2858	7.5
14	102678	0.20107	2835	6.0
15	129026	0.18972	2740	6.9
16	46526	0.20716	2883	5.5
17	71802	0.20579	2873	6.3
18	659551	0.20033	2829	4.9
19	165828	0.19242	2763	6.1
20	73874	0.19895	2818	5.4
21	20371	0.18508	2699	5.5
22	21982	0.17386	2595	5.3
23	33164	0.21021	2907	6.4
24	86486	0.18406	2690	5.1
25	99148	0.20434	2861	4.4
26	54554	0.20049	2830	5.6
27	52435	0.17947	2648	3.8
28	45325	0.20018	2828	4.3
29	75391	0.18983	2741	3.0
30	77047	0.20775	2888	4.7
31	32181	0.19856	2814	3.1
32	50218	0.19811	2811	3.3
33	28491	0.20148	2838	4.3
34	21801	0.19768	2807	4.6
35	22466	0.20144	2838	5.9
36	48990	0.20013	2827	3.3
37	26535	0.20445	2862	5.8
38	114112	0.18364	2686	2.1
39	41973	0.20083	2833	3.4
40	57549	0.20210	2843	2.6
41	26869	0.25312	3204	2.7
42	49986	0.19811	2811	3.0
43	20567	0.19924	2820	4.6
44	5467	0.19417	2778	9.2
45	29042	0.20106	2835	4.2
46	9255	0.18565	2704	6.7
47	18597	0.20277	2849	4.3
48	112700	0.17900	2644	2.3
49	84858	0.19285	2767	2.8
50	14867	0.17617	2617	8.2
51	24908	0.19765	2807	3.7
52	11178	0.19419	2778	5.5
53	91255	0.17807	2635	4.3
54	28338	0.20395	2858	4.7
55	24855	0.18937	2737	4.8
56	7761	0.18757	2721	9.0
57	12436	0.19563	2790	6.5
58	12571	0.19849	2814	5.4
448392 Granite, Kangersuneq				
1	318831	0.19069	2748	3.5
2	361175	0.18986	2741	2.7
3	406129	0.19945	2822	3.3
4	163666	0.18800	2725	3.6
5	205935	0.19380	2775	3.1
6	227282	0.19148	2755	3.0
7	123658	0.18830	2727	3.1
8	294942	0.18738	2719	5.1
9	407109	0.19415	2778	5.0
10	481882	0.19342	2771	5.1
11	212302	0.18706	2716	4.7
12	407464	0.19766	2807	3.0
13	491512	0.19950	2822	4.2
14	94032	0.18905	2734	3.0
15	173984	0.18392	2689	4.9
16	109933	0.18320	2682	5.7
17	50994	0.19030	2745	4.6
18	13465	0.18864	2730	6.2
19	21101	0.17697	2625	6.4
20	99478	0.18431	2692	5.8
21	108982	0.18687	2715	3.9
22	33255	0.18969	2739	5.7
23	192965	0.18985	2741	6.8
24	280376	0.18859	2730	6.1
25	287725	0.18761	2721	5.1
26	101087	0.18975	2740	4.7
27	85412	0.18695	2716	4.3
28	125421	0.18639	2711	6.2
29	45496	0.18854	2730	5.7
30	75470	0.18108	2663	4.9
31	40021	0.18483	2697	4.9
32	48564	0.19087	2750	5.6
33	101631	0.18754	2721	3.2
34	117730	0.18292	2679	2.5
35	49211	0.18807	2725	3.8
36	112930	0.18847	2729	2.9
37	202637	0.18826	2727	2.2
38	102831	0.18893	2733	2.2
39	55266	0.19174	2757	2.8
40	45349	0.18639	2711	4.5
41	104416	0.18742	2720	3.3
42	188642	0.18481	2696	2.2
43	97849	0.18797	2724	2.6
44	145946	0.17859	2640	4.0
448394 Metasediment, Kangersuneq				
1	695411	0.16006	2456	3.6
2	52863	0.20417	2860	5.3
3	443404	0.11180	1829	3.8
4	1104248	0.11717	1913	4.4
5	579803	0.11532	1885	4.7
6	231966	0.12351	2008	4.9
7	362937	0.10979	1796	3.1
8	303451	0.11334	1854	3.9
9	277637	0.11090	1814	3.1
10	380962	0.12251	1993	3.9
11	115636	0.16115	2468	6.0
12	461330	0.11598	1895	3.5
13	493717	0.19532	2787	3.7
14	207687	0.17408	2597	5.3
15	393460	0.11112	1818	2.7
16	242631	0.10929	1788	4.9
17	132013	0.19838	2813	4.9
18	178574	0.10859	1776	6.1
19	303683	0.10774	1762	4.1
20	241139	0.15569	2409	7.4
21	51484	0.12627	2047	5.5
22	53211	0.12080	1968	7.7
23	53531	0.11660	1905	6.9
24	23896	0.19593	2793	6.2
25	79706	0.11458	1873	6.4
26	89308	0.11277	1845	6.3
27	63147	0.11176	1828	8.6
28	12586	0.19431	2779	6.5
29	100961	0.13800	2202	7.0
30	12592	0.16853	2543	9.7
31	57066	0.11124	1820	8.5
32	51764	0.11438	1870	10.1
33	218430	0.11295	1847	7.4
34	78169	0.10868	1777	9.7
35	96773	0.11345	1855	8.4
36	143102	0.11037	1806	6.7
37	33237	0.13986	2225	6.4
38	92186	0.10819	1769	9.7
39	80332	0.12802	2071	8.3
40	35510	0.19386	2775	8.0
41	11684	0.18283	2679	7.4
42	21389	0.19620	2795	8.2
43	14702	0.19528	2787	9.7
44	19762	0.19659	2798	6.5
45	36375	0.11197	1832	9.0
46	17548	0.18024	2655	11.7
47	9064	0.19962	2823	10.9
48	11530	0.19199	2759	7.8
49	64234	0.11111	1818	10.3
50	7566	0.16671	2525	11.0
51	38371	0.10619	1735	9.1
52	15464	0.18496	2698	9.1
53	15534	0.14855	2329	9.3
54	27618	0.11461	1874	8.4
55	15853	0.19890	2817	9.4
56	10902	0.18316	2682	11.0
57	8905	0.20952	2902	9.4
58	6493	0.18680	2714	10.5
59	16248	0.19267	2765	8.7
60	43736	0.14480	2285	6.4
61	48133	0.11266	1843	12.3
62	52656	0.12037	1962	10.7
63	88558	0.11566	1890	7.2
64	65717	0.10988	1797	8.8
65	14964	0.15276	2377	8.5
66	59777	0.11635	1901	7.3
67	23849	0.16781	2536	8.6
68	16825	0.19548	2789	12.3
69	17260	0.14321	2266	8.8
70	28538	0.19178	2757	10.3
71	65355	0.11192	1831	8.4
72	58939	0.12654	2050	9.6
73	69509	0.11151	1824	6.8
74	49893	0.13319	2140	8.6
75	76541	0.11448	1872	8.1
76	67611	0.11351	1856	8.0
77	58817	0.10691	1747	8.9
78	69641	0.11468	1875	11.3
79	57943	0.11116	1818	4.7
463129 Synkinematic granite, Saqqarput				
1	2283739	0.18759	2721	3.0
2	1266859	0.19890	2817	3.6
3	344375	0.18904	2734	4.1
4	531257	0.18883	2732	5.5
5	565174	0.19441	2780	4.6
6	247679	0.18844	2729	4.9
7	460352	0.20656	2879	3.8
8	1058356	0.19510	2786	3.2
9	405853	0.18296	2680	6.8
10	554081	0.17660	2621	3.0
11	1363965	0.20876	2896	4.0
12	935603	0.19609	2794	2.7
13	605520	0.18625	2709	2.6
14	516471	0.17880	2642	5.1
15	822166	0.18954	2738	5.5
16	655511	0.20436	2861	4.0
17	755390	0.19587	2792	5.0
18	127005	0.18594	2707	5.9
19	422927	0.19261	2765	4.8
20	653950	0.19183	2758	4.0
21	1135912	0.19679	2800	2.9
22	1096015	0.19497	2785	2.4
23	653314	0.19170	2757	2.6
24	228993	0.20892	2897	7.4
25	221510	0.21878	2972	9.2
26	346159	0.20045	2830	6.6
27	37048	0.16944	2552	11.9
28	97269	0.17974	2650	10.8
29	85210	0.18521	2700	8.7
30	172975	0.18213	2672	8.2
31	171017	0.17446	2601	9.0
32	165639	0.18002	2653	5.5
33	133709	0.18851	2729	7.8
34	182742	0.18315	2682	5.2
35	125199	0.18194	2671	7.0
36	169034	0.19244	2763	7.5
37	85182	0.16778	2536	9.4

Table 1 *(continued)*

Spot	^{206}Pb (cps)	^{207}Pb/^{206}Pb	Age (Ma)	2σ %
38	101924	0.18113	2663	7.6
39	178145	0.20233	2845	8.9
40	35771	0.18557	2703	8.3
41	23866	0.19033	2745	10.0
42	78620	0.22740	3034	11.3
43	88660	0.20740	2885	7.8
44	264622	0.18784	2723	6.5
45	219347	0.19029	2745	5.2
46	215885	0.18648	2711	9.4
47	117234	0.17897	2643	9.0
48	29425	0.18849	2729	8.9
49	59458	0.18317	2682	10.0
50	44706	0.19343	2772	11.5
51	47511	0.20920	2899	14.7
52	52220	0.18199	2671	10.6
53	58597	0.17855	2639	12.7
54	47047	0.18403	2690	6.8
55	85100	0.19408	2777	8.0
56	150838	0.18512	2699	9.1
57	42220	0.18152	2667	8.4
58	182300	0.17444	2601	6.3
59	181857	0.19158	2756	5.8
60	656182	0.18446	2693	3.8
61	1625878	0.19433	2779	4.0
62	1033362	0.19004	2742	7.1
463257 Metasediment, Amitsoq				
1	94060	0.20316	2852	4
2	126332	0.19611	2795	4
3	245874	0.21538	2946	4
4	154787	0.20172	2840	4
5	68216	0.19982	2825	4
6	428099	0.18536	2701	4
7	100464	0.18737	2719	4
8	106081	0.19619	2794	4
9	178863	0.20711	2883	4
10	72018	0.19715	2808	4
11	102336	0.18203	2671	4
12	218440	0.21010	2907	4
13	144435	0.20135	2837	4
14	73200	0.20617	2875	4
15	103837	0.17190	2575	4
16	100257	0.15132	2361	4
17	120574	0.20468	2864	4
18	88636	0.20786	2889	4
19	129707	0.20434	2861	4
20	133092	0.21288	2928	4
21	176443	0.20885	2897	4
22	48385	0.19377	2774	5.2
23	61486	0.19210	2760	8.2
24	60275	0.22028	2983	3.6
25	44550	0.20247	2846	6.8
26	30952	0.20191	2842	5.9
27	7392	0.18113	2663	8.0
28	20571	0.19351	2772	8.6
29	15357	0.19909	2819	6.7
30	31747	0.20691	2881	7.0
31	22596	0.20038	2829	8.1
32	35613	0.20326	2853	7.7
33	15204	0.20568	2872	10.5
34	24804	0.19424	2778	8.2
35	17027	0.19728	2804	5.8
36	21866	0.19494	2784	8.4
37	13148	0.20815	2891	9.3
38	27502	0.20821	2892	6.1
39	26648	0.20452	2863	8.3
40	27263	0.18701	2716	10.7
41	46499	0.14869	2331	6.7
42	36471	0.20245	2846	6.7
43	64587	0.20102	2834	8.7
44	31986	0.20332	2853	8.9
45	46174	0.21292	2928	8.9
46	61284	0.20775	2888	6.6
47	41436	0.20439	2862	6.8
48	72510	0.20430	2861	5.1
49	67124	0.20347	2854	7.9
50	37221	0.19866	2815	7.0

Spot	^{206}Pb (cps)	^{207}Pb/^{206}Pb	Age (Ma)	2σ %
464435 Metasediment, Naternaq				
1	620630	0.12031	1961	4
2	184109	0.14293	2261	4
3	177844	0.12013	1959	4
4	508546	0.12356	2019	4
5	521502	0.11208	1833	4
6	560514	0.11545	1887	4
7	455565	0.10976	1795	4
8	294092	0.11916	1944	4
9	407244	0.12342	2006	4
10	217026	0.11556	1889	4
11	240050	0.11948	1948	4
12	285058	0.12258	1995	4
13	651523	0.11831	1938	4
14	367681	0.12552	2036	4
15	337595	0.12582	2041	4
16	465635	0.11732	1917	4
17	321964	0.12267	1995	4
18	1150971	0.11774	1922	4
19	266990	0.12383	2013	4
20	374761	0.12502	2030	4
21	297903	0.12321	2002	4
22	87395	0.11806	1927	4.3
23	88706	0.12335	2005	6.5
24	53359	0.13734	2194	6.5
25	72472	0.11727	1915	5.8
26	16174	0.13058	2106	4.4
27	125924	0.11860	1935	4.6
28	81398	0.11940	1947	6.3
29	93208	0.11402	1864	6.3
30	131504	0.12001	1956	4.2
31	107212	0.12410	2016	6.6
32	66177	0.12687	2055	7.7
33	72338	0.11608	1897	4.1
34	163168	0.11450	1872	4.4
35	92298	0.12172	1982	5.5
36	220614	0.12305	2001	4.3
37	112247	0.12249	1993	5.7
38	76097	0.11662	1905	4.7
39	76847	0.11907	1942	4.1
40	39338	0.11918	1944	6.8
41	51130	0.11856	1935	6.6
42	86970	0.12690	2055	5.0
43	128237	0.11865	1936	5.3
44	47126	0.12236	1991	5.5
45	84328	0.11894	1940	5.6
46	307611	0.12127	1975	5.0
47	115975	0.11797	1926	6.9
48	149629	0.12005	1957	7.5
49	385671	0.11759	1920	7.7
50	454534	0.12076	1967	6.8
51	245715	0.11875	1937	7.4
52	320479	0.12160	1980	6.4
53	1098422	0.10860	1776	7.8
54	578352	0.12047	1963	4.1
55	186864	0.11804	1927	7.0
56	79299	0.11614	1898	5.5
57	255968	0.10900	1783	3.3
58	707747	0.11876	1938	7.4
59	97872	0.12173	1982	6.5
60	109798	0.11649	1903	5.4
61	489175	0.12003	1957	4.0
470515 Pegmatite NE of Kangaatsiaq				
1	149998	0.11231	1837	3.3
2	114249	0.11111	1818	2.3
3	128681	0.11066	1810	2.5
4	249115	0.11405	1865	2.5
5	174468	0.11307	1849	2.2
6	188664	0.11253	1841	2.7
7	118304	0.11223	1836	3.0
8	69708	0.11414	1866	4.3
9	107108	0.11379	1861	3.5
10	57749	0.11019	1803	5.2
11	255076	0.11091	1814	2.7
12	112190	0.11350	1856	4.7
13	145495	0.11459	1873	3.2

Spot	^{206}Pb (cps)	^{207}Pb/^{206}Pb	Age (Ma)	2σ %
14	162431	0.11214	1834	4.2
15	42424	0.11157	1825	5.5
16	109374	0.11367	1859	4.3
17	52552	0.11218	1835	6.4
18	67018	0.11372	1860	5.2
19	38574	0.11173	1828	5.3
20	184531	0.11162	1826	2.5
21	420598	0.11279	1845	2.5
22	675700	0.11206	1833	1.7
480041 Quartz diorite, Qasigiannguit				
1	130744	0.19864	2815	5.2
2	127784	0.19639	2796	4.7
3	30286	0.19684	2800	4.6
4	28769	0.20120	2836	4.7
5	41484	0.19738	2805	4.7
6	19837	0.20222	2844	7.0
7	35270	0.19516	2786	5.5
8	48190	0.20117	2836	5.6
9	35231	0.19155	2756	5.0
10	93023	0.19849	2814	4.8
11	36116	0.19465	2782	4.8
12	82370	0.19490	2784	10.4
13	58322	0.19959	2823	7.2
14	61328	0.19932	2821	6.7
15	58943	0.19951	2822	11.6
16	25024	0.19642	2797	3.7
17	61436	0.19260	2765	5.7
18	56976	0.19778	2808	7.2
19	43379	0.19673	2799	5.3
20	68466	0.19216	2761	7.7
480054 Tonalite intruding mafic complex				
1	8174	0.20380	2857	10.3
2	10419	0.19353	2772	7.4
3	18592	0.20474	2864	5.5
4	213185	0.15919	2447	5.9
5	17238	0.19681	2800	5.3
6	11204	0.20444	2862	6.4
7	17603	0.20266	2848	7.2
8	36568	0.20791	2889	9.5
9	42107	0.20580	2873	6.5
10	30492	0.19888	2817	7.1
11	25591	0.20251	2847	7.2
12	14106	0.20374	2856	6.4
13	18218	0.20025	2828	4.4
14	20117	0.19869	2816	5.8
15	42704	0.20836	2893	6.8
16	29583	0.20336	2853	7.6
17	23900	0.19738	2805	9.0
483631 Granite intruding metasediment				
1	259347	0.19195	2759	3.1
2	155094	0.19256	2764	2.4
3	94380	0.19393	2776	3.3
4	33706	0.18539	2702	3.7
5	57040	0.18930	2736	3.2
6	42007	0.19204	2760	3.5
7	71104	0.19592	2793	3.8
8	33803	0.19616	2794	4.1
9	79316	0.19110	2752	3.9
10	13550	0.18486	2697	7.3
11	57313	0.19407	2777	4.3
12	56128	0.19155	2756	3.1
13	56620	0.19591	2792	3.4
14	101430	0.19250	2764	3.6
15	41779	0.19211	2760	3.4
16	367814	0.19593	2793	2.0
17	118779	0.18771	2722	2.7
18	26473	0.16345	2492	13.9
19	45218	0.19626	2795	3.6
20	76399	0.19586	2792	3.6
21	24409	0.18865	2730	4.7

Table 2. Zircon ion probe U-Th-Pb data from sample 464435, Naternaq

Spot #	U ppm	Th ppm	Pb ppm	Th/U measured	f^{206} %	$^{207}Pb/^{206}Pb$	σ %	$^{207}Pb/^{235}U$	σ %	$^{206}Pb/^{238}U$	σ %	Disc. % (conv.)	Ages (Ma) $^{207}Pb/^{206}Pb$	σ	$^{207}Pb/^{235}U$	σ	$^{206}Pb/^{238}U$	σ
1	404	161	167	0.40	0.37	0.1160	0.36	5.390	1.81	0.3370	1.77	–1.4	1898	6	1935	16	1970	30
2	384	170	170	0.44	0.02	0.1162	0.33	5.727	1.80	0.3575	1.77	4.4	1894	13	1875	17	1858	29
3	235	121	101	0.51	1.34	0.1159	0.75	5.338	1.93	0.3341	1.78	–2.2	1911	6	1898	16	1886	29
4	411	178	173	0.43	0.24	0.1170	0.33	5.483	1.81	0.3398	1.77	–1.5	1892	6	1906	16	1918	29
5	489	195	208	0.40	0.24	0.1158	0.32	5.534	1.80	0.3466	1.77	1.6	1916	6	1902	16	1890	29
6	360	123	149	0.34	0.02	0.1174	0.33	5.511	1.80	0.3406	1.77	–1.6	1895	6	1906	16	1917	29
7	416	163	176	0.39	0.04	0.1160	0.31	5.537	1.80	0.3463	1.77	1.3	1909	6	1921	16	1932	30
8	413	178	178	0.43	0.03	0.1169	0.31	5.629	1.80	0.3494	1.77	1.4	1860	7	1775	15	1704	27
9	653	281	239	0.43	0.70	0.1137	0.40	4.743	1.82	0.3025	1.77	–9.5	1901	7	1901	16	1900	29
10	237	88	99	0.37	0.04	0.1163	0.39	5.500	1.81	0.3429	1.77	0.0	1896	7	1883	16	1872	29
11	239	108	101	0.45	0.05	0.1174	0.39	5.521	1.81	0.3410	1.77	–1.6	1918	7	1904	16	1891	29
12	448	224	194	0.50	0.03	0.1170	0.39	5.539	1.81	0.3434	1.77	–0.5	1911	7	1907	16	1903	29
13	2192	1713	975	0.78	0.15	0.1165	0.17	5.337	1.78	0.3323	1.77	–3.3	1903	3	1875	15	1849	2

Errors on ratios and ages are quoted at 1σ level.
f^{206} %: The fraction of common ^{206}Pb, estimated from the measured ^{204}Pb.
Disc. % (conv.): Degree of discordance of the zircon analysis (at the centre of the error ellipse).

that the northern and eastern parts of the study area are strongly reworked by Nagssugtoqidian deformation and amphibolite facies metamorphism.

Geochronological targets and methods

Both Archaean and Palaeoproterozoic supracrustal sequences are known to exist within the Nagssugtoqidian orogen (Marker *et al.* 1999; Nutman *et al.* 1999). Depositional ages of such supracrustal belts may be constrained by the ages of detrital zircons in their sedimentary components, since the youngest grains define their maximum age of deposition; conversely, the age of a magmatic rock that has intruded the supracrustal sequence may serve to define a lower depositional age limit. Ideally, both metasediment and cross-cutting magmatic rocks from the same outcrop should be analysed to best constrain the timing of deposition. However, cross-cutting intrusive rocks of appropriate age (i.e. other than late Palaeoproterozoic pegmatites) were not generally present. The direct dating of Archaean or Palaeoproterozoic deformation by dating e.g. synkinematic granitoids requires the rather scarce occurrence of an intrusive rock that unequivocally both cuts and is affected by a single fabric.

Ten samples from the Kangaatsiaq–Qasigiannguit area, mainly provided by members of the GEUS mapping groups in 2001–2002, have been analysed by quadrupole laser ablation inductively coupled mass spectrometry (LA-ICP-MS) at the University of Texas at Austin (zircon Pb-Pb data, Table 1); additional ion probe U-Pb zircon data from one metasedimentary rock were obtained at the NORDSIM laboratory, Naturhistoriska Riksmuseet, Stockholm (Table 2). Analytical details are given in the appendix. The samples were collected from seven different, dismembered metasedimentary sequences (four samples of metasediment and four samples of cross-cutting granitoid rocks), and from intrusive granite and orthogneiss that constrain the timing of deformation (two samples). All ages of rocks presented in this manuscript have been calculated using Isoplot/Ex (Ludwig 1999) and are reported with 2-sigma uncertainties.

The main advantage of using the LA-ICP-MS technique for zircon geochronology is that each analysis only lasts about two minutes, whereas the analytical time on an ion microprobe is typically around 15–20 minutes. This becomes an important factor when analysing detrital rocks, where analysis of a large number of detrital grains is essential to achieve good statistics. The major limitation of the LA-ICP-MS technique employed is that U-Pb ratios could not be measured, and only $^{207}Pb/^{206}Pb$ ages are obtained. A direct indication of concordance therefore is not available, and all the ages obtained should be interpreted conservatively to represent minimum ages of crystallisation or metamorphism. Furthermore, common Pb corrections cannot be carried out due to interference in the plasma of ^{204}Hg from the carrier gases. A test of the LA-ICP-MS instrument used in this study was carried out by Connelly *et al.* (2006), who analysed zircons from the Itilli diorite, Disko Bugt, West Greenland using both LA-ICP-MS and ID-TIMS methods and found that the $^{207}Pb/^{206}Pb$ age of 3019 ± 23 Ma obtained with the laser instrument compared well with its ID-TIMS age of 3030 +8/–5 Ma.

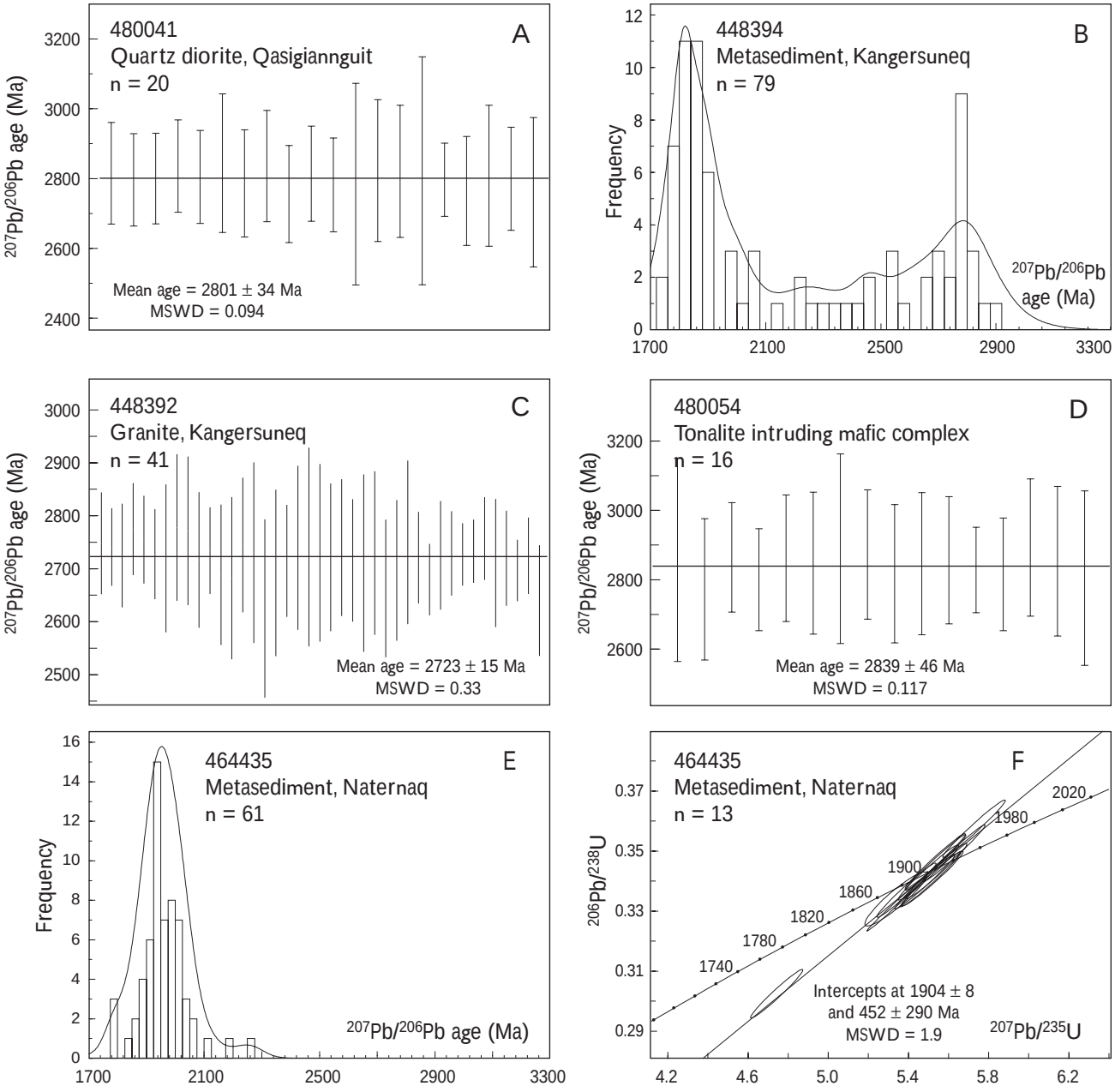

Fig. 2. Zircon age data from the Kangaatsiaq–Qasigiannguit region. A, C, D, G, J, K: Weighted average plots of LA-ICP-MS $^{207}Pb/^{206}Pb$ age data of igneous rocks. B, E, H, I: Probability density plots of LA-ICP-MS $^{207}Pb/^{206}Pb$ age data of metasediments. F: Ion probe U-Pb age data (concordia plot), sample 464435.

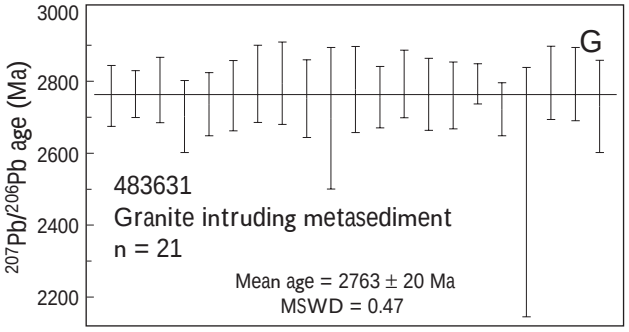

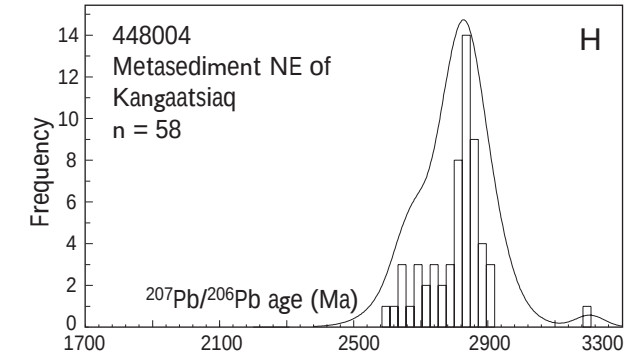

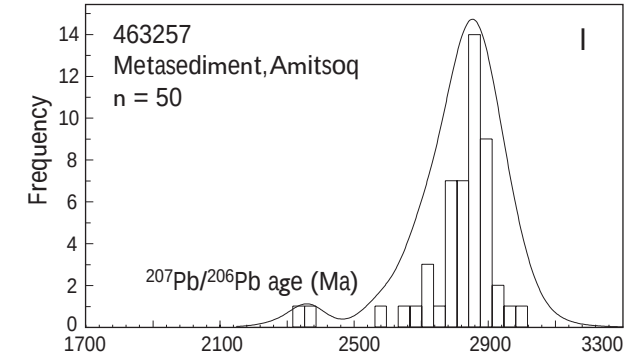

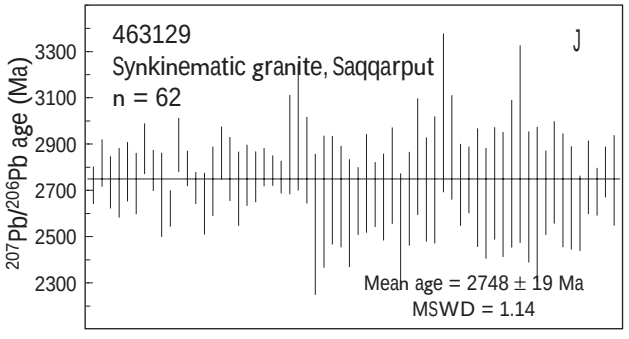

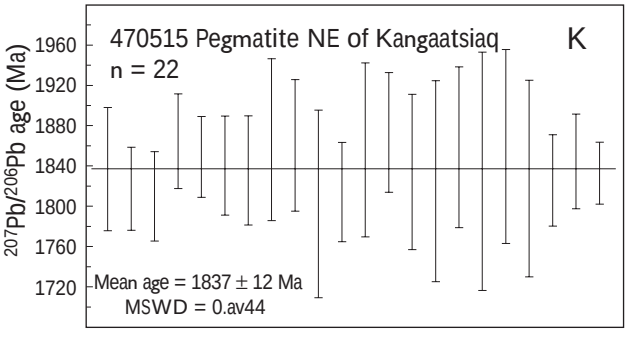

Geochronological age constraints of metasedimentary belts

The study area contains numerous, dismembered, discontinuous belts of metasedimentary rocks that may be either Archaean or Palaeoproterozoic in age. While the main focus of this work was to constrain their timing of deposition, provenance information gained through the detrital zircons permits regional correlation of these metasedimentary belts. The analysed samples are presented in Tables 1–2 and Fig. 2 and discussed below from north to south.

Sample 480041, quartz diorite intruding metasedimentary and metavolcanic rocks at Qasigiannguit

Sample 480041 of a homogeneous, grey, medium-grained quartz diorite was collected 3 km east of Qasigiannguit at 68°48.83′N, 51°08.05′W (Fig. 1). The rock consists of plagioclase, quartz, hornblende and biotite and has a strong linear fabric. The quartz diorite forms a 3–4 km long elongate body exposed on the top of the ridge facing Qasigiannguit. Its contact relationships are generally equivocal due to deformation, but at the south-western margin the contact appears to be intrusive into a metasedimentary-metavolcanic sequence.

The zircons from this sample are clear and stubby. Twenty grains were analysed, which yield consistent $^{207}Pb/^{206}Pb$ ratios corresponding to a weighted mean age of 2801 ± 34 Ma (MSWD = 0.094, Fig. 2A). The age is interpreted as the crystallisation age of the quartz diorite, implying that the supracrustal sequence it cuts must also be Archaean.

Samples 448394, metasediment and 448392, intruding granite on the south coast of Kangersuneq

Sample 448394 (68°46.24′N, 50°52.16′W) from a pelitic metasedimentary rock and sample 448392 (68°46.20′N, 50°51.55′W) of a granite that cuts the metasedimentary belt, were collected *c.* 200 m apart on the south coast of Kangersuneq (Fig. 1). After the analytical results were obtained, the locality was revisited in 2003 and the previously reported field relations confirmed (Jeroen van Gool, personal communication 2003).

The zircons from the metasediment are brownish, elongate, 100–200 µm long, and in many cases cracked and showing clear signs of dissolution. The least altered and, presumably, least disturbed zircons were chosen for anal-

yses. In several cases it was possible to distinguish broad rims containing more U than the cores, and in such cases both core and rim were analysed. Seventy-nine spots were analysed and yield an age spectrum with a large peak at 1850 Ma and a smaller one at 2800 Ma (Fig. 2B). A range of intermediate ages (2500–2100 Ma) between the two peaks are also present (see below). The Archaean peak comprises only analyses from cores, whereas the 1850 Ma peak consists of analyses from both cores and rims.

The zircons from the granite are typically brown, and larger than those in the metasediment. In size they range from 100–350 µm and occur both as slender and somewhat stubby crystals. Core–rim zonation is observed in the majority of the zircons. Of 44 grains analysed from the granite, 41 yielded a consistent pattern of $^{207}Pb/^{206}Pb$ ratios corresponding to an average age of 2723 ± 15 Ma (MSWD = 0.33) (Fig. 2C); both cores and rims were analysed in several grains without observing any age variations. The remaining three grains yield ages from 2822 to 2807 Ma and are most likely inherited. Due to the homogeneity of the zircon population it is highly unlikely that the zircons are detrital grains inherited from the metasediment. They are also unlikely to have been inherited from the orthogneisses adjacent to the metasediment, as these do not generally contain such young zircons. Therefore, the age of 2723 ± 15 Ma is interpreted as the emplacement age of the granite, and the metasediment must also be of Archaean age. The 1850 Ma peak for the zircons in the metasediment is therefore interpreted to date Nagssugtoqidian metamorphism, and the 2500–2100 Ma ages most likely represent Archaean zircons that have suffered Pb-loss; alternatively the latter analyses might represent accidental mixtures of cores and rims.

Sample 480054, tonalite intruding mafic complex *c.* 25 km south-east of Kangersuneq

Sample 480054, a biotite-hornblende tonalite, was collected from a relatively undeformed tonalitic body *c.* 2 km^2 in size at 68°35.53′N, 50°30.28′W within a large mafic supracrustal complex near the Inland Ice about 25 km south-east of Kangersuneq (Fig. 1). The tonalite is light grey in colour, medium- to coarse-grained, homogeneous, and has a weak linear fabric. It is feldspar-phyric with phenocrysts up to 2 cm in diameter. Near the contacts with the surrounding mafic rocks the tonalite contains xenoliths of the mafic supracrustal rocks, and its intrusive nature is unequivocal. Dykes of tonalite, 50 cm to 2 m wide, extend from the main tonalite body into rocks of the surrounding large mafic complex.

The tonalite sample yielded a population of large, euhedral, mostly prismatic, clear to yellow zircons. Seventeen spots on zircon grains were analysed, and sixteen of them generated a consistent spectrum of $^{207}Pb/^{206}Pb$ ratios corresponding to an average age of 2839 ± 46 Ma (MSWD = 0.117) (Fig. 2D). The consistent $^{207}Pb/^{206}Pb$ ratios indicate that little or no Pb-loss has occurred. The age result is therefore interpreted to closely reflect the crystallisation age of the tonalite, and the mafic complex intruded by the tonalite must consequently also be Archaean.

Sample 464435, metasedimentary rock from the Naternaq supracrustal belt

Naternaq (Lersletten) is an extensive Quaternary outwash plain with scattered outcrops of Precambrian basement gneisses and supracrustal rocks (Østergaard *et al.* 2002). A sample of very fine-grained mica schist was collected from the extensive Naternaq supracrustal belt at 68°24.10′N, 51°56.70′W (Fig. 1). The zircons are elongate, 50–150 µm long, and vary in colour from clear to slightly brown. All 61 analyses carried out yield Palaeoproterozoic $^{207}Pb/^{206}Pb$ ages ranging from 2261 to 1776 Ma, with the main peak of $^{207}Pb/^{206}Pb$ ages around 1950 Ma (Fig. 2E). While it is possible that some of the younger grains may be metamorphic, we interpret the majority of the grains to be detrital because of the igneous appearance of the zircons and because they are older than any metamorphic event so far described in the Nagssugtoqidian orogen (e.g. Connelly *et al.* 2000, earliest metamorphism at *c.* 1870 Ma). Furthermore, it seems unlikely that a zircon population from a metasedimentary rock would only comprise metamorphic grains and not contain a single detrital grain. Consequently this requires a Palaeoproterozoic deposition age for the metasedimentary unit at Naternaq.

In order to confirm the obtained $^{207}Pb/^{206}Pb$ LA-ICP-MS ages, zircons from this sample were also analysed on the CAMECA IMS 1270 ion microprobe at the NORDSIM Laboratory, Swedish Museum of Natural History, Stockholm. The thirteen ion probe analyses yield a cluster of ages on the concordia diagram of Fig. 2F (Table 2), with an upper intercept isochron age of 1904 ± 8 Ma (MSWD = 1.9). The ion probe age is thus slightly younger than the *c.* 1950 Ma peak obtained by LA-ICP-MS, but the two data sets overlap within the large analytical error of the latter method, and the apparent older LA-ICP-MS age could be due to common Pb for which we were unable to correct. In conclusion, the ion probe data clearly demonstrate that the zircons are older than any metamorphic ages hitherto obtained from the Nagssug-

toqidian orogen. The most likely interpretation is that the sediment at Naternaq was derived from the magmatic arc that formed in the central part of the orogen between 1920 and 1870 Ma (Kalsbeek *et al.* 1987; Kalsbeek & Nutman 1996; Whitehouse *et al.* 1998; Connelly *et al.* 2000). The new age data from the Naternaq supracrustal belt have important consequences for the structural interpretation of the Naternaq area, documenting the existence of large Palaeoproterozoic folds.

Sample 483631, granite vein intruding metasediment on strike with the Naternaq supracrustal sequence

A sample (483631) of an 8 cm wide vein of muscovite-biotite granite vein was collected east of Naternaq at 68°31.04′N, 51°17.87′W (Fig. 1). The granite vein is deformed but clearly intrudes mica schist on strike with the eastern part of the Naternaq supracrustal belt.

Most of the zircons in sample 483631 are long, prismatic grains with a distinct core-rim zonation and range from clear to brownish in colour. Twenty-two analyses were carried out, mostly on cores, but also on a few rims. All except one analysis yielded consistent $^{207}Pb/^{206}Pb$ ratios corresponding to an average age of 2763 ± 20 Ma (MSWD = 0.47, Fig. 2G). One core analysis yielded a $^{207}Pb/^{206}Pb$ age of 2467 ± 158 Ma, which may be due to Pb-loss. The analyses demonstrate that the granite is Archaean. The regional basement does not generally contain orthogneisses with such young ages and, therefore, limits the possibility that the zircons in the granite were inherited. It follows that the supracrustal rocks east of Naternaq on strike with the Naternaq supracrustal belt must also be of Archaean age.

Sample 448004, metasedimentary belt near Kangaatsiaq

Sample 448004 of a quartz-rich metasedimentary rock was collected north-east of Kangaatsiaq at 68°21.15′N, 53°13.18′W (Fig. 1). The zircons vary from elongate to stubby but all have been rounded during transport. They are clear and between 50 to 200 µm in length. A weak igneous zonation is present in the majority of the grains. Fifty-eight spots were analysed, and both core and rim were analysed in several grains. The age population ranges from 2909 to 2595 Ma, with a single grain yielding an age of 3200 Ma (Fig. 2H). A peak is present around 2850 Ma, which is a common age for polyphase orthogneisses within the Nagssugtoqidian orogen (Kalsbeek *et al.* 1987; Kalsbeek & Nutman 1996; Whitehouse *et al.* 1998; Connelly & Mengel 2000; Hollis *et al.* 2006, this volume). The scatter of younger ages from 2800 to 2595 Ma most likely results from variable degrees of Pb loss. We cannot with certainty assign an age of deposition to this sediment, as the data are compatible with both Archaean and Palaeoproterozoic sedimentation.

Sample 463257, quartz-rich metasedimentary sequence at Amitsoq

Sample 463257 of a medium- to fine-grained, quartz-rich metasedimentary rock with abundant small garnets was collected at the head of the fjord Amitsoq at 68°05.78′N, 52°30.99′W (Fig. 1). It is part of an extensive metasedimentary sequence, which is significantly more quartz-rich than all other metasedimentary rocks reported from the Kangaatsiaq map area, although similar rocks have been observed in the central Nagssugtoqidian orogen (Jeroen van Gool, personal communication 2003).

The zircons are clear, 50–250 µm in length and vary from elongate to stubby, and have been rounded during transport. Most zircons show clear igneous zonation, and some contain a high-U metamorphic rim. This rim was unfortunately too thin to analyse with the LA-ICP-MS. All except two of the 50 analysed grains yield Archaean ages, with two exceptions interpreted to have suffered Pb-loss. The zircons show very little age variation, with a major peak of $^{207}Pb/^{206}Pb$ ages at around 2850 Ma (Fig. 2I). This age is comparable to that of the surrounding regional orthogneisses, and indicates that the detritus may be locally derived. However, it is only possible to conclude that the sediment was deposited after 2850 Ma.

Dating of deformation using synkinematic granitic rocks

Sample 463129, synkinematic granite vein at Saqqarput

A sample of synkinematic granite (463129) was collected at Saqqarput at 68°09.22′N, 52°42.65′W (Fig. 1). The granite occurs as fine- to medium-grained, subconcordant veins in the orthogneiss. Sixty-two analyses yielded $^{207}Pb/^{206}Pb$ ratios corresponding to an average $^{207}Pb/^{206}Pb$ age of 2748 ± 19 Ma (MSWD = 1.14; Fig. 2J). This is interpreted to be the crystallisation age of the granite since, as in sample 483631 described above, it is unlikely that zircons

of this age are inherited. Some of the observed deformation in the host basement orthogneisses must, therefore, also be Archaean in age.

Sample 470515, pegmatite north-east of Kangaatsiaq

A sample of pegmatite (470515) was collected north-east of Kangaatsiaq at 68°20.23′N, 59°00.17′W (Fig. 1). The pegmatite forms a 020° trending vertical sheet cutting orthogneiss. The pegmatite is a member of a conjugate set of pegmatites within the Kangaatsiaq map area that indicate late, regional N–S orientated compression (Ian Alsop, personal communication 2002), and itself contains evidence of ductile sinistral shear along its margins; the regional foliation is deflected into sinistral shear fabrics, indicating that the pegmatite emplacement took place later than the foliation formation in the gneisses, but while the host rock was still hot enough to behave in a ductile manner.

The sample contains large, brownish, prismatic zircons that vary from slender to short and stubby in shape. Twenty-two spots were analysed on thirteen grains. Both rims and cores were analysed on several grains, but no age variation was documented between the two. All analyses yield the same result within uncertainties; the average $^{207}Pb/^{206}Pb$ ratio corresponds to an age of 1837 ± 12 Ma (MSWD = 0.44) (Fig. 2K). This is interpreted to be the emplacement age of the pegmatite, and is considered to date the late Nagssugtoqidian N–S compression.

Discussion and conclusions

The zircon ages obtained from this study show that metasedimentary rocks in the Kangaatsiaq–Qasigiannguit region are predominately Archaean in age. The best age constraints come from the four Archaean granitoid rocks that cut four different supracrustal belts. Only one metasediment was analysed from these belts and yields an Archaean detrital peak of *c.* 2800 Ma and a Palaeoproterozoic peak of *c.* 1850 Ma. The Palaeoproterozoic peak is attributed to the growth of metamorphic zircon during Nagssugtoqidian metamorphism. Similarly, the occurrences of ages between 2800–1850 Ma are attributed to Pb-loss from detrital grains and/or mixed analysis of detrital and metamorphic zircon. Two of the three remaining metasedimentary rocks yield only Archaean detrital ages with peaks between 2800 and 2900 Ma, which are similar to the ages of the basement orthogneisses in the Nagssugtoqidian orogen (Kalsbeek *et al.* 1987; Kalsbeek & Nutman 1996; Whitehouse *et al.* 1998; Connelly & Mengel 2000) and may indicate that the sedimentary sequences were derived from local sources. While it is tempting to conclude that these metasediments might also themselves be of Archaean age, the lack of cross-cutting granites from these locations only permits the conclusion that they must be younger than 2850 Ma. Thus, the sediments could have been deposited either in the Archaean at around 2850–2750 Ma (i.e., before the regional 2.75 Ga metamorphism documented within the Nagssugtoqidian orogen), or during the Palaeoproterozoic (most likely before the formation of the Arfersiorfik–Sisimiut arc; Kalsbeek *et al.* 1987; Kalsbeek & Nutman 1996; Whitehouse *et al.* 1998; Connelly *et al.* 2000).

The remaining sample of metasediment (464435), collected from the Naternaq supracrustal belt, is the only metasediment in this study which is interpreted to be of Palaeoproterozoic age. Similar rocks which crop out south of Sydostbugten to the north-east have previously been interpreted as along-strike equivalents of the Naternaq supracrustal belt, although the intervening area is partly concealed by Quaternary deposits (Fig. 1). However, the discordant Archaean granitic vein (483631) that cuts the metasedimentary rocks south of Sydostbugten requires that the two belts contain rocks of different age.

It is interesting to note that all the Archaean detrital ages obtained match the ages between 2850 and 2800 Ma of the Archaean basement gneisses in the central Nagssugtoqidian orogen. This distinguishes the metasedimentary rocks of the study area from metasedimentary rocks in the Rinkian belt to the north, which include detrital zircons that are as old as 3600 Ma (Thrane *et al.* 2003).

The predominance of Archaean metasedimentary rocks unfortunately precludes them from being useful marker horizons to partition Archaean and Palaeoproterozoic deformation. Nevertheless, the 2748 ± 19 Ma synkinematic granite (463129) from Saqqarput south-east of Kangaatsiaq dates large fold structures in the northern Nagssugtoqidian basement at around this age, which overlaps with the previously defined age of Archaean deformation and metamorphism in the central part of the orogen (e.g. Connelly & Mengel 2000).

The new age data place several constraints on the timing and style of Palaeoproterozoic metamorphism and deformation in the region. The Palaeoproterozoic sediment at Naternaq (sample 464435) was probably metamorphosed and deformed shortly after its deposition, in line with the significant *c.* 1850 Ma metamorphic peak in the Archaean sediment from Kangersuneq (sample 448394). The metamorphic zircon age from this sample

is not very precise, and TIMS analyses would be necessary to obtain an exact age of the metamorphism. However, it correlates with previous estimates for the timing of deformation and metamorphism both north and south of the study area (Kalsbeek *et al.* 1987; Kalsbeek & Nutman 1996; Whitehouse *et al.* 1998; Connelly *et al.* 2000; Thrane *et al.* 2003; Connelly *et al.* 2006). Furthermore, a late phase of N–S-directed shortening is dated at 1837 ± 12 Ma by a synkinematic pegmatite (470515). The age of this pegmatite may correlate with the 1821 Ma D2 deformation event defined in the central Nagssugtoqidian orogen by Connelly *et al.* (2000), and with 1821–1823 Ma deformation east of Ilulissat in the north (Connelly *et al.* 2006).

Acknowledgements

Funding by the Carlsberg Foundation (Thrane) and the National Science Foundation (grant EAR-0337594 to Connelly) is gratefully acknowledged. We thank Ian Alsop (University of St. Andrews), Adam A. Garde and Jeroen van Gool (GEUS) for providing samples. We also thank John Lansdown (The University of Texas at Austin) for assisting in collecting the LA-ICP-MS data, and Julie A. Hollis and Adam A. Garde (GEUS) for re-analysing sample 464435 zircons on the ion microprobe. Allen P. Nutman and Åke Johansson are thanked for their constructive comments, and Adam A. Garde and A.K. Higgins are thanked for help with the geological introduction.

References

Árting, U.E. 2004: A petrological study of basic dykes and sills of assumed Palaeoproterozoic age in central western Greenland, 122 pp., two appendices. Unpublished M.Sc. thesis, University of Copenhagen, Denmark.

Connelly, J.N. & Mengel, F.C. 2000: Evolution of Archean components in the Nagssugtoqidian orogen, West Greenland. Geological Society of America Bulletin 112, 747–763.

Connelly, J.N., van Gool, J.A.M. & Mengel, F.C. 2000: Temporal evolution of a deeply eroded orogen: the Nagssugtoqidian orogen, West Greenland. Canadian Journal of Earth Sciences 37, 1121–1142.

Connelly, J.N., Thrane, K., Krawiec, A.W. & Garde, A.A. 2006: Linking the Palaeoproterozoic Nagssugtoqidian and Rinkian orogens through the Disko Bugt region of West Greenland. Journal of the Geological Society (London) 163, 319–335.

Garde, A.A. 2004: Geological map of Greenland, 1:100 000, Kangaatsiaq 68 V.1 Syd. Copenhagen: Geological Survey of Denmark and Greenland.

Glassley, W.E. & Sørensen, K. 1980: Constant P_S-T amphibolite to granulite facies transition in Agto (West Greenland) metadolerites: implications and applications. Journal of Petrology 21, 69–105.

Hollis, J.A., Keiding, M., Stensgaard, B.M., van Gool, J.A.M. & Garde, A.A. 2006: Evolution of Neoarchaean supracrustal belts at the northern margin of the North Atlantic Craton, West Greenland. In: Garde, A.A. & Kalsbeek, F. (eds): Precambrian crustal evolution and Cretaceous–Palaeogene faulting in West Greenland. Geological Survey of Denmark and Greenland Bulletin 11, 9–31 (this volume).

Kalsbeek, F. & Nutman, A.P. 1996: Anatomy of the Early Proterozoic Nagssugtoqidian orogen, West Greenland, explored by reconnaissance SHRIMP U-Pb dating. Geology 24, 515–518.

Kalsbeek, F., Pidgeon, R.T. & Taylor, P.N. 1987: Nagssugtoqidian mobile belt of West Greenland: a cryptic 1850 Ma suture between two Archaean continents – chemical and isotopic evidence. Earth and Planetary Science Letters 85, 365–385.

Ludwig, K.R. 1999: Isoplot/Ex version 2.00 – A geochronological toolkit for Microsoft Excel. Berkeley Geochronology Center, Special Publication 2.

Marker, M., Whitehouse, M., Scott, D., Stecher, O., Bridgwater, D. & van Gool, J.A.M. 1999: Deposition, provenance and tectonic setting for metasediments in the Palaeoproterozoic Nagssugtoqidian orogen, West Greenland: a key for understanding crustal collision. Abstracts EUG 10, Strasbourg, France.

Mazur, S., Piazolo, S. & Alsop, G.I. 2006: Structural analysis of the northern Nagssugtoqidian orogen, West Greenland: an example of complex tectonic patterns in reworked high-grade metamorphic terrains. In: Garde, A.A. & Kalsbeek, F. (eds): Precambrian crustal evolution and Cretaceous–Palaeogene faulting in West Greenland. Geological Survey of Denmark and Greenland Bulletin 11, 163–178 (this volume).

Nutman, A.P., Kalsbeek, F., Marker, M., van Gool, J.A.M. & Bridgwater, D. 1999: U-Pb zircon ages of Kangâmiut dykes and detrital zircons in metasediments in the Palaeoproterozoic Nagssugtoqidian orogen (West Greenland): clues to the pre-collisional history of the orogen. Precambrian Research 93, 87–104.

Østergaard, C., Garde, A.A., Nygaard, J., Blomsterberg, J., Nielsen, B.M., Stendal, H. & Thomas, C.W. 2002: The Precambrian supracrustal rocks in the Naternaq (Lersletten) and Ikamiut areas, central West Greenland. Geology of Greenland Survey Bulletin 191, 24–32.

Piazolo, S., Alsop, G.I., van Gool, J. & Nielsen, B.M. 2004: Using GIS to unravel high strain patterns in high grade terranes: a case study of indentor tectonics from West Greenland. In: Alsop, G.I. *et al.* (eds): Flow processes in faults and shear zones. Geological Society Special Publication (London) 224, 63–78.

Schuhmacher, M., de Chambost, E., McKeegan, K.D., Harrison, T.M. & Migeon, H. 1994: In situ dating of zircon with the CAMECA ims 1270. In: Benninghoven, A. (ed.): Secondary Ion Mass Spectrometry SIMS IX, 919–922. Chichester: Wiley.

Thrane, K., Connelly, J.N., Garde, A.A., Grocott, J. & Krawiec, A. 2003: Linking the Palaeoproterozoic Rinkian and Nagssugtoqidian belts of central W. Greenland: implications of new U-Pb and Pb-Pb ages. European Union of Geosciences Meeting, Geophysical Research Abstracts, CD 5, Abstract # 09275.

van Gool, J.A.M. *et al.* 2002: Precambrian geology of the northern Nagssugtoqidian orogen: mapping in the Kangaatsiaq area. Geology of Greenland Survey Bulletin 191, 13–23.

Whitehouse, M.J., Claesson, S., Sunde, T. & Vestin, J. 1997: Ion microprobe U-Pb zircon geochronology and correlation of Archaean gneisses from the Lewisian Complex of Gruinard, north-western Scotland. Geochimica et Cosmochimica Acta 61, 4429–4438.

Whitehouse, M.J., Kalsbeek, F. & Nutman, A.P. 1998: Crustal growth and crustal recycling in the Nagssugtoqidian orogen of West Greenland: constraints from radiogenic isotope systematics and U-Pb zircon geochronology. Precambrian Research 91, 365–381.

Wiedenbeck, M., Allé, P., Corfu, F., Griffin, W.L., Meier, M., Oberli, F., von Quardt, A., Roddick, J.C. & Spiegel, W. 1995: Three natural zircon standards for U-Th-Pb, Lu-Hf, trace element and REE analyses. Geostandards Newsletter 19, 1–23.

Williams, I.S. 1998: U-Th-Pb geochronology by Ion Microprobe. In: McKibben, M.A., Shanks III, W.C. & Ridley, W.I. (eds): Applications of microanalytical techniques to understanding mineralising processes. Reviews in Economic Geology 7, 1–35.

Manuscript received 15 October 2004; revision accepted 9 September 2005

Appendix

Analytical methods

Rock samples were crushed to mineral size under clean conditions using a jaw crusher and a disc pulveriser, and initial mineral separation was made using a Wilfley table at the University of Copenhagen or the University of Texas at Austin. All subsequent procedures, including sieving, heavy liquids and magnetic separation, were conducted at the University of Texas at Austin. Mineral fractions were characterised using a binocular reflected light microscope, a transmitted light petrographic microscope (with condenser lens inserted to minimise edge refraction), and a scanning cathodoluminescence (CL) imaging system on a JEOL 730 scanning electron microscope. Selected zircons of comparable size were hand picked and placed on two-sided tape, collared, and covered with epoxy. The zircons in the resulting mount were ground to approximately two thirds of their original thickness and polished. CL imaging was used to characterise the zircons before analysis.

Laser ablation analysis utilised a Merchantek 213nm YAG-laser connected to a Micromass quadrupole mass spectrometer (Platform). Fractionation and inherent detector non-linearity were accounted for by analysing zircons already well characterised by TIMS. Corrections necessary to obtain the correct $^{207}Pb/^{206}Pb$ ratios for these internal laboratory standards, covering a range of intensities and isotopic ratios, were applied to unknowns. Standards were run throughout each session. Blanks and off-peak baselines were also determined throughout each analytical session. Selecting and analysing only the highest quality zircons minimised the need for common Pb corrections using measured ^{204}Pb, a procedure made impossible by high ^{204}Hg counts. A single zircon analysis comprises approximately 450 ten-microsecond scans of $^{207}Pb/^{206}Pb$. Ratios reflecting the moving average of twenty ^{207}Pb and ^{206}Pb measurements are first plotted on a graph to check for anomalous ratios throughout a run. Those with high ratios at the beginning are presumed to reflect common Pb and are removed from further consideration. A jump from one ratio plateau to another during one analysis is interpreted to reflect piercing a core or rim of different age. Only data from one plateau at a time were considered. In cases where the beam pierces the grain too deeply and ejecta are not effectively emitted towards the end of an analysis, the signal intensity and commonly also isotope ratios change dramatically. Data from the late part of such runs were also rejected.

With this first assessment of data complete, the ^{207}Pb and ^{206}Pb data were then passed through a 4-sigma filter to remove highly anomalous counts before being passed through a more rigorous 2-sigma filter. The averages of the remaining individual measurements (typically < 5% rejection) of ^{207}Pb and ^{206}Pb provided the final $^{207}Pb/^{206}Pb$ ratio and consequent age. Given the transient signal inherent in LA-ICP-MS and sequential acquisition required by the single collector, standard statistics on multiple blocks of scans is not applicable.

A major limitation of our LA-ICP-MS protocol is that U abundances are not measured; instead only $^{207}Pb/^{206}Pb$ ratios are obtained. A direct indication of concordance is, therefore, not available and all the ages obtained should conservatively be interpreted to represent minimum ages for crystallisation.

A single sample was analysed using the CAMECA IMS 1270 ion microprobe at the NORDSIM laboratory, Naturhistoriska Riksmuseet, Stockholm. The sample was prepared in the same way as the samples analysed by LA-ICP-MS. Reference zircon 91500 from Ontario, Canada, with a weighted average $^{207}Pb/^{206}Pb$ age of 1065 Ma (Wiedenbeck *et al.* 1995), was included in the mount and used as standard. Analytical procedures and common lead corrections are similar to those described by Schuhmacher *et al.* (1994) and Whitehouse *et al.* (1997). Calibrations of Pb/U ratios are based on the observed relationship between Pb/U and UO_2/U and follow procedures similar to those used by the SHRIMP group at the Australian National University (Williams 1998).

^{207}Pb-^{206}Pb dating of magnetite, monazite and allanite in the central and northern Nagssugtoqidian orogen, West Greenland

Henrik Stendal, Karsten Secher and Robert Frei

Pb-isotopic data for magnetite from amphibolites in the Nagssugtoqidian orogen, central West Greenland, have been used to trace their source characteristics and the timing of metamorphism. Analyses of the magnetite define a Pb-Pb isochron age of 1726 ± 7 Ma. The magnetite is metamorphic in origin, and the 1726 Ma age is interpreted as a cooling age through the closing temperature of magnetite at ~600°C. Some of the amphibolites in this study come from the Naternaq supracrustal rocks in the northern Nagssugtoqidian orogen, which host the Naternaq sulphide deposit and may be part of the Nordre Strømfjord supracrustal suite, which was deposited at around 1950 Ma ago.

Pb-isotopic signatures of magnetite from the Arfersiorfik quartz diorite in the central Nagssugtoqidian orogen are compatible with published whole-rock Pb-isotopic data from this suite; previous work has shown that it is a product of subduction-related calc-alkaline magmatism between 1920 and 1870 Ma. Intrusion of pegmatites occurred at around 1800 Ma in both the central and the northern parts of the orogen. Pegmatite ages have been determined by Pb stepwise leaching analyses of allanite and monazite, and source characteristics of Pb point to an origin of the pegmatites by melting of the surrounding late Archaean and Palaeoproterozoic country rocks. Hydrothermal activity took place after pegmatite emplacement and continued below the closure temperature of magnetite at 1800–1650 Ma. Because of the relatively inert and refractory nature of magnetite, Pb-isotopic measurements from this mineral may be of help to understand the metamorphic evolution of geologically complex terrains.

Keywords: Pb isotopes, magnetite, Nagssugtoqidian orogen, Palaeoproterozoic, pegmatites, Pb stepwise leaching, supracrustal rocks

---

H.S. & K.S., *Geological Survey of Denmark and Greenland, Øster Voldgade 10, DK-1350 Copenhagen K, Denmark.*
E-mail: *hst@geus.dk*
R.F., *Geological Institute, University of Copenhagen, Øster Voldgade 10, DK-1350 Copenhagen K, Denmark.*

As part of the research programme 2000–2003 in the Nagssugtoqidian orogen of West Greenland by the Geological Survey of Denmark and Greenland (GEUS), an assessment was made of the mineral resource potential of the region between Maniitsoq (Sukkertoppen; 66°N) and the southern part of Nuussuaq (70°15′N; Stendal *et al.* 2004). The present study comprises Pb-isotopic analyses of magnetite from amphibolites, hydrothermally altered amphibolites, the Arfersiorfik quartz diorite (see below), skarn, ultramafic rocks and pegmatites. Magnetite was chosen as a medium for analysis because of its abundance in amphibolites, even though the concentration of Pb in magnetite is generally low. In addition, an attempt was made to date monazite and allanite from pegmatites by the Pb stepwise leaching (PbSL) technique (Frei & Kamber 1995). The Pb-isotopic study of the amphibolites covers the Attu, Kangaatsiaq and Qasigiannguit regions (Fig. 1). The analysed pegmatites are from the Nordre

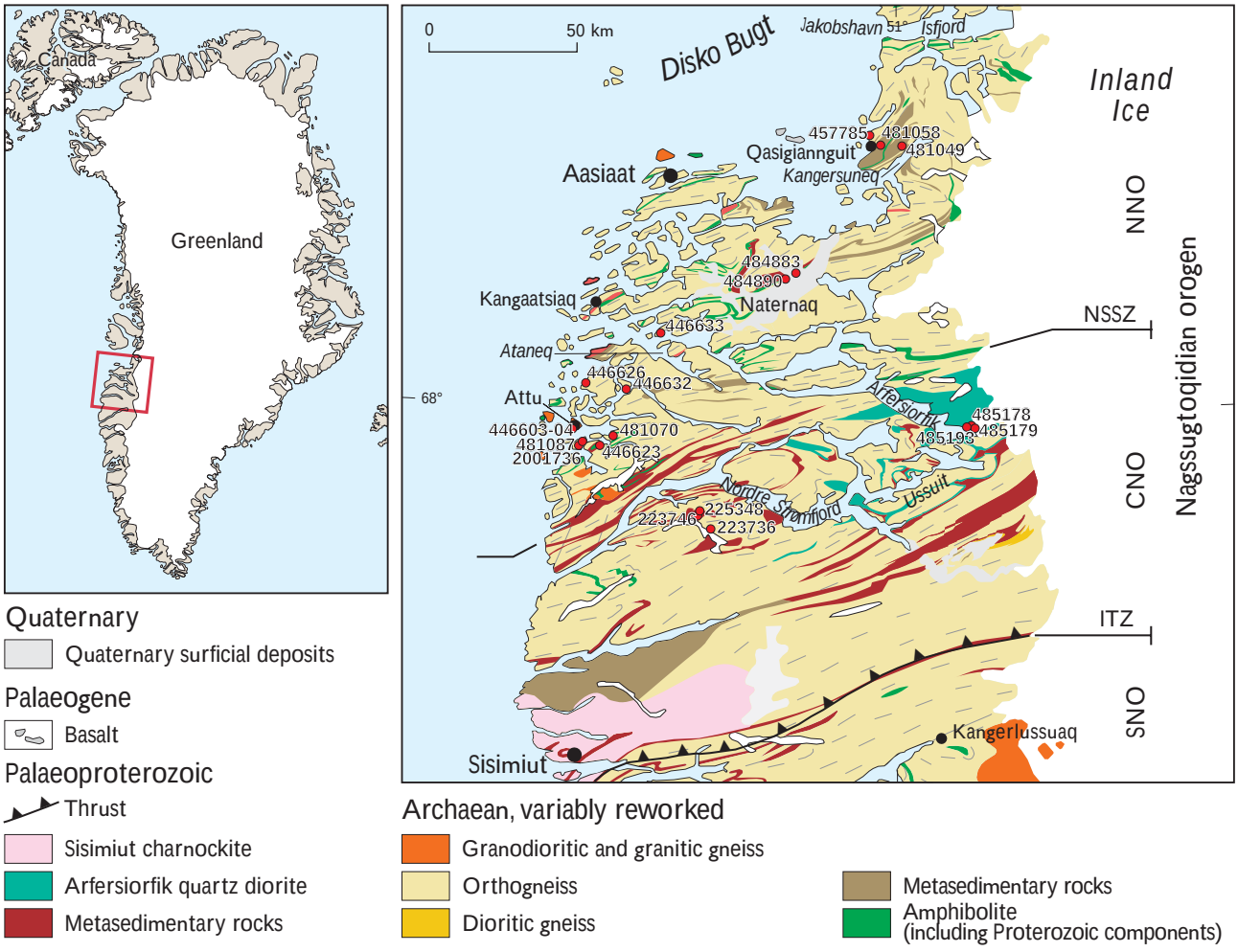

Fig. 1. Geological map of central West Greenland, modified from van Gool *et al.* (2002). Red dots with numbers refer to samples analysed. CNO, Central Nagssugtoqidian orogen; NNO, Northern Nagssugtoqidian orogen; SNO, Southern Nagssugtoqidian orogen; ITZ, Ikertôq thrust zone; NSSZ, Nordre Strømfjord shear zone.

Strømfjord (Nassuttooq), Attu and Qasigiannguit areas. The aims of the study were (1) to use Pb-isotopic signatures of magnetite in an attempt to outline the metamorphic history of the region; (2) to characterise the hydrothermal overprinting in terms of its timing and Pb source; and (3) to place the results within the evolutionary frame of the Nagssuqtoqidian orogen.

Regional geological setting

The study region comprises the Palaeoproterozoic Nagssugtoqidian orogen, a major collisional belt situated just north of the North Atlantic Craton (van Gool *et al.* 2002), as well as the southernmost part of the contemporaneous Rinkian fold belt (Garde & Steenfelt 1999; Connelly *et al.* 2006). Most of the region consists of Archaean orthogneisses, variably reworked during the Nagssugtoqidian and Rinkian tectonothermal events. Several thin belts of supracrustal rocks occur within the reworked Archaean gneiss terrain of the Nagssugtoqidian orogen (Fig. 1). Granitoid rocks and numerous pegmatites intrude the gneisses. Formations of Palaeoproterozoic age are limited to the Sisimiut igneous suite, Arfersiorfik quartz diorite, and minor supracrustal sequences including the Naternaq supracrustal belt (Connelly *et al.* 2000; Thrane & Connelly 2006, this volume).

The metamorphic grade is amphibolite facies, except for an area south of Ataneq in the south-western part of the northern Nagssugtoqidian orogen (NNO; Fig. 1) and in most of the central Nagssugtoqidian orogen (CNO), where granulite facies rocks predominate. The gneisses are intensely folded and show a general E–W to NE–SW strike. Deformation of the Archaean gneisses in the NNO

decreases gradually northwards, from high-strain to more open structures in the Archaean rocks. Steeply and shallowly dipping shear and fault zones are common in contact zones between different rock types. Major fault and shear zones generally strike NNE–NE. The gneisses of the NNO are late Archaean, with ages between 2870 and 2700 Ma (Kalsbeek & Nutman 1996; Connelly & Mengel 2000; Thrane & Connelly 2006, this volume). However, older rocks with ages ~3150 Ma appear to be present in the Attu area (Stendal *et al*. 2006, this volume). Only a few younger Palaeoproterozoic ages have been obtained from the NNO, including an undeformed pegmatite between Attu and Aasiaat with an intrusion age of about 1790 Ma (Connelly & Mengel 2000).

The geological history of the study area can be summarised as follows (van Gool *et al*. 2002):

- Deposition of supracrustal rocks: 2200–1950 Ma
- Continental breakup – the Kangâmiut dyke swarm: 2040 Ma
- Drifting – sediment deposition (supracrustal rocks) in the Nordre Strømfjord area: 2000–1920 Ma
- Subduction – calc-alkaline magmatism, giving rise to the Sisimiut and Arfersiorfik igneous suites: 1920–1870 Ma
- Peak metamorphism during collision (D1 and D2): 1860–1840 Ma
- Large scale folding (D3): ~1825 Ma
- Shearing in steep belts (D4): ~1775 Ma
- Slow cooling following the shearing, with closing temperature of rutile (420°C) at around 1670 Ma (Connelly *et al.* 2000). Based on ^{40}Ar-^{39}Ar and U-Pb data for several minerals, Willigers *et al.* (2001) estimated cooling temperatures around 500°C at ~1700 Ma, 410°C at ~1640 Ma, and 200°C at ~1400 Ma.

Previous investigations

The Geological Survey, university research groups as well as exploration companies have been working in central West Greenland for decades and have collected significant amounts of data on the mineral potential of the region (Stendal *et al*. 2002, 2004; Stendal & Schønwandt 2003; Schjøth & Steenfelt 2004; Steenfelt *et al*. 2004). Whole-rock Pb-Pb, Rb-Sr and Sm-Nd isotopic data from the study area have been presented by Kalsbeek *et al.* (1984, 1987, 1988), Taylor & Kalsbeek (1990) and Whitehouse *et al.* (1998), while e.g. Kalsbeek & Nutman (1996), Connelly & Mengel (2000), Connelly *et al.* (2000), Hollis *et al*. (2006, this volume) and Thrane & Connelly (2006, this volume) have published zircon U-Pb geochronological data.

Pb-isotopic work has been carried out on sulphide separates, mainly pyrite, from a mineralisation in the Disko Bugt region north of the study area (Stendal 1998). In the latter study, two distinct mineralisation types in the Archaean rocks were identified – a syngenetic, and at least one epigenetic type of ore formation. Pb-isotopic data of sulphides from Proterozoic rocks yield a well-defined linear trend in a Pb-Pb isochron diagram, with a slope corresponding to an age of ~1900 Ma, and indicative of a primitive (i.e. low μ) source character of Pb in that mineralisation.

Local geology and descriptions of the investigated rocks

During this study Pb-isotopic analyses were carried out on magnetite from amphibolite (four samples), banded iron formation (one sample), hydrothermally altered amphibolite and calc-silicate skarn rock (four samples), the Arfersiorfik quartz diorite (three samples), magnetite skarn (one sample), ultramafic rock (one sample) and pegmatite (one sample). In addition, one amphibolite, one altered amphibolite and one sample of banded iron formation were subjected to PbSL procedures (Frei & Kamber 1995), and allanite (two samples) and monazite (three samples) from pegmatites were analysed by PbSL in an attempt to date their emplacement. Brief descriptions of the investigated rocks are given below.

Amphibolitic rocks

Amphibolites occur together with garnet-mica schists/gneisses in supracrustal sequences, interlayered with orthogneiss. Some amphibolite layers in the gneiss terrain can be followed continuously along strike for up to tens of kilometres. They are heterogeneous in composition. They are found in three associations: (1) rusty weathering, medium-grained garnet amphibolite layers (*c*. 0.5 m thick) folded together with the orthogneisses, (2) dark, fine-grained amphibolite, occurring as layers up to 10 m thick, and (3) medium-grained, commonly garnetiferous, layered amphibolite. Layered amphibolites are the most common, and occur as units up to 200 m thick, although layers only 10–20 m thick are more common. The three different types of amphibolite form separate outcrops and do not occur together. The Pb-isotopic analyses reported in this paper refer to magnetite from the layered amphibolites (type 3).

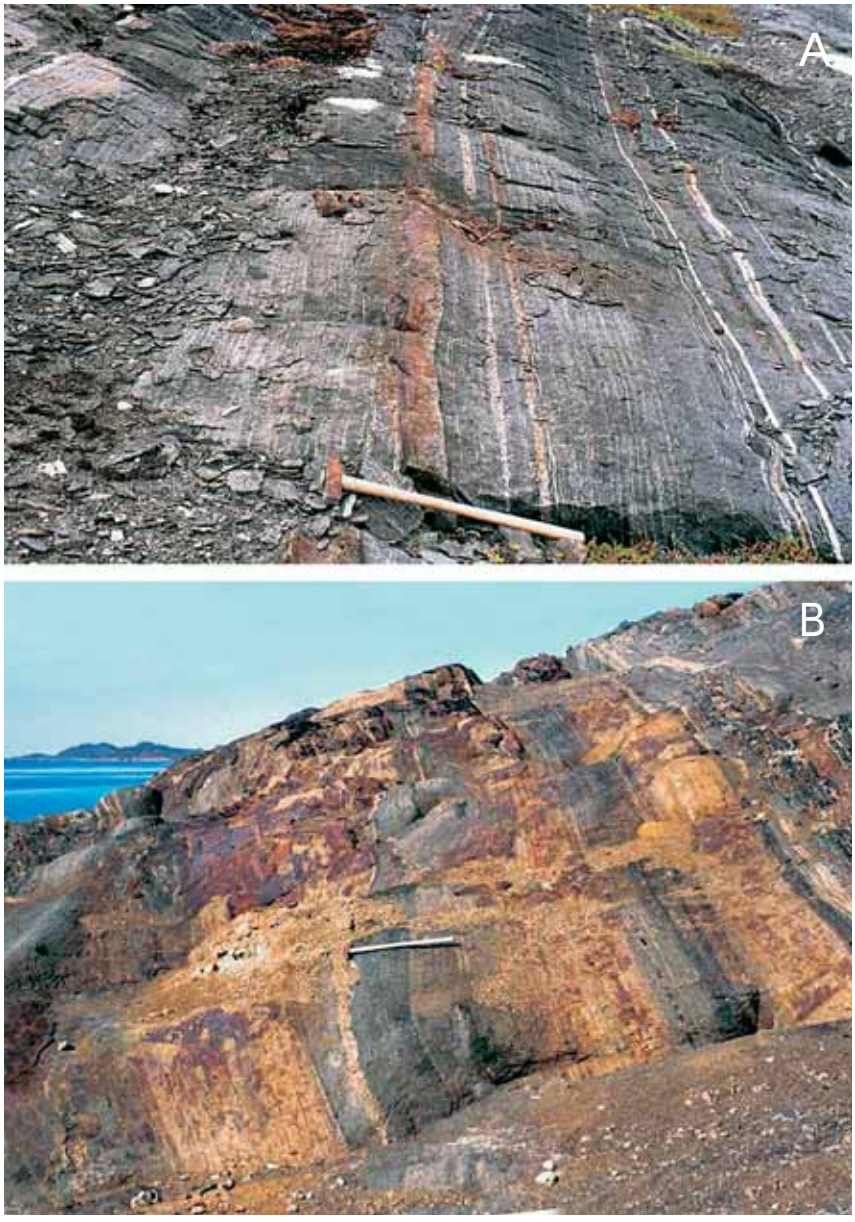

Fig. 2. Amphibolite (A) and hydrothermally altered amphibolite (B) from the Attu area.

The supracrustal sequences consist of garnet-mica schist/gneiss, together with amphibolite (Fig. 2a) and rusty weathering layers *c*. 1 m thick of quartz-garnet rich gneiss with some iron sulphides (1 vol.%). Within the layered amphibolite sequences, magnetite-bearing horizons 1–10 m thick occur. The magnetite occurs in laminae 1–10 mm thick, alternating with quartz-feldspar laminae of the same thickness. Alteration is common within the layered amphibolites.

Altered amphibolite

Some amphibolites have been hydrothermally altered and sulphide mineralised and may contain calc-silicates. This type of amphibolite is dominated by layered garnet-rich amphibolite, interlayered with magnetite-bearing and rusty weathering layers, with disseminated pyrite (Fig. 2b). The layers are generally 0.5–2 m thick; in some cases layered amphibolite is intercalated with rusty weathering layers 10–30 cm thick, consisting of quartz-bearing mica schist with iron sulphides and staining of malachite. Within the altered amphibolite calc-silicate minerals are found in zones 1–2 m thick or as smaller lenses, comprising hornblende, diopside, garnet and magnetite.

Fig. 3. Banded iron formation sequence from the Naternaq area.

Banded iron formation at Naternaq

The supracrustal belt at Naternaq (Fig. 1) consists of metavolcanic rocks interlayered with pelitic and psammitic schists and gneisses, marble units, exhalites and chert-rich layers with minor quartzite and banded iron formation. In total, these units define a supracrustal sequence up to 3 km thick, which is folded into a major shallowly dipping WSW-trending antiform. The supracrustal sequence can be traced for approximately 30 km along strike and is intruded by granite sheets and pegmatite veins. Østergaard *et al.* (2002) and Stendal *et al.* (2002) give detailed descriptions of the stratigraphy of the supracrustal rocks. The banded iron formation (Fig. 3) occurs locally associated with the amphibolite in zones composed of centimetre-thick layers of magnetite and siderite quartz and calc-silicates. The depositional environment is of a sedimentary type comprising true sediments, submarine volcanic rocks and exhalites. A range of variably altered conformable horizons of very fine-grained siliceous and sulphide rich lithologies associated with either amphibolite or marble are interpreted as volcanogenic-exhalitic rocks (Østergaard *et al*. 2002; Stendal *et al.* 2002).

Arfersiorfik quartz diorite

The Arfersiorfik quartz diorite (Kalsbeek *et al.* 1987) is located in the eastern part of the fjord Arfersiorfik (Fig. 1) and covers several hundreds of square kilometres. Within the quartz diorite body, magnetite occurs in hornblende-rich rocks (hornblende, quartz, feldspar, and chlorite) and often shows paragenetic relation with iron sulphides (predominantly pyrrhotite). The Arfersiorfik quartz diorite was emplaced in the period 1920–1870 Ma (Kalsbeek *et al.* 1987; Connelly *et. al.* 2000).

Ultramafic rocks near Qasigiannguit

An ultramafic body 300 × 300 m large is located on the north side of Kangersuneq, forming rusty weathered hills. On its eastern and western sides the ultramafic body is bounded by fault zones, invaded by pegmatites. On its northern and southern sides it is bordered by amphibolite and garnet amphibolite, respectively. Because of the penetrative weathering it is difficult to sample fresh material from the ultramafic body. In its centre, an intensely rusty weathered and eroded 'joint' zone cuts the ultramafic rocks. This contains 1–10 vol.% magnetite.

Magnetite-rich skarn at Qasigiannguit

Near Qasigiannguit a skarn rock is found in the contact zone striking 66° and dipping 77°SE between mica schist and quartzite and a marble-calc-silicate sequence. It comprises magnetite skarn (0.5 m thick) in close contact with the mica schist and quartzite. Towards the south-east the magnetite skarn is followed by alternating layers of calc-silicate rocks and marble (including a quartzitic, sulphide-rich layer), followed by a pegmatite body.

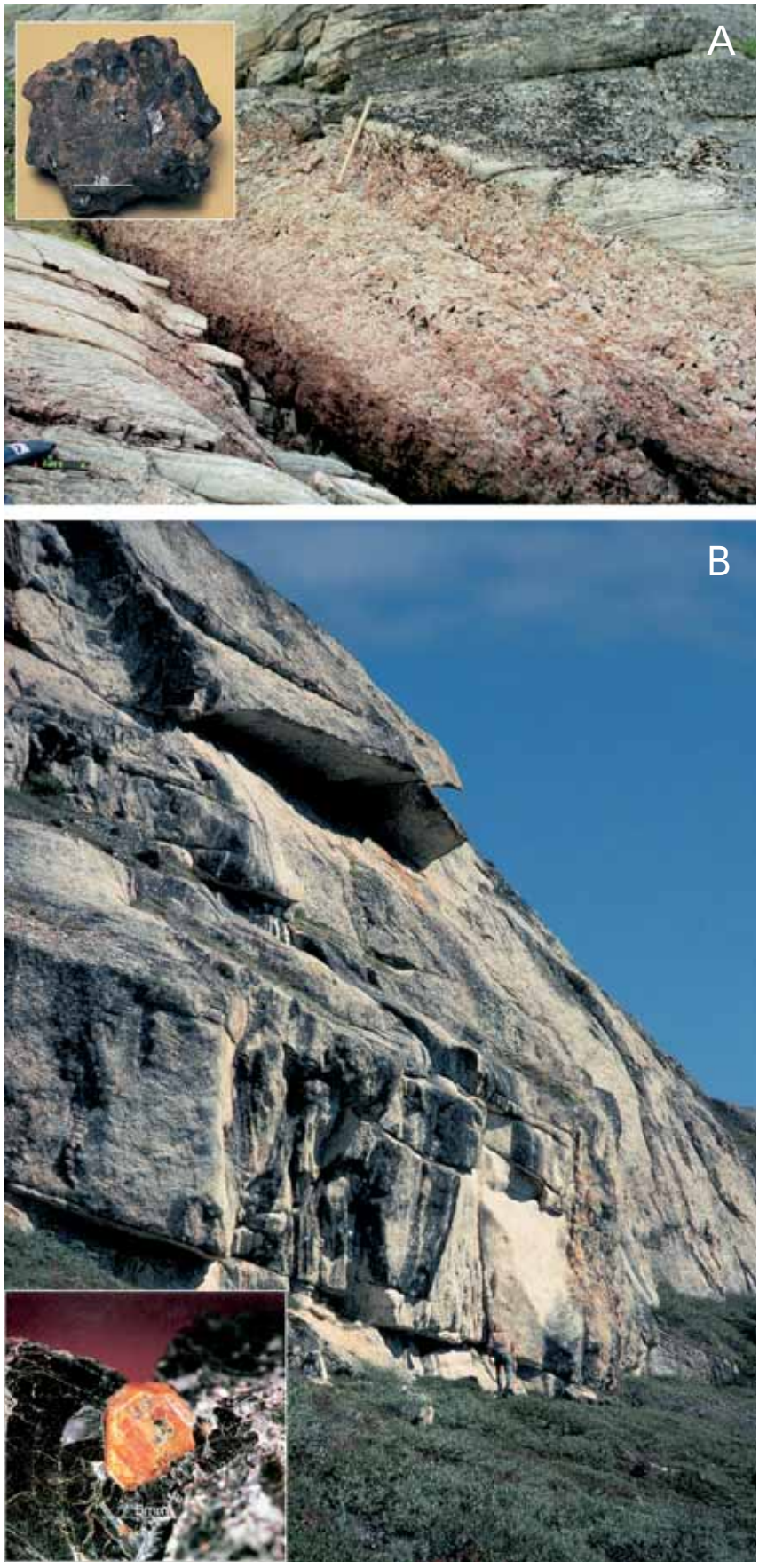

Fig. 4. Pegmatites and minerals analysed. A: Pink discordant pegmatite and allanite (inset) from the Attu area. B: White pegmatite and monazite (inset) from the Nordre Strømfjord (Nassuttooq) area.

Pegmatites

Pink pegmatites. Throughout the study area, especially in the outer fjord zone from south of Attu northward to Kangaatsiaq, the country rocks are intruded by granite and by pink pegmatites with alkali feldspar crystals commonly more than 10 cm in size. The pegmatites occur mostly as discordant decimetre- to metre-thick bodies within the gneisses, at contacts between major lithological units, and within supracrustal rocks where they are clearly cross-cutting. The dominant minerals in the pink pegmatite are alkali feldspar, quartz, biotite and subordinate allanite, titanite, apatite, magnetite and Fe-sulphides (Fig. 4a). Zonation is occasionally seen with quartz-rich centres bounded by alkali feldspar-rich parts.

White pegmatites. White pegmatites are generally concordant (but locally discordant) to the foliation of the adjacent country rocks, typically grey gneiss and supracrustal rocks. The pegmatites are 5–20 m wide and 50–200 m long with a general trend of NW–SE all over the Nordre Strømfjord and Ussuit areas. Gradational contacts to the host rocks are common. Quartz and feldspar dominate the white pegmatites, with garnet, biotite, monazite, magnetite and zircon as characteristic minor constituents. Monazite is found as 0.5–5 mm orange crystals that mainly occur in plagioclase- and biotite-rich pegmatites (Fig. 4b). Monazite crystals are euhedral and occur in lens-shaped layers accompanied by biotite, set in a granoblastic matrix of primarily plagioclase (Secher 1980).

Analytical methods

Pb isotope analyses for this study were carried out at the Danish Centre for Isotope Geology, Geological Institute, University of Copenhagen. Mineral fractions were separated from dry split aliquots of crushed and sieved (100–200 µm) rock powders using a hand magnet, a Frantz isodynamic separator and heavy liquid techniques. No further purification was carried out, and the mineral fractions may contain minor proportions of foreign minerals. Pb was separated conventionally on 0.5 ml glass columns charged with anion exchange resin, followed by a clean up on 200 µl Teflon columns. A standard HBr-HCl solution recipe was applied in both column steps. Total procedural blanks for Pb amounted to < 120 pg which is considered insignificant for the measured Pb-isotopic results, relative to the amount of sample Pb estimated from the mass spectrometer signal intensities. Isotope analyses were

Table 1. Pb isotope ratios of magnetite from different rock types

Sample	Locality	Latitude N	Longitude W	Rock	$^{206}Pb/^{204}Pb$	± 2σ*	$^{207}Pb/^{204}Pb$	± 2σ	$^{208}Pb/^{204}Pb$	± 2σ	r1 **	r2†
Magnetite from amphibolite and banded iron formation												
446626	Ataneq	68°.061	53°.510	Amphibolite	18.815	0.026	15.549	0.022	44.971	0.068	0.973	0.953
446632	Ataneq	68°.047	53°.179	Amphibolite	28.204	0.042	16.518	0.026	38.467	0.066	0.971	0.906
446623	Attu	67°.837	53°.408	Amphibolite	17.522	0.025	15.404	0.024	38.344	0.066	0.961	0.880
481070	Attu	67°.915	53°.231	Amphibolite	17.388	0.019	15.376	0.018	41.241	0.053	0.978	0.936
484883	Naternaq	68°.398	51°.941	BIF in amphibolite	54.587	0.028	19.316	0.012	36.871	0.030	0.942	0.886
Magnetite from altered amphibolite and calc-silicate rock												
446633	Niaqornaarsuk	68°.217	53°.028	Altered amphibolite	26.387	0.505	16.465	0.316	47.423	0.908	0.998	0.999
446603	Attu	67°.927	53°.622	Altered amphibolite	18.398	0.030	15.620	0.026	41.710	0.074	0.978	0.956
446604	Attu	67°.927	53°.622	Altered amphibolite	18.256	0.046	15.638	0.042	40.443	0.122	0.930	0.845
484890	Naternaq	68°.408	51°.935	Calc-silicates (skarn)	16.534	0.009	15.372	0.010	35.562	0.028	0.957	0.913
Magnetite from the Arfersiorfik quartz diorite												
485178	Arfersiorfik	67°.970	50°.430	Quartz diorite	17.790	0.016	15.469	0.016	36.703	0.049	0.919	0.782
485179	Arfersiorfik	67°.967	50°.412	Quartz diorite	18.071	0.018	15.498	0.016	36.343	0.041	0.975	0.954
485193	Arfersiorfik	67°.956	50°.594	Hornblenditic rock	17.007	0.013	15.456	0.013	37.124	0.037	0.959	0.902
Magnetite from pegmatite												
481087	Attu	67°.890	53°.517	Pegmatite	28.393	0.043	16.602	0.026	189.024	0.311	0.982	0.971
Magnetite from ultramafic rock and skarn												
481049	Qasigiannguit	68°.801	50°.973	Ultramafic rock	25.827	0.039	16.103	0.025	51.334	0.084	0.979	0.949
481058	Qasigiannguit	68°.800	51°.169	Magnetite skarn	35.124	0.024	17.028	0.013	38.847	0.035	0.968	0.929

BIF: Banded iron formation.

* Errors are 2σ absolute (Ludwig 1990).

** r1 = $^{206}Pb/^{204}Pb$ versus $^{207}Pb/^{204}Pb$ error correlation (Ludwig 1990).

† r2 = $^{206}Pb/^{204}Pb$ versus $^{208}Pb/^{204}Pb$ error correlation (Ludwig 1990).

Table 2. Pb-Pb step leaching data for magnetite, allanite, and monazite in banded iron formation, amphibolite and pegmatites in the Nagssugtoqidian orogen

Code	Acid	Time	$^{206}Pb/^{204}Pb$	± 2σ *	$^{207}Pb/^{204}Pb$	± 2σ *	$^{208}Pb/^{204}Pb$	± 2σ *	r1	r2
Magnetite, banded iron formation within amphibolite 484883, locality 68°.398 N, 51°.941 W										
[1]	1 N HBr	30'	48.234	0.030	18.615	0.014	37.418	0.032	0.968	0.919
[2]	1 N HBr	1 h	120.002	0.091	26.407	0.022	3.862	0.005	0.978	0.760
[3]	4 N HBr	3 h	94.120	0.363	23.247	0.090	37.841	0.149	0.995	0.987
[4]	8 N HBr	6 h	30.176	0.239	16.809	0.134	35.387	0.282	0.994	0.994
[5]	8 N HBr	12 h	18.799	0.062	15.506	0.052	34.534	0.116	0.991	0.987
[6]	HF	12 h	18.799	0.124	15.539	0.103	35.013	0.233	0.995	0.993
Magnetite, amphibolite 446632, locality 68°.047 N, 53°.179 W										
[1]	1 N HBr	30'	19.932	0.026	15.621	0.021	37.462	0.055	0.970	0.920
[2]	1 N HBr	1 h	38.765	0.032	17.639	0.016	39.167	0.040	0.978	0.946
[3]	4 N HBr	3 h	35.439	0.060	17.098	0.030	42.830	0.079	0.982	0.948
[4]	8 N HBr	6 h	37.099	0.150	17.595	0.072	36.972	0.154	0.993	0.979
[5]	8 N HBr	12 h	40.431	0.219	18.100	0.099	34.544	0.189	0.994	0.994
[6]	HF	12 h	28.265	0.083	16.910	0.051	34.598	0.106	0.987	0.977
Magnetite, altered amphibolite 446633, locality 68°.217 N, 53°.027 W										
[1]	1 N HBr	30'	25.206	0.021	16.298	0.015	45.932	0.047	0.971	0.914
[2]	1 N HBr	1 h	27.276	0.170	16.492	0.104	47.555	0.300	0.993	0.990
[3]	4 N HBr	3 h	25.359	0.022	16.261	0.016	45.944	0.049	0.975	0.948
[4]	8 N HBr	6 h	26.018	0.024	16.333	0.016	46.646	0.051	0.968	0.936
[5]	8 N HBr	12 h	27.705	0.073	16.539	0.046	48.236	0.138	0.965	0.937
Allanite, pegmatite 2001-736, locality 67°.883 N, 53°.523 W										
[1]	1 N HBr	30'	22.579	0.029	15.860	0.021	137.787	0.193	0.982	0.960
[2]	1 N HBr	1 h	21.528	0.013	15.728	0.011	123.978	0.101	0.971	0.939
[3]	4 N HBr	3 h	79.398	1.929	22.265	0.542	1360.842	33.070	0.999	1.000
[4]	8 N HBr	6 h	2527.779	37.253	295.424	4.391	52501.990	774.512	0.992	0.999
[5]	8 N HBr	12 h	7804.112	133.916	882.216	15.164	161163.864	2767.112	0.999	1.000
[6]	HF	12 h	551.839	2.322	74.260	0.322	11002.171	46.823	0.973	0.994
[7]	HF	2 d	111.336	0.543	25.175	0.136	1948.881	9.628	0.901	0.991
Allanite, pegmatite 457785, locality 68°.834 N, 51°.226 W										
[1]	1 N HBr	30'	36.910	1.617	17.616	0.772	538.548	23.595	1.000	1.000
[2]	1 N HBr	1 h	44.614	0.389	18.318	0.160	714.245	6.237	0.998	0.999
[3]	4 N HBr	3 h	26.321	0.210	16.341	0.130	270.923	2.164	0.998	0.999
[4]	8 N HBr	6 h	21966.303	527.491	2410.934	57.939	328786.908	7897.797	0.999	1.000
[5]	8 N HBr	12 h	26.193	0.574	17.165	0.390	161.467	3.639	0.964	0.972
[6]	HF	12 h	15.058	1.448	15.006	1.443	39.562	3.805	1.000	1.000
[7]	HF	2 d	27.000	0.230	15.806	0.207	186.650	2.183	0.651	0.729
Monazite, pegmatite 223736, locality 67°.680 N, 52°.565 W										
[1]	1 N HBr	30'	136.776	2.665	28.301	0.574	6619.883	131.103	0.960	0.984
[2]	1 N HBr	1 h	222.475	3.796	37.330	0.643	12548.515	214.343	0.991	0.999
[3]	4 N HBr	3h	219.227	2.039	36.918	0.346	12871.792	120.474	0.992	0.995
[4]	8 N HBr	6 h	184.897	2.055	33.259	0.373	10581.910	118.035	0.993	0.997
[5]	8 N HBr	12 h	89.680	0.811	23.046	0.213	3554.756	32.275	0.979	0.998
[6]	HF	12 h	39.412	0.038	17.328	0.018	88.489	0.099	0.980	0.957
[7]	HF	2 d	261.196	1.366	41.737	0.220	175.006	0.931	0.994	0.987
Monazite, pegmatite 223746, locality 67°.674 N, 52°.456 W										
[1]	1 N HBr	30'	20.955	0.097	15.264	0.071	156.248	0.733	0.995	0.994
[2]	1 N HBr	1 h	26.768	0.169	16.158	0.103	315.778	2.010	0.997	0.997
[3]	4 N HBr	3h	215.079	2.560	37.781	0.451	5263.963	62.733	0.997	0.999
[4]	8 N HBr	6 h	2978.834	188.060	343.540	21.694	75533.892	4768.946	1.000	1.000
[5]	8 N HBr	12 h	6392.913	99.502	721.057	11.259	157988.821	2460.811	0.997	1.000
[6]	HF	12 h	468.603	5.974	66.525	0.919	10731.171	137.428	0.923	0.996
[7]	HF	2 d	2161.547	97.250	254.541	11.458	51062.309	2297.561	1.000	1.000
Monazite, pegmatite 225348, locality 67°.833 N, 52°.323 W										
[1]	1 N HBr	30'	139.662	2.160	29.676	0.459	1656.012	25.630	1.000	1.000
[2]	1 N HBr	1 h	140.039	1.416	29.481	0.299	1544.411	15.642	0.996	0.999
[3]	4 N HBr	3h	877.104	4.121	108.678	0.517	12440.807	58.889	0.990	0.997
[4]	8 N HBr	6 h	25.459	0.418	16.750	0.456	225.146	4.515	0.604	0.820
[5]	8 N HBr	12 h	40549.054	1970.494	4458.008	222.550	602889.998	29313.071	0.973	1.000
[6]	HF	12 h	8037.949	261.731	893.317	29.098	122611.734	3993.108	1.000	1.000
[7]	HF	2 d	4389.260	60.969	493.058	6.880	66031.253	918.275	0.996	0.999

* Errors are 2σ absolute (Ludwig 1990). For explanations of r1 and r2, see Table 1.

Table 3. Pb isotope ages, μ1-values, and intercepts with the Stacey & Kramers (1975) Pb-isotopic growth curve for magnetite, allanite, and monazite from amphibolite, BIF and pegmatites

Sample	Rock	Mineral	Method	Age (Ma)	± 2σ	MSWD	Intercept (Ma) with Stacey & Kramers (1975)	μ1	± 2σ
5 samples	Amphibolite/BIF	Magnetite	Bulk	1726	6.5	1.38	2140	7.89	0.02
484883	BIF	Magnetite	PbSL	1756	36	8.70	2401	7.7	0.11
223736	Pegmatite	Monazite	PbSL	1797	13	4.44	2925	7	0.05
223746	Pegmatite	Monazite	PbSL	1816	16	41.7	2784	7.24	0.12
225348	Pegmatite	Monazite	PbSL	1787	11	76.9	2271	7.81	1.00
447783	Pegmatite	Allanite	PbSL	1785	9.2	12.9	2335	7.76	0.00
2001-736	Pegmatite	Allanite	PbSL	1818	12	53.8	2453	7.66	0.02

BIF: Banded iron formation; PbSL: Pb step leaching.

carried out on a VG Sector 54-IT instrument. Fractionation for Pb was controlled by repetitive analysis of the NBS 981 standard (values of Todt *et al*. 1993) and amounted to 0.103 ± 0.007% / amu (2 σ; n = 11). Stepwise Pb leaching (PbSL) experiments followed methods described in Frei & Kamber (1995).

The programmes and parameters of Ludwig (1990) were used for the isochron calculations. Model first-stage μ_1 values were calculated using 4.55 Ga for the age of the earth. All age and isotope data in this paper are given with 2 σ precisions.

Results

The Pb-isotopic results are given in Tables 1–3. The uranogenic Pb-isotopic composition of magnetite from the amphibolites (four samples; squares in Fig. 5) together with the banded iron formation (Naternaq; one sample outside the range of Fig. 5) define an isochron with an age of 1726 ± 7 Ma (2 σ; MSWD = 1.4; model μ_1 = 7.89 ± 0.02), which corresponds to a late stage in the metamorphic evolution of the Nagssugtoqidian orogen (cf. Willigers *et al*. 2002). This isochron intercepts the Stacey & Kramers (1975) Pb-isotopic growth curve at ~2140 Ma.

Four mineral separates from altered amphibolite, represented by calc-silicate rich phases and by hydrothermally altered and mineralised samples, have Pb-isotopic compositions that plot above the 1726 Ma isochron (diamonds in Fig. 5). This more radiogenic Pb-isotopic composition indicates admixture of a more evolved Pb component into the alteration fluids. The Pb-isotopic compositions of magnetite from an ultramafic rock and a magnetite skarn from the Qasigiannguit area plot below the isochron (out-

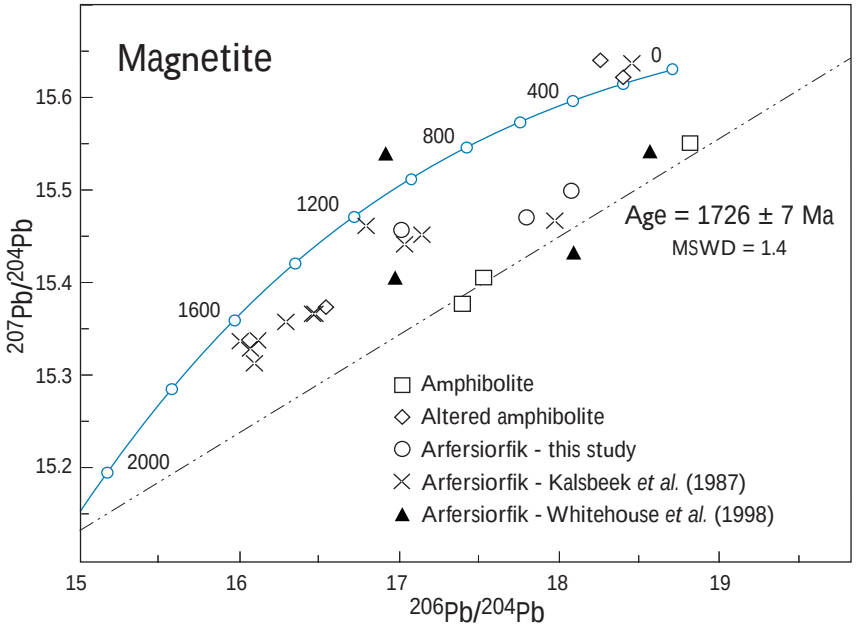

Fig. 5. $^{206}Pb/^{204}Pb$-$^{207}Pb/^{204}Pb$ diagram. Squares, Pb isotope ratios of magnetite from amphibolites; diamonds, magnetite from altered amphibolites (data from sample 446632 outside the range of Fig. 5, see Table 1). *Arfersiorfik quartz diorite:* circles, this study; crosses, data from Kalsbeek *et al*. 1987; filled triangles, data from Whitehouse *et al*. 1998. The isochron intercepts the Stacey & Kramers (1975) Pb-isotopic growth curve (blue) at ~2140 Ma.

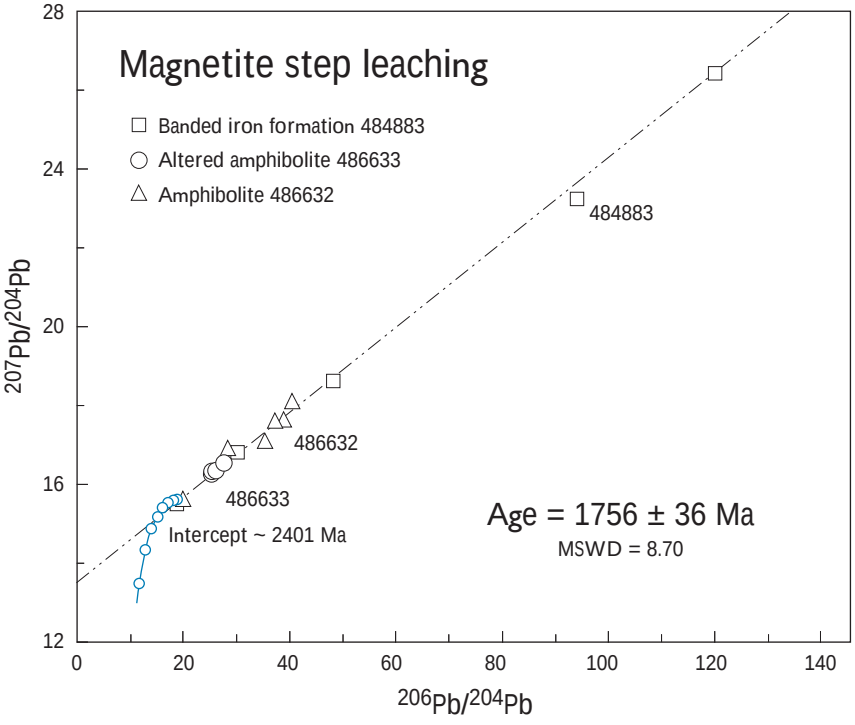

Fig. 6. $^{206}Pb/^{204}Pb$-$^{207}Pb/^{204}Pb$ diagram of step leaching results of magnetite for three samples. The errorchron intercepts the Stacey & Kramers (1975) Pb-isotopic growth curve (blue) at ~2400 Ma.

side the range of Fig. 5; see Table 1), suggesting a slightly more primitive Pb source.

The uranogenic vs. thorogenic isotopic patterns (not shown in a figure) are complex and do not add to a better understanding of the uranogenic Pb-isotopic data. As expected, they reflect differences in U/Th ratios among the different samples analysed.

The Arfersiorfik quartz diorite has been dated at ~1920 Ma (Kalsbeek *et al.* 1987). Three magnetite samples from this igneous suite have been included in the present study. The uranogenic Pb-isotopic compositions of these magnetites (circles in Fig. 5) are similar to the whole-rock Pb-isotopic signatures (crosses in Fig. 5; data from Kalsbeek *et al.* 1987). Four additional whole-rock analyses (filled triangles in Fig. 5; data of Whitehouse *et al.* 1998) show wider scatter than the data of Kalsbeek *et al.* (1987) and the results of this study.

The PbSL data obtained on magnetite from three of these samples are shown in Fig. 6. A regression for the steps defined by the sample of banded iron formation, 484883 (excluding step 3; Table 1) yields a best-fit line with a slope corresponding to an age of 1756 ± 36 Ma (MSWD = 8.70; model μ_1 = 7.70 ± 0.11; lower intercept with the Stacey & Kramers Pb-isotopic growth curve at ~2400 Ma), similar to the age obtained from the amphibolites. PbSL analyses of two other samples (446632, amphibolite and 446633, altered amphibolite) are closely scattered around the 1756 correlation line.

PbSL data obtained on allanite from a pink pegmatite (sample 2001-736) resulted in a well-defined errorchron with an age of 1818 ± 12 Ma (MSWD = 53.8; model μ_1 = 7.66 ± 0.02; lower intercept with the Stacey & Kramers Pb-isotopic growth curve at ~2450 Ma; Fig. 7A). The thorogenic vs. uranogenic isotopic pattern (Fig. 7B) reveals that essentially only one phase has dominantly contributed Pb to the leaching acids, as a nearly perfect linear relationship is indicated by the data points. This points to a more or less constant Th/U in the recovered Pb fractions. For this reason, the age of 1818 ± 12 Ma can be interpreted with great confidence to represent the emplacement age of the pegmatite. The Pb-isotopic composition of magnetite (sample 481087, Table 1) from this pegmatite plots on the allanite isochron (Fig. 7A), indicating preservation of isotopic equilibrium between these two phases.

PbSL data on monazite from a white pegmatite (sample 223736) also yield an errorchron, the slope of which corresponds to an age of 1797 ± 13 Ma (MSWD = 4.44; model μ_1 = 7.00 ± 0.05; lower intercept with the Stacey & Kramers Pb-isotopic growth curve at ~2925 Ma; Fig. 8A). The thorogenic vs. uranogenic isotopic pattern (Fig. 8B) again indicates a predominantly single phase that contributed Pb to the leaching acids, as the data points define a near perfect linear relationship. Consequently, with great confidence, the age of 1797 ± 13 Ma is interpreted as the intrusion age of this pegmatite.

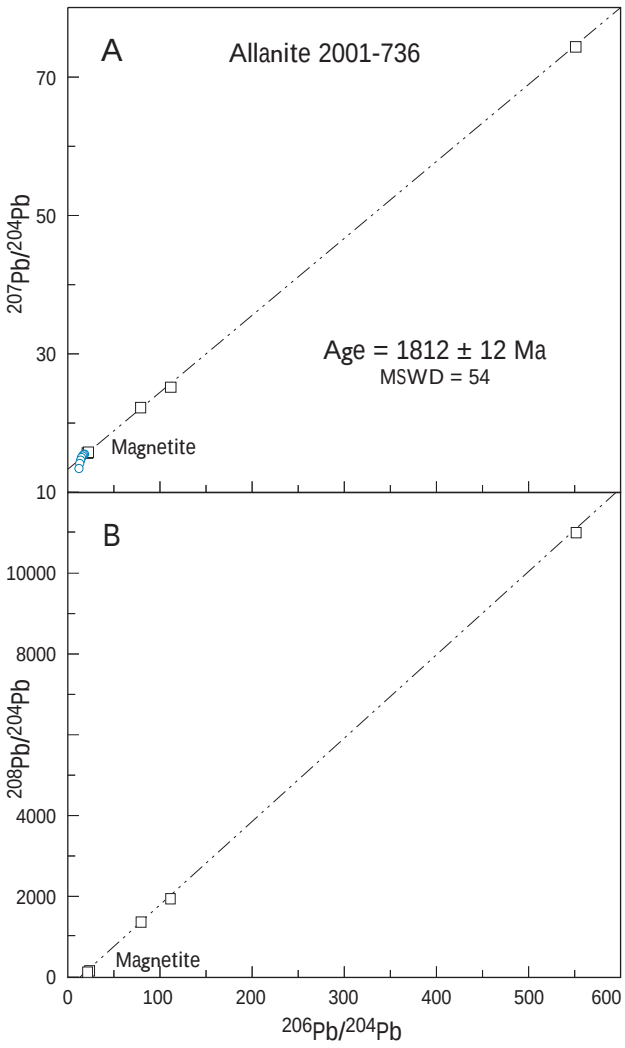

Fig. 7. Step leaching $^{206}Pb/^{204}Pb$-$^{207}Pb/^{204}Pb$ and $^{208}Pb/^{204}Pb$-$^{206}Pb/^{204}Pb$ diagrams of allanite from red pegmatite (sample 2000736). The errorchron intercepts the Stacey & Kramers (1975) Pb-isotopic growth curve (blue) at ~2925 Ma.

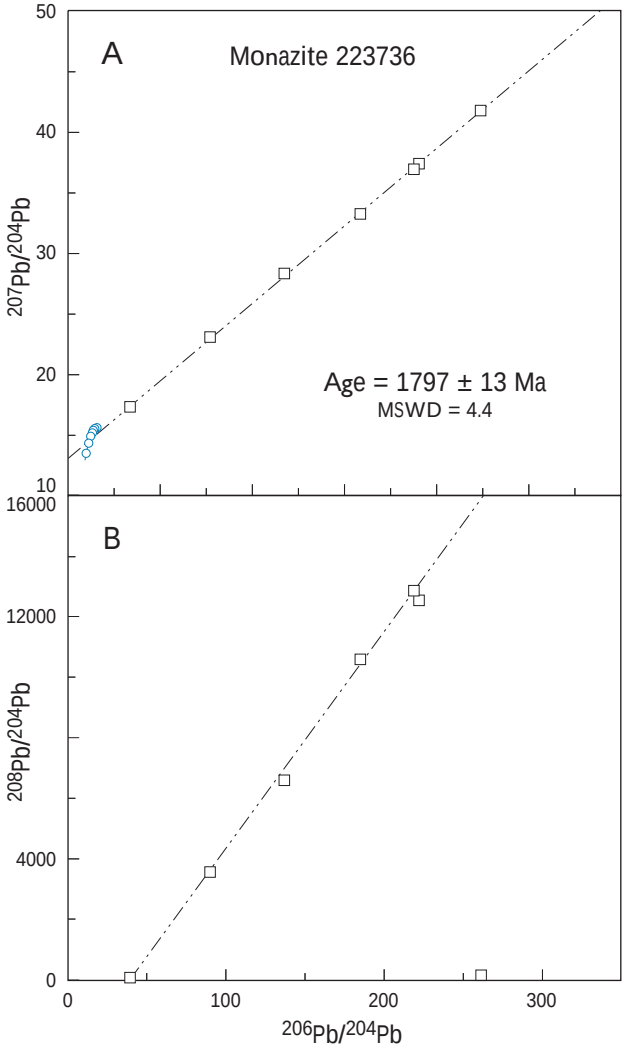

Fig. 8. Step leaching $^{206}Pb/^{204}Pb$-$^{207}Pb/^{204}Pb$ and $^{208}Pb/^{204}Pb$-$^{206}Pb/^{204}Pb$ diagrams of monazite from white pegmatite (sample 223736). The errorchron intercepts the Stacey & Kramers (1975) Pb-isotopic growth curve (blue) at ~2453 Ma.

Three more step-leaching experiments were performed on allanite (1) and monazite (2) separates from other pegmatites (Fig. 9). The ages defined by the respective errorchrons are similar to the ones presented above, and are close to 1800 Ma. Results of the isochron calculations are listed in Table 3.

Discussion

The age defined by the Pb-isotopic compositions of magnetite from the amphibolites (1726±7 Ma) is younger than the latest major tectonometamorphic event in the region (D4, strike-slip shearing and granite intrusion at 1780–1770 Ma; see Connelly *et al.* 2000 and van Gool *et al.* 2002), and may be interpreted as a cooling age after the D4 event. Metamorphic conditions in the CNO reached temperatures above 650°C at 1800 Ma and approximately 540°C by *c.* 1740 Ma (Connelly & Mengel 2000; Connelly *et al.* 2000; Willigers *et al.* 2001). Slow cooling followed with closing temperatures of rutile (420°C) around 1670 Ma (Connelly *et al.* 2000). Based on ^{40}Ar-^{39}Ar and U-Pb data of several minerals, Willigers *et al.* (2001) estimated cooling temperatures around 500°C at ~1700 Ma, 410°C at ~1640 Ma and 200°C at ~1400 Ma. A continuous magnetite-ulvöspinel solid solution series exists, with exsolution taking place below 600°C (Deer *et al.* 1966; Ramdohr 1969). Thus, the ages of the magnetite may date

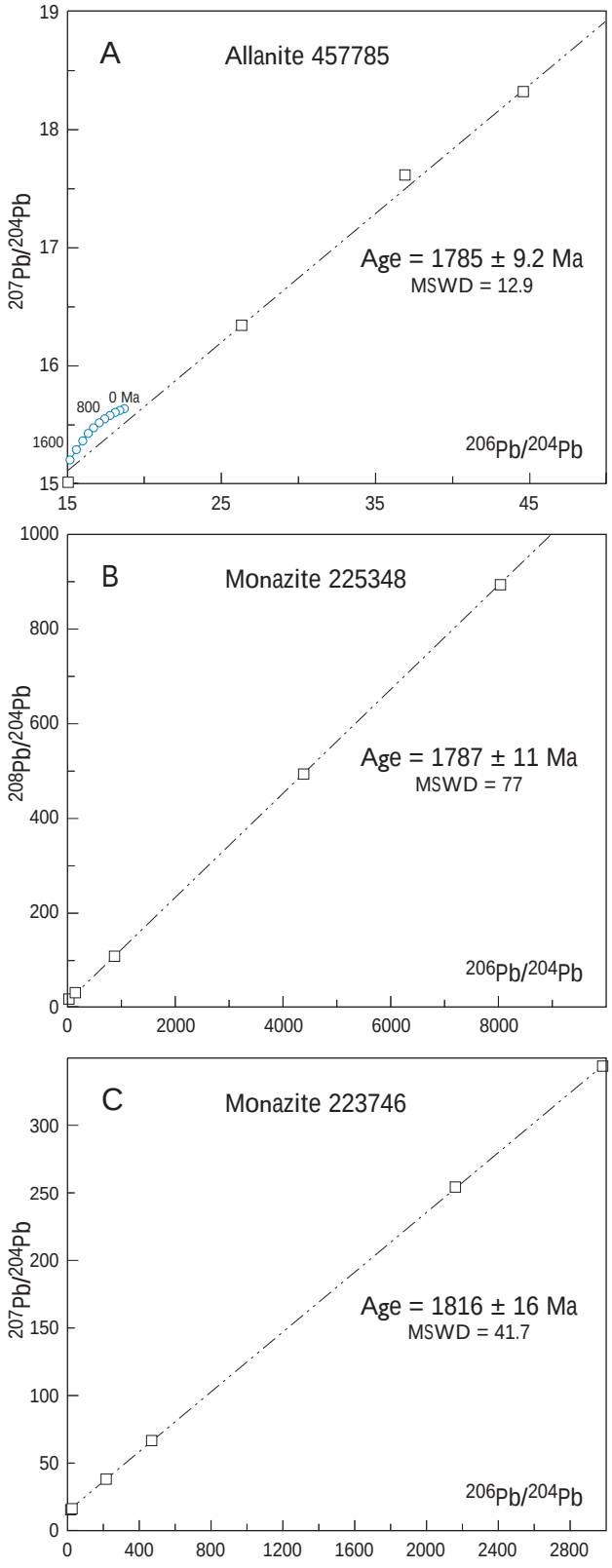

Fig. 9. Step leaching $^{206}Pb/^{204}Pb$-$^{207}Pb/^{204}Pb$ diagrams of monazite from white pegmatite (samples 225348 and 223736) and allanite from pink pegmatite (sample 447783). The errorchron intercepts of the Stacey & Kramers (1975) Pb-isotopic growth curve (blue) are given.

the timing where exsolution in magnetite ceased (< 1800 Ma), that is, after peak metamorphic conditions.

Model first-stage μ_1 values associated with Pb-Pb isochrons have been used elsewhere in Greenland to judge the influence of Pb from Archaean sources on the Pb-isotopic characteristics of Palaeoproterozoic igneous rocks (e.g. Kalsbeek & Taylor 1985). Rocks derived from Proterozoic sources commonly have model μ_1 values around 8, while contamination with Pb from Archaean sources tends to lower the μ_1 values. The high μ_1 value (7.89; Table 3) obtained for the amphibolite isochron and the lower intercept with Stacey & Kramers (1975) Pb-isotopic growth curve at 2140 Ma suggest a mainly Palaeoproterozoic Pb source for the amphibolites. This source is probably also related to the origin of the supracrustal rocks. Detrital zircon U-Pb ages of metasedimentary rocks of the Nordre Strømfjord suite (2200–1950 Ma; Nutman *et al*. 1999) and the Naternaq supracrustal belt (*c*. 1950–1900 Ma, Thrane & Connelly 2006, this volume) indicate erosion of a predominantly Palaeoproterozoic hinterland. It implies that the stratabound, semi-massive sulphide deposits associated with banded iron formation at Naternaq (Stendal *et al*. 2004) were also deposited during Palaeoproterozoic time.

The results of allanite and monazite PbSL experiments indicate pegmatite formation around 1800 Ma in both the CNO (at Nordre Strømfjord) and NNO (at Attu and Qasigiannguit). This is in agreement with ages reported by Kalsbeek & Nutman (1996) and Connelly *et al.* (2000), which are slightly younger (1780–1770 Ma) or within error overlapping those reported here. The pegmatites were emplaced after post-collisional deformation, large scale folding, and shear zone formation (D3) which ended around 1825 Ma (van Gool *et al.* 2002).

The wide range in model μ_1 values (7.00–7.81) and lower intercepts with the Stacey & Kramers (1975) Pb-isotopic growth curve (2271–2925 Ma) indicate variable contributions of Archaean and Palaeoproterozoic country rocks to the petrogenesis of the pegmatites: Pegmatite sample 223736 (μ_1 = 7.00; lower intercept at 2925 Ma) may largely consist of remelted Archaean country rock, whereas sample 225348 (μ_1 = 7.81; lower intercept at 2271 Ma) appears to be mainly derived from Palaeoproterozoic sources.

Hydrothermal activity in the region probably continued after the time of pegmatite emplacement and after the magnetite had cooled through its closing temperature (~600°C), which means that the temperatures of the hydrothermal fluids ranged from 650°C to 400°C in the period 1800–1650 Ma.

The Pb-isotopic signatures of the ultramafic rock and

the magnetite skarn from the Qasigiannguit area do not lend themselves to deduce whether these formations were formed during the Palaeoproterozoic or represent remnants of Archaean origin.

It has been suggested that many of the epigenetic gold and copper occurrences in the Ataa area north-east of Disko Bugt, about 75 km north of Jakobshavn Isfjord (Fig. 1), are contemporaneous with the peak metamorphism at ~1900 Ma in that area (Stendal 1998). This 1900 Ma metamorphic-hydrothermal event is not reflected in the magnetite Pb-isotopic data of the present study area.

Conclusions

Pb-isotopic data of magnetite can be related to the general geological evolution of the Nagssugtoqidian orogen and are thus a useful tool for studying the metamorphic history of Palaeoproterozoic events in West Greenland. A drawback of magnetite Pb-isotopic analysis, however, is the generally low Pb concentration in this mineral, which makes analysis difficult.

Magnetite in the amphibolites was formed during several stages of metamorphism. The isochron age of ~1726 Ma probably represents a cooling age after a prominent late tectonometamorphic event in the region dated at ~1775 Ma. The isotopic data suggest a Palaeoproterozoic (mantle?) source for the Pb in the amphibolites. The Nordre Strømfjord supracrustal suite, formed by erosion of a similar juvenile Palaeoproterozoic hinterland, was deposited between 2000 and 1920 Ma. It is suggested that the Naternaq sulphide deposit is part of this supracrustal suite.

Calc-alkaline magmatism related to subduction (1920–1870 Ma; Connelly *et al*. 2000) gave rise to the formation of the Arfersiorfik quartz diorite. The Pb-isotopic signature of magnetite from these rocks is comparable with that of whole-rock samples.

Allanite and monazite PbSL analyses yield pegmatite formation ages of ~1800 Ma for both the Nordre Strømfjord, Attu and Qasigiannguit regions. The formation of pegmatites is therefore post-collisional. The pegmatites were formed by melting of the local country rocks; Pb-isotopic data indicate that variable proportions of Late Archaean and Palaeoproterozoic age contributed to their petrogenesis. Hydrothermal activity continued after pegmatite emplacement and after closure of magnetite, at 1800–1650 Ma.

Acknowledgements

The authors acknowledge F. Kalsbeek for inspiring suggestions, and P.M. Holm and an anonymous reviewer for further improvements of the manuscript. This paper also contains contributions from several colleagues at GEUS, all of whom are acknowledged for their work. A special thanks goes to K. Markussen, Attu, for information about the allanite-bearing pegmatite south of the village.

References

Connelly, J.N. & Mengel, F.C. 2000: Evolution of Archean components in the Paleoproterozoic Nagssugtoqidian orogen, West Greenland. Geological Society of America Bulletin 112, 747–763.

Connelly, J.N., van Gool, J.A.M. & Mengel, F.C. 2000: Temporal evolution of a deeply eroded orogen: the Nagssugtoqidian orogen, West Greenland. Canadian Journal of Earth Sciences 37, 1121–1142.

Connelly, J.N., Thrane, K., Krawiec, A.W., & Garde, A.A. 2006: Linking the Palaeoproterozoic Nagssugtoqidian and Rinkian orogens through the Disko Bugt region of West Greenland. Journal of the Geological Society, London 163, 319–335.

Deer, W.A., Howie, R.A. & Zussman, J. 1966: An introduction to the rock-forming minerals, 528 pp. London: Longman.

Frei, R. & Kamber, B.S. 1995: Single mineral Pb-Pb dating. Earth and Planetary Science Letters 129, 261–268.

Garde, A.A. & Steenfelt, A. 1999: Precambrian geology of Nuussuaq and the area north-east of Disko Bugt, West Greenland. Geology of Greenland Survey Bulletin 181, 6–40.

Hollis, J.A., Keiding, M., Stensgaard, B.M., van Gool, J.A.M. & Garde, A.A. 2006: Evolution of Neoarchaean supracrustal belts at the northern margin of the North Atlantic Craton, West Greenland. In: Garde, A.A. & Kalsbeek, F. (eds): Precambrian crustal evolution and Cretaceous–Palaeogene faulting in West Greenland. Geological Survey of Denmark and Greenland Bulletin 11, 9–31 (this volume).

Kalsbeek, F. & Nutman, A.P. 1996: Anatomy of the early Proterozoic Nagssugtoqidian Orogen, West Greenland, explored by reconnaissance SHRIMP U-Pb zircon dating. Geology 24, 515–518.

Kalsbeek, F. & Taylor, P.N. 1985: Isotopic and chemical variations in granites across a Proterozoic continental margin – the Ketilidian mobile belt of South Greenland. Earth and Planetary Science Letters 73, 65–80.

Kalsbeek, F., Taylor, P.N. & Henriksen, N. 1984: Age of rocks, structures, and metamorphism in the Nagssugtoqidian mobile belt, West Greenland – field and Pb-isotope evidence. Canadian Journal of Earth Sciences 21, 1126–1131.

Kalsbeek, F., Pidgeon, R.T. & Taylor, P.N. 1987: Nagssugtoqidian mobile belt of West Greenland: cryptic 1850 Ma suture between two Archaean continents – chemical and isotopic evidence. Earth and Planetary Science Letters 85, 365–385.

Kalsbeek, F., Taylor, P.N. & Pidgeon, R.T. 1988: Unreworked Archaean basement and Proterozoic supracrustal rocks from northeastern Disko Bugt, West Greenland: implications for the nature of Proter-

ozoic mobile belts in Greenland. Canadian Journal of Earth Sciences 25, 773–782.

Ludwig, K.R. 1990: ISOPLOT for MS-DOS – A plotting and regression program for radiogenic isotope data, for IBM-PC compatible computers, version 2.03. United States Geological Survey, Open File Report OF-88-0557, 40 pp.

Nutman, A.P., Kalsbeek, F., Marker, M., van Gool, J.A.M. & Bridgwater, D. 1999: U-Pb zircon ages of Kangâmiut dykes and detrital zircons in metasediments in the Palaeoproterozoic Nagssugtoqidian orogen (West Greenland). Clues to the pre-collisional history of the orogen. Precambrian Research 93, 87–104.

Østergaard, C., Garde, A.A., Nygaard, J., Blomsterberg, J., Nielsen, B.M., Stendal, H. & Thomas, C.W. 2002: The Precambrian supracrustal rocks in the Naternaq (Lersletten) and Ikamiut areas, central West Greenland. Geology of Greenland Survey Bulletin 191, 24–32.

Ramdohr, P. 1969: The ore minerals and their intergrowths, 1174 pp. Oxford: Pergamon Press.

Schjødt, F. & Steenfelt, A. 2004: Mineral resources of the Precambrian shield of central West Greenland (66° to 70°15′ N). Part 1. Compilation of geoscience data. Danmarks og Grønlands Geologiske Undersøgelse Rapport 2004/16, 45 pp.

Secher, K. 1980: Distribution of radioactive mineralisation in central West Greenland. Rapport Grønlands Geologiske Undersøgelse 100, 61–65.

Stacey, J.S. & Kramers, J.D. 1975: Approximation of terrestrial lead isotope evolution by a two-stage model. Earth and Planetary Science Letters 26, 207–221.

Steenfelt, A., Stendal, H., Nielsen, B.M. & Rasmussen, T.M. 2004: Gold in central West Greenland – known and prospective occurrences. Geological Survey of Denmark and Greenland Bulletin 4, 65–68.

Stendal, H. 1998: Contrasting Pb isotopes of Archaean and Palaeoproterozoic sulphide mineralisation, Disko Bugt, central West Greenland. Mineralium Deposita 33, 255–265.

Stendal, H. & Schønwandt, H.K. 2003: Precambrian supracrustal rocks and mineral occurrences, north-east Disko Bugt. Danmarks og Grønlands Geologiske Undersøgelse Rapport 2003/24, 57 pp.

Stendal, H., Blomsterberg, J., Jensen, S.M., Lind, M., Madsen, H.B., Nielsen, B.M., Thorning, L. & Østergaard, C. 2002: The mineral resource potential of the Nordre Strømfjord – Qasigiannguit region, southern central West Greenland. Geology of Greenland Survey Bulletin 191, 39–47.

Stendal, H., Nielsen, B.M., Secher, K. & Steenfelt, A. 2004: Mineral resources of the Precambrian shield of central West Greenland (66° to 70°15′). Part 2. Mineral occurrences. Danmarks og Grønlands Geologiske Undersøgelse Rapport 2004/20, 212 pp.

Stendal, H., Frei, R. & Stensgaard, B.M. 2006: A lead isotope study of an Archaean gold prospect in the Attu region, Nagssugtoqidian orogen, West Greenland. In: Garde, A.A. & Kalsbeek, F. (eds): Precambrian crustal evolution and Cretaceous–Palaeogene faulting in West Greenland. Geological Survey of Denmark and Greenland Bulletin 11, 53–60 (this volume).

Taylor, P.N. & Kalsbeek, F. 1990: Dating the metamorphism of Precambrian marbles: Examples from Proterozoic mobile belts in Greenland. Chemical Geology 86, 21–28.

Thrane, K. & Connelly, J.N. 2006: Zircon geochronology from the Kangaatsiaq–Qasigiannguit region, the northern part of the 1.9–1.8 Ga Nagssugtoqidian orogen, West Greenland. In: Garde, A.A. & Kalsbeek, F. (eds): Precambrian crustal evolution and Cretaceous–Palaeogene faulting in West Greenland. Geological Survey of Denmark and Greenland Bulletin 11, 87–99 (this volume).

Todt, W., Cliff, R.A., Hanser, A. & Hofmann, A.W. 1993: Re-calibration of NBS lead standards using a 202Pb + 205Pb double spike. Terra Abstracts 5, Supplement 1.

van Gool, J.A.M., Connelly, J.N., Marker, M. & Mengel, F. 2002: The Nagssugtoqidian orogen of West Greenland: tectonic evolution and regional correlations from a West Greenland perspective. Canadian Journal of Earth Sciences 39, 665–686.

Whitehouse, M.J., Kalsbeek, F. & Nutman, A.P. 1998: Crustal growth and crustal recycling in the Nagssugtoqidian orogen of West Greenland: constraints from radiogenic isotope systematics and U-Pb zircon geochronology. Precambrian Research 91, 365–381.

Willigers, B.J.A., Krogstad, E.J. & Wijbrans, J.R. 2001: Comparison of thermochronometers in a slowly cooled granulite terrain: Nagssugtoqidian orogen, West Greenland. Journal of Petrology 42, 1729–1749.

Manuscript received 28 October 2004; revision accepted 19 December 2005

New hornblende and muscovite $^{40}Ar/^{39}Ar$ cooling ages in the central Rinkian fold belt, West Greenland

Ann-Sofie Sidgren, Laurence Page and Adam A. Garde

The Palaeoproterozoic Rinkian fold belt in West Greenland consists of reworked Archaean basement, mainly orthogneiss, and the unconformably overlying Palaeoproterozoic Karrat Group. Both parts were intensely deformed and metamorphosed at around 1.87 Ga, at which time the crustal anatectic Prøven igneous complex was emplaced into the northern part of the belt. Seven new hornblende and muscovite $^{40}Ar/^{39}Ar$ cooling ages are presented from the central–northern parts of the Rinkian fold belt. Four $^{40}Ar/^{39}Ar$ hornblende ages ranging from 1795 ± 3 to 1782 ± 3 Ma were obtained from amphibolite and hornblendite enclaves in the Archaean orthogneiss, and two from relict dyke fragments in the latter that may be of Palaeoproterozoic age. Three $^{40}Ar/^{39}Ar$ muscovite ages of 1681 ± 6 Ma, 1686 ± 3 Ma and 1676 ± 3 Ma were obtained from samples of Karrat Group metagreywacke, andalusite schist and metasiltstone. The new $^{40}Ar/^{39}Ar$ ages, from hornblende and muscovite respectively, are very uniform and probably unrelated to local metamorphic grade and structural history, and are interpreted as regional late orogenic cooling ages. The new hornblende ages are significantly older than those previously obtained from the central and northern parts of the adjacent Nagssugtoqidian orogen to the south, and point to different uplift histories, which may suggest that the orogeny was not synchronous in the two regions.

Keywords: Ar-Ar, geochronology, Rinkian, Palaeoproterozoic, West Greenland

---

A.-S.S. & L.P., *Department of Geology, Geobiosphere Science Center, Lund University, Sölvegatan 12, S-223 62 Lund, Sweden.*
E-mail: *Ann-Sofie.Sidgren@bd.lst.se*
A.A.G., *Geological Survey of Denmark and Greenland, Øster Voldgade 10, DK-1350 Copenhagen K, Denmark.*

This paper presents seven new hornblende and muscovite $^{40}Ar/^{39}Ar$ cooling ages from the central part of the Palaeoproterozoic Rinkian fold belt in West Greenland. The new data set provides insight into the cooling history of the Rinkian fold belt and can also be used to address its temporal relationship with the adjacent Nagssugtoqidian orogen to the south, from which other $^{40}Ar/^{39}Ar$ cooling ages have previously been published.

Most of central and northern West Greenland consists of Archaean continental crust which was intensively reworked during the Palaeoproterozoic. This reworking was first recognised in central West Greenland between 66° and 69°N by Ramberg (1949), who established the Nagssugtoqidian mobile belt (now called the Nagssugtoqidian orogen) in this area. Escher & Pulvertaft (1976) subsequently proposed that a separate Palaeoproterozoic mobile belt, the Rinkian fold belt, existed in central and northern West Greenland between 69° and 75°N (see inset map of Fig. 1). They noted that the latter region was dominated by an overall flat-lying tectonic foliation with superimposed large domes, and considered that these structures were of a different nature from the generally steep foliations and tight folds that had previously been identified in the Nagssugtoqidian belt. In contrast to the collisional structures recognised within the Nagssugtoqidian orogen, it was thought that the Rinkian deformation had taken place without significant crustal shortening.

Furthermore, whereas the collisional Nagssugtoqidian

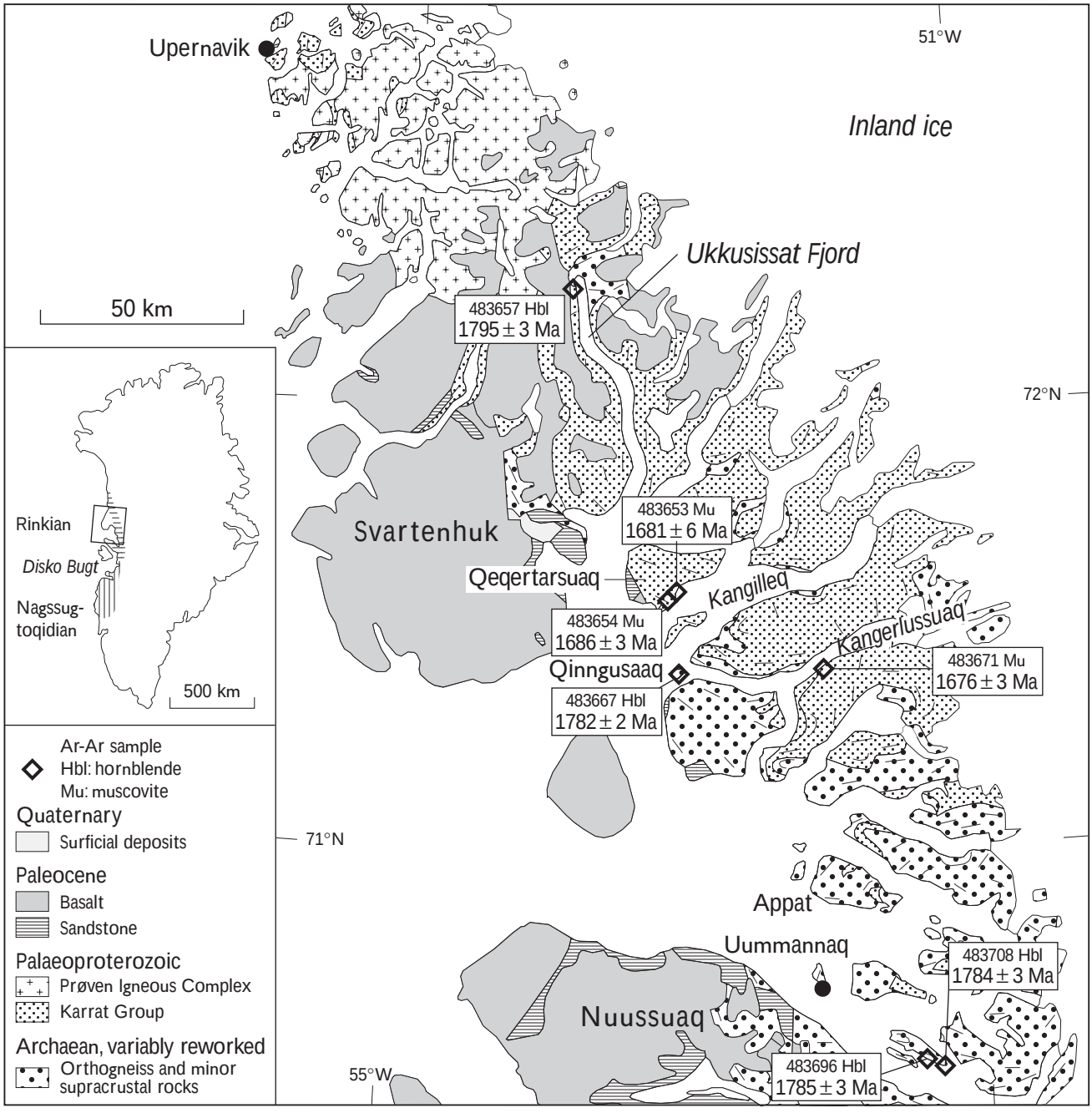

Fig. 1. Map of the central Rinkian fold belt showing the locations of samples collected for $^{40}Ar/^{39}Ar$ age determination. The index map shows the position of Fig. 1 and the approximate extent of Nagssugtoqidian and Rinkian reworking in West Greenland. Modified from Garde *et al.* (2004).

orogen was originally believed only to comprise Archaean supracrustal and infracrustal rocks, the Rinkian fold belt contains a widespread, metamorphosed and deformed cover sequence, the *c.* 2 Ga old Karrat Group, which was unconformably deposited on the Archaean basement gneisses (Garde & Pulvertaft 1976; Henderson & Pulvertaft 1987; Kalsbeek *et al.* 1998). The lowest parts of the Karrat Group consist of quartzite, marble and minor amphibolite (the Qeqertarsuaq and Marmorilik Formations), which are overlain by a very uniform sequence of metagreywacke, the Nukavsak Formation, which is several kilometres thick and occurs throughout most of the Rinkian belt (Fig. 1; Henderson & Pulvertaft 1987). The geochemistry of the Karrat Group and studies of its detrital zircons indicate that the Karrat Group was derived from a mixed source including Palaeoproterozoic magmatic arc

rocks and Archaean basement rocks, and that it was deposited at around 2.0–1.9 Ga ago (Kalsbeek *et al.* 1998; Thrane *et al.* 2003).

The Rinkian fold belt also incorporates the Prøven igneous complex, a very large plutonic complex of granitic and microdioritic crustal melts that were emplaced under granulite facies conditions into the middle to upper crust in the Upernavik region of the Rinkian belt and is also found as the Cumberland batholith on adjacent Baffin Island, Canada. The pluton has previously yielded a Rb-Sr whole rock isochron age of 1860 ± 25 Ma with a high initial $^{87}Sr/^{86}Sr$ ratio (Kalsbeek 1981) and has recently also been studied by Thrane *et al.* (2005). The latter produced a more precise zircon U-Pb ion probe age of 1869 ± 9 Ma and obtained negative εNd values from the pluton (calculated at 1870 Ma) ranging between –5.2 and –4.3. In agreement with the previous Rb/Sr data this shows that the plutonic complex contains a large Archaean continental crustal component. It is therefore questionable whether the Prøven igneous complex – Cumberland batholith is subduction-related as has been proposed by Canadian workers. Thrane *et al.* (2005) suggest it represents a crustal melt, induced by upwelling hot asthenospheric mantle.

Pulvertaft (1986), Henderson & Pulvertaft (1987), Grocott & Pulvertaft (1990) and Garde & Steenfelt (1999b) have described the structural evolution in various parts of the Rinkian fold belt, and recognised large-scale thrusts in its southern part. Following new field work in 2002–2003, the structural evolution in the Uummannaq region is at present regarded as consisting of four main phases (briefly outlined by Garde *et al.* 2003, 2004). Deformation began with tight folding and possibly thrusting (D1), which developed prior to cleavage formation. This was followed by NE- to E-directed thrusting and ductile tectonic transport (D2) accompanied by formation of a penetrative schistosity, and then by NW- to W-directed tectonic transport (D3) and intensification of the pre-existing schistosity. Lastly, very large, upright to overturned, dome-shaped anticlines and tight synclinal cusps were developed during continued shortening of the now strongly tectonically layered crust; these large structures are only locally accompanied by a new tectonic fabric. The Prøven igneous complex was emplaced at a late stage of the main fabric-forming events and gave rise to a wide metamorphic aureole that was overprinted on rocks that were already regionally metamorphosed at high grade.

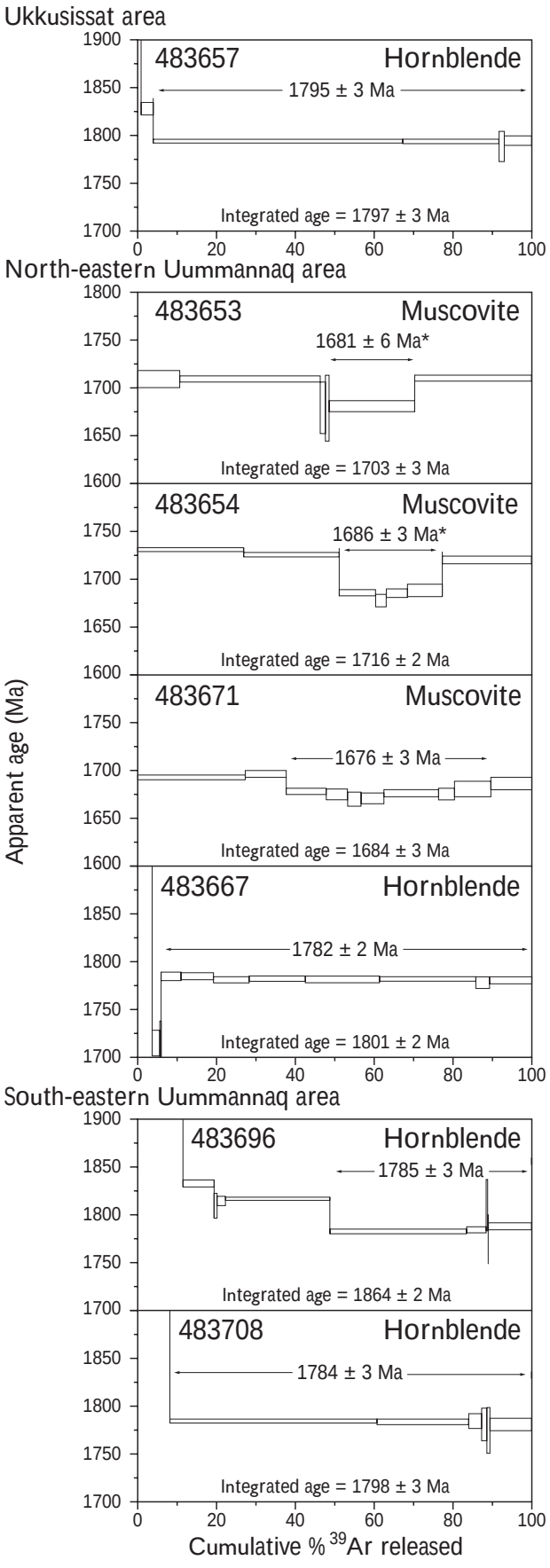

Fig. 2. $^{40}Ar/^{39}Ar$ plateau age spectra from the Rinkian fold belt. Ages with an asterisk (*): $^{40}Ar/^{39}Ar$ plateau age representing less than 50% of total ^{39}Ar release. Ages without an asterisk: $^{40}Ar/^{39}Ar$ plateau age.

Table 1. ^{40}Ar-^{39}Ar analytical data for step heating experiments on amphiboles and muscovites from the Rinkian fold belt

Step	Pwr/T°C	Ca/K	Cl/K	$^{36}Ar/^{39}Ar$	$\%^{36}Ar(Ca)$	$^{40*}Ar/^{39}Ar$	Mol ^{39}Ar	% Step	$\%^{39}Ar$ Cumulated	$\%^{40*}Ar$	Age (Ma)	±Age (2σ)
483653 Muscovite (J = 0.01071 ± 0.00001):												
C	1.4	0.00001	0.001	0.00011	0	147.485	0.093	10.9	10.9	100	1709.6	4.4
D	1.4	0.1461	0.004	0.00008	26.5	147.544	0.306	35.6	46.4	100	1710	1.7
•E	1.5	1.9453	0.021	0.00097	27.6	143.552	0.011	1.2	47.7	99.9	1679.9	13.4
•F	1.6	2.875	0.004	0.00041	96.1	143.488	0.009	1	48.7	100	1679.4	17.2
•G	1.9	0.4853	0.003	0.00010	68.7	143.739	0.187	21.7	70.3	100	1681.3	2.7
H	4	0.3402	0.004	0.00019	24.8	147.664	0.256	29.7	100	100	1710.9	1.6
Integrated (total fusion) age:											1703	3
(•) Plateau age:								23.9			1681	6
483654 Muscovite (J = 0.01071 ± 0.00001):												
A	1.4	0.005	0.003	0.00106	0.1	150.444	0.767	26.9	26.9	99.8	1731.6	1.0
B	1.5	0.006	0.005	0.00033	0.2	149.670	0.692	24.3	51.2	99.9	1725.9	1.2
•C	1.6	0.0499	0.009	0.00063	1.1	144.382	0.265	9.3	60.5	99.9	1686.2	1.5
•D	1.7	0.9006	0.020	0.00077	16.1	143.337	0.075	2.6	63.1	99.9	1678.2	3.3
•E	1.8	0.1521	0.007	0.00147	1.4	144.323	0.153	5.4	68.5	99.7	1685.7	2.2
•F	1.9	0.357	0.009	0.00015	32.9	144.706	0.251	8.8	77.3	100	1688.6	3.1
G	2.3	0.0741	0.003	0.00003	35.7	148.939	0.648	22.7	100	100	1720.4	2.1
Integrated (total fusion) age:											1716	2
(•) Plateau age:								26.1			1686	3
483657 Hornblende (J = 0.01071 ± 0.00001):												
A	1.8	11.847	0.123	0.04105	4	184.220	0.019	1	1	94	1965.7	11.4
B	1.9	11.642	0.027	0.00559	28.7	163.894	0.059	3.1	4.1	99.3	1828.5	3.3
•C	2	10.312	0.013	0.00193	73.5	159.127	1.198	63.2	67.3	99.9	1794.7	1.1
•D	2	10.03	0.014	0.00155	89	159.084	0.463	24.4	91.7	100	1794.4	1.3
•E	2.1	11.862	0.043	0.00182	90	158.317	0.028	1.5	93.2	100	1788.9	8.0
•F	2.6	11.62	0.018	0.00223	71.9	159.178	0.130	6.8	100	99.9	1795.1	2.3
Integrated (total fusion) age:											1797	3
(•) Plateau age:								95.9			1795	3
483667 Hornblende (J = 0.01071 ± 0.00001):												
A	1.8	14	0.277	0.08890	2.2	501.205	0.011	0.5	0.5	95.1	3339.8	25.5
B	1.9	8.88	-0.010	0.01236	9.9	166.723	0.006	0.2	0.7	98.1	1848.2	27.0
C	2	8.133	0.066	0.00845	13.3	196.061	0.068	3	3.7	98.9	2041	3.3
D	2	8.823	0.082	0.01454	8.4	148.220	0.042	1.8	5.5	97.4	1715.1	6.7
E	2.1	5.161	0.073	0.01482	4.8	146.685	0.009	0.4	5.9	97.2	1703.6	17.3
•F	2.2	8.525	0.054	0.00482	24.4	157.760	0.118	5.2	11	99.3	1784.9	2.3
•G	2.2	9.17	0.048	0.00241	52.4	157.782	0.188	8.2	19.2	99.8	1785.1	1.7
•H	2.3	8.683	0.050	0.00316	37.8	157.288	0.206	9	28.2	99.6	1781.6	1.6
•I	2.3	8.979	0.056	0.00234	53	157.382	0.328	14.3	42.5	99.8	1782.2	1.4
•J	2.4	8.623	0.055	0.00105	113.4	157.274	0.432	18.8	61.3	100	1781.5	1.9
•K	2.6	8.346	0.056	0.00150	77	157.395	0.561	24.4	85.8	99.9	1782.3	1.1
•L	2.8	9.598	0.067	0.00374	35.4	156.861	0.081	3.5	89.3	99.5	1778.5	3.0
•M	4	10.4	0.062	0.00273	52.5	157.231	0.246	10.7	100	99.8	1781.1	1.9
Integrated (total fusion) age:											1801	2
(•) Plateau age:								94.1			1782	2
483671 Muscovite (J = 0.01071 ± 0.00001):												
A	1.4	0.2482	0.005	0.00153	2.2	145.263	0.449	27.4	27.4	99.7	1692.9	1.2
B	1.5	0.7642	0.007	0.00189	5.6	145.703	0.168	10.3	37.6	99.6	1696.2	1.9
•C	1.5	0.3775	0.007	0.00197	2.6	143.327	0.168	10.2	47.8	99.6	1678.2	1.6
•D	1.6	0.4299	0.017	0.00377	1.6	142.856	0.089	5.4	53.3	99.2	1674.6	2.8
•E	1.6	1.5215	0.010	0.00180	11.7	142.234	0.057	3.5	56.7	99.7	1669.8	3.7
•F	1.7	0.9017	0.017	0.00144	8.7	142.377	0.093	5.7	62.4	99.7	1670.9	3.0
•G	1.7	0.2113	0.005	0.00004	79.6	143.047	0.230	14	76.4	100	1676	1.7
•H	1.8	1.123	0.015	0.00144	10.7	142.970	0.065	4	80.4	99.7	1675.4	23.0
•I	2	0.4492	0.005	0.00121	5.1	143.638	0.152	9.3	89.7	99.8	1680.5	4.2
J	2.3	0.2898	0.004	0.00172	2.3	144.357	0.169	10.3	100	99.7	1686	3.2
Integrated (total fusion) age:											1684	3
(•) Plateau age:								52.1			1676	3

J: irradiation parameter. $^{40*}Ar$: radiogenic ^{40}Ar.
Steps marked with dot (•) are included in the plateau age for each sample.

Table 1 *(continued)*

Step	Pwr/T°C	Ca/K	Cl/K	$^{36}Ar/^{39}Ar$	$\%^{36}Ar(Ca)$	$^{40*}Ar/^{39}Ar$	Mol ^{39}Ar	% Step	$\%^{39}Ar$ Cumulated	$\%^{40*}Ar$	Age (Ma)	± Age (2σ)
483696 Hornblende (J = 0.01071 ± 0.00001):												
A	1.9	4.9568	0.167	0.02251	3	557.080	0.091	1.9	1.9	98.9	3501.9	4.4
B	2	5.6395	0.198	0.00248	31.3	176.447	0.447	9.5	11.5	99.7	1914.4	1.3
C	2.1	5.7159	0.202	0.00177	44.4	164.542	0.370	7.9	19.4	99.8	1833	1.7
D	2.2	5.9588	0.197	0.00468	17.5	161.233	0.042	0.9	20.3	99.3	1809.7	6.6
E	2.2	5.7368	0.198	0.00147	53.9	161.903	0.098	2.1	22.3	99.9	1814.5	2.5
F	2.3	5.3872	0.190	0.00107	69.3	162.278	1.212	26.4	48.8	99.9	1817.1	1.0
•G	2.3	5.3337	0.184	0.00097	75.5	157.503	1.620	34.6	83.4	100	1783.1	1.3
•H	2.4	5.3052	0.209	0.00097	75.2	157.732	0.242	5.2	88.5	100	1784.7	1.6
•I	2.6	6.2547	0.255	0.00436	19.8	161.354	0.017	0.4	88.9	99.4	1810.6	13.4
•J	2.9	7.1602	0.246	0.00815	12.1	156.396	0.009	0.2	89.1	98.7	1775.1	13.0
•K	4	5.4765	0.189	0.00181	41.7	158.216	0.511	10.9	100	99.8	1788.2	1.6
Integrated (total fusion) age:											1864	2
(•) Plateau age:								51.2			1785	3
483708 Hornblende (J = 0.01071 ± 0.00001):												
A	1.9	7.672	0.051	0.00834	12.7	181.053	0.134	8.2	8.2	98.8	1945	2.2
•B	2	9.5527	0.062	0.00197	66.7	157.766	0.855	52.6	60.8	99.9	1785	1.0
•C	2.1	9.6506	0.062	0.00317	42	157.637	0.376	23.2	84	99.7	1784.1	1.5
•D	2.2	8.7213	0.062	0.00050	241.2	157.711	0.054	3.3	87.3	100.1	1784.6	3.8
•E	2.3	10.597	0.109	0.00836	17.5	157.274	0.024	1.5	88.7	98.7	1781.5	8.4
•F	2.4	13.824	0.144	0.00502	38	156.401	0.012	0.7	89.5	99.4	1775.2	12.1
•G	2.7	10.368	0.067	0.00298	47.9	157.265	0.171	10.5	100	99.7	1781.4	3.3
Integrated (total fusion) age:											1798	3
(•) Plateau age:								91.8			1784	3

Whereas the tectonic model of Grocott & Pulvertaft (1990) operated with four contractional and three extensional events in an epicontinental marginal basin, four main phases of deformation that developed during progressive crustal shortening are now recognised. It has been debated in recent years whether the previous distinction between the Rinkian and Nagssugtoqidian belts in West Greenland is meaningful in tectonic terms (e.g. Garde & Steenfelt 1999a; van Gool *et al.* 2002), and it has now been proposed that the two belts represent the northern and southern parts of a common, more than 1100 km wide collisional orogen, separated by a suture located in the Disko Bugt region (Fig. 1; Connelly *et al.* 2005). The continuous crustal shortening in the Rinkian fold belt throughout its tectonic evolution is in agreement with a setting within the northern of two colliding plates at some distance from the suture, and thus in accordance with the proposed tectonic linkage to the Nagssugtoqidian orogen. However, the $^{40}Ar/^{39}Ar$ data presented in the following section may be interpreted to indicate that the tectono-metamorphic events in the Rinkian and Nagssugtoqidian belts were not contemporaneous.

Descriptions of samples and results of $^{40}Ar/^{39}Ar$ age determinations

Four hornblende samples and three muscovite samples were collected at the head of Ukkusissat Fjord close to the Prøven igneous complex, between Svartenhuk and Uummannaq, and close to the north coast of Nuussuaq (Fig. 1). Sample numbers refer to the data base of the Geological Survey of Denmark and Greenland.

Ukkusissat Fjord near the Prøven igneous complex

A sample with hornblende was collected south of the Prøven igneous complex, within the high-grade contact metamorphic aureole where extensive partial melting has been observed, particularly within the Karrat Group (Grocott & Pulvertaft 1990). The sample (483657, Fig. 1) comes from a homogeneous, medium-grained, amphibolitic relict dyke within the regional flat-lying tonalitic orthogneiss basement. The amphibolite dyke is approximately one metre thick, a few metres long, and has been isoclinally folded. The sample is mostly composed of light to dark green hornblende between 0.5 and 1 mm in diameter, together with some plagioclase and minor phases

such as biotite, titanite and zoizite. The biotite is intergrown with hornblende, and the plagioclase is partly altered to sericite. The obtained plateau age is 1795 ± 3 Ma (Fig 2; Table 1).

North-eastern Uummannaq

Four samples were collected in the Kangilleq–Kangerlussuaq area, 75–100 km north of Uummannaq (Fig. 1). This area was less intensely affected by Rinkian metamorphism than other areas investigated in this study, with chlorite schist locally preserved on the north coast of Qeqertarsuaq.

Samples 483653 and 483654, both from the Nukavsak Formation, were collected at two localities close to each other near the southern end of Qeqertarsuaq (Fig. 1). Sample 483653 (Fig. 1) is a greywacke consisting of biotite, sillimanite, quartz, muscovite and small amounts of tourmaline and zircon. It is a fine-grained rock, where biotite and muscovite together define the main tectonic foliation. Fibrolitic sillimanite occurs in broom-shaped clusters close to muscovite. It was difficult to obtain a good separate from this sample because the muscovite is very fine grained, intergrown with biotite, and sometimes has altered rims. This sample yielded a u-shaped spectrum, with a minimum which yields an age of 1681 ± 6 Ma and represents 24% of the total ^{39}Ar-release (Fig. 2; Table 1).

Sample 483654 (Fig. 1) is a fine-grained andalusite schist with centimetre-sized andalusite poikiloblasts in a matrix of biotite and quartz, minor tourmaline and muscovite. Partial recrystallisation of andalusite to fibrolite was observed. The biotite shows two different orientations implying growth both during D2 and D3 deformation. The muscovite crystals are very small and often occur close to biotite, but sometimes also in small separate clusters. This sample gave a u-shaped spectrum, with a minimum representing 26% of the total ^{39}Ar-release and yielding an age of 1686 ± 3 Ma (Fig. 2; Table 1).

Sample 483667 (Fig. 1) was collected from a decimetre-thick, boudinaged, homogeneous amphibolite band in tonalitic reworked orthogneiss on Qinngusaaq (Fig. 1). Folds, lineations, δ- and σ-shaped porphyroclasts and foliations representing both D2–D3 and D4 occur at the sampling locality. The light to dark brownish-green hornblende forms well-crystallised medium-grained aggregates with interstitial plagioclase partly altered to sericite. Small grains of pale green pyroxene, probably diopside, occur together with the hornblende. A hornblende plateau age of 1782 ± 2 Ma was obtained (Fig. 2; Table 1).

Sample 483671 (Fig. 1) consists of fine-grained metasandstone to metasiltstone from the Nukavsak Formation with quartz, biotite, muscovite and sillimanite as main minerals. Biotite, muscovite and sillimanite define the main tectonic foliation, where sillimanite often occurs in clusters containing small muscovite and biotite grains. At this locality, quartz pods display distinct asymmetries in two different directions. The asymmetric pods on rock faces with SW–NE orientations suggest top-to-NE tectonic transport (during D2), whereas rock faces with SE–NW orientations suggest transport to the NW (during D3) and contain biotite lineations with that trend. Muscovite from this rock, presumably grown during D3, gave a plateau age of 1676 ± 3 Ma (Fig. 2; Table 1).

South-east of Uummannaq

Two samples with hornblende were collected from the Archaean basement south-east of the Uummannaq area, close to the north coast of Nuussuaq (Fig. 1). Sample 483696 (Fig. 1) comes from a hornblenditic layer in a leucogabbro that occurs as enclaves in quartzo-feldspathic orthogneiss. The sample consists almost exclusively of light to dark green, medium- to coarse-grained hornblende. The hornblende plateau age is 1785 ± 3 Ma (Fig. 2; Table 1).

Sample 483708 (Fig. 2) comes from an amphibolite dyke that cuts the fabric of the surrounding augen gneiss and is probably Palaeoproterozoic in age. Both the amphibolite and the host gneiss are intensely deformed. This sample has biotite and hornblende growing together, feldspars partly altered to sericite, and minor amounts of quartz. The hornblende plateau age is 1784 ± 3 Ma (Fig. 2; Table 1).

Discussion and conclusions

The results from this study provide the first published constraints on cooling ages of hornblende and muscovite in the central Rinkian belt. Hornblende ^{40}Ar/^{39}Ar plateau age spectra from samples 483657, 483667 and 483708 yield ages between 1795 and 1782 Ma. These ages all form well-defined plateaus, and the plateaus represent more than 90% of total ^{39}Ar release. Sample 483696 yielded a plateau age of 1785 Ma for 51% of the total ^{39}Ar release, and is consistent with the other hornblende ages. Muscovite samples 483653 and 483654 both yield u-shaped age spectra with minima representing less than 50% of the total ^{39}Ar release, at 1681 and 1686 Ma respectively. Sample 483671 provides a plateau age of 1676 Ma defined by

52% of the total ^{39}Ar release. The muscovite plateau age spectrum for sample 483671 is consistent with the minima provided by samples 483653 and 483654. These taken together suggest a relatively consistent muscovite cooling age below 350°C of *c*. 1680 Ma in the central Rinkian belt.

The obtained hornblende and muscovite ages at 1795–1782 and 1686–1676 Ma, respectively, are remarkably uniform, although they cover a distance of *c*. 200 km in chlorite to sillimanite grade amphibolite facies terrain across the entire central part of the Rinkian fold belt. This ^{40}Ar/^{39}Ar age study shows that the temperatures reached during the Palaeoproterozoic tectonothermal reworking were everywhere sufficiently high to reset the ^{40}Ar/^{39}Ar hornblende and muscovite systems in the rocks examined. The ages date the cooling below the closure temperature of Ar diffusion in hornblende and muscovite after the Palaeoproterozoic metamorphic event, and the data suggest a slow cooling rate of *c*. 1.5°C/Ma between *c*. 1780 and 1680 Ma, using closure temperatures of 500°C for hornblende and 350°C for muscovite (McDougall & Harrison 1999).

Due to recent recalculation of the primary and secondary standards used in ^{40}Ar/^{39}Ar geochronological experiments (Renne *et al.* 1998), the previously published ^{40}Ar/^{39}Ar ages from the Nagssugtoqidian belt (Rasmussen & Holm 1999; Willigers *et al.* 2001, 2002), which use the older standard age, have to be multiplied by 1.009 in order to compare directly with the new ^{40}Ar/^{39}Ar ages presented here from the Rinkian belt. In the northern part of the Nagssugtoqidian orogen, Willigers *et al*. (2001, 2002) obtained ^{40}Ar/^{39}Ar hornblende ages of 1756–1733 Ma (recalculated from 1740–1717 Ma) and muscovite ages of *c*. 1715 Ma (recalculated from 1700 Ma). In the central part of the orogen still farther south, their hornblende ages range between *c*. 1750–1700 Ma and muscovite ages between *c*. 1765–1715 Ma (recalculated from 1750–1700 Ma). In the Disko Bugt area (Fig. 1), where Connelly *et al.* (2005) proposed a suture between the two belts, a set of ^{40}Ar/^{39}Ar and K-Ar hornblende age data reported by Rasmussen & Holm (1999) scatter between Archaean ages and a K-Ar age of *c*. 1765 Ma, revealing that temperatures during the Palaeoproterozoic thermal event were not sufficiently high in all parts of this area to reset the K-Ar isotope system (Rasmussen & Holm 1999).

The uniformity of the new ^{40}Ar/^{39}Ar ages from the central and northern Rinkian fold belt suggests that the ages are largely unrelated to the metamorphic grade and to the structural history of the geographical locations of the samples, with the possible exception of sample 483657 from Ukkusissat Fjord (see below). Accordingly, the ^{40}Ar/^{39}Ar data are interpreted as regional, late orogenic cooling ages which are not directly related to the tectono-metamorphic history of the individual samples. This conclusion is supported by (in part unpublished) U-Pb zircon ages of syn- to late-kinematic Palaeoproterozoic pegmatites from the same region, which are older than 1800 Ma (Thrane *et al*. 2003; K. Thrane, personal communication 2004).

Willigers *et al*. (2002) reached the same conclusion from their ^{40}Ar/^{39}Ar studies of the central and northern Nagssugtoqidian orogen reported above, pointing out that their study area represents a section of middle to lower crust that was only slowly exhumed by erosion.

In preserved upper crustal levels of younger orogens it is commonly possible to date specific tectonic events using the ^{40}Ar/^{39}Ar method, because the dated units were either transported rapidly to these crustal levels and are not yet eroded away, or the minerals grew at temperatures near or below their closing temperature and thus constrain the age of the prograde tectonothermal event itself. The 1795 ± 3 Ma age of the hornblende from Ukkusissat Fjord (sample 483657, about 12 Ma older than the other hornblende ages) may point to early uplift of this particular area, which is a domain of early NE-directed D2 thrusting that was not affected by the subsequent NW-directed tectonic transport during D3.

The cooling rate of *c*. 1.5°C/Ma documented by this study (using hornblende and muscovite closure temperatures of 500°C and 350°C) is only slightly slower than the 2–3°C/Ma reported by Willigers *et al.* (2001, 2002) from the central Nagssugtoqidian orogen, but considerably slower than rates between 5° and 7°C/Ma reported by the latter authors from the northern Nagssugtoqidian orogen. Willigers *et al.* (2001, 2002) used less accepted closure temperatures of 580°C and 410°C for hornblende and muscovite, respectively, implying a difference of 170°C between hornblende and muscovite closure temperatures. The latter temperature gap is larger than the 150°C used in this study, but this makes little difference to the calculation of cooling rates.

The uniform ^{40}Ar/^{39}Ar hornblende ages resulting from the present investigation are significantly older than those in both the northern and central parts of the Nagssugtoqidian orogen (Willigers *et al*. 2001, 2002). As regards muscovite, the Rinkian muscovite ages are younger than muscovite ages in the northern Nagssugtoqidian belt, but older than those in the central Nagssugtoqidian orogen (Willigers *et al.* 2001, 2002). The fact that Rinkian hornblende ages are older than those in the Nagssugtoqidian orogen shows that cooling below 500°C took place earlier in the Rinkian fold belt than in both the central and northern parts of the Nagssugtoqidian orogen. It is therefore

plausible that uplift began significantly earlier in the Rinkian belt but was slower than in the Nagssugtoqidian orogen, which may in turn suggest that the main phases of compression and peak metamorphism in the two belts were not synchronous.

These interpretations are consistent with the observation by Taylor & Kalsbeek (1990) that Pb-Pb whole-rock isochron ages of marbles in the two belts (interpreted as representing recrystallisation of the marbles during peak metamorphism) differ significantly from each other. Marbles collected on Appat island in the central Rinkian belt (Fig. 1) yielded a Pb-Pb isochron of 1881 ± 20 Ma, whereas an age of 1845 ± 23 Ma was obtained from marbles in the central part of the Nagssugtoqidian orogen. Our interpretations are also consistent with the fact that the $^{40}Ar/^{39}Ar$ data reported here show no signs of having been affected by a contact metamorphic aureole around the Prøven igneous complex. The intrusion age of the latter at 1869 ± 9 Ma is coeval with the youngest members of the Arfersiorfik complex and Sisimiut charnockite in the central Nagssugtoqidian orogen (Connelly *et al.* 2000; van Gool *et al.* 2002). The Prøven igneous complex has intruded rocks belonging to the Karrat Group that were already intensely deformed and metamorphosed prior to the intrusion, but before the last major deformation and peak metamorphism (Thrane *et al.* 2005); the Prøven igneous complex represents a crustal melt that was apparently not related to subduction processes. In contrast, the Arfersiorfik complex and Sisimiut charnockite in the south represent I-type magmas that were related to precollision subduction.

Notwithstanding the overall structural and geochronological evidence for a direct linkage between the Rinkian fold belt and the Nagssugtoqidian orogen, the age relationships outlined above may imply that collision-related deformation, metamorphism and magmatic activity took place in the northern Rinkian belt while subduction was still going on south of the recently proposed suture in the Disko Bugt region. It may be speculated that such diachronism is also reflected in the dissimilar $^{40}Ar/^{39}Ar$ cooling ages from the Rinkian and Nagssugtoqidian parts of the entire Palaeoproterozoic orogenic complex in West Greenland. Alternatively, the different Rinkian and Nagssugtoqidian cooling ages might relate to different depths of burial. However, this is not supported by the uniform hornblende $^{40}Ar/^{39}Ar$ cooling ages found within the Rinkian belt itself, regardless of geographical distance and metamorphic facies; further discussion of large-scale plate-tectonic implications is beyond the scope of the present paper.

Analytical procedure

Four hornblende and three muscovite separates from the central Rinkian belt have been dated with the $^{40}Ar/^{39}Ar$-method. The hornblende separates were obtained from amphibolite and diorite, and muscovite from metasedimentary rocks, by crushing, sieving and handpicking. The hornblende and muscovite samples selected for $^{40}Ar/^{39}Ar$ geochronology were irradiated together with the DRA-2 sanidine standard (25.26 Ma; Wijbrans *et al.* 1995, recalculated following Renne *et al.* 1998), for 35 hours at the NRG-Petten HFR RODEO facility in Petten, The Netherlands. J-values (the irradiation parameter) were calculated with a precision of 0.5%.

The $^{40}Ar/^{39}Ar$ geochronology laboratory at the University of Lund employs a Micromass 5400 mass spectrometer with a Faraday cup and an electron multiplier. A metal extraction line, which contains two SAES C50-ST101 Zr-Al getters and a cold finger cooled to *c.* –155°C by a Polycold P100 cryogenic refrigeration unit, is also present. One or two grains of hornblende or muscovite were loaded into a copper planchette that consists of several 3 mm holes. Samples were step-heated using a defocused 50W CO^2 laser. Sample clean-up time was 5 minutes, using the two hot Zr-Al SAES getters and the cold finger. The laser was rastered over the samples to provide even heating of all grains. The entire analytical process is automated and runs on a Macintosh computer with software developed at the Berkeley Geochronology Center by Al Deino and modified for the laboratory at the University of Lund. Time zero regressions were fitted to data collected from 10 scans over the mass range of 40 to 36. Peak heights and backgrounds were corrected for mass discrimination, isotopic decay and interfering nucleogenic Ca-, K-, and Cl-derived isotopes. Isotopic production values for the cadmium lined position in the Petten reactor are $^{36}Ar/^{37}Ar^{(Ca)} = 0.000270$, $^{39}Ar/^{37}Ar^{(Ca)} = 0.000699$, and $^{40}Ar/^{39}Ar^{(K)} = 0.00183$. ^{40}Ar blanks were calculated before every new sample and after every three sample steps. ^{40}Ar blanks were between 5.0 and 3×10^{-16}. Blank values for masses 39 to 36 were all less than 7×10^{-18}. Blank values were subtracted for all incremental steps from the sample signal. The laboratory was able to produce very good incremental gas splits, using a combination of increasing time at the same laser output, followed by increasing laser output. Age plateaus were determined using the criteria of Dalrymple & Lanphere (1971), which specify the presence of at least three contiguous incremental heating steps with statistically indistinguishable ages and constituting greater than 50% of the total ^{39}Ar released during the experiment. Inverse isochrons yield ages statistically indis-

tinguishable from those given by the plateaus and are not presented here. $^{40}Ar/^{39}Ar$ plateau age spectra are presented in Fig. 2 and the analytical data in Table 1.

Acknowledgements

The authors thank J.N. Connelly, J. Grocott, M. Hand, K.J.W. McCaffrey and K. Thrane for discussions leading to the preparation of this manuscript, which also draws on their collective field observations in 2002–2003. We are grateful to J. Grocott and Å. Johansson for critical reviews.

References

Connelly, J.N., van Gool, J.A.M. & Mengel, F.C. 2000: Temporal evolution of a deeply eroded orogen: the Nagssugtoqidian orogen, West Greenland. Canadian Journal of Earth Sciences 37, 1121–1142.

Connelly, J.N., Thrane K., Krawiec, A. & Garde A.A. 2005: Linking the Palaeoproterozoic Nagssugtoqidian and Rinkian orogens through the Disko Bugt region of West Greenland. Journal of the Geological Society (London) 162, 1–17.

Dalrymple, G.B & Lanphere, M.A. 1971: $^{40}Ar/^{39}Ar$ technique of K-Ar dating: a comparison with the conventional technique. Earth and Planetary Science Letters 12, 300–308.

Escher, A. & Pulvertaft, T.C.R. 1976: Rinkian mobile belt of West Greenland. In: Escher, A. & Watt, W.S. (eds): Geology of Greenland, 105–119. Copenhagen: Geological Survey of Greenland.

Garde, A.A. & Pulvertaft, T.C.R. 1976: Age relations of the Precambrian Mârmorilik Marble Formation, central West Greenland. Rapport Grønlands Geologiske Undersøgelse 80, 49–53.

Garde, A.A. & Steenfelt, A. 1999a: Precambrian geology of Nuussuaq and the area north-east of Disko Bugt, West Greenland. Geology of Greenland Survey Bulletin 181, 6–40.

Garde, A.A. & Steenfelt, A. 1999b: Proterozoic tectonic overprinting of Archaean gneisses in Nuussuaq, West Greenland. Geology of Greenland Survey Bulletin 181, 141–154.

Garde, A.A., Grocott, J., Thrane, K. & Connelly, J.N. 2003: Reappraisal of the Rinkian fold belt in central West Greenland: Tectonic evolution during crustal shortening and linkage with the Nagssugtoqidian orogen. Geophysical research Abstracts 5 (EGS-AGU-EUG Joint Assembly), 09411.

Garde, A.A., Connelly, J.N., Grocott, J., Hand, M., McCaffrey, K.J.W. & Thrane, K. 2004: Crustal shortening and granite emplacement in the Rinkian fold belt, West Greenland, and implications for Palaeoproterozoic Laurentian evolution. Danmarks og Grønlands Geologiske Undersøgelse Rapport 2004/17, 16–18.

Grocott, J. & Pulvertaft, T.C.R. 1990: The Early Proterozoic Rinkian belt of central West Greenland. In: Lewry, J.F. & Stauffer, M.R. (eds): The Early Proterozoic Trans-Hudson orogen of North America. Geological Association of Canada Special Paper 37, 443–463.

Henderson, G. & Pulvertaft, T.C.R. 1987: Geological Map of Greenland, 1:100 000, Mârmorilik 71 V.2 Syd, Nûgâtsiaq 71 V.2 Nord, Pangnertôq 72 V.2 Syd. Descriptive text, 72 pp., 8 plates. Copenhagen: Geological Survey of Greenland.

Kalsbeek, F. 1981: The northward extent of the Archaean basement of Greenland – a review of Rb-Sr whole-rock ages. Precambrian Research 14, 203–219.

Kalsbeek, F., Pulvertaft, T.C.R. & Nutman, A.P. 1998: Geochemistry, age and origin of metagreywackes from the Palaeoproterozoic Karrat Group, Rinkian Belt, West Greenland. Precambrian Research 91, 383–399.

McDougall, I. & Harrison, T.M. 1999: Geochronology and thermochronology by the $^{40}Ar/^{39}Ar$ method. Oxford: Oxford University Press.

Pulvertaft, T.C.R. 1986: The development of thin thrust sheets and basement-cover sandwiches in the southern part of the Rinkian belt, Umanak district, West Greenland. Rapport Grønlands Geologiske Undersøgelse 128, 75–87.

Ramberg, H. 1949: On the petrogenesis of the gneiss complexes between Sukkertoppen and Christianshaab, West Greenland. Meddelelser Dansk Geologisk Forening 11, 312–327.

Rasmussen, H. & Holm, P.M. 1999: Proterozoic thermal activity in the Archaean basement of Disko Bugt region and eastern Nuussuaq, West Greenland: evidence from ^{40}Ar–^{39}Ar mineral age investigations. Geology of Greenland Survey Bulletin 181, 55–64.

Renne, P.R., Swisher, C.C., Deino, A.L., Karner, D.B., Owens, T.L. & DePaolo, D.J. 1998: Intercalibration of standards, absolute ages and uncertainties in $^{40}Ar/^{39}Ar$ dating. Chemical Geology 145, 117–152.

Taylor, P.N. & Kalsbeek, F. 1990: Dating the metamorphism of Precambrian marbles: examples from Proterozoic mobile belts in Greenland. Chemical Geology (Isotope Geoscience Section) 86, 21–28.

Thrane, K., Connelly, J.N., Garde, A.A., Grocott, J. & Krawiec, A.W. 2003: Linking the Palaeoproterozoic Rinkian and Nagssugtoqidian belts of central West Greenland: implications of new U-Pb and Pb-Pb zircon ages. Geophysical Research Abstracts 5 (EGS-AGU-EUG Joint Assembly), 09275 only.

Thrane, K., Baker, J., Connelly, J.[N.] & Nutman, A.P. 2005: Age, petrogenesis and metamorphism of the syn-collisional Prøven igneous complex, West Greenland. Contributions to Mineralogy and Petrology 149, 541–555.

van Gool, J.A.M., Connelly, J.N., Marker, M. & Mengel, F.C. 2002: The Nagssugtoqidian orogen of West Greenland: tectonic evolution and regional correlation from a West Greenland perspective. Canadian Journal of Earth Sciences 39, 665–686.

Wijbrans, J.R., Pringle, M.S., Koppers, A.A.P & Scheveers, R. 1995: Argon geochronology of small samples using the Vulkaan argon laserprobe. Proceedings of the Koninklijke Nederlandse Akademie van Wetenschappen 98, 185–218.

Willigers, B.J.A., Krogstad, E.J. & Wijbrans, J.R. 2001: Comparison of thermochronometers in a slowly cooled granulite terrain: Nagssugtoqidian orogen, West Greenland. Journal of Petrology 42, 1729–1749.

Willigers, B.J.A., van Gool, J.A.M., Wijbrans, J.R., Krogstad, E.J. & Mezger, K. 2002: Posttectonic cooling of the Nagssugtoqidian orogen and a comparison of contrasting cooling histories in Precambrian and Phanerozoic orogens. Journal of Geology 110(5), 503–517.

Manuscript received 21 June 2004; revision accepted 15 March 2005

Presentation and interpretation of structural data from the Nagssugtoqidian orogen using a GIS platform: general trends and features

Jeroen A.M. van Gool and Sandra Piazolo

In this contribution we present data collected by more than 50 international geologists involved in geological mapping and research projects in the Nagssugtoqidian orogen of West Greenland, organised by the Geological Survey of Denmark and Greenland and the Danish Lithosphere Centre. Using a geographical information system (GIS) as a framework for visualisation and analysis of structural and lithological data, it is now possible to give a unique overview of thousands of data points, employed here within a study area of approximately 160 × 180 km in the central and northern Nagssugtoqidian orogen. The GIS methodology allows comparison, integration and analysis of datasets in terms of subject, space, and scale. This is extremely helpful in the recognition of geological patterns, such as terrain or domain boundaries and map-scale structures. Analysis of the available structural data shows clear differences in deformation patterns between the core and the northern segment of the Nagssugtoqidian orogen. One of the most prominent features is the ENE-striking Nordre Strømfjord shear zone, which transects the orogen from the coast to the Inland Ice. The data also clearly document a change from predominantly steeply dipping, ENE–WSW-trending fabrics and large, elongate structural domains in the core of the orogen, to large, open fold patterns and moderately to shallowly dipping fabrics in smaller structural domains in the north.

Keywords: geographical information systems, Nagssugtoqidian orogen, West Greenland, structural data, structural domains

J.A.M.v.G. & S.P., *Geological Survey of Denmark and Greenland, Øster Voldgade 10, DK-1350 Copenhagen K, Denmark.* E-mail: *jvg@geus.dk*

S.P., *Geological Survey of Denmark and Greenland, Øster Voldgade 10, DK-1350 Copenhagen K, Denmark.* Present address: *Department of Geology and Geochemistry, Stockholm University, 10691 Stockholm, Sweden.*

Over the past ten years the Nagssugtoqidian orogen in central West Greenland (Fig. 1) has been the subject of intense geological research, involving both bedrock mapping and research into the Palaeoproterozoic and Archaean tectonic evolution of the region. This has led to a major improvement in the understanding of the tectonic development of the Nagssugtoqidian orogen (Kalsbeek & Nutman 1996; Connelly *et al*. 2000; van Gool *et al*. 2002). The research was undertaken in two projects, organised by the Danish Lithosphere Centre (DLC) from 1994 to 1999 and the Geological Survey of Denmark and Greenland (GEUS) from 2000 to 2003, respectively. Approximately 35 international geologists from institutions on three continents participated in the field work of these projects, with changing teams from year to year. During these projects a very large amount of data was collected, including structural measurements, lithological observations, intrusive relationships, information about metamorphic mineral assemblages, etc. Other structural data were collected during previous work in part of the region in

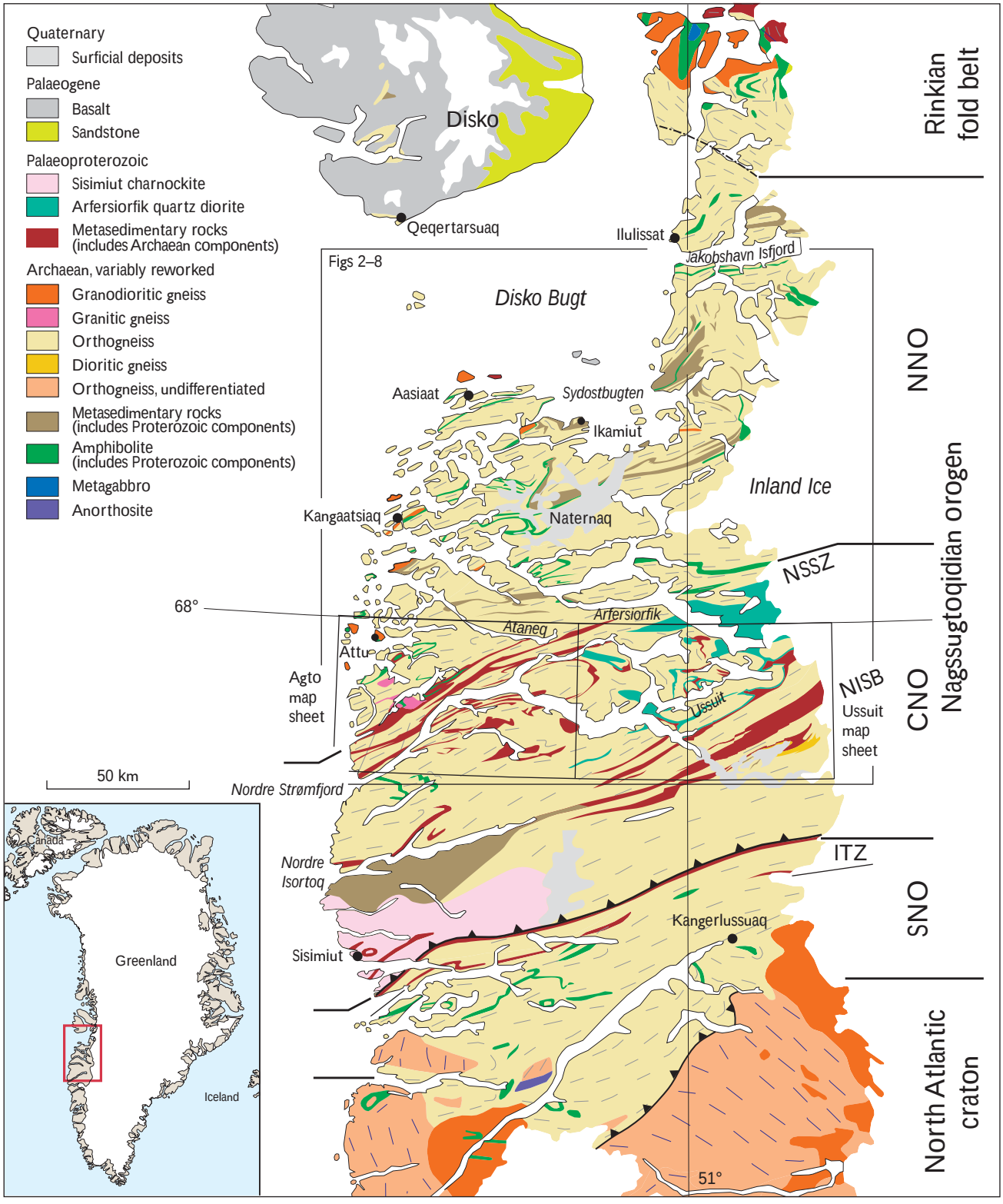

Fig. 1. Schematic geological map of central West Greenland (modified from van Gool *et al.* 2002), depicting the Nagssugtoqidian orogen. ITZ, Ikertôq thrust zone; NISB, Nordre Isortoq steep belt; NSSZ, Nordre Strømfjord shear zone; SNO, CNO and NNO, respectively, the southern, central and northern Nagssugtoqidian orogen. Small boxes outline the locations of the Agto and Ussuit map sheets; Large box indicates the location of Figs 2–8.

the 1960s and 1970s by the former Geological Survey of Greenland (GGU, now part of GEUS). Part of this was used by the collectors in their individual research or in small groups, and for the compilation of a published geological map, However, to date only a fraction of the total dataset has been made accessible in publications, and most of the original data collected prior to 2001 are only available for further analysis if extracted from the individual geologists' field diaries and field maps. With traditional methods it would be highly impractical and tedious to obtain an overview of all the structural data collected over time from the Nagssugtoqidian orogen in West Greenland, and a rigorous conventional analysis of the complete dataset would be close to impossible. Hence, alternative methods of data compilation and analysis were required.

Since 2001 GEUS' mapping projects have included systematic collection of structural data which are available digitally. The data from all participants are recorded in field diaries and on maps, stored electronically in spreadsheets, and subsequently entered in a geographical information system (GIS) for further presentation and analysis. In this way all data from an entire group of geologists can be accessed as a whole and used for map production and data analysis.

GIS methods has already proved useful in several disciplines including mineral exploration on local to global scales (e.g. Bonham-Carter *et al.* 1990; Goodwin *et al.* 1996; Knox-Robinson & Wyborn 1997; Harris *et al.* 2001), palaeontology (e.g. Carrasco & Barnosky 2000), and environmental assessment (e.g. True *et al.* 1999; Books 2000; Wilson *et al.* 2000).

In this paper we demonstrate the application of GIS data management, visualisation and methods of analysis in a large-scale and long-term international project, including data from two previous mapping projects in the region. We present for the first time in a digital format a set of more than 10 000 structural orientation measurements and observations collected by more than 50 geologists in the Nagssugtoqidian orogen over a period of 40 years. Such a presentation can (a) provide a very helpful overview of the data itself, (b) help to identify where future research efforts may be scientifically interesting, and (c) show how these together with geological and geophysical maps can define structural domains and illustrate the large-scale structural variations through an important part of the orogen.

The Nagssugtoqidian orogen

The Nagssugtoqidian orogen in West Greenland is a Palaeoproterozoic collisional belt, dominated by Archaean gneisses that were reworked at amphibolite and granulite facies during the Palaeoproterozoic orogeny (van Gool *et al*. 2002). It forms the northern boundary of the North Atlantic craton in southern Greenland, and is bound to the north by the contemporaneous Rinkian fold belt. It consists of three tectonic segments, referred to as the southern, central and northern Nagssugtoqidian orogen (SNO, CNO and NNO; Fig. 1), which respectively consist of a southern parautochthonous foreland, a high-grade core, and a transition zone to the Rinkian fold belt. Juvenile Palaeoproterozoic magmatic arc rocks and supracrustal sequences occur mainly in narrow belts within the CNO. The Nagssugtoqidian orogen is characterised by a dominant ENE–WSW structural trend, which culminates in a number of linear belts: the Ikertôq thrust zone, the Nordre Isortoq steep belt, and the Nordre Strømfjord shear zone. These are interpreted as crustal-scale structures and alternate with areas dominated by large fold structures. Detailed investigations in the core of the orogen have shown that during the Nagssugtoqidian orogeny this region originally underwent a phase of NW-vergent thrusting, followed by folding now recognised predominantly as isoclinal folds (van Gool *et al.* 2002). A second fold phase resulted in upright, ENE-trending folds on a scale of tens of kilometres, with associated development of extension lineations plunging shallowly ENE. Finally, a phase of sinistral strike-slip shearing on the steep flanks of the large fold structures resulted in the above mentioned prominent linear belts. It is therefore only the latest deformation phases that generated the main ENE–WSW-trending tectonic fabric of the orogen (van Gool *et al*. 2002).

The area discussed in this study extends from 67°N in the Nordre Strømfjord region to 69°10′N at Jakobshavn Isfjord and covers the northern part of the CNO and most of the NNO (Fig. 1).

Structural data

Origin of the data

The structural data have been derived from two different sources. The data north of 68°N were collected during recent GEUS mapping projects (2001–2003), while the data from south of 68°N have been extracted from published GGU and GEUS maps, collected during previous GGU, DLC and GEUS projects. During the recent GEUS

mapping projects, data were collected in the northern Nagssugtoqidian orogen. Structural measurements and other geological data were noted in field diaries together with their geographical coordinates using global positioning system (GPS) receivers. These data were subsequently entered in spreadsheets and imported into ArcView®. The geographical distribution of the structural data reflects the way they were collected along shorelines and on inland traverses. There may be several measurements at any one location, whereas no data were obtained in areas between traverses (which were often located many kilometres apart). In this study, we have restricted our analysis to the structural measurements. However, a combination of these data with other information, e.g. lithological and geophysical data, would make this GIS-based analysis tool even more powerful.

The southern part of the study area, south of 68°, is covered by two 1:100 000 scale maps, which were compiled prior to the digital storage of field data. The Agto map sheet in the west (Olesen 1984) consists of analogue data (but was recently digitised), whereas the Ussuit map sheet in the east was produced in digital format (Fig. 1; van Gool & Marker 2004). The structural data from the Agto and Ussuit map sheets are stored in GEUS' Geogreen map database and were extracted from this for the present study. However, these structural data only represent a fraction of the original data collected in the field. During the map compilations, the original structural data recorded on field maps or noted field diaries were filtered such that only representative measurements were shown on the final map; each measurement typically covers an area of a few square kilometres. Thus, the southern part of the data compilation map in this paper shows an even distribution of data, and a much lower data density, compared to the more recently compiled areas in the north. The fact that the Agto map sheet only contains very few lineation measurements compared to the surrounding regions also reflects a change in focus since the 1960s and 1970s, when measurement of lineations was not considered a high priority. A large gap in the data coverage occurs in the east, from Arfersiorfik fjord to the north almost up to Sydostbugten (Fig. 1); this area was not covered by the mapping programmes by GGU and GEUS.

Definition of terms

In the descriptions below the general *orientation* of a structural element is its three-dimensional orientation with respect to true north and horizontal, as defined by the combination of strike, dip direction and dip for planar structures, and plunge direction and plunge for linear structures. the term *trend* is used as the direction along the strike of a planar structure (without indication of dip direction), or the direction of plunge of a linear structure, without distinction between plunges up or down this direction. The trend is always expressed as two opposite directions (e.g. NE–SW).

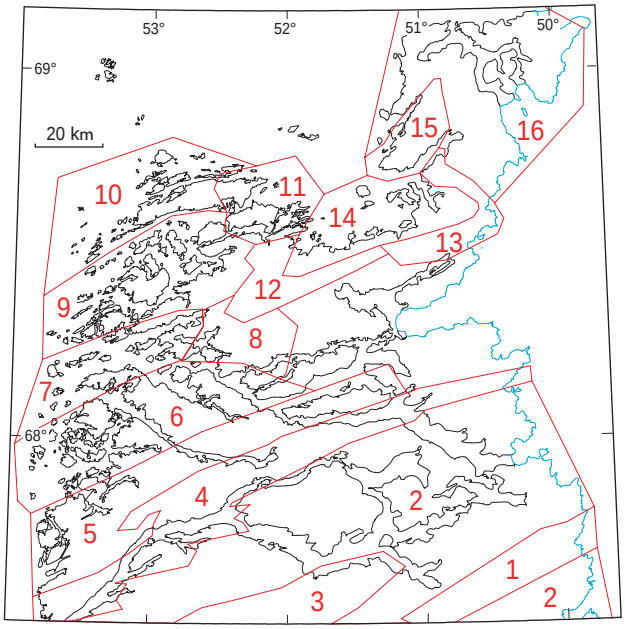

Fig. 2. Structural domains in the central and northern Nagssugtoqidian orogen, based on structural orientation data. Domain numbers refer to those used in Table 1, Fig. 8, and the main text.

Methods of data presentation

For map presentation of the data we have used ArcView® version 3.2. In addition, stereographic projections and statistical analysis for the determination of great circles and point maxima were prepared with StereoNett (J. Duyster, unpublished freeware). Once the structural dataset has been incorporated into the GIS database, the ArcView® Geoprocessing extension can be used to easily select subsets of data in areas with irregular shapes (Fig. 2), or alternatively functions like ArcView® Query Builder can be used to select data with certain characteristics.

The data were plotted on a topographic map using conventional structural symbols, whereas orientations and dip angles were colour-coded. For foliations and lineations, four maps with different colour codes were plotted (Figs 3–7). Having attempted several different ways of displaying variations of dip/plunge directions on maps, we found

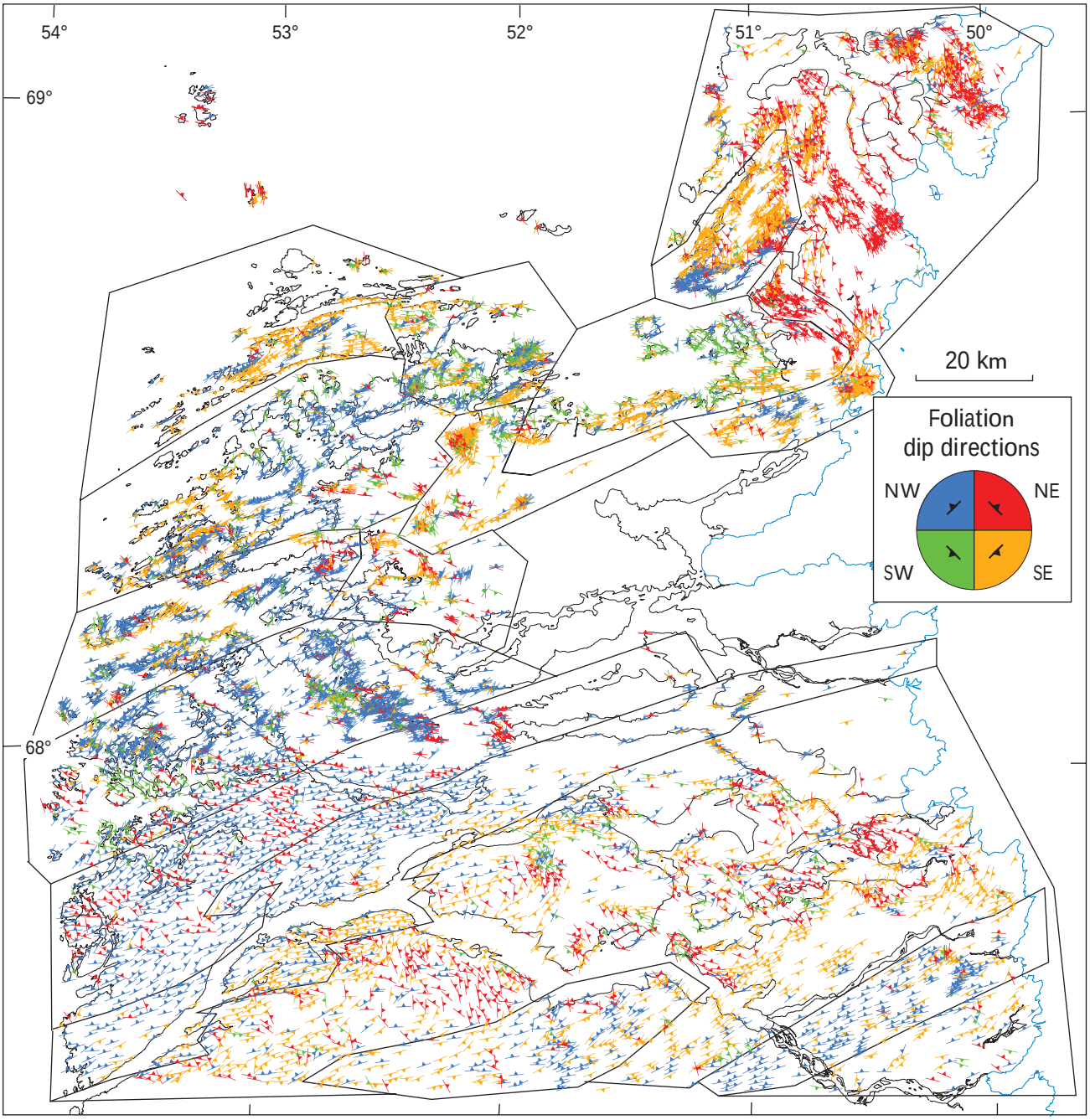

Fig. 3A. Foliation data, using four different colours to represent dip directions in the four quadrants of 0–90°, 90–180°, 180–270° and 270–360°.

that the regional trends were best shown using a subdivision into colour-coded quadrants. This gives a clear indication of variations on a regional scale and displays features that conventional plots of structural data would not have easily revealed. Other features of the data could be highlighted with other methods of coding, or by plotting them on a different scale. The GIS program allows the user to change the coding criteria and colours with a limited number of key strokes, and thus forms a powerful, user-friendly tool of analysis.

We plotted one map for each of the planar and linear datasets (Figs 3A, 5A), using differently coloured symbols for dip/plunge directions within each of four different quadrants: directions between 0–90° (NE quadrant) are shown in red, 90–180° (SE quadrant) in orange, 180–270° (SW quadrant) in green, and 270–360° (NW quad-

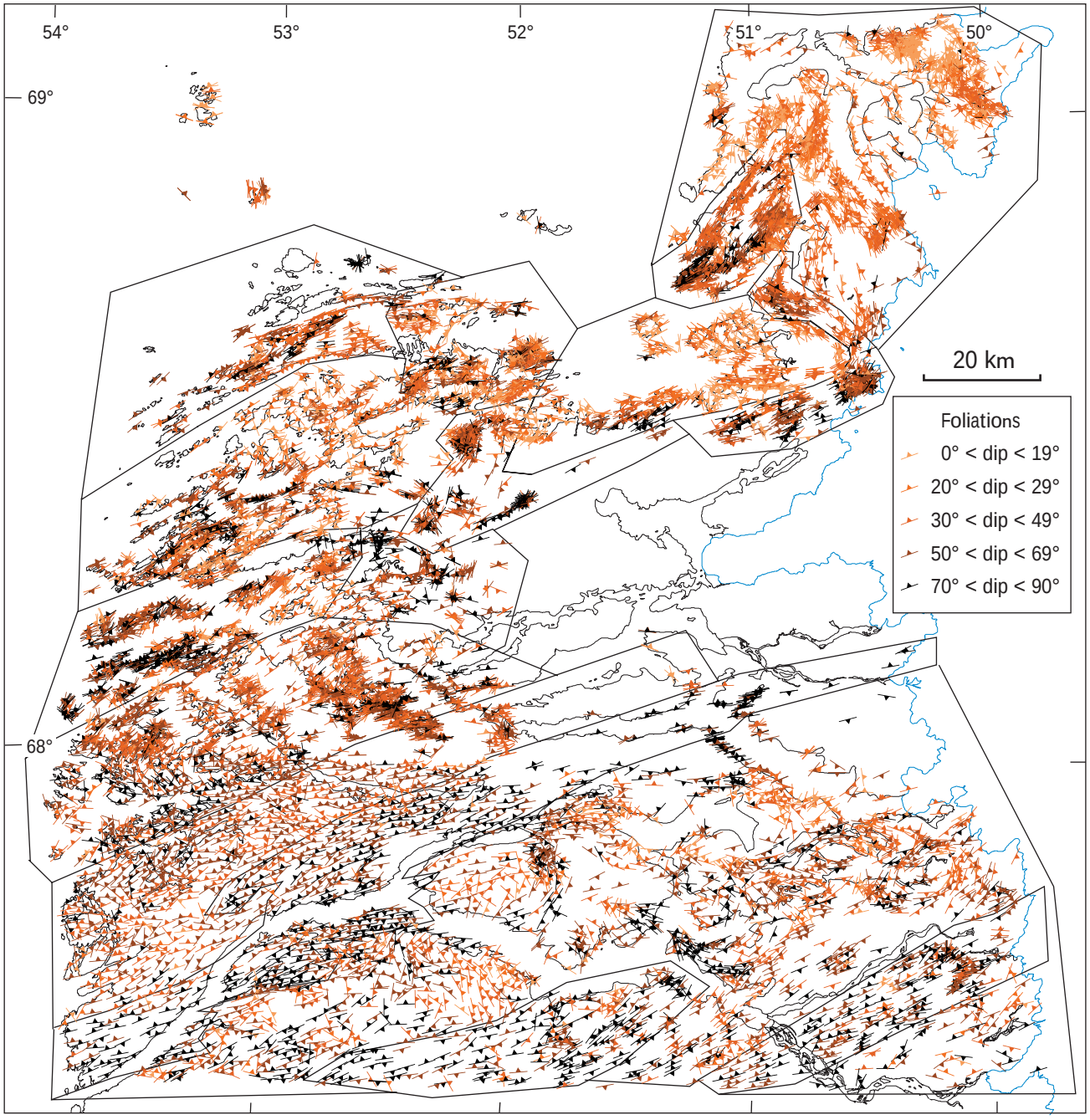

Fig. 3B. Foliation data, using colour intensity to reflect dip angle. Darker colours indicate steeper dip angles.

rant) in blue. We also plotted foliations, lineations and fold axes, respectively, in three maps where the colour intensity reflects the steepness of the dip/plunge (Figs 3B, 5B, 7). Here the light orange colour indicates shallow dips/plunges, and darker brown to black colours indicate progressively steeper dips/plunges.

The data were also plotted in a third way by combining the two just described methods. The different colours were maintained for the dip/plunge directions within each of the four quadrants, combined with colour intensity to display the variations in dip. The foliation data were split into two separate plots to show more detail and avoid clutter: Fig. 4A shows the overall ENE–WSW-trending structures (blue and orange), whereas Fig. 4B contains the overall ESE–WNW-trending structures (red and green). A similar method was used for the lineations, however, on

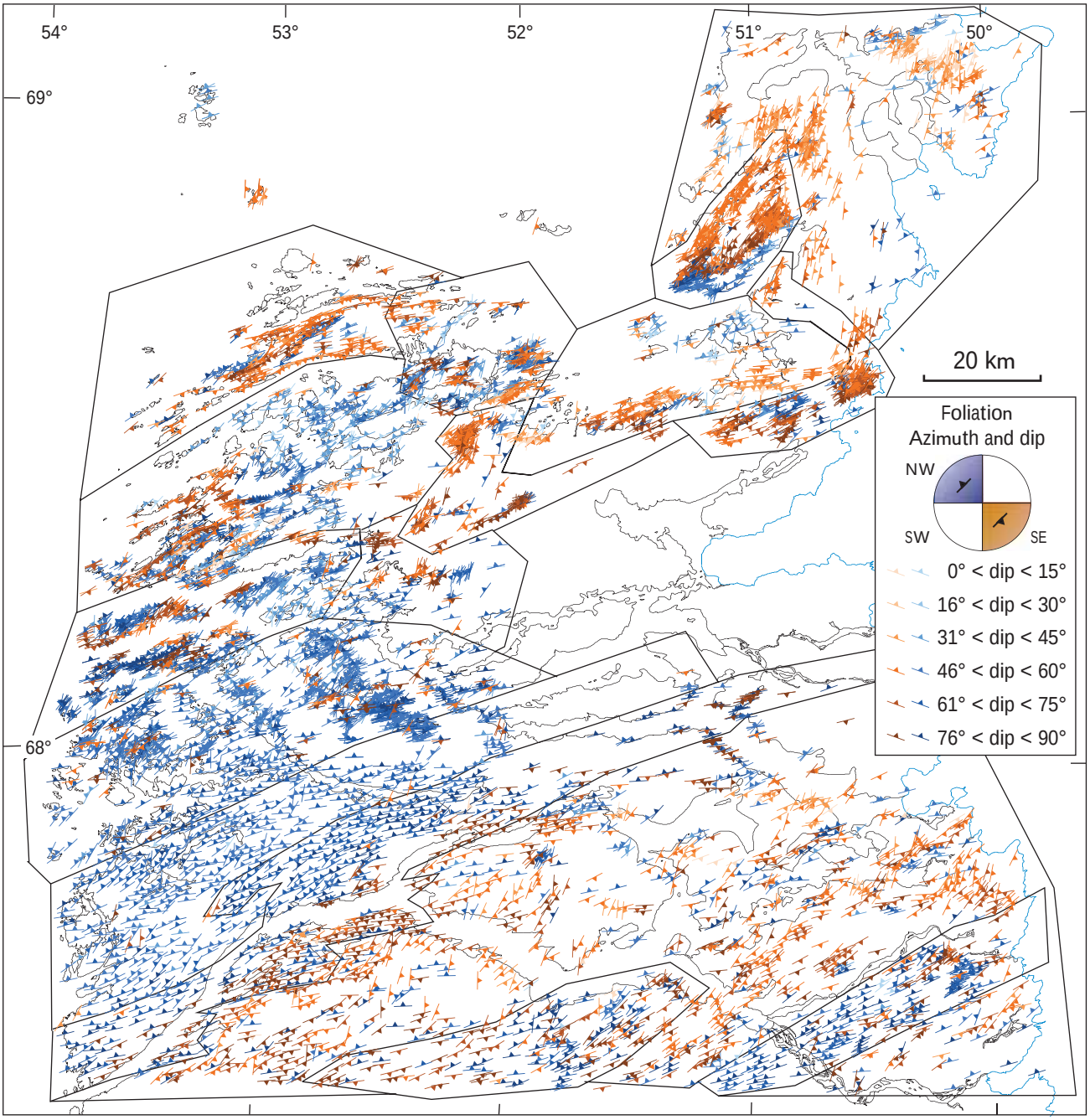

Fig. 4A. Foliation data, using blue and orange colours for NE–SW trends with NW and SE dips, respectively, combined with colour intensity to reflect dip angle. See Fig. 4B for NW–SE trends.

the scale of presentation many of the red and green lineations (ENE–WSW-trending) would overlap. Therefore, the green symbols were plotted separately (Fig. 6A), whereas the red symbols were included with the blue and orange ones (Fig. 6B); there are relatively few blue and orange symbols and therefore less cluttering.

There are significantly less measurements of fold axes than of other structural elements. Therefore we were not able to use their orientations for analysis of regional trends, and the fold axes are only colour coded for plunge angle (Fig. 7).

In some areas the very high data density causes a saturation with the colour of the main orientation on the scale of presentation. Although the main trends can still be seen, minor orientation components may be obscured. This problem can be overcome by zooming in on smaller areas

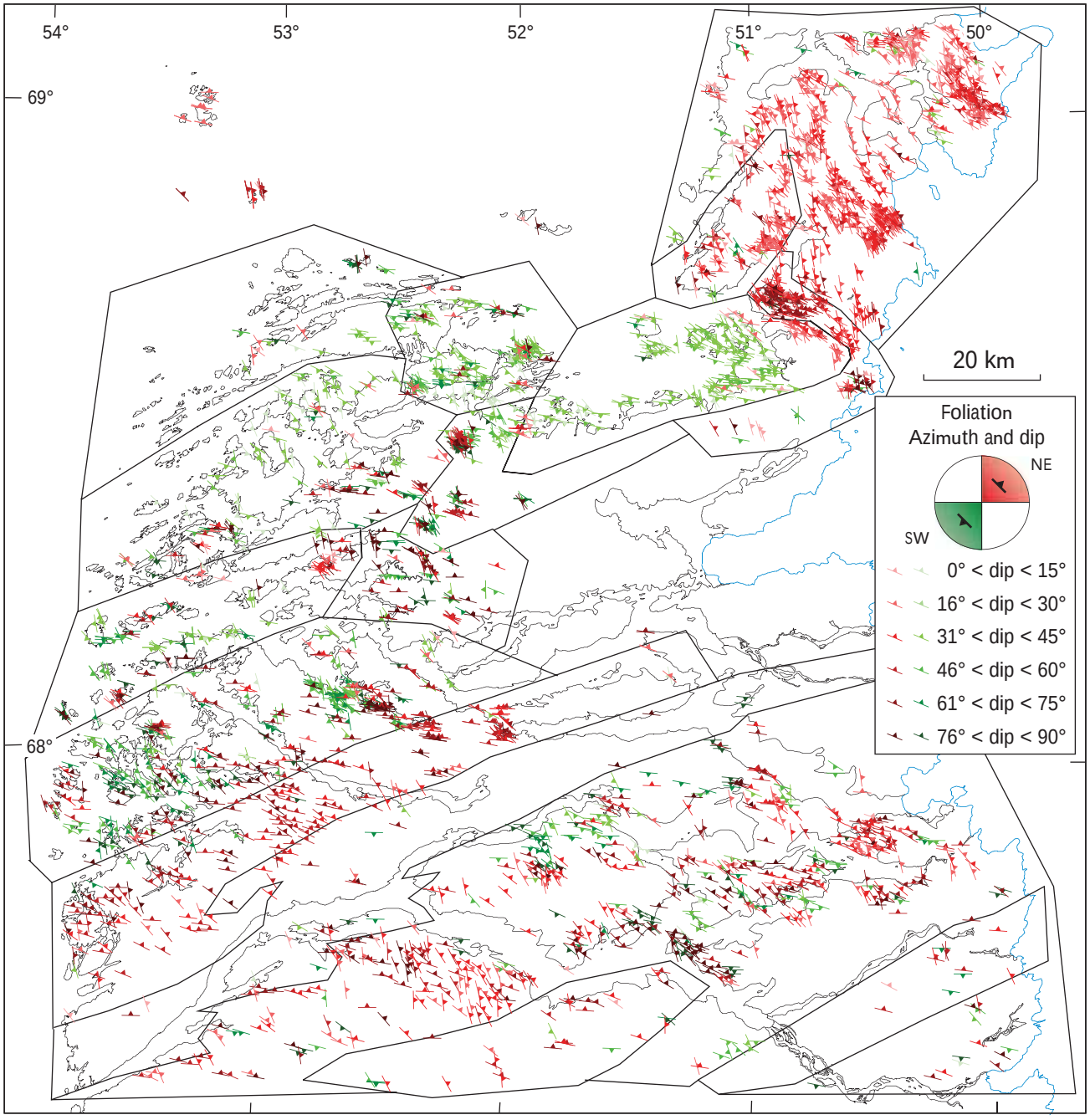

Fig. 4B. Foliation data, using red and green colours for NW–SE trends with NE and SW dips, respectively, combined with colour intensity to reflect dip angle. See Fig. 4A for NE–SW trends.

and printing on a different scale, revealing the full range of the data (e.g. Mazur *et al.* 2006, this volume).

Structural domains

Apart from the general variations in structural style, it is apparent that there are well defined areas with distinct structural patterns. We therefore divided the whole study area into 16 structural domains (Fig. 2), within each of which the structural characteristics are largely consistent and more or less distinct from those of adjacent domains. this subdivision is exclusively based on visual evaluation of the plotted data. A more rigorous approach for the definition of domains would have been possible, for example the method by Vollmer (1990) based on eigenvalue cal-

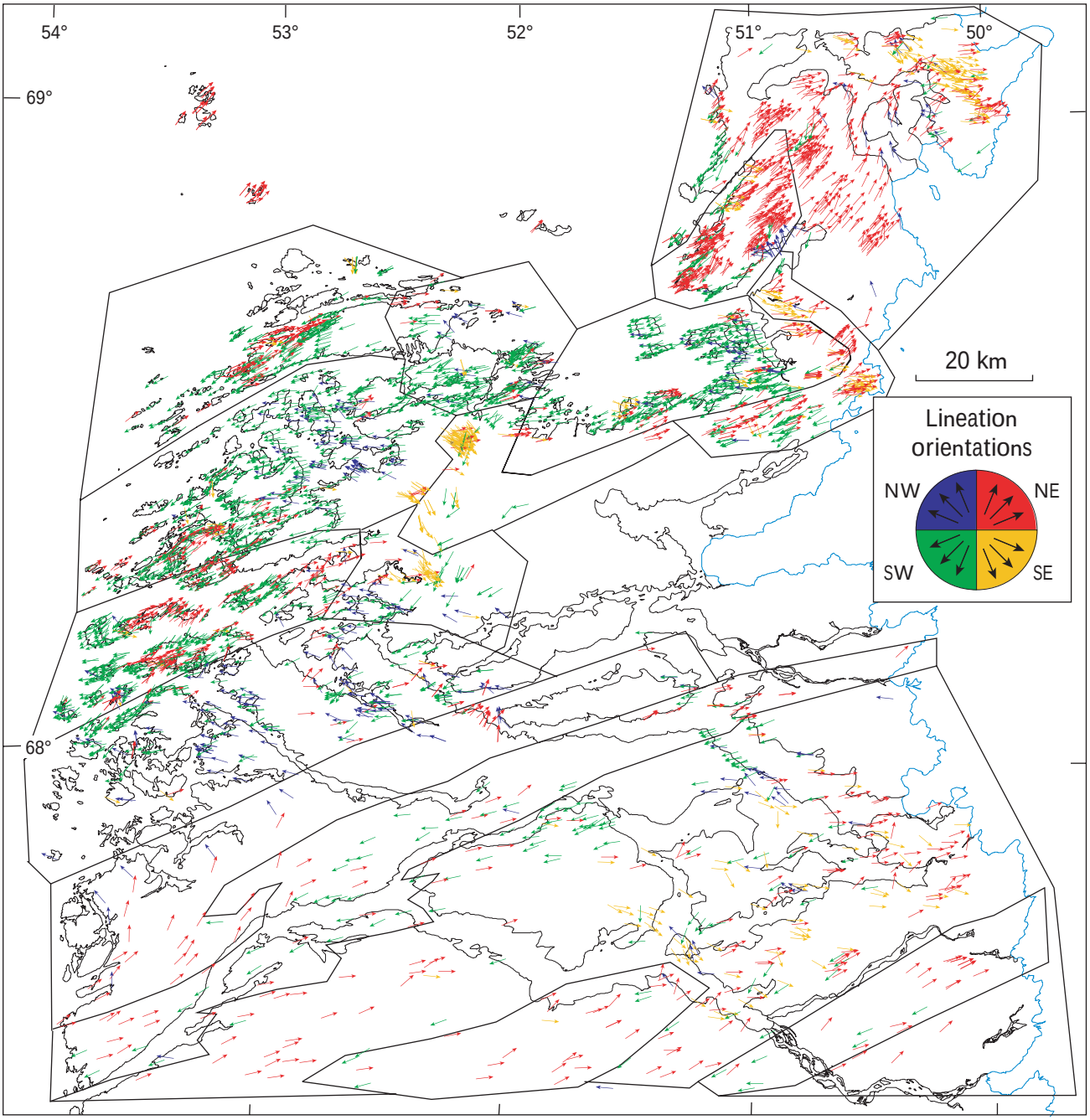

Fig. 5A. Lineation data, using four different colours to represent plunge directions in the four quadrants of 0–90°, 90–180°, 180–270° and 270–360°. See also Fig. 5B.

culations of data in small subsets, but is beyond the scope of the present study. The domains are presented schematically in Fig. 2, and their outlines are also shown in Figs 3–8. The structural data for each of the domains were extracted and plotted as equal area, lower hemisphere stereographic projections (Fig. 8). Foliations were plotted as poles to planes and contoured, and the orientation of the maximum density of data indicated in each plot. Great circles were calculated where visual inspection of the contoured data suggested that a great circle distribution exists. Calculations of great circle and fold axis orientations are based on the orientations of the three eigenvectors of the data. The large number of data in the contoured plots results in an accentuation of the high concentrations, while smaller populations that define separate structures are less visible. However, these are included in the calculations of

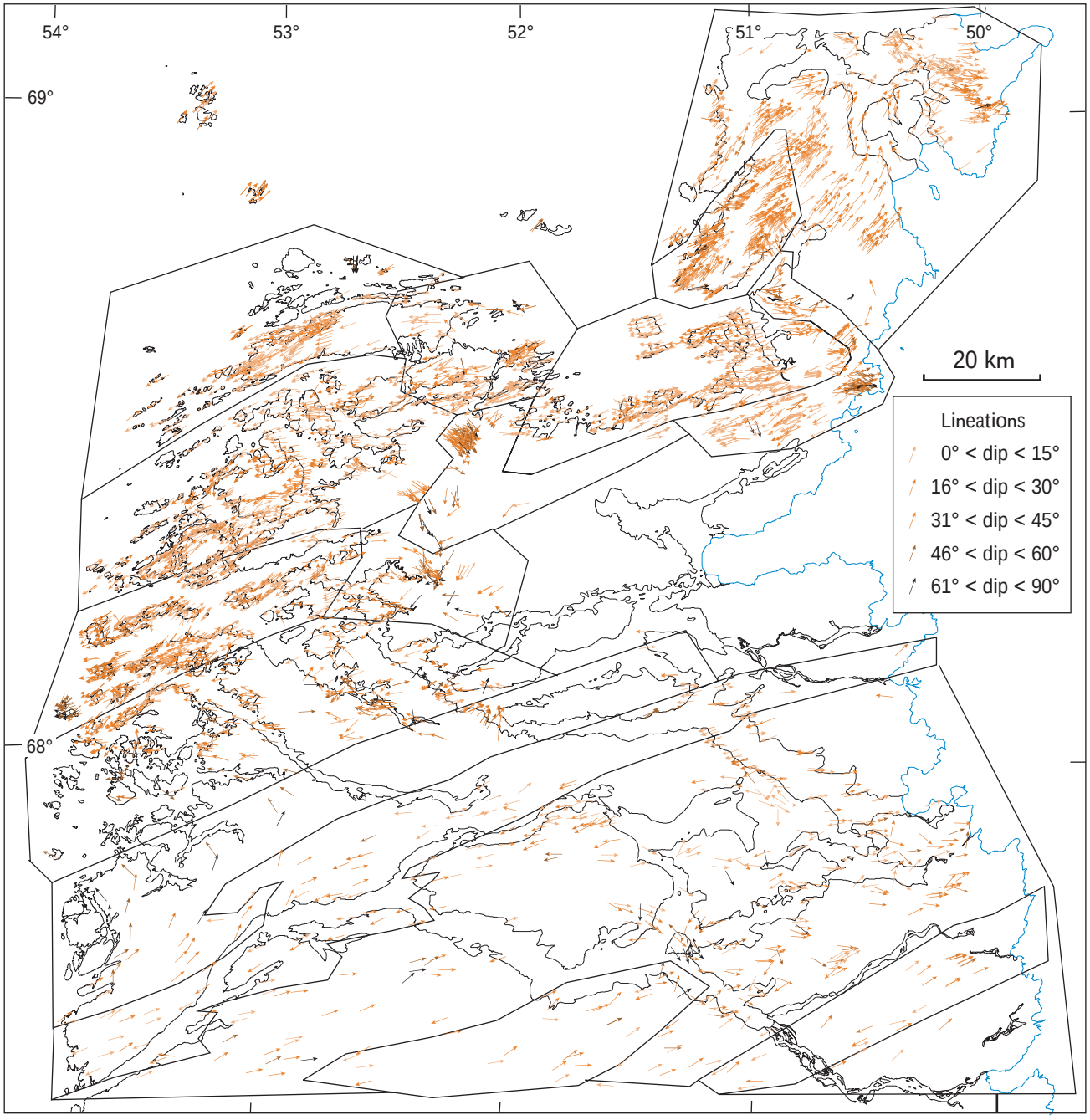

Fig. 5B. Lineation data, using colour intensity to reflect steepness of plunge. See also Fig. 5A.

the great circles and fold axes, and therefore the calculated great circle may diverge from the one defined by the maximum orientations, as in domains 7, 9 and 14 (Fig. 8). Lineations were plotted and contoured, with indication of the orientation of the maximum concentration of data (Fig. 8B). Table 1 contains short descriptions of the characteristics of each domain regarding foliation, linear data and general geology.

Results

The main variations in the structural patterns within the study area are described in the following sections, using structural maps and stereographic projections (Figs 3–8). The structural variations are apparent at a first glance as clustering of data and variations in colours; they reflect the nature of the large-scale tectonic evolution of the orogen, which is discussed in a final section.

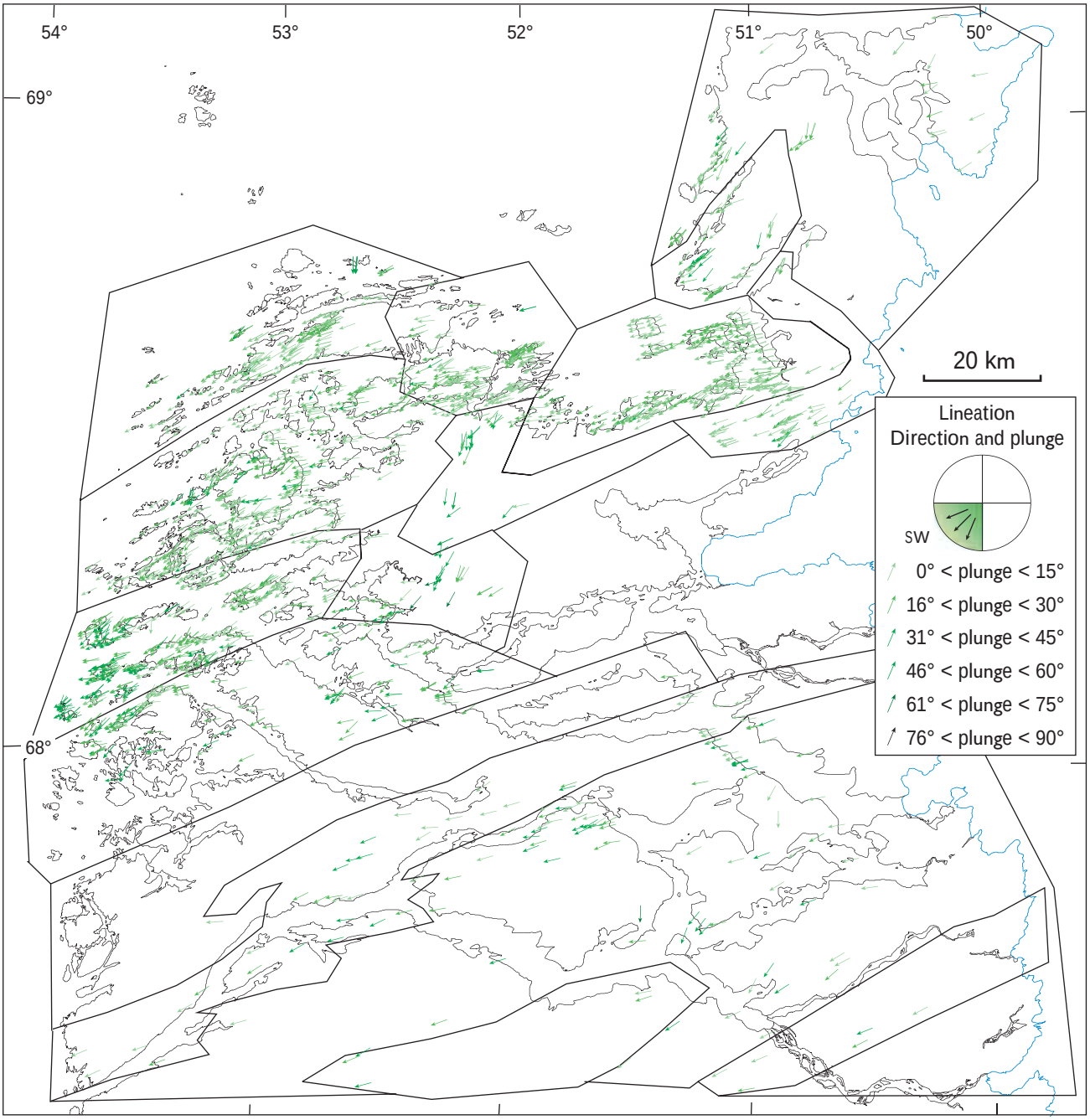

Fig. 6A. Lineation data, using green colour to represent SW directions and colour intensity to reflect steepness of plunge. See Fig. 6B for NW, NE and SE directions.

Foliations

Overviews of the orientations of the planar fabrics are shown in Figs 3, 4. The predominant foliation trend is ENE–WSW, shown in orange and blue colours. Linear belts in this direction, dominated by steeply dipping foliations, alternate with broader regions characterised by strongly variable orientations. These belts and regions with different structural characteristics have previously been referred to as steep belts and flat belts, respectively (Marker *et al.* 1995). The distinct alternation between such distinct linear belts and folded regions diminishes towards the north, and the predominant general ENE–WSW trend becomes progressively weaker, as reflected by the increase of red- and green-coloured symbols. This is apparent especially in the north-eastern corner of the study region, where the foliations are dominated by NE dip directions

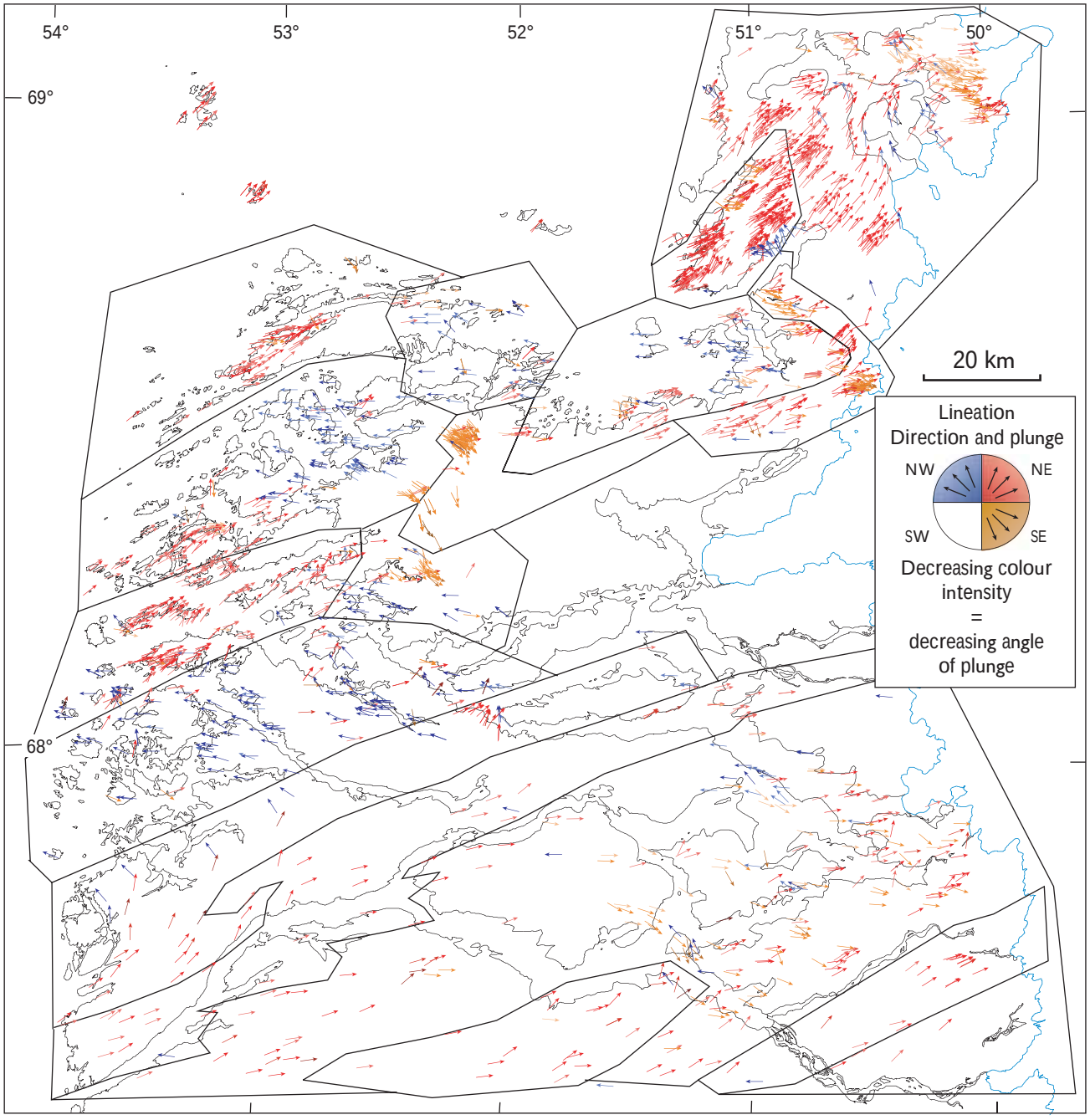

Fig. 6B. Lineation data, using blue, red and orange colours for NW, NE and SE orientations, respectively, combined with colour intensity to reflect steepness of plunge. See Fig. 6A for SW directions.

shown in red. Coupled with this progressive change towards the north there is an overall decrease in the dip angle, as expressed by an increasing amount of light orange-coloured symbols.

In the south, the two main linear belts, the Nordre Isortoq steep belt in domain 1 and the Nordre Strømfjord shear zone in domain 4, are characterised by a near-uniform ENE–WSW-trending foliation, a marked absence of NW–SE-trending foliations, and steep dip angles. A third linear belt in the north, the Naternaq belt in domains 12 and 13 and the northern part of domain 7, is discontinuous and less well defined. Smaller, discontinuous shear zones also occur in the NNO e.g. in domains 10 and 15; these are indicated by strong clustering and alignment of symbols of the same colour, but not necessarily by steep dips. Dip directions of the overall ENE–WSW-trending

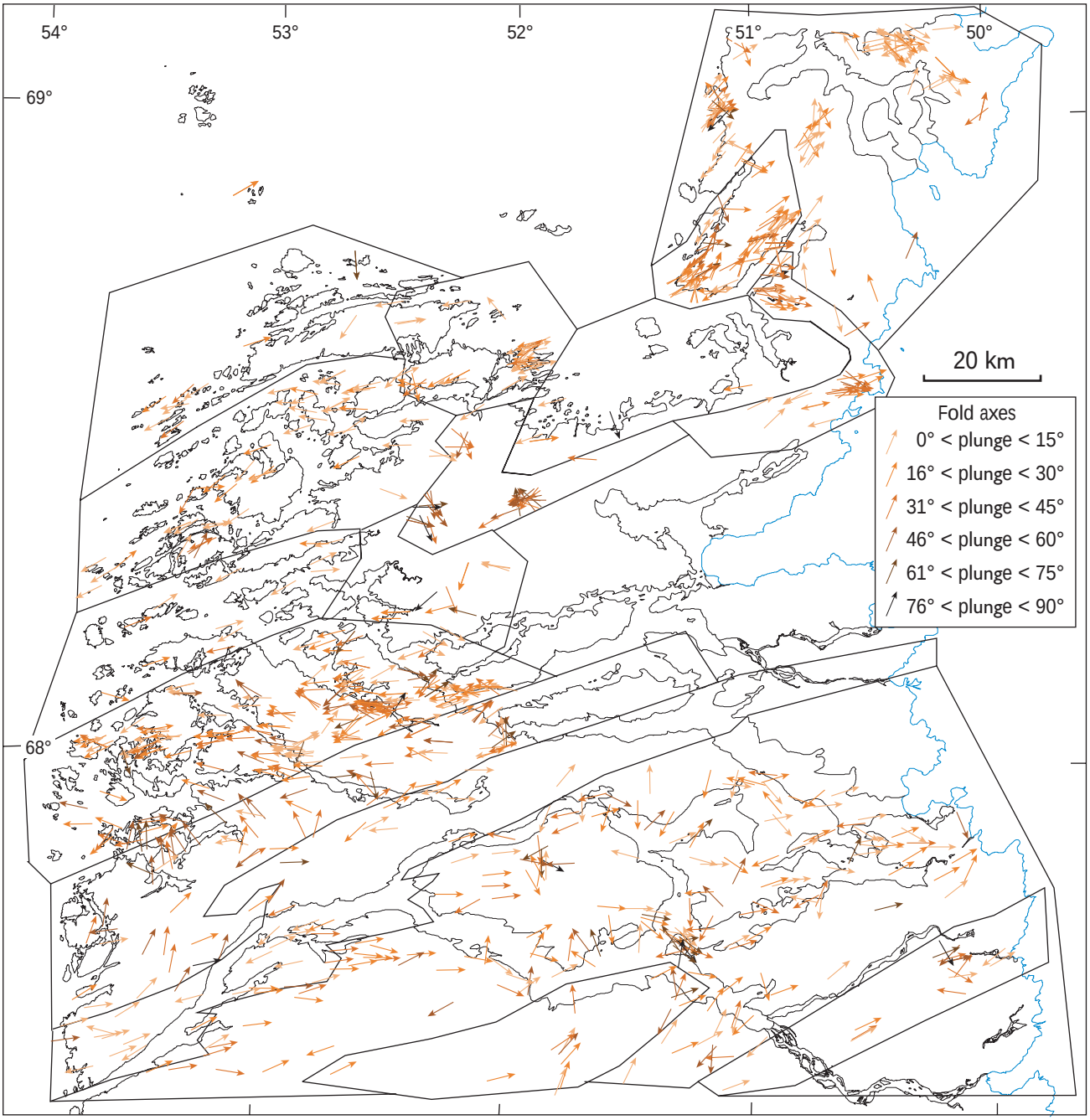

Fig. 7. Fold axis data, using colour intensity to reflect steepness of plunge.

structures (in blue and orange colours, Fig. 3A) show a clear regional pattern of alternating NW and SE dip directions. In the south, switches in dip directions are associated with the two main linear belts such that the intervening area, which forms a large anticlinorium (van Gool *et al*. 2002), is characterised by predominant SSE dips (in orange), while NNW dips (in blue) prevail to the north and south. NW–SE-trending foliations are predominant in two distinct areas in the north-east: one in the extreme north-eastern corner with predominating NE-dipping foliations (in red), and another around Sydostbugten, characterised by SW-dipping foliations (in green). Farther south only two areas of uniform dip directions are recognised, one around Attu with predominant SW dips (in green), and another forming a belt north of the Nordre Strømfjord shear zone, which has uniform NW dips (in blue).

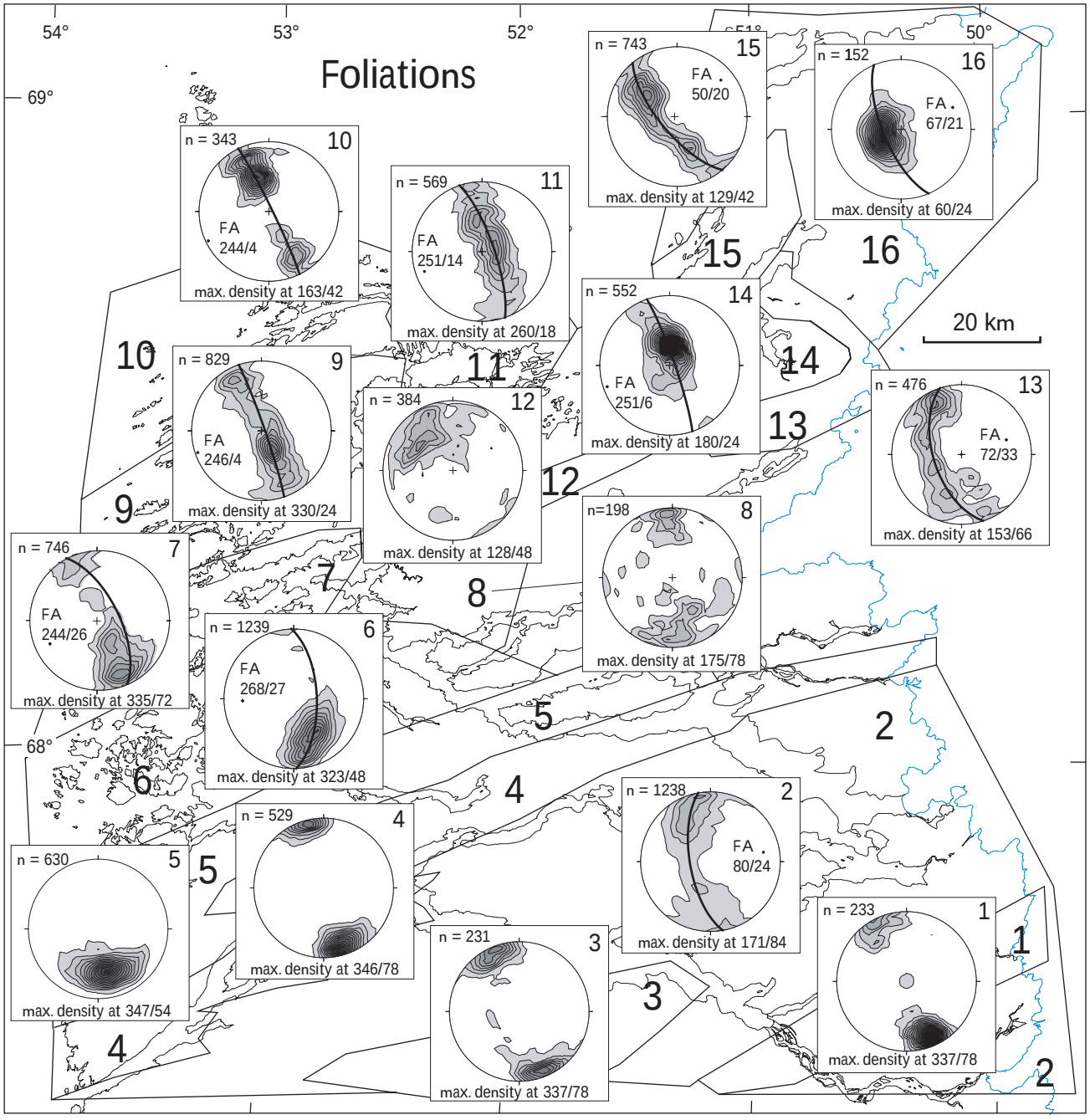

Fig. 8A. Characterisation of structural domains from Fig. 2 with stereographic projections of foliations within each domain. Poles to foliations plotted on lower hemisphere, equal angle nets and contoured at 1, 2, 3, etc. times random distribution. The number of data points (n) and orientation of maximum density are indicated for each plot. FA, calculated fold axis.

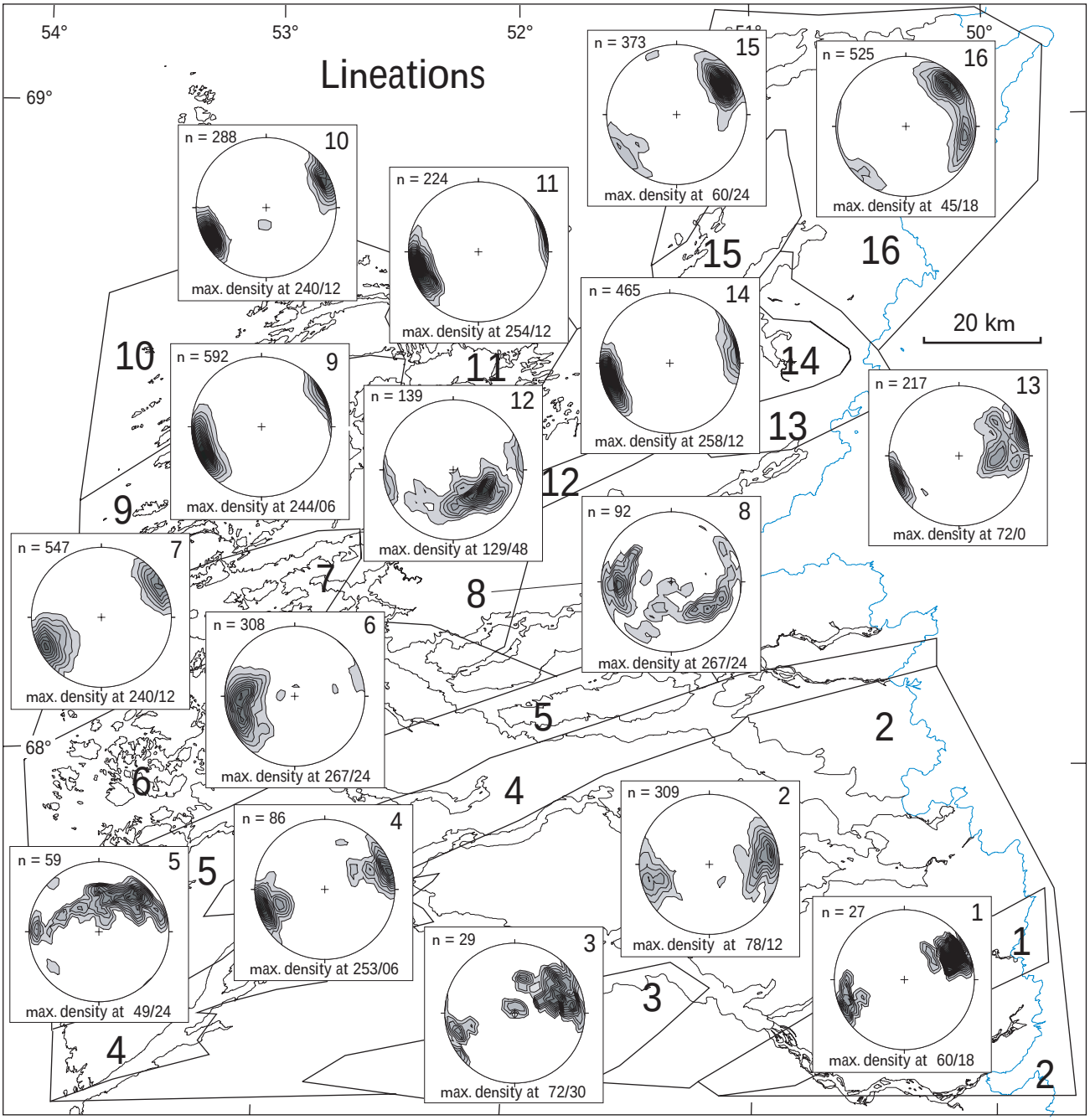

Fig. 8B. Characterisation of structural domains from Fig. 2 with stereographic projections of lineations within each domain. Data plotted on lower hemisphere, equal angle nets and contoured at 1, 2, 3, etc. times random distribution. The number of data points (n) and orientation of maximum density are indicated for each plot.

Table 1. Summary of characteristic features of the structural domains

Domain	Foliation	Lineation	Geology	Synopsis
1	Steep N-dipping foliation with consistent orientation. A sharp transition to S-dipping foliations at the northern boundary of the belt.	Consistent, predominant shallow ENE plunge.	Nordre Isortoq steep belt (shear zone), predominant sinistral shear. Mainly paragneiss.	High-strain strike-slip zone constrained by metasedimentary rocks.
2	Foliation curved along shallowly ENE-plunging folds on a scale of tens of kilometres. Dips variable, SE dips predominating over NE and less common SW dips.	Variable lineations, with predominant shallow ENE plunges, parallel with fold axes. Shallow, SE-plunging lineations in a c. 10 km wide zone south of the NSSZ.	Northern CNO flat belt of interleaved Archaean orthogneisses and Proterozoic ortho- and paragneisses.	Anticlinorium between two shear zones. Lineation constant in spite of intense folding. Only one zone where lineations plunge SE, locally steeply.
3	Steep foliation. Both northerly and southerly dips. Few folds on scales of 0.5–1 km.	Lineations mainly shallowly ENE-plunging. Some variation in fold hinges, especially near the eastern domain boundary.	Steep belt within the northern CNO flat belt; tightly interleaved ortho- and paragneisses.	Steep zone with tight folds within the larger domain 2 with large fold structures. Steep zone discontinuous to the east, and concentrated in an area dominated by two metasedimentary belts.
4	Steep foliations with consistent orientations, slightly oblique to the trend of the linear belt. Northerly dips predominate. Near the southern boundary a sharp transition to SSE-dipping foliations.	Subhorizontal lineations, the majority WSW-plunging in contrast with surrounding areas.	NSSZ. Interleaved ortho- and paragneisses.	Sinistral strike slip zone5 km wide. Obliquity of foliation fits with sinistral shear.
5	Gradual northward transition from steep dips close to the NSSZ to shallower NNW dips. The foliation locally curves into the shear zone. NE dips are mixed with the dominant NNW dips in most of the area. The plentiful data points on the stereonet (Fig. 8A)obscure orientations (mainly NE-dipping) away from the maximum.	Progressive change from shallow ENE plunges near the NSSZ towards steep NE and N plunges in the north-west.	Archaean orthogneisses and horizons of supracrustal amphibolite.	Region with shallow, N-dipping structures.
6	Intensely folded region with 5–10 km large folds, mainly W-plunging. Northerly and westerly dips predominate in contrast to domain 5.	Mixed orientations with a cluster of shallowly SE-plunging lineations. In the west progressive change in orientation continues from domain 5. More variable orientations in the east.	Archaean indentor, ortho- and paragneiss as in domain 5. Large fold structures.	Overall W- and WSW-plunging folds. Two sets of lineations, one variable, the other consistently WSW-plunging, parallel with fold axis.
7	Variable strike. NNW dips less predominant than in domain 5. Folding. Dips mainly moderate, but steep in the south-west. Fig. 8A displays a girdle over shallow, WSW-plunging fold structures. A calculated great circle is discordant to the measured maxima, which align on a steeper great circle.	Rather consistent ENE-trending lineations. ENE plunges in the east become shallower and mixed with WSW-plunging domains in the west, followed by moderate to steep WSW plunges at the coast. Locally steep lineations in fold cores.	Archaean orthogneisses and metasedimentary rocks define a poorly sampled linear zone at the northern boundary of the indentor block of Piazolo *et al.* (2004). A few kilometre-sized fold structures.	Predominantly straight and steep foliations with ENE trends, but variable dip directions, and consistently shallow lineations. Misalignment of foliation girdle and calculated great circle (Fig. 8A) indicates complex fold pattern: along-strike variation of lineations (and presumably fold axes) and local folds with steep axes disturb the stereographic plot. Non-consistent dip directions and dips in the northern linear zone suggest intense folding.
8	Foliations outline the large fold structure visible on Fig. 1. Southerly dips predominate in the northern part (green and orange/brown, Fig. 3A). A zone with NW dips (blue) runs through the domain centre. Mixed dip directions in the south. Dips moderate to steep. Irregular stereonet pattern (Fig. 8A), with remnants of a great circle distribution similar to that in domains 6 and 7.	Steep SW- and SE-plunging lineations around a large central fold core. Mainly E–W-trending lineations in the west in transition to domain 7. Variable lineations in the east. Two maxima of shallow W plunges and steeper SE plunges (Fig. 8B), the latter possibly with a small circle distribution.	Orthogneisses interleaved with supracrustal amphibolite. A fold interference pattern occurs south of the main fold at the western end of the Naternaq belt.	Mixed structural patterns including ENE-trending fold limbs and fold interference patterns. The core of the large fold with the steep lineations is located along the southern extension of a NNE-trending belt of steep lineations on the western limb of the Naternaq supracrustal belt.

CNO: Central Nagssugtoqidian orogen. NNO: Northern Nagssugtoqidian orogen. NSSZ: Nordre Strømfjord shear zone.

Table 1 *(continued)*

Domain	Foliation	Lineation	Geology	Synopsis
9	Consistent ENE trend with both NNW and SSE dip directions. Large fold structures in the east. Steep dips, shallower towards north. Great circle distribution with shallowly NNW-dipping and subordinate steep, SSW-dipping flanks tentatively interpreted as due to asymmetric S-vergent folds (Fig. 8A).	Predominant subhorizontal ENE–WSW-trending lineations, gradually changing to E–W in the east, where large-scale folds occur. Very strong preferred ENE–WSW subhorizontal orientation, with a tail towards E–W trends displayed on Fig. 8B.	Region around Kangaatsiaq with metasedimentary rocks, amphibolite and granite within the regional grey gneiss.	Transition from predominant steep, northerly dips in the CNO to shallower, variable dips and large fold structures in the north. From east to west a large swing from ENE–SSW to E–W trends. Lineations uniform also in the area of large folds.
10	Mainly steep S dips with consistent trend. As in domain 9, ENE-WSW-trending foliation in the west swings towards E–W in the east. At the southern boundary a linear belt with moderate S dip. Partial great circle distribution; no dip directions within the NE quadrant (Fig. 8A).	Consistent ENE–WSW-trending subhorizontal lineations, with indistinct domains of respectively easterly and westerly plunges. Strong point maximum on stereonet with shallow WSW plunges (Fig. 8B).	Straight zone of predominant orthogneisses around Aasiaat, bounded to the south by a high-strain zone.	Very consistent foliation trends, the northernmost widespread steeply dipping foliations, and very persistent lineations.
11	Foliations outline a W-plunging antiform *c.* 10 km large. The northern part of its northern limb appears overturned towards N. Great circle distribution with predominant shallow to moderate dips on stereonet (Fig. 8A).	Shallow plunges of lineations, mainly towards W. Subordinate NW plunges on northern fold limb. Fig. 8B shows strong point maximum parallel with calculated fold axis.	Ikamiut supracrustal rocks. Large antiform with 1 km-scale parasitic folds on its southern limb. Northern limb poorly exposed and undersampled.	Data consistent with a shallowly W-plunging antiform becoming progressively tighter westward (but not easily traced into domain 10).
12	Foliations outline a fold with a folded, overall moderately SE-dipping western main limb. The high-strain southern limb dips steeply S. Large spread on stereonet (Fig. 8A).	Moderately SE-plunging lineations on the western limb, with isolated SSW plunges in hinge zone. Very few measurements on the southern limb, with shallow WSW plunges.	Western Naternaq belt. Steep paragneisses folded on 20 km-scale. Mainly data from isoclinal fold on western limb; less from straight southern limb.	Western limb of Naternaq supracrustal belt, forming a distinct zone, apparently transecting the overall ENE-trending fabric, and with uncommon SE-plunging lineations and fold axes.
13	Eastern continuation of steep, high-strain southern limb of fold from domain 12 and large E-plunging antiform. NW dips more common in the north, dips shallower near hinge. The northern limb has moderate to steep NE dip. Fig. 8A shows a well-defined great circle and NE-plunging calculated fold axis.	Lineations shallow and ENE- or WSW-plunging on the southern limb. Variable plunges on the eastern limb between NE and ESE. The latter orientation most common in hinge areas. Fig. 8B clearly shows these three separate populations.	Steeply dipping, straight gneisses in eastern Naternaq belt. A large E-plunging antiform at the eastern end, and a north-eastern fold limb with only minor metasedimentary rocks.	Consistent lineation trend in antiform, but opposite plunge directions on the limbs. Steeper lineations in the fold hinge.
14	Irregular foliation in the core of the eastern Naternaq fold, forming an E–W-trending whaleback structure. Fig. 8A shows a point maximum and partial girdle which do not fit the calculated great circle (see the main text).	Predominant subhorizontal WSW plunges, except ENE plunges at the eastern domain margin along the eastern limb of the map-scale fold. Fig. 8B shows a single strong point maximum.	Predominantly orthogneiss, cut by flat-lying shear zones.	Very consistent lineation trends, also through the antiform in the east. Direction of plunge flips over in the east, perhaps indicating two generations of lineations.
15	Foliations define a large, open NE-trending synform with steepest orientations in the core, bounded by straight belts. An antiform occurs in the south-east, with its southern limb in domain 13. A well-defined great circle on Fig. 8A indicates cylindrical, NE-plunging folds.	Strong predominance of ENE-plunging lineations along the synform axis. Consistent SE plunges south-east of the shear zone. Consistent moderate NW plunge in the antiform near head of fjord. Fig. 8B shows a fairly well defined point maximum close to the calculated fold axis.	Synform with strongly migmatitic paragneiss and a core of migmatitic orthogneiss. High-strain zones to the north-west and south-east.	The south-eastern limb of the synform, overturned to the north-west and becoming very tight towards north-east. Distinctly different lineations in the underlying, folded shear zone.
16	The foliation defines large, open, NE-plunging folds besides a large antiform surrounding the synform of domain 15. The stereonet data (Fig. 8A) display a point maximum with a partial great circle distribution.	Predominant shallow, NE-plunging lineations and a small population of slightly steeper, E-plunging lineations in the north-eastern domain corner. The lineations swing, following the folds.	Archaean orthogneiss with thin sheets of pelitic rocks and supracrustal amphibolite. Also areas of very weakly foliated porphyritic granodiorite.	The NE-dipping orientations and open folds are significantly different from elsewhere in NNO. The shear zone exposed on either side of the synform in domain 15 does not continue in domain 16.

The stereographic projections of the foliations clearly reflect two trends (Fig. 8A). The plots from the southern part of the study area define alternating point maxima and great circle distributions, reflecting, respectively, the linear belts and the fold-dominated regions. In contrast, in most of the NNO the plots mainly display (partial) great circle distributions or otherwise irregular patterns, indicating the lack of extensive linear belts in the north. Furthermore, the stereographic projections reflect the northward decrease in dip angle: in the CNO the point maxima indicate dip angles around 80°, whereas the NNO is characterised by point maxima indicating dip angles in the range 20–40°.

Lineations

Overviews of the linear fabrics are shown in Figs 5, 6. The highly uneven data density in the lineation maps (Fig. 5A, B) reflects that the southern and northern parts of these maps have been compiled from different sources, i.e. published maps in the south and complete field datasets in the north. Nevertheless, it is apparent that the dominant trend is ENE–WSW, as indicated by the predominant red and green colours (Fig. 5). Outside the linear belts, gradual changes in the lineation trends on a scale of 10–50 km or more are seen, for example between Attu and Nordre Strømfjord, at western Ussuit, and in the north-east of the study area. Several smaller areas are dominated by E–W trends, for example east of Attu, south-east of Sydostbugten, and south of Jakobshavn Isfjord.

Most lineations plunge 0–30°, with markedly steeper plunges in regions of map-scale fold interference structures and fold hinges. This is prominent west of Ataneq, north-west of Attu, and in the eastern part of domain 13. These regions are also characterised by orientations that diverge from the general ENE–WSW trend.

The structural maps (Fig. 6) stereographic projections (Fig. 8B) clearly show that WSW-plunging lineations predominate in most of the NNO (north of the Nordre Strømfjord shear zone) except for small clusters of NE-plunging lineations and the area east and north-east of Sydostbugten, where the plunge is towards ENE (domains 13, 15 and 16); there is a sharp break between these two plunge directions east of Sydostbugten. The same pattern is shown by the fold axes calculated from the great circle girdles of the foliations (Fig. 8A). South of the Nordre Strømfjord shear zone (in the CNO), the point maxima of the lineations and calculated fold axes consistently indicate shallow ENE plunges.

Fold axes

Orientations of fold axes are shown on Fig. 7. The symbols are colour-coded for plunge angle in order to facilitate comparison with the lineation data. The orientations of the fold axes mimic the general characteristics of the lineations, being generally subparallel with the latter. Their distribution in clusters reflects a higher density of measurements in areas of map-scale fold hinges, where outcrop-scale folds are more common.

Tectonic implications

The structural data presented in this paper show that the tectonic style changes significantly across the central and northern parts of the Nagssugtoqidian orogen. While the CNO is dominated by steep, linear and continuous belts separated by well-defined areas of large-scale folding, the NNO does not contain such continuous, linear belts, whereas 20–80 km-scale folds are abundant. The main change in tectonic style occurs across the Nordre Strømfjord shear zone. More specifically, the southern part of the study area (the CNO and the Nordre Strømfjord shear zone) is dominated by alternating linear belts and folded regions. The corresponding structural domains follow the main strike of the linear belts and are continuous from the coast to the Inland Ice. The linear belts themselves are dominated by sinistral strike-slip deformation. In contrast, the domains in the NNO are generally less elongate and reflect the lack of linear belts of similar dimensions as in the CNO. Small high-strain zones are observed locally, e.g. along the northern and southern margins of domain 15 and with several examples in domains 7, 9 and 10. Shear sense indicators are rare and inconsistent in the NNO, and the overall deformation in this region seems to be predominantly coaxial (Piazolo *et al.* 2004; Mazur *et al*. 2006, this volume). The change in tectonic style is interpreted to be a result of (a) differences in localisation of strain as high-strain, steep belts, (b) different deformation kinematics (strike-slip wrench tectonics in the south, coaxial deformation in the north), and (c) variations in the intensity of deformation. We consider that the overall Palaeoproterozoic strain is significantly lower in the NNO than in the CNO. The NNO commonly preserves shallow dips, which presumably predominated after the original phase of thrusting. Besides, the two latest deformation phases, which are responsible for the steep foliation in the CNO, are less intense in the NNO (van Gool *et al.* 2002; Piazolo *et al.* 2004; Mazur *et al.* 2006, this volume). These observations may account for the previously

outlined differences in the mode of strain localisation. The data presented here furthermore show that the change in style is rather abrupt across the Nordre Strømfjord shear zone, and thus support the interpretation by Sørensen (1983) and Sørensen *et al.* (2006, this volume) that this structure is of crustal scale and has a significant offset – a notion that has previously been questioned by Hanmer *et al.* (1997).

It is well established in the literature that the structural pattern of the CNO is fully attributed to Nagssugtoqidian deformation (van Gool *et al*. 2002). In contrast, the NNO is currently interpreted as having only in part been affected by Palaeoproterozoic deformation, and the Nagssugtoqidian strain is furthermore partitioned into smaller regions (Piazolo *et al*. 2004; Mazur *et al*. 2006, this volume). A significant part of the deformation in the NNO thus seems to be of Archaean age, and its overall structural style defined by interference between Archaean and Palaeoproterozoic structures. Therefore, like Mazur *et al.* (2006, this volume) we suggest that the change in tectonic style from south to north reflects partitioning of Nagssugtoqidian strain. This is clearly illustrated by the smaller and less elongate structural domains in the NNO, and by the significant change of the general trend of both foliations and lineations towards the north-eastern corner of the study area, where we consider that the influence of the Palaeoproterozoic deformation diminishes rapidly. This interpretation is supported by the relatively low metamorphic temperatures recorded by Hollis *et al.* (2006, this volume) in some parts of the NNO.

It is beyond the scope of this contribution to explore the details of the structural domains that we have outlined. However, three other contributions in the present volume of Geological Survey of Denmark and Greenland Bulletin deal with the specific nature of some of these domains. Sørensen *et al*. (2006, this volume) investigate the character of the Nordre Strømfjord shear zone and adjacent areas in domains 4 and 5, Mazur *et al*. (2006, this volume) focus on the partioning of structures within domains 6, 7 and 8, and Hollis *et al*. (2006, this volume) describe structures within domains 11 and 15.

Conclusions

The application of a GIS computer program enables us to visualise large amounts of structural data in a variety of ways. Thus, we can rapidly obtain an overview of large datasets that are otherwise difficult to manage, and delineate areas with consistent tectonic trends. Although the methods applied here de not reveal features that are not present in the original geological maps, they can substantially facilitate the detection and description of structural trends and variations. In addition, stereographic plots of each of the domains can quickly be produced and analysed. In the present case, the methods greatly helped to subdivide the central and northern Nagssugtoqidian orogen into distinct structural domains with specific individual characters.

The investigation of the large-scale structural trends in the central and northern Nagssugtoqidian orogen revealed distinct changes in the tectonic style from south to north. In the core of the orogen, the ENE-striking Nordre Strømfjord shear zone from the coast to the Inland Ice forms the most prominent feature. The tectonic character of the orogen changes across this structure from predominantly ENE-tending, steep fabrics in the south to large fold patterns and generally flat structures in the north, with a marked decrease in the main dip angle from *c*. 80° south of the shear zone, to *c*. 20–40° in the north. In addition, a significant decrease in the intensity of deformation is apparent, coupled with a decreasing proportion of the strain localised in linear belts. We interpret these patterns as reflecting a general northward decrease in the Palaeoproterozoic tectonic overprint on Archaean structures, as well as strain partitioning in smaller regions. Hence, some of the structural domains in the NNO are largely unaffected by pervasive Palaeoproterozoic deformation.

Acknowledgements

Reviews by John Grocott and Ken McCaffrey are gratefully acknowledged.

References

Bonham-Carter, G.F., Agterberg, F.P. & Wright. D.F. 1990: Weights of evidence modelling: a new approach to mapping mineral potential. Geological Survey of Canada Paper 89, 171–183.

Books, C.J. 2000: Defining groundwater system recharge and vulnerability areas in regions of suburban expansion; overview of the northern Illinois example. Abstracts with Programs – Geological Society of America 33, 45 only.

Carrasco, M.A. & Barnosky, A.D. 2000: MIOMAP: a GIS-linked database to assess the effects of tectonic and climatic changes on mammalian evolution. Abstracts with Programs – Geological Society of America 32, 15 only.

Connelly, J.N., van Gool, J.A.M. & Mengel F.C. 2000. Temporal evolution of a deeply eroded orogen: the Nagssugtoqidian orogen, West Greenland. Canadian Journal of Earth Sciences 37, 1121–1142.

Goodwin, P.B, Choiniere, M.E., Harris, F.W. & Dean, B.P. 1996: Im-

proving exploration with geographical information system (GIS) technology. American Association of Petroleum Geologists Bulletin 80, 1297.

Hanmer, S., Mengel, F., Connelly, J. & van Gool, J.[A.M.] 1997: Significance of crustal-scale shear zones and syn-kinematic mafic dykes in the Nagssugtoqidian orogen, SW Greenland: a re-examination. Journal of Structural Geology 19, 59–75.

Harris, J.R., Wilkinson, K., Heather, K., Fumerton, S., Bernier, M.A., Ayer, J. & Dahn, R. 2001: Application of GIS processing techniques for producing mineral prospectivity maps – A case study: mesothermal Au in the Swayze Greenstone Belt, Ontario, Canada. Natural Resources Research 10, 91–124.

Hollis, J.A., Keiding, M., Stensgaard, B.M., van Gool, J.A.M. & Garde, A.A. 2006: Evolution of Neoarchaean supracrustal belts at the northern margin of the North Atlantic Craton, West Greenland. In: Garde, A.A. & Kalsbeek, F. (eds): Precambrian crustal evolution and Cretaceous–Palaeogene faulting in West Greenland. Geological Survey of Denmark and Greenland Bulletin 11, 9–31 (this volume).

Kalsbeek, F. & Nutman, A.P. 1996: Anatomy of the Early Proterozoic Nagssugtoqidian orogen, West Greenland, explored by reconnaissance SHRIMP U-Pb dating. Geology 24, 515–518.

Knox-Robinson, C.M. & Weyborn, L.A.I. 1997: Towards a holistic exploration strategy: using geographic information systems (GIS) as a tool to enhance exploration. Australian Journal of Earth Sciences 44, 453–463.

Manatschal, G., Ulfbeck, D. & van Gool, J.[A.M.] 1998. Change from thrusting to syncollisional extension at a mid-crustal level: an example from the Palaeoproterozoic Nagssugtoqidian orogen (West Greenland). Canadian Journal of Earth Sciences 35, 802–819.

Marker, M., Mengel, F., van Gool, J. & field party 1995: Evolution of the Palaeoproterozoic Nagssugtoqidian orogen: DLC investigations in West Greenland. Rapport Grønlands Geologiske Undersøgelse 165, 100–105.

Mazur, S., Piazolo, S. & Alsop, G.I. 2006: Structural analysis of the northern Nagssugtoqidian orogen, West Greenland: an example of complex tectonic patterns in reworked high-grade metamorphic terrains. In: Garde, A.A. & Kalsbeek, F. (eds): Precambrian crustal evolution and Cretaceous–Palaeogene faulting in West Greenland. Geological Survey of Denmark and Greenland Bulletin 11, 163–178 (this volume).

Olesen, N.Ø. 1984: Geological map of Greenland, 1:100 000, Agto 67 V.1 Nord. Copenhagen: Geological Survey of Greenland.

Piazolo, S., Alsop, G.I., van Gool, J.A.M. & Nielsen, B.M. 2004: Using GIS to unravel high strain patterns in high grade terranes: a case study of indentor tectonics from West Greenland In: Alsop, G.I. *et al.* (eds.): Flow processes in faults and shear zones. Geological Society Special Publication (London) 224, 63–78.

Sørensen, K. 1983: Growth and dynamics of the Nordre Strømfjord Shear Zone. Journal of Geophysical Research 88, 3419–3437.

Sørensen, K., Glassley, W., Korstgård, J. & Stensgaard, B.M. 2006: The Nordre Strømfjord shear zone and the Arfersiorfik quartz diorite in Arfersiorfik, the Nagssugtoqidian orogen, West Greenland. In: Garde, A.A. & Kalsbeek, F. (eds): Precambrian crustal evolution and Cretaceous–Palaeogene faulting in West Greenland. Geological Survey of Denmark and Greenland Bulletin 11, 145–161 (this volume).

True, M.A., Slawski, J.J. & Hibner, B.A. 1999: Assessment of environmental hazards in western Siberian oil fields using remotely sensed imagery from U.S. and Russian national security systems. Proceedings of the Thematic Conference on Geologic Remote Sensing 13, 13–20.

van Gool, J.A.M. & Marker, M. 2004: Geological map of Greenland, 1:100 000, Ussuit 67 V.2 Nord. Copenhagen: Geological Survey of Denmark and Greenland.

van Gool, J.A.M., Connelly, J.N., Marker, M. & Mengel, F.C. 2002: The Nagssugtoqidian orogen of West Greenland: tectonic evolution and regional correlations from a West Greenland perspective. Canadian Journal of Earth Sciences 39, 665–686.

Vollmer, F.W. 1990: An application of eigenvalue methods to structural domain analysis. Geological Society of America Bulletin 102, 786–791.

Wilson, C.E., Scott, H.D., Norman, R.J., Slaton, N.A. & Frizzell, D.L. 2000: Spatial distribution of irrigation water quality parameters in Desha County, Arkansas. Abstracts with Programs, Geological Society of America 32, 45 only.

Manuscript received 4 November 2004; revision accepted 20 December 2005

The Nordre Strømfjord shear zone and the Arfersiorfik quartz diorite in Arfersiorfik, the Nagssugtoqidian orogen, West Greenland

Kai Sørensen, John A. Korstgård, William E. Glassley and Bo Møller Stensgaard

The Nordre Strømfjord shear zone in the fjord Arfersiorfik, central West Greenland, consists of alternating panels of supracrustal rocks and orthogneisses which together form a vertical zone up to 7 km wide with sinistral transcurrent, ductile deformation, which occurred under middle amphibolite facies conditions. The pelitic and metavolcanic schists and paragneisses are all highly deformed, while the orthogneisses appear more variably deformed, with increasing deformation evident towards the supracrustal units. The *c*. 1.92 Ga Arfersiorfik quartz diorite is traceable for a distance of at least 35 km from the Inland Ice towards the west-south-west. Towards its northern contact with an intensely deformed schist unit it shows a similar pattern of increasing strain, which is accompanied by chemical and mineralogical changes. The metasomatic changes associated with the shear zone deformation are superimposed on a wide range of original chemical compositions, which reflect magmatic olivine and/or pyroxene as well as hornblende fractionation trends. The chemistry of the Arfersiorfik quartz diorite suite as a whole is comparable to that of Phanerozoic plutonic and volcanic rocks of calc-alkaline affinity.

Keywords: aeromagnetic data, Arfersiorfik quartz diorite, deformation, geochemistry, Nagssugtoqidian, Nordre Strømfjord shear zone, West Greenland

K.S. & B.M.S., *Geological Survey of Denmark and Greenland, Øster Voldgade 10, DK-1350 Copenhagen K, Denmark.*
E-mail: *ks@geus.dk*
J.A.K., *Department of Earth Sciences, University of Aarhus, DK-8000 Århus C, Denmark.*
W.E.G., *Lawrence Livermore National Laboratory, L-646, Livermore, CA 94550, California, USA.*

The *c*. 1850 Ma Nagssugtoqidian orogen in central West Greenland, originally defined by Ramberg (1949), is built up of both Palaeoproterozoic and reworked Archaean rocks, and contains several prominent shear zones of Nagssugtoqidian age (Bak *et al.* 1975a; Connelly *et al.* 2000; van Gool *et al*. 2002). These are roughly ENE–WSW-trending, approximately linear zones of intensely deformed rocks with well-developed planar and linear tectonic fabrics. The shear zones may be up to 20 km wide and have a strike length of more than 150 km, the approximate width of the ice-free coast of West Greenland. One of the most prominent shear zones, the Nordre Strømfjord shear zone (Fig. 1), was described in detail by Bak *et al.* (1975b) and Sørensen (1983), and is a main subject of this paper.

The Nordre Strømfjord shear zone was recognised by previous authors as a sinistral shear zone mainly on the basis of deflection of fabrics and lithologies. A general observation was that open structures outside the zone become closed and brought into parallelism within the zone. This is apparent both in the field and especially so on regional geological maps and aerial photographs. A systematic change in the orientation of planar fabrics across the shear zone indicated that the zone is wedge-shaped in vertical profile, suggesting that the zone narrows upwards,

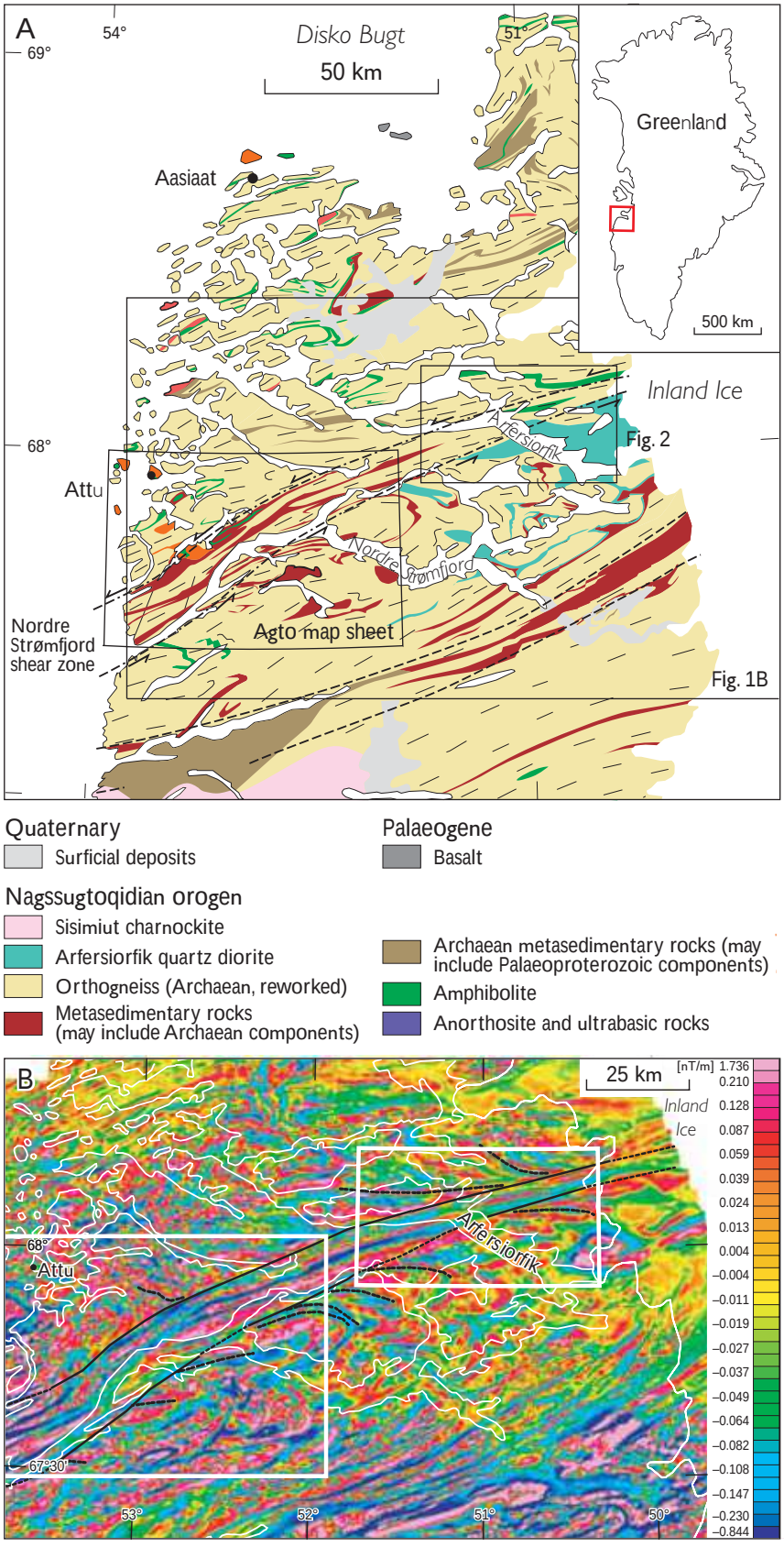

Fig. 1. A: Simplified geological map of the Nagssugtoqidian orogen. Index map of Greenland shows the location of Fig. 1A. Black frames, locations of the Agto map sheet (Olesen 1984) and the inner Arfersiorfik region investigated during field work in 2002 (Fig. 2). B: Aeromagnetic map of the Nordre Strømfjord shear zone from the coast to the western margin of the Inland Ice (shown as the vertical gradient of the total magnetic field intensity, nT/m). Anticlockwise rotation of lithologies into the shear zone is shown by curved stippled lines. The established and inferred boundaries of the high-strain part of the shear zone (full and stippled lines) are positioned where these rotating lithologies attain orientations which are indistinguishable from those within the central part of the shear zone itself. The magnetic anomaly field was obtained by subtracting the regional aeromagnetic data from the international geomagnetic reference field (Rasmussen & van Gool 2000). Nominal flight altitude of the survey: 300 m above sea level, with gentle drape flying over areas with high relief. The survey was flown along N–S flight lines 500 m apart and along orthogonal tielines at 5 km intervals. nT = nanotesla (magnetic flux density).

and conversely widens deeper in the crust. This interpretation is supported by the observation that the deepest part of the shear zone, which is exposed in the west near the coast, is more than twice as wide as its more high-level, eastern end near the Inland Ice (Bak *et al.* 1975a, b).

The western part of the Nordre Strømfjord shear zone was mapped in detail within the Agto map sheet (Olesen 1984). In this paper we report an investigation of its eastern part, conducted in 2002 in the inner part of the fjord Arfersiorfik.

Our investigations were in part intended to resolve conflicting interpretations of the nature of the shear zone. Although all previous published work on the shear zone had reached similar conclusions regarding its magnitude and structural character, a different hypothesis was presented in a subsequent reconnaissance study by Hanmer *et al.* (1997a, b), who re-interpreted the pre-existing data and purported that the shear zone was smaller than previously mapped and accommodated less lateral displacement than previously accepted. Our premise was that detailed field work aimed at resolving the spatial relationships of structural elements, rather than relying on previously collected data, would expand our knowledge of the characteristics of the shear zone and would enable rigorous testing of the two previous hypotheses.

The early work (Bak *et al.* 1975a, b; Sørensen 1983) showed the shear zone to be a large-scale synmetamorphic, sinistral transcurrent zone with a distinct wedge shape in its western, syn-granulite facies part. In that area, the shear zone is *c.* 15 km wide. It was also suggested that the shear zone deformation occurred simultaneously with large-scale metasomatism (Sørensen & Winter 1989). Prior to the present study, the general outline and extent of the Nordre Strømfjord shear zone between the Agto map sheet and the Inland Ice was drawn by Bak *et al.* (1975b) and Sørensen (1983), based on work by Henderson (1969) and interpretation of aerial photographs. Now, the extent of the zone of high strain between the coast and the Inland Ice can be demonstrated to correlate with anticlockwise rotation of lithologies into the shear zone, which is clearly visible on a new aeromagnetic data set (Nielsen & Rasmussen 2004). The age of the shear zone seems to be bracketed by the 1.85 Ga age of regional metamorphism (Hickman & Glassley 1984; Connelly *et al.* 2000) and postkinematic pegmatite ages of 1.76 Ga (Connelly *et al.* 2000; Stendal *et al.* 2006, this volume). Apart from the shear zone, the area we investigated in 2002 also encompasses a major part of the Arfersiorfik quartz diorite (AQD), first observed by Noe-Nygaard & Ramberg (1961) and later described by Henderson (1969). The latter author visited the area in connection with reconnaissance work leading to the publication of the 1:500 000 scale geological map Nussuaq – Søndre Strømfjord (Escher 1971). The Arfersiorfik quartz diorite was subsequently studied by Kalsbeek *et al.* (1984, 1987) and Kalsbeek (2001), who interpreted it as a subduction-related calc-alkaline intrusive suite and obtained an age of intrusion of 1.92 Ga (see also the section on petrology).

Along its shores, the Arfersiorfik fjord system offers excellent exposures of the shear zone and its surroundings. The authors spent three weeks in the region in the summer of 2002, conducting their investigations from a single camp with transport by inflatable dinghy, supplemented by half a day's helicopter reconnaissance in the area between inner Arfersiorfik and the Inland Ice. The area covered during the field work is shown in Fig. 2. The main aims of the field work were to investigate the shear zone in the inner part of Arfersiorfik and to investigate the relationships between the shear zone and the Arfersiorfik quartz diorite; as can be seen from Fig. 2, the shear zone constitutes the northern boundary of the AQD for a distance of at least 35 km between the Inland Ice and inner Arfersiorfik. Laboratory investigations of the approximately 110 samples collected during field work have not yet been finalised, and this account is therefore of preliminary nature.

A transect through the shear zone

The lithology and structure of the shear zone are illustrated by way of a schematic profile covering the area between Akunnaaq and Sarfaarsuk (Fig. 3), a distance of *c.* 8 km, corresponding to a distance of *c.* 7 km as measured perpendicular to the shear zone trend. The shear zone is expressed by two principal characteristics: lithological units are all planar and vertically oriented, and the lithological variability per unit length across strike is much more pronounced than in the surrounding rocks north and south of the zone. In the field, these features are best displayed along the eastern shore of the small fjord Orlerfik (Fig. 2). Lithologically, the shear zone can be described as a succession of supracrustal schist and gneiss units alternating with siliceous and intermediate orthogneisses of the AQD. The profile of Fig. 3 is described in the following from south to north. Further details about the AQD are described in a later section.

To the south of the shear zone (within the area of investigation, Fig. 2) the AQD is seen to rest with low-angle boundaries on siliceous gneisses, often with an intervening screen of schist. We agree with van Gool *et al.* (1999) that this surface is of tectonic, probably thrust or ductile

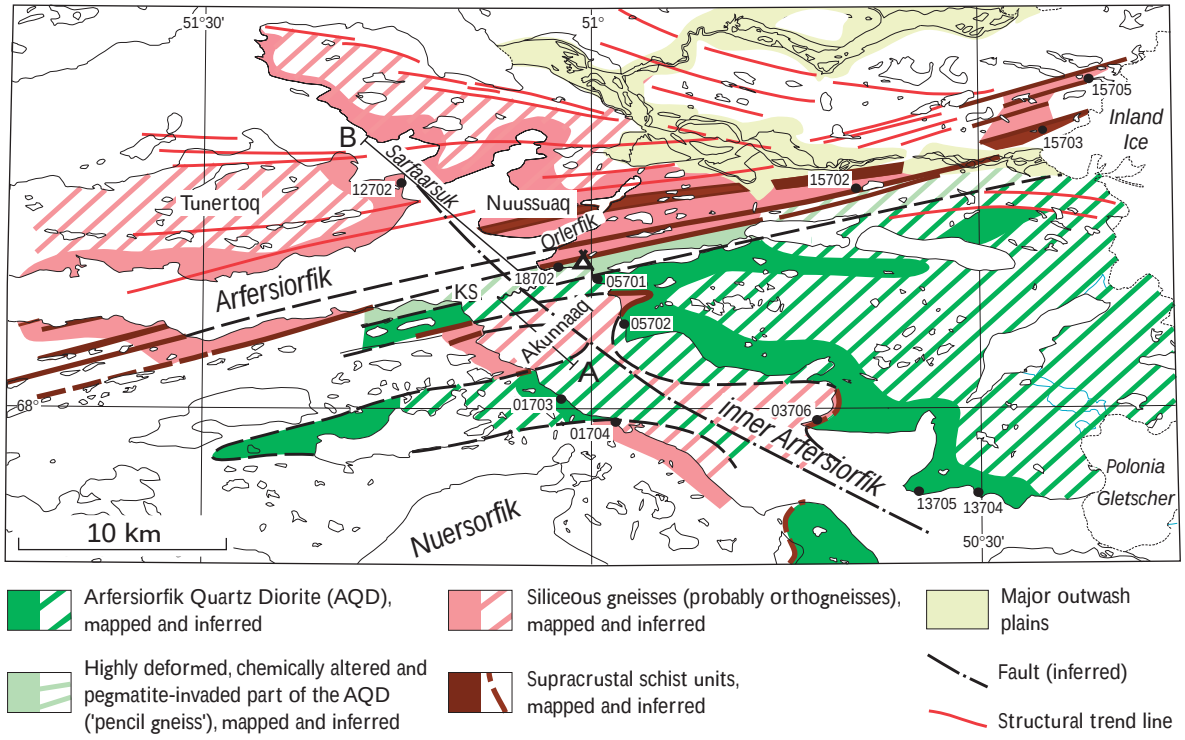

Fig. 2. Simplified geological map of the inner Arfersiorfik region, showing the authors' 2002 field work along full-coloured coasts (see also Fig. 1). Compare the mapped geology with the magnetic patterns on Fig. 7, shown at the same scale. Red lines, structural trend lines mainly from aeromagnetic data. KS, Kangimut Sammisoq (near map centre). Five digit numbers, locality numbers mentioned in the text. Two antiformal folds east of the inferred fault along inner Arfersiorfik are outlined by the AQD contact overlying siliceous gneisses north of localities 05702 and 03706. The axial trace of the intervening synformal fold meets the coast near loc. 01703. Tent symbol, position of camp during 2002 field work. Inland geology near Nuersorfik from van Gool & Marker (2004).

thrust nature. Farther to the south, in the area between the heads of Nordre Strømfjord and Arfersiorfik, a thin (up to 500 m) sheet of AQD with tectonic contacts occurs with Archaean siliceous gneisses both above and below the AQD sheet (the Ussuit unit; Manatschal *et al.* 1998; van Gool *et al.* 1999). The geometry of this bounding surface is interpreted as outlining a series of folds. Only the northern limb of the northernmost synformal structure is contained within the composite profile of Fig. 3. Folding of the AQD was observed by Henderson (1969) and later elaborated upon by Passchier *et al.* (1997) and van Gool *et al.* (1999). At the localities outside the shear zone where the AQD can be seen in contact with the structurally underlying siliceous gneisses (localities 01702,

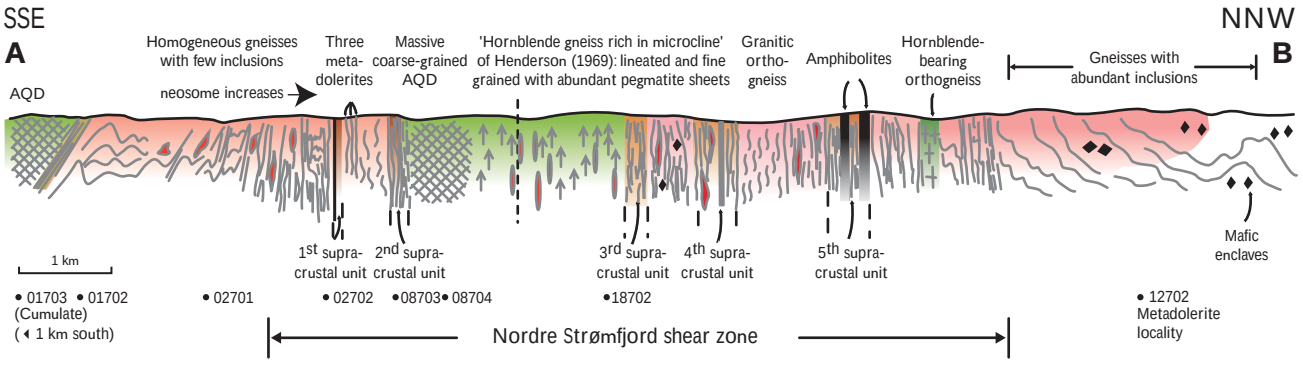

Fig. 3. Schematic profile A–B through the Nordre Strømfjord shear zone in the inner Arfersiorfik from Akunnaaq in the south to Sarfaarsuk in the north (Figs 2, 7). Localities and lithologies have been projected onto the profile plane along the strike direction of the shear zone. Locality numbers mentioned in the text appear beneath the profile. For colour code, consult caption to Fig. 2.

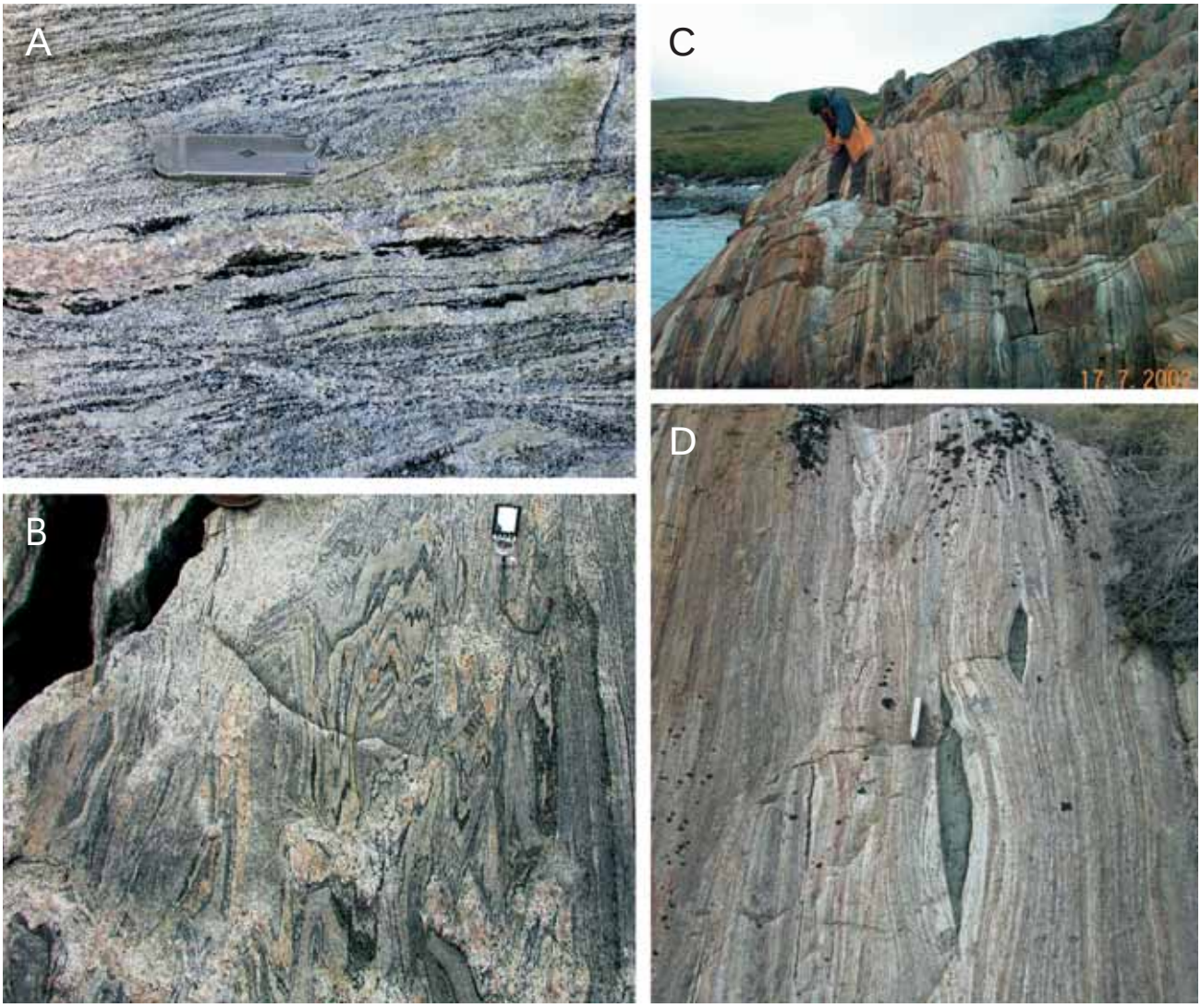

Fig. 4. Siliceous gneisses between localitiess 17701 and 02702 (Figs 2–3) illustrating progressive deformation towards the first supracrustal unit. A: Coarsely banded biotite gneiss, loc. 17701 (knife 10 cm long). B: Finely banded gneiss with generally steeply oriented foliation, but apparently variable deformation intensity at outcrop scale, loc. 02701 (compass 10 cm long). C: Extreme planar fabric and fine-scale layering in siliceous gneiss near the first supracrustal schist unit, loc. 02702. D: Detail from the same locality with lenticular ultramafic inclusions (knife 10 cm long).

01704, 03706, 05701, Figs 2, 3), the contacts are all tectonised, and with a well-developed, folded planar fabric. Original intrusive features have been obliterated except at loc. 05702 (Fig. 2), where xenoliths of pelitic schist can be seen within the AQD, clearly indicating intrusion of the quartz diorite into a pre-existing metamorphosed sedimentary sequence.

From loc. 01702 (Fig. 3) and towards the north, siliceous gneisses become progressively more deformed and contain an increasing amount of granitic material. For a distance of almost 1 km to the south of the first supracrustal schist unit, the gneisses display a subvertical planar fabric and contain abundant layers of leucocratic, in places pegmatitic, material. These gneisses appear highly strained. The transition within these gneisses, from 01701 to 02702 (Fig. 3), is the best exposed transition zone developed in siliceous gneisses in the area that we have visited. The structural development of these gneisses is illustrated in Fig. 4A–C.

The first supracrustal unit (Fig. 3) comprises a predominant lithology of mafic schists with calc-silicate and ultramafic lenses. Pelitic schists are subordinate. At locality 08703, a second thin supracrustal unit of pelitic schist (thickness 25 m) occurs along the boundary to the AQD. The gneisses to the north of the first supracrustal unit contain abundant layers of homogeneous amphibolite,

Fig. 5. Arfersiorfik quartz diorite. A: Coarse-grained metamorphosed quartz diorite with pervasive linear fabric. A minor dextral shear zone deforms the linear fabric (compass 10 cm long). B: Extreme linear fabric developed in AQD close to its northern boundary ('pencil gneiss'; knife 20 cm long).

with locally preserved discordant relationships to the host gneiss structures. These discordant amphibolites were undoubtedly originally dolerite dykes. Farther to the north, the gneisses are nearly devoid of amphibolites and are characterised by wavy and folded migmatitic structures without the pronounced planar fabric seen in the gneisses adjacent to the first supracrustal unit.

The contact between the second supracrustal unit and the AQD is vertical. Coarse-grained segregations of granitic pegmatite in the schist appear to be smeared out and pulled apart. The AQD near this contact is syntectonically recrystallised and displays layering on a centimetre scale. The AQD farther to the north of the contact becomes relatively coarse grained and in places preserves undeformed magmatic structures (see a later section with more details on the petrology of the AQD). These relatively coarse-grained AQD rocks become progressively tectonised towards the north, developing a very pronounced L-tectonite fabric. Pegmatite sheets also become abundant, and the AQD itself becomes progressively more leucocratic. Henderson (1969 p. 7) describes this transition with these words: "In the inner part of Arfersiorfik a zone of basic gneiss of a type not found elsewhere in the area was encountered. This is a hornblende gneiss rich in microcline. It contains numerous pegmatites", and further, "A large folded quartz diorite body dominates the inner part of Arfersiorfik ... On its northern side it is in contact with the hornblende gneiss rich in microcline mentioned previously" (Henderson 1969, p. 11). We interpret the "hornblende gneiss rich in microcline" as the northernmost, most highly deformed (and most chemically altered) equivalent of the much less deformed and more igneous appearing AQD to the south of the shear zone. Nevertheless, the AQD to the south of the shear zone is in most places also a tectonite; a mineral lineation is nearly always present in the rock. Textures viewed on sections perpen-

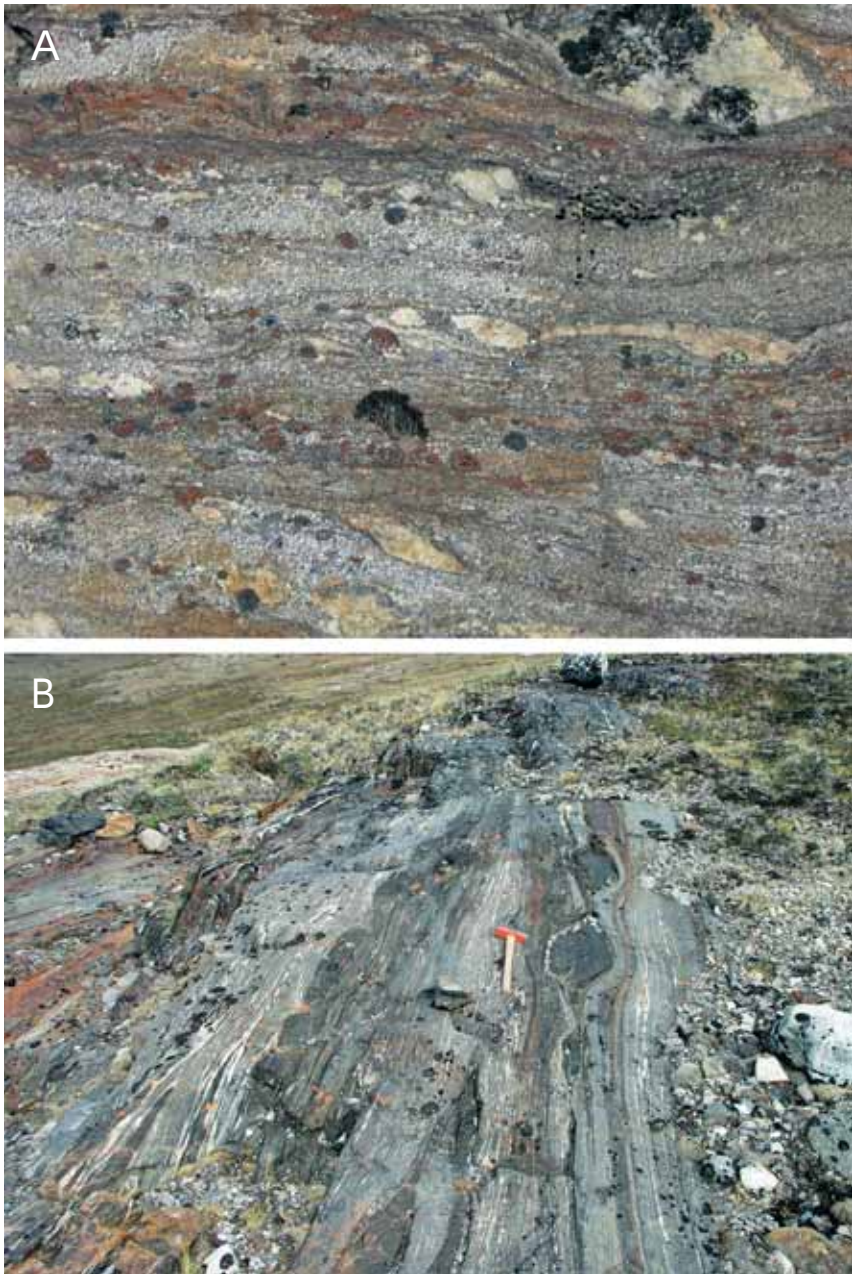

Fig. 6. Pelitic and mafic schists from supracrustal unit near the Inland Ice visited during helicopter reconnaissance, loc. 15705 (Fig. 2). A: Two-mica sillimanite schist with abundant 'winged' feldspar blasts indicating sinistral sense of shear. Long dimension of photo *c.* 75 cm. B: Amphibolitic schist with boudins of garnet-bearing ultramafic rock (hammer *c.* 50 cm long).

dicular to the lineation appear igneous, while a pronounced tectonic lineation is seen in other orientations (Fig. 5). The transition from the more magmatic appearing AQD to the "hornblende gneiss rich in microcline" is gradual, and the continuity of these rocks is evident on either side of Arfersiorfik.

Between the third and fourth supracrustal units siliceous gneisses of varying heterogeneity and apparent degree of shear zone deformation occur, all with a vertical planar structure. Basic inclusions are common in this gneiss unit.

The fourth supracrustal unit as exposed on the eastern shore of Orlerfik is a lithologically variable assemblage of pelitic schists and gneisses, amphibolitic schists, and calc-silicate gneiss. Overall, the rocks appear highly deformed. The pelitic rocks typically contain numerous layers and lenses of pegmatitic material up to 8 m thick. Cordierite was observed in the schists, and a lens of tourmalinite was also found. Near the Inland Ice, at loc. 15703 (Fig. 2), a centimetre-thick marble layer, the only occurrence of marble seen during field work, was observed in a pelitic schist thought to be the merged equivalent of the third and fourth supracrustal units at Orlerfik.

The gneisses between the fourth and fifth supracrustal

units are quartzofeldspathic. A rather homogeneous, granitic orthogneiss 1 km wide occurs immediately to the north of the fourth supracrustal unit. It contains a few mafic inclusions which appear to be metadolerites. This gneiss, although foliated, has not developed the typical shear zone fine layering, and it is clearly an orthogneiss. Towards the north, quartzofeldspathic gneisses with numerous granitic layers and bands form the boundary towards the fifth supracrustal unit. The finely banded shear zone planar structure is developed in places. The gneisses between the fourth and fifth supracrustal unit thus appear to be progressively deformed towards the north.

The fifth supracrustal unit is well exposed at Orlerfik and along the western shore of the Nuussuaq peninsula. On Nuussuaq, this unit forms an elongate ridge of strongly rusty weathering rocks. In fresh exposures in the tidal zone, the rusty weathering rock can be seen to be a fine-grained graphite- and sulphide-bearing darkish grey gneiss. In this unit, finely banded amphibolitic schists are prominent, along with pelitic sillimanite-bearing schists. Calc-silicate rocks are seen as well, as also described by Henderson (1969). Pegmatitic layers are abundant. We were unable to confirm the marble layer occurring on the western half of the Nuussuaq peninsula on Henderson's (1969) map. We found, instead, a complex of light-coloured, in some places greenish, anthophyllite-phlogopite-diopside-bearing metamorphosed ultramafic rocks.

It appears that all the supracrustal units, although structurally continuous, change lithologically along strike, consisting of various combinations of pelitic schists and gneisses, graphite-sulphide gneisses, calc-silicate rocks, mafic schists and ultramafic lenses. In all the supracrustal units deformation appears to be intense. Both pelitic and mafic rocks are finely schistose (Fig. 6). Ultramafic and skarn lenses may be rather massive and homogeneous, but they are small in size and volumetrically minor. Overall, the supracrustal units are schistose throughout, and differ in this way from the intervening siliceous gneisses, which are heterogeneously deformed on a 100 m scale.

To the north of the fifth supracrustal unit only scattered exposures of gneiss are found at Orlerfik. Along several localities near the northern boundary of the shear zone, at Orlerfik and along the south coast of Tunertoq, a homogeneous, hornblende-bearing orthogneiss is encountered. In places it is reminiscent of the AQD. Farther north of the shear zone in the area around Sarfaarsuk, gneisses with a complex history occur, as indicated by several generations of granitic and pegmatitic veins and layers, and mafic and ultramafic layers and lenses. At locality 12702 (Fig. 2), a number of mafic layers are clearly folded metadolerites, and at this locality it can be seen how new layering develops concomitantly with deformation. Along this layering the thin metadolerites can be seen to be displaced, and it seems evident that new layering develops in the siliceous gneisses at small angles to the older layering. Without the metadolerites it would be impossible to discriminate between new and old layering.

Aeromagnetic data

The entire Nordre Strømfjord shear zone and adjacent areas are covered by regional aeromagnetic data (Figs 1B, 7) acquired during the project *Aeromag 1999* (see text to Fig. 1B and Rasmussen & van Gool 2000). The aeromagnetic map proved very useful for delineation of lithologies and structures in the field, and in general there is a very clear correlation between observed surface geology and the aeromagnetic anomaly patterns.

The Arfersiorfik quartz diorite is associated with a variable magnetic signature. The best exposed part of the AQD is located in inner Arfersiorfik just north of Polonia Gletscher (Fig. 7). This part is denoted the core zone of the AQD complex and is characterised by a distinct positive anomaly (300–490 nT). Here an unusually large amount of magnetite was found, both as millimetre-scale magnetite needles and as magnetite grains 1–3 cm large. A pronounced decrease in the magnetic intensity of the AQD is observed just north-west of the core zone. The magnetic signature of the AQD changes towards the shear zone, where the fine-grained, pegmatite-bearing and strongly linear AQD (the 'pencil gneiss') that forms the northernmost 1–2 km of the body exhibits strong negative anomalies. These changes in magnetic signature appear to reflect metamorphic and metasomatic processes associated with the shear zone development. The demagnetising effects reflect the formation of titanite and biotite at the expense of Fe-Ti-oxides, which is synchronous with shear zone evolution. Detailed thin section observations show that the modal abundances of titanite and magnetite/ilmenite are strongly negatively correlated. Comparison of titanite-rich samples and magnetite/ilmenite-rich samples with the vertical gradient of the magnetic anomaly field (obtained from the map shown in Fig. 7) shows that the titanite-rich samples consistently occur within negative changes in the gradient, while the magnetite/ilmenite-rich samples occur within positive gradients. Further work is underway to evaluate the reliability of this correlation.

In general, the supracrustal schist units are associated with negative anomalies in the total magnetic field intensity. Within the shear zone, the schist units are characterised by pronounced, linear short-wavelength negative ano-

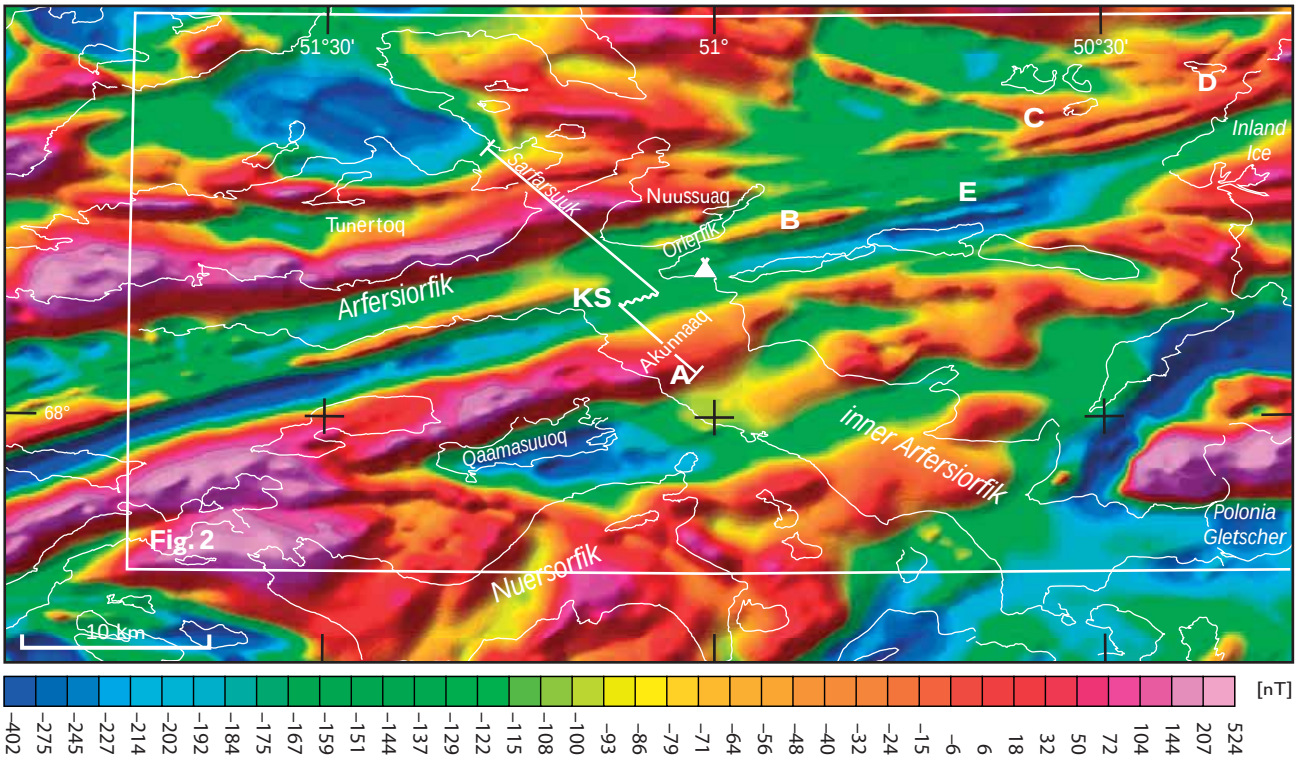

Fig. 7. Total magnetic field intensity map of the study area. A, Akunnaaq; KS, Kangimut Sammisoq; B, magnetic high coinciding with the orthogneisses between the fourth and fifth supracrustal units; C–D, lithological boundary between siliceous gneisses and supracrustal schists; E, possible magnetic expression of merged fourth and fifth supracrustal units. The position of the camp site used during the field work is shown with a tent symbol. Compare the magnetic patterns with the mapped geology on Fig. 2 (white frame), shown at the same scale. nT: nanotesla, a unit of magnetic flux density.

malies (–150 to –300 nT). At Kangimut Sammisoq (KS on Fig. 7) and towards the west-south-west the AQD and juxtaposed schists form a coherent negative anomaly, which can be traced for a considerable distance towards west-south-west into the Agto map sheet area (Olesen 1984). Within the latter area the anomaly reflects supracrustal rocks only. The negative anomalies of the supracrustal schists probably reflect the absence of Fe-Ti oxides and the abundance of iron sulphides and graphite, which yields a weak magnetic response.

In general, gneiss lithologies in the area are expressed as positive magnetic anomalies. Because of their greater volume, the gneisses are associated with broader wavelength anomalies than the supracrustal units. However, the shape of the anomalies associated with the gneiss units within the shear zone are of short wavelength and elongate (Fig. 7). Where a significant strain gradient in the siliceous gneisses is observed, e.g. northwards from Akunnaaq along the western shore of inner Arfersiorfik (from loc. 01702 to 02702, Fig. 3), this transition is not visible in the magnetic field (A on Fig. 7). In general, it appears that even large changes in strain adjacent to and within the shear zone do not have a clear magnetic signature in the siliceous gneisses. While the magnetic lows associated with supracrustal units are in general persistent along strike, the highs associated with the siliceous gneisses in places outline lenticular structures, the most obvious example being the magnetic high which can be seen to coincide with the orthogneisses between the fourth and fifth unit (B on Fig. 7).

The general map structure

Although we have not carried out regional mapping, some map scale observations follow from our work. From the Inland Ice and for a distance of at least 35 km towards the south-west (i.e. in the area between the Inland Ice and the bend of Arfersiorfik towards south-east west of Nuussuaq), the AQD is bounded to the north by the shear zone, and probably with a continuous screen of supracrustal schists along its northern boundary. Towards this bounding schist, the AQD becomes progressively deformed, developing a pronounced linear fabric and undergoing a number of

mineralogical changes, described below. These mineralogical changes are reflected in a change in magnetic signature. The change is less dramatic to the east of Arfersiorfik than it is to the west of the fjord, and this signature can be followed from the fjord to the Inland Ice and beneath the ice for at least another 30 km. Based on aeromagnetic data covering the entire Greenland including the Inland Ice, Nielsen (2004) and Nielsen & Rasmussen (2004) suggest a 125 km eastward extension of the AQD beneath the ice.

The outcrop pattern and orientations of the boundary between the AQD and the structurally underlying schists and gneisses are in accord with a structural model involving relatively open folding, as marked on Fig. 2. On Henderson's (1969) map, a 'tongue' of siliceous gneisses projects from the eastern shore of the fjord 20 km eastwards into the AQD. During helicopter reconnaissance by us, this eastward-reaching gneiss was nowhere to be seen. Along the shores of Arfersiorfik, there is an antiformal closure of AQD over siliceous gneisses with an intervening schist screen, but this cannot extend inland for more than 2 km. The entire triangular area bounded by Arfersiorfik, the shear zone, and the Inland Ice is most likely only underlain by AQD. The map pattern west of inner Arfersiorfik differs from the pattern described above. Along the shoreline south of Kangimut Sammisoq the southern boundary of the AQD is vertical, and south of the boundary, gneisses and the schists of the first supracrustal unit are also vertically oriented and possess a well-developed planar shear zone fabric. We interpret this difference in map pattern as reflecting intersections with the shear zone boundary at two different levels.

Petrology

Arfersiorfik quartz diorite

The Arfersiorfik quartz diorite was first mapped in the study area by Henderson (1969), who noted that it varies from a homogeneous, coarse-grained igneous rock in its central region which lacks evidence of deformation, to a compositionally banded gneiss near its margins. Further work by Kalsbeek *et al.* (1984, 1987) and Kalsbeek (2001) supported the general descriptions of Henderson and provided a considerable body of evidence regarding the age and chemical composition of the body. Our observations expand on these earlier results.

Within the 'greater AQD igneous complex' we have observed a number of lithologies indicative of a complex igneous history (Fig. 8). At loc. 01703 (Fig. 2) we observed a locally developed layered cumulate sequence (Fig. 8A) in gradational igneous contact with quartz diorite that contains blocks of more mafic igneous rocks. The cumulate sequence consists of numerous cycles of pyroxene-olivine cumulate layers grading into plagioclase-pyroxene anorthositic layers. This rhythmic layering grades upward into massive dioritic and quartz-dioritic rocks that contain plagioclase-porphyritic mafic xenoliths. At the same structural level, but farther north at loc. 08704, mafic enclaves (Fig. 8B) occur within leucocratic quartz diorite. In places, these enclaves contain plagioclase-porphyritic xenoliths similar to those observed at loc. 01703. We interpret these enclaves to be evidence of mixing of magmas, similar to that reported for other igneous bodies (e.g. Gagnevin *et al.* 2004; Healy *et al.* 2004; Janousek *et al.* 2004). The presence of both cumulate rocks and mixed mafic magmas at approximately the same structural level suggests that these sites represent the lower levels of the igneous complex that makes up the AQD suite.

At loc. 13705 clear evidence of at least two separate magmas in an undeformed state is preserved, with a later diorite exhibiting well-developed chilled margins against an earlier quartz diorite (Fig. 8D). Whether this implies that the AQD is actually a collection of numerous smaller intrusions or a major igneous body with local, small and rare later intrusive phases can only be resolved with more detailed field work. At loc. 18702 (Fig. 2) we have also observed a finely banded rock, apparently developed by extreme deformation of a sequence of pillow lavas (Fig. 8D). This latter occurrence was found close to the northern boundary of the AQD and may represent the upper part of the 'greater AQD igneous complex'. Within the thin sheet of AQD to the south of the localities that we examined, an occurrence of metavolcanic rocks was reported by Manatschal *et al.* (1998), which supports the interpretation that exposures of the AQD suite represent a variety of deep to near-surface original positions.

In thin section, the mineralogy of the AQD suite is invariably modified by metamorphic recrystallisation. Textural features suggest that the AQD originally consisted of hornblende and pyroxene diorites and quartz diorites. In those rocks with primary pyroxenes, the ortho- and clinopyroxenes are partially to completely recrystallised to intergrowths of plagioclase, hornblende, quartz, magnetite, ilmenite and sometimes biotite. In instances where the pyroxene is completely replaced by amphibole, the amphibole is densely filled with inclusions of magnetite/ilmenite. In the hornblende diorites and quartz diorites the original igneous amphiboles are generally inclusion-free and tend to have more brownish pleochroic colours. In some cases, plagioclase crystals exhibit well-preserved

Fig. 8. Extent of lithological variation within the 'greater Arfersiorfik quartz diorite complex'. A: Igneous layering at loc. 01703 (Fig. 2), where an assemblage of undeformed cumulates and related rocks from the AQD suite is set in a host of tectonised (lineated) AQD (pencil *c.* 15 cm long). B: Igneous textured AQD with hornblende-rich pods indicating fractionation or magma mingling. Observe light grey xenolith within hornblende rich phase immediately north-east of centre of photo (fist for scale). C: Dark coloured igneous rock (left) chilling against lighter coloured rock (right), loc. 13705 (Fig. 2; compass 10 cm long). D: Part of a pegmatite sheet (right) within a banded amphibolitic rock (left) interpreted as strongly deformed pillow lava (hammer handle *c.* 50 cm long).

igneous oscillatory zoning, but usually this is partially to completely replaced by metamorphic zoning. Cummingtonite-hornblende intergrowths are relatively common and are identical to similar features described from dioritic rocks affected by amphibolite facies metamorphism in other parts of the world, e.g., Tanzania (Haslam & Walker 1971), USA (New Hampshire, Brady 1974; the Grand Canyon, Clark 1978), and Australia (New South Wales, Stephensen & Hensel 1979). Recrystallisation of the AQD occurred within middle to upper amphibolite facies, as indicated by the hornblende-biotite-plagioclase ± garnet association, the instability of ortho- and clinopyroxene with amphibole, and the development of cummingtonite-hornblende intergrowths.

The chemical variability of the AQD suite (Fig. 9) is typical of that of other calc-alkaline igneous complexes, as noted previously by Kalsbeek *et al.* (1987) and Kalsbeek (2001) who demonstrated similarities between these rocks and the Sierra Nevada batholith. Including their data, we have expanded the comparison to that of the Cascades of Washington State, USA, the Mt Lassen complex of California, and the southwest Pacific island arc

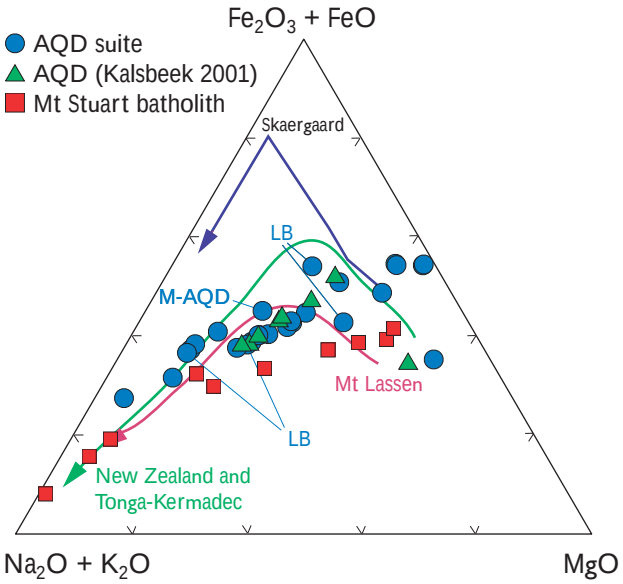

Fig. 9. AFM diagram comparing Arfersiorfik quartz diorite chemistry (including the large boulder samples labelled 'LB') to that of other calc-alkaline systems. The trend for the Skaergaard igneous complex is shown for comparison. Mt Stuart data from Erikson (1977). All other trends from Best (1982). The sample labelled M-AQD is the mylonitised quartz diorite sample mentioned in the text.

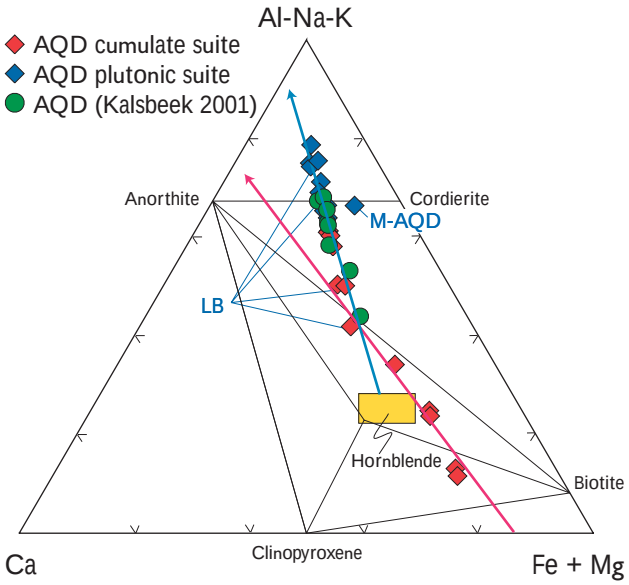

Fig. 10. ACF atomic triangular diagram showing the chemical variation in the Arfersiorfik quartz diorite based on our data (including the boulder samples LB and data reported by Kalsbeek 2001). Red symbols, samples collected within cumulate localities. Blue and green symbols, collected by us and Kalsbeek (respectively) from the non-layered igneous complex. Note the kink in the trend of chemical evolution and the overlap between the non-layered and cumulate rocks of the Arfersiorfik quartz diorite. Red arrowed line, the trend of magmatic evolution implied by the cumulate samples, reflecting fractionation of some combination of olivine and/or orthopyroxene with clinopyroxene in the most primitive cumulate suite. Blue arrowed line, that suite of samples for which chemical variability can be ascribed to hornblende fractionation. Yellow box: outline of the range of likely hornblende compositions. M-AQD, mylonitised quartz diorite sample mentioned in the text.

system. The compositional range of the AQD suite is large, varying from ultramafic (within the cumulate complex) to quartz-dioritic and quartz-monzonitic. The compositional evolution of the magma appears to have been controlled by crystal fractionation of olivine and/or pyroxenes when the cumulates were forming, but eventually reaching the stage where hornblende fractionation dominated the chemical evolution of the magma (Fig. 10). The one sample that deviates from these trends is labelled M-AQD. This is a fine-grained biotite-plagioclase-quartz mylonite produced by local granulation of coarse-grained AQD. Further study of this sample is underway to understand the controls on this alteration process.

We noted that in the near vicinity of the Nordre Strømfjord shear zone chemical modification of the AQD appears to be significant. Development of K-feldspar-rich mineral assemblages is common, and often accompanied by the association calcite-titanite. These rocks occur in the same region in which Henderson (1969) noted the presence of K-feldspar-rich gneisses. The magnitude, extent and significance of these chemically unusual rocks are under investigation. Metasomatism at the AQD margin and minor shear zones within the AQD were described by Kalsbeek *et al.* (1987).

Included in Figs 9, 10 are four analyses (labelled LB) from samples of large boulders in outwash from glacial deposits, collected several hundred metres east of our camp (see Fig. 2). In the field, the samples bear striking similarity to AQD lithologies. As is evident from the figures, these rocks are chemically indistinguishable from the AQD suite, supporting evidence from aeromagnetic data discussed above that the AQD extends under the ice for some distance.

Late garnet granite

The southernmost samples collected (loc. 13704, Fig. 2) are from a site at which peraluminous garnet granite exhibits classic intrusive relationships into granodioritic to quartz-dioritic gneisses of the AQD. This granite contains stoped blocks of gneisses within the upper 30 m of its upper boundary zone (Fig. 11), and dykes and sills from the granite invade the gneiss. The granite itself contains

Fig. 11. Peraluminous garnet- and muscovite-bearing granite at loc. 13704 (Fig. 2) intruding into Arfersiorfik quartz diorite and interpreted as the roof zone of a pluton with rafts of country rock and sheets of granite above. Looking north-north-east. Height of section *c.* 150 m.

delicate, primary muscovite rosettes and myrmekitic intergrowths with no evidence of deformation. The intrusive relationships and the preservation of delicate primary igneous structures suggest that the granite invaded postkinematically, and that it could provide excellent samples for establishing a minimum age for the time of cessation of tectonic activity in the region.

Late stage, low-grade metamorphism

A suite of samples from the AQD in the region south of the Nordre Strømfjord shear zone contain postkinematic mineral assemblages of the prehnite-pumpellyite and lower greenschist facies overprinting the higher grade metamorphic mineral assemblages that define the amphibolite facies metamorphism. This late-stage, low-grade metamorphism is associated with brittle fracturing and veining, and local piemontite and base metal mineralisation. The timing of this low-grade metamorphism remains unresolved.

Strain variation within the Nordre Strømfjord shear zone

Earlier work within the Agto map sheet (Fig. 1; Bak *et al.* 1975b; Sørensen 1983) concluded that the Nordre Strømfjord shear zone reflects sinistral transcurrent movement. It was also concluded from the fanning of planar structures that the shear zone is wedge-shaped within the Agto map sheet. The present work has shown that in the inner part of Arfersiorfik such fanning is not obvious, perhaps because the zone here is only half as wide as near the coast in the Agto map sheet area. The planar structures within the shear zone are vertical (Fig. 3) with an extremely limited variation of dips (Fig. 12), and linear structures are horizontal. The justification for drawing the schematic profile (Fig. 3) with vertical lithological boundaries throughout the shear zone is evident from the stereograms of Fig. 12.

The horizontal orientation of linear structures is also in accordance with a horizontal movement direction and with the orientation of linear structures in the western part of the shear zone (Bak *et al.* 1975b). The sinistral shear sense, already inferred by Bak *et al.* (1975b) and further discussed and analysed by Sørensen (1983), is obvious from the large-scale anticlockwise rotation seen in

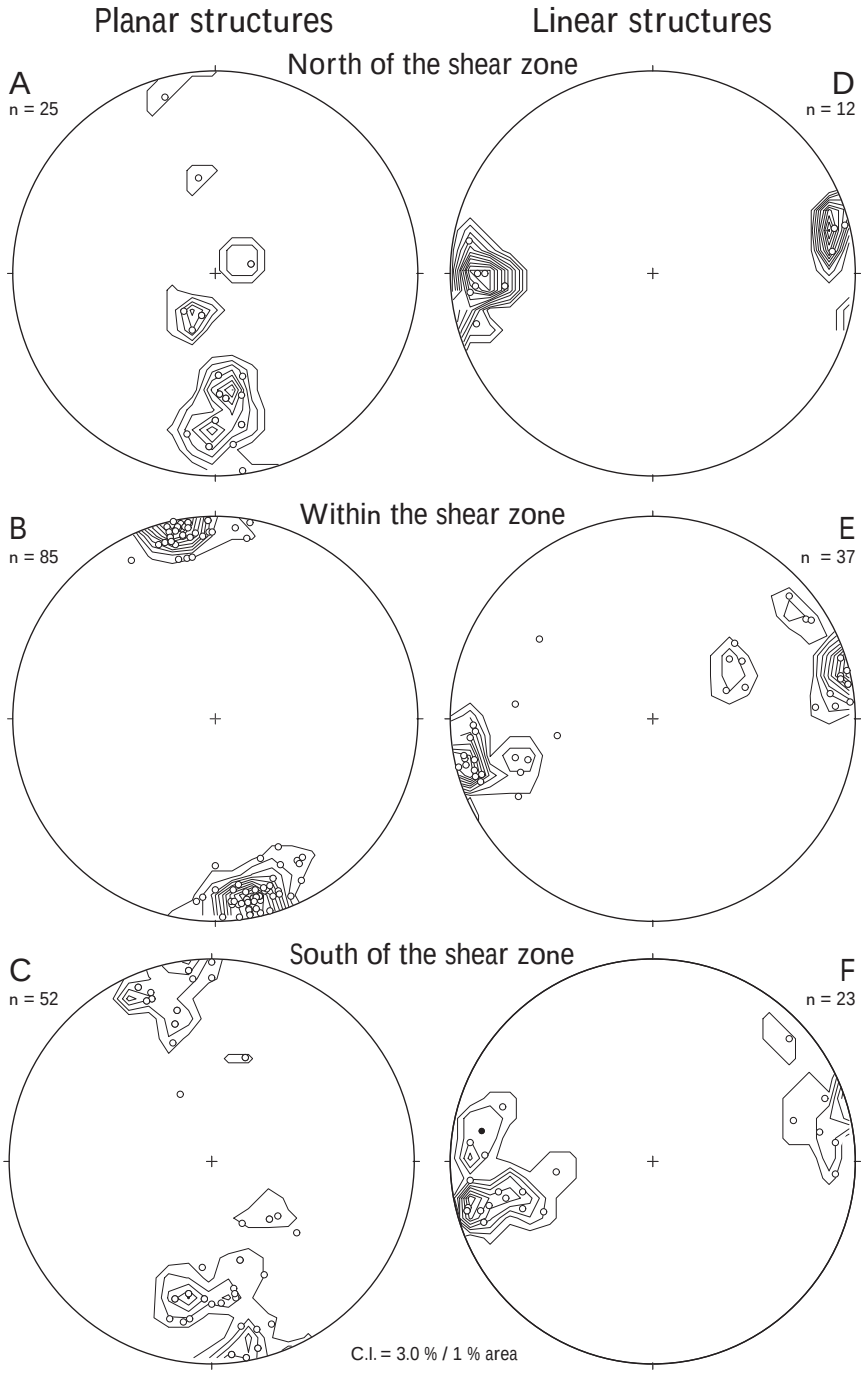

Fig. 12. Stereograms of planar and linear structures from within and outside the Nordre Strømfjord shear zone. While linear structures (D–F) outside and within the shear zone do not differ in orientation, planar structures (A–C) within the shear zone are seen to be extremely concentrated as opposed to the wider spread of planar structures along girdles perpendicular to the linear structures outside the zone. Equal area lower hemisphere projections. Contour interval = 3% of plotted points per 1% of stereogram area.

the aeromagnetic data (Figs 1, 7). Small-scale shear sense indicators confirm this pattern (Fig. 6). They do not occur abundantly, and as the large-scale features of the entire shear zone from the coast to the Inland Ice leave no doubt about the sinistral nature of movement, we have made no systematic investigations of small-scale shear sense indicators.

It was suggested by Sørensen (1983, fig. 14) that the shear zone between Arfersiorfik and the Inland Ice could be divided into an central part bounded by two marginal zones. He furthermore speculated (p. 3432) that the strain profile at the Inland Ice was suggestive of superposition of two mechanisms, one responsible for most of the deformation in the marginal zones, and another responsible for the major part of the strain in the central part of the shear zone. The rotation on which this suggestion was based is also evident, for example, on the aeromagnetic data between labels C and D on Fig. 7, and from there

farther towards the west-south-west. Our field work demonstrates that this line is in fact a lithological boundary between siliceous gneisses and supracrustal schists. A corresponding boundary may be placed at the boundary between the 'pencil type' AQD and the schist that we have termed the third supracrustal unit on Fig. 3, and thus like the northern line of rotation coincides with a lithological boundary. Throughout the shear zone all the supracrustal units are highly and penetratively deformed, whereas the intervening orthogneisses are heterogeneously deformed. Furthermore, where visited by the authors, the boundaries to the central part of the shear zone do in fact correspond to lithological boundaries involving supracrustal schists. In addition, the intervening siliceous gneisses, as judged from the aeromagnetic map, may in places form augen-like features, as for example, immediately north of E on Fig. 7. The eastern tip of this positive magnetic anomaly was visited by helicopter (loc. 15702). Immediately east of this locality the fourth and fifth supracrustal units can be seen to be separated by a few tens of metres of siliceous gneiss, a unit which is almost 2 km wide along Orlerfik 15 km to the west. To the east of this locality, a wide negative magnetic anomaly can be seen to underlie unexposed ground (E on Fig. 7). We interpret this as the magnetic expression of the merged supracrustal units four and five. Our work in Arfersiorfik therefore suggests a model for strain variation that is fundamentally different from the model developed by Sørensen (1983) for the western, lower crustal and most high-grade part of the shear zone. Where the latter model suggests continuity of lithologies from wall to wall of the shear zone, our observations in Arfersiorfik indicate that ~~a~~discontinuities~~y~~ in strain may be associated with boundaries between schists and orthogneisses. It is furthermore suggested by the aeromagnetic data that the intervening siliceous gneisses may form augen-like features. The change in deformation mechanism suggested by Sørensen (1983) may therefore reflect ductility contrasts between the supracrustal schist units and the siliceous gneisses and not the superposition of two different deformation mechanisms.

Mineral occurrences

Two dominating types of mineral occurrences have been found in the inner part of Arfersiorfik: (1) occurrences of disseminated to massive pyrrhotite in supracrustal mica schist units and (2) occurrences of iron sulphides in the contact/fault zones between the AQD and juxtaposed supracrustal units. The former type is associated with strongly foliated amphibolite, biotite ± graphite ± sillimanite schist and paragneiss. The pyrrhotite is found either as horizons up to 0.5 m thick or as lenticular bodies or pods up to 1 × 2 m in outcrop size. This type of occurrence is only found in the supracrustal rock units within the shear zone. Similar occurrences exist west of the investigated area all the way to the outer coast just north of the mouth of Nordre Strømfjord. This occurrence type is interpreted as syn-genetic volcanic-associated exhalative sulphide deposited in a volcanic arc environment. The highest analytical values of gold and base metals obtained from samples of disseminated sulphides in pelitic schist are the following figures: 38 ppb Au, 45 ppm As, 497 ppm Zn, 3813 ppm Cu and 456 ppm Ni. All samples have elevated Mn concentrations, up to 2.9 wt% Mn. The second type of mineral occurrence is widespread in the inner part of Arfersiorfik, both within and outside the shear zone. The zones hosting the sulphides are often associated with alteration, and in many cases a high degree of silicification is observed. It is unknown if this type is strictly epigenetic, caused by hydrothermal activity along the contact or in the fault zones between the AQD and the minor supracrustal units, or if it is a product of hydrothermal remobilisation of syngenetic iron sulphides in the supracrustal rock units. For more details and description of mineral occurrences in central West Greenland see Steenfelt *et al.* (2004) and Stendal *et al.* (2004).

Conclusions

Our investigations of the Nordre Strømfjord shear zone in the eastern part of Arfersiorfik suggest that deformation and displacement at this crustal level are primarily a function of lithology, with large displacements effected by ductile flow in the supracrustal sequences. The large mass of Arfersiorfik quartz diorite between Arfersiorfik and the Inland Ice is bordered to the north by the shear zone, probably with a supracrustal schist unit along this boundary. The latter is indicative of the extreme deformation that can be taken up in the supracrustal rocks. Towards this boundary the tectonite fabric of the AQD becomes further accentuated, and near its northern boundary the AQD differs both chemically, mineralogically and structurally from the AQD to the south of the shear zone. We have both found cumulate rocks originating from near the base of the original magmatic AQD complex and metavolcanic rocks interpreted as belonging to its top part, whose less deformed equivalents are most probably covered by the Inland Ice. The chemical variation of the AQD suite is wide and comparable to that of Cenozoic calc-alkaline igneous suites.

Acknowledgements

Concise reviews by Graham Leslie and Chris Pulvertaft and financial support by the Carlsberg Foundation are gratefully acknowledged. The Air Greenland helicopter pilot and the crew on board M/S Milandt (Aasiaat) are thanked for efficient transport and practical help. Chemical analyses were carried out by XRF on glass discs at the Department of Earth Sciences, University of Aarhus, Denmark.

References

Bak, J., Grocott, J., Korstgård, J.A., Nash, D., Sørensen K. & Watterson, J. 1975a: Tectonic implications of Precambrian shear belts in western Greenland. Nature 254, 566–569.

Bak, J., Korstgård, J.[A.] & Sørensen, K. 1975b: A major shear zone within the Nagssugtoqidian of West Greenland. Tectonophysics 27, 191–209.

Best, M.G. 1982: Igneous and Metamorphic Petrology, 630 pp. San Francisco: W.H. Freeman.

Brady, J.B. 1974: Coexisting actinolite and hornblende from West-Central New Hampshire. American Mineralogist 59, 529–535.

Clark, M.D. 1978: Amphibolitic rocks from the Precambrian of Grand Canyon: mineral chemistry and phase petrology. Mineralogical Magazine 42, 199–207.

Connelly, J.N., van Gool, J.A.M. & Mengel, F.C. 2000: Temporal evolution of a deeply eroded orogen: the Nagssugtoqidian Orogen, West Greenland. Canadian Journal of Earth Sciences 37, 1121–1142.

Erikson, E.H. Jr. 1977: Petrology and petrogenesis of the Mount Stuart batholith – plutonic equivalent of the high-alumina basalt association?. Contributions to Mineralogy and Petrology 60, 183–207.

Escher, A. 1971: Geological Map of Greenland, 1:500 000, Søndre Strømfjord – Nûgssuaq, sheet 3. Copenhagen: Geological Survey of Greenland.

Gagnevin, D., Daly, J.S. & Poli, G. 2004: Petrographic, geochemical and isotopic constraints on magma dynamics and mixing in the Miocene Monte Capanne monzogranite (Elba Island, Italy). Lithos 78, 157–195.

Hanmer, S., Mengel, F., Connelly, J. & van Gool, J.[A.M.] 1997a: Significance of crustal-scale shear zones and synkinematic dykes in the Nagssugtoqidian orogen, SW Greenland: a re-examination. Journal of Structural Geology 19, 59–75.

Hanmer, S., Mengel, F., Connelly, J. & van Gool, J.[A.M.] 1997b: Significance of crustal-scale shear zones and synkinematic dykes in the Nagssugtoqidian orogen, SW Greenland: a re-examination. (Corrigendum). Journal of Structural Geology 19, I.

Haslam, H.W. & Walker, B.G. 1971: A metamorphosed pyroxenite at Nero Hill, Central Tanzania. Mineralogical Magazine 38, 58–63.

Healy, B., Collins, W.J. & Richards, S.W. 2004: A hybrid origin for the Lachlan S-type granites: the Murrumbidgee Batholith example. Lithos 78, 197–216.

Henderson, G. 1969: The Precambrian rocks of the Egedesminde–Christianshåb area (sheets 68V.1 and 68V.2). Rapport Grønlands Geologiske Undersøgelse 23, 1–37.

Hickman, M.H. & Glassley, W.E. 1984: The role of metamorphic fluid transport and the Rb-Sr isotopic resetting of shear zones: evidence from Nordre Strømfjord, West Greenland. Contributions to Mineralogy and Petrology 87, 265–281.

Janousek, J., Braithwaite, C.J.R., Bowes, D.R. & Gerdes, A. 2004: Magma-mixing in the genesis of Hercynian calc-alkaline granitoids: an integrated petrographic and geochemical study of the Sazava intrusion, Central Bohemian Pluton, Czech Republic. Lithos 78, 67–99.

Kalsbeek, F. 2001: Geochemical comparison between Archaean and Proterozoic orthogneisses from the Nagssugtoqidian orogen, West Greenland. Precambrian Research 105, 165–181.

Kalsbeek, F., Taylor, P.N. & Henriksen, N. 1984: Age of rocks, structures and metamorphism in the Nagssugtoqidian mobile belt – field and Pb-isotopic evidence. Canadian Journal of Earth Sciences 21, 1126–1131.

Kalsbeek, F., Pidgeon, R.T. & Taylor, P.N. 1987: Nagssugtoqidian mobile belt of West Greenland: a cryptic 1850 Ma suture between two Archaean continents – chemical and isotopic evidence. Earth and Planetary Science Letters 85, 365–385.

Manatschal, G., Ulfbeck, D. & van Gool, J.[A.M.] 1998: Change from thrusting to syncollisional extension at a mid-crustal level: an example from the Palaeoproterozoic Nagssugtoqidian Orogen (West Greenland). Canadian Journal of Earth Sciences 35, 802–819.

Nielsen, B.M. 2004: Crustal architecture and spatial distribution of mineral occurrences in the Precambrian shield of central West Greenland based on geophysical and geological data. Danmarks og Grønlands Geologiske Undersøgelse Rapport 2004/26, 63 pp., 8 appendices. Ph.D. thesis, Department of Earth Sciences, University of Aarhus, Denmark.

Nielsen, B.M & Rasmussen, T.M. 2004: Mineral resources of the Precambrian shield of central West Greenland (66° to 70°15′N). Part 3. Implications of potential field data for the tectonic framework. Danmarks og Grønlands Geologiske Undersøgelse Rapport 2004/21, 165 pp., 1 CD-ROM.

Noe-Nygaard, A. & Ramberg, H. 1961: Geological reconnaissance map of the country between latitudes 69°N and 63°45′N, West Greenland. Meddelelser om Grønland 123, 1–9.

Olesen, N.Ø. 1984: Geological map of Greenland, 1:100 000, Agto, 67 V.1 Nord. Copenhagen: Geological Survey of Greenland.

Passchier, C.W., den Brok, S.W.J., van Gool, J.A.M., Marker, M. & Manatschal, G. 1997: A laterally constricted shear zone system – the Nordre Strømfjord steep belt, Nagssugtoqidian Orogen, W. Greenland. Terra Nova 9, 199–202.

Ramberg, H. 1949: On the petrogenesis of the gneiss complexes between Sukkertoppen and Christianshaab, West Greenland. Meddelelser fra Dansk Geologisk Forening 11, 312–327.

Rasmussen, T.M. & van Gool, J.A.M. 2000: Aeromagnetic survey in southern West Greenland: project Aeromag 1999. Geology of Greenland Survey Bulletin 186, 73–77.

Sørensen, K. 1983: Growth and dynamics of the Nordre Strømfjord Shear Zone. Journal of Geophysical Research 88, 3419–3437.

Sørensen, K. & Winter, J.D. 1989: Deformation and mass transport in the Nordre Strømfjord Shear Zone, Central West Greenland. In: Bridgwater, D. (ed.): Fluid movements – element transport and the composition of the deep crust, 171–185. Amsterdam: Kluwer Academic Publishers.

Steenfelt, A., Stendal, H., Nielsen, B.M. & Rasmussen, T.M. 2004: Gold in central West Greenland – known and prospective occurrences. Geological Survey of Denmark and Greenland Bulletin 4, 65–68.

Stendal, H., Nielsen, B.M., Secher, K. & Steenfelt, A. 2004: Mineral resources of the Precambrian shield of central West Greenland (66° to 70°15′N). Part 2. Mineral occurrences. Danmarks og Grønlands Geologiske Undersøgelse Rapport 2004/20, 212 pp.

Stendal, H., Secher, K. & Frei, R. 2006: ^{207}Pb-^{206}Pb dating of magnetite, monazite and allanite in the central and northern Nagssugtoqidian orogen, West Greenland. In: Garde, A.A. & Kalsbeek, F. (eds): Precambrian crustal evolution and Cretaceous–Palaeogene faulting in West Greenland. Geological Survey of Denmark and Greenland Bulletin 11, 101–114 (this volume).

Stephensen, N.C.N. & Hensel, H.D. 1979: Intergrown calcic and Fe-Mg amphiboles from the Wongwibinda metamorphic complex, N.S.W., Australia. Canadian Mineralogist 17, 11–23.

van Gool, J.A.M., Kriegsman, L.M., Marker, M. & Nichols, G.T. 1999: Thrust stacking in the inner Nordre Strømfjord area, West Greenland: Significance for the tectonic evolution of the Palaeoproterozoic Nagssugtoqidian orogen. Precambrian Research 93, 71–86.

van Gool, J.A.M., Connelly, J.N., Marker, M. & Mengel, F.C. 2002: The Nagssugtoqidian Orogen of West Greenland: tectonic evolution and regional correlations from a West Greenland perspective. Canadian Journal of Earth Sciences 39, 665–686.

van Gool, J.A.M. & Marker, M. 2004: Geological Map of Greenland, 1:100 000, Ussuit, 67 V.2 Nord. Copenhagen: Geological Survey of Denmark and Greenland.

Manuscript received 5 November 2004; revision accepted 1 November 2005

Structural analysis of the northern Nagssugtoqidian orogen, West Greenland: an example of complex tectonic patterns in reworked high-grade metamorphic terrains

Stanislaw Mazur, Sandra Piazolo and G. Ian Alsop

Structural analysis of the deeply eroded northern flank of the Palaeoproterozoic Nagssugtoqidian orogen shows marked regional variations in both the orientation and type of fabrics, as is characteristic of Precambrian high-grade terrains subjected to polyphase deformation. Here we investigate the relationship between strain, metamorphic grade, and the resulting structural patterns. The study area south of Aasiaat in West Greenland consists of amphibolite- to granulite-grade Archaean orthogneisses and relatively thin supracrustal units. The regional foliation displays a WSW–ENE to SW–NE strike associated with steep to moderate dips towards the WNW or SSE. Lineation trends are WSW–ENE and generally plunge gently towards the WSW. Mesoscopic fold hinges are usually colinear with the regional lineation. A systematic change in the plunge of lineations occurs across the south-western part of the study area. Towards the south, the lineation plunge progressively increases, despite the generally uniform strike of foliation. This southward increase of lineation pitch is typically associated with the transition from L > S or L = S shape fabrics in rocks characterised by a low pitch, to S > L or S fabrics in the zone of moderate to high pitch. The structural patterns point to subdivision of the study area into a southern domain mostly characterised by S or S > L shape fabrics and a moderate to high angle of lineation pitch, and a northern domain showing L > S or L = S fabrics and low angles of lineation pitch. This subdivision corresponds well with the map scale boundary between granulite facies rocks in the south and amphibolite facies rocks farther north. The observed structural pattern may be explained by two alternative tectonic models: (1) northward indentation of the previously cooled granulite block into the rheologically weaker amphibolite domain, and (2) strain partitioning within a mid-crustal transpression zone. In model 2 the northern domain represents a localised zone dominated by strike-slip kinematics, whereas the southern domain shows evidence of mostly coaxial shortening. Recent geochronology supports the indentator model in spite of limited available data. Despite the details and structural complexities of the two tectonic models, the granulite and amphibolite facies domains seem to form autochthonous segments of a crustal section linked by a transitional zone that was only reactivated and reworked during indentation or transpression. The Nagssugtoqidian compression was effectively transferred across this zone towards the northern amphibolite domain that suffered penetrative deformation during the Palaeoproterozoic event. The N–S shortening was accommodated through folding, indentation and/or strike-slip displacements, rather than by thrusting and folding as seen south of the study area.

Keywords: deformation, GIS, Nagssugtoqidian orogen, transpression, indentation tectonics, West Greenland

S.M., *Institute of Geological Sciences, University of Wroclaw, Maxa Borna 9, 50-204 Wroclaw, Poland.*
E-mail: *smazur@ing.uni.wroc.pl*
S.P., *Geological Survey of Denmark and Greenland, Øster Voldgade 10, DK-1350 Copenhagen K, Denmark.* Present address: *Department of Geology and Geochemistry, Stockholm University, 10691 Stockholm, Sweden.*
G.I.A., *School of Geography and Geosciences, University of St. Andrews, Fife KY16 9AL, UK.*

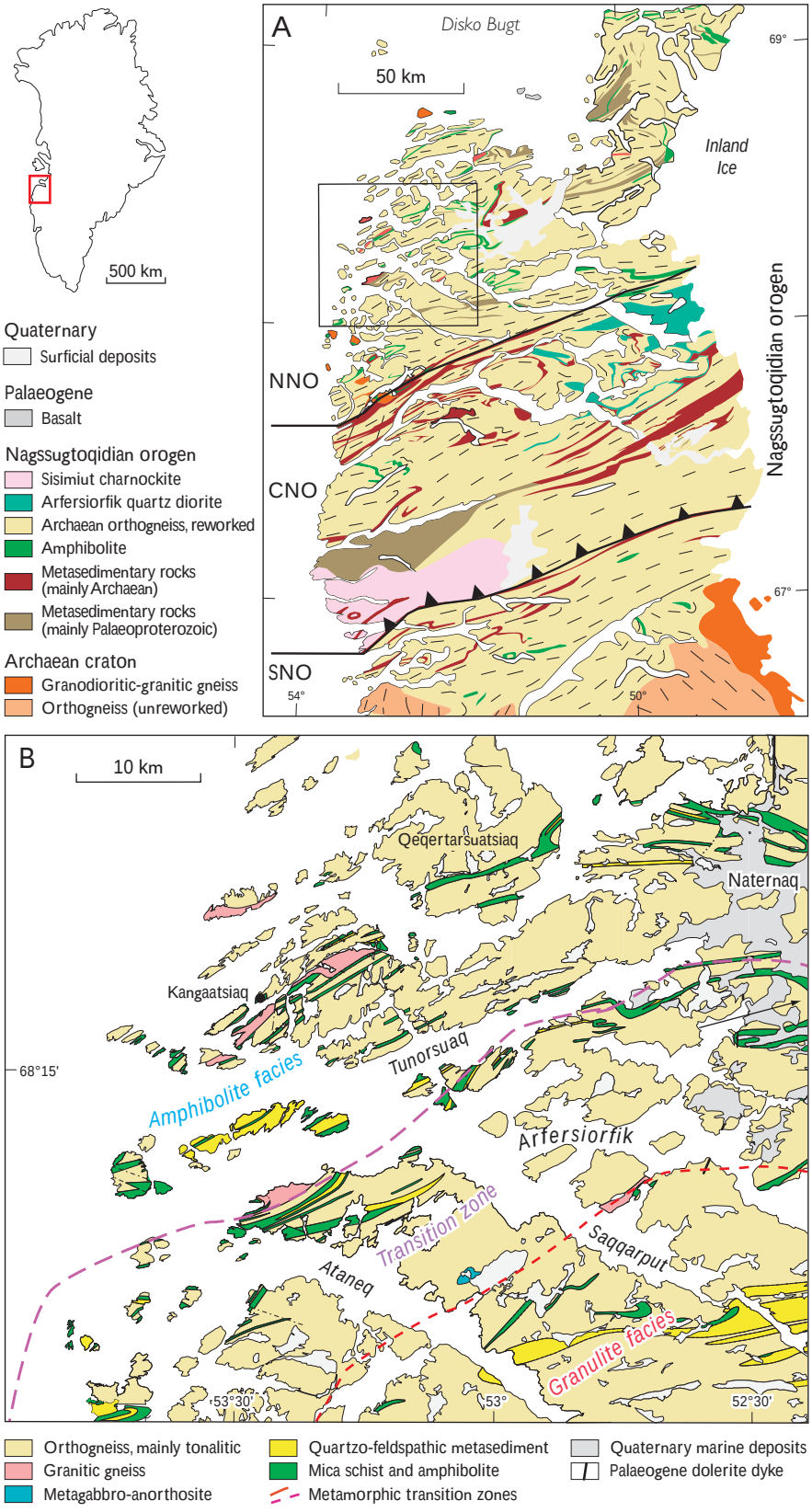

Fig. 1. A: Schematic geological map of the Nagssugtoqidian orogen and adjacent foreland (modified from van Gool *et al*. 2002b). Outlined box shows location of the study area. SNO, southern Nagssugtoqidian orogen; CNO, central Nagssugtoqidian orogen; NNO, northern Nagssugtoqidian orogen. B: Simplified geological map of most of the study area (modified from van Gool *et al*. 2002a).

The deeply eroded northern flank of the Palaeoproterozoic Nagssugtoqidian orogen is exposed south of Aasiaat in central West Greenland (Fig. 1). These rocks bear record of tectono-thermal processes that operated at mid-crustal levels in a collisional setting and controlled the distribution of strain and metamorphic facies. The area shows a complex structural pattern that varies significantly from south to north. The aim of this work is to describe the regional variation of structural elements and to investigate the relationship between strain, metamorphic grade and the orientation of deformational structures. This then leads to the consideration of two different tectonic models, which have been developed to account for the observed structural pattern: (1) an indentor model proposed originally by Piazolo *et al.* (2004), and (2) a transpression zone model.

The study area covers the Kangaatsiaq geological map sheet at scale 1:100 000 (Garde 2004), mapped in 2001–2002 by the Geological Survey of Denmark and Greenland (GEUS; van Gool *et al.* 2002b). The directional and fabric type structural data sets were analysed using Geographic Information Systems (GIS) based techniques that proved to be a powerful tool in the investigation of complex structural patterns. Some of the structural data collected during this field campaign were presented by Piazolo *et al.* (2004) to illustrate the application of GIS in a multidisciplinary approach to survey high-grade terrains. Our present study focuses on a more detailed analysis and interpretation of the structural relationships of the investigated area, a high-grade Precambrian terrain affected by more than one deformation phase, and whose interpretation is not unequivocal.

Geological setting

The study area covers over 3000 km^2, and extends from 68°N–68°30′ N and 52°W–53°15′ W, between the fjord of Ataneq in the south and the island of Qeqertarsuatsiaq in the north (Fig. 1). The area comprises the northern, *c.* 300 km wide exposure of the roughly E–W-trending Nagssugtoqidian orogen (Fig. 1). In the broadest sense, this tectonic belt resulted from a continent–continent collision between the Archaean North Atlantic Craton to the south and an Archaean continental mass to the north (e.g. Kalsbeek *et al.* 1987; Connelly *et al.* 2000; van Gool *et al.* 2002a). The orogen is generally characterised by E–W-trending kilometre-scale folds and ENE–WSW-trending linear belts which overprint an Archaean fabric. On the basis of the grade of metamorphic reworking, Ramberg (1949) and later Marker *et al.* (1995) distinguished southern, central and northern segments of the Nagssugtoqidian orogen (SNO, CNO and NNO respectively; Fig. 1). Detailed structural investigations within the CNO show that deformation in this area is dominated by thrust tectonics (Manatschal *et al.* 1998; van Gool *et al.* 1999).

The investigated area lies within the NNO and is composed of amphibolite- to granulite-grade Archaean orthogneisses interlayered with relatively thin metasedimentary units (Fig. 1). This region is transected by major fjord systems that allow data collection along well-exposed coastal sections. Reconnaissance studies (Noe-Nygaard & Ramberg 1961; Henderson 1969; Marker *et al.* 1995; Kalsbeek & Nutman 1996; Mengel *et al.* 1998; Connelly *et al.* 2000) provided initial information on the structural style of the study area. A comprehensive description of the structural pattern was recently presented by Piazolo *et al.* (2004) and interpreted in terms of indentor tectonics with a rigid granulite-grade domain moving northwards into a rheologically weaker amphibolite facies domain.

Although quartzofeldspathic orthogneiss dominates in the investigated area, the overall map pattern is governed by discontinuous NE–SW-trending supracrustal belts (Fig. 1). These 2–3 km thick sequences comprise several distinct lithological types: (a) monotonous, garnet-bearing quartzofeldspathic paragneiss locally containing subordinate mafic volcanic and metapelitic intercalations; (b) pelitic to semipelitic schist with or without garnet and sillimanite, including thin quartzofeldspathic layers and rarely quartzite; and (c) layered mafic to intermediate metavolcanic successions with calc-silicate bands and/or pods.

Previous studies have demonstrated that the metamorphic grade of the NNO decreases northwards and is predominantly amphibolite facies, with granulite facies rocks preserved only in the south-western corner of the study area near the boundary with the CNO (e.g. Marker *et al.* 1995). The contact between these two facies is transitional over a distance of 10–12 km and forms a zone nearly parallel to the strike of the regional foliation (Fig. 1). The granulite facies gneisses are typically pyroxene-bearing and enclose frequent melt pockets and cross-cutting veins. Thermobarometric analyses point to a peak temperature of 800 ± 30°C at medium pressures of 6–7.5 kbar (Piazolo *et al.* 2004). The amphibolite facies gneisses are lighter coloured and contain fewer biotite-bearing melt veins. They reveal peak metamorphism conditions of 650 ± 30°C at 4–5 kbar (Piazolo *et al.* 2004). Within the supracrustal amphibolites, crystallisation of amphibole, usually developed along foliation planes, indicates a syntectonic fluid flux and associated metamorphism. No relics of earlier granulite facies assemblages are preserved in these rocks. Thrane & Connelly (2006, this volume) carried out seve-

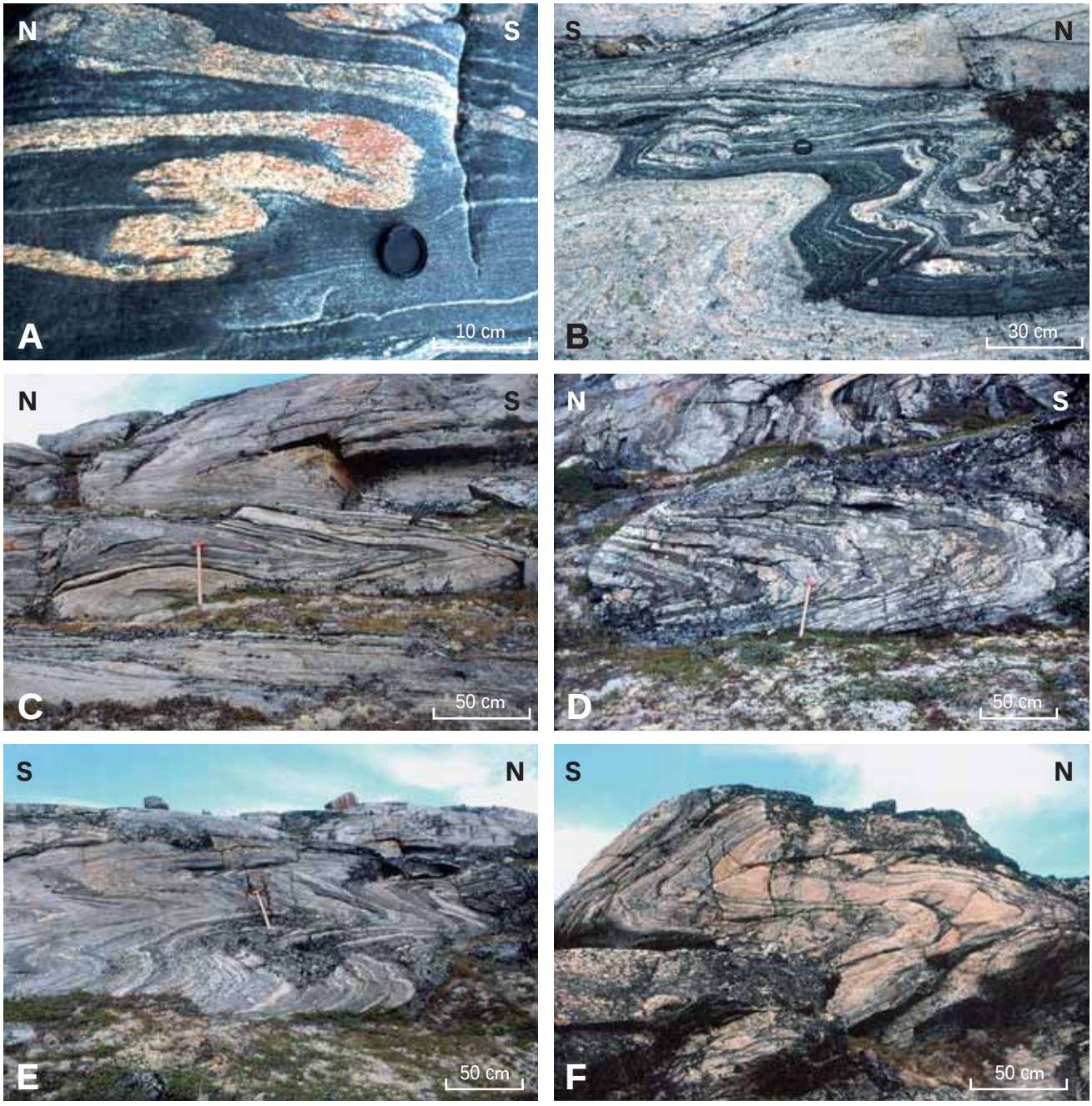

Fig. 2. Examples of mesoscopic folds in the orthogneisses and metasediments of the study area. A: Main foliation S_1 of orthogneiss developed parallel to the axial plane of isoclinal F_1 fold. B: Lithological boundaries and originally cross-cutting basic dykes folded by F_1 isoclinal fold and showing extensive migmatisation. C: S_1 foliation folded into isoclinal folds during the same progressive D_1 event. D: S_1 foliation and its subsequent folding accompanied by pervasive migmatisation. E: S_1 foliation locally folded by F_3 folds of variable geometry with fold axes developed subparallel to the lineation. F: S_1 foliation of the orthogneiss folded by the F_3 fold with fold axes parallel to the lineation and S-directed asymmetry. N, north; S, south.

ral laser ablation and ion probe age determinations of zircon from within and adjacent to the present study area. Deformation in the south-western part of the area is constrained by the emplacement age of 2748 ± 19 Ma for a synkinematic granite which intrudes the orthogneiss. A Palaeoproterozoic deposition age of *c*. 1950 Ma was obtained from a metasediment within the Naternaq supracrustal belt (Fig. 1), and broad rims of zircons from an Archaean sediment from Kangersuneq yielded a metamorphic age of *c*. 1850 Ma, suggesting that major Nagssugtoqidian deformation and metamorphism occurred at around this time. Thrane & Connelly (2006, this volume) also obtained an age of 1837 ± 12 Ma for a vertical, straight pegmatite north-east of Kangaatsiaq trending 020° and displaying sinistral shear along its margins, that is thought to date a late phase of overall N–S-directed Palaeoproterozoic shortening.

Characteristics of directional structures

The main foliation (S_1) is axial planar to rare isoclinal F_1 folds that fold lithological boundaries as well as cross-cutting basic dykes (Fig. 2A). These dykes have been rotated into parallelism with the foliation on the fold limbs (Fig. 2B). The S_1 foliation was itself later folded into isoclinal folds, although this refolding may reflect the same progressive D_1 deformation event since no overprinting fabric is associated with it (Fig. 2C). A characteristic feature of these folds is the broad parallelism of their axial planes to the regional foliation S_1. A L_1 mineral lineation is developed on the foliation planes and is usually defined by a parallel alignment of amphibole crystals and/or elongated quartz-feldspar and biotite aggregates. The lineation is well developed in the amphibolite facies rocks but rather weak in the granulite facies gneisses. In the transition zone between the amphibolite and granulite domains (Fig. 1B), no mutually cross-cutting mineral lineations were detected and no evidence for fabric superimposition was observed. The L_1 lineation is only rarely associated with kinematic indicators that are commonly symmetric and must have resulted from coaxial strain and/or a finite strain combining the effects of several strain increments. Asymmetric fabrics have been observed only in zones of steeply dipping foliation, and typically indicate a sinistral rotational shear component in the present-day coordinates (Fig. 3). Restoration of the steep foliation attitude to more gentle regional dips would result in the same indicators implying a top-to-the-west or WSW sense of shear.

The S_1 foliation and its subsequent folding during the presumed progressive D_1 event, were accompanied by a

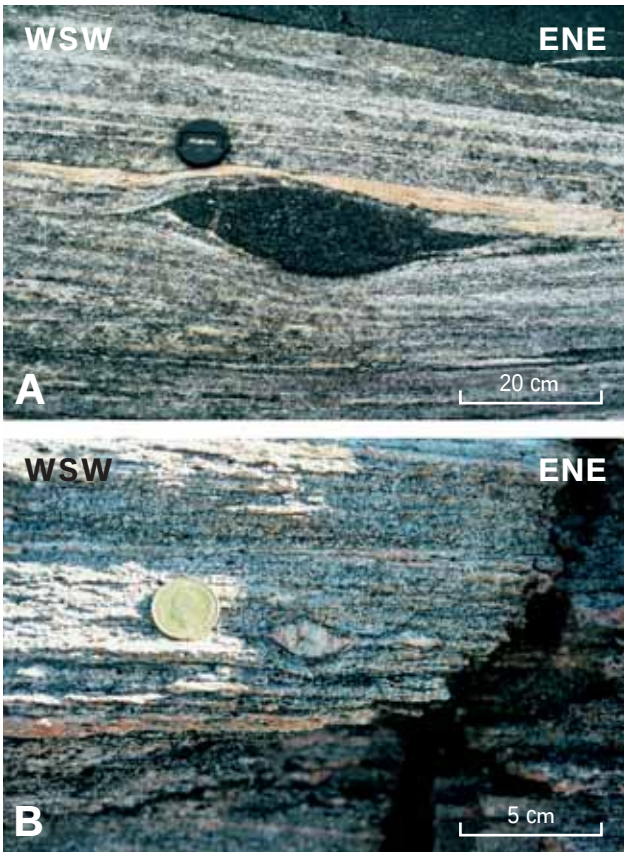

Fig. 3. Examples of sinistral (top-to-the WSW) kinematic indicators in the orthogneisses of the study area. The lineation is plunging towards WSW on north-dipping foliation planes. A: Sheared, asymmetric amphibolite enclave. B: Sigmoidal K-feldspar porphyroclast.

long-lasting pervasive migmatisation. This is demonstrated by the common occurrence of migmatite layers or patches that are variably deformed and show mutually cross-cutting relationships. Some of them are parallel to the main foliation S_1 (Fig. 2D) whereas others define discordant veins or dykes oblique to the regional fabric. Between these two end members are a range of cross-cutting veins that are deformed and reoriented to varying degrees. In the metasedimentary rocks of the Naternaq (Lersletten) area, the S_1 regional foliation is refolded by F_2 folds characterised by steep to subvertical fold hinges. These folds are developed at kilometre- to centimetre-scale and, in a few cases, map scale F_2 folds can be seen refolding F_1 (A.A. Garde & J.A. Hollis, personal communication 2003). F_2 folds are found exclusively within the metasedimentary belts and at their contacts with the adjacent gneisses. At a mesoscopic scale, they are represented by folds plunging steeply towards the SE and in few cases towards the north. A moderate to strong, SE-plunging mineral lineation is associated with the hinges of F_2 folds, locally deviating

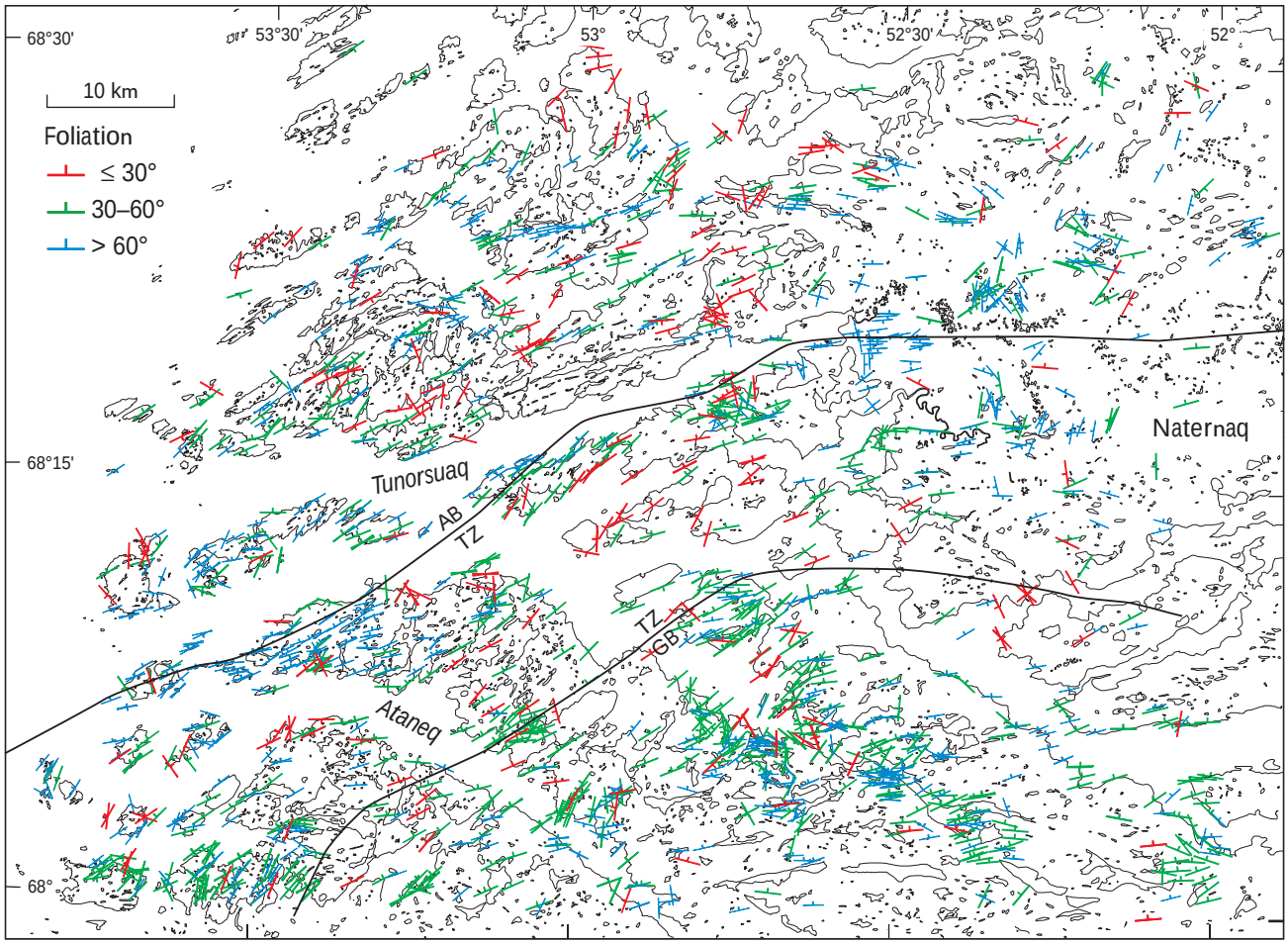

Fig. 4. Representation of foliation trends and dip directions in the study area. GB, granulite block; TZ, transition zone; AB, amphibolite block.

from its regional trend although it remains the only lineation present. An S_2 cleavage axial planar to F_2 is rarely, and only weakly, developed. Beyond Naternaq, the S_1 foliation is refolded by F_3 folds of variable, often complex geometry with gently plunging fold axes developed subparallel to the L_1 lineation (Fig. 2E). The frequency of such folds increases northwards within the amphibolite-grade rocks. Associated F_3 axial planes are locally marked by a subtle S_3 cleavage, accentuated by local mica aggregates and discrete joints which cut the main S_1 foliation. The distinction between F_2 and F_3 folds is primarily based on their different geometries since they both fold the regional fabric S_1 and are not associated with penetrative axial cleavages or intersection lineations. The hinges of F_2 folds are relatively steep and oblique to the regional lineation, whereas F_3 axes are gently inclined and run parallel to the lineation L_1. The F_3 mesoscopic folds are frequently asymmetric with fairly uniform SSE vergence in the area south and west of Kangaatsiaq (Fig. 2F).

Orientation of directional structures

On the map scale, the regional foliation displays a WSW–ENE to SW–NE strike associated with steep to moderate dips towards the NNW or SSE (Fig. 4). Shallow-dipping foliations (< 30°) are rare and randomly distributed throughout the study area. Their variable directions suggest that they are associated with the hinge zones of F_3 folds developed at different scales (Fig. 4). Moderately and steeply dipping foliations show a distinctly discrete grouping within the investigated area. The former predominate in the south-eastern corner of the area, corresponding with the granulite-grade block, whereas the steeply dipping foliations are developed in its central part, forming a wide belt along Tunorsuaq (Fig. 4). This belt coincides with a transition zone between the granulite and amphibolite facies domains and partly with the south-eastern margin of the latter (see Figs 1, 4). The strike of foliation dipping steeper than 30° remains fairly consistent throughout the area, while the dip direction varies only in the case of sub-

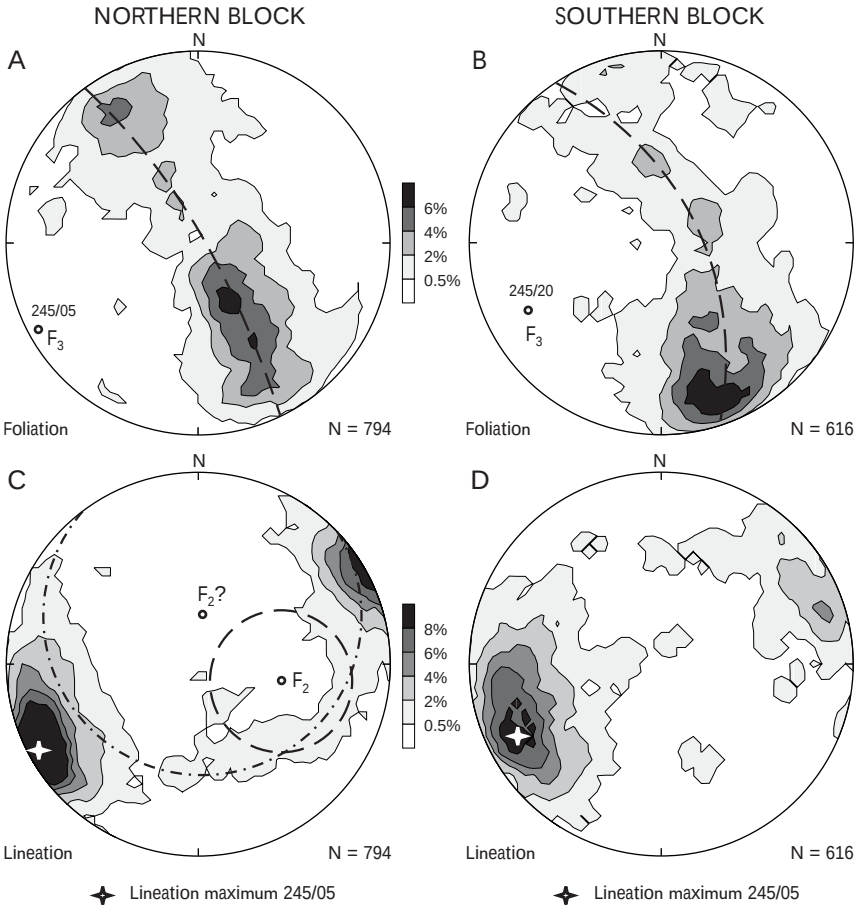

Fig. 5. Attitudes of foliation S_1 and stretching lineation L_1 in the northern amphibolite facies block (A, C), and southern granulite facies block (B, D). The positions of the poles to the foliation girdles and maximum of lineation measurements are indicated in stereoplots A, B and C, D, respectively.

vertical planes (> 60°). On stereoplots, the poles to foliation are scattered along a regular girdle produced by the F_3 folds (Fig. 5).

In the southern granulite facies block the vast majority of foliation measurements cluster in one maximum, suggesting that late folding is insignificant or absent in this area (Fig. 5). This maximum corresponds to the foliation dipping moderately to steeply towards the NNW, while the axis of the foliation girdle plunges gently to the WSW at 20°. In the northern, amphibolite facies block measurements are more evenly distributed along the foliation girdle, providing evidence for the regional importance of F_3 folding (Fig. 5). In contrast to the southern block, the stereographic girdle axis is almost subhorizontal. Although the foliation patterns in the southern and northern blocks are fairly similar, a striking difference occurs within the latter between the rheologically competent orthogneisses and relatively incompetent supracrustal formations (Fig. 6). The orthogneisses reveal a regular girdle perfectly controlled by a cylindrical geometry of the F_3 folds. In contrast, the less competent supracrustal rocks display a pronounced foliation scatter, reflecting a complex interference between the effects of the (possibly noncylindrical) F_2 and F_3 folding.

The lineation trends WSW–ENE over the whole study area, and frequently plunges gently towards the WSW (Fig. 7). Shallow lineations (< 15°) are concentrated in the northern and central parts of the investigated area (Fig. 7), and commonly coincide with the subvertical foliation within the amphibolite facies block and the associated transition zone towards the granulite facies block. Conversely, lineations plunging steeper than 15° group largely in the south-eastern corner of the area, corresponding with the granulite block, and show mostly WSW-directed plunges. Mesoscopic F_3 fold hinges are usually colinear with the regional lineation, and this is also the case at the larger scale since the lineation maxima are located near the pole of the foliation girdle on stereoplots (cf. Fig. 5). In the amphibolite facies block, the lineation is shallow and relatively well grouped in the maximum representing the subhorizontal WSW–ENE trend. A significant scatter occurs only in the Naternaq area, which is displayed on the map by relatively steeply plunging lineations (Fig. 7) and on stereoplots by data distribution along a small cir-

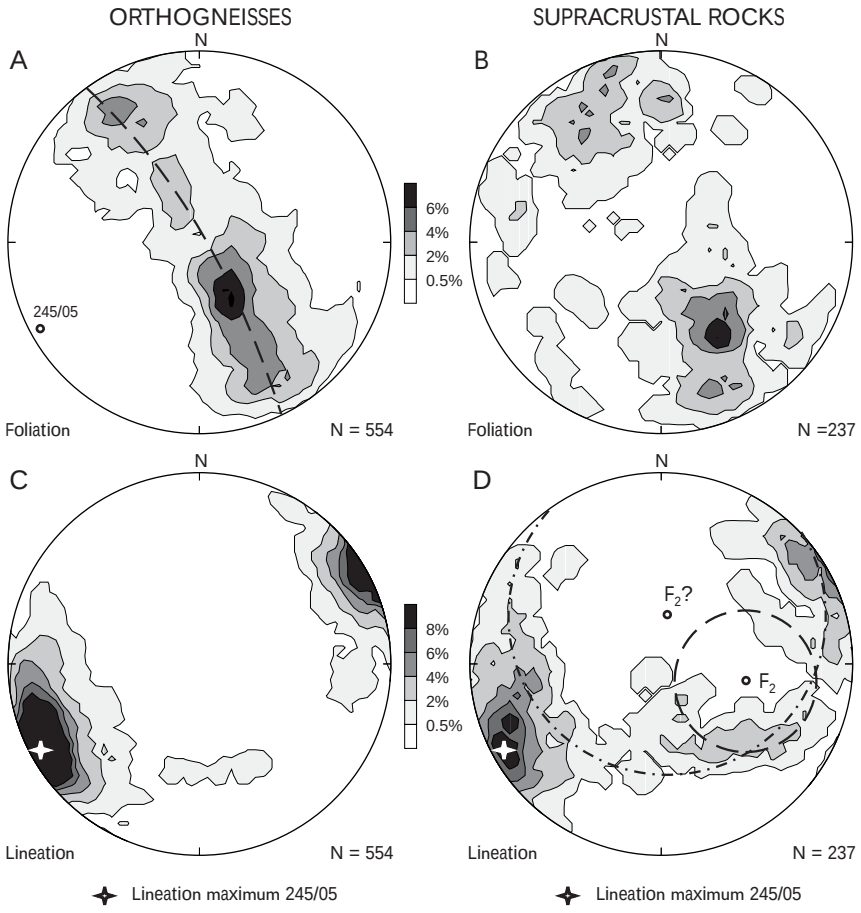

Fig. 6. Attitudes of foliation (S_1) and stretching lineation (L_1) in the orthogneisses (A, C) and supracrustal rocks (B, D) of the northern amphibolite facies block. The position of the pole to the foliation girdle and maximum of lineation measurements are indicated in stereoplots A and C, D, respectively.

cle (Fig. 5). A dispersal of lineation measurements is produced in that area by steeply plunging F_2 fold hinges whose orientation corresponds to the centre of a small circle defined by the scatter of the lineation (Fig. 5). Two different small circles can be delineated on the stereoplot (Fig. 5) based on the lineation scatter. One is centred at the orientation of F_2 hinges steeply inclined to the SE that are relatively frequent as mesoscopic structures. The second is developed around the nearly vertical north-plunging F_2 hinges rarely found in the outcrops but probably important at the map scale. The lineation scatter induced by the F_2 folding is very clear in the supracrustal rocks, whereas it is almost absent in the orthogneisses (Fig. 6). This relationship is consistent with the field observation that the F_2 folds are developed almost exclusively in the metasediments. In the southern block the lineation is slightly steeper than in the north and shows a mean plunge of *c.* 20°. Its maximum is more diffuse than in the amphibolite-grade block and more lineations are relatively steep (> 15°). Nevertheless, the average lineation trend defined by the position of maxima on stereoplots is exactly the same for the amphibolite and granulite facies domains (Fig. 5).

In order to better understand the geometric relationships between planar and linear fabric elements during deformation, they may be directly compared on fabric topology plots in terms of fabric trends and lineation pitch (see Alsop & Holdsworth 2004 for a review). The angle of pitch may be defined as the angle that a line makes with the strike of a surface, when measured within that plane (Fig. 8A). A significant variation in the angle of lineation pitch on the regional foliation surface is observed (Fig. 8B); this may be caused by two independent factors: (1) variable plunge of the lineation, and (2) variable dip direction of the foliation. The latter feature seems to be a consequence of local folding, since a high pitch angle (> 45°) is most characteristic for SW-dipping foliations (Fig. 9) that represent the hinges of F_3 folds (Fig. 5). On the other hand, a majority of measurements correspond to foliation dipping to the NW or SE that reveals a low or moderate pitch angle (Fig. 9). Such a foliation pattern is consistent with the regional attitude of foliation inclined towards the NW and only locally reoriented on limbs of the F_3 folds. Since the F_3 folds are only of minor significance in the southern part of the study area characterised by higher pitch values (Fig. 8), and the majority of lineations were measured on steep to subvertical foliation sur-

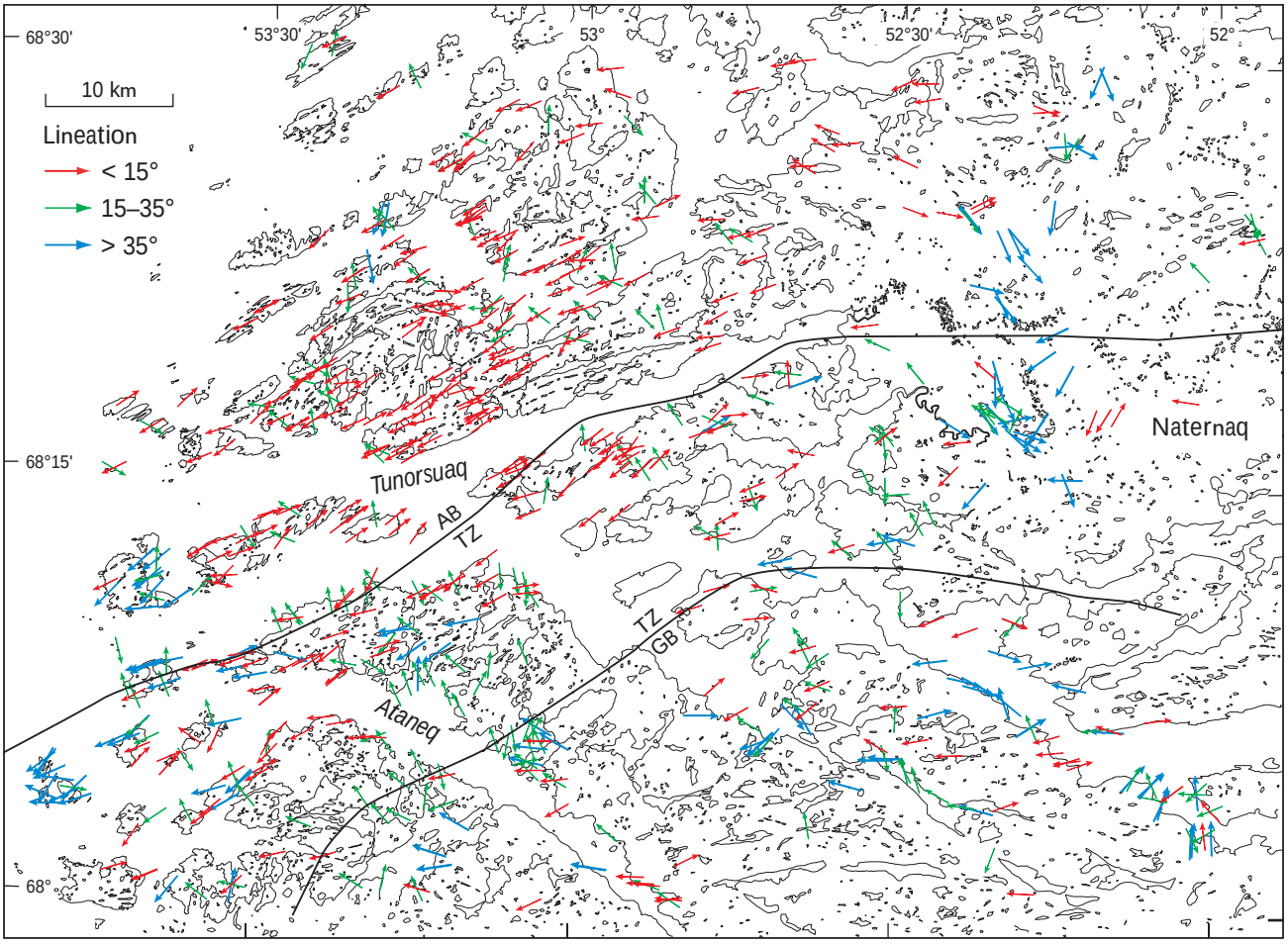

Fig. 7. Representation of lineation trends and plunge directions of the study area. GB, granulite block; TZ, transition zone; AB, amphibolite block.

faces, the broad scatter of the pitch angles can be attributed to variations in the lineation plunge (Fig. 10). Only a minority of measurements plot away from the line that indicates the similarity of pitch and plunge angles (Fig. 10). Thus, the change of foliation strike plays a less important role in the distribution of pitch angles. The low pitch angle (< 15°) is characteristic of the central and northern parts of the study area (Fig. 8), corresponding to the amphibolite facies block and the transition zone to the granulite facies block. This is the area that is additionally characterised by the steep foliations and shallow lineation plunge. The higher pitch angles (exceeding 15°) are more common in the south-east corner of the study area within the granulite facies gneisses, where they are related to relatively steep lineations occurring on the moderately to steeply inclined foliation.

A systematic change in the plunge of lineations can be observed across the south-western part of the study area (Fig. 7). The steep SW–NE-striking foliation around Tunorsuaq is associated with the gently plunging lineation that defines a low angle of pitch on the foliation. Towards the south, however, the plunge of lineation becomes progressively steeper despite the generally uniform strike of foliation (Fig. 4). A pitch versus lineation trend diagram (Fig. 11) demonstrates that the increase in pitch is unrelated to the change of lineation trend. This means that lineations are typically not reoriented on fold limbs, and that folds, if present, are mostly colinear with lineation. Furthermore, in the north-western part of the area the lineations plunge gently to the SW and NE to define a series of culminations and depressions, that are clearly illustrated by the opposing plunges on the south side of Tunorsuaq and the outer islands to the west-south-west (Fig. 7). This sinuosity of lineations and associated fold hinges defines a large-scale whaleback pattern consistent with a dominantly subhorizontal and approximately N–S contractional strain (cf. Piazolo *et al.* 2004).

The finite planar (S) and linear (L) shape fabrics within a high-strain rock may be qualitatively described (Flinn 1978). Consequently, the relative dominance of these re-

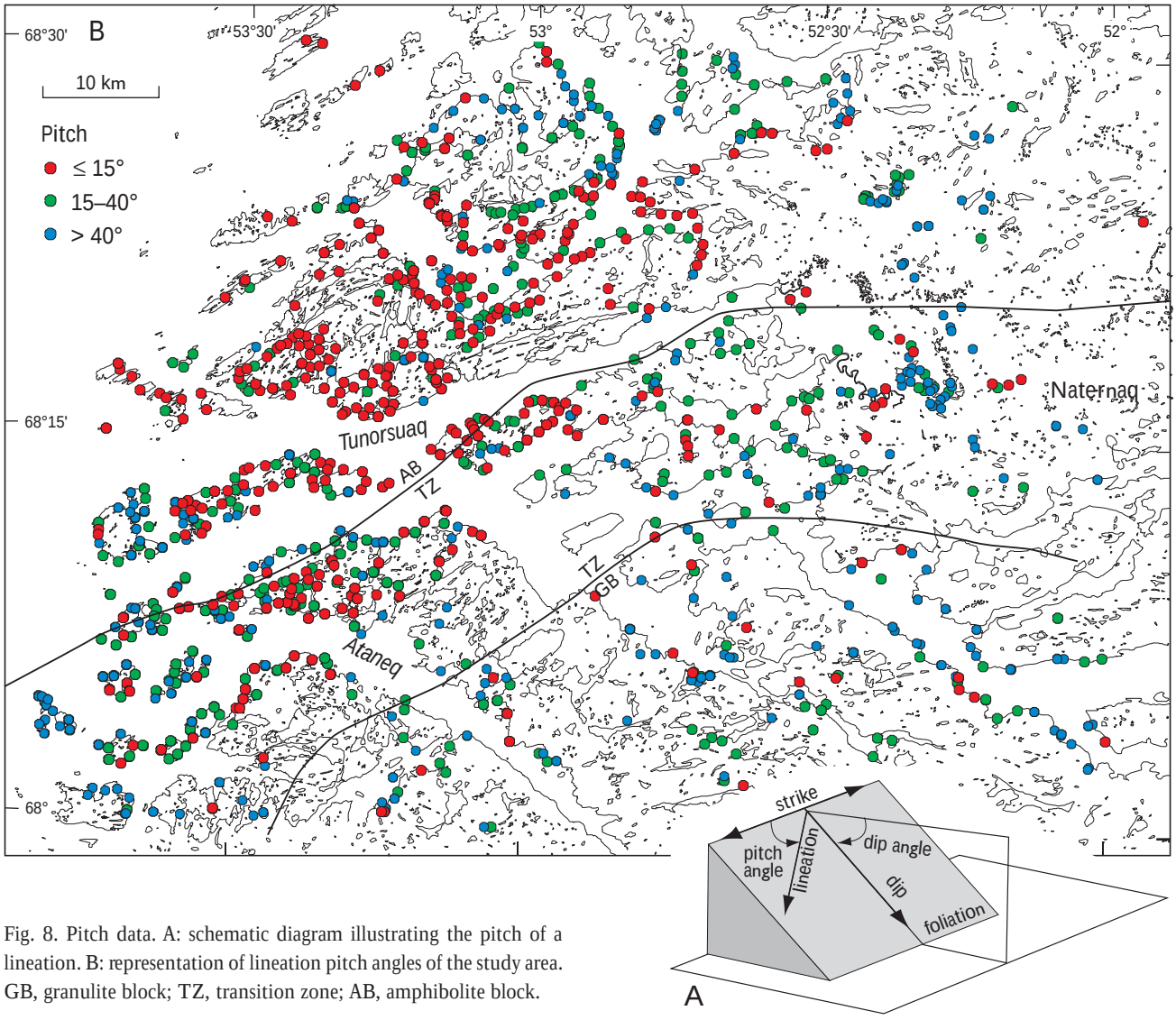

Fig. 8. Pitch data. A: schematic diagram illustrating the pitch of a lineation. B: representation of lineation pitch angles of the study area. GB, granulite block; TZ, transition zone; AB, amphibolite block.

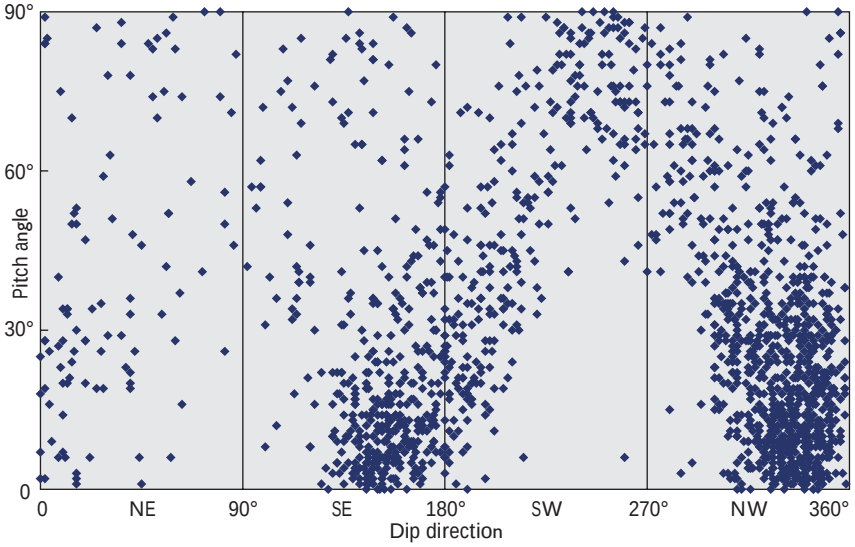

Fig. 9. Plot of lineation pitch angle vs. dip direction of foliation, showing the change of pitch as a consequence of local folding.

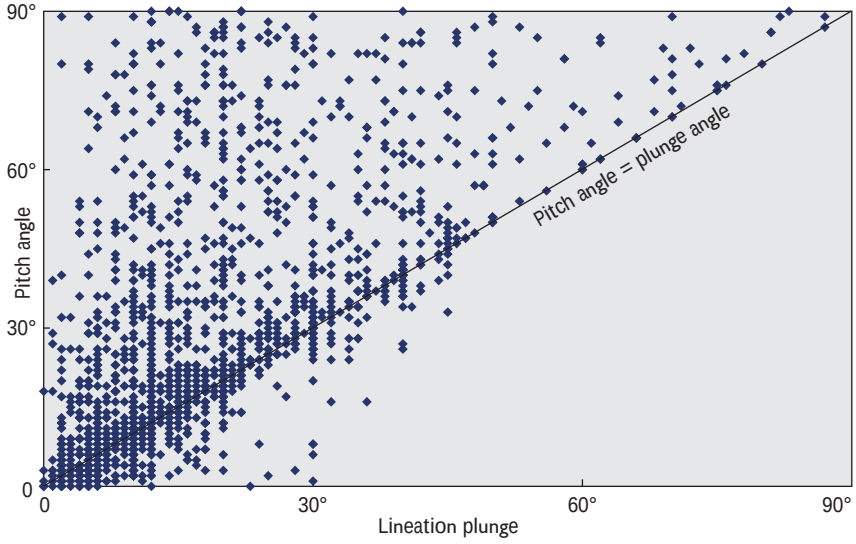

Fig. 10. Plot of lineation pitch angle vs. lineation plunge, showing the contribution of changing lineation plunge to the total variation of pitch. Measurements located on the straight line connecting the lower left and upper right corners of the plot have been taken on vertical foliation planes.

spective components enables a distinction to be made between fabrics that are foliation dominated (S tectonite), lineation dominated (L tectonite) or contain a combination of foliation and lineation (SL tectonite). The pattern shown by the spatial distribution of fabric types in the study area is clearly differentiated. The north-western part of the area is dominated by LS and L > S fabric types whereas the south-eastern part reveals a vast preponderance of S or S > L types (Fig. 12). The southward increase of lineation pitch is typically associated with the transition from L > S or LS shape fabrics in rocks characterised by a low pitch, to S > L or S fabrics in the zone of moderate to high pitch. Constrictional fabrics, i.e. L and L > S fabrics, are typical of rocks with shallowly plunging lineations on the steep foliation belonging to the amphibolite facies block and the transition zone to the granulite facies block. The latter is dominated by the flattening fabric types, i.e. S and S > L fabrics, which are common in rocks containing steeply plunging lineations.

Discussion

Three main observations can be made concerning the data presented above: (1) structural elements, i.e. lineations, foliations, folding and fabric type, vary with lithology, (2) two broad domains with different structural patterns can be distinguished, and (3) the structural style in the NNO is markedly different to that previously described from the CNO, e.g. by Manatschal *et al.* (1998) and van Gool *et al.* (1999).

The observed scarcity of mineral lineations in the gran-

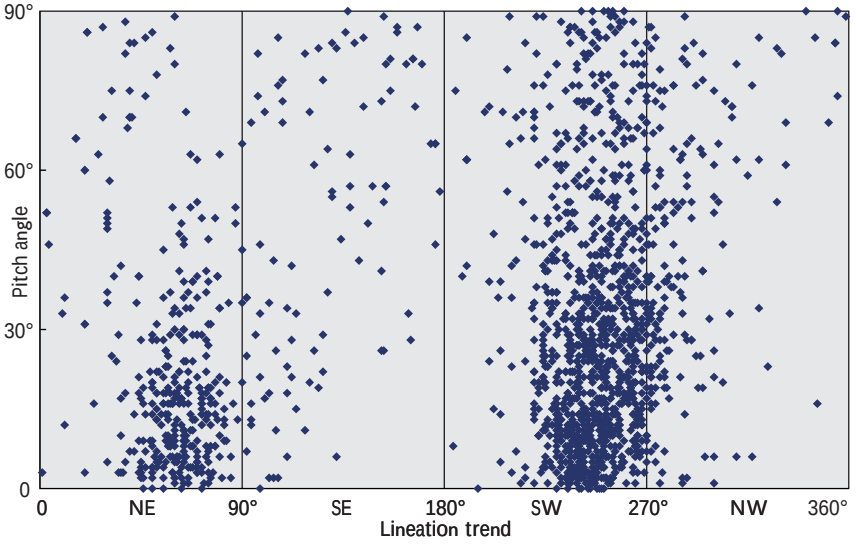

Fig. 11. Plot of lineation pitch angle vs. lineation trend, showing the variation of pitch despite the uniform trend of lineation.

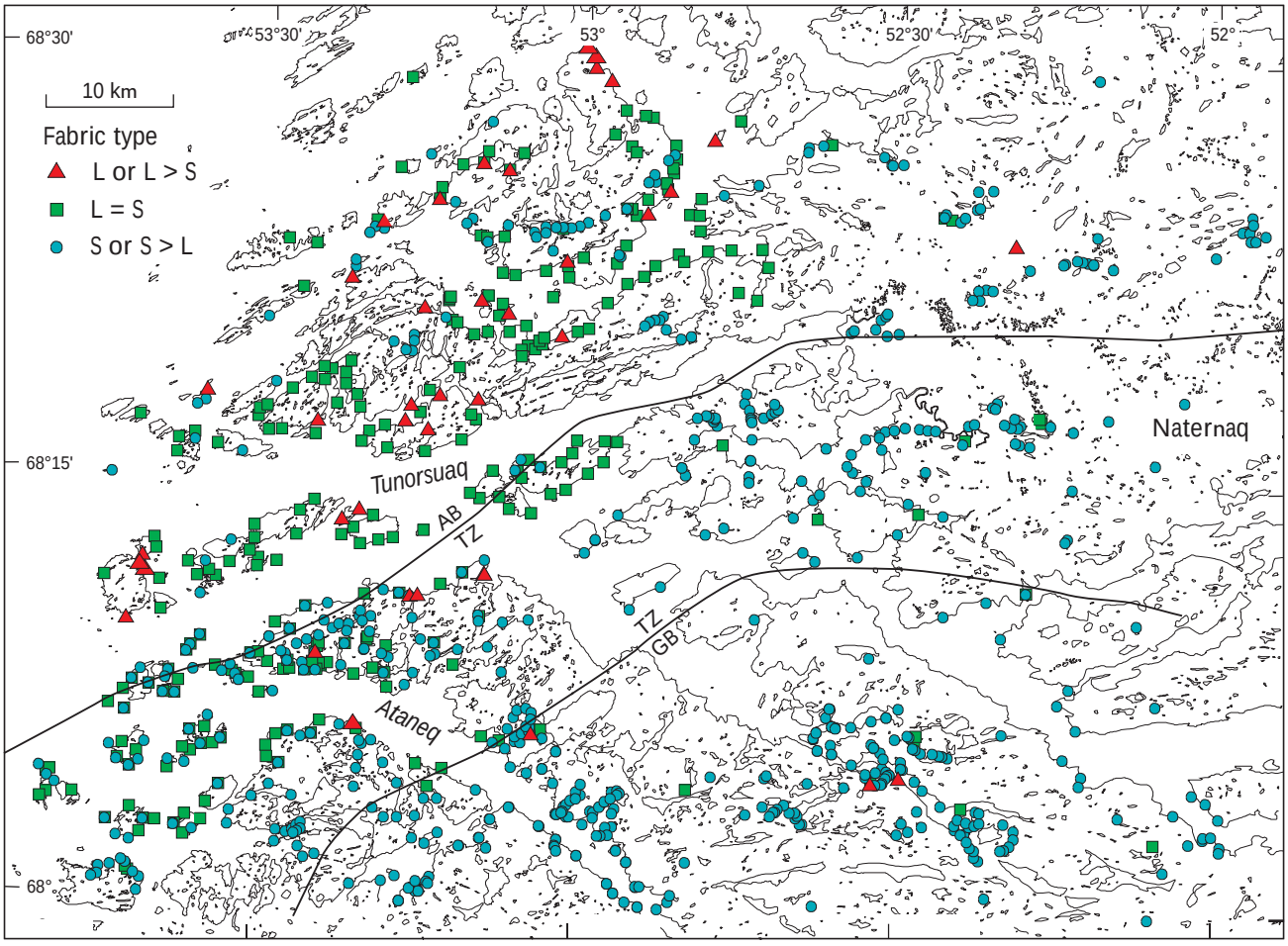

Fig. 12. Spatial distribution of fabric types (terminology af Flinn 1978). GB, granulite block; TZ, transition zone; AB, amphibolite block.

ulite facies gneisses could be attributed to the absence of minerals with a high shape aspect ratio. If such minerals are lacking, lineations of the type that forms by rigid rotation or due to growth parallel to the maximum extension direction or transport direction can hardly develop. Nevertheless, aggregate lineations that form by dynamic recrystallisation and material transfer should be expected in the granulite facies gneisses. Since even these lineations are lacking in the southern block, it seems that the scarcity of linear structures in this area is not only a function of lithology but also reflects specific features of deformation history. In the northern block, a significant strain partitioning between orthogneisses and supracrustal formations is indicated by the effects of F_2 folding in metasedimentary rocks and the resultant scatter of foliation and lineations in these rocks (Fig. 6). This points to the concentration of deformation in rheologically weak metasedimentary belts that accommodate the bulk of strain induced during F_2 folding. The competent orthogneisses experienced only subsequent F_3 folding, when they were deformed together with associated less competent supracrustal rocks.

At the western limb of the Naternaq supracrustal belt, there is a structural discordance with another E–W-trending supracrustal unit farther to the west. This structural discordance may suggest the presence of some kind of 'stockwerke tectonics' (Wegmann 1935), in addition to the inferred strain partitioning between the orthogneisses and metasedimentary rocks. The application of the 'stockwerke' model to the Naternaq belt itself remains an intriguing problem that cannot be resolved at present, due to the lack of sufficient information on the time relationship between the structural discordance and the main phase(s) of folding and metamorphism.

Disregarding the local complexity at Naternaq, the general structural pattern described in this paper allows subdivision of the study area into two main domains: (1) a southern domain mostly characterised by S or S > L shape fabrics and a moderate to high angle of pitch, and (2) a northern domain showing L > S or LS fabrics and low

angles of lineation pitch. This subdivision compares well with the map scale variation of the metamorphic grade from granulite facies in the south to amphibolite facies further north. The contact between these two facies is transitional and forms a gently curved boundary that is subparallel to the strike of the regional foliation (Piazolo *et al.* 2004). This division of the study area into two contrasting blocks, indicated by the structural data and variation of metamorphic grade, can be explained by two models, namely (1) an indentor model, and (2) a transpressive deformation model, the relevance of which is briefly discussed below.

The indentor model, originally developed by Piazolo *et al.* (2004), invokes a twofold deformation history. During the first event the southern block was subjected to a coaxial flattening under granulite facies conditions (Fig. 13B – time A). A fairly uniform strain developed at that time and is manifested by prevailing S or S > L shape fabrics. During the second event (Fig. 13B – time B) the previously cooled granulite grade block acted as an indentor, with the amphibolite facies domain being plastered and moulded around the rigid block. The structural pattern and mineral assemblages of the southern domain were only modified in a transition zone that experienced retrogression to the amphibolite facies. At the same time, the amphibolite grade northern domain was subjected to mostly coaxial strain, including an important constrictional component. The resultant structural grain in the amphibolite facies rocks mimics the geometry shown by the boundaries of the southern block.

The alternative model (Fig. 13C) explains the observed structural relationships in terms of strain partitioning within a transpression zone (for a review of transpression see Holdsworth *et al.* 2002, and references therein). In this model, the different structural patterns documented in the northern and southern domains were produced during a single deformation event. Consequently, the model implies a continuity of the structural grain across the transitional zone as well as a gradual change in the orientation of directional structures, fabric type and kinematics of strain. The southern domain was mostly subjected to coaxial flattening, resulting in S or S > L shape fabrics with a moderately plunging lineation. The northern domain was deformed in a wrench-dominated regime, characterised by a constrictional or plane strain with a significant rotational strike-slip component. Hence, the northern block reveals L > S and LS shape fabrics and shallowly plunging lineations. A sinistral sense of displacement assumed in the model is consistent with rare observations in the field of kinematic indicators with the appropriate asymmetry.

The indentor model explains the arcuate swing of the structural grain around the granulite facies block, the map scale geometry of which may appear to control the foliation and lineation patterns within the amphibolite facies block further north. A serious weakness of the indentor model is the lack of evidence for fabric overprinting in the boundary zone between the two domains despite the assumed twofold deformation. However, high strain in the transitional zone could account for the obliteration of interference patterns and the apparent continuity of structural grain. The transpression zone model accounts for the presence of steep (F_2) fold hinges in the Naternaq supracrustal belt that are expected to develop within the wrench-dominated part of the transpressive system. The model also explains the contrast of structural style between the northern and southern domain without a detectable tectonic boundary or an overlap of structural patterns. Consequently, it is consistent with an apparent continuous transition linking the structural patterns within the granulite and amphibolite blocks. The somewhat steeper plunge of lineations within the granulite facies domain may indicate a greater component of coaxial strain in that area. However, the potential strain partitioning, as revealed by the lineation pattern, is relatively weak for a transpression zone. The partitioning of strain that takes place between the orthogneisses and supracrustal rocks within the northern amphibolite facies block is consistent with both of the discussed models. In addition, both models are consistent with a dominantly subhorizontal and approximately N–S contractional strain in the northern block causing the small-scale porpoising and large-scale whalebacking of lineations and associated fold hinges.

Thus, even a detailed structural analysis does not allow us to determine unequivocally which of the two models is the more appropriate. Nevertheless, the presented structural models can be indirectly verified by geochronological data, which constrain the age of peak metamorphism and associated deformation in the northern amphibolite facies block as Palaeoproterozoic (Thrane & Connelly 2006, this volume). Furthermore, the late Archaean crystallisation age of syndeformational granites emplaced at Saqqarput (Fig. 1) and at the southern margin of the NNO (Connelly & Mengel 2000; Thrane & Connelly *op. cit.*), points to a lack of significant deformation in the southern block from the late Archaean onwards. This is in conflict with the coincidence of deformation between the northern and southern blocks required by the transpression model and, thus, supports the indentor model. This is corroborated by the occurrence of undeformed but metamorphosed mafic dykes of likely Palaeoproterozoic origin emplaced at the southern margin of the investigated area (Glassley & Sørensen 1980; Árting 2004).

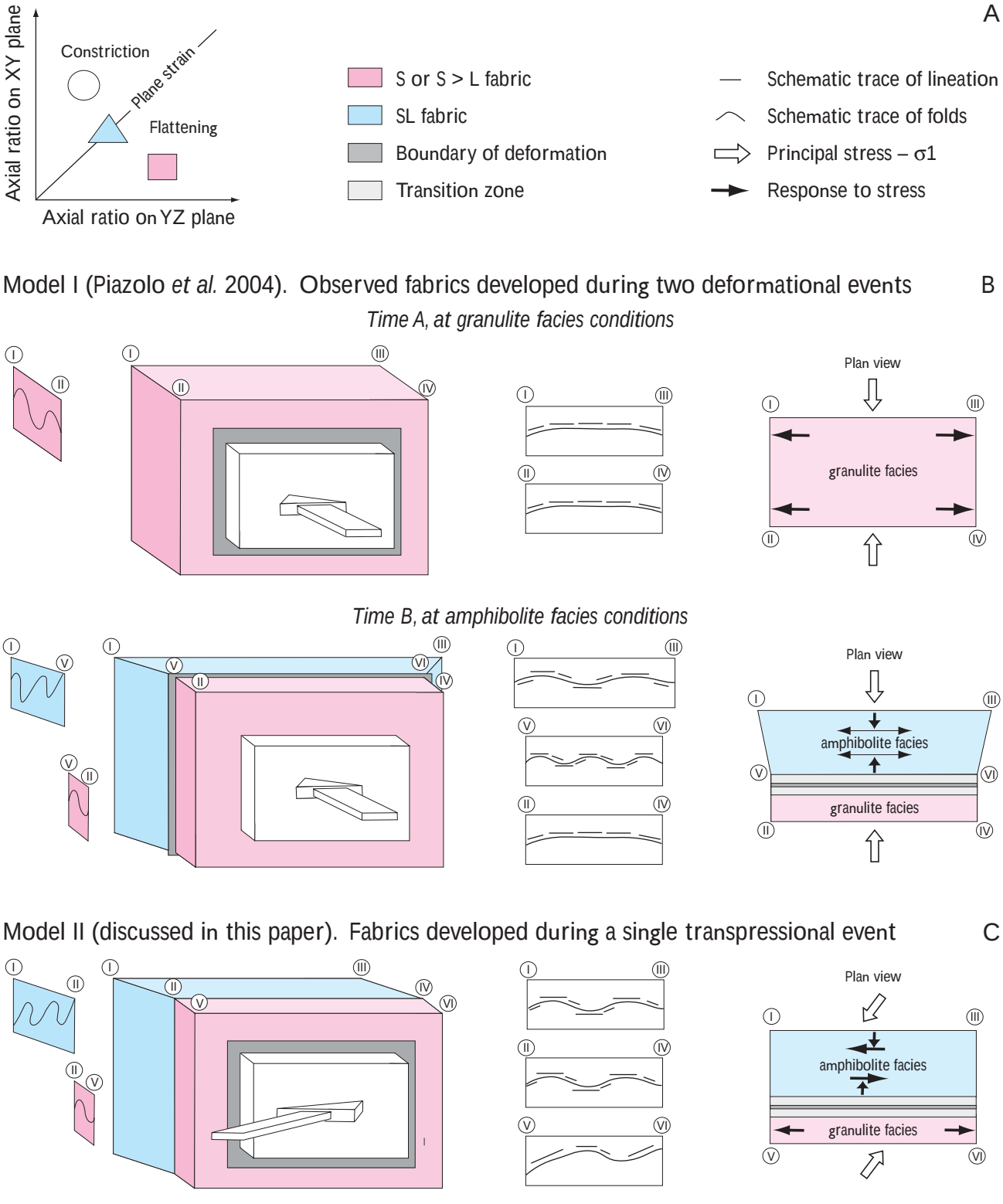

Fig. 13. Schematic indentor and transpression zone models with expected fabric types and fold patterns. A: Flinn graph with schematic qualitative descriptions of the finite planar (S) and linear (L) shape fabrics. B: Indentor model. C: Transpression zone model.

The F_3 folding apparently postdates the juxtaposition of the granulite and amphibolite blocks and had a relatively minor influence on their contact zone. The northward increase in intensity of F_3 folding is readily explained by the rheological weakness of the amphibolite facies domain during cooling. The origin of F_3 folds provides evidence for prolonged, approximately N–S-directed compression, the age of which is roughly constrained by the previously mentioned 1837 ± 12 Ma pegmatite (Thrane & Connelly 2006, this volume).

Our structural data also show that compressional stress related to the growth of the Nagssugtoqidian orogen was effectively transferred across the lower crust, and that the amphibolite facies domain south of Aasiaat was subjected to the penetrative Palaeoproterozoic deformation. Therefore, this area represents an integral part of the Nagssugtoqidian orogen despite the obvious paucity of Palaeoproterozoic crustal components. In contrast to the southern part of the orogen, the overall N–S shortening induced by the Nagssugtoqidian collision was accommodated in the study area through indentation and folding, in contrast to the central part of the orogen that displays significant thrust tectonics.

Concluding remarks

The indentor and transpression-driven tectonic models discussed in this paper share a number of features which shed a new light on the evolution of the northernmost Nagssugtoqidian orogen. The granulite and amphibolite facies blocks distinguished in the study area appear to be (par)autochthonous, and their boundary is only reactivated and reworked during indentation or transpression.

The area studied shows excellent examples of Precambrian deformation that are characterised by significant strain partitioning into less competent metasedimentary rocks. The presence or absence of lineations may be influenced significantly by lithology and metamorphic grade. Complex structural patterns may not always conclusively reveal the structural history on their own, hence geochronological data are essential in distinguishing between different deformation models such as transpression or indentation. In addition, it is apparent that the tectonic styles of the lower to middle crust can be highly variable within the same orogen. Deformation may vary from thrust-dominated in the central portion to folding associated with indentation or transpression on its flanks.

Acknowledgements

Critical reviews by C.R.L. Friend and an anonymous reviewer as well as constructive comments by A.A. Garde helped us to improve the manuscript, and are gratefully acknowledged. Structural information acquired from other members of the GEUS field parties in 2001–2002 significantly contributed to the data base used in this paper.

References

Alsop, G.I. & Holdsworth, R.E. 2004: The geometry and topology of natural sheath folds: a new tool for structural analysis. Journal of Structural Geology 26, 1561–1589.

Árting, U.E. 2004: A petrological study of basic dykes and sills of assumed Palaeoproterozoic age in central western Greenland, 122 pp., two appendices. Unpublished M.Sc. thesis, University of Copenhagen, Denmark.

Connelly, J.N. & Mengel, F.C. 2000: Evolution of Archean components in the Paleoproterozoic Nagssugtoqidian orogen, West Greenland. Geological Society of America Bulletin 112, 747–763.

Connelly, J.N., van Gool, J.A.M. & Mengel, F.C. 2000: Temporal evolution of a deeply eroded orogen: the Nagssugtoqidian orogen, West Greenland. Canadian Journal of Earth Sciences 37, 1121–1142.

Flinn, D. 1978: Construction and computation of three-dimensional progressive deformations. Journal of the Geological Society (London) 135, 291–305.

Garde, A.A. 2004: Geological map of Greenland, 1:100 000, Kangaatsiaq 68 V.1 Syd. Copenhagen: Geological Survey of Denmark and Greenland.

Glassley, W.E. & Sørensen, K. 1980: Constant *Ps*-*T* amphibolite to granulite facies transition in Agto (West Greenland) metadolerites: implications and applications. Journal of Petrology 21, 69–105.

Henderson, G. 1969: The Precambrian rocks of the Egedesminde–Christianshåb area, West Greenland. Rapport Grønlands Geologiske Undersøgelse 23, 37 pp.

Holdsworth, R.E., Tavarnelli, E., Clegg, P., Pinheiro, R.V.L., Jones, R.R. & McCaffrey, K.J.W. 2002: Domainal deformation patterns and strain partitioning during transpression: an example from the Southern Uplands terrane, Scotland. Journal of the Geological Society (London) 159, 401–415.

Kalsbeek, F. & Nutman, A.P. 1996: Anatomy of the Early Proterozoic Nagssugtoqidian orogen, West Greenland, explored by reconnaissance SHRIMP U-Pb dating. Geology 24, 515–518.

Kalsbeek, F., Pidgeon, R.T. & Taylor, P.N. 1987: Nagssugtoqidian mobile belt of West Greenland: a cryptic 1850 Ma suture between two Archaean continents – chemical and isotopic evidence. Earth and Planetary Science Letters 85, 365–385.

Manatschal, G., Ulfbeck, D. & van Gool, J.[A.M.] 1998: Change from thrusting to syncollisional extension at a mid-crustal level: an example from the Palaeoproterozoic Nagssugtoqidian orogen (West Greenland). Canadian Journal of Earth Sciences 35, 802–819.

Marker, M., Mengel, F., van Gool, J.[A.M.] & field party 1995: Evolution of the Palaeoproterozoic Nagssugtoqidian orogen: DLC investigations in West Greenland. Rapport Grønlands Geologiske Undersøgelse 165, 100–105.

Mengel, F., van Gool, J.A.M., Krogstad, E. & the 1997 field crew 1998: Archaean and Palaeoproterozoic orogenic processes: Danish Lithosphere Centre studies of the Nagssugtoqidian orogen, West Greenland. Geology of Greenland Survey Bulletin 180, 100–110.

Noe-Nygaard, A. & Ramberg, H. 1961: Geological reconnaissance map of the country between latitudes 69°N and 63°45´N, West Greenland, 1:500 000. Geological Map Grønlands Geologiske Undersøgelse 1, 9 pp., 2 maps. (Also Meddelelser om Grønland 123(5).)

Piazolo, S., Alsop, G.I., van Gool, J.[A.M.] & Nielsen, B.M. 2004: Using GIS to unravel high strain patterns in high grade terranes: a case study of indentor tectonics from West Greenland. In: Alsop, G.I. *et al.* (eds): Flow processes in faults and shear zones. Geological Society Special Publication (London) 224, 63–78.

Ramberg, H. 1949: On the petrogenesis of the gneiss complexes between Sukkertoppen and Christianshaab, West Greenland. Meddelelser fra Dansk Geologisk Forening 11, 312–327.

Thrane, K. & Connelly, J.N. 2006: Zircon geochronology from the Kangaatsiaq–Qasigiannguit region, the northern part of the 1.9–1.8 Ga Nagssugtoqidian orogen, West Greenland. In: Garde, A.A. & Kalsbeek, F. (eds): Precambrian crustal evolution and Cretaceous–Palaeogene faulting in West Greenland. Geological Survey of Denmark and Greenland Bulletin 11, 87–99 (this volume).

van Gool, J.A.M., Kriegsman, L., Marker, M. & Nichols, G.T. 1999: Thrust stacking in the inner Nordre Strømfjord area, West Greenland: significance for the tectonic evolution of the Palaeoproterozoic Nagssugtoqidian orogen. Precambrian Research 93, 71–86.

van Gool, J.A.M. *et al.* 2002a: Precambrian geology of the northern Nagssugtoqidian orogen, West Greenland: mapping in the Kangaatsiaq area. Geology of Greenland Survey Bulletin 191, 13–23.

van Gool, J.A.M., Connelly, J.N., Marker, M. & Mengel, F.C. 2002b: The Nagssugtoqidian orogen of West Greenland: tectonic evolution and regional correlations from a West Greenland perspective. Canadian Journal of Earth Sciences 39, 665–686.

Wegmann, C.E. 1935: Zur Deutung der Migmatite. Geologische Rundschau 26, 305–350.

Manuscript received 17 June 2004; revision accepted 14 June 2005

Magnetic anomalies and metamorphic boundaries in the southern Nagssugtoqidian orogen, West Greenland

John A. Korstgård, Bo Møller Stensgaard and Thorkild M. Rasmussen

Within the southern Nagssugtoqidian orogen in West Greenland metamorphic terrains of both Archaean and Palaeoproterozoic ages occur with metamorphic grade varying from low amphibolite facies to granulite facies. The determination of the relative ages of the different metamorphic terrains is greatly aided by the intrusion of the 2 Ga Kangâmiut dyke swarm along a NNE trend. In Archaean areas dykes cross-cut gneiss structures, and the host gneisses are in amphibolite to granulite facies. Along Itilleq strong shearing in an E–W-oriented zone caused retrogression of surrounding gneisses to low amphibolite facies. Within this Itivdleq shear zone Kangâmiut dykes follow the E–W shear fabrics giving the impression that dykes were reoriented by the shearing. However, the dykes remain largely undeformed and unmetamorphosed, indicating that the shear zone was established prior to dyke emplacement and that the orientation of the dykes here was governed by the shear fabric. Metamorphism and deformation north of Itilleq involve both dykes and host gneisses, and the metamorphic grade is amphibolite facies increasing to granulite facies at the northern boundary of the southern Nagssugtoqidian orogen. Here a zone of strong deformation, the Ikertôq thrust zone, coincides roughly with the amphibolite–granulite facies transition. Total magnetic field intensity anomalies from aeromagnetic data coincide spectacularly with metamorphic boundaries and reflect changes in content of the magnetic minerals at facies transitions. Even the nature of facies transitions is apparent. Static metamorphic boundaries are gradual whereas dynamic boundaries along deformation zones are abrupt.

Keywords: aeromagnetic data, magnetic anomalies, metamorphic facies, Nagssugtoqidian orogen, West Greenland

J.A.K., *Department of Earth Sciences, University of Aarhus, Høegh-Guldbergsgade 2, DK-8000 Århus C, Denmark.*
E-mail: *john.korstgard@geo.au.dk*
B.M.S. & T.M.R., *Geological Survey of Denmark and Greenland (GEUS), Øster Voldgade 10, DK-1350 Copenhagen K, Denmark.*

The establishment of the Palaeoproterozoic Nagssugtoqidian orogen in West Greenland (Ramberg 1949) is based on the deformation and metamorphism of the Kangâmiut dykes, dated at 2.04 Ga by Nutman *et al.* (1999). South of the southern Nagssugtoqidian front (SNF in Fig. 1), in the southern Nagssugtoqidian foreland, Kangâmiut dykes are undeformed and cross-cut gneiss structures. North of the front, gneisses and dykes have been metamorphosed and deformed together during the Nagssugtoqidian orogeny. Here, gneiss structures and dyke margins are concordant and dykes transformed into amphibolites. This is the simple story upon which Ramberg (1949) based his definition of the 'Nagssugtoqides'. Ramberg also divided the Nagssugtoqidian orogen into three metamorphic complexes based on the metamorphic grade of the rocks. Thus the Egedesminde complex was the northernmost amphibolite facies complex, the Isortoq complex the central granulite facies complex, and the Ikertôq complex the southernmost amphibolite facies complex. The current division of the orogen (Fig. 1) is based on structural criteria, and division boundaries now follow major structural features (Marker *et al.* 1995). The current division therefore deviates considerably from Ramberg's original division for the northern and central Nagssugtoqidian orogen, whereas the

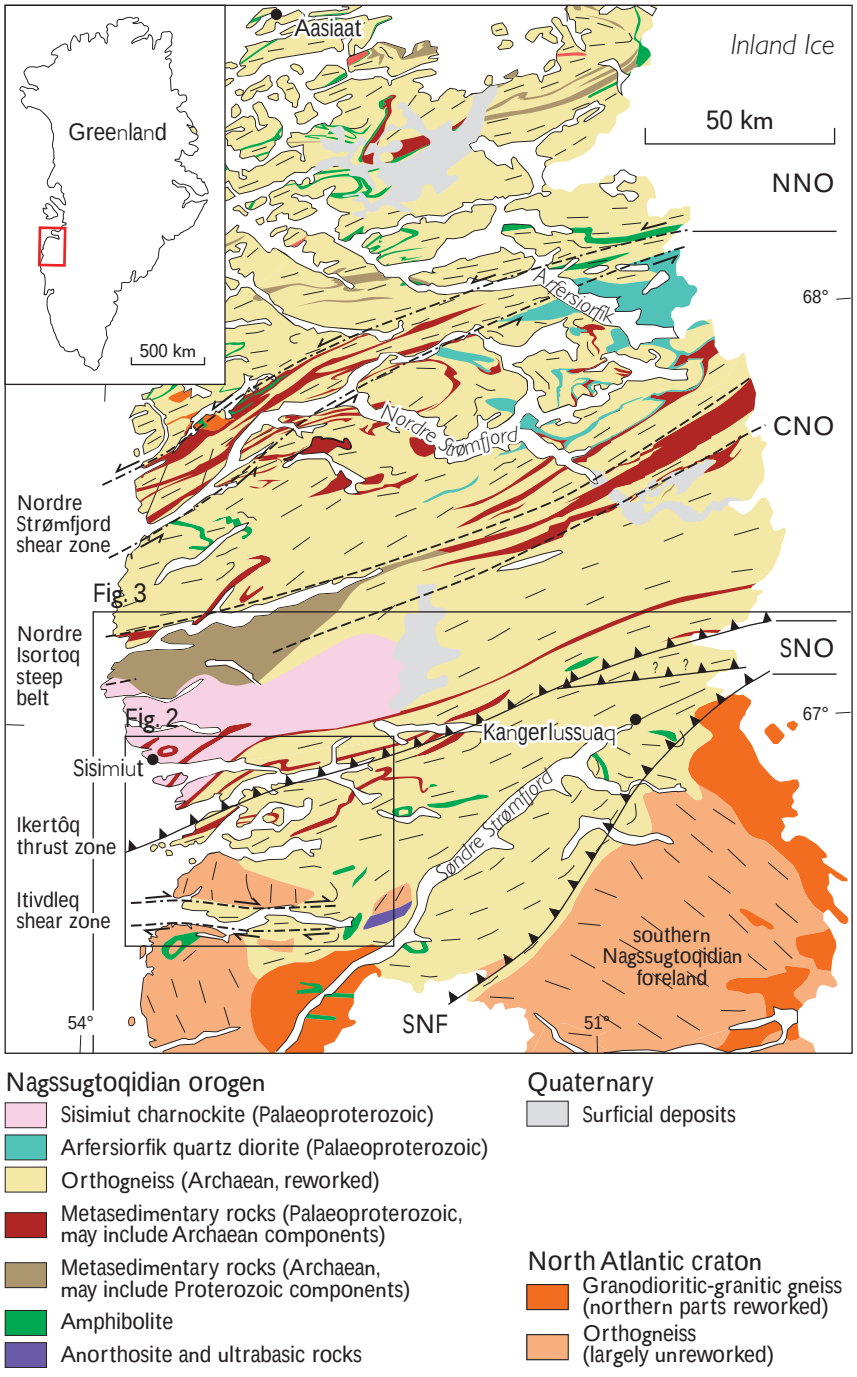

Fig. 1. Schematic geology of the southern part of the Nagssugtoqidian orogen and adjacent forelands (modified from Escher & Pulvertaft 1995 and Marker *et al.* 1995). SNO, southern Nagssugtoqidian orogen; CNO, central Nagssugtoqidian orogen; NNO, northern Nagssugtoqidian orogen; SNF, southern Nagssugtoqidian front. The locations of thrust and shear zones are defined from trends observed in the aeromagnetic data; note that the E–W-trending thrust zone with question marks north of Kangerlussuaq is uncertain, as this structure has not been confirmed by geological mapping. Black frames show the locations of Figs 2, 3.

southern Nagssugtoqidian orogen corresponds almost exactly to Ramberg's original Ikertôq complex.

The southern Nagssugtoqidian orogen (SNO in Fig. 1) in the coastal region between Sisimiut and Itilleq consists mainly of quartzofeldspathic gneisses of granodioritic to tonalitic composition. Several supracrustal layers occur, particularly in the northern part of the SNO. The supracrustal rocks are mainly garnet-biotite schists, rusty weathering biotite gneisses and amphibolites. The metamorphic grade is low amphibolite facies to granulite facies, and due to the fortunate timing of the intrusion of the Kangâmiut dykes it is possible to assign relative ages to the different metamorphic terrains in the region.

Pre-dyke metamorphism and deformation

South of and immediately north of Itilleq, the Kangâmiut dykes are largely undeformed, unmetamorphosed and

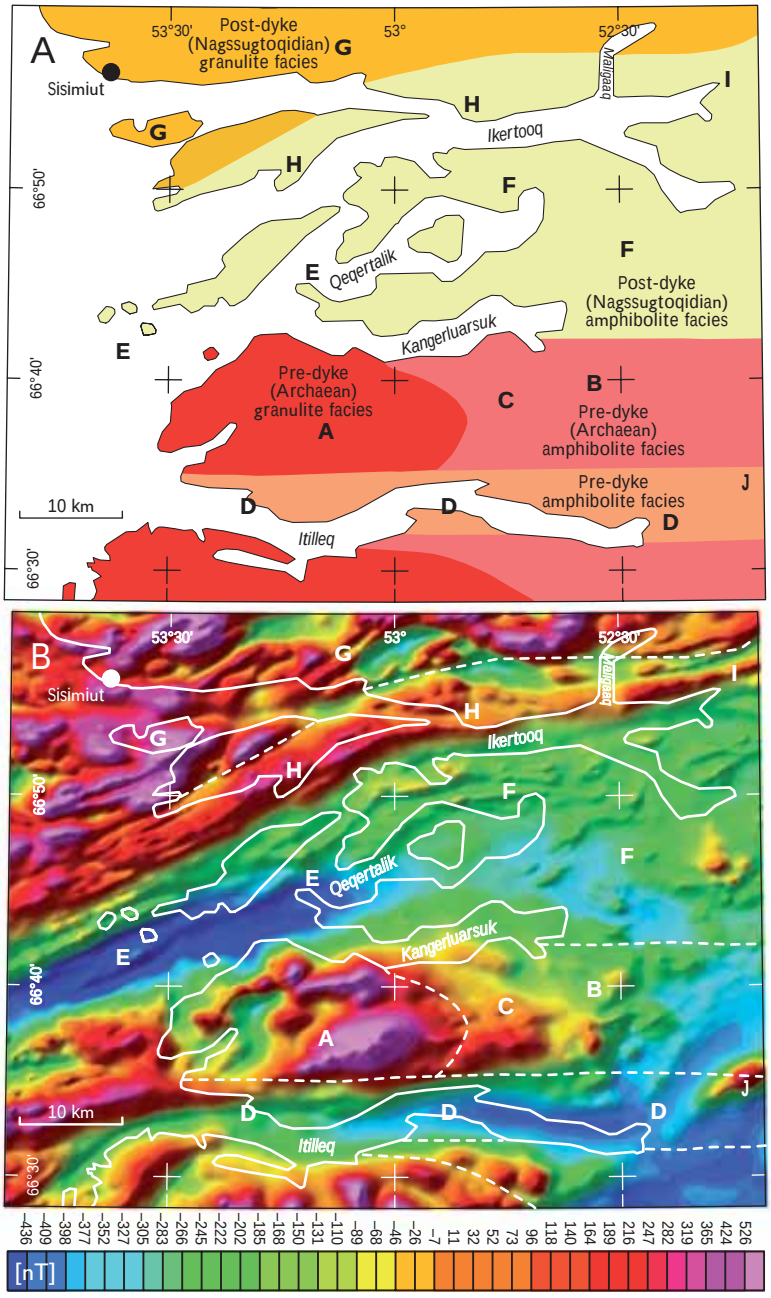

Fig. 2. Correlation between metamorphic facies and aeromagnetic anomaly patterns in the Itilleq–Ikertooq region. White lines indicate approximate metamorphic facies boundaries based on geological field work; labels A–J are explained in the text. A: Distribution and relative ages of metamorphic facies. B: Total intensity magnetic field anomaly map. Shadow of magnetic field pattern modelled from a light source with inclination 45° and declination 315°.

cross-cut gneiss structures. The main dyke direction is NNE–SSW, and a subordinate direction is E–W to ESE–WNW (Fig. 1). Upon entering the Itilleq area, the dyke trends are E–W, parallel to the fjord. This change in trend also corresponds to a change in foliation trend in the host gneisses. However, the dykes are still largely undeformed and unmetamorphosed within this E–W trend. The metamorphic grade of host gneisses north and south of Itilleq is granulite facies in western parts and amphibolite facies in eastern parts (Fig. 2A). However, all along the E–W trend in Itilleq, gneisses are in low amphibolite facies.

The dyke behaviour in the Itilleq region led to the interpretation that prior to intrusion of the Kangâmiut dykes the area was stabilised in amphibolite-granulite facies with a variable northerly trend of the foliation (Grocott 1979; Korstgård 1979). At some point prior to dyke intrusion an E–W zone of strong deformation was established along Itilleq, downgrading gneisses to low amphibolite facies (epidote-muscovite). Within this Itivdleq shear zone, dykes intruded along the shear fabrics and show a variety of primary pinch-and-swell structures (Nash 1979). Outside the shear zone, dyke margins are straight-sided indicating that dykes intruded along brittle fractures.

Post-dyke metamorphism and deformation

Farther north of Itilleq, from Kangerluarssuk and northwards (Fig. 2A), dykes are thoroughly deformed and parallel to country rock structures. Both dykes and country rock structures are in amphibolite facies. Foliation trends are variable ENE–WSW around west-plunging fold axes.

Continuing northwards the metamorphic grade increases and reaches granulite facies north of Ikertooq fjord (Fig. 2A). In addition, gneiss structures and metamorphosed dykes take on a pervasive E–W orientation (Ikertôq thrust zone, Fig. 1) with a steeply N-dipping foliation and N-plunging stretching lineations.

The interpretation of field observations in the northern SNO is that the metamorphism and deformation are post-dyke, the metamorphic transition is prograde, and the Ikertôq thrust zone represents a zone of southward ductile thrusting whereby deeper-seated rocks are brought up from the north.

Facies transitions

Within the Itilleq–Ikertooq region four types of facies transitions or boundaries are recognised. Two of these are prograde and two are associated with strong deformation in ductile shear zones.

The amphibolite–granulite facies transition in the Archaean areas around Itilleq is prograde and static in the sense that the boundary was not established as a result of a deformational event, but reflects static equilibration of the mineral assemblages to the conditions that prevailed when the rocks were at their deepest crustal level. During later uplift the rocks escaped any significant metamorphic changes due to the absence of deformation, and the metamorphism reflects their initial Archaean state.

The granulite to low amphibolite facies and amphibolite to low amphibolite facies transitions along Itilleq are retrograde and dynamic in the sense that they were established as a direct consequence of the deformation along the Itivdleq shear zone. Mineral assemblages in the shear zone were equilibrated to the metamorphic conditions of a higher crustal level than reflected in the surrounding gneisses, and the shearing triggered this re-equilibration.

The amphibolite–granulite facies transition north of Ikertooq is both prograde and dynamic. It can be considered as a displaced prograde and static transition brought up into a sub-vertical position by the overthrust movement along the Ikertôq thrust zone (Fig. 1).

Magnetisation

Comparing the magnetic anomaly map for the area (Fig. 2B) with the metamorphic map (Fig. 2A) a striking coincidence of magnetisation and metamorphic boundaries is evident. More information on the magnetic field data and the geological interpretations can be found in Rasmussen & van Gool (2000), Nielsen (2004) and Nielsen & Rasmussen (2004).

Strong magnetisation in pre-dyke Archaean granulite facies areas just north of Itilleq (A in Fig. 2B) is attributed to a higher content of magnetite or other magnetic minerals. A likely explanation for this is production of magnetite by the breakdown of hydrous (Fe, Mg)-Al-silicates (e.g. biotite, amphibole) during the transition from amphibolites to granulite facies according to the general reaction: hydrous (Fe, Mg)-Al-silicates ± SiO_2 ± O_2 = K-feldspar + (Fe, Mg)-silicates ± magnetite + H_2O. The lower magnetisation in pre-dyke Archaean amphibolite facies areas (B in Fig. 2B) relative to pre-dyke Archaean granulite facies areas indicates no additional production of magnetite. The gradual increase in magnetic intensity (C in Fig. 2B) marks the gradual prograde facies transition.

The elongate low magnetic anomaly coincident with the Itivdleq shear zone (D in Fig. 2B) is caused by extensive breakdown of magnetic minerals. This may be due to chemical breakdown during metamorphic retrogression to pre-dyke amphibolite facies aided by circulating fluids in the shear zone, and mechanical destruction of the magnetic mineral grains. The abrupt changes in anomaly patterns from D to A (Fig. 2B) across the metamorphic facies transition and deformation boundary are a response to the dynamic nature of this boundary.

Previously suggested possible shearing south of Ikertooq (E in Fig. 2B; Grocott 1979; Korstgård 1979) contemporaneous with the shearing at Itilleq (D in Fig. 2B) is supported by similarities in the character of the anomaly patterns. The post-dyke amphibolite facies areas at, and south of, Ikertooq (F in Fig. 2B) indicate the Palaeoproterozoic retrogression to amphibolite facies and deformational reworking. The boundary between the pre-dyke Archaean amphibolite facies and the post-dyke amphibolite facies areas does not have a well-defined magnetic signature (between B and F in Fig. 2B).

The increase in magnetisation north of Ikertooq (G in Fig. 2B) corresponds to rocks metamorphosed under granulite facies conditions after dyke intrusion and brought up by overthrusting. The offset between the mapped facies boundary north of Ikertooq (Fig. 2A) and the boundary between high and low magnetisation (H in Fig. 2B) can be explained as partially due to non-exposed post-dyke

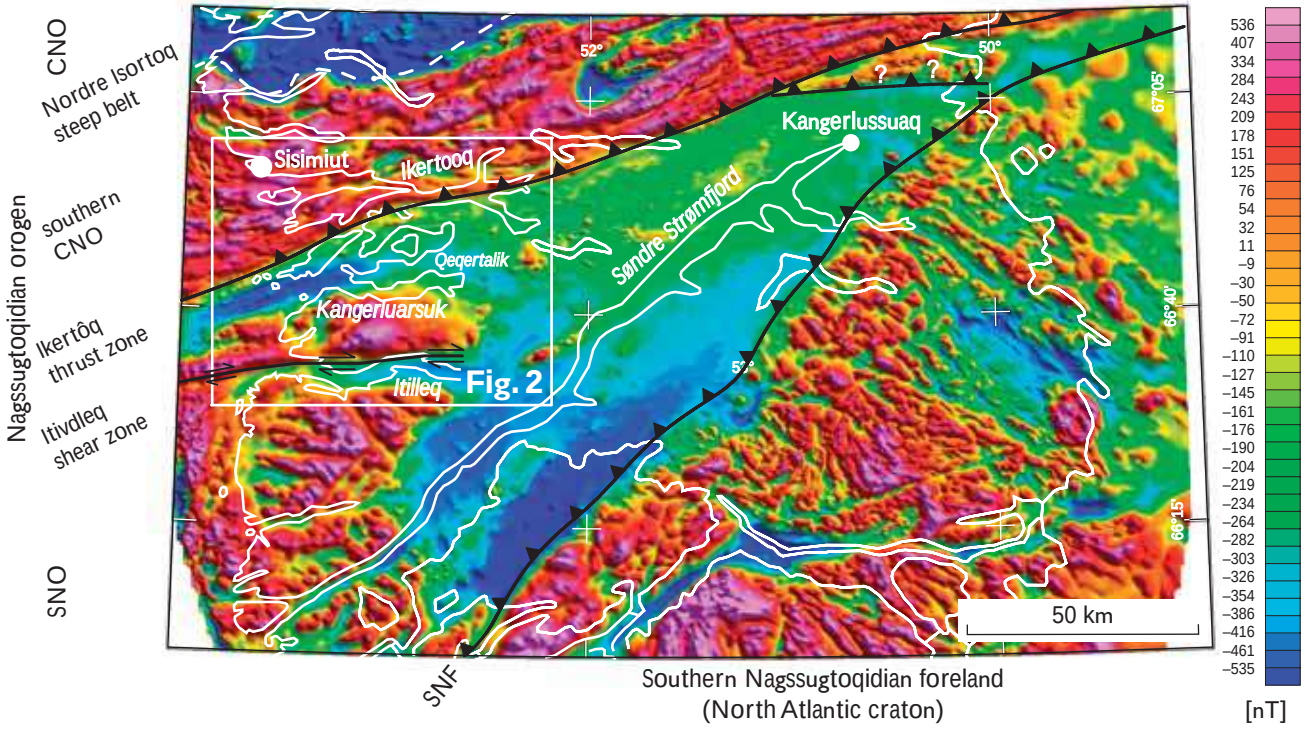

Fig. 3. Total intensity magnetic field anomaly map of the south-eastern part of the Nagssugtoqidian orogen and its foreland, with the location of the Itilleq–Ikertooq region (white frame, Fig. 2). Abbreviations as for Fig. 1; shadow on magnetic data as for Fig. 2. The E–W-trending thrust zone with question marks north of Kangerlussuaq is uncertain, as this structure has not been confirmed by geological mapping.

granulite facies rocks, and partially to the effect of stacked thrust panels of post-dyke amphibolite and granulite facies rocks with alternating low and high magnetic intensity anomalies (I in Fig. 2B). Isolated high intensity anomalies can be correlated with distinct lithologies or intrusives (e.g. an anorthosite complex at J in Fig. 2B). The presence or absence of Kangâmiut dykes is not reflected in the aeromagnetic data.

The observed correlations between metamorphic facies, deformation and magnetisation can be extended to other areas of the SNO (Fig. 3) provided that the background gneisses are lithologically fairly homogeneous, as is generally the case in the southern Nagssugtoqidian orogen. Where gneiss lithologies are more variable, such as in the Nordre Isortoq steep belt (Fig. 1) and the Nordre Strømfjord shear zone (Sørensen *et al*. 2006, this volume) correlations tend to depend on lithology rather than metamorphic grade.

Acknowledgements

The authors thank Graham Leslie and Chris Pulvertaft for their concise and constructive reviews.

References

Escher, J.C. & Pulvertaft, T.C.R. 1995: Geological map of Greenland, 1:2 500 000. Copenhagen: Geological Survey of Greenland.

Grocott, J. 1979: Controls of metamorphic grade in shear belts. In: Korstgård, J.A. (ed.): Nagssugtoqidian geology. Rapport Grønlands Geologiske Undersøgelse 89, 47–62.

Korstgård, J.A. (ed.) 1979: Nagssugtoqidian geology. Rapport Grønlands Geologiske Undersøgelse 89, 146 pp.

Marker, M., Mengel, F., van Gool, J. & field party 1995: Evolution of the Palaeoproterozoic Nagssugtoqidian orogen: DLC investigations in West Greenland. Rapport Grønlands Geologiske Undersøgelse 165, 100–105.

Nash, D. 1979: An interpretation of irregular dyke forms in the Itivdleq shear zone, West Greenland. In: Korstgård, J.A. (ed.): Nagssugtoqidian geology. Rapport Grønlands Geologiske Undersøgelse 89, 77–83.

Nielsen, B.M. 2004: Crustal architecture and spatial distribution of mineral occurrences in the Precambrian shield of central West Greenland based on geophysical and geological data. Danmarks og Grønlands Geologiske Undersøgelse Rapport 2004/26, 63 pp., 8 appendices. Ph.D. thesis 2004. Department of Earth Sciences, University of Aarhus, Denmark.

Nielsen, B.M. & Rasmussen, T.M. 2004: Mineral resources of the Precambrian shield of central West Greenland (66° to 70°15′N). Part

3. Implications of potential field data for the tectonic framework. Danmarks og Grønlands Geologiske Undersøgelse Rapport 2004/21, 165 pp.

Nutman, A.P., Kalsbeek, F., Marker, M., van Gool, J.A.M. & Bridgwater, D. 1999: U-Pb zircon ages of Kangâmiut dykes and detrital zircons in metasediments in the Palaeoproterozoic Nagssugtoqidian Orogen (West Greenland): clues to the pre-collisional history of the orogen. Precambrian Research 93, 87–104.

Ramberg, H. 1949: On the petrogenesis of the gneiss complexes between Sukkertoppen and Christianshaab, West Greenland. Meddelelser fra Dansk Geologisk Forening 11, 312–327.

Rasmussen, T.M. & van Gool, J.A.M. 2000: Aeromagnetic survey in southern West Greenland: project Aeromag 1999. Geology of Greenland Survey Bulletin 186, 73–77.

Sørensen, K., Korstgård, J.A., Glassley, W.E. & Stensgaard, B.M. 2006: The Nordre Strømfjord shear zone and the Arfersiorfik quartz diorite in the inner Arfersiorfik, the Nagssugtoqidian orogen, West Greenland. In: Garde, A.A. & Kalsbeek, F. (eds): Precambrian crustal evolution and Cretaceous–Palaeogene faulting in West Greenland. Geological Survey of Denmark and Greenland Bulletin 11, 145–161 (this volume).

Manuscript received 10 November 2004; revision accepted 1 November 2005

Faults and fractures in central West Greenland: onshore expression of continental break-up and sea-floor spreading in the Labrador – Baffin Bay Sea

Robert W. Wilson, Knud Erik S. Klint, Jeroen A.M. van Gool, Kenneth J.W. McCaffrey, Robert E. Holdsworth and James A. Chalmers

The complex Ungava fault zone lies in the Davis Strait and separates failed spreading centres in the Labrador Sea and Baffin Bay. This study focuses on coastal exposures east of the fault-bound Sisimiut basin, where the onshore expressions of these fault systems and the influence of pre-existing basement are examined. Regional lineament studies identify five main systems: N–S, NNE–SSW, ENE–WSW, ESE–WNW and NNW–SSE. Field studies reveal that strike-slip movements predominate, and are consistent with a ~NNE–SSW-oriented sinistral wrench system. Extensional faults trending N–S and ENE–WSW (basement-parallel), and compressional faults trending E–W, were also identified. The relative ages of these fault systems have been interpreted using cross-cutting relationships and by correlation with previously identified structures. A two-phase model for fault development fits the development of both the onshore fault systems observed in this study and regional tectonic structures offshore. The conclusions from this study show that the fault patterns and sense of movement on faults onshore reflect the stress fields that govern the opening of the Labrador Sea – Davis Strait – Baffin Bay seaway, and that the wrench couple on the Ungava transform system played a dominant role in the development of the onshore fault patterns.

Keywords: faults and fractures, extensional tectonics, wrench systems, sedimentary basins, basement reactivation, West Greenland

R.W.W., K.J.W.M. & R.E.H., *Reactivation Research Group, Department of Earth Sciences, University of Durham, Durham DH1 3LE, UK.* E-mail: *robert.wilson@durham.ac.uk*
K.E.S.K., J.A.M.v.G. & J.A.C., *Geological Survey of Denmark and Greenland, Øster Voldgade 10, DK-1350 Copenhagen K, Denmark.*

Introduction

Pre-existing heterogeneities in the continental crust, such as shear zones and terrain boundaries, have long been known to influence the structure and development of later deformation events (Butler *et al*. 1997; Holdsworth *et al*. 1997, and references therein). The sedimentary basins of the Labrador Sea – Baffin Bay region are situated west of Greenland (Fig. 1) and are early Cenozoic failed spreading centres (Chalmers & Pulvertaft 2001), separated by the Davis Strait. The orientation of the Davis Strait relative to the proposed spreading centres in the Labrador Sea and Baffin Bay is consistent with the geometry of an 'extensional transform zone' (Taylor *et al*. 1994). Steep basement fabrics of the Nagssugtoqidian orogen trend highly obliquely to these offshore structures (Fig. 1) and coincide with this 'step-over zone' in the Davis Strait. Fault systems fundamental to the development of sedimentary basins in the Davis Strait are exposed onshore in West Greenland. In this project, the onshore fault systems of central West Greenland were studied in order to improve

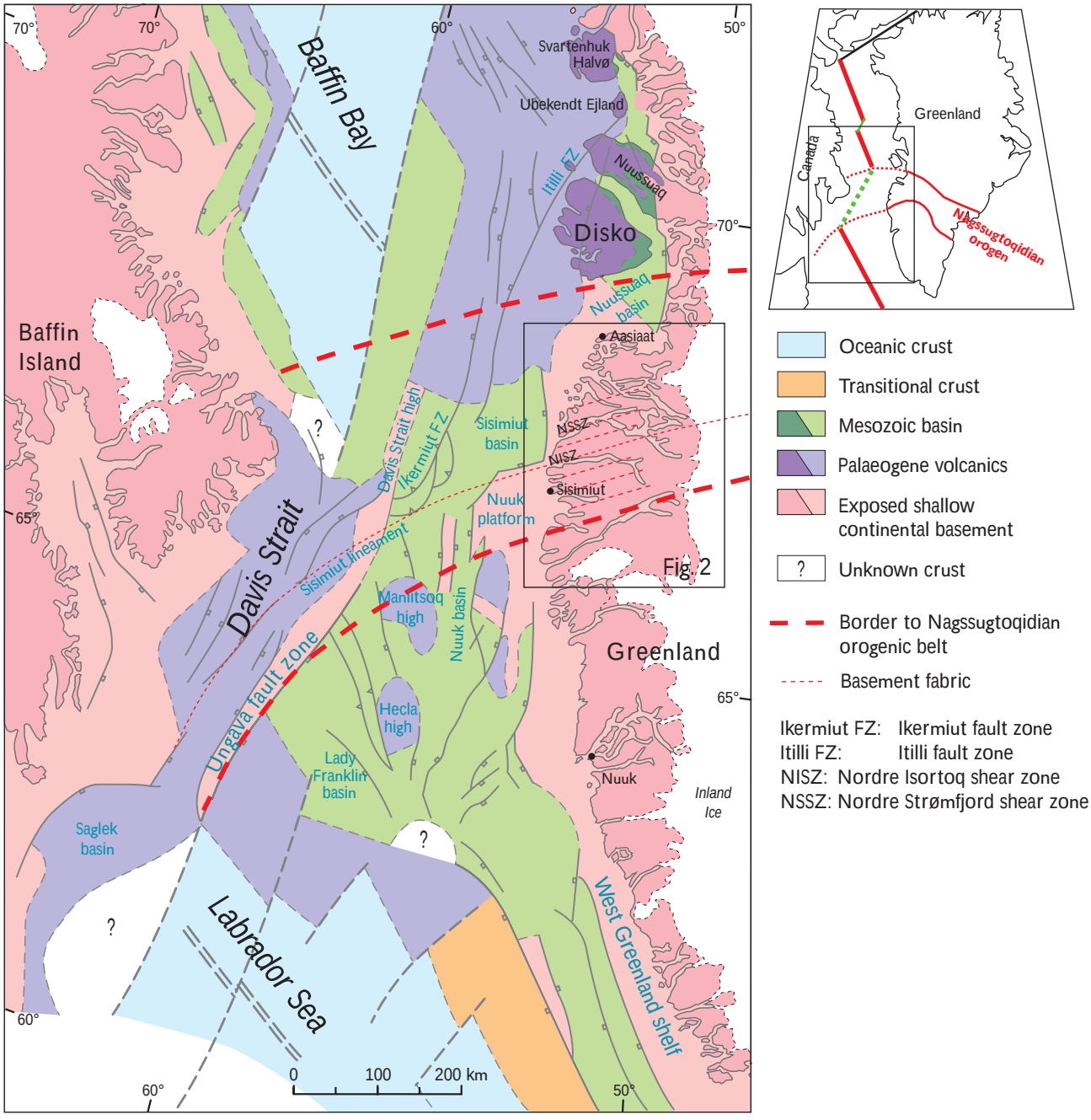

Fig. 1. Regional tectonic map of the offshore geology of the Labrador Sea – Baffin Bay area between Canada and Greenland. Modified from Chalmers & Pulvertaft (2001).

Facing page:

Fig. 2. Geological map of the Nagssugtoqidian orogen of central West Greenland (modified from Escher & Pulvertaft 1995). A: Outline map of Greenland highlighting the region covered in Fig. 2B. B: Geological map of the Nagssugtoqidian orogen showing main lithological units and basement structures. C: Topographic contour map of the central coastal area showing the field camps chosen for this study (camps 0 to 4); black dashed lines highlight major topographic escarpments. D: 3-D model view of NNE-trending coastal escarpment, constructed in ArcGIS by draping a Landsat image onto a topographic model. Abbreviations used: SNO, CNO and NNO are the southern, central and northern Nagssugtoqidian orogen, respectively. ITZ, Ikertôq thrust zone; NISZ, Nordre Isortoq shear zone; NSSZ, Nordre Strømfjord shear zone.

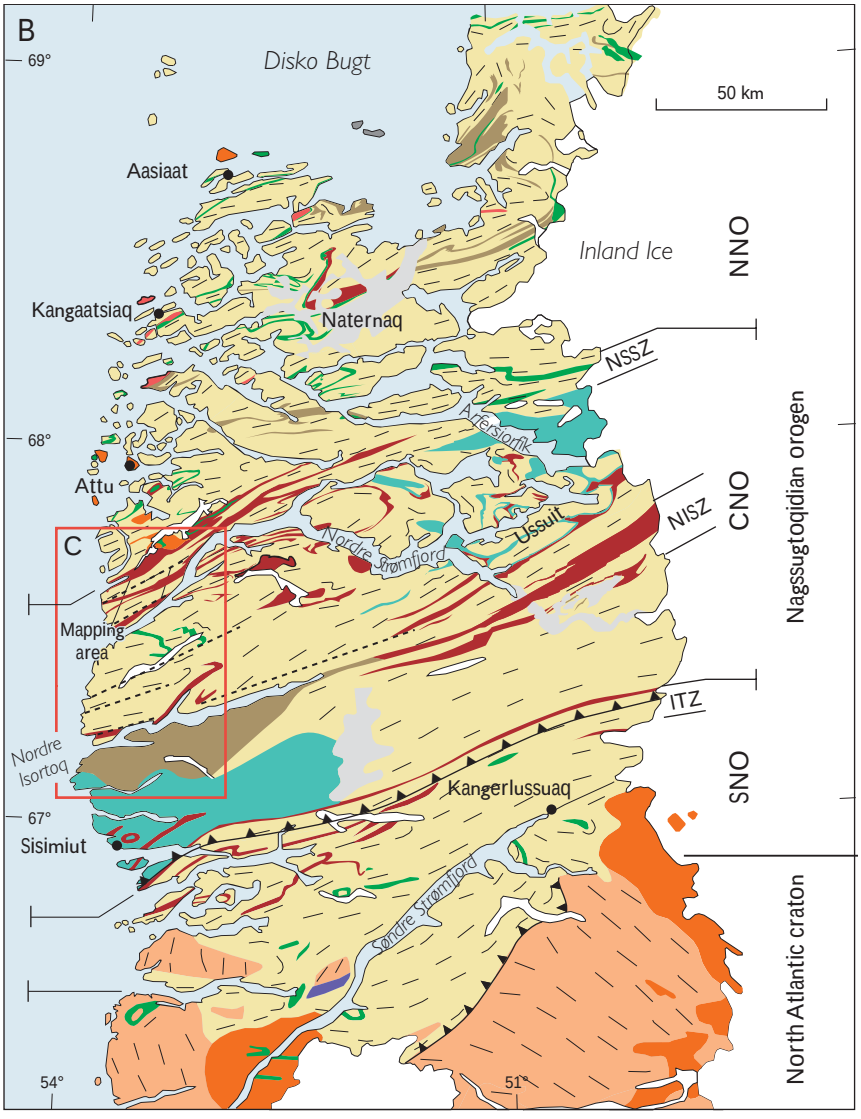

Surficial Quaternary deposits

PROTEROZOIC

- Calc-alkaline intrusions Arfersiorfik and Sisimiut suites
- Granitic intrusions
- Metasedimentary rocks
- Archaean gneisses reworked in the Palaeoproterozoic

ARCHAEAN

- Supracrustal rocks
- Metasedimentary rocks
- Anorthosite and ultrabasic rocks
- Granitic intrusions
- Orthogneisses
- Thrusts
- Basement fabrics

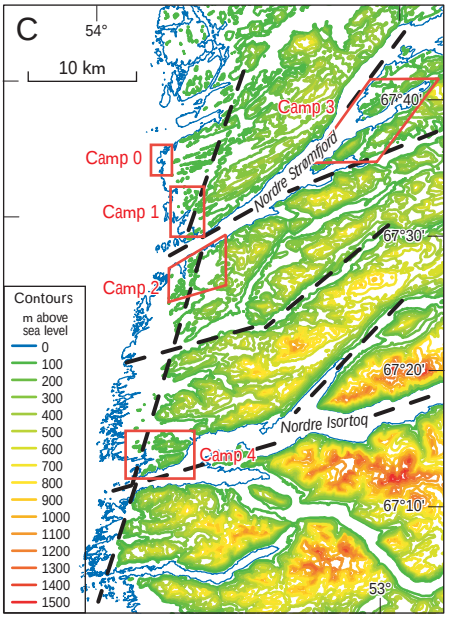

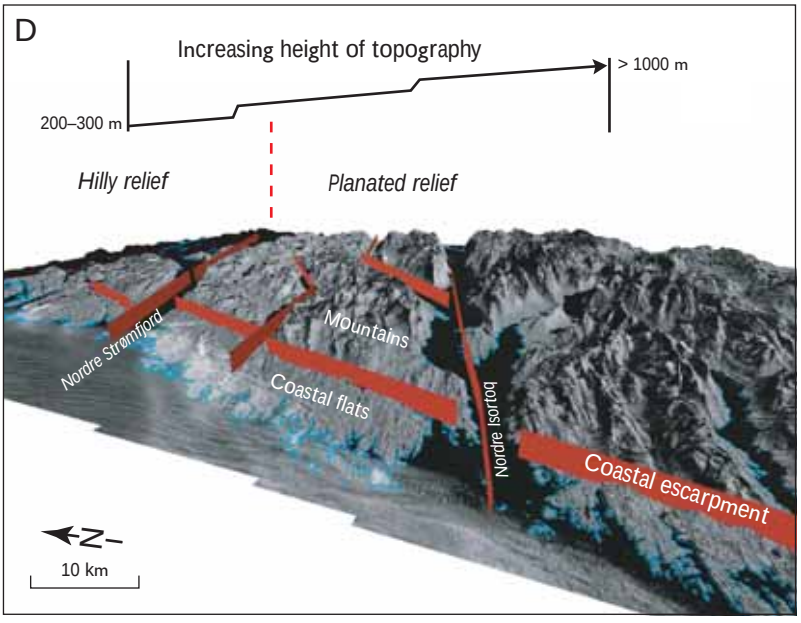

the understanding of the role played by basement reactivation in offshore basin development.

In the summer of 2003 field work was carried out in an area along the coast stretching from Nordre Strømfjord (Nassuttooq) in the north, to Nordre Isortoq in the south (Figs 2, 3). This area was selected because it is believed that two ENE-striking Palaeoproterozoic shear zones, the Nordre Strømfjord shear zone and the Nordre Isortoq shear zone, were reactivated and played an important role in the development of the Mesozoic to Tertiary sedimentary basins. The western projection of the Nordre Isortoq shear zone appears to coincide with the southern faulted boundary of the Sisimiut basin offshore (Figs 1, 2). In addition, the offshore basins occur close to the coast in this area, and the offshore extensional faults that drop the top of the basement down to 3 km below sea level, within 10 km west of the coast, are believed to correlate with fault escarpments onshore in this area.

Tectonic and geological setting

Offshore

The Labrador Sea and Baffin Bay formed during divergent plate motion between Greenland and North America during the early Cenozoic (Chalmers & Pulvertaft 2001, and references therein). The extensional basins of Baffin Bay and the Labrador Sea are separated by a bathymetric high in the Davis Strait (Fig. 1). This transverse ridge is interpreted as a complex sinistral-shear transform fault zone, known as the Ungava fault system (Fig. 1; Chalmers *et al*. 1995). Extensional faulting and tectonic subsidence are thought to have commenced in the early Cretaceous, at the same time as sea-floor spreading in the North Atlantic south of the Charlie Gibbs fracture zone. Opening started during the Paleocene (Chian & Louden 1994; Chalmers & Laursen 1995), and sea-floor spreading appears to have ceased by the Oligocene.

Interpretation of seismic reflection data has revealed the existence of a number of sedimentary basins offshore western Greenland (Chalmers *et al*. 1995; Whittaker 1995). One such basin is the deep Sisimiut basin, located in the Davis Strait to the west of the Nordre Strømfjord region (Fig. 1). At about 10 km west of the coast, the top of the basement is at *c*. 3 km depth, while there is no cover preserved on top of basement exposed onshore. Therefore, the eastern border of the basin must be a major fault, but it is located too close to the coast to have been surveyed by a seismic experiment. The orientation of this bounding fault is likely to follow the NNE–SSW trend of the coastline. The western margin of the Sisimiut basin is the NNE–SSW-trending Ikermiut fault zone (Fig. 1), a transpressional flower structure developed along the transform fault (Ungava fault zone) between the North American and Greenland plates (Fig. 2) formed during the Palaeogene (i.e. it cuts early Eocene strata; Chalmers & Pulvertaft 2001). The Nukik platform lies to the south of the Sisimiut basin and is separated from it by a line of ENE- and E-trending faults that coincide with the offshore extension of the Nordre Isortoq shear zone onshore (Figs 1, 2). It has therefore been proposed that the faults at the southern margin of the basin developed by reactivation of basement shear zone structures in the central Nagssugtoqidian orogen. These faults affect Mesozoic sediments and are overstepped by Paleocene sediments, so that the latest significant movement on them must have been prior to the end of the Paleocene.

Onshore

Onshore exposures in central West Greenland, from Søndre Strømfjord in the south to Disko Bugt in the north, comprise high-grade gneisses of the Palaeoproterozoic Nagssugtoqidian orogen (Fig. 2; Ramberg 1949; van Gool *et al*. 2002). The Nagssugtoqidian orogen is a 300 km wide belt of predominantly Archaean orthogneisses, Palaeoproterozoic paragneisses and intrusive rocks, that were reworked during Palaeoproterozoic orogenesis (van Gool *et al*. 2002). These basement rocks form ENE-trending linear belts of steeply dipping gneisses, some of which are crustal-scale shear zones (i.e. the Nordre Strømfjord and Nordre Isortoq shear zones, Fig. 2), which alternate with zones dominated by kilometre-scale fold structures (van Gool *et al*. 2002). The Nagssugtoqidian orogen is divided into three tectonic segments: the southern, central and northern Nagssugtoqidian orogen (Fig. 2; Marker *et al*. 1995). The onshore research in this study lies entirely within the granulite facies orthogneisses of the central Nagssugtoqidian orogen, which is bound to the north by the

Facing page:

Fig. 3. Lineament map of the main study area derived from lineament mapping of a Landsat TM image at 1:100 000 scale (total 1284 lineaments), using ArcGIS. The main rose diagram (bottom right) shows the distribution of lineaments for this map, while smaller rose diagrams (left) show results from aerial photograph analyses (at 1:20 000 scale) for each field camp. Green, system 1; blue, system 2; red, system 3; yellow, system 4; purple, system 5. Red box shows the position of Fig. 4.

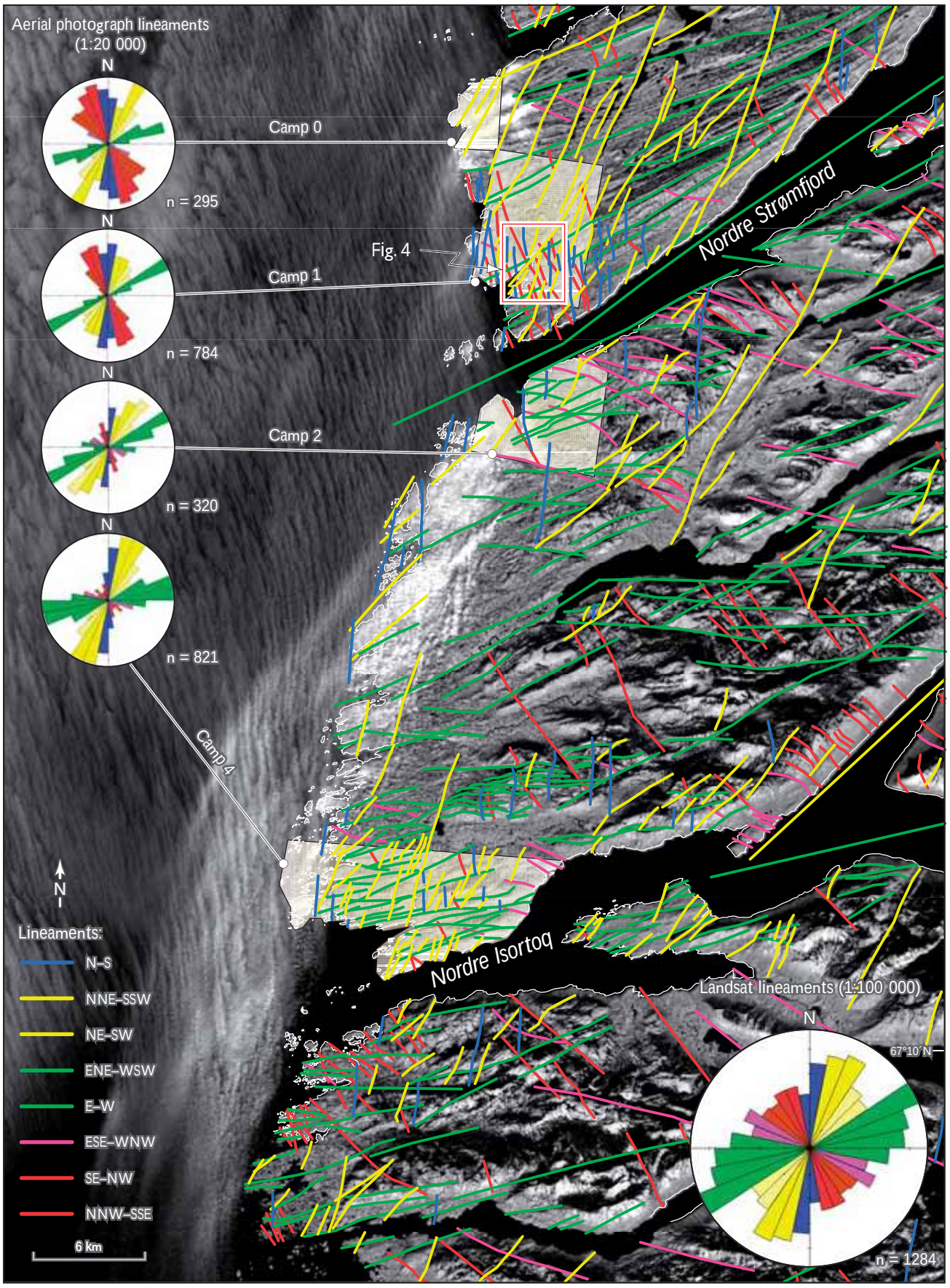
Aerial photograph lineaments
(1:20 000)
N
Camp 0
n = 295
N
Fig. 4
Camp 1
n = 784
N
Camp 2
n = 320
N
n = 821
Camp 4
Nordre Strømfjord
Nordre Isortoq
N
Lineaments:
N–S
NNE–SSW
NE–SW
ENE–WSW
E–W
ESE–WNW
SE–NW
NNW–SSE
6 km
Landsat lineaments (1:100 000)
N
67°10´N
n = 1284

Nordre Strømfjord shear zone (Marker *et al.* 1995; van Gool *et al.* 2002) and to the south by the Ikertôq thrust zone (Fig. 2).

Indirect topographic evidence from geomorphological investigations has suggested that late (Mesozoic or Cenozoic) onshore fault movements may have occurred (Bonow 2004). For example, in some of the larger inlets and valleys, characteristic recent shelly marine sands can be observed up to 30 m above sea level. These are likely to have been uplifted due to isostatic rebound following glacial retreat. However, variations in elevation of these palaeoshorelines may also result from differential vertical fault movements or differential unloading. On the larger scale, the Nordre Strømfjord shear zone marks a major change between two landscape types (Japsen *et al.* 2002). South of the Nordre Strømfjord shear zone topography is planated, with flat mountain tops forming a plateau that gradually increases in height southwards from 500 to 1000 m (Fig. 2C, D). In contrast, north of the Nordre Strømfjord shear zone, the land has a hilly relief with a relatively flat and low-lying topography with isolated hills up to 300 m high. Locally, the change in landscape type occurs across a more than 500 m high, ENE–WSW-oriented escarpment that drops down to the north (Fig. 2).

There is also a pronounced NNE–SSW-oriented escarpment almost 1 km high that drops down to the west between Nordre Strømfjord and Nordre Isortoq (Fig. 2). This major escarpment separates low-lying (50–150 m high) coastal flats to the west from the much higher (500 m+) mountains to the east (Fig. 2) and can be traced for over 80 km, from Sisimiut in the south to Nordre Strømfjord in the north. Similar escarpments can be observed in the near offshore on both bathymetric and horizon maps of depth to basement, thus supporting the theory that onshore structures reflect those offshore.

Methods

The present study combines regional to outcrop-scale mapping and regional studies of remotely sensed data to determine fault-fracture geometries, distribution, relative timing and kinematics in selected key areas of central West Greenland.

Regional studies comprised satellite image and aerial photograph analysis at a variety of scales (1:500 000; 1:100 000; 1:20 000) in order to identify lineaments and other geological structures (e.g. variations in lithology, fabric intensity, faults, fractures).

Field investigations were carried out in the well-exposed Precambrian basement rocks in key areas of interest that were identified during aerial photograph analysis prior to departure. A number of field camps were used during the mapping (Fig. 2C). Camp 0 was located at Inussuk, a site visited previously in 2002 (Japsen *et al.* 2002). Camps 1 and 2 were located on the north and south shores of Nordre Strømfjord, while camp was on the north shore of Nordre Isortoq. Camp 3 was farther inland, and is not analysed further in this study.

During field work, fault and fracture systems were mapped, and the following structural data were collected for statistical/structural analysis:

- Fault attributes including: orientation; kinematics; fault surface characteristics; mineralisation.
- Relative age relationships.
- Structural/statistical analyses to determine kinematic patterns.

Over 200 pseudotachylite and mica-bearing fault-rock samples were also collected from different fault sets at various localities in order to date the fault movements using $^{40}Ar/^{39}Ar$ geochronology (results to be discussed elsewhere). All field data were geospatially located (to 5 m resolution) using Global Positioning System (GPS) waypoint collection, and were subsequently stored in a computer database with links to Geographic Information System (GIS) based maps.

Fault and fracture characterisation

Fractures include all brittle structures such as joints, fissures, cracks, veins, etc. that are not faults, bedding or cleavage surfaces, and are larger than the grain size of the rock. In general, fractures are defined as dominantly tensile (mode I) cracks, and as such, they are associated with characteristic stress, strain and displacement fields. They are distinguished from small faults by distinctive surface textures and lack of shear displacements. *Faults* are mapped where distinct offsets have been identified, often with a development of slip striae on the surface (slickenlines). Criteria for determining the sense of movement were based on methods outlined in McClay (1987) and Petit (1987).

In the present study faults were classified as:

- Normal (extensional dip / oblique-slip fault).
- Reverse (compressional dip / oblique-slip fault).
- Strike-slip faults (dextral or sinistral).

The classification of faults and fractures into systems was primarily based on the orientation of the structures (i.e.

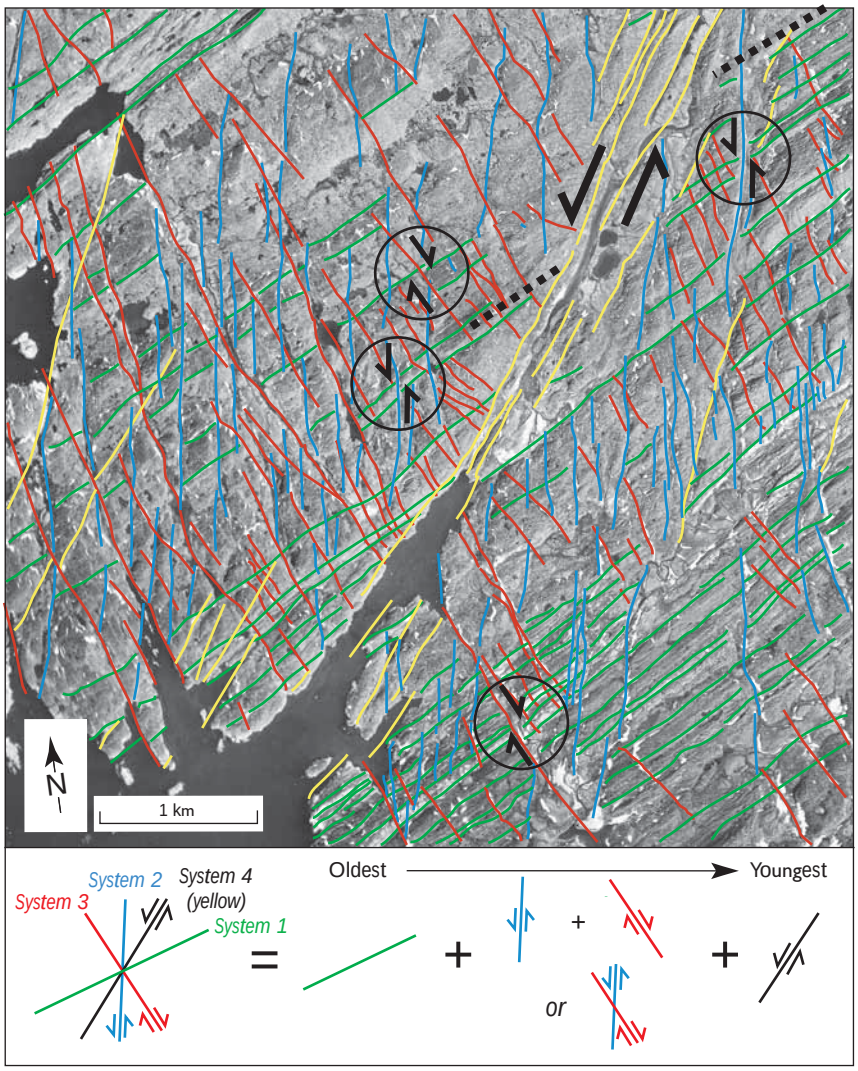

Fig. 4. Age relationships interpreted from cross-cutting relationships of lineament systems derived from aerial photographs for camp 1. Four dominant lineament trends are apparent: N–S (system 2), NNE–SSW (system 4), ENE–WSW (system 1), and NNW–SSE (system 3). Through cross-cutting relationships a relative order of fault development is apparent, as indicated across the bottom of the image.

trend of lineament or strike of plane). Structures with different orientations can reflect different deformation phases, but in complex fault zones developed in three-dimensional (3-D) strain fields, multiple fault and fracture orientations may develop during a single event (see e.g. De Paola *et al*. 2005). Therefore further classification needs to be applied, either through systematic fracture properties (such as surface type or mineralisation), or through kinematic studies, in order to determine if only one or several phases of deformation are apparent.

Fault and fracture measurement technique

In order to accurately classify the fault and fracture systems, populations of at least 50 fractures/faults were measured at most localities. Faults were classified according to type (normal/reverse dip-slip faults or dextral/sinistral strike-slip faults). Fault orientations and the directions of slickenlines (when observed) were measured, and the following characteristics recorded:

- *Surface shape:* The overall fracture shape (metre-scale) was described as listric, planar, undulating or irregular.
- *Surface roughness character:* The surface roughness character (millimetre scale) was described as smooth, rough or slickenside (striae).
- *Other features:* Some fractures/faults have a filling of iron oxide precipitates, quartz crystals, epidote, or preferential growth of other crystals on the surface showing the slip direction. Special types of fractures such as conjugate shear fractures, en échelon fractures, plumose jointing etc. were noted if present.

Lineament mapping

Lineament maps for the central Nagssugtoqidian orogen (Fig. 3) were plotted from Landsat TM images and aerial photographs at a variety of scales (1:500 000 and 1:100 000 for Landsat images and 1:20 000 for aerial photographs). Images were georeferenced and displayed in a GIS environment and the lineaments picked by hand. After interpretation, lineaments were then refined using digital terrain model (DTM) analysis and compared to pre-existing geological maps of the region (e.g. Henriksen *et al*. 2000). As the data are stored in a GIS, attribute data for each lineament (i.e. trend; length; offset; other features) were also measured or calculated and stored. Spatial analysis and rose plotting tools in ArcView GIS were used to analyse the orientation (Fig. 3) and spatial distribution of these structures.

A more detailed analysis of selected areas was then carried out at 1:20 000 scale using aerial photographs. As image resolutions are much higher in aerial photographs (2 m pixel size), particular attention was paid to how the lineaments interact with topography (e.g. V-ing into valleys, etc.) to gain a better understanding of their overall geometry. Generally all lineaments picked appear to have a steep dip as only minor interactions with topography were observed. Attention was also paid to cross-cutting relationships between lineaments in an attempt to determine the relative timing of structures (Fig. 4).

Lineament systems

In total 1284 lineaments have been identified from Landsat TM images (pixel size 30 m) at 1:100 000 scale (Fig. 3). Lineaments derived from both Landsat and aerial photographs have been grouped into systems based on their orientation. Five main lineament systems (N–S, NNE–SSW, ENE–WSW, ESE–WNW, and NNW–SSE) have been identified (Fig. 3; Table 1).

System 1 structures (green; Figs 3, 4) are oriented ENE–WSW (~060–090° trend), and are pervasively distributed across the region. This system has a trend similar to the Nordre Strømfjord and Nordre Isortoq fjords, and lies parallel to the regional basement fabric (foliation, gneissic banding, and shear zones; van Gool *et al*. 2002). Note that as these lineaments may represent either faults or basement fabrics, care must be taken when analysing these quantitatively. In an attempt to minimise the amount of oversampling, only the most pronounced lineaments (e.g. most weathered out) that mark a distinct change in structure were mapped, while those that are clearly basement fabrics (i.e. those showing ductile features such as folds) were not.

System 2 lineaments (blue; Figs 3, 4) are N–S oriented (trend ~350–010°), and often show sinistral offsets of pre-existing structures (basement fabrics). This system can be traced from Nordre Isortoq to the northernmost part of the investigated area (Fig. 3), and previous investigations indicated that they may continue as far north as Aasiaat, Disko and Nuussuaq (Japsen *et al*. 2002). The fault zones are closely spaced (100–500 m), and strike-slip separations of up to 30 m have been observed.

System 3 lineaments (red; Figs 3, 4) are NNW–SSE oriented (trend ~140–170°). They are closely spaced (50–100 m), and offsets of marble beds show net dextral separations in the order of 20–40 m (Fig. 4). This system is most pronounced in the Nordre Strømfjord shear zone, and less dominant in the Nordre Isortoq shear zone (see rose diagrams in Fig. 3).

System 4 lineaments (yellow; Figs 3, 4) are oriented NNE–SSW (trend ~010–040°) and are strongly developed in the Nordre Strømfjord shear zone region (camps 0 and 1, Fig. 3). These structures show apparent sinistral strike-slip separations of up to 400 m in the westernmost part of the study area. The spacing between them increases from approximately 500 m at the coast, to approximately 2 km farther inland. The same lineament directions were encountered at camps 2 and 4, south of Nordre Strømfjord, where these structures are shorter and more discontinuous, possibly due to differences in rock type and fabric between the two areas.

System 5 lineaments (purple; Fig. 3) consist of E–W to ESE–WNW (trend ~090–120°) -oriented structures. The valleys that distinguish this system are generally 10–30 m wide and have a curved trend. This system appears to be mostly localised into two specific areas: the first of these lies in the fold belt south of Nordre Strømfjord (Fig. 3), and the second is located south of Sisimiut (Fig. 1).

Relative timings

Figure 4 shows an aerial photograph of an area around camp 1 where an apparent order of lineament development can be deduced. The oldest structures appear to be system 1 (green), and in this area these structures appear to be basement fabrics in the form of alternating layers of semipelite and marble up to 100 m thick (Henriksen *et al*. 2000). System 2 (blue) structures show sinistral offsets of these lithological layers, while system 3 structures (red) show dextral displacements. In Fig. 4, system 3 structures appear to dominantly cross-cut system 2 structures, but this is not always the case as in some areas the reverse is true (system 2 cross-cutting/displacing system 3). As there

Table 1. Main characteristics for each fault system, identified from remote sensing and outcrop studies

Lineament system	Orientation	Sense of movement	Comments
System 1	ENE–WSW	• Normal (dip-slip) • Reverse (dextral oblique-slip) • Dextral and sinistral strike-slip	• Basement-parallel to subparallel • Multiple phases of movement
System 2	N–S	• Sinistral strike-slip • Normal (dip-slip)	• Closely spaced (100–500 m) • Displacements range between 0.2 and 30 m for individual faults • May show an en échelon to irregular trend
System 3	NNW–SSE	• Dextral strike-slip • Normal (dip-slip and oblique-slip)	• Dominant fracture/joint trend is associated with this system • Closely spaced (50–100 m) • Marble layers show displacements in the order of 20–40 m
System 4	NNE–SSW	• Sinistral strike-slip	• Major subvertical faults and fault zones • Generally associated with wide (> 50 m) valleys • Exposed fault cores show complex fracture sets associated with strike-slip movements
System 5	E–W to ESE–WNW	• Dextral strike-slip	• Localised to the fold belt south of Nordre Strømfjord and north of the Nordre Isortoq shear zone • Prominent structures at regional scale (i.e. from Landsat and aerial photos) but not at outcrop • Spatially associated with compressional faults (i.e. system 1 reverse faults)

is evidence for systems 2 and 3 mutually cross-cutting each other, and also because apparent movements are compatible with a conjugate system of strike-slip faults, it is possible that they are contemporaneous. Cross-cutting all other systems are the NNE-trending system 4 lineaments, suggesting that they are likely to be the youngest structures, or at least have experienced the most recent movements.

Other areas show a similar pattern of events, although some system 1 structures show evidence for younger movements (reactivation?), especially in areas around camps 2 and 4. System 5 is not represented in Fig. 4 as it was not observed at camp 1. This system is marked by quite wide (30–50 m) valleys, thus making its displacements difficult to determine; however, as it is quite pronounced, it may be a more recent system.

Field observations

Four key areas were chosen for detailed fracture and fault analysis in the field (Fig. 3), based on their structural interest (i.e. their potential to enable all systems to be analysed) and accessibility. The first objective of the field work was identification of the lineaments picked from the aerial photographs. In most cases field observations proved that the lineaments correspond to major fault structures, many of which are weathered out to leave gorges and river valleys (Fig. 5A–C). However, whilst many of the ENE–WSW-oriented system 1 structures are faults, others also correspond to basement fabric features, such as strongly foliated zones, lithological contacts and shear zones (Fig. 5D). Therefore care must be taken in any quantitative geometric or spatial analysis of this system.

After a regional reconnaissance from each field camp, detailed structural analysis was carried out. Ninety outcrop locations were investigated in the four camps, distributed along the coast between Nordre Isortoq and just north of Nordre Strømfjord (Fig. 2). In total *c.* 1700 faults and fractures were measured and described.

Fault geometries

A wide range of *fracture* orientations were observed (Fig. 6A), with dominantly N–S and NNW–SSE strikes and an overall mean fracture plane of 167/89E. Various *fault* orientations can be separated out in the field (dominant trends are N–S and ENE–WSW), showing a range of slip movements and shear senses (Fig. 6B–F). Dominant fault movements appear to be strike-slip (71% of faults recorded show strike-slip movements), although extensional and compressional faults were also apparent.

Fig. 5. Field identification of lineaments picked from Landsat and aerial photographs. A: Two major gorges/valleys trending ENE and NNE near camp 1; these correspond to major lineament systems 1 and 4, respectively. Fault core exposed within the NNE-trending stream bed (system 4) shows evidence for sinistral strike-slip faulting (Fig. 5B); fault movements on the ENE-trending basement-parallel valley (system 1) were not identified. B: Photograph of subhorizontal, sinistral strike-slip slickenlines observed within the fault core of the NNE-trending fault (system 4) identified in Fig. 5A. C: Some ENE-trending (system 1) lineaments correspond to basement fabrics such as steeply dipping (and tightly folded) marble units. D: Other basement parallel lineaments, however, do show evidence for brittle fault movement, as identified in this ENE-trending fault core (fault movement criteria defined by secondary fracture indicators, i.e. RM and lunate fractures, outlined in Petit 1987).

A set of ENE–WSW-oriented faults (green planes/mean poles in Fig. 6) appear to reactivate strong basement fabrics in the Nordre Strømfjord and Nordre Isortoq shear zones. These faults correspond to system 1 lineaments and exhibit various forms of fault movement (e.g. extensional, compressional and strike-slip; Fig. 6B–F). Faults corresponding to systems 2 (N–S, blue), 3 (NNW–SSE, red) and 4 (NNE–SSW, yellow) can also be easily distinguished from the fault data in Fig. 6. However, lineament system 5 (E–W to ESE–WNW, purple) is not apparent. As previously discussed this system appears to be a more geographically localised system (i.e. local to areas south of the Nordre Strømfjord and Nordre Isortoq shear zones), and correspond to zones dominated by reverse fault movements (Fig. 6B) and a small number of ESE-trending dextral strike-slip faults (Fig. 6E).

Fault systems corresponding to lineament systems 2, 3 and 4 appear to consist of parallel fault zones separated by non-faulted, but generally strongly fractured rock. The fault zones range typically between 1 and 50 m in width (Fig. 5B) and consist of multiple parallel faults with variable spacing. These zones are commonly located in pronounced valleys and gorges (Fig. 5A), so characterisation of fault planes was often difficult as the valley floors are generally covered by recent sediment and vegetation.

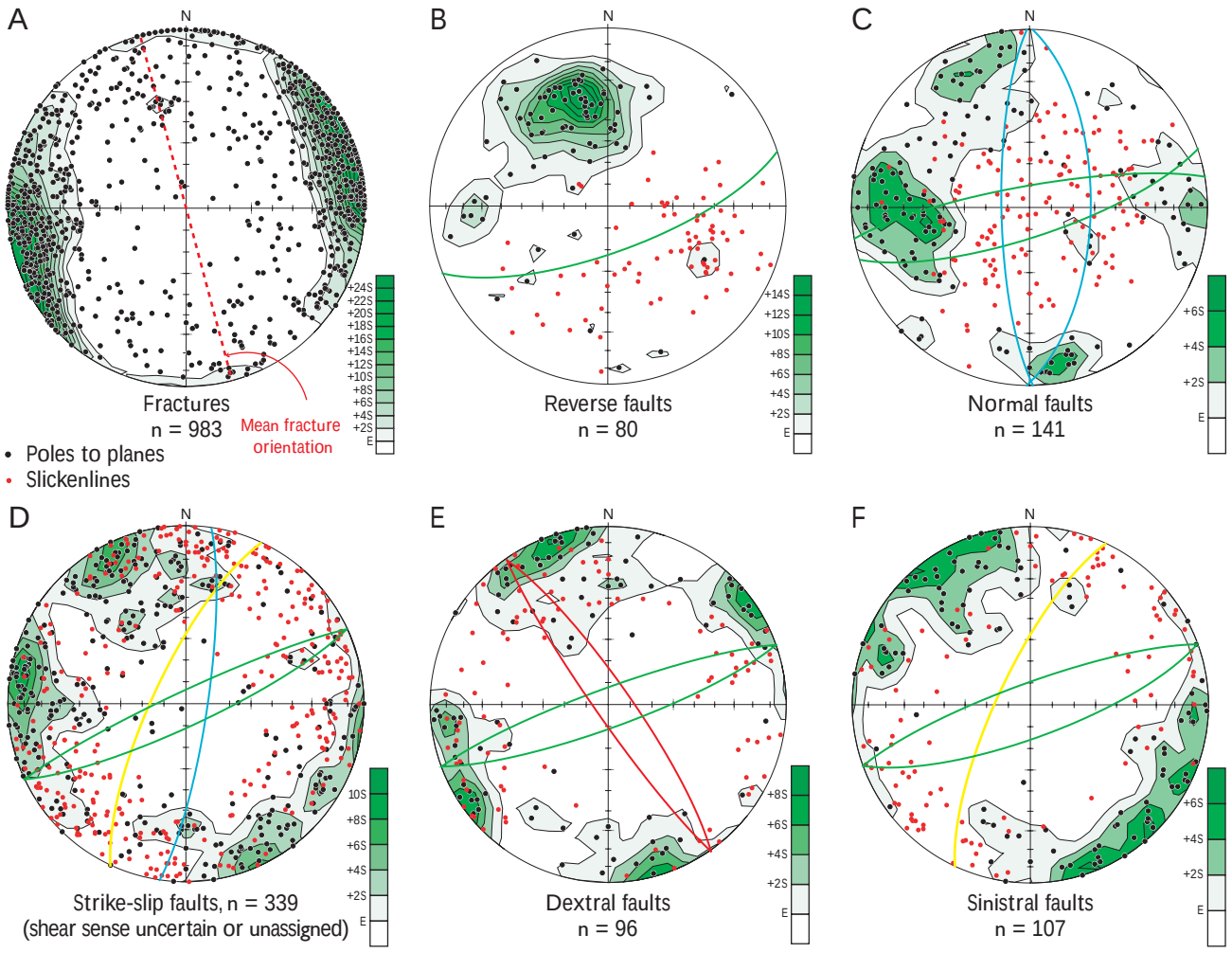

Fig. 6. Lower hemisphere, equal area stereographic projections of all fault and fracture data collected at camps 1, 2 and 4 (total number of measurements = 1746). A: Fractures (i.e. planes showing no evidence for slip). B: Reverse faults. C: Normal faults. D: Strike-slip faults with undetermined sense of movement. E: Dextral strike-slip faults. F: Sinistral strike-slip faults. Black dots, poles to planes of fault and fracture surfaces. Red dots, slickenlines. Mean fault planes are also shown, coloured according to lineament/fault systems identified in Fig. 3. Poles to fault and fracture surfaces are contoured using a Gaussian weighting function; n, number of measurements for each plot. In the labels, E corresponds to the background value (calculated as number of points/100), while S = standard deviations above this value.

Fault kinematics

In addition to the characterisation of the faults and fractures in terms of their trend and distribution, they can also be described according to their movement patterns (see Table 1). The nature and timing of tectonic events that are responsible for the formation of these fault-fracture systems is quite complex. Multiple directions of slickenlines on several fault surfaces indicate that many faults were either reactivated or that individual faults exhibit curved movement trajectories consistent with complex strain histories.

Strike-slip faulting

Strike-slip slickenlines account for 71% of those observed and were observed on all main fault geometries or systems. Multiple orientations of strike-slip faulting are common in wrench-dominated fault systems due to the development of Riedel, P and X shears (e.g. Woodcock & Schubert 1994).

Basement parallel faults (system 1, green) show both dextral and sinistral movements (note, RM structures – Petit 1987 – associated with R-shears suggest dextral movements on basement faults in Fig. 5D). NNW-trending (system 3, red) faults appear to correspond to dextral movements. N-trending faults (system 2, blue) appear to

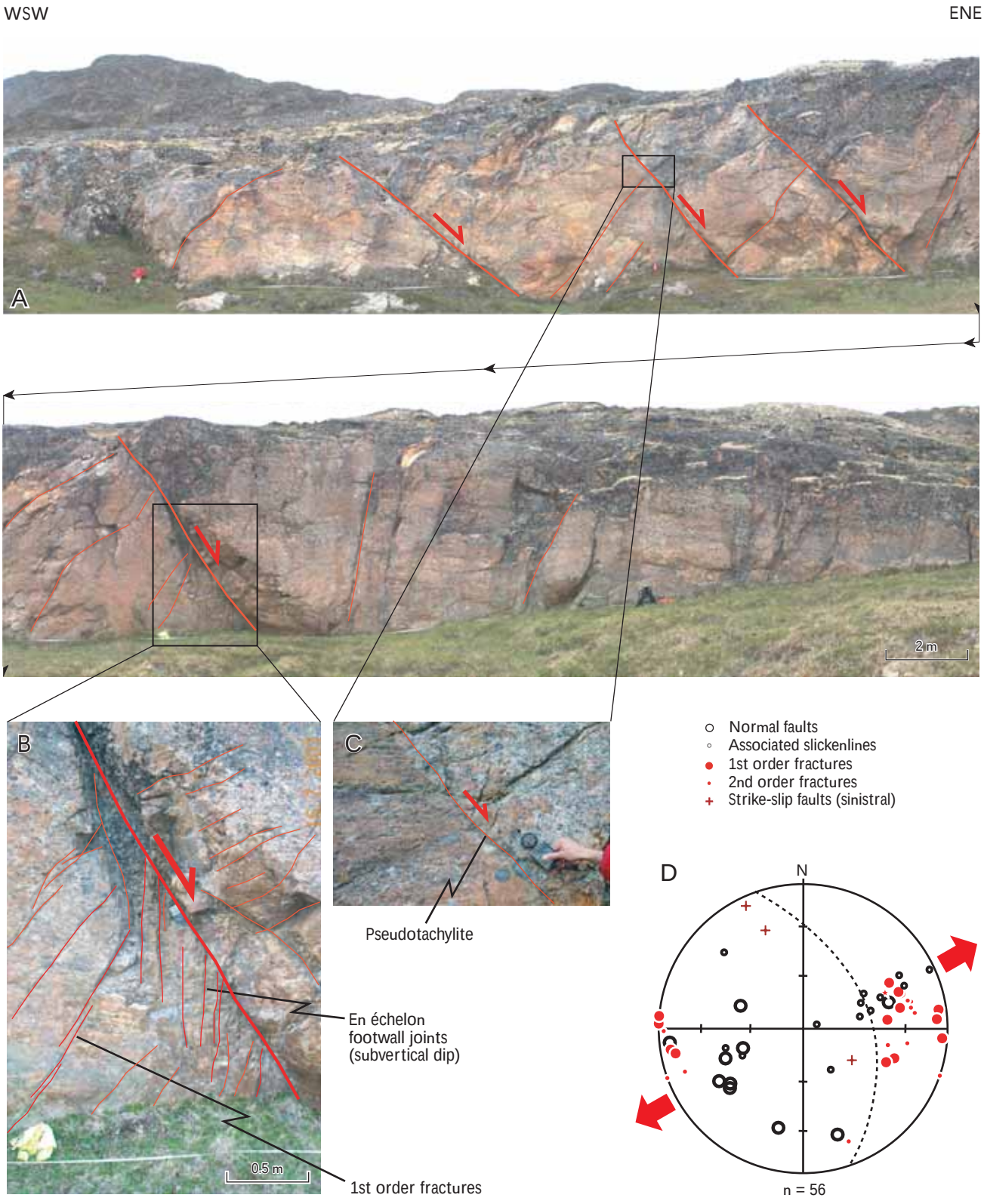

Fig. 7. A: Panoramic photograph showing exposures of a series of parallel ENE-dipping extensional faults, in the vicinity of camp 1. B and C: close-up photographs showing en échelon fracturing on the footwall of normal faults and pseudotachylite fault exposure in more detail. D: Lower hemisphere, equal area stereographic projection of poles to planes, and associated slickenlines, for faults and fractures observed at the outcrop of Fig. 7A. Fault orientations and kinematics suggest ENE–WSW extension as indicated by stress arrows (red); n, number of measurements.

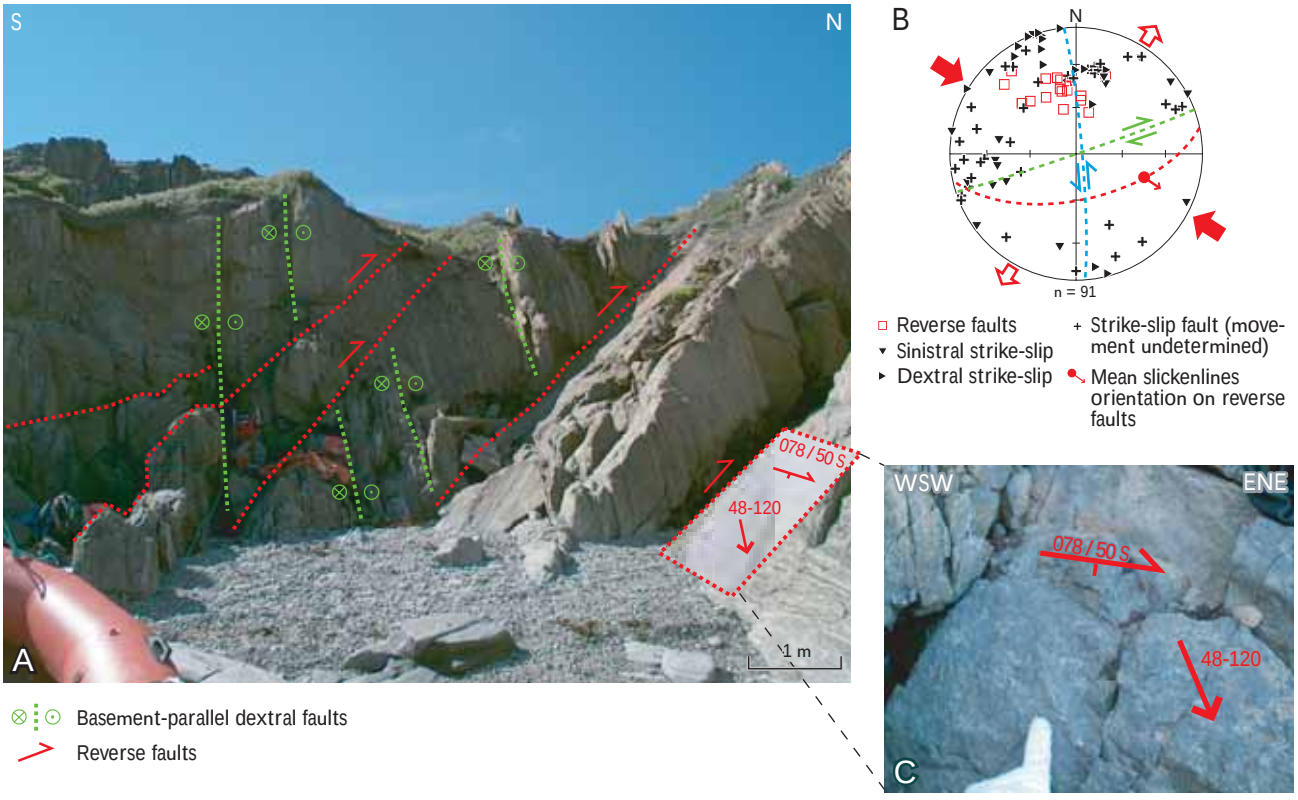

Fig. 8. A: Exposure of a localised set of reverse faults near camp 4. B: Lower hemisphere, equal area stereographic projections of poles to structures observed at the locality of Fig. 8A. Three dominant fault sets are apparent: basement parallel – i.e. ENE-trending – reverse and dextral strike-slip faults, and a set of sinistral faults oriented N–S (e.g. along the large rock face in shadow). Slickenline orientations and relative fault movements suggest ESE–WNW compression as indicated by stress arrows (red); n, number of measurements. C: Photograph of surface of reverse fault, showing dextral-oblique slickenlines (mean slickenline orientation 45/120, see stereonet). Note that faults coloured in red here highlight thrust faults and do not refer to system 3 faults as in other figures.

show both dextral and sinistral movements, while NNE-trending faults (system 4, yellow) are sinistral structures (Fig. 6D–F).

Extensional faulting

Although all five fault systems show dominantly strike-slip movements, normal and oblique-slip components of displacement were also recorded on some sets. These faults appear to have two dominant orientations, N–S (system 2) and ENE–WSW (system 1; Fig. 6C). In some areas NNW–SSE (system 3) -oriented structures also appear to be normal faults (Fig. 7), but these are not the dominant orientations in bulk analyses (Fig. 6). Field observations suggest that strike-slip movements post-date dip-slip.

Compressional faulting

Reverse faults (Figs 6B, 8) appear to be confined to areas close to camps 2 and 4, and to be spatially associated with system 5 lineaments. These faults strike parallel or sub-parallel to basement structures (ENE–WSW to E–W, Fig. 6B) and exhibit dextral-oblique slickenlines, which plunge towards the ESE (Figs 6B, 8).

As these compressional or thrust faults are only found on the southern shore of Nordre Strømfjord and the northern shore of Nordre Isortoq (i.e. abutting against major basement shear zones) it is possible that these structures are the result of local transpressional thrust faulting, which may be linked to steps in the en échelon sinistral fault system (system 4). Field observations suggest these compressional faults post-date most other fault and fractures. However, at camp 4, a N–S sinistral strike-slip fault appears to cross-cut these thrusts (Fig. 8B).

Fractures and joints

A diverse array of fracture orientations was recorded. Dominant orientations vary from NW–SE through to NNE–SSW. The orientation of the mean plane is NNW–SSE. All fractures recorded showed no evidence for shear movement (i.e. rough surfaces and with no apparent offsets) and are thus interpreted as opening mode 1 fractures and suggesting extension directions varied from *c.* E–W to NE–SW.

Interpretation and discussion

An overall summary of each of the fault systems identified through remote sensing (i.e. lineament mapping) and field studies is presented in Table 1. In this section we discuss the possible interpretations and implications of these observations.

Fault development

System 1 (ENE–WSW) faults and fractures appear to be the oldest structures, however multiple slip vectors and apparent fault movements suggest that there has been activity on this system during later tectonic episodes (note that system 1 faults are apparent in all stereoplots for all fault types, Fig. 6B–F). These lie parallel to the pre-existing Nagssugtoqidian basement fabric, which dates at *c.* 1.8 Ga (van Gool *et al.* 2002).

Cross-cutting relationships interpreted from analysis of aerial photographs suggest that the next systems to develop were systems 2 and 3 (Fig. 5). It is difficult to determine if one of these systems predates the other as mutually cross-cutting relationships can be seen; however, it does appear that system 3 is the more pervasive system and thus may be more recent.

Strike-slip movements and offsets on systems 2 (N–S) and 3 (NNW–SSE) suggest that, if active at the same time, these would represent a strike-slip conjugate system. In such cases the inferred extension vector would trend ENE–WSW, subparallel to system 1 foliation-parallel faults. This extension vector is also consistent with the dip-slip fault movements seen locally on these same fault systems.

These strike-slip movements appear to be preceded by dip-slip extensional movements. System 2 (N–S) is the dominant extensional fault orientation in the area (Fig. 6C), while some localities showed small populations where NNW–SSE-oriented extensional faults represent the preferred trend (e.g. Fig. 7). These faults are indicative of E–W to ENE–WSW extension. This extension cannot, however, explain the apparent basement-parallel (system 1) extensional faults, which suggest an apparent NNW–SSE extension. These ENE-trending normal faults have also been observed in seismic interpretations and are thus important structures regionally.

These two extensional fault sets show a quadrimodal fault distribution, i.e. four sets of fault planes (Fig. 6C). If regarded as two separate fault sets, this geometry would suggest two separate extension directions (E–W and NNW–SSE); however an alternative to this is that these faults formed contemporaneously under three-dimensional strain (Reches 1983; Nieto-Samaniego & Alaniz-Alvarez 1997). As one set of normal faults trends parallel to a pre-existing plane of weakness (e.g. basement fabric) it is likely that basement reactivation played a role in the development of these faults, and that this has lead to formation of extensional faults oblique to the regional extension. The regional tectonic setting would fit with 3-D strain as the area borders the transfer zone between two extensional basins, i.e. is a transtensional deformation zone (Dewey 2002; De Paola *et al.* 2005).

Geoffroy *et al.* (1998) recorded similar fault geometries and kinematics farther north in Disko and Nuussuaq (Fig. 1). Their interpretation is that strike-slip and dip-slip faulting developed during a single tectonic episode of WSW–ENE extension, which is in agreement with a model of 3-D transtensional strain.

As the stereoplots in Fig. 6 show, strike-slip faults are the dominant fault type in the area (as mentioned above, 71% of all faults measures are strike-slip) and these appear to post-date extensional movements. All fault systems show evidence for strike-slip movements. System 1 (ENE–WSW) exhibits both dextral and sinistral senses of shear, systems 3 (NNW–SSE) and 5 (ESE–WNW) show dextral shear, while systems 2 (N–S) and 4 (NNE–SSW) are dominated by sinistral shear movements. System 4 faults (NNE–SSW) appear to cross-cut all other fault sets, and are characterised by major fault zones (Fig. 5). These major sinistral strike-slip structures lie subparallel to the sinistral Ikermiut and Ungava fault zones that dominate the Davis Strait offshore (Fig. 1). Assuming a ~NNE-trending sinistral wrench system for the study area, strike-slip fault movements on each system appear to correlate closely with synthetic (R) and antithetic (R') Reidel shears, and also with synthetic P and antithetic X shears typical of a plane strain wrench tectonic regime (Fig. 9; Woodcock & Schubert 1994).

Compressional faults appear to be relatively late structures (although cross-cut by ~N–S-trending sinistral faults) and are localised in areas of strong basement fabric (i.e.

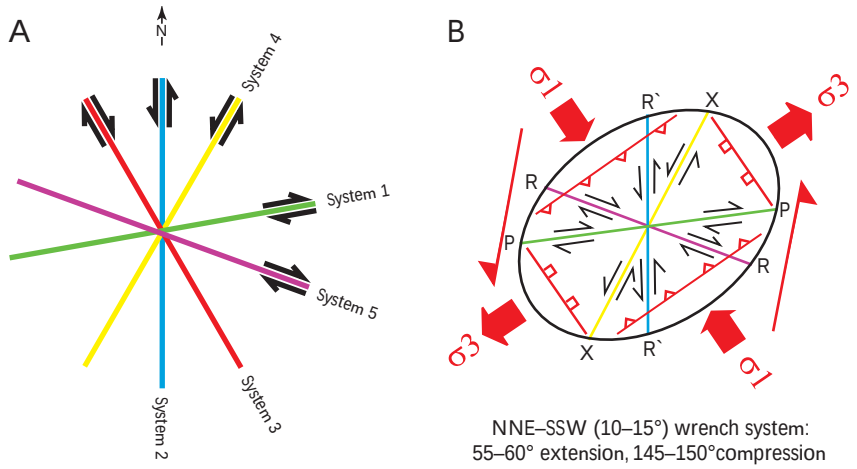

Fig. 9. A: Diagram showing fault systems and their corresponding movements. B: Strain ellipse for a NNE–SSW (~010–190°) -oriented sinistral wrench system, showing Riedel (R and R'), P and X shears (Woodcock & Schubert 1994). Also shown are the regional stress vectors (σ1 and σ3). Systems 2 (sinistral) and 5 (dextral) correspond to R' and R shears, while systems 1 (dextral) and 4 (sinistral) correspond to P and X shears. System 3 corresponds to normal fault sets in Fig. 9B; however, dominant movements on this system were dextral.

shear zones). These faults strike parallel to basement fabrics and indicate an oblique compression (from the ESE or SE; Fig. 8). Offshore there is evidence for thrusting in a similar orientation along the Ikermiut fault zone (Fig. 1). Positive flower structures have been identified (Chalmers & Pulvertaft 2001) and are interpreted as inversion structures formed at a restraining bend during sinistral strike-slip along the Ungava transform fault, during the early Eocene (*c.* 54–49 Ma, Chalmers & Pulvertaft 2001). If trends of basement shear zones (outlined in Fig. 2) are continued alongstrike offshore they appear to coincide with these transpression zones within the Ikermiut fault zone. It is possible that thrusts observed onshore have formed in a similar way to those offshore with basement shear zones acting as restraining bend structures, thus leading to localised compressional zones. Furthermore, slickenlines on the reverse faults suggest a compression from the ESE or SE (Figs 6B, 8), which is consistent with the compressional axis for a sinistral wrench system (i.e. NE–SW extension and NW–SE compression; Fig. 9).

Regional comparison and implications

A key prerequisite for building tectono-stratigraphic models is being able to date each tectonic event. As all onshore exposures in this part of West Greenland are in Precambrian basement rocks, there are no stratigraphic markers for constraining the timing of Phanerozoic tectonic events. Relative timing has been inferred from various cross-cutting relationships in the field and from lineament analysis, but is open to different interpretations. In the absence of age data that constrain the absolute age(s) of fault activity, comparisons with offshore models and with data collected in other onshore areas are used here to infer ages for events in our tectonic model (see Table 2 for a summary).

Regional onshore correlations

Farthernorth in the region of Disko and Nuussuaq, onshore faulting episodes can be dated relative to the deposition of basaltic lavas and the sedimentary systems during Campanian to Eocene times (Geoffroy *et al.* 1998; Storey *et al.* 1998; Chalmers *et al.* 1999; Dam *et al.* 2000). Dam & Sønderholm (1998), Dam *et al.* (2000) and Dam (2002) document at least three phases of faulting recorded in the sedimentary record prior to Paleocene volcanism. Cretaceous–Paleocene sediments on Nuussuaq show distinctunconformities, with incised valleys and submarine canyons, reflecting disturbances in early Campanian, Maastrichtian and early Paleocene times. These unconformities and channels are thought to have formed in response to structural movements associated with regional NE–SW rifting (and also the arrival of the North Atlantic plume in the latter two cases).

$^{40}Ar/^{39}Ar$ dating has revealed that volcanism commenced in West Greenland between 60.9 and 61.3 Ma and that 80% of the Paleocene lava pile was erupted in less than 1 Ma (Storey *et al.* 1998). These lavas show a distinct coastal flexure (Geoffroy *et al.* 1998, 2001; Larsen & Pulvertaft 2000), presently expressed by seaward dipping basalt lavas. This flexure has an arcuate course, striking NW–SE in southern Svartenhuk Halvø and northern Ubekendt Ejland, turning through N–S in south-west Ubekendt Ejland to NE–SW in north-west Nuussuaq and finally to N–S in north-west Disko (Fig. 1; Geoffroy *et al.* 1998, 2001; Larsen & Pulvertaft 2000). Numerous dykes cut these lavas (e.g. see figs 4 and 5 in Larsen & Pulvertaft 2000), and so do various fault sets (Geoffroy *et al.* 1998). The timing of the various phases of volcanic eruption, dyke emplacement, and block faulting relative to one another is still a matter of debate. Geoffroy *et al.* (1998) presented detailed structural evidence suggesting that fault and dyke intrusion on Disko took place during tilting of lava sys-

Table 2. Proposed event stratigraphic model and apparent correlation with offshore events

Event #	Timing and event	Offshore tectonic structures	Onshore tectonic structures
5 (Youngest)	Pliocene to Pleistocene tilting	• Subsidence	• Uplift? • Possible reactivation of systems 1–4 as normal faults
4	Eocene Labrador sea-floor spreading (Ungava system)	• N- to NNE-trending sinistral transverse fault system (Ungava fault zone). • Local transpressional and transtensional faulting (e.g. Ikermiut fault zone)	• Faults consistent with NNE-oriented sinistral wrench system: NNE-trending (system 4) faults and basement-parallel (system 1) faults active as antithetic X and synthetic P shears • Systems 2 (reactivation) and 5 active as Reidel shears • Local transpressional thrust faulting observed near camps 2 and 4, associated with steep basement fabrics
3	Late Cretaceous to early Paleocene extension	• N-trending faults in Davis Strait (E–W extension) leading to formation of the Sisimiut Basin offshore	• Systems 1, 2 (and 3?) faults all active as extensional faults during NE–SW to ENE–WSW extension (3D strain)?
2	Early or middle to late Cretaceous extension and thermal subsidence	• NW-trending normal faults in the Labrador Sea (SW–NE extension) • WSW–ENE faults bordering the Sisimiut basin to the south were active offshore during events 2 and/or 3	• Uncertain?
1 (Oldest)	Proterozoic and later localised reactivation	• Uncertain?	• Possible system 1 ENE–WSW foliation-parallel faulting prior to late Mesozoic?

tems. Geoffroy *et al.* (2001) then stated that NW–SE-oriented, flexure-parallel dykes in southern Svartenhuk yield dates of around 54.6 ± 0.6 Ma. This suggests that most of the coastal flexure is of Eocene age (or later?). Further evidence for this comes from north-west Nuussuaq where tilted lavas (Larsen & Pulvertaft 2000) have been dated at ~53 Ma (Storey *et al.* 1998).

Systems 2 (N–S) and 3 (NNW–SSE) extensional faults in this study appear comparable to faults that cross-cut these Paleocene basalt lavas (Geoffroy *et al.* 1998). Taking the dates outlined above for dyke emplacement which is believed to be associated with faulting, it would appear that our system 2 and 3 faults were active during Eocene times. Taking all these onshore tectonic timings into account it would then appear that the faults observed may have been active from late Cretaceous (Maastrichtian) through to Eocene times (Dam & Sønderholm 1998; Geoffroy *et al.* 1998, 2001; Chalmers *et al.* 1999; Dam *et al.* 2000; Larsen & Pulvertaft 2000; Dam 2002).

Normal fault orientations similar to systems 2 (N–S) and 3 (NNW–SSE) occur in and around the Nuussuaq basin (Fig. 1; Geoffroy *et al.* 1998; Chalmers *et al.* 1999) and are consistent with either ENE–WSW (Geoffroy *et al.* 1998) or E–W (Chalmers *et al.* 1999) extension. Chalmers *et al.* (1999) proposed that the N–S faults formed by E–W-oriented crustal extension, while associated ESE–WNW faults formed as a consequence of reactivation of shear zones in the underlying basement. Normal faults are dominantly N–S onshore (Fig. 6C), fitting with this model proposed by Chalmers *et al.* (1999). However, this implies that while Baffin Bay in the north and Labrador Sea in the south were undergoing ENE–WSW extension (deduced from dominant fault trends and earliest magnetic anomaly trends, Chalmers & Pulvertaft 2001), southern West Greenland and the Nuussuaq basin were undergoing E–W extension. A better explanation is that the Davis Strait at this time (i.e. prior to the onset of sea-floor spreading) lay in a transfer/step-over zone between two extensional basins, and that it was strongly influenced by basement fabrics such that this region experienced complex 3-D strain associated with regional ENE–WSW extension (Fig. 10). Onshore normal fault sets form a quadrimodal fault distribution (four sets of fault planes, Fig. 6C) consistent with 3-D strain.

This faulting is then subsequently dissected by N–S (system 2) and NNE–SSW (system 4) -oriented faults during the Eocene (Chalmers *et al.* 1999). The Itilli fault zone (Fig. 1) is one such NNE–SSW-oriented structure cutting through north-west Nuussuaq. This fault zone appears to be a left-lateral splay from the northern extension of the Ungava fault zone in the Davis Strait (Chalmers *et al.* 1999).

STAGE 1:
Late Cretaceous–Paleocene extension (NE–SW to ENE–SSW). Pre-existing basement anisotropy (Nagssugtoqidian orogenic belt) appears to influence fault patterns in the Davis Strait. Possible strain partitioning between basement-parallel and N–S-trending normal faults.

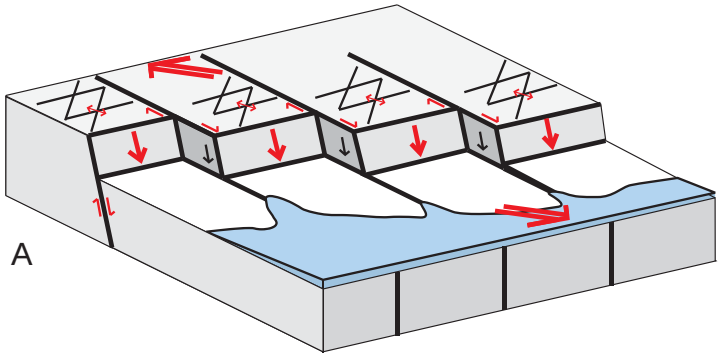

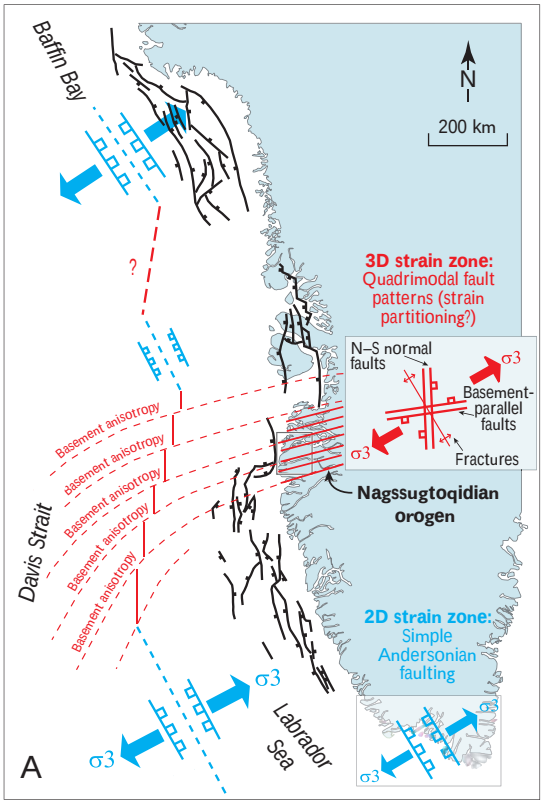

STAGE 2:
NNE-trending Eocene sinistral wrench system (NE to ENE extension, SE to SSE compression) reactivating earlier extensional faults and basement-parallel structures (e.g. thrust faults at camp 4, and the Ikermiut fault zone).

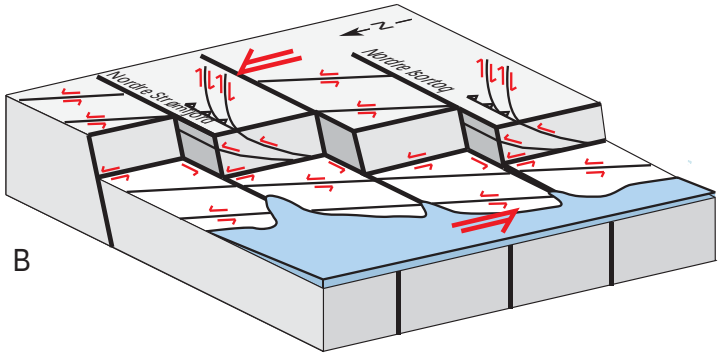

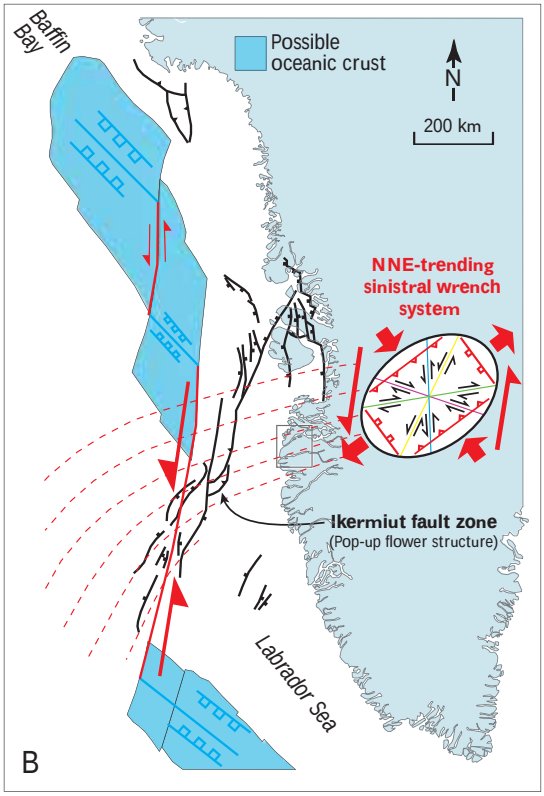

Fig. 10. Proposed two-stage tectonic model for the tectonic evolution of upper Mesozoic – Cenozoic extension within the Nagssugtoqidian orogen. Stage 1(A): N- and ENE-trending normal faults and dextral basement reactivation due to ENE–WSW extension. Stage 2 (B): N- and NNE-trending sinistral strike-slip faulting, and associated strike-slip wrench tectonic systems, with compressional structures (reverse faults) forming in zones of basement anisotropy (e.g. shear zones). Block diagrams show schematic cartoons outlining fault patterns observed onshore, while maps show the regional context, based on correlations between onshore and offshore fault structures.

Correlation with fault structures offshore

Fault patterns offshore in the Davis Strait exhibit similar *c.* N–S and ENE–WSW dominant orientations. The south and east bounding faults to the Sisimiut basin strike ENE–WSW and N–S respectively (Fig. 1). Significantly, the southern margin of the Sisimiut basin is coincident both in orientation and location with a major basement shear zone (the Nordre Isortoq shear zone), and is likely to have exerted a similar structural control to that interpreted for onshore. Block faulting has been dated via drilling as having taken place between the late Campanian and late Paleocene (Christiansen *et al.* 2001; Dalhoff *et al.* 2003), indicating that these extensional faults are of similar age to those associated with valley incision on Nuussuaq and north Disko (Dam & Sønderholm 1998; Dam *et al.* 2000; Dam 2002).

The Ungava fault zone with its associated fault systems (e.g. the Ikermiut fault zone) is the most prominent structure in the Davis Strait (Chalmers & Pulvertaft 2001). This NNE–SSW-oriented structure is interpreted as a transform fault zone showing sinistral shear, and has been linked to the Itilli fault zone (Fig. 1; Chalmers *et al.* 1999). System 4 (NNE–SSW) faulting onshore, around Nordre Strømfjord, is consistent with late sinistral strike-slip movements, and it is reasonable to suggest that this system is of similar age. As already discussed, offshore evidence for sinistral strike-slip movements can be seen in the Ikermiut fault zone on the western margin of the Sisimiut basin (Chalmers & Pulvertaft 2001) where transpressional thrusts (similar to compressional flower structures modelled in Dooley *et al.* 1999) appear to have formed in the restraining bend of a strike-slip fault (see fig. 6 of Chalmers & Pulvertaft 2001). These thrusts cut early Eocene mudstones, but are overlain by late Eocene sediments, providing further evidence for timing of these movements. This sinistral shear is thus a consequence of left-lateral movement of the Canadian plate relative to the Greenland plate along the Ungava transform system during sea-floor spreading in the Labrador Sea (Fig. 1).

Evidence for neotectonic faulting?

Chalmers (2000) presented evidence for Neogene uplift in offshore areas of central West Greenland, while recent onshore topographic and apatite fission-track data analysis has identified similar Neogene activity (Japsen *et al.* 2002, 2005). A common observation in this field area is the presence of raised beaches and palaeoshorelines, up to elevations 30 m above present sea levels (Fig. 5A). They are probably the result of isostatic readjustment following the removal of Pleistocene ice load. Topographically, the region appears to be divided into blocks, split by ENE-trending fjords and NNE-trending escarpments (Fig. 2C). These must be quite recent features as they have not been eroded during glacial activity (and may in fact be a consequence of it). The trend of system 4 faults (and also locally those of system 2) is generally parallel to the pronounced NNE-trending escarpment from Nordre Isortoq to Nordre Strømfjord onshore, and also to a similarly trending scarp near offshore (identified in bathymetry maps), and it is possible that these faults have been reactivated as normal faults during a recent tectonic event. This conjecture still needs to be verified, as the main escarpments were not studied in detail during our field work.

Summary

The observed fault and fracture systems reflect a brittle tectonic history that is ultimately related to far-field plate movements, uplift and basin formation. The development of Mesozoic to Cenozoic basins offshore West Greenland appears to be strongly controlled by faults. Therefore, knowledge of the fracture systems in the exposed Precambrian basement provides a valuable insight into fault geometries and kinematics during the development of offshore basins and potential hydrocarbon reservoirs. It also provides insights into the possible influence of basement reactivation.

Several possible tectonic-event models may be constructed for this region given the lack of definite ages for structures. Table 2 shows a basic summary of the relative timings of fault systems identified in this study relative to regional offshore tectonic models, while Fig. 10 presents a model for fault development based on the observations and correlations made in this study. The absolute timing of the fault activity onshore, as deduced from correlation to other fault systems with known ages, needs to be tested by dating of fault rock samples. A simple two-stage model has been outlined to explain the complex fault patterns exhibited in onshore exposures of the central Nagssugtoqidian orogen (Fig. 10).

The brittle tectonic evolution of the region appears to be dominated by NE–SW extension, which is consistent with the opening of the Labrador Sea and Baffin Bay. Only slight variations in the regional stress field are required to account for the diversity of fault orientations. According to Chalmers & Pulvertaft (2001) there was a 15° counter

clockwise rotation in spreading direction between the Paleocene and the Eocene in the Labrador Sea as opening started between Greenland and Europe, which is consistent with the two-stage model outlined in Fig. 10. In the early stages of opening, faulting was dominated by extensional structures (under 3-D strain conditions), favouring an E–W to ENE–WSW extension (Fig. 10A); however, as the Ungava transform fault developed, faulting became more wrench dominated (2-D plane strain), and suggests NE–SW extension (Fig. 10B). Variations in fault geometry reflect these changes in the regional stress field. However, the influence of basement structure also appears to have played an important role throughout (e.g. extensional faults not normal to the extension direction, and the apparent localised compressional zones associated with intense basement fabrics). Although most faults observed onshore trend highly obliquely to basement fabrics, fault patterns do appear to vary in areas of intense pre-existing structure (such as the Nordre Strømfjord and Nordre Isortoq shear zones) which suggest that the fabrics within the Nagssugtoqidian orogen may have had some influence on the fault complexity of the Davis Strait.

The conclusions from this study show that the fault patterns and sense of movement on faults onshore reflect the stress fields that govern the opening of the Labrador Sea – Davis Strait – Baffin Bay seaway, and that the wrench couple on the Ungava transform system played a dominant role in the development of the onshore fault patterns.

Acknowledgements

The authors would like to thank BP (Norway) and Statoil (UK) for providing additional funding for this field research, and to NERC for funding R.W.W.'s Ph.D. research (NER/S/S/2001/06740). Thorough and insightful reviews from S. Bergh and T.C.R. Pulvertaft and additional help from the latter concerning numerous details are greatly appreciated. The bulletin editors, A.A. Garde and F. Kalsbeek, are also thanked for their helpful and encouraging comments.

References

Bonow, J.M. 2004: Palaeosurfaces and palaeovalleys on North Atlantic previously glaciated passive margins – reference forms for conclusions on uplift and erosion. Ph.D. thesis. Thesis in Geography with Emphasis on Physical Geography 30, 17 pp. + 4 articles. Stockholm University, Sweden.

Butler, R.W.H., Holdsworth, R.E. & Lloyd, G.E. 1997: The role of basement reactivation in continental deformation. Journal of the Geological Society (London) 154, 69–71.

Chalmers, J.A. 2000: Offshore evidence for Neogene uplift in central West Greenland. Global and Planetary Change 24, 311–318.

Chalmers, J.A. & Laursen, K.H. 1995: Labrador Sea: the extent of continental crust and the timing of the start of sea floor spreading. Marine and Petroleum Geology 12, 205–217.

Chalmers, J.A. & Pulvertaft, T.C.R. 2001: Development of the continental margins of the Labrador Sea: a review. In: Wilson, R.C.L. *et al*. (eds): Non-volcanic rifting of continental margins: a comparison of evidence from land and sea. Geological Society Special Publication (London) 187, 77–105.

Chalmers, J.A., Dahl-Jensen, T., Bate, K.J. & Whittaker, R.C. 1995: Geology and petroleum prospectivity of the region offshore southern West Greenland. Rapport Grønlands Geologiske Undersøgelse 165, 13–21.

Chalmers, J.A., Pulvertaft, T.C.R., Marcussen, C. & Pedersen, A.K. 1999: New insight into the structure of the Nuussuaq basin, central West Greenland. Marine and Petroleum Geology 16, 197–224.

Chian, D. & Louden, K.E. 1994: The continent-ocean crustal transition across the southwest Greenland margin. Journal of Geophysical Research 99, 9117–9135.

Christiansen, F.G., Bojesen-Koefoed, J.A. & Chalmers, J.A. 2001: Petroleum geological activities in West Greenland in 2000. Geology of Greenland Survey Bulletin 189, 24–33.

Dalhoff, F., Chalmers, J.A., Gregersen, U., Nøhr-Hansen, H., Rasmussen, J.A. & Sheldon, E. 2003: Mapping and facies analysis of Paleocene – Mid-Eocene seismic sequences, offshore southern West Greenland. Marine and Petroleum Geology 20, 935–986.

Dam, G. 2002: Sedimentology of magmatically and structurally controlled outburst valleys along rifted volcanic margins: examples from the Nuussuaq basin, West Greenland. Sedimentology 49, 505–532.

Dam, G. & Sønderholm, M. 1998: Sedimentological evolution of a fault-controlled early Paleocene incised-valley system, Nuussuaq Basin, West Greenland. In: Shanley, K.W. & McCabe, P.J. (eds): Relative role of eustasy, climate, and tectonism in continental rocks. Society of Economic Paleontologists and Mineralogists Special Publication 59, 109–121.

Dam, G., Nøhr-Hansen, H., Pedersen, G.K. & Sønderholm, M. 2000: Sedimentary and structural evidence of a new early Campanian rift phase in the Nuussuaq Basin, West Greenland. Cretaceous Research 21, 127–154.

De Paola, N., Holdsworth, R.E., McCaffrey, K.J.W. & Barchi, M.R. 2005: Partitioned transtension: an alternative to basin inversion models. Journal of Structural Geology 27, 607–625.

Dewey, J.F. 2002: Transtension in arcs and orogens. International Geology Review 44, 402–439.

Dooley, T., McClay, K. & Bonora, M. 1999: 4D evolution of segmented strike-slip fault systems: applications to NW Europe. In: Fleet, A.J. & Boldy, S.A.R. (eds): Petroleum geology of Northwest Europe, Proceedings of the 5th Conference, 215–225. London: Geological Society.

Escher, J.C. & Pulvertaft, T.C.R. 1995: Geological map of Greenland, 1:2 500 000. Copenhagen: Geological Survey of Greenland.

Geoffroy, J., Gélard, J.P., Lepvrier, C. & Olivier, P. 1998: The coastal flexure of Disko (West Greenland), onshore expression of the 'oblique reflectors'. Journal of the Geological Society (London) 155, 463–473.

Geoffroy, J. *et al*. 2001: Southeast Baffin volcanic margin and the North American – Greenland plate separation. Tectonics 20, 566–584.

Henriksen, N., Higgins, A.K., Kalsbeek, F. & Pulvertaft, T.C.R. 2000: Greenland from Archaean to Quaternary. Descriptive text to the geological map of Greenland, 1:2 500 000. Geology of Greenland Survey Bulletin 185, 93 pp.

Holdsworth, R.E., Butler, C.A. & Roberts, A.M. 1997: The recognition of reactivation during continental deformation. Journal of the Geological Society (London) 154, 73–78.

Japsen, P., Bonow, J., Klint, K.E.S. & Jensen, F.K. 2002: Neogene uplift, erosion and resedimentation in West Greenland. Field report summer 2002. Danmarks og Grønlands Geologiske Undersøgelse Rapport 2002/71, 114 pp.

Japsen, P., Green, P.F. & Chalmers, J.A. 2005: Separation of Palaeogene and Neogene uplift on Nuussuaq, West Greenland. Journal of the Geological Society (London) 162, 299–314.

Larsen, J.G. & Pulvertaft, T.C.R. 2000: The structure of the Cretaceous–Palaeogene sedimentary-volcanic area of Svartenhuk Halvø, central West Greenland. Geology of Greenland Survey Bulletin 188, 40 pp.

Marker, M., Mengel, F., van Gool, J. and field party 1995: Evolution of the Palaeoproterozoic Nagssugtoqidian orogen: DLC investigations in West Greenland. Rapport Grønlands Geologiske Undersøgelse 165, 100–105.

McClay, K.R. 1987: The mapping of geological structures (Geological Society of London handbook), 161 pp. London: John Wiley and Sons.

Nieto-Samaniego, A.F. & Alaniz-Alvarez, S.A. 1997: Origin and tectonic interpretation of multiple fault patterns. Tectonophysics 279, 197–206.

Petit, J.-P. 1987: Criteria for the sense of movement on fault surfaces in brittle rocks. Journal of Structural Geology 9, 597–608.

Ramberg, H. 1949: On the petrogenesis of the gneiss complexes between Sukkertoppen and Christianshaab, West Greenland. Meddelelser fra Dansk Geologisk Forening 11, 312–327.

Reches, Z. 1983: Faulting of rocks in three-dimensional strain fields. II. Theoretical analysis. Tectonophysics 95, 133–156.

Storey, M., Duncan, R.A., Pedersen, A.K., Larsen, L.M. & Larsen, H.C. 1998: $^{40}Ar/^{39}Ar$ geochronology of the West Greenland Tertiary volcanic province. Earth and Planetary Science Letters 160, 569–586.

Taylor, B., Crook, K. & Sinton, J. 1994: Extensional transform zones and oblique spreading centres. Journal of Geophysical Research 99(B10), 19707–19718.

van Gool, J.A.M., Connelly, J.N., Marker, M. & Mengel, F.C. 2002: The Nagssugtoqidian orogen of West Greenland: tectonic evolution and regional correlations from a West Greenland perspective. Canadian Journal of Earth Sciences 39, 665–686.

Whittaker, R.C. 1995: A preliminary assessment of the structure, basin development and petroleum potential offshore central West Greenland. Open File Series Grønlands Geologiske Undersøgelse 95/9, 33 pp., 6 maps.

Woodcock, N.H. & Schubert, C. 1994: Continental strike-slip tectonics. In: Hancock, P.L. (ed.): Continental deformation, 251–263. Oxford: Pergamon Press.

Manuscript received 26 October 2004; revision accepted 1 November 2005

Danmarks og Grønlands Geologiske Undersøgelse (GEUS)

Geological Survey of Denmark and Greenland
Øster Voldgade 10, DK-1350 Copenhagen K
Denmark

Geological Survey of Denmark and Greenland Bulletin is a new series started in 2003 to replace the two former bulletin series of the Survey, viz. *Geology of Greenland Survey Bulletin* and *Geology of Denmark Survey Bulletin*. The twenty-one volumes published since 1997 in those two series are listed below after the new bulletin series. The new series, together with *Geological Survey of Denmark and Greenland Map Series*, now forms the peer-reviewed scientific series of the Survey.

Geological Survey of Denmark and Greenland Bulletin (new series)

1 The Jurassic of Denmark and Greenland, 948 pp. (28 articles), 2003.
Edited by J.R. Ineson & F. Surlyk. 500.00

2 Fish otoliths from the Paleocene of Denmark, 94 pp., 2003.
By W. Schwarzhans. 100.00

3 Late Quaternary environmental changes recorded in the Danish marine molluscan faunas, 268 pp., 2004.
By K.S. Pedersen. 200.00

4 Review of Survey activities 2003, 100 pp. (24 articles), 2004.
Edited by M. Sønderholm & A.K. Higgins. 180.00

5 The Jurassic of North-East Greenland, 112 pp. (7 articles), 2004.
Edited by L. Stemmerik & S. Stouge. 160.00

6 East Greenland Caledonides: stratigraphy, structure and geochronology, 93 pp. (6 articles), 2004.
Edited by A.K. Higgins and F. Kalsbeek. 160.00

7 Review of Survey activities 2004, 80 pp. (19 articles), 2005.
Edited by M. Sønderholm & A.K. Higgins. 180.00

8 Structural analysis of the Rubjerg Knude Glaciotectonic Complex, Vendsyssel, northern Denmark, 2005.
By S.A.S. Pedersen. 300.00

9 Scientific results from the deepened Lopra-1 borehole, Faroe Islands, 156 pp. (11 articles), 2006.
Edited by J.A. Chalmers and R. Waagstein. 240.00

10 Review of Survey activities 2005, 68 pp. (15 articles), 2006.
Edited by M. Sønderholm & A.K. Higgins.

11 Precambrian crustal evolution and Cretaceous–Palaeogene faulting in West Greenland, 204 pp. (12 articles), 2006.
Edited by A.A. Garde & F. Kalsbeek.

Geological Survey of Denmark and Greenland Map Series (new series)

1 Explanatory notes to the Geological map of Greenland, 1:500 000, Humboldt Gletscher, Sheet 6, 48 pp., 2004.
By P.R. Dawes 280.00

2 Explanatory notes to the Geological map of Greenland, 1:500 000, Thule, Sheet 5 (1991), 97 pp. + map, 2006.
By P.R. Dawes. 300.00

Geology of Greenland Survey Bulletin (discontinued)

176 Review of Greenland activities 1996, 112 pp. (18 articles), 1997.
Edited by A.K. Higgins & J.R. Ineson. 200.00

177 Accretion and evolution of an Archaean high-grade grey gneiss – amphibolite complex: the Fiskefjord area, southern West Greenland, 115 pp., 1997.
By A.A. Garde. 200.00

178 Lithostratigraphy, sedimentary evolution and sequence stratigraphy of the Upper Proterozoic Lyell Land Group (Eleonore Bay Supergroup) of East and North-East Greenland, 60 pp., 1997.
By H. Tirsgaard & M. Sønderholm. 200.00

179 The Citronen Fjord massive sulphide deposit, Peary Land, North Greenland: discovery, stratigraphy, mineralization and structural setting, 40 pp., 1998.
By F.W. van der Stijl & G.Z. Mosher. 200.00

180 Review of Greenland activities 1997, 176 pp. (26 articles), 1998.
Edited by A.K. Higgins & W.S. Watt. 200.00

181 Precambrian geology of the Disko Bugt region, West Greenland, 179 pp. (15 articles), 1999.
Edited by F. Kalsbeek. 240.00

182 Vertebrate remains from Upper Silurian – Lower Devonian beds of Hall Land, North Greenland, 80 pp., 1999.
By H. Blom. 120.00

183 Review of Greenland activities 1998, 81 pp. (10 articles), 1999.
Edited by A.K. Higgins & W.S. Watt. 200.00

184 Collected research papers: palaeontology, geochronology, geochemistry, 62 pp. (6 articles), 1999. 150.00

185 Greenland from Archaean to Quaternary. Descriptive text to the Geological map of Greenland, 1:2 500 000, 93 pp., 2000.
By N. Henriksen, A.K. Higgins, F. Kalsbeek & T.C.R. Pulvertaft. 225.00

186 Review of Greenland activities 1999, 105 pp. (13 articles), 2000.
Edited by P.R. Dawes & A.K. Higgins. 225.00

187 Palynology and deposition in the Wandel Sea Basin, eastern North Greenland, 101 pp. (6 articles), 2000.
Edited by L. Stemmerik. 160.00

188 The structure of the Cretaceous–Palaeogene sedimentary-volcanic area of Svartenhuk Halvø, central West Greenland, 40 pp., 2000.
By J. Gutzon Larsen & T.C.R. Pulvertaft. 130.00

189 Review of Greenland activities 2000, 131 pp. (17 articles), 2001.
Edited by A.K. Higgins & K. Secher. 160.00

190 The Ilímaussaq alkaline complex, South Greenland: status of mineralogical research with new results, 167 pp. (19 articles), 2001.
Edited by H. Sørensen. 160.00

191 Review of Greenland activities 2001, 161 pp. (20 articles), 2002.
Edited by A.K. Higgins, K. Secher & M. Sønderholm. 200.00

Geology of Denmark Survey Bulletin (discontinued)

36 Petroleum potential and depositional environments of Middle Jurassic coals and non-marine deposits, Danish Central Graben, with special reference to the Søgne Basin, 78 pp., 1998.
By H.I. Petersen, J. Andsbjerg, J.A. Bojesen-Koefoed, H.P. Nytoft & P. Rosenberg. 250.00

37 The Selandian (Paleocene) mollusc fauna from Copenhagen, Denmark: the Poul Harder 1920 collection, 85 pp., 2001.
By K.I. Schnetler. 150.00

Prices are in Danish kroner exclusive of local taxes, postage and handling

Note that information on the publications of the former Geological Survey of Denmark and the former Geological Survey of Greenland (amalgamated in 1995 to form the present Geological Survey of Denmark and Greenland) can be found on the Survey's website: *www.geus.dk*